CRACK TIP OPENING DISPLACEMENT (CTOD) IN SINGLE EDGE NOTCHED BEND (SEN(B))

A thesis submitted for the degree of

Doctor of Philosophy

by

WeeLiam Khor

MACE

Brunel University London

April 2018

Acknowledgement

To my dear parents, sisters and aunt, Terry, Sharon, Shirley, Ashley and Ai Hwa, I am very grateful for all the unconditional love and support. My supervisors, Dr. Philippa Moore, Chris Brown and Dr. Henryk Pisarski, thank you very much for guiding me though this long journey with your knowledge and experience. Dear Dr. Simon Smith, your patience with all the unexpected 'pop-up' technical discussions is deeply appreciated. To the lively laboratory technicians, Jerry, Phil, Dan, Mark, Ashley, Tom and Dianne, thank you for making my time at the office interesting. And to Dr. HweiYang Tan and Muhammad Shaheer, thanks for the mental support when I need them most.

I tried to keep this short and would like to apologize for those whose name had been omitted. Without all your help and support this piece of work would struggle to complete. And finally, a very special thank you to C.

Abstract

This thesis investigates the quantity Crack Tip Opening Displacement (CTOD) as a means to assess fracture toughness when measured in the Single Edge Notched Bend (SENB) specimen setup. A particular objective is to assess the effectiveness of the test when used for high strain-hardening materials (e.g. stainless steels). This has been an increasing concern as the current available methods were generally designed for lower strain hardening structural steel.

Experimental work on CTOD tests included silicone casting of the crack, and constant displacement tests were also performed. The silicone castings enable physical measurement of the crack under an optical microscope. Results from a series of Finite Element (FE) models were validated from the experiments. δ_5 surface measurements were obtained using Digital Image Correlation (DIC) as a courtesy of TWI, which were compared to surface CTOD measurements from the silicone castings. In addition to the experiments and Finite Element modelling, archived test data from TWI was processed, showing analytical differences between current Standard CTOD equations.

CTOD calculations from BS 7448, ISO 12135, ASTM E1820 and WES 1108 were compared to the experimental and FE modelling results. For high strain hardening material, CTOD predicted by Standard equations (apart from those in BS 7448 and single point CTOD from ISO 12135) were lower than the values determined from silicone measurements and modelling. This potentially leads to over conservative values to be used in Engineering Critical Assessments (ECA) or material approval.

Based on a series of different strain hardening property models, a relationship between strain hardening and the specimen rotational factor, r_p was established. An improved equation for the calculation of CTOD is proposed, which gave good estimation of the experimental and Finite Element modelling results. The improved equation will be proposed for future amendments of the ISO 12135 standard.

The results of this research enable the accurate fracture characterisation of a range of engineering alloys, with both low and high strain hardening behaviour in both the brittle and ductile fracture regime.

Introduction

Many factors contribute to the failure of an engineering component, i.e. flaw or inclusion in material, cyclic fatigue loading and residual stresses in the material. One of the most notable failure cases in history is the brittle fracture of Liberty Ships in 1940's, where 1031 of 2078 ships experienced brittle related damage (Kobayashi & Onoue 1943). The lack of understanding in fracture at the time did not recognize material strength at low temperature and the effects due to weldments, which led to an expensive lesson in fracture. This incident led to more research in fracture mechanics, with two notable researches by Rice (1968) and Wells (1961).

Fracture mechanics is a study of the material's fracture resistivity, consisting two main parts: - linear elastic fracture mechanics (LEFM) and elastic plastic fracture mechanics (EPFM). Linear elastic fracture mechanics describes the material's fracture resistance within the elastic yielding region, mainly represented by stress intensity factor, K; the elastic plastic fracture mechanics considers post yielding where the crack deforms plastically, represented by the J-integral and crack tip opening displacement, CTOD.

Experimentally, the fracture parameters K, J and CTOD are assessed through fracture toughness tests, where specimens are extracted from the actual structures and tested in a laboratory environment. Fracture toughness is typically used in Engineering Critical Assessments (ECA), where fracture mechanics theories are applied to evaluate the fitness of a structure for operation purposes. The tests are conducted in a controlled lab environment, where load and displacement feedback are used to infer the equivalent fracture toughness value. Normally, a fatigue crack is induced onto the specimen to represent the crack in a real operating environment. There are numerous different setup for fracture toughness testing, e.g. compact tension (C(T)), single edge notched bend (SEN(B)) and single edge notched tension (SEN(T)).

The BS 7448-1 and ASTM E1820 are two of the most popular standards specifying methods of estimating fracture toughness, including CTOD. However, the equations do not agree with each other due to the different assumptions adapted for the formulation of the equations. This issue is known and thus researchers at the Japanese Welding Engineering Society, JWES proposed a new CTOD equation with the intention of estimating CTOD accurately.

A series of fracture toughness tests were designed to validate the CTOD estimations using three materials with different strain hardening properties. To obtain a physical representative of CTOD, the crack in the specimens were casted using silicone compound, which gives a physical negative of the crack. The physical CTOD can be measured from the crack replica by using an optical microscope. The CTOD measured on the crack replica is considered the actual CTOD and was used as the baseline comparison against other methods. In addition to the experiments, finite element models were used to predict CTOD based on the material used in the experiments.

Chapter 5.1 gives an analytical comparison between the different CTOD equations. Based on the resources available at TWI, data from 137 parent material SEN(B) tests were calculated using the CTOD equations from BS, ASTM and JWES. JWES overestimate BS for low strain hardening materials but underestimate higher strain hardening materials, whereas the ASTM consistently underestimate BS. Comparing the elastic and plastic CTOD, for low CTOD values, the elastic component of CTOD is dominant, and *vice versa* for high CTOD values.

Chapter 6.1 describes the variation of CTOD across the specimen thickness in 20mm thick austenitic stainless steel. It was well known that fracture toughness varies across the crack front, but the standards did not explicitly specify the location for the assessment of CTOD. Experimentally, CTOD is affected by the curved crack front due to fatigue pre-cracking. An alternative definition of CTOD based on surface measurements, δ_5 was extracted from seven specimens, compared to CTOD measured from the middle of the silicone replica. Additionally, CTOD was extracted from a straight crack front FE model to show the effect of crack front curvature.

In Chapter 7.1, the accuracy of the CTOD equations are validated based on CTOD measured from the middle of the crack. The FE models representing the test specimens managed to give good estimation of CTOD. Comparing the CTOD based on the equations to the silicone replica and FE measurements, it was found that the equations generally underestimate CTOD, apart from the BS equation for higher strain hardening properties. The ASTM equation was seen to give lower estimation of CTOD regardless of the material strain hardening. The JWES equation seemed to give a good compromise between underestimation and accuracy for all strain hardening.

Chapter 8.1 shows the effect of strain hardening on the CTOD tearing resistance curve, also described as the CTOD R-curve. The ISO, ASTM and BS equations were based on different assumptions and employed different crack correction factors for CTOD. Measurements from the silicone replica show that the material's resistance to tearing increase with strain hardening property. Similar to that observed in Chapter 7.1, the BS equation overestimate the high strain hardening R-curve, and ASTM underestimate all R-curves. Despite not designed for R-curves, the JWES equation estimated the R-curves with adequate accuracy.

The role of the rotational factor, r_p in the determination of CTOD is described in Chapter 9.1. r_p was extracted from both experiment and FE models shows that r_p is not constant as assumed by BS and JWES. Including the effects of strain hardening in r_p, r_p increases with reducing strain hardening. The constant r_p used by BS and JWES falls within the range of the r_p corrected for strain hardening. The corrected r_p estimated the silicone replica CTOD accurately despite some minor overestimation.

Chapter 10.1 provides a discussion for the overall work. The implication of the different definition of CTOD and its effect on a propagating crack is explained. The necessity of the crack correction factor for R-curves is discussed. The chapter also explains the validity of the similar triangles concept and strain hardening correction for CTOD.

Contents

List of figures

List of tables

Nomenclature

A_p= Plastic work, area under P vs. V_p, Nmm
a_0= Original crack length, mm
a_0/W= Crack length- specimen width ratio
B=Specimen thickness, mm
B_0= Remaining ligament ahead of the crack tip, W-a_0, mm
B_N= Net specimen thickness in the remaining ligament ahead of the crack tip, mm
b= Position across the crack in the thickness direction
CMOD= Crack mouth opening displacement, mm
E= Modulus of elasticity, MPa
ERR= percentage error, %
FE= Finite element
G= Griffith's energy release rate
J= Path independent strain energy around the crack, also called J-integral, Nmm^{-1}
J_{el}= Elastic component of J, Nmm^{-1}
J_{pl}= Plastic component of J, Nmm^{-1}
K= Stress intensity factor, $Nmm^{-3/2}$
k= Proportionality constant
m= Factor relating CTOD to J or K (sometimes referred to as a "constraint" factor)
P= Load, kN
q= Load line displacement, mm
r, θ= Polar coordinates described in Figure 1.04
r_p= Rotational factor
$r_{p\,sh}$= strain hardening corrected r_p
S= Specimen span, mm
SENB= Single edge notched bend
T= Temperature, °C
V_g= clip gauge opening displacement, mm
V_p= Plastic component of the clip gauge opening displacement, mm
W= Specimen width, mm
W_s= work needed for the formation of new surfaces
w= Strain energy density
w_f= Fracture energy
X= crack growth correction factor for BS 7448-4
Y_{ASTM}=crack growth correction factor for ASTM E1802
Y_{ISO}=crack growth correction factor for ISO 12135
z= Vertical height above the crack mouth where displacement is measured, mm
δ= Crack tip opening displacement, CTOD, mm
δ_0= CTOD based on the opening of the original crack tip, mm
δ_{45}= CTOD measured based on the 45° intercept from the blunted crack tip in FE, mm
δ_5= Displacement between two points, positioned 5mm apart horizontally at the original crack tip of the specimen surfaces, mm
δ_{el}= Elastic component of CTOD, mm
δ_{FE}= CTOD measured from the middle thickness of the FE model based on the opening of the original crack tip, mm
$\delta_{FE\,corr}$= δ_{FE} with applied correction factor validated to experimental results, mm

δ_{pl}= Plastic component of CTOD, mm
δ_{sh}= Strain hardening corrected CTOD based on $r_{p\,sh}$
δ_{SRC}= CTOD measured from the middle thickness of the silicone replica based on the original crack tip, mm
σ_{eng}= Engineering stress, MPa
σ_{ij}= Stress tensor, MPa
σ_{true}= True stress, MPa
σ_{uts}= Ultimate tensile stress, MPa
σ_{y}= 'Flow' stress defined in ASTM E1820, $(\sigma_{ys}+\sigma_{uts})/2$, MPa
σ_{ys}= 0.2% yield/ proof stress, MPa
σ_{ys}/σ_{uts}= Tensile ratio
ε_{eng}= Engineering strain
ε_{ij}= Strain tensor
ε_{true}= True strain
η_{pl}= Geometrical based calibration factor for J
v= Poisson's ratio
μ= tearing modulus
Π= potential energy of the crack
Π_0= total potential energy of the un-cracked plate
γ_s= surface energy, $(\gamma_s+\gamma_p)$

Chapter 1

Literature review

1.1 Introduction

During the design process of a component or structure, it is often assumed that the material is isotropic and free from flaws. However this is nearly impossible to achieve as flaws are often introduced during the fabrication process. When the component or structure is in operation, fatigue loading could lead to an increase of flaw size. When the flaw achieves a critical size or critical load is experienced, unstable brittle fracture could occur. Unstable brittle fracture is least desirable as there would be almost no indication before failure takes place. It is important that these flaws can be assessed using an engineering approach to determine the fitness of the flawed component/ structure for operation.

Historically, many accidents happened due to the lack of fracture mechanics consideration. The DeHavilland Comet aircraft incident (Wanhill 2002), Titanic (SSC n.d.) and the Liberty ship (Kobayashi & Onoue 1943) incident are few of the well-known cases caused by fatigue and brittle fracture. Much money is lost, reliability jeopardized and more importantly many innocent lives are sacrificed. It is believed that most of these incidents could be avoided if the concept of fracture mechanics is properly applied and the flaws accessed accordingly. Fracture mechanics is the theoretical description of the behaviour of cracks in materials.

The concept of fracture mechanics was first investigated and developed around the First World War. The first approach to brittle fracture was introduced by Griffith (1921), while the study of fracture mechanics approach to real structures is still being improved today. In the industry, fracture mechanics is applied to real structures in the use of fracture toughness testing and engineering critical assessments.

Fracture toughness is the study of the material's resistivity to crack extension. Fracture toughness is described by several parameters: K, J and CTOD (crack tip opening displacement). There are many factors that affect the fracture toughness of a material, i.e. temperature, specimen geometry and tensile properties. Fracture toughness testing standards are published with the objective to standardize the testing procedure, ensuring consistent test results. Two different parties testing the same material under similar conditions according to the same standard should yield similar and comparable result.

This literature review describes the main concepts of fracture mechanics, an introduction to fracture toughness testing, and it's implication on fitness-for-service assessments.

1.2 Fracture mechanics

1.2.1 Overview

Fracture mechanics is the study of flaws and cracks. The crack propagating mechanism and energy absorbed by the crack are two examples studied in fracture mechanics. The two main areas of fracture mechanics are described as linear elastic fracture mechanics and elastic-plastic fracture mechanics.

The basic approach to fracture mechanics is established in the 1920's based on experiments on glass material, intended to explain the failure of brittle materials (Griffith 1921). Linear elastic fracture mechanics is applicable when the material operates within the yield limit. However some yielding in unavoidable during real operations. Therefore elastic-plastic fracture mechanics is often applied alongside linear elastic fracture mechanics for analysis of problems in real engineering structures.

This section gives an overall introduction to fracture mechanics, covering different loading modes, the condition of the crack tip, fracture parameters, modes of fracture and factors affecting fracture toughness.

1.2.2 Loading modes

There are three basic loading conditions of a crack, Mode I, II and III loading (Figure 1.01). In real operating conditions, cracks could experience a combination of two or all three modes of loading. The crack tip for Mode I loading experiences tensile stress; the crack tip for Mode II and Mode III loading experiences in-plane shearing and out-of-plane shearing respectively. Mode I loading is the most common loading mode used for fracture toughness evaluation.

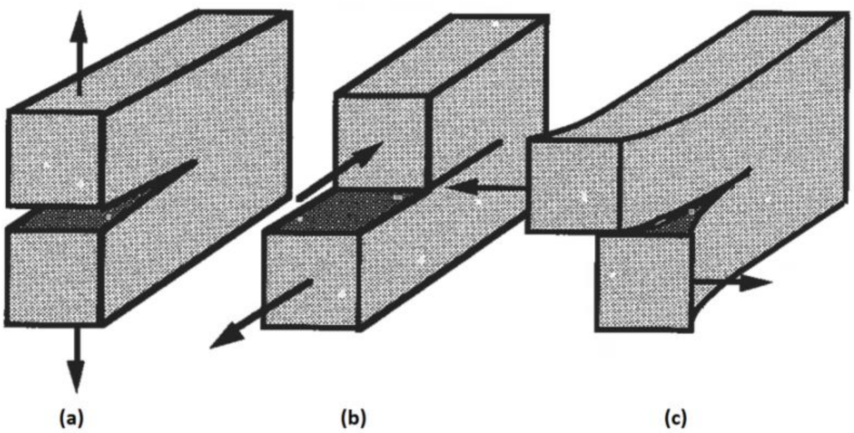

Figure 1.01 Three basic crack loading mechanism: - (a) Mode I, opening, (b) Mode II, in-plane shear, (c) Mode III, out-of-plane shear (Anderson 2008, p.43)

1.2.3 Flaw and voids

When an operating structure or component fails in fracture, it is often found that the fracture initiates from a flaw or voids. Flaw and voids introduce a non-load bearing region within an isotropic material, where stress flows around it when loaded.

Consider a plate of infinite length with a circular hole under uniaxial loading (see Figure 1.02(a)). The hole will not bear any load, representing a crack. The remaining ligament would experience higher stress than the regions without a hole. Stress would be highest at the side of the hole as shown in Figure 1.02(b). Based on the observation of the stress distribution across the region with a hole, it shows that the material at the sides of the hole with maximum stress will be the fracture initiation point.

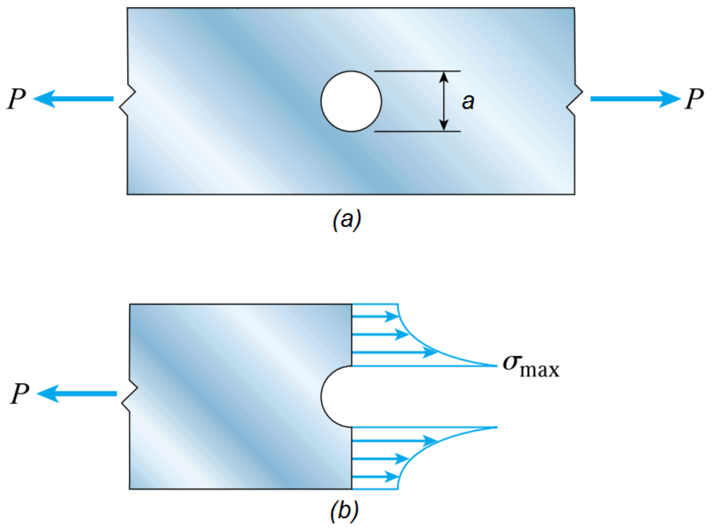

Figure 1.02 Illustrating the effects of a void in an isotropic material: - (a) a circular hole in an infinite length plate under uniaxial tension, (b) stress distribution across the cross section (Gere 2004, p.140)

1.2.4 Fracture parameters, *K*, *J* and CTOD

Fracture mechanics is often described in terms of fracture toughness parameters, *K*, *J* and CTOD. Material failing elastically is generally described using the stress intensity factor, K, which is the intensity of the elastic crack-tip field. *J* is described by the energy absorbed by the crack tip region. CTOD is the measure of the opening at the crack tip due to the opening of the crack. The fracture parameters are the measure of the material's resistance to fracture. The material would fail when the crack driving force exceeds the fracture toughness of the material.

1.3 Linear elastic fracture mechanics, LEFM

Linear elastic fracture mechanics, LEFM describes the condition of the crack when the stress experienced is within the yield limit. Deformation in the linear elastic region is recoverable and not permanent. However, small scale yielding (SSY), which is permanent deformation, occurs under the elastic yield limit as well. However, deformation due to SSY is small compared to the linear elastic deformation and generally neglected.

1.3.1 Griffith's energy balance criteria

One of the best known early developments in fracture mechanics was conducted by an English aeronautical engineer A.A. Griffith in the 1920s, where investigation of brittle fracture was performed on glass. Applying the concept of the First Law of Thermodynamics, it was assumed that the total energy experienced by the crack would be in equilibrium to the load applied on the crack. Therefore, under equilibrium, there is no change in total energy until the crack achieves the critical point for the initiation of crack growth. When the crack grows, energy is released from the crack, and therefore the energy applied on the crack and the energy experienced by the crack is no longer in equilibrium. The energy release due to crack growth was described as the Griffith energy release rate,

$$G = -\frac{d\Pi}{dA}$$

Π is the potential energy of the crack and A is the area. Consider an infinitely wide plate with a through thickness crack subjected to remote tensile stress in plane stress condition as in Figure 1.03.

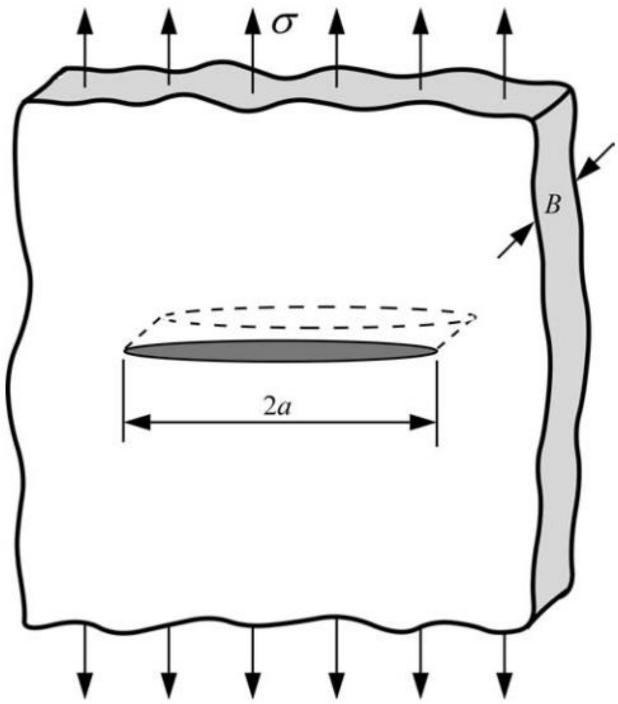

Figure 1.03 An infinitely wide plate with a through thickness ellipse crack subjected to remote tensile stress
(Anderson 2008, p.30)

For the crack to grow there must be sufficient potential energy to overcome the surface energy. Under equilibrium conditions, the Griffith energy balance is expressed as

$$\frac{d\Pi}{dA} + \frac{dW_s}{dA} = 0 \qquad \text{Eq. 1.01}$$

Π is the potential energy due to remote tensile stress and internal strain energy, W_s is the amount of work needed for the formation of new surfaces and dA is the incremental increase of crack area. For an ellipse shaped crack in plane stress, where the crack width in the stress loading direction approaches 0, Griffith solved the strain energy solution for a crack in an isotropic material, simplified by Anderson (2008, p.29) as

$$\Pi = \Pi_0 - \frac{\pi\sigma^2 a^2 B}{E}$$

Π_0 is described as the total potential energy of the un-cracked plate. The creation of a new crack require the formation of two new surfaces, and therefore the total work required to extend the existing crack is described as

$$W_s = 2(2aB\gamma_s)$$

γ_s is the surface energy of the material. Solving the differential equation gives

$$-\frac{d\Pi}{dA} = \frac{\pi\sigma^2 a}{E} \qquad \text{Eq. 1.02}$$

And

$$\frac{dW_s}{dA} = 2\gamma_s \qquad \text{Eq. 1.03}$$

Substituting Eq. 1.02 and Eq. 1.03 into the Griffith energy balance (Eq. 1.01), the fracture stress, σ_f is obtained as

$$\sigma_f = \sqrt{\frac{2\gamma_s E}{\pi a}} \qquad \text{Eq. 1.04}$$

Eq. 1.04 is applicable to isotropic linear elastic materials, as the Inglis (1913) and Griffith's (1921) analysis is based on the elastic stress solution at the crack tip. For small scale yielding situations, to account for the plastic flow, γ_s is replaced with ($\gamma_s + \gamma_p$) in Eq. 1.04, *w*here γ_p is the plastic component of the surface energy. This modification leads to

$$\sigma_f = \sqrt{\frac{2(\gamma_s + \gamma_p)E}{\pi a}} = \sqrt{\frac{2w_f E}{\pi a}}$$

w_f is defined as the fracture energy, depending on the property of the material. In small scale yielding situation, the crack would grow in an isotropic material when $\sigma > \sigma_f$ at the crack tip.

1.3.2 Stress intensity factor, K

For a cracked body subjected to external loading, solutions had been derived describing the stress field near the crack tip. In a linear isotropic material, setting the crack tip as the origin of the polar coordinate axis, the first order stress field could be described as (Anderson 2008, p.42)

$$\sigma_{ij} = \left(\frac{k}{\sqrt{r}}\right) f_{ij}(\theta) + \cdots \qquad \text{Eq. 1.05}$$

σ_{ij} is the stress tensor, f_{ij} is a dimensionless function, k is the proportionality constant, while r and θ are polar coordinates defined in Figure 1.04. The stresses ahead of the crack tip is proportional to $r^{-1/2}$, which leads to stress singularity ($\sigma_{ij} \approx \infty$) when r approaches 0.

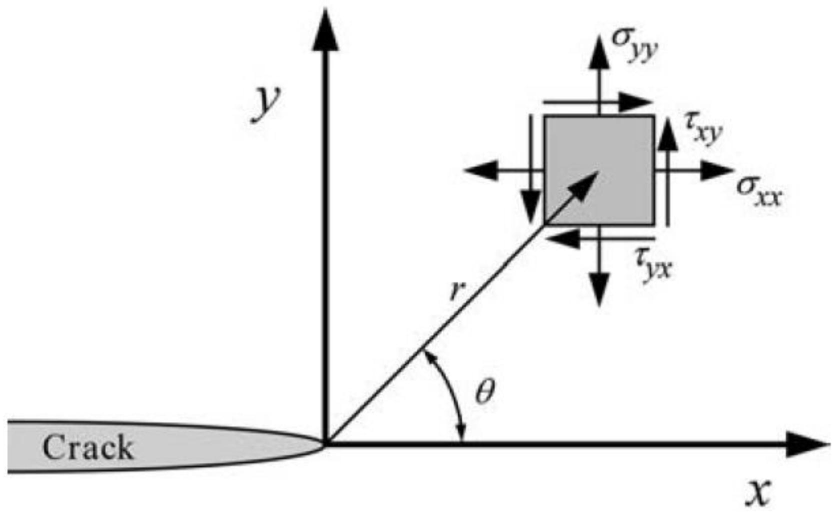

Figure 1.04 Polar coordinates of the stresses ahead of the crack tip (Anderson 2008, p.43)

To be able to define stress at the point of singularity, the stress intensity factor, K is introduced as

$$K = k\sqrt{2\pi} \qquad \text{Eq. 1.06}$$

K is normally described as K_I, K_{II} and K_{III} corresponding to the mode I, II and III crack opening modes. Replacing k in the stress field near the crack tip (Eq. 1.05) using the definition of K (Eq. 1.06) gives

$$\sigma_{ij} = \left(\frac{K}{\sqrt{2\pi r}}\right) f_{ij}(\theta) + \cdots \qquad \text{Eq. 1.07}$$

In Mode I loading, when $\theta \approx 0$, the primary terms in Eq. 1.07 gives

$$\sigma_{xx} = \sigma_{yy} = \frac{K_I}{\sqrt{2\pi r}} \qquad \text{Eq. 1.08}$$

Considering an infinitely wide plate containing a flaw in biaxial tension (see Figure 1.05), Westergaard (1939) derived the stresses as

$$\sigma_{xx} = \sigma_{yy} = \frac{\sigma\sqrt{a}}{\sqrt{2x^*}} \qquad \text{Eq. 1.09}$$

Where $x^* = x - a = r$. Comparing Eq. 1.08 to Eq. 1.09, the stress intensity factor for Mode I loading, K_I could then be described as

$$K_I = \sigma\sqrt{\pi a} \qquad \text{Eq. 1.10}$$

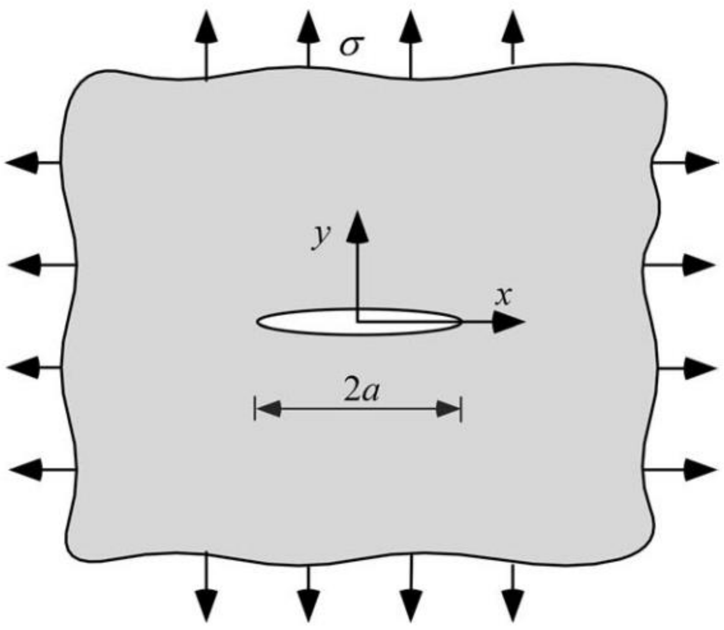

Figure 1.05 An infinite plate containing a through thickness flaw loaded in biaxial tension (Anderson 2008, p.97)

Based on Eq. 1.10, the stress intensity factor can be defined in a general form

$$K = Y\sigma\sqrt{\pi a}$$

Y is a dimensionless constant which varies due to different loading condition and crack geometry. In the cases of fracture toughness specimens, the stress intensity factor is described as a function of crack to width ratio, *a/ W*.

$$K_I = \frac{P}{BW^{0.5}} \times f\left(\frac{a}{W}\right)$$

1.3.3 Relationship between *G* and *K*

G and *K* are two different parameters describing the crack. *G* is an energy parameter based on strain energy; *K* is derived using local stresses near the crack tip. To unify *G* and *K*, consider Eq. 1.02

$$G = \frac{\pi \sigma^2 a}{E}$$

And Eq. 1.10,

$$K_I = \sigma \sqrt{\pi a}$$

The relationship between *G* and *K* could be described as

$$G = \frac{K^2}{E'}$$

E' is E for plane stress, where $E' = E/(1-v^2)$ for plane strain.

1.4 Elastic-plastic fracture mechanics

The Griffith energy criterion and stress intensity factor are parameters used to describe fracture toughness of isotropic elastic materials. However, it would not be as useful on material exhibiting plastic deformation, as the crack tip would deform plastically after the fracture stress (Eq. 1.04) is achieved, instead of failing in cleavage. To account for the plastic properties of the material, two parameters were used: - displacement based CTOD and energy based *J*.

1.4.1 Crack tip opening displacement, CTOD

The Crack Opening Displacement (COD, now known as Crack Tip Opening Displacement, CTOD) is a fracture criterion was introduced by Wells (1961, 1969) based on experiments using notched tension bars. CTOD is a measure of the physical opening of an original crack tip in a standard fracture toughness test specimen at the point of stable or unstable crack extension. Material exhibiting elastic-plastic properties would experience plastic deformation at the crack tip before fracture. The maximum opening of the crack tip before cleavage fracture or plastic collapse is the CTOD.

There are a number of definitions used to describe CTOD. One of the best-known definition for CTOD is the opening of the original crack tip when the crack opens due to loading. It is a measure of displacement of the crack tip, where the original crack tip (produced by machining or fatigue pre-cracking) experiences blunting as the crack opens, resulting in a finite displacement at the original crack tip (see Figure 1.06).

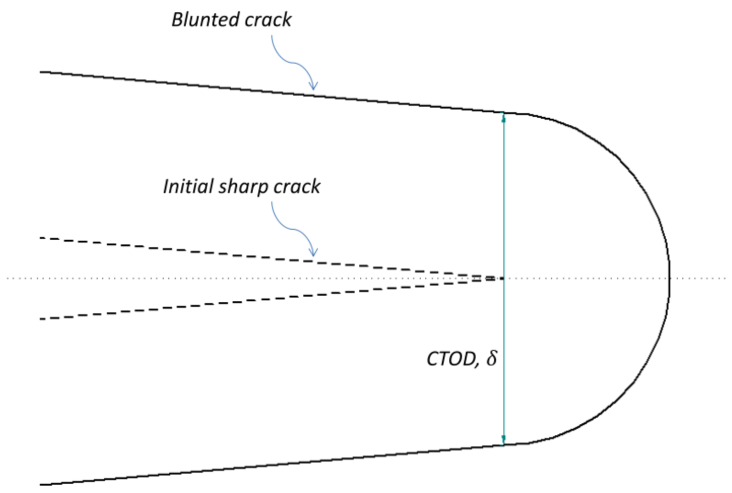

Figure 1.06 Definition of CTOD using the COD approach

An alternate definition for CTOD, δ_{45} is known as the 45° CTOD at the crack tip. δ_{45} defines CTOD based on the displacement of the intercept of the crack face and a pair of imaginary line set at 45° from the blunted crack tip (see Figure 1.07). This definition is proposed by Shih (1981) based on *J*-CTOD conversion, described in Chapter 1.4.3. This definition is often used in finite element analysis.

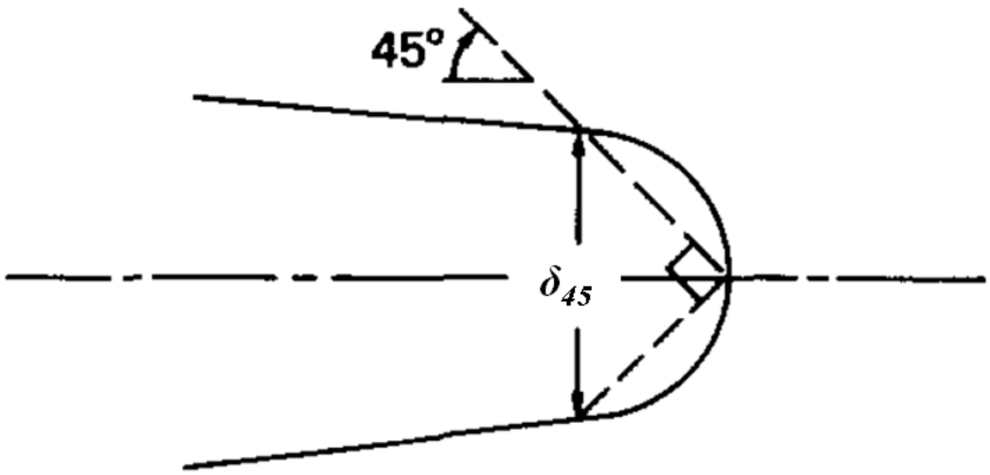

Figure 1.07 The definition of δ_{45} (Kumar et al. 1981)

The CTOD concept was first proposed as the opening of the original crack tip, as described in Figure 1.06. The theoretical derivation was based on the crack tip stress and displacement field in Mode I crack opening.

Consider σ_{yy} in a Mode I loading (coordinates as in Figure 1.04),

$$\sigma_{yy} = \frac{K_I}{\sqrt{2\pi r_y}} \qquad \text{Eq. 1.11}$$

By replacing σ_{yy} with σ_{ys} in Eq. 1.11, Irwin (1968) rearranged the equation for to allow the estimation of the plastic zone length

$$r_y = \frac{1}{2\pi}\left(\frac{K_I}{\sigma_{ys}}\right)^2 \qquad \text{Eq. 1.12}$$

r_y is the length

Based on the displacement field solution, the displacement in the y direction from the crack tip, u_y is given as (Anderson 2008, p.43)

$$u_y = \frac{\kappa+1}{2\mu} K_I \sqrt{\frac{r_y}{2\pi}} \qquad \text{Eq. 1.13}$$

In which *κ= (3– v)/ (1+ v)* for plane stress. *v* is the Poisson ratio. Substituting Eq. 1.12 into Eq. 1.13, u_y can be expressed as

$$u_y = \left(\frac{4}{(1+v)2\mu}\right)\left(\frac{{K_I}^2}{2\pi\sigma_{ys}}\right)$$

μ is the tearing modulus of the material. The Young's modulus, *E* is related to *v and μ* as E= *2μ (1+ v)*. CTOD, *δ* is twice the displacement of u_y, described as,

$$\delta = 2u_y = \left(\frac{4}{E}\right)\left(\frac{{K_I}^2}{\pi\sigma_{ys}}\right) = \frac{4G}{\pi\sigma_{ys}} \qquad \text{Eq. 1.14}$$

Combining the numerical constants from Eq. 1.14, a general equation for small-scale yielding CTOD can be described as

$$\delta = \frac{K^2}{m\sigma_{ys}E} = \frac{G}{m\sigma_{ys}} \qquad \text{Eq. 1.15}$$

m is defined as a dimensionless constant which depends on the plane stress (*m*≈ 1) and plane strain-ness (*m*≈ 2) of the crack tip (Anderson 2008, p.105).

1.4.2 J-integral, path independent energy around the crack

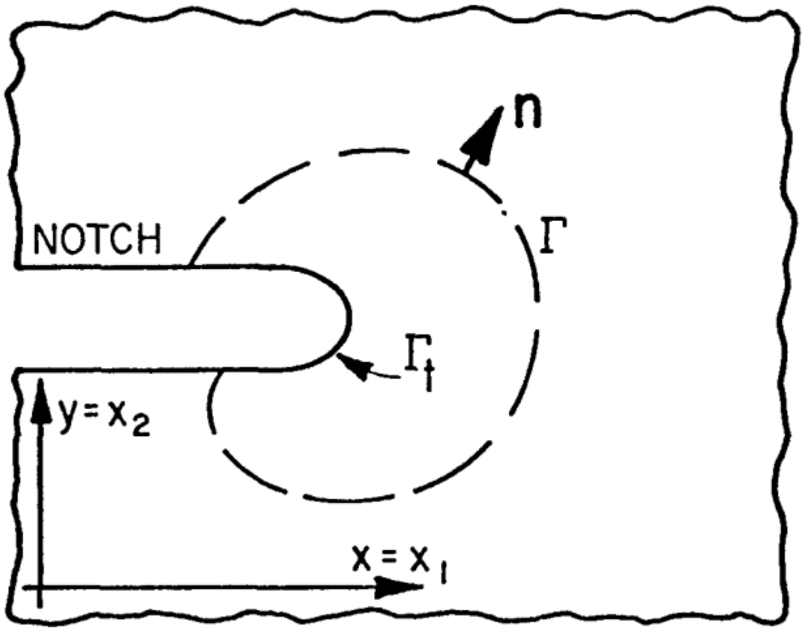

Figure 1.08 Contour around a crack in an infinitesimally wide plate in 2-D, used to describe the concept of *J* (Rice 1968)

The *J*-integral energy approach was proposed by Rice (1968) based on the strain energy density around the crack tip. J defines the path independent strain energy release rate of a crack, applicable to linear and non-linear elastic material.

Consider a notch in a plate with infinitesimal width (Figure 1.08), Γ is a vanishing small arbitrary path around the notch within the material, and Γ_1 denotes the path around the open notch (refer Figure 1.08). The strain energy density, w is defined by

$$w = w(x,y) = w(\varepsilon) = \int_0^{\varepsilon} \sigma_{ij}\varepsilon_{ij} \qquad \text{Eq. 1.16}$$

σ_{ij} = stress tensor

ε_{ij} = strain tensor

The traction vector, T acts in an outward normal direction along the path Γ, described as

$$T = \sigma_{ij} n_j \qquad \text{Eq. 1.17}$$

Considering the overall strain energy of the plate without the strain energy surrounded by Γ, J can then be described as (Rice 1968)

$$J = \int_{\Gamma} \left(w dy - T \frac{\partial u}{\partial x} ds \right)$$

u = displacement vector

ds = length increment along Γ

Experimentally, the *J*-integral can be measured by arranging strain gauges in a manner where it forms a contour around the crack tip. However this method is complicated and troublesome. It is difficult to place strain gauges around the same contour manually with accuracy.

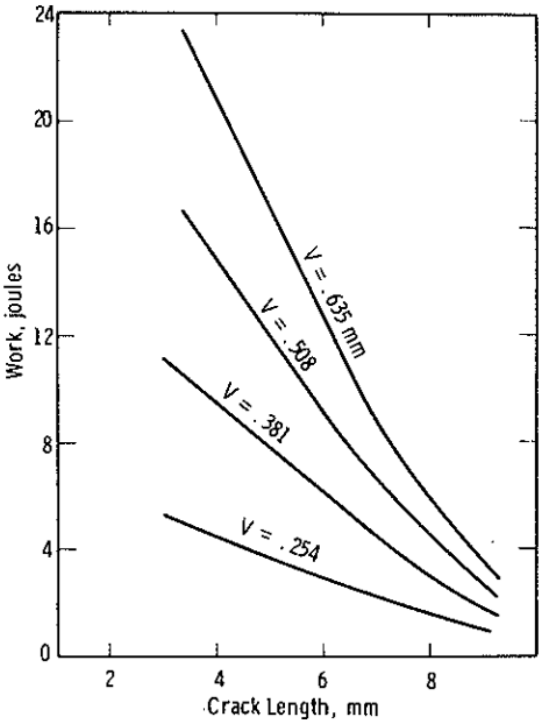

Figure 1.09 Work vs. crack length for different displacement loading (Landes & Begley 1972)

For *J* to be used as fracture criterion, an alternative description was given to *J* in terms of energy release rate (Begley & Landes 1972; Landes & Begley 1972). The equation is given as,

$$J = -\frac{\Pi}{dA} = -\frac{1}{B}\frac{dU}{da}$$

dA is the change in cross section area ahead of the crack tip. *J* is defined as the negative of the gradient of work, dU divided by crack length increment, da, per unit thickness, B (Landes & Begley 1972; Dawes 1979). The relationship is shown in Figure 1.09, where *V* is the corresponding fixed displacement.

When applied experimentally on fracture toughness specimens (Chapter 1.5.2), the general relationship for *J* can be described as (Zhu 2009)

$$J = \frac{\eta}{BB_o}\int_0^{\Delta} Pd\Delta = \frac{\eta A}{BB_o} \qquad \text{Eq. 1.18}$$

η = dimensionless calibration constant, a function of *a/ W*

A = work applied on the specimen

BB_o is the cross-sectional area of the un-cracked specimen.

In the case of deeply cracked SEN(B) specimens (Rice et al. 1973; Zhu 2009)

$$J = \frac{2}{BB_o}\int_0^{\Delta} Pd\Delta = \frac{2A}{BB_o}$$

The notch depth must be of sufficient depth to ensure that plasticity is confined to the unbroken ligament ahead of the crack (Rice et al. 1973).

1.4.3 Relationship between J and CTOD

J and CTOD are both fracture parameters, and therefore it would be useful if both parameters can be related from one to another. Shih (1981) described the relationship between *J* and CTOD as

$$\delta_{45} = d_n \frac{J}{\sigma_y}$$

By comparing it to the equations in the standardized equations (further described in Chapter 1.7.1), it could be found that

$$\delta = \frac{J}{m\sigma_y}$$

Where d_n could be described as

$$d_n = \frac{1}{m}$$

m is a dimensionless function which considers the crack length- specimen width ratio and tensile properties of the material.

1.5 Fracture toughness testing

1.5.1 Introduction

Fracture toughness is described as the material’s resistance to fracture, and is typically used in Engineering Critical Assessments (ECA) to evaluate the fitness of an engineering structure in respect to fracture avoidance (Shen et al. 2004; Gordon et al. 2013; Sarzosa et al. 2015; BSI 2014a; API 2007). It is important that fracture toughness is evaluated appropriately, as it is the main variable for flaw acceptance (Anderson & Osage 2000). Overestimation of fracture toughness could possibly lead to the acceptance of a flaw which is beyond its critical size, jeopardizing the safety of the structure.

Two of the most commonly used specimen configurations in fracture toughness tests are the Single Edge Notched Bend, SEN(B) and Compact Tension, C(T) specimen setup, described in Chapter 1.5.2. Generally, the universal testing machine which is capable of applying tensile or compression loading is used for the tests, using the appropriate testing apparatus for the particular specimen configuration (example Figure 1.10). Typically, fatigue loading is applied on the specimen to generate a crack in the material and loaded in a manner where Mode I loading is experienced at the crack. The load-displacement trace obtained from the test is used to calculate fracture toughness (*K*, *J* or CTOD) of the specimen (Chapter 1.8).

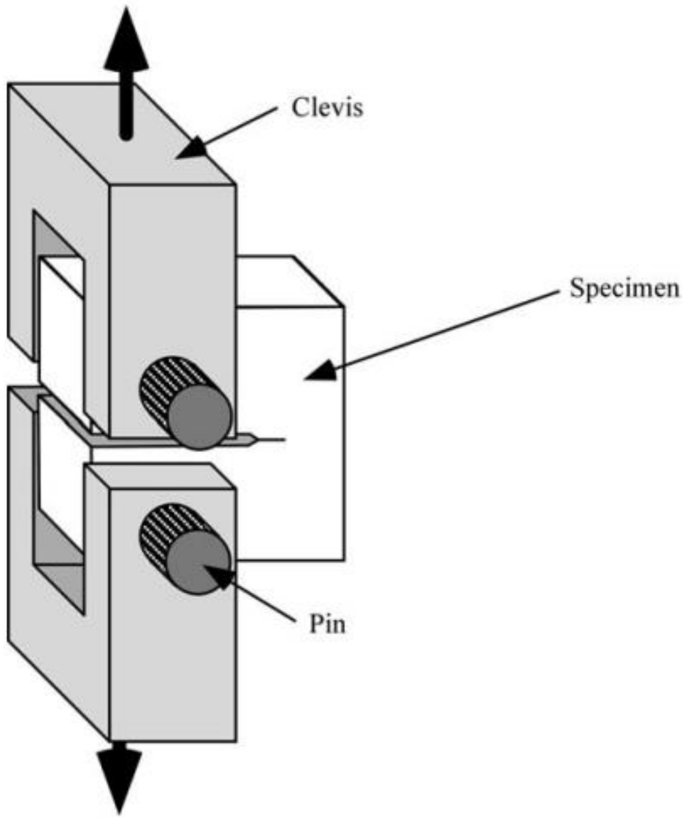

Figure 1.10 Apparatus for C(T) testing (Anderson 2008, p.302)

1.5.2 Fracture toughness specimens

Specimens of different geometries are used to measure fracture toughness of a material. Several of the many factors affecting the selection of specimen geometries are: - loading condition, wall thickness and welds of the sample extracted from the structure. Different specimen geometry has different levels of constraint (Figure 1.11). Some specimens are easy to machine, whereas some specimens require little material. Some of the common specimen configurations had been standardized so that repeatable results could be obtained by different testing parties.

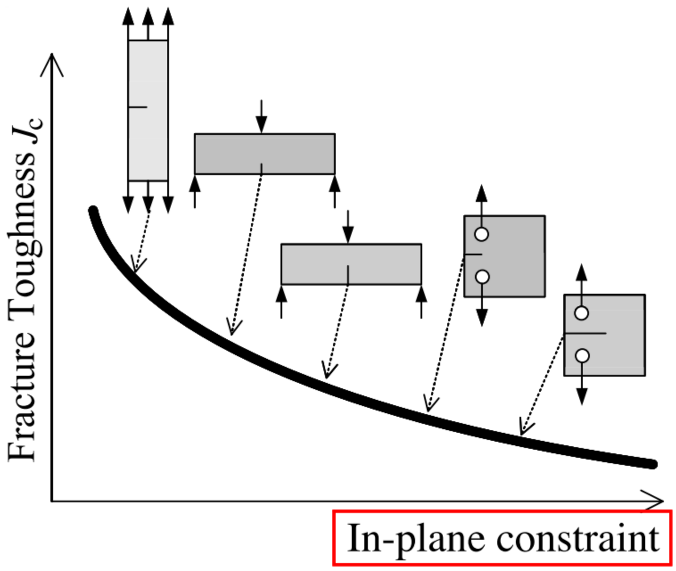

Figure 1.11 In-plane constraint vs. fracture toughness for different specimen geometry and loading condition (Meshii et al. 2016)

1.5.2.1 Single edge notched bend, SEN(B)

A SEN(B) test is one of the most commonly used fracture toughness test configuration (Figure 1.12). This test configuration is standardized by major standardizing committees, e.g. BS 7448, ASTM E1820 and ISO 12135. SEN(B) specimens are highly constrained, meaning that the test results will not overestimate the actual material fracture toughness behaviour of a sharp crack under typical service loading conditions. Additionally, the SEN(B) specimens are rectangular and therefore are straight forward and easy to manufacture.

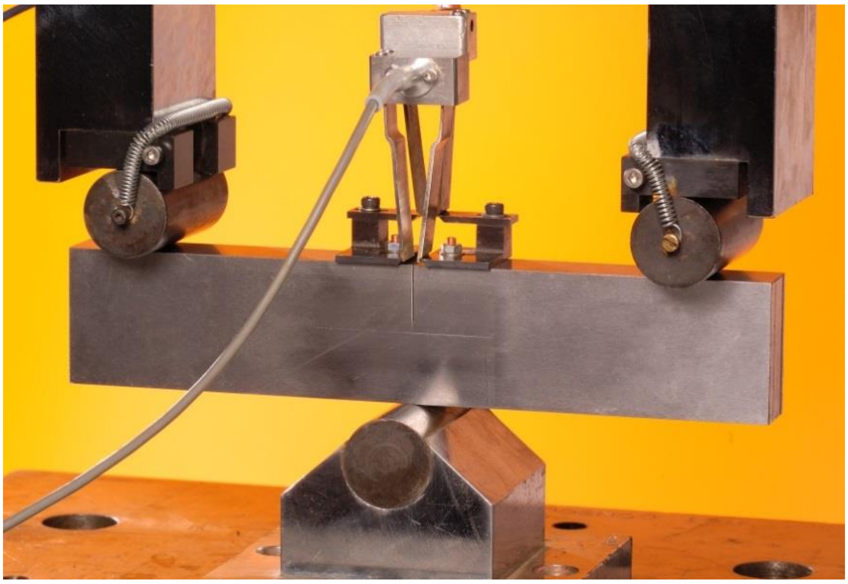

Figure 1.12 A fatigue pre-cracked SEN(B) specimen with double clip gauged attached to elevated knife edges (image from TWI)

1.5.2.2 Compact tension, C(T)

The C(T) test, like the SEN(B) test, is commonly used and standardized by major standardizing committees (Figure 1.13). Compared to SEN(B) specimens, C(T) specimens have a slightly higher constraint, therefore would give lower fracture toughness for the same material thickness and temperature compared to SEN(B).

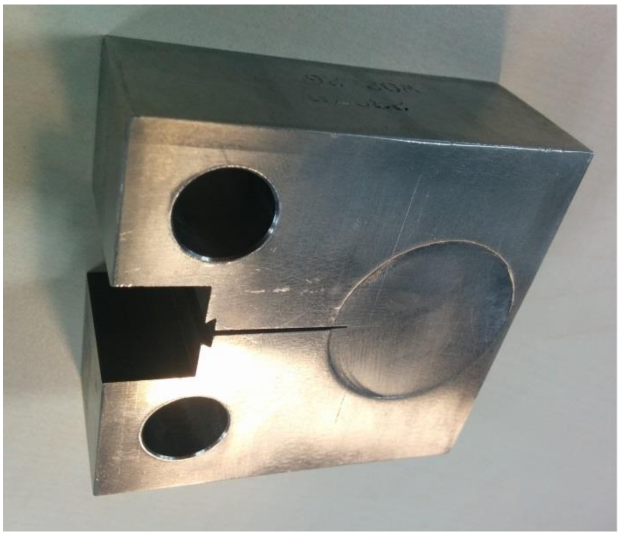

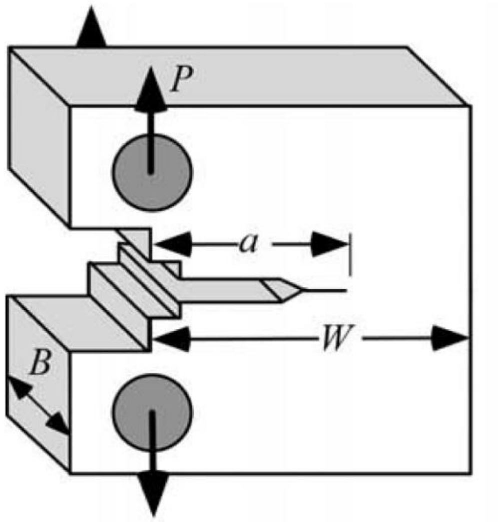

Figure 1.13 An integral knife edge C(T) specimen with local compression (left), loading schematic and geometry of C(T) testing (Anderson 2008, p.300)

The advantage of the C(T) specimen compared to SEN(B) is the material required to manufacture the specimen for the same specimen thickness (see Figure 1.14). However, due to the complexity of the specimen geometry, it requires more time and cost to manufacture.

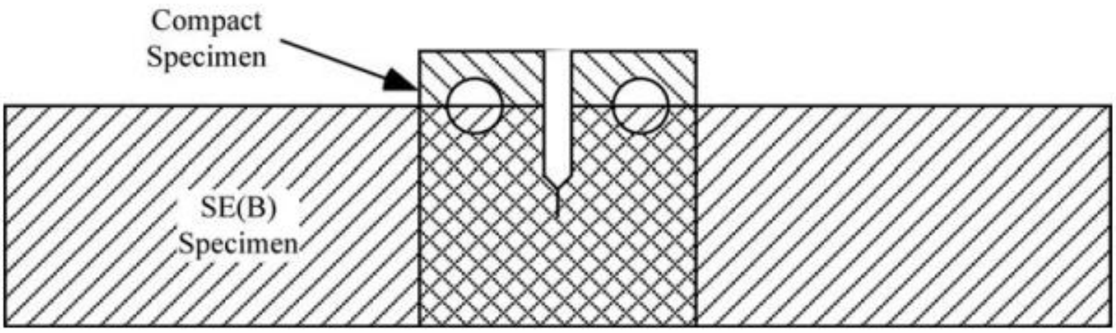

Figure 1.14 Comparison of SEN(B) and C(T) specimen of same a_0/ W (Anderson 2008, p.301)

1.5.2.3 Single edge notched tension, SEN(T)

The SEN(T) test configuration is a comparatively new design of standard fracture toughness test specimen (Figure 1.15). This configuration has lower constraint compared to SEN(B) and C(T), and should produce results more similar to a how a crack behave in real structures (particularly for flaws in pipeline girth welds), whilst not being over-conservative. A SEN(T) standard was published recently by the BSI (2014b) and there is a recommended procedure for SEN(T) testing by DNV (2006).

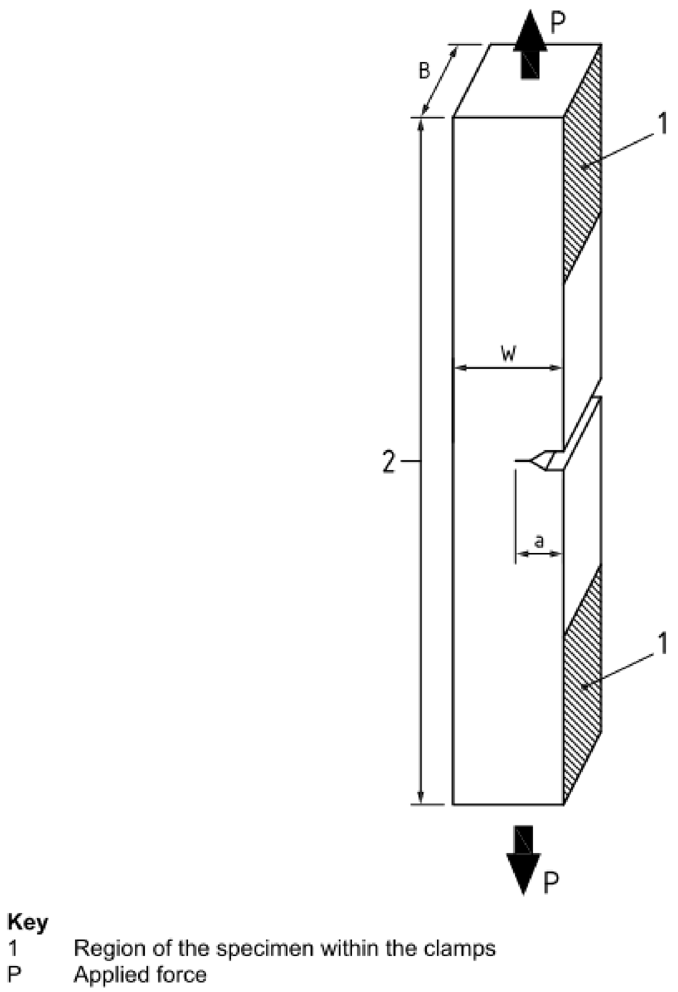

Figure 1.15 Loading schematic and geometry of a SEN(T) specimen (BSI 2014b)

1.5.2.4 Non-standardized fracture toughness configurations

Some fracture toughness specimen configurations have not been standardized, due to being more complicated for analysis, or the lack of research in the particular configuration. The middle-cracked tension, M(T) and double-edge notched tension, DE(T) specimen are few of many examples of non-standardized fracture toughness configuration (Figure 1.16). These configurations are sometimes used when it could describe the actual crack and loading conditions of the actual component more accurately than the standardized fracture toughness specimens. Lower specimen constraint would lead to lower conservativism in the test results, further described in Chapter 1.5.6.

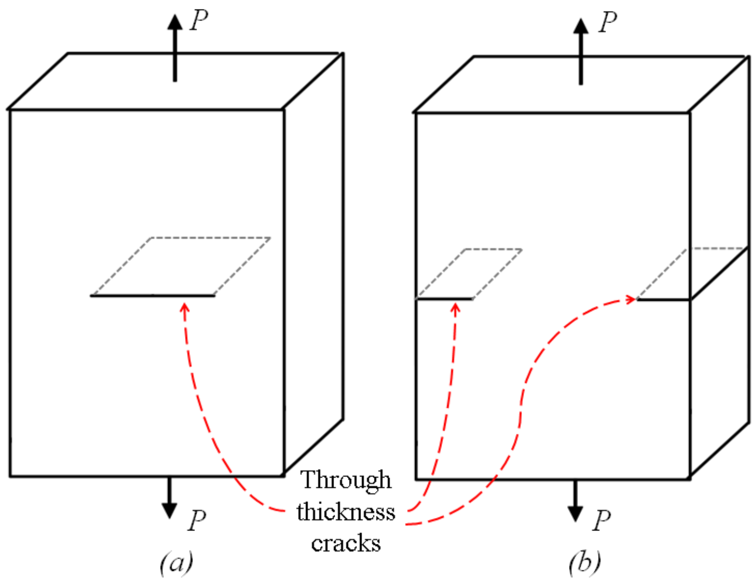

Figure 1.16 Examples of non-standardized fracture toughness configurations (a) middle-cracked tension and (b) double-edge cracked tension.

1.5.3 Temperature effect

The tensile yield stress of a material is a function of temperature (BSI 2014a; JWES 1995). As shown in Figure 1.17, temperature affects the flow stress of the material. Flow stress, σ_{flow} is the function of yield and ultimate tensile stress and is a value between the two stresses. A simplified definition of $\sigma_{flow} = (\sigma_{ys} + \sigma_{uts})/2$ is used in ASTM (2014). As temperature increases, σ_{flow} decreases. Cleavage fracture occurs when σ_{flow} is equivalent or greater than the fracture stress, $\sigma_{fracture}$. When $\sigma_{flow} < \sigma_{fracture}$, micro void coalescence is experienced by the material, thus leading to ductile crack tearing.

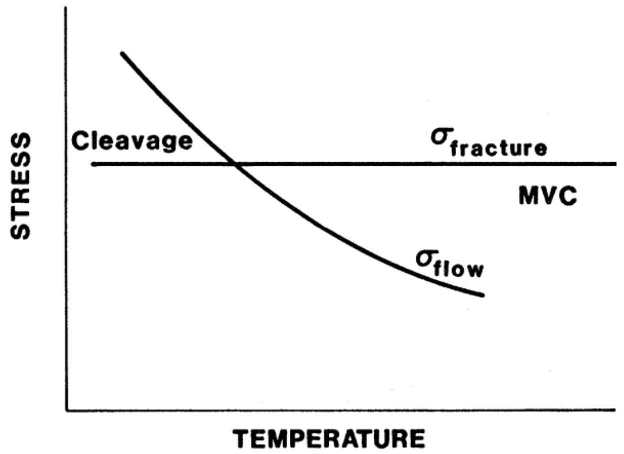

Figure 1.17 The effect of temperature on σ_{flow} (Anderson 1984, p.32)

At low temperatures, the material yield strength increases; at high temperature, the material yield strength decreases (BSI 2014a; JWES 1995). Although the material yield strength is increased at low temperatures, the ductility of the material is lowered, and is therefore is more susceptible to brittle fracture. On the contrary, increased temperature decreases the yield strength but increases ductility, leading to the material failing in a ductile manner.

1.5.4 Ductile-brittle transition

As mentioned in Chapter 1.5.3, the change in temperature affects the yield and ultimate tensile stress of the material. Figure 1.18 exhibits a generalization of the fracture toughness transition over temperature. At extremely low temperature, notably in region 1, materials tend to fail in cleavage. Linear elastic fracture mechanics is dominant in region 1. Region 2 and 3 is considered the ductile-brittle transition region. Failure in this region is generally influenced by the combination of cleavage and MVC. In region 4 where the temperature is higher than other regions, the material fails in a plastic ductile manner.

Despite the generalized trend, scatter is often observed on the actual fracture toughness obtained from different temperature. Figure 1.19 shows a collection of fracture toughness data for C-Mn welded metal, tested at various temperatures. At very low temperatures *($T< -100°C$)*, the measured *K* is fairly consistent (Moskovic 1993). The scatter of data increases as temperature increases. The most scatter is seen at about *$T\approx 20°C$.* Majority data exhibiting cleavage fracture falls in the region *$-10°C< T< 30°C$.* As the fracture toughness is least consistent in the ductile-brittle transition region, it would be most accurate to fracture toughness tests on the actual material at temperature of interest. An idealised curve for the relationship between temperature and fracture toughness is shown in Figure 1.20.

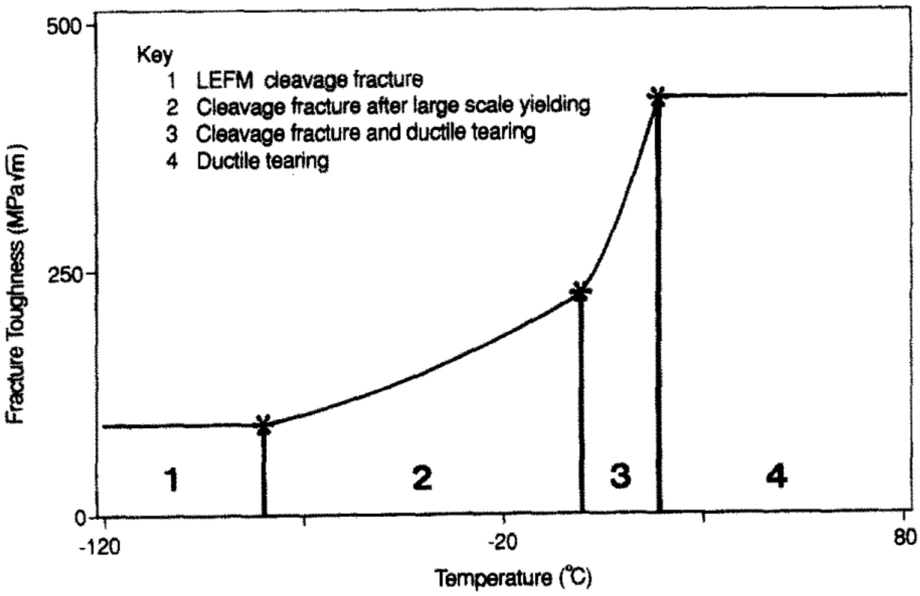

Figure 1.18 Generalization of the variation of fracture toughness for different temperature (Moskovic 1993)

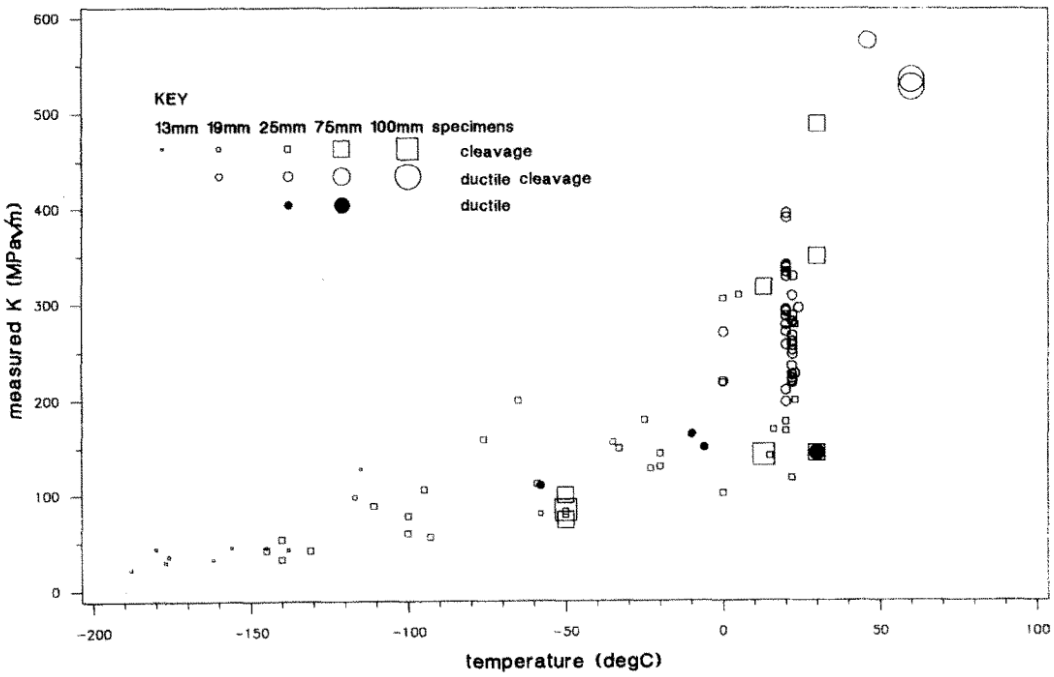

Figure 1.19 Collection of fracture toughness data at different temperature (Moskovic 1993)

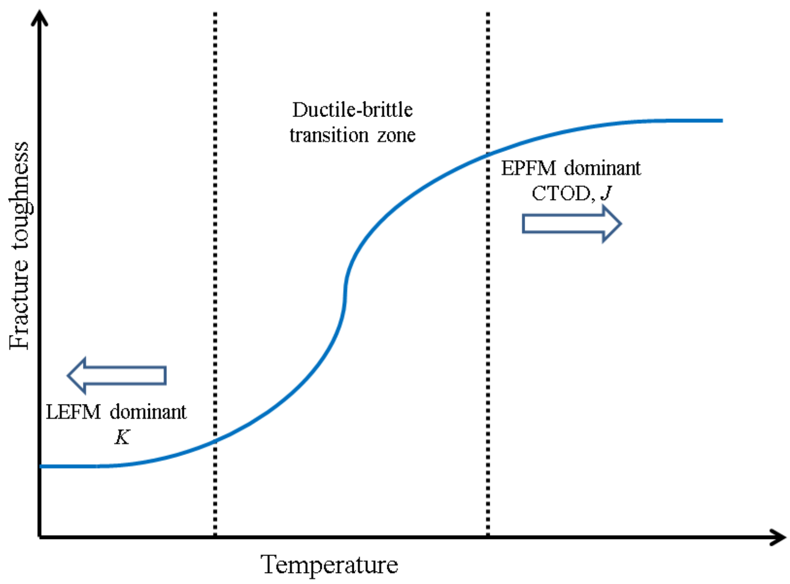

Figure 1.20 Effects of temperature on fracture toughness

1.5.5 Thickness effect

Thickness of the material is one of the main considerations in fracture analysis. When performing fracture toughness tests to assess real structures, it is often recommended that the test specimen thickness is similar to the actual structure. The main reason is that it is non-conservative to predict the fracture toughness of a thicker specimen using a thinner specimen.

There are two explanations on how specimen size would affect fracture toughness: the ‘weakest link’ initiation of cleavage fracture and tri-axial stresses at the crack tip. The ‘weakest link’ concept is based on the assumption that when a defect is initiated at the crack tip, it would extend across the material in a cleavage manner (Hunt & McCartney 1979; Anderson 1984). The 'weakest link' is distributed across the material, therefore when the specimen size increases, the 'weakest link' sampling area increases, leading to higher probability for cleavage fracture.

The tri-axial stress concept is based on plane strain condition experienced at the crack tip. Considering a mode I loading, no stress is experienced on the side surface of the crack, in the direction normal to the plane of crack opening (σ_z), which is plane stress dominant. The plane strain dominant region in the centre of the material experiences the highest σ_z. Figure 1.21 shows the typical plastic zone distribution across the crack tip. The semi-conical shape shows that the plastic zone is the widest on the sides of the crack, tapers as it moves into the middle of the material and converges. Plane stress dominant region gives a larger plastic zone compared to the plane strain region. As the thickness increases, the semi-conical plane stress affected plastic zone size remains relatively the same, leading to a longer region of 'converged' smaller plane strain dominated plastic zone. The plane strain region experience higher tri-axial stresses, leading to higher fracture toughness compared to the plane stress region.

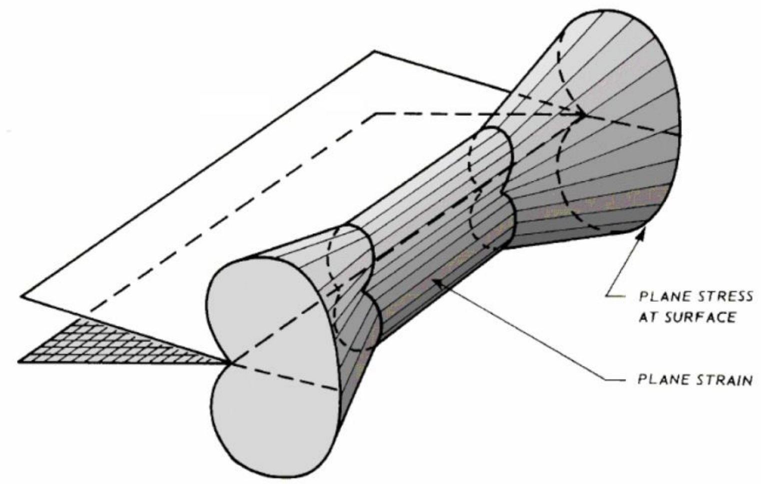

Figure 1.21 Typical distribution of plastic zone across the crack tip (Janssen et al. 2004, p.74)

As the specimen size increases, the plane strain dominant plastic region increases, and therefore it is more susceptible to fracture. This means thicker specimens are more constrained than smaller specimen. Therefore it would be safe to test for fracture toughness using a specimen of the same thickness as to the assessed component.

1.5.6 Constraint effect

In fracture mechanics, constraint describes the level of restrictiveness of the crack. Several parameters affect the constraint level of the crack: - specimen geometry, crack length, material thickness and loading condition. Higher constraint causes the material to behave in a more brittle manner compared to lower constraint under similar conditions, exhibiting lower resistance to fracture. In the laboratory environment, fracture toughness assessments conducted on test specimens representing real structures generally experience higher constraint, giving conservative results. Figure 1.22 exhibits the effect of constraint on fracture toughness with temperature.

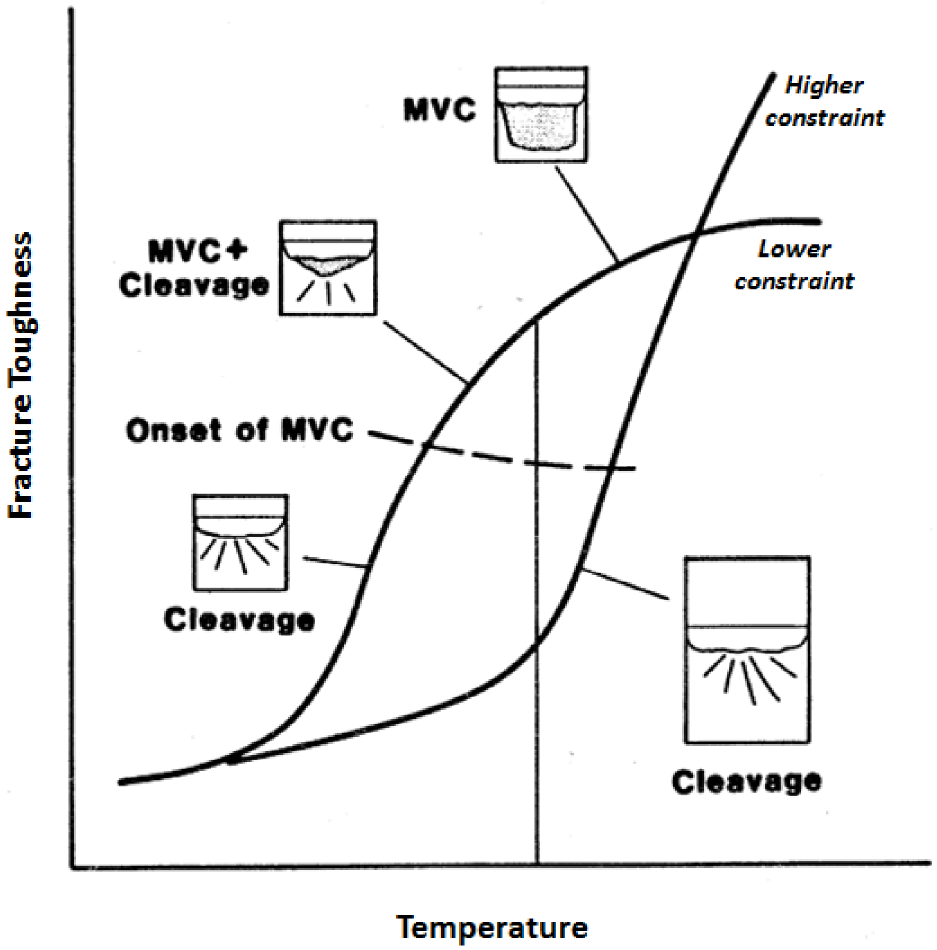

Figure 1.22 The effect of constraint on fracture toughness (Anderson 1984)

1.6 Fracture toughness testing standards

For the purpose of replicating the fracture toughness test with consistency, several standards had been published for single point (*K*, *J* and *CTOD)* and R-curve estimation. However, sometimes the different standardizing bodies estimate the same parameter using different approaches. Table 1.01 shows the standards and testing parameters covered by the standards.

Table 1.01 Current active quasistatic fracture toughness standards

Standards	Origin	Fracture toughness parameters covered	Material type
BS 7448-1	British Standards Institution	K_{Ic}, J, $CTOD$	Parent material
BS 7448-4	British Standards Institution	R-curve	Parent material
ASTM E1820	American Society for Testing and Materials	K_{Ic}, J, $CTOD$, R-curve	Parent material and weld material
ISO 12135	International Organization for Standardization	K_{Ic}, J, $CTOD$, R-curve	Parent material
BS EN ISO 15653	British Standards Institution	J, $CTOD$ ($0.1 \le a_0/W \le 0.45$)	Weld material
WES 1108	Japan Welding Engineering Society	$CTOD$	Parent material

1.7 Calculating fracture toughness

1.7.1 General equations of the standard fracture toughness estimation

Based on the load-displacement feedback obtained from the tests, *K*, *J* and CTOD are calculated. For specimen failing without significant ductile deformation, the stress intensity factor, *K* is used as the fracture toughness parameter. The *K* equation is generally theoretical, where

$$K = \frac{PS}{BW^{1.5}} \times f\left(\frac{a_0}{W}\right)$$

For elastic-plastic specimens, fracture toughness is described in terms of *J* and CTOD. The standards specify that fracture toughness is calculated by the addition of two components: - the elastic component and the plastic component (Wu 1989). The total J is described as

$$J = J_{elastic} + J_{plastic}$$

The elastic component of *J* is described as

$$J_{elastic} = \frac{K^2(1 - v^2)}{E}$$

Whereas plastic component of *J* is described as

$$J_{plastic} = \frac{\eta A_p}{BB_N}$$

η is a dimensionless calibration factor which varies depending on the specimen geometry and specimen crack length. The η factors used in the standards are calibrated using FEA.

Similar to *J*, CTOD is described in two parts,

$$\delta = \delta_{elastic} + \delta_{plastic}$$

The elastic component of CTOD can be described as

$$\delta_{elastic} = \frac{K^2(1-v^2)}{mE\sigma_{ys}}$$

Two different methods are used for the calculation of plastic CTOD: - geometrical estimation and *J*-CTOD conversion. The geometrical estimation for the plastic component of CTOD is (further described in Chapter 1.7.2),

$$\delta_{plastic} = \frac{r_p(W-a)V_p}{\left[r_p(W-a)+a+z\right]}$$

The *J*-CTOD conversion is given as

$$\delta_{plastic} = \frac{J}{m\sigma_y}$$

The equations for the calculation of CTOD are described in Table 1.02 based on the standards.

Table 1.02 Standardized CTOD and J estimation equations

Standards	***Year***	***Equation***
BS7448-1[1]	‘91	
ASTM E1290	’93 ‘99	$\delta = K^2\frac{(1-v^2)}{2\sigma_{ys}E} + \frac{r_pB_oV_p}{r_pB_o+a_0+z}$
ASTM E1820	‘01	
ASTM E1820[1]	‘14	$\delta = \frac{J}{m\sigma_y}$
ASTM E1290	’07 ‘08	
BSI EN ISO 15653[1]	‘10	$J = \frac{K^2(1-v^2)}{E} + \frac{\eta_{pl}A_p}{B_NB_o}$
BSI EN ISO 15653[1] (*0.1≤ a_0/W≤0.45*)	‘10	
ISO 12135[1]		$\delta = K^2\frac{(1-v^2)}{2\sigma_{ys}E} + \frac{(0.6\Delta a+0.4B_o)V_p}{0.4W+0.6(a_0+\Delta a)+z}$
BS 7448-4[1]	‘97	

1.7.2 Geometrical estimation of CTOD based on specimen rotation

When a SEN(B) specimen is loaded under three-point bending, the crack tip would experience tensile stress, whereas there would be a region in the un-cracked ligament which experiences

[1] These standards are currently active

compression. In the calculation of the plastic component of CTOD in BS 7448-1, ISO 12135, ASTM E1290-93 and E1820-01, it is assumed that the specimen flanges rotate about a stationary point within un-cracked ligament ahead of the crack tip, a distance ahead of the crack tip equal to $r_p \times B_0$, where r_p is the rotational factor and B_0 is the remaining ligament ahead of the crack tip. This concept is introduced by Dawes (1979), based on a 2-D derived plastic hinge model assuming plane strain condition in the equation (Lin et al. 1982).

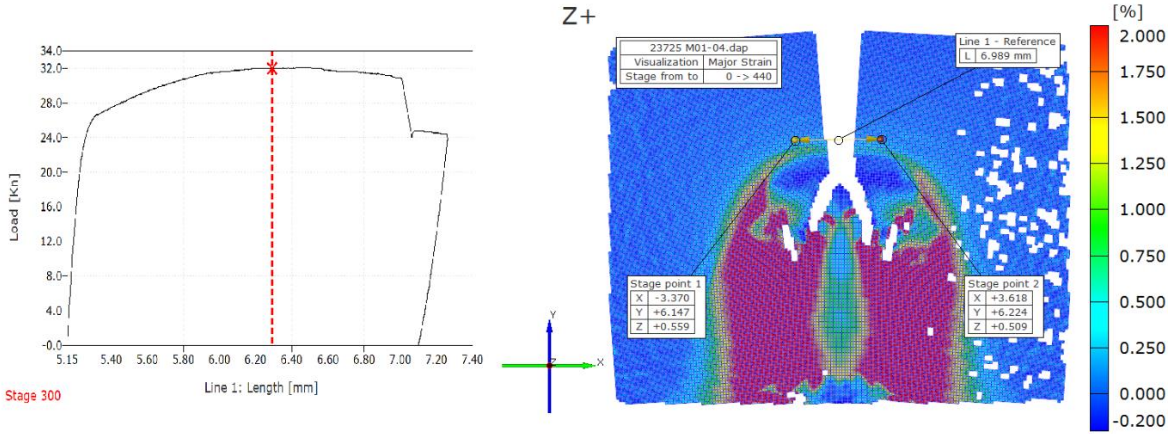

Figure 1.23 Strain distribution near the crack tip on a SEN(B) specimen observed using the Digital Image Correlation technique (Haslett et al. 2015)

According to the assumption of slip line theory, the deformation is assumed as rigid arms rotating about a circular rotational point (Cotterell 2002). Green's (Green & Hundy 1956; Green 1956) observation on photo-elastic images of notched bend specimens showed that the yielding pattern are similar to that predicted in a slip-line field. Digital Image Correlation observation on a SEN(B) specimen showed that the strain distribution near the crack tip shows similarity to that described in the slip line field theory by Green (Figure 1.23).

The determination of the rotational factor is based on the geometrical analysis of the specimen. Consider a deformed SEN(B) specimen (Figure 1.24), the distance of the rotational point from the CMOD, H is defined in terms of rotational factor, $r_p(W - a) + a$ (Lin et al. 1982).

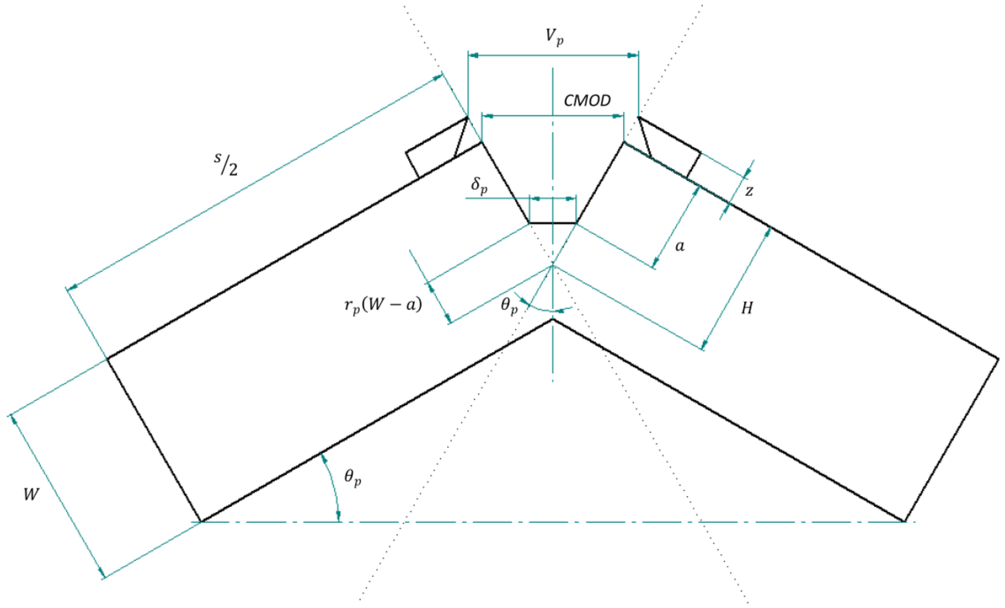

Figure 1.24 Diagram for the evaluation of the geometrical based CTOD

From Figure 1.24, it is shown that

$$r_p = \frac{H-a}{W-a} \qquad \text{Eq. 1.19}$$

$$V_p = 2\left[r_p(W-a) + a + z\right] \sin\theta_p \qquad \text{Eq. 1.20}$$

$$\delta_p = 2r_p(W-a)\sin\theta_p \qquad \text{Eq. 1.21}$$

Rearranging Eq. 1.20 into Eq. 1.21 gives (Lin et al. 1982)

$$\delta_p = \frac{r_p(W-a)V_p}{\left[r_p(W-a) + a + z\right]}$$

Anderson et al. (1985) showed that r_p is independent of the geometry of the specimen for the same material. Wells (1971) shown that in the case of the SEN(B) specimen geometry, initially the rotational point would be close to the crack tip (*r_p< 0.1),* which would extend and converge to a point within the unbroken ligament ahead of the crack tip (*r_p≈ 0.45)* as load is applied and after general yielding (Figure 1.25). BS 7448 used a constant value of r_p= 0.4 in the calculation of CTOD. The basis for the determination of *r_p= 0.4* for SEN(B) was not in the public domain, but it is understood that this value is determined through extensive experiments and should underestimate the actual CTOD (Wu 1983).

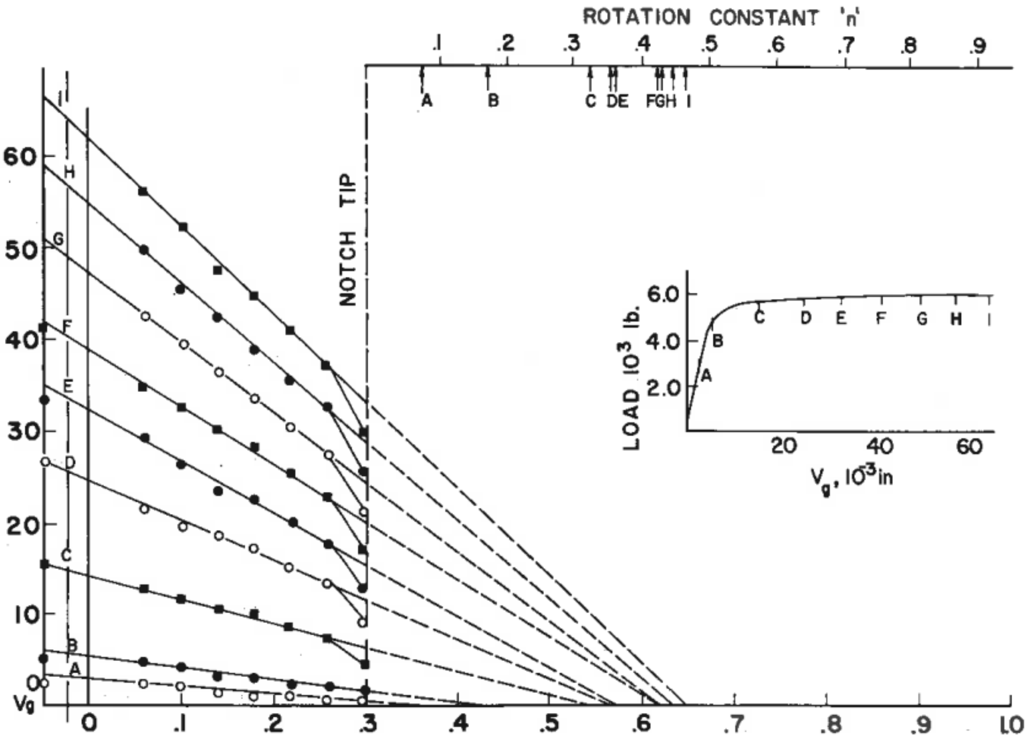

Figure 1.25 Rotational factor (rotational constant) at different point of loading (Wells 1971)

1.7.3 Experimental *J* equation for SEN(B) specimens

Zhu (2009) showed that Eq. 1.18 can be used as a general equation for the experimental assessment of *J*. The η factor is used to calibrate the equation to the respective specimen geometry. The η function is dependent on the specimen geometry, loading condition and calibrated to the type of displacement (CMOD or LLD).

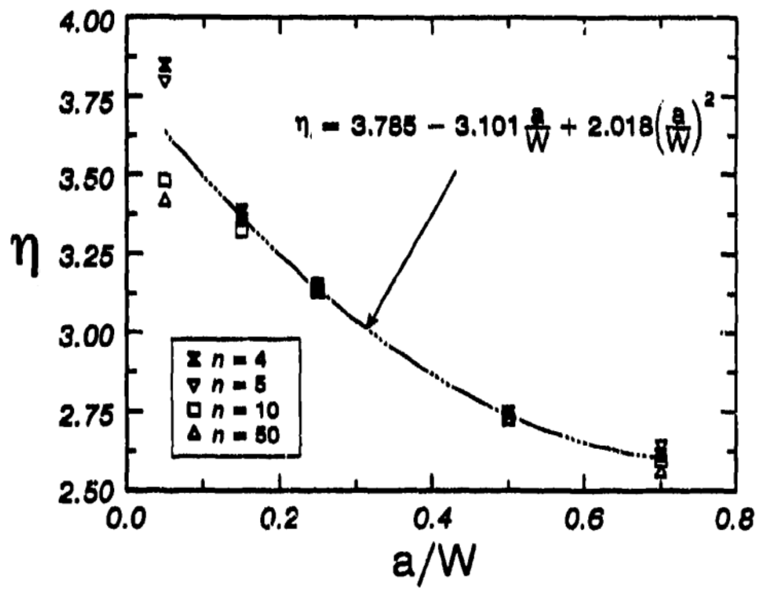

Figure 1.26 η factor vs. *a/W* for based on *4≤n≤50* and CMOD (Kirk & Dodds Jr. 1993)

To prevent repetition, this chapter would describe the η calibration based on CMOD. In the case of SEN(B) setup, the first η calibration was provided by Kirk & Dodds Jr. (1993). The calibration was based on finite element analysis and it was found that the η factor calibrated to CMOD is consistent and independent of strain-hardening (see Figure 1.26).

The first CMOD based η factor used for J is

$$\eta = 3.785 - 3.101\left(\frac{a_0}{W}\right) + 2.018\left(\frac{a_0}{W}\right)^2$$

The estimation above is used in the superseded ASTM E 1290-08.

Zhu et al. (2008) performed an investigation on the η factor calibrated by a number of different independent investigators. Different modelling techniques were applied: - 3-D FEA data for based on the average J_{pl} across the crack front (Kim et al. 2004; Donato & Ruggieri 2006; Nevalainen & Dodds Jr. 1995), 3-D FEA based on the J_{pl} on the mid thickness J_{pl} (Donato & Ruggieri 2006) and 2-D FEA (Kirk & Dodds Jr. 1993). Despite the different techniques applied, the results were similar and thus an average of the estimations based on CMOD is given as (Figure 1.27)

$$\eta_{pl} = 3.667 - 2.199\left(\frac{a_0}{W}\right) + 0.437\left(\frac{a_0}{W}\right)^2$$

The refined equation above is utilized in the current active ASTM E1820.

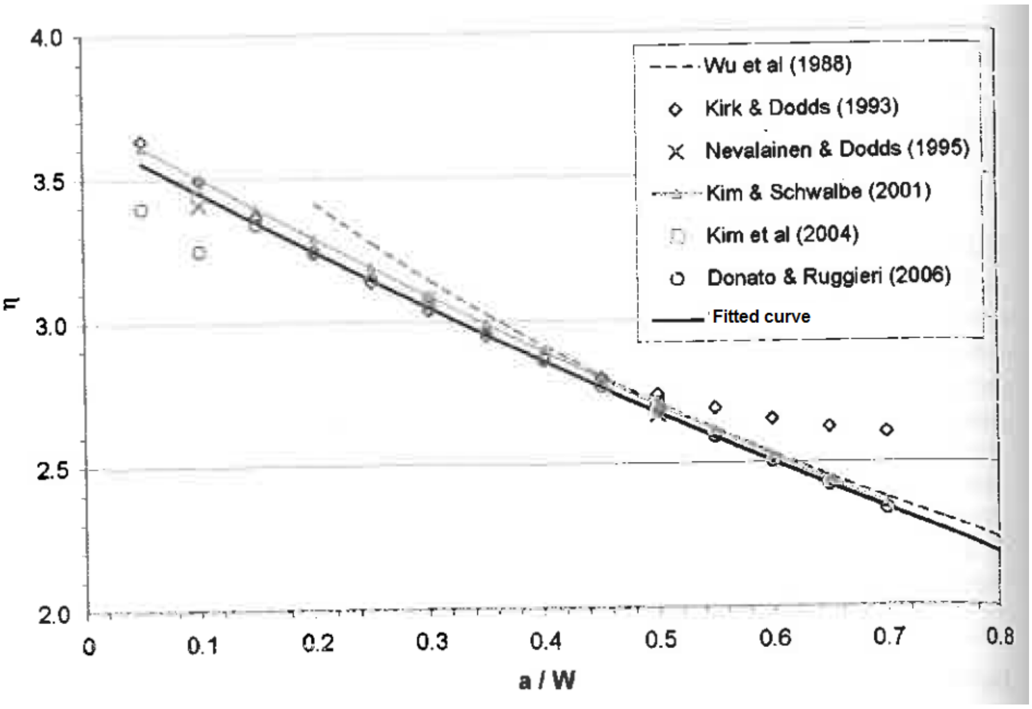

Figure 1.27 Compilation of CMOD based η vs. *a/W* from different researchers (Zhu et al. 2008)

1.8 Data obtained from fracture toughness testing

1.8.1 Load-displacement data

The load and displacement data obtained from fracture toughness tests are used to calculate fracture toughness. Figure 1.28 shows an idealized load-displacement diagram obtained from a fracture toughness test.

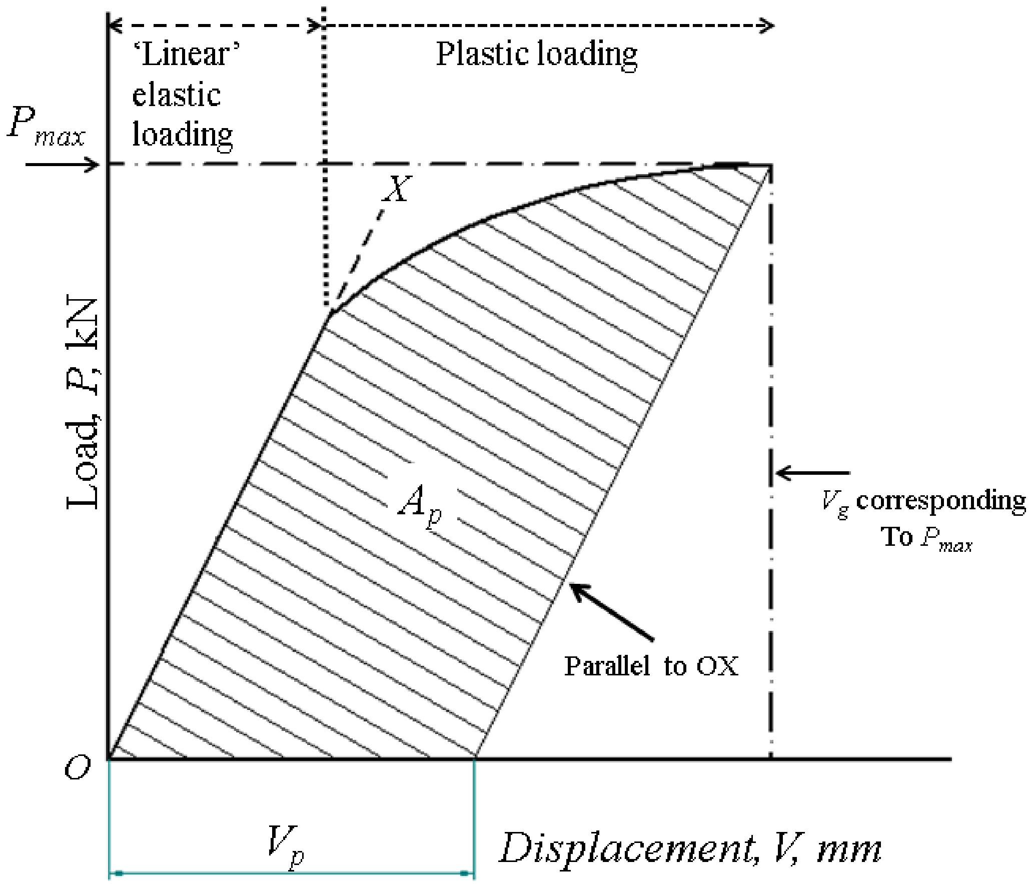

Figure 1.28 Idealized load-displacement diagram obtained from a test

1.8.2 Methods of measuring displacement

Displacement data is obtained by one of two of the following methods: - relative opening of the crack mouth opening displacement (CMOD) or the displacement loading of the specimen, referred as the load-line displacement. Sometimes these can be measured directly, and sometimes are inferred indirectly from other measurement methods during the test.

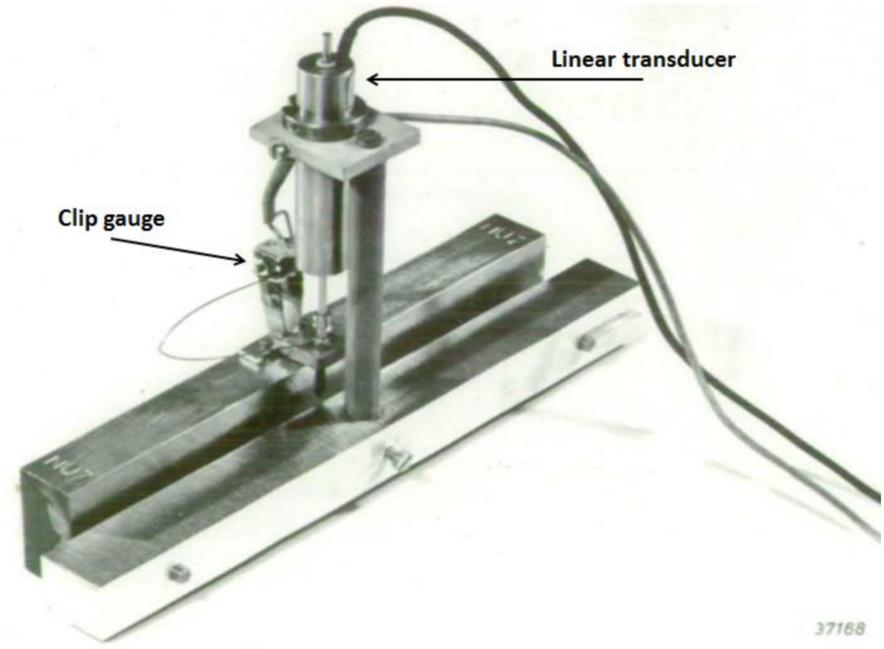

Figure 1.29 Clip gauge and linear transducer used to measure displacement (Dawes 1979)

1.8.2.1 Crack mouth opening displacement, CMOD

The CMOD is defined as the opening displacement at the top end of the crack. CMOD can be measured directly by using the integral knife method (see Figure 1.30) or estimated using the double clip gauge technique (see Figure 1.31). The knife edges for the clip gauges are mounted on steel shims and welded to the notch mouth.

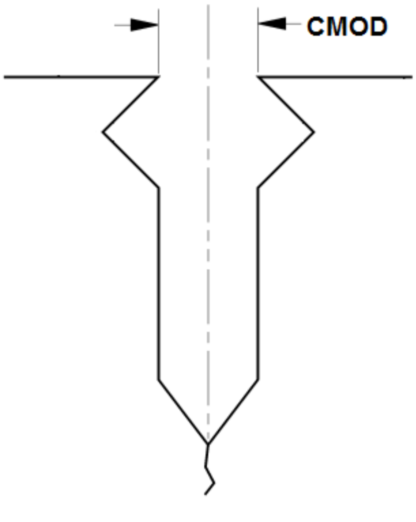

Figure 1.30 Diagram of the integral knife to measure CMOD directly using a clip gauge

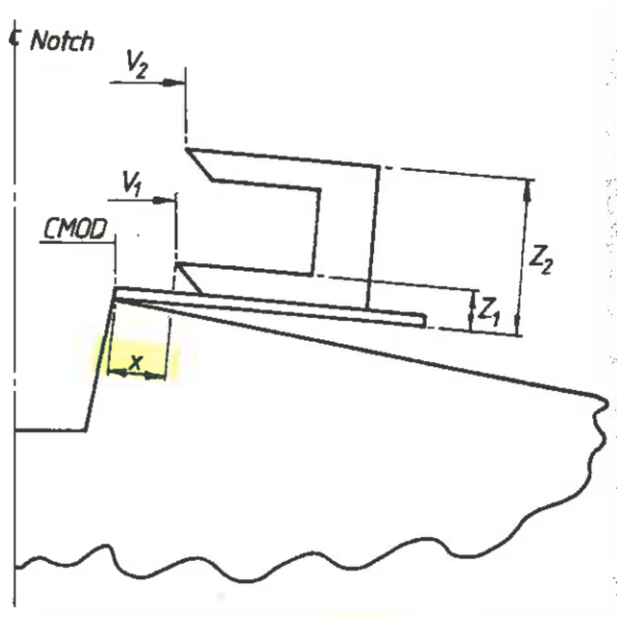

Figure 1.31 Diagram for the double clip gauge technique (Dawes et al. 1992)

The displacement of knife edged does not represent the actual CMOD. However, an estimation was provided by Dawes et al. (1992) for the estimation of CMOD, given as

$$CMOD = V_1 - z_1\left(\frac{V_2 - V_1}{z_2 - z_1}\right) - 2x\cos\left(\sin^{-1} 0.5\left(\frac{V_2 - V_1}{z_2 - z_1}\right)\right) + 2x$$

Studying the equations from the current ASTM E1820, it requires CMOD data for J_{pl} calculation, whereas ASTM E1290-08 (now superseded) allows CMOD estimation using clip gauge data mounted above the CMOD. Both J_{pl} equations are compared below

$$J_{pl\ in\ ASTM\ E1290-08} = \frac{\eta A_p}{BB_o\left(1+\frac{[\alpha+z]}{0.8a_0+0.2W}\right)} \qquad \text{Eq. 1.22}$$

$$J_{pl\ in\ ASTM\ E1820-11e} = \frac{\eta_{pl}A_p}{B_N B_o} \qquad \text{Eq. 1.23}$$

α= 0 for SEN(B) specimen setup and A_p is the defined as the area under the P vs V_p (see Figure 1.28). By analysing the SEN(B) diagram (Figure 1.24), both CMOD and clip gauge displacement measured above the CMOD can be described as

$$CMOD = H\sin\theta \qquad \text{Eq. 1.24}$$

and

$$V_p = (H + z)\sin\theta \qquad \text{Eq. 1.25}$$

Relating Eq. 1.24 and Eq. 1.25,

$$CMOD = V_p \frac{H}{H+z} = \frac{V_p}{1+{}^{z}/_{H}} = \frac{V_p}{1+\frac{z}{r_p(W-a)+a}} \quad \text{Eq. 1.26}$$

Comparing Eq. 1.22 and Eq. 1.23, it can be seen that Eq. 1.26 is applied in ASTM E1290-08, where

$$A_p = \int_0^{CMOD} P \times dCMOD = P \times \frac{1}{1+\frac{z}{r_p(W-a)+a}} dV_p \quad \text{Eq. 1.27}$$

When $r_p = 0.2$,

$$CMOD = \frac{V_p}{1+\frac{z}{0.8a+0.2W}} \quad \text{Eq. 1.28}$$

The constant $r_p = 0.2$ applied in Eq. 1.28 is based on reverse calculation. Eq. 1.28 is applied in ASTM E1290-08 to obtain a CMOD estimate based on clip gauge opening measured above the CMOD.

1.8.2.2 Load-line displacement, LLD

The load-line displacement (LLD) is the measure of displacement loading applied on the specimen. LLD for SEN(B) specimen setup can be obtained by measuring the relative vertical displacement of an appropriate point in the specimen, i.e. notch mouth. Typically, direct measurement could be obtained using the comparator bar technique (see Figure 1.32), where a linear transducer is used to measure the displacement of the crack mouth position in the vertical direction (see Figure 1.29).

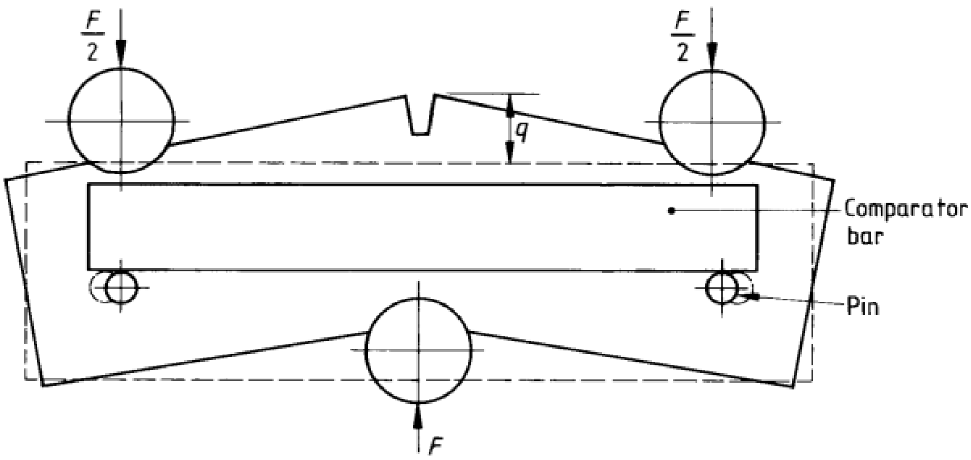

Figure 1.32 Comparator bar technique for the load-line displacement

Alternatively, the load-line displacement could be estimated using the double clip gauge technique with the following equation (ISO 2016),

$$q = \frac{S}{4}\left(\frac{V_2 - V_1}{z_2 - z_1}\right)$$

It should be noted that the machine loading displacement or the ram displacement can give an approximation of the LLD. However, it is not suitable in SEN(B) testing due to the bend loading of the specimen. The machine loading displacement or the ram displacement is unable to separate the elastic and plastic displacement of the SEN(B) specimen and the elastic displacements caused by the loading fixtures and testing machines. These factors are accumulative and would eventually result in an overestimation of the true load-line displacement (BSI 1991; ISO 2016).

1.8.3 Modes of fracture

There are two main modes of fracture of cracks under quasistatic loading: - fracture under unstable crack propagation (often described as brittle fracture) and fracture with stable ductile tearing. Brittle fracture is often associated with cleavage, where fracture propagates along the material grain. Generally, there is a certain amount of micro void coalescence (MVC) associated with fracture with stable ductile tearing, where crack tip tearing occur as tiny voids ahead of the crack tip grow and connect. Intergranular cracking can occur in both fracture modes (Anderson 1984).

In materials failing in a brittle manner, the rate of crack propagation is very high after the initiation of crack tearing. Material failing in stable ductile tearing and MVC are generally more ductile. As the crack propagates, the limit of maximum bearable load decreases, but the rate of crack propagation will be much lower compared to brittle fracture.

1.8.4 Pop-ins, arrested crack propagation

Typically, the theoretical derivations of the equations were based on isotropic, homogenous material. However, flaws within the material are unavoidable during the manufacturing process. Voids, inclusions, heat affected zone and local brittle zones are several examples contributing to inhomogeneity in real materials. This inhomogeneity of the material can lead to crack initiation, as well as a subsequent barrier to unstable crack propagation, described as crack arrest.

The crack arrest phenomenon is often observed when the material exhibits ‘pop-ins’ during the test. ‘Pop-ins’ are often experienced when a brittle crack is arrested by tougher material, or when the crack extension is interfered by the material flaw or inclusion (Pisarski 1987). Figure 1.33 shows the crack faces of the test specimen, where the initiation of pop-in leads to unstable crack extension, arrested by a region of higher toughness material (dotted line).

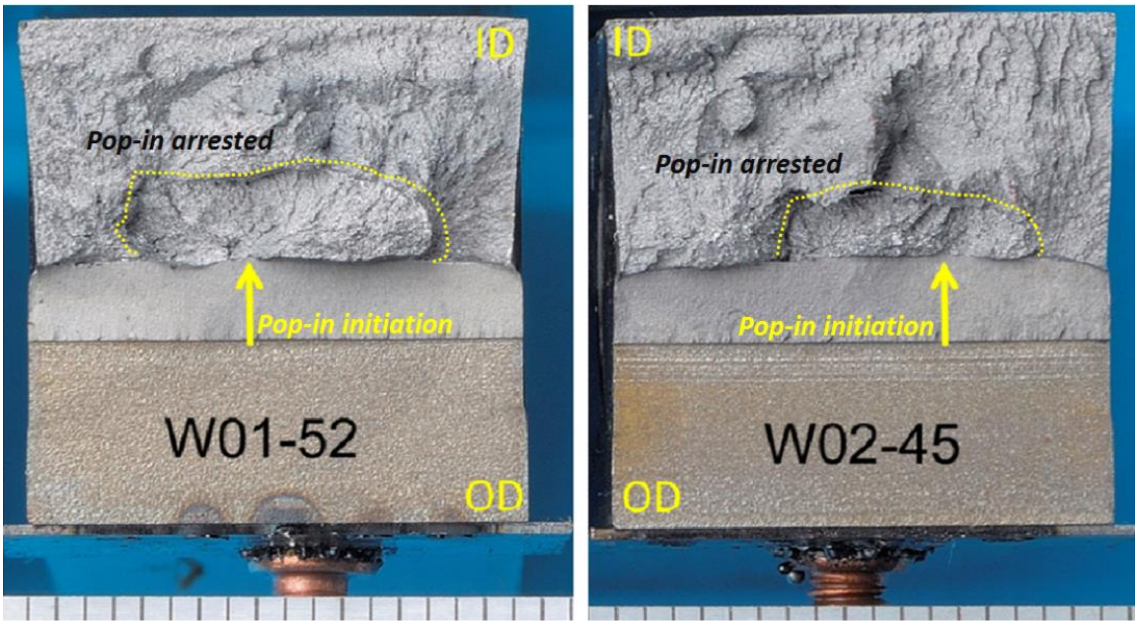

Figure 1.33 Crack faces showing initiation locations of pop-ins and the region where the unstable crack extension is arrested (yellow dotted lines) (Moore & Nicholas 2013)

During a fracture toughness test, the occurrence of pop-ins is often observable from the load-displacement diagram. Figure 1.34 shows several different patterns of pop-ins that can be observed from the load-displacement diagram. Test specimens exhibiting 'pop-ins' generally end up with their fracture toughness dominated by the pop-in event as the assessment point, as the inhomogeneity of the material might be due to local brittle zones or foreign particles/ voids.

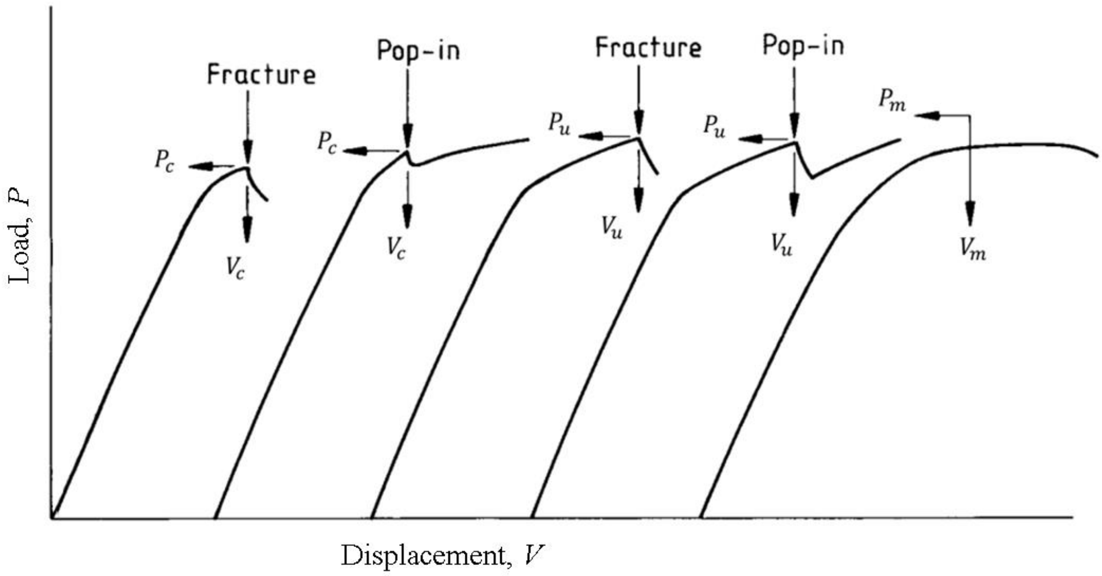

Figure 1.34 Typical idealised 'pop-in' patterns observed from the test data (BSI 1991)

1.9 Fracture toughness test results

The single point fracture toughness test would measure the fracture toughness of the material when maximum load in experienced; the R-curve would give a measure of the material's resistance to tearing. The single point and R-curve assessments are described in the following chapter.

1.9.1 Single point fracture toughness

In single point fracture toughness test (see Figure 1.35), load is applied on the specimen using displacement control. Displacement would increase gradually until the point where the maximum load is achieved or the specimen fractures. Data for the maximum load achieved and clip gauge displacement is used to calculate *K*, *J* or CTOD.

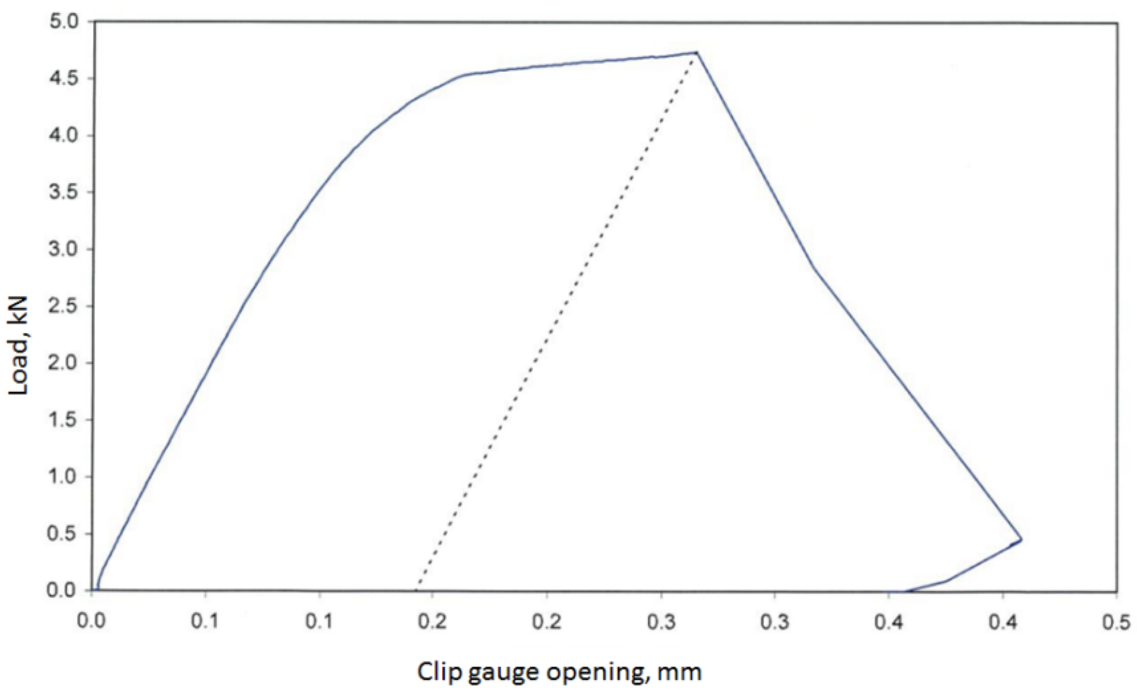

Figure 1.35 Typical load-displacement diagram for single point fracture toughness test (TWI archive 17163 W03-03)

1.9.2 Tearing resistance curve, R-curve

When generating a tearing resistance curve, the test is usually called an R-curve test. The R-curve is a measure of fracture toughness with increasing crack tearing, also described as the material's resistance to tearing. The R-curve gives an estimate of a growing crack, where the fracture toughness is evaluated as the crack grows in a stable ductile manner, causing the effective toughness ahead of the crack tip to increase over a small amount of crack growth, instead of the single critical assessment point in the single point fracture toughness test. The typical data used for the generation of an R-curve is shown in Figure 1.36.

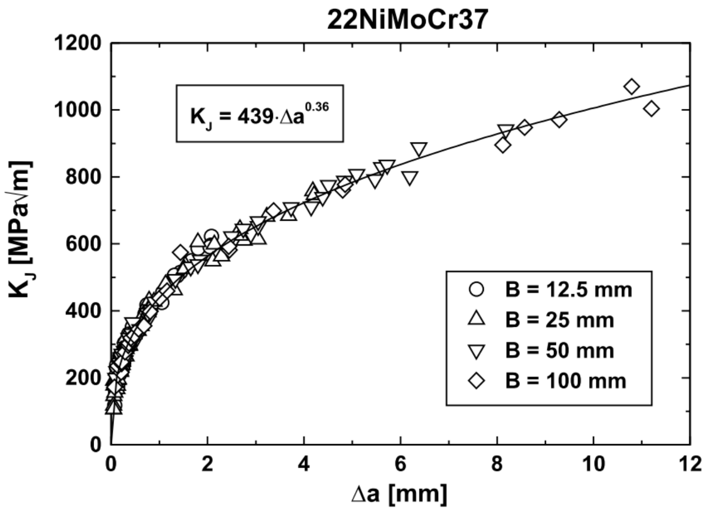

Figure 1.36 Multi-specimen R-curve based on *K* for 22NiMoCr37 C(T) specimens (Wallin 2002)

An R-curve can be built based on data obtained from two different methods: single specimen unloading compliance method or the multi-specimen method. Both methods provide comparable results (Zhu & Leis 2008). The unloading compliance method requires only one specimen, often performed when there are limited specimens; whereas the multi-specimen method requires a minimum of 6 specimens to build a valid R-curve (BSI 1997).

1.9.2.1 Multiple-specimen method

Different from the unloading compliance method, the multiple-specimen method requires multiple specimens tested to different loading points using the single point test method. Fracture toughness calculated based on the single point test method from the specimens are then plotted based on the respective crack extension observed on the specimen crack faces (see Figure 1.37).

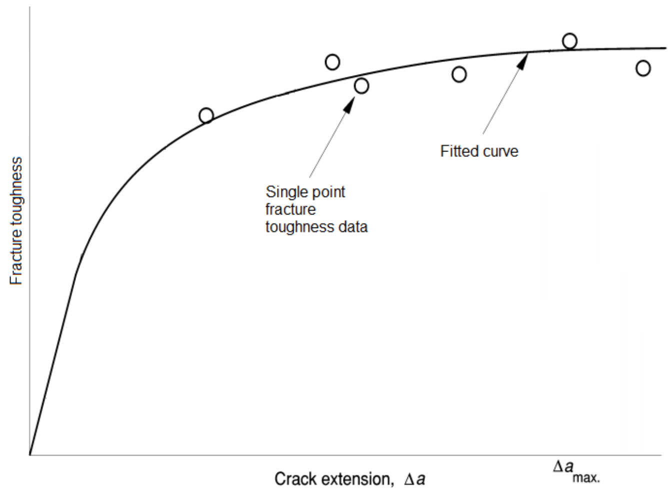

Figure 1.37 Multi-specimen R-curve

1.9.2.2 Unloading compliance method

The unloading compliance method is performed by first loading the specimen to the load of interest, followed by partially unloading the specimen, then reloading the specimen to the next point. This cycle is repeated for all the points before the test is ended. During the partial unloading and reloading cycle, the specimen behaves in an elastic manner, where elastic compliance (related to the unloading slope) is used for the prediction of the instantaneous crack length. The repeatedly unloading-reloading points (Figure 1.38) gives crack length estimations at different levels of plastic strain. Fracture toughness could then be estimated as the crack grows (Willoughby 1981). Typically, side-grooves are machined onto the sides of the crack to minimize the effects of shear lips during the unloading-reloading cycle.

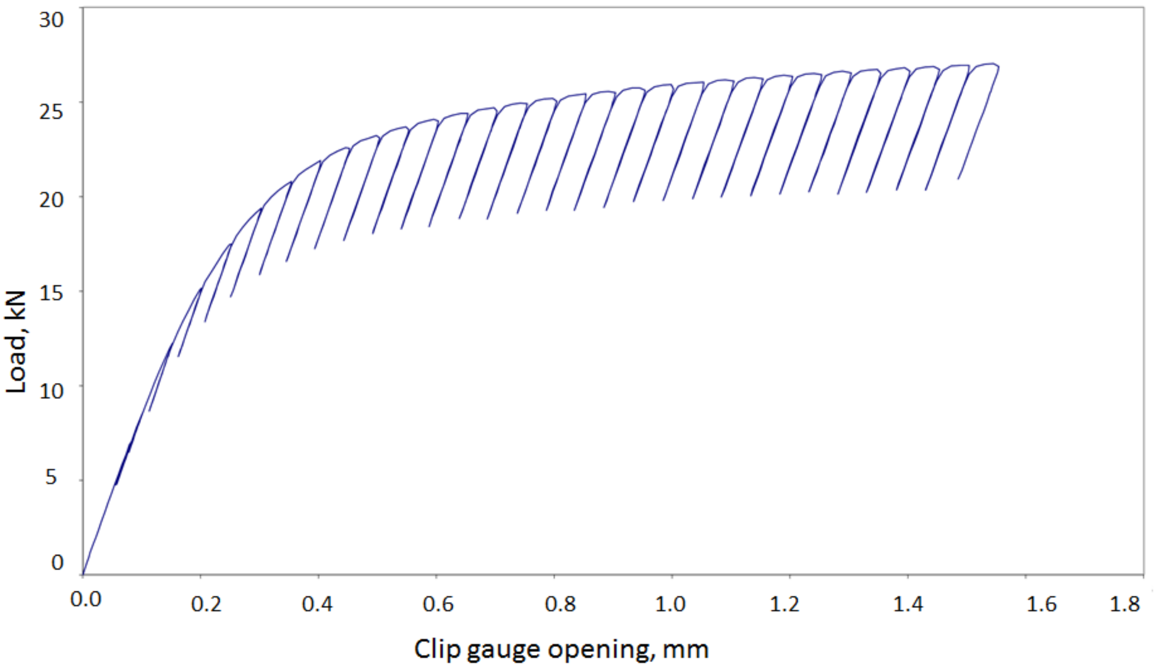

Figure 1.38 Typical load-displacement diagram for unloading compliance R-curve test (TWI archive 22160 W01-04)

1.10 Material tensile performance

Evaluating the fracture toughness equations, it is found that the tensile properties and the ductile flow of the material determine the material performance in quasistatic fracture toughness. It is important that the tensile properties are accessed accordingly. As seen in Figure 1.39, high strain rate could increase the yield stress significantly.

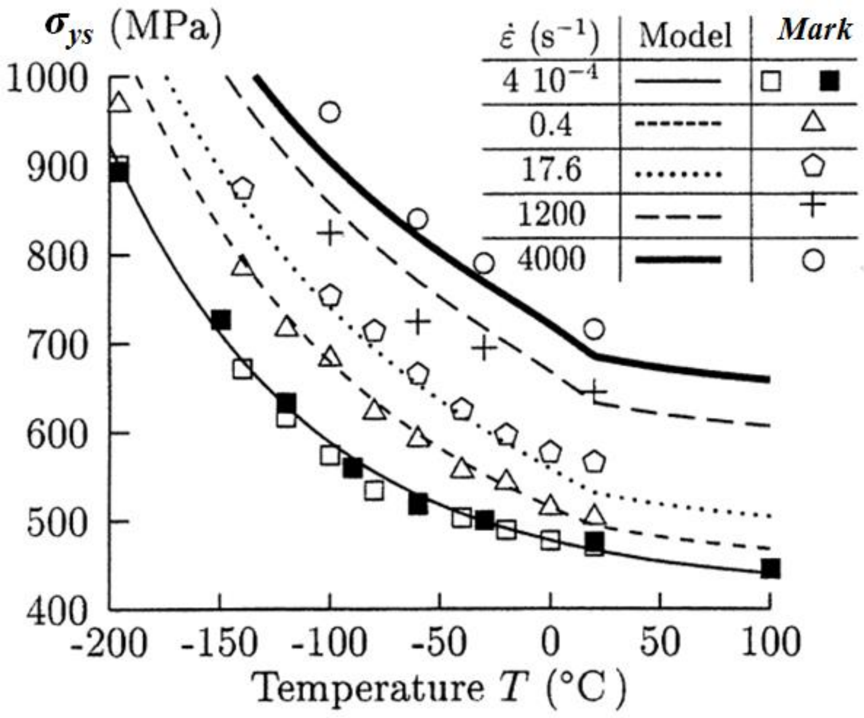

Figure 1.39 The effect of strain rate on yield stress (Tanguy et al. 2007)

The variation of tensile properties has direct effect on the fracture toughness of the material. The increase of yield stress would give lower fracture toughness, and the increase of the ratio between yield stress and tensile stress (described as tensile ratio) would increase the ductility of the material, often contributing to higher fracture toughness.

1.10.1 Strain/ work hardening

Deformation occurs when load is applied on a material. When the experienced stress is within the elastic limit (yield stress), linear deformation occurs and the material can return to the original form elastically when unloaded; when the amount of stress exceeds the elastic limit, plastic/permanent deformation is takes place. The total strain experienced by the material after deformation is the sum of elastic strain and plastic strain (Hosford 2010). In an idealized situation, when the stress is removed, the elastic strain would be recovered, whereas the plastic strain would remain (Higdon et al. 1978).

The stress-strain curve shape varies for different materials; therefore it is convenient to have an idealized stress-strain curve to simplify analysis, particularly in numerical modelling. Several idealized curve are shown in Figure 1.40: (a) no work-hardening, (b) linear work-hardening (c) power law, (d) improved power law approximation, (e) saturation model by Voce. Most metals display trends similar to (c), (d) and (e) instead of linear or no work-hardening (Hosford 2010).

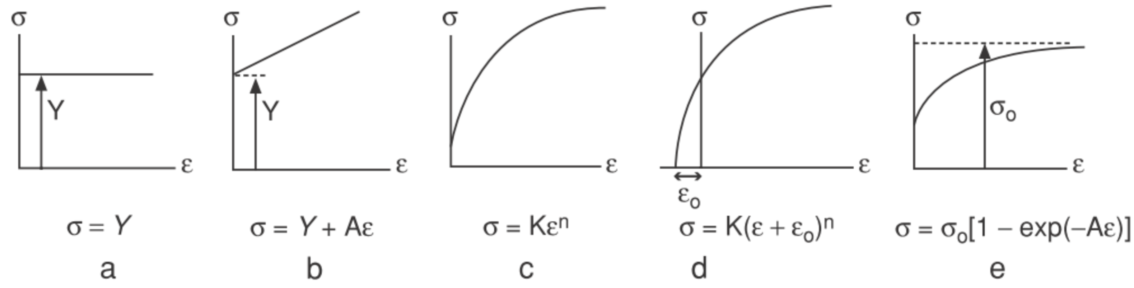

Figure 1.40 Mathematical approximations of the true stress-strain curve (Hosford 2010)

Generally the basic power law approximation (c) is used for analysis. Linearizing the equation,

$$\ln \sigma = \ln K + n \ln \varepsilon$$

Where n is the strain hardening exponent which characterizes the loading curve. Materials with low *n* values tend to be less ductile; more ductile for higher *n* values. Figure 1.41 shows an idealized true stress-true strain power law curve for different strain hardening exponent, *n*.

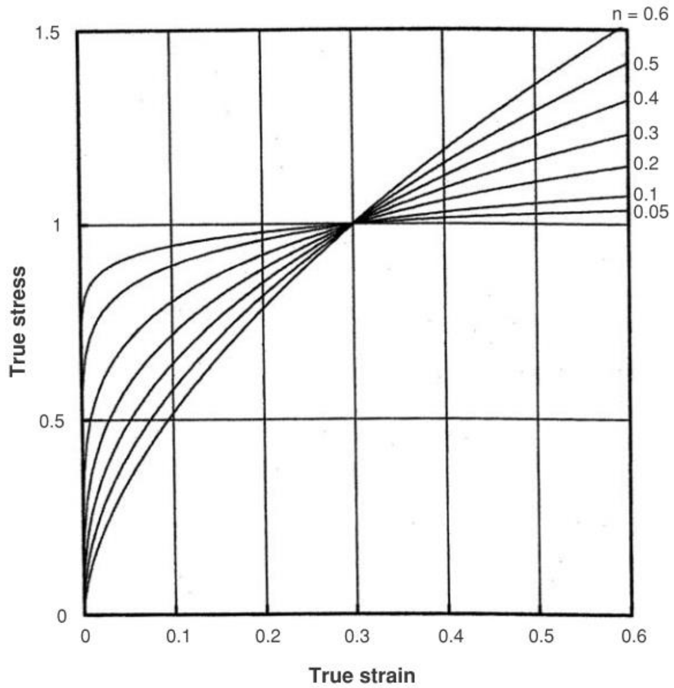

Figure 1.41 True stress vs. true strain of $\sigma = K\varepsilon^n$ (Hosford 2010)

1.11 Fitness-for-service assessment

When the structure or equipment in the oil, gas, petrochemical or power industry had been operating through its design lifespan, corrosion, fabrication imperfections, flaws or changes in material properties are sometimes unavoidable. If all imperfections are replaced or repaired regardless of severity, the cost of restoration bared by the operating company would be enormous.

Fitness-for-service (FFS) assessment (also known as Engineering Critical Assessment, ECA) is an engineering assessment procedure used to evaluate the fitness of an operating structure or equipment. The FFS evaluation of crack-like flaws is typically based on fracture toughness tests performed in a condition similar to the operating component. FFS serves as a mechanism to set weld flaw acceptance criteria, and or decide if the concerned subject requires repair, replacement or modification to be fit for operation (Selva 2012).

It is important for fracture toughness to be assessed to the highest accuracy. An underestimation of fracture toughness would sometimes result in unnecessary repairs on fit components; whereas overestimation of fracture toughness could miss-assess a critical flaw, leading to potential catastrophic fracture of the component in operation.

1.12 **Conclusion**

The fracture toughness concept for fracture resistance testing had been around for decades. The K_{Ic} critical stress intensity factor is mainly theoretical and consistent in all standards.

CTOD is a physical displacement of the crack tip, and there are two different approaches for estimation: - geometrical rotational factor approach and *J*-CTOD conversion (δ_{45}). It is unsure which approach is most appropriate or accurate, as δ_{45} is often associated to studies in FEA and less appropriate experimentally. The limitation of the δ_{45} definition for CTOD is described in Chapter 4.5.

Fracture toughness testing had been used many years in the industry. Although laboratory results are often conservative, it is important that the fracture toughness is estimated as accurately as possible. An over conservative estimation of fracture toughness could lead to meaningless money and manpower spent on a structurally fit component. The accuracy of the single point CTOD equations is investigated in Chapter 7.1, and R-curves in Chapter 8.1. Additionally, the suitability of the geometrical rotational factor approach for CTOD is studied in Chapter 9.1.

Chapter 2

Experimental Methods

2.1 Introduction

This study is focused in the investigation of the physical CTOD in SEN(B) specimen setup. The physical CTOD is obtained by casting the crack using a silicone replication compound, and measured optically using a microscope. Based on the physical CTOD, the accuracy and reliability of estimations from the standardised equations and FE model are examined.

This chapter describes the experimental work including fracture toughness tests, crack replication and physical measurements of the crack. Fracture toughness tests were performed on three different steel materials, machined to standard SEN(B) geometries. Three different fracture toughness tests were performed in three-point bend setup using a universal testing machine: -

- standard single point test
- standard unloading compliance test
- modified single point test

Single point and R-curve data were obtained from the standard tests, whereas a 2-part silicone compound was injected into the crack in the modified single point test to cast the crack. This technique produces a physical ‘negative’ of the crack.

The standard test results serve as a baseline to check the validity of the modified single point test. The silicone replica extracted from the modified single point test represents the physical crack of the specimen. The silicone replica was then sectioned at various points and measurements were made on the cross section of the sectioned silicone replica. CTOD measurements obtained from the sectioned cross section surface of the silicone replica correspond to the physical CTOD. The data extracted from the tests were analysed in the subsequent chapters.

2.2 Specimen design and manufacture

While there are several different established specimen setups used for fracture toughness testing: - CT, SEN(B) and SEN(T) (Chapter 1.5.2), this research focuses on the estimation of CTOD in the SEN(B) setup. The advantages of the SEN(B) setup are the simplicity of the geometry for manufacture and maturity of the configuration in this setup within standards.

The different steel materials were obtained in plate form. The steel plates were cut to rectangular steel blocks, then milled precisely to $B\times 2B$ and $B\times B$ geometries, where $B=$ 20mm. The milled steel blocks were notched using the electric discharge machining technique, EDM. The notches were machined parallel to the steel plate rolling direction, Y-X direction as shown in Figure 2.01.

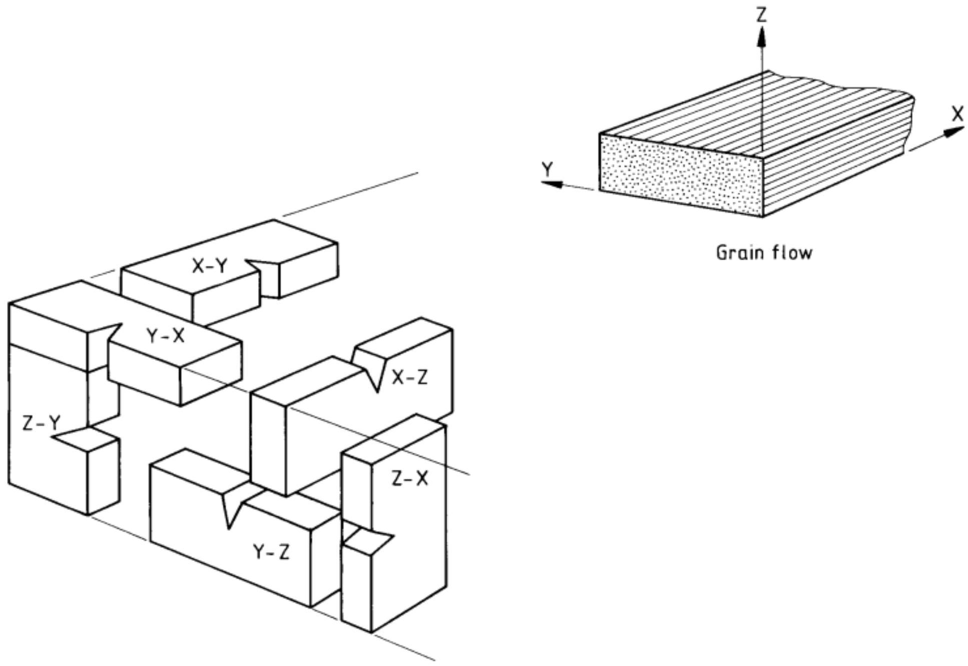

Figure 2.01 Fracture plane identification in rectangular base material (BSI 1991)

2.3 Fatigue pre-cracking

In the fracture toughness tests, a fatigue crack was introduced into the machined SEN(B) specimen before the specimens were tested. The intention of introducing a fatigue crack into the specimen is to replicate a real crack condition in the tests, as the machined notch is not sufficiently sharp to simulate a real crack. A machined crack tip would have higher crack tip radius compared to a fatigued crack, leading to higher fracture toughness (Taggart et al. 1976; Spink et al. 1973; Nowak-Coventry et al. 2015).

After the specimens were machined to their respective specimen setup, a fatigue crack was introduced to the specimens. The fatigue pre-cracking process was performed in a three-point-bend configuration (see Figure 2.02). An Instron 1603 fatigue machine with a load cell of 20kN was used for fatigue cracking.

Fatigue pre-cracking was performed by introducing cyclic loading on the SEN(B) specimen. The length of the intended crack length is marked on the sides of the specimen and the crack extension is observed optically as fatigue loading was performed (Figure 2.03). The loadings are halted when the crack extension on the side of the specimen achieves the intended crack length.

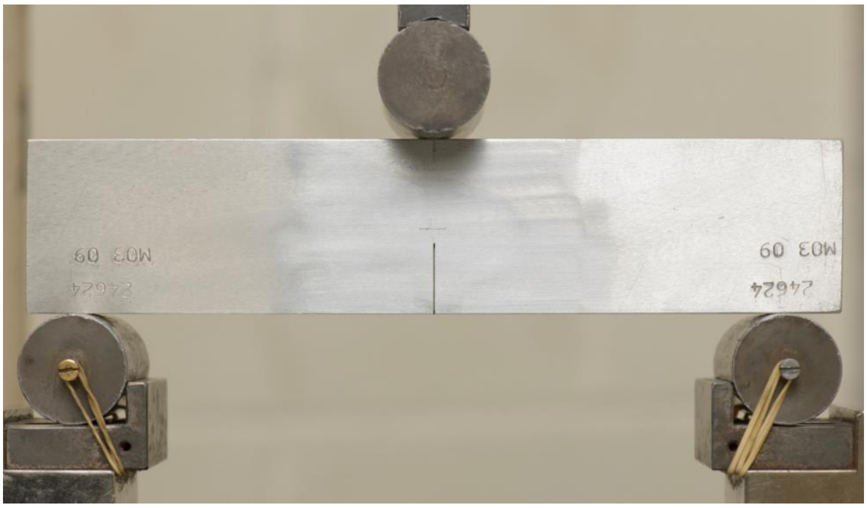

Figure 2.02 Fatigue pre-cracking in a three-point-bend configuration

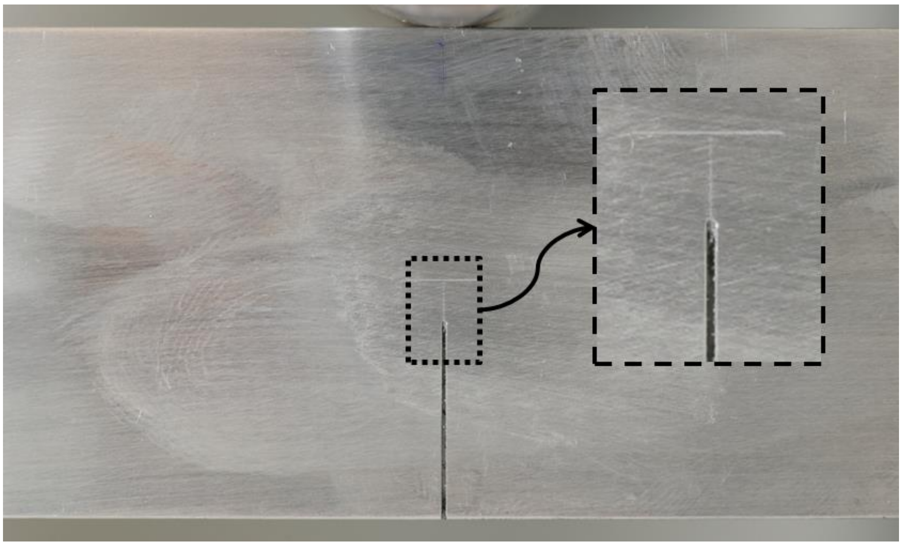

Figure 2.03 Fatigue pre-crack observed on the side of the specimen

There are several conditions imposed in BS 7448-1 on the pre-cracking procedure. The pre-cracking force applied on the final 1.3mm of the pre-cracking extension shall be below

$$F_{pre} = \frac{B(W-a)^2(\sigma_{ys}+\sigma_{uts})}{4S}$$

and

$$\frac{\Delta K_{pre}}{E} = 3.2 \times 10^{-4} m^{0.5}$$

Where the pre-cracking stress intensity factor is defined as

$$K_{pre} = \frac{FS}{BW^{1.5}} \times f\left({}^{a_0}/_{W}\right)$$

$f(a_0/W)$ is a dimensionless geometrical factor, which is described as below for SEN(B) configuration

$$f\left({}^{a_0}/_{W}\right) = \frac{3\left({}^{a_0}/_{W}\right)^{0.5}\left[1.99 - \left({}^{a_0}/_{W}\right)\left(1 - {}^{a_0}/_{W}\right)\left(2.15 - 3.93\,{}^{a_0}/_{W} + 2.7\,{}^{a_0{}^2}/_{W^2}\right)\right]}{2\left(1 + 2\,{}^{a_0}/_{W}\right)\left(1 - {}^{a_0}/_{W}\right)^{1.5}}$$

The fatigue pre-cracking force and stress intensity factors applied on the specimens complied to the standardized limits above. The pre-cracking force and stress intensity factor limit were intended to ensure a sufficiently small plastic zone ahead of the crack tip, so that the plastic zone size will not affect the fracture toughness of the specimen (Nowak-Coventry et al. 2015).

2.4 Material properties and specimen numbering

The main theme of the research is the validation of CTOD for material of different strain hardening exponents. Three different steel materials were chosen for the experiments due to different strain hardening properties. Mechanical and chemical properties were tested for the materials. Mechanical properties were obtained testing round tensile specimens in a uniaxial tensile machine, tested in accordance to BS EN ISO 6892-1:2009. Mechanical properties and the engineering stress strain curve for the materials were shown in Figure 2.04 and Table 2.01. The true stress-strain curve used in FE modelling is shown in Figure 2.05.

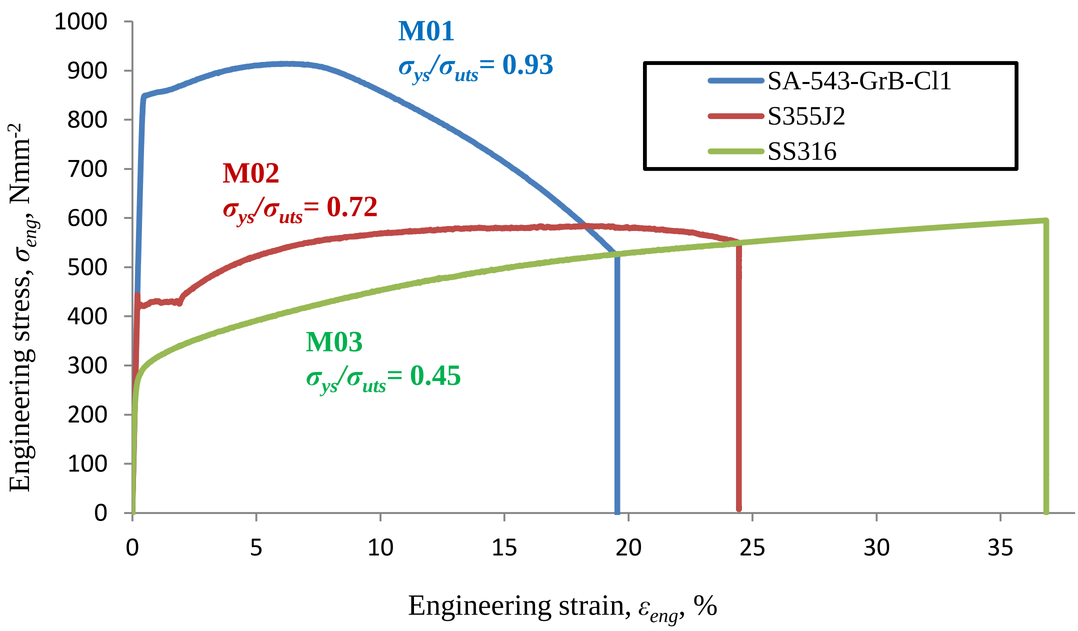

Figure 2.04 Engineering stress-strain curve obtained from the tensile test

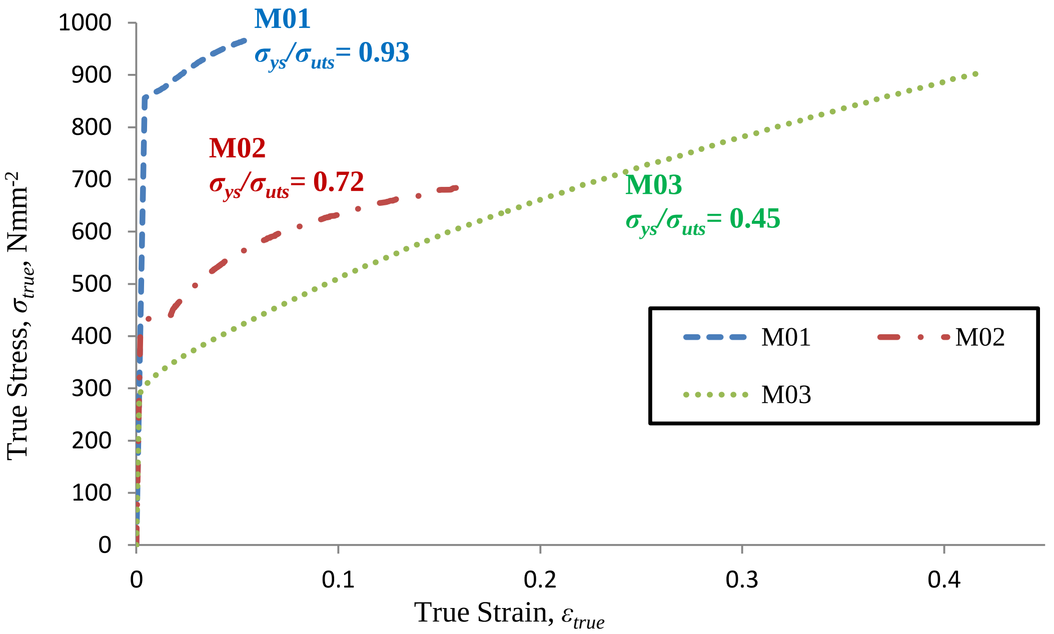

Figure 2.05 True stress-strain curve obtained from the tensile test

Table 2.01 Mechanical properties obtained from tensile test

Material	**M01**	**M02**	**M03**
Steel Grade	*SA-543-GrB-Cl1*	*S355J2*	*SS316*
Strain hardening, *n*[2]	*0.095*	*0.2*	*0.53*
Strain hardening designation	*Low*	*Medium*	*High*
Plate thickness, mm	*26*	*31*	*21*
0.2% offset proof strength, MPa	*850*	*421*	*286*
Tensile strength, MPa	*914*	*585*	*595*
Tensile ratio, σ_{ys}/σ_{uts}	*0.93*	*0.72*	*0.45*
Modulus of Elasticity, GPa	*217*	*205*	*205*
Elongation, %	*19.5*	*31.5*	*67.5*

In order to confirm the different steel grades, a cube was machined from each of the three materials. The cubes were tested for chemical composition using the spark discharge machine. Based on the chemical composition, the different materials could be confirmed. The chemical compositions of all three materials were shown in Table 2.02.

[2] Strain hardening was estimated by fitting the offset power law, $\sigma=K(\varepsilon+\varepsilon_0)^n$ to the true stress-true strain curve

Table 2.02 Chemical properties by weight percentage

Steel Grade	M01	M02	M03
C	0.17	0.17	0.021
Si	0.38	0.4	0.26
Mn	0.29	1.46	1.76
P	0.007	0.014	0.037
S	0.005	0.005	0.003
Cr	1.46	0.012	17.4
Mo	0.46	<0.003	1.94
Ni	2.95	0.02	10.1
Al	0.014	0.033	<0.01
As	<0.004	<0.004	<0.01
B	<0.0003	0.0004	<0.001
Co	0.008	0.007	0.19
Cu	0.018	0.012	0.37
Nb	0.004	0.019	<0.01
Pb	<0.005	<0.005	<0.002
Sn	<0.004	<0.004	0.01
Ti	0.007	0.003	<0.005
V	0.012	0.005	0.06
W	<0.01	<0.01	0.07
Zr	<0.005	<0.005	
Ca	<0.0003	0.0004	<0.001
Ce	<0.002	<0.002	
Sb	< 0.002	< 0.002	

2.5 Specimen numbering

Each specimen tested experimentally was uniquely numbered for identification. As an example, for 'M02-04', 'M02' would correspond to material S355J2, whereas '04' corresponds to the specimen's unique numbering. The designated numbering of the specimens and the specimen configuration is shown in Table 2.03.

Table 2.03 Specimen numbering with description

Specimen Number	Description	Setup and geometry
M01-04	Single specimen unloading compliance without side grooves	nominally 20mm×40mm B×2B SEN(B) specimen
M01-05	Interrupted SEN(B) test with silicone crack replication	
M01-07	Single point SEN(B) test	
M05-06	Interrupted SEN(B) test with silicone crack replication	
M05-07	Single specimen unloading compliance with side grooves	
M02-03	Single point SEN(B) test	nominally 20mm×40mm B×2B SEN(B) specimen
M02-04	Single specimen unloading compliance without side grooves	
M02-05	Interrupted SEN(B) test with silicone crack replication	
M02-06	Single specimen unloading compliance with side grooves	
M02-07	Interrupted SEN(B) test with silicone crack replication	
M02-08	Interrupted SEN(B) test with silicone crack replication	
M02-09	Interrupted SEN(B) test with silicone crack replication	
M03-03	Single point SEN(B) test	nominally 20mm×40mm B×2B SEN(B) specimen
M03-04	Single specimen unloading compliance without side grooves	
M03-05	Interrupted SEN(B) test with silicone crack replication	
M03-06	Interrupted SEN(B) test with silicone crack replication	
M03-07	Single specimen unloading compliance with side grooves	

2.6 Fracture toughness test programme

SEN(B) specimens were machined and fatigue loaded to a nominal crack length-specimen width ratio, a_0/W of 0.5. The side grooved specimens were machined to 0.1 of the thickness on each sides of the specimen after fatigue pre-cracking was performed. Three different tests were performed: - standard single point fracture toughness test, modified single point fracture toughness test and standard unloading compliance fracture toughness test.

The standard single point test provides standard load-displacement data for fracture toughness calculation; whereas the estimated crack extension could be calculated using data from the standard unloading compliance test. Silicone compound was used to create a physical crack casting on the modified single point tests, where the silicone replicas are the exact representative of the crack and enables direct measurement of the crack dimensions by sectioning after removal from the test specimen.

2.7 Standard single point test

In a single point fracture toughness test, applied load, crosshead (machine) and clip gauge displacement data were recorded. Fracture toughness was calculated based on the point of maximum load or the onset of unstable crack extension.

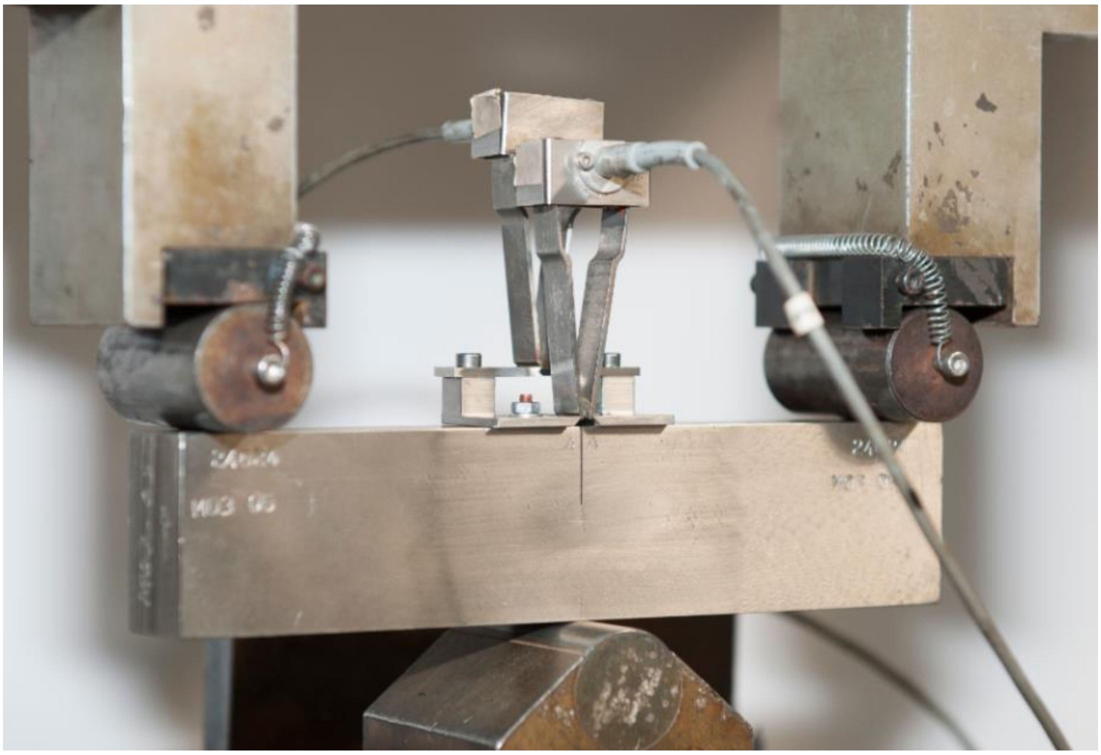

Figure 2.06 SEN(B) specimen with clip gauges in a three-point-bend setup, showing the double clip gauge configuration

The SEN(B) specimens were designed to be loaded in a three-point bend setup, where the loading span, $S = 4W$. The SEN(B) specimens were positioned on the testing jig as in Figure 2.06, fitted to the universal testing machine. Two clip gauges, V_{g1} and V_{g2} were positioned on the knife edges, located 2mm and 12mm above the crack mouth respectively. The clip gauges records the displacement data above the crack mouth opening, whereas the machine records the load reaction force exerted by the specimen. The universal testing machine, Instron B107 with a load cell of 500KN was set to displacement control (crosshead displacement) for the tests, where the rate of displacement was set at 0.1mms^{-1}. This displacement loading rate gives a constant increasing K rate within 0.5MPam$^{0.5}$s^{-1} to 3.0MPam$^{0.5}$s^{-1}, valid to BS 7448-1. The specimen was loaded to the point beyond the point of maximum force before unloading the specimen to end the test. Figure 2.07 shows an idealised load-displacement data obtained from a three-point-bend test.

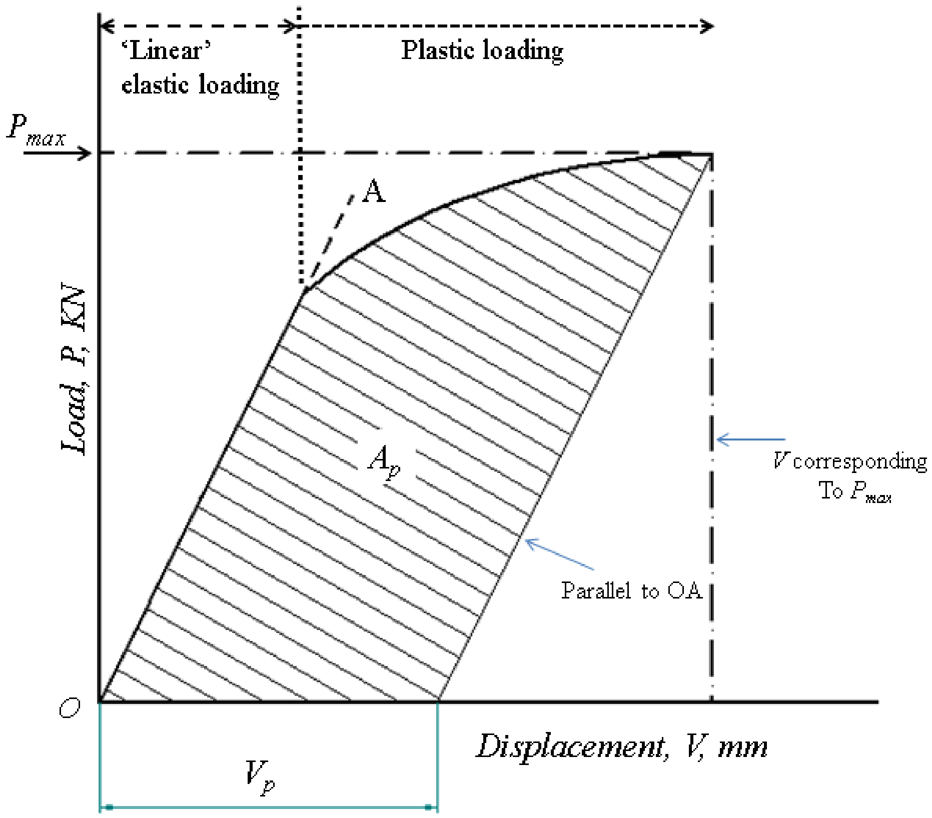

Figure 2.07 Idealized load-displacement diagram obtained from a test

After the end of test, the specimens were heat tinted in an oven at 400°C (Figure 2.08). Heat tinting allows the exposed crack face to oxidise, showing a darker shade. This technique gives a clear contrast between the cracked material and the unbroken ligament. The heat tinted specimens were frozen in liquid nitrogen then broken into two parts, exposing the crack faces. Liquid nitrogen freezes the specimen so that it fractures in brittle cleavage, where a distinct line between the end of tearing during the test and the start of brittle cleavage fracture due to freezing is obvious. The crack faces allow observation and measurement of the crack.

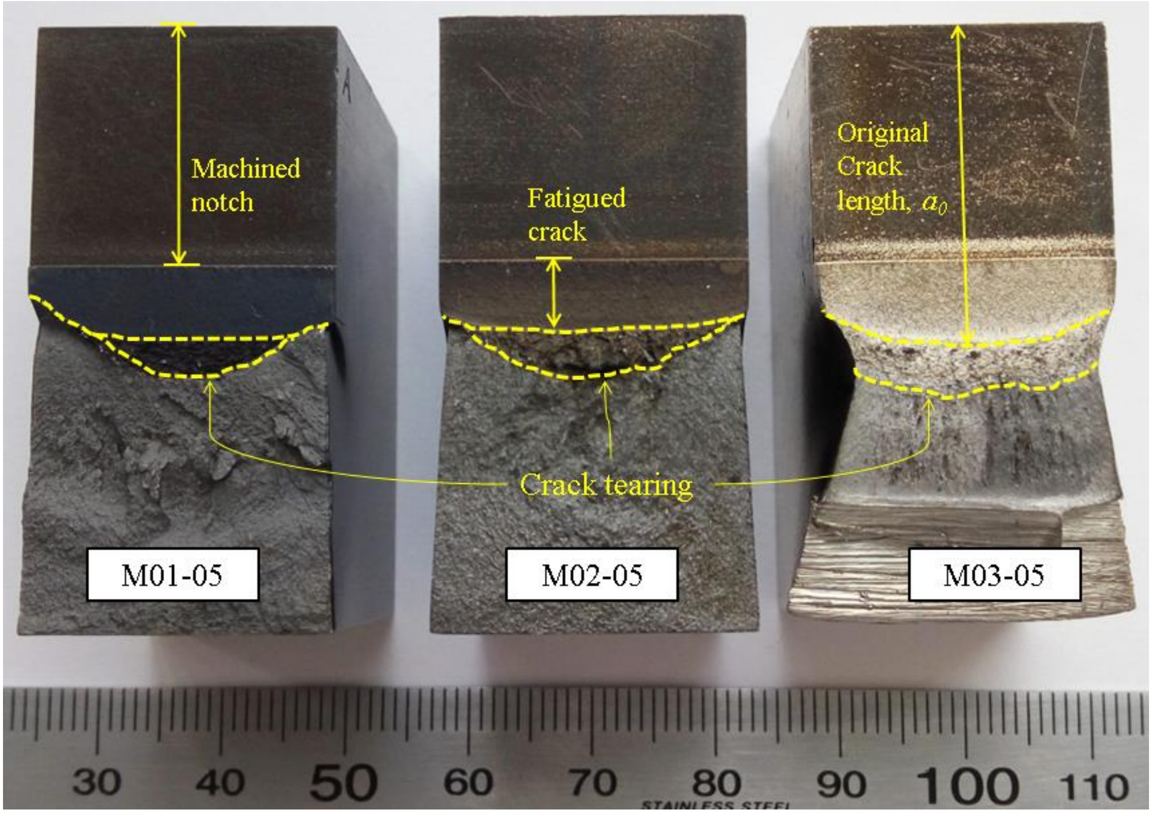

Figure 2.08 Heat tinted crack faces, allowing easy identification of the start and end of crack tearing

2.8 Unloading compliance test

The main objective of the unloading compliance test in this research is to estimate the crack extension as the specimen is loaded. This allowed prediction of suitable load points to cast the crack replicas. Similar to the single point test, the SEN(B) specimens were tested in a three-point-bend setup. Instead of continuous loading to the end of test, the specimens were loaded to a certain point, partially unloaded, before reloading then unloading again. The load-unloading sequence was repeated to the end of test. A typical unloading compliance load-displacement data is shown in Figure 2.09. The elastic compliance (gradient of the straight portion on the unloading-reloading) was used to estimate the crack length extension as the specimen was loaded. These estimations are calibrated against physical measurements from the crack face, showing the initial and final crack lengths. Fracture toughness was plotted with the crack extension, which gives data points to fit the resistance curve, R-curve (Figure 2.10).

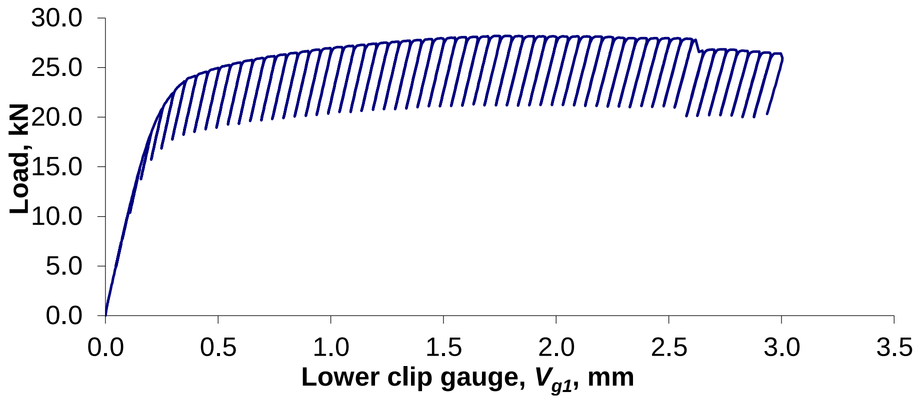

Figure 2.09 Typical load-displacement data obtained from unloading compliance test

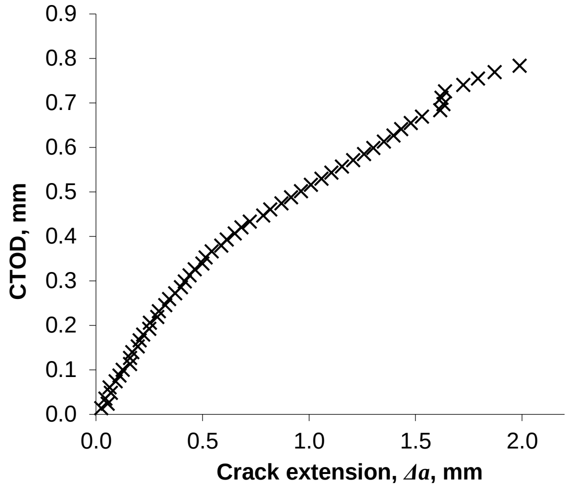

Figure 2.10 Typical R-curve for CTOD, generated from the unloading compliance data shown in Figure 2.09

2.9 Modified single point test for crack casting

The different CTOD equations were formulated based on different assumptions (Chapter 1.7), leading to different values calculated (Chapter 5.3 and 7.3). By replicating the actual crack, the physical replicas were extracted, enabling measurements to be used for the validation of different CTOD equations. This technique had been used in research and showed promising results (Robinson & Tetelman 1975; Robinson & Tetelman 1976; Wang et al. 1997; Robinson & Tetelman 1974; Tagawa et al. 2014; Kawabata et al. 2016). Using 2-part silicone compound (Microset RF101), it is possible to make a casting of the actual crack. Microset RF101 has a resolution of 0.1µm, 5 minute cure time and less than 0.1% shrinkage, which means that the cured replica is an accurate representation of the actual crack.

The single point SEN(B) test procedure was modified to allow for the crack casting process. Initially, the specimens were loaded in the same manner as the standard single point test. At selected displacement points based on the clip gauge opening, the machine loading was paused and the specimens were held in crosshead displacement control. While held, the clip gauge readings were paused and the clip gauges removed. The sides of the crack were sealed using tape, while a tiny ‘exhaust’ hole was made at the crack tip, which helped to reduce the probability of trapped air bubbles around the crack tip region. The silicone compound was injected into the crack from one side of the specimen slowly, allowing the silicone compound to completely fill the void. A syringe was used to induce vacuum on the ‘exhaust’ holes, removing a minimal amount of silicone compound along with any air bubbles near the sides of the crack tip (Figure 2.11). The crack was fully filled with the silicone compound and left to cure.

Figure 2.11 Syringe with a rubber seal was used to induce vacuum at the sides of the crack tip while the silicone compound is being injected

After 5 minutes of curing time for the silicone compound, the clip gauges were replaced and the displacement loggings were resumed. The specimen was loaded to the next displacement of interest, then paused and held in displacement control. The clip gauges readings were again paused and clip gauges removed, along with the tapes sealing the sides of the crack. The cured silicone replica was carefully removed (Figure 2.12). The procedure above was repeated casting a new crack replica for the consecutive selected points.

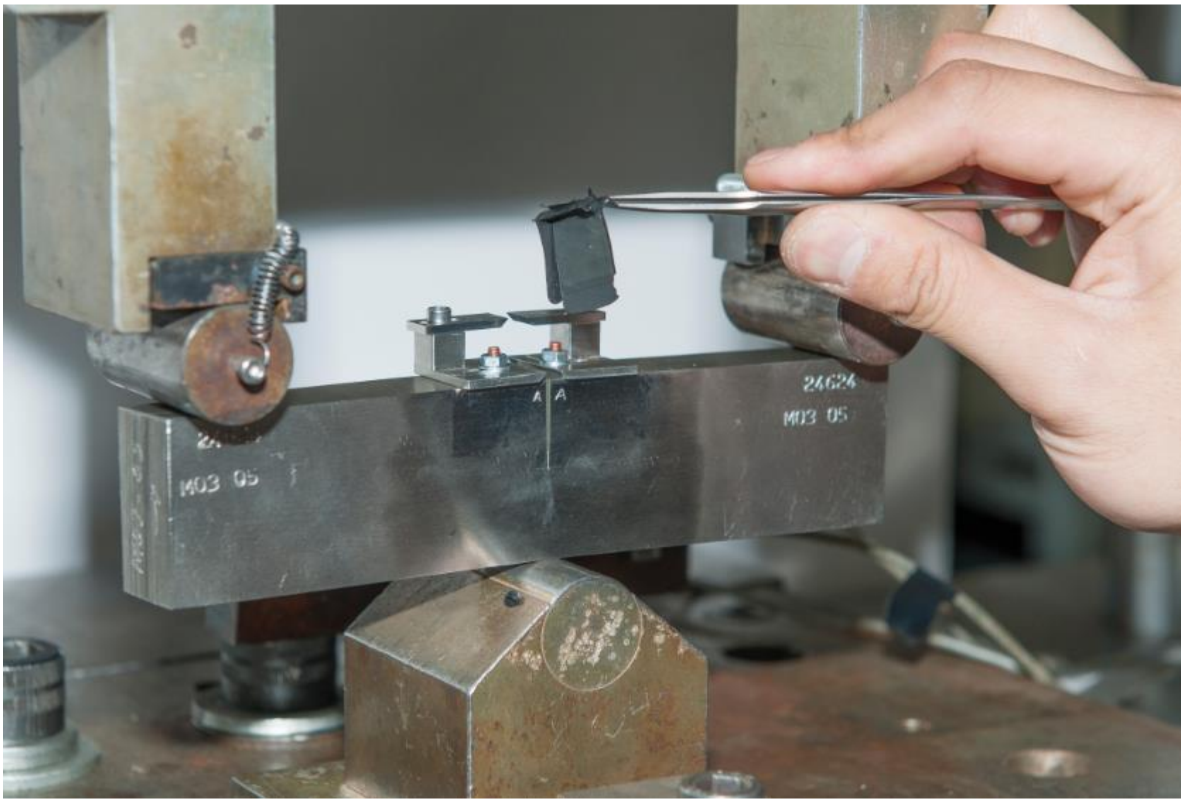

Figure 2.12 Silicone replica carefully extracted from the specimen

2.10 Measurement on the silicone replicated crack

The silicone replicated crack (SRC) extracted from the modified single point tests were labelled according to the specimen number and the corresponding clip gauge opening where it was extracted. The silicone replica was sliced at different positions, allowing measurement to be taken on the exposed cross section.

For the physical measurements, an optical microscope, Olympus SZX9 with x0.5 magnification main objective lens was used to capture images of the sample for measurements. The samples were placed on a flat levelled surface, where the location of interest was focused using the highest magnification, x57. The magnification was then reduced to x6.3, where the whole fatigue crack could be observed in the image without the need of image stitching. An image of the crack was captured using the Leica DFC 295 camera mounted to the microscope, and processed using the Leica Core software. The Leica Core software was calibrated to measure distance based on the pixels on the image. This image capturing procedure was slightly modified from the typical method to reduce human error, further explained in the Section 2.11.

The measurement of the original crack length, a_0 is required for the determination of CTOD. By measuring the crack face of the test specimens, a_0 was the sum of the machined crack length (Figure 2.13) and the fatigue crack length (Figure 2.14).

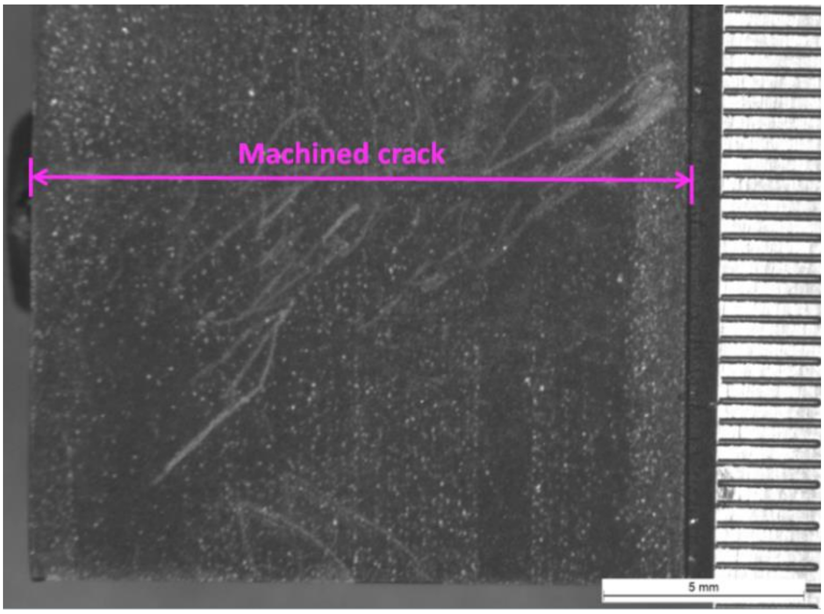

Figure 2.13 Length of the machined crack measured on the crack face (horizontal)

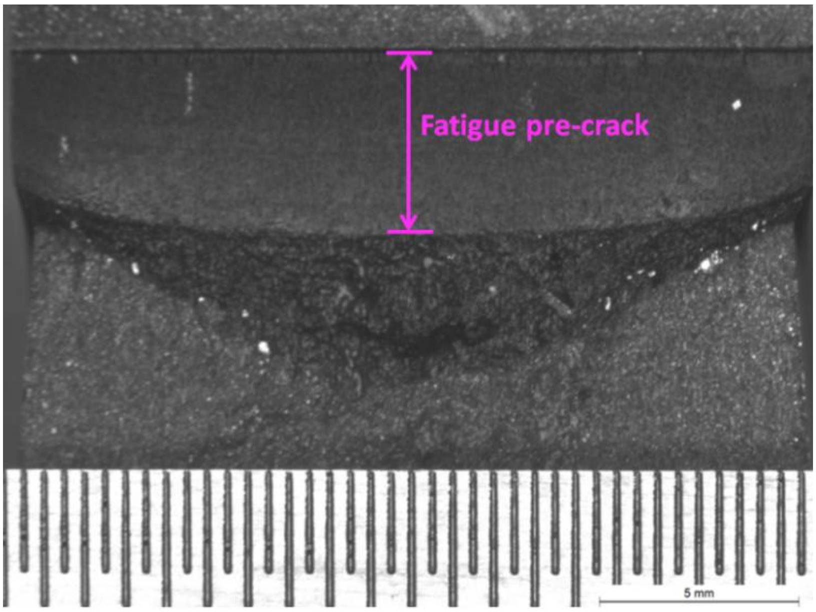

Figure 2.14 Length of the fatigue pre-crack measured on the crack face (vertical)

The sectioning of the silicone replicated crack (SRC) was based on a coordinate system defining the position across the specimen thickness, *b*, with *b*= 0 being the mid-point of the replica, and the outer sides being defined as *b*= 1 and -1. The SRC was sliced at *b*= 0 into two equal portions or at *b*= -0.5, 0 and 0.5 into four equal portions depending on the analysis required (Figure 2.15). The cross section of the SRC was mounted under the optical microscope for image capture and measurement. Using the Leica Core software, a_0 was measured on the image, which determines the position where CTOD was measured (Figure 2.16).

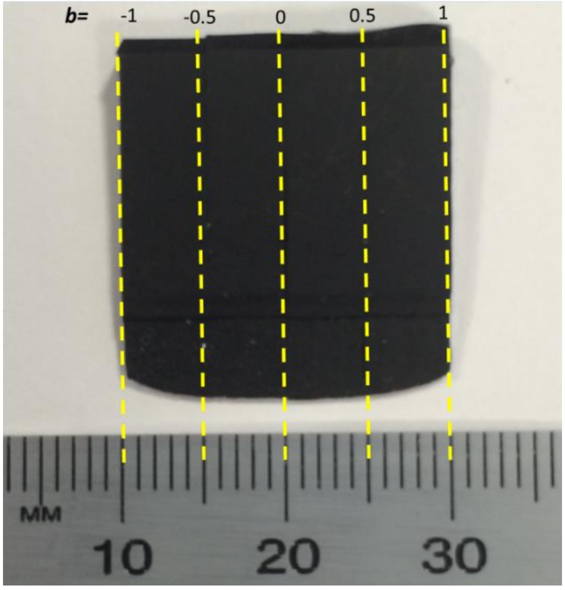

Figure 2.15 Measured sections across the thickness of the specimen

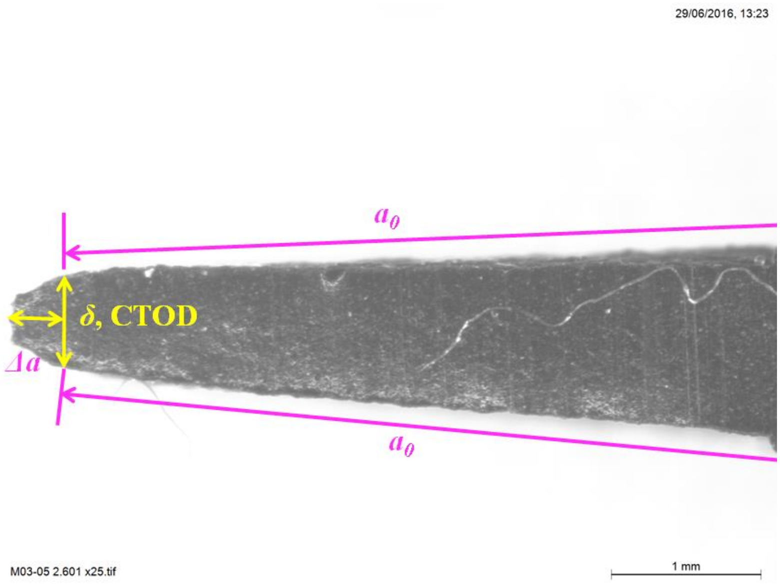

Figure 2.16 Measurement on the sliced cross section of the silicone crack replica (M03-05, V_{g1}= 2.601mm, middle of the crack, *b*= 0, ×25 magnification)

2.11 Calibration to minimize inconsistency in measurement

The optical microscope was used for physical measurement of the silicone replicas. Generally, the image was first focused on the region of interest at the highest magnification, and then reduced to the intended magnification, then adjusted for image sharpness. This method gives a sharp image, but the measurements were less consistent. The measurements were calibrated to the distance between the pixels, and sharpness adjustment at the reduced magnification introduces large human error.

Aware of the shortcomings of the method above, a modified procedure had been introduced to reduce human error, improving consistency and accuracy. First, the highest magnification was set and focused on the region of interest, then reduced to the intended magnification without further adjusting focal point for image sharpness. Although the image will not always be sharp, this is not an issue with respect to accurate CTOD measurement. The modified method was validated by measuring distance on a metal ruler on various elevations.

A rule with mm scale was measured on 0mm, 14mm and 30mm elevation attached to a block magnet. The method to determine levelling and metal ruler attachment is shown in Figure 2.17 and Figure 2.18.

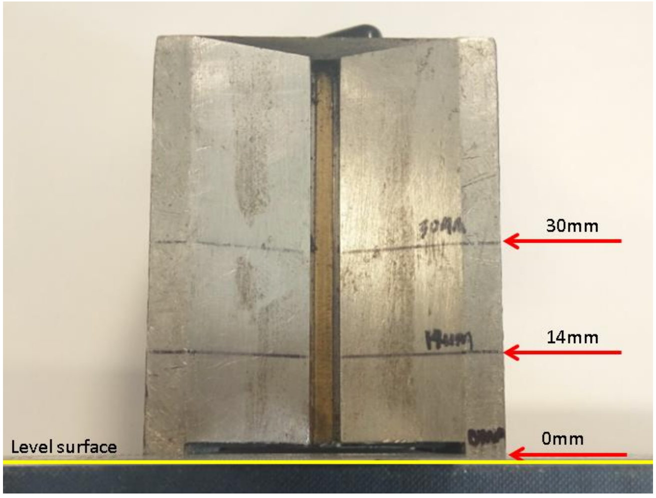

Figure 2.17 Side view of the block magnet, exposing the different levelling for attachment of the metal ruler

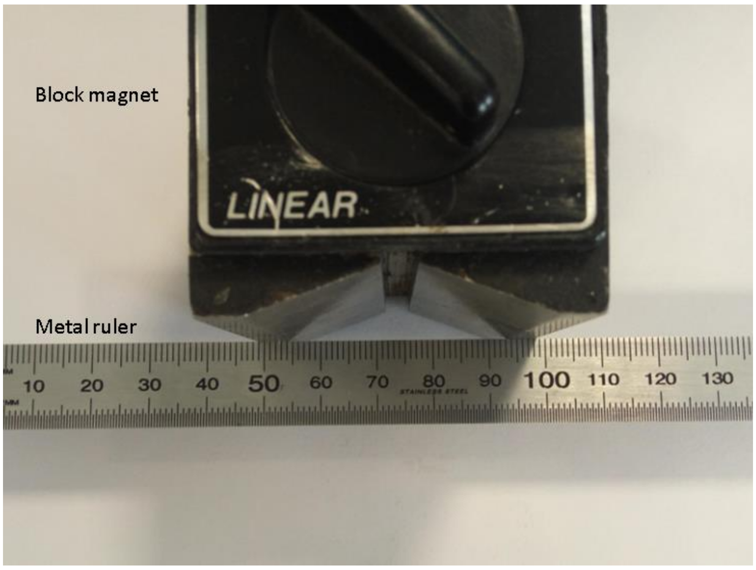

Figure 2.18 Top view of the block magnet with the metal ruler at 14mm levelling

The rule was placed at 0mm elevation using a block magnet. Magnification was increased to maximum, x57 and focused for sharpness. The magnification was adjusted to x6.3 and the image was captured. Images were captured at three different elevations, 0mm, 14mm and 30mm (Figure 2.19). Measuring the distance between 50mm and 60mm, it was found that the measurements obtained were consistent (Figure 2.19). This image focusing procedure was applied to all images captured using the optical microscope for measurement purposes.

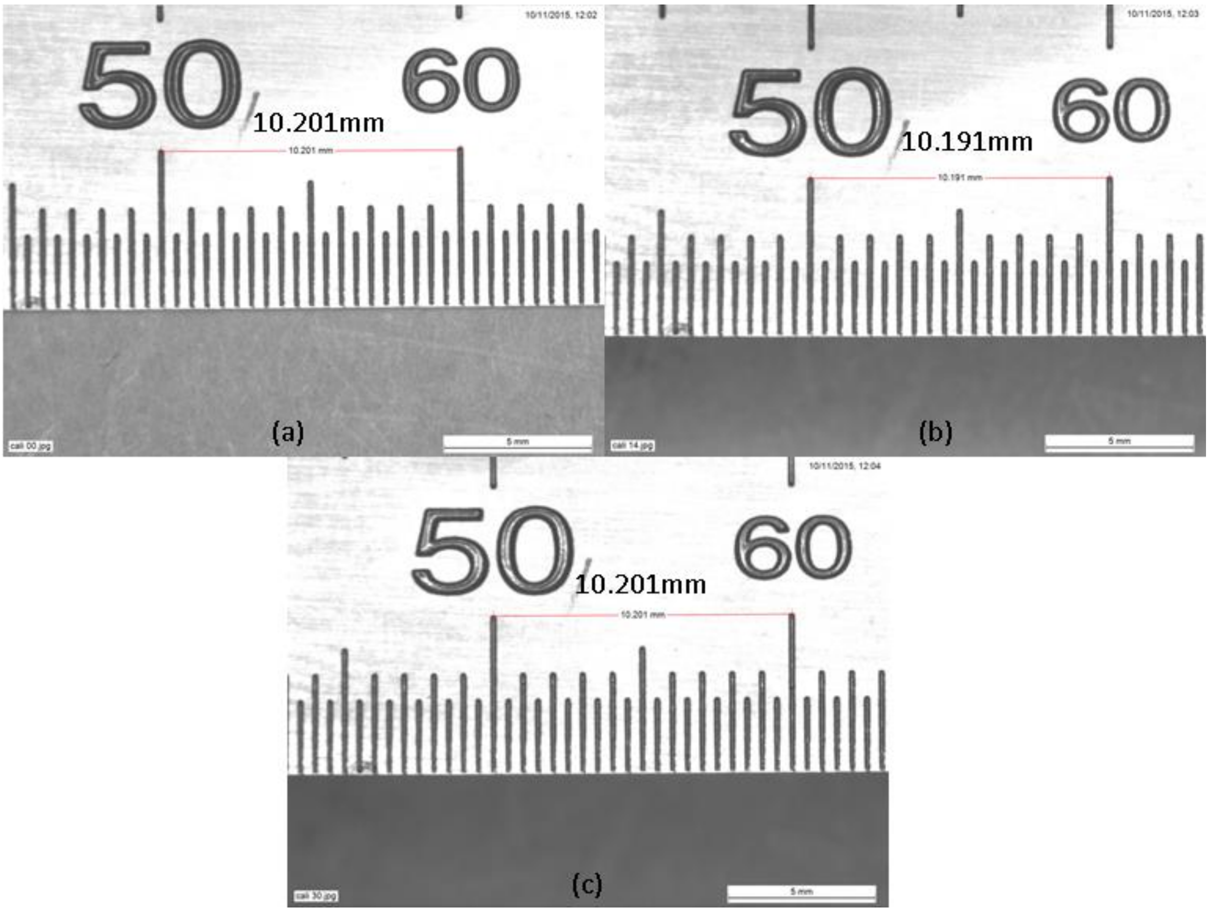

Figure 2.19 Calibration photos of the metal ruler on (a) level surface (b) 14mm elevation (c) 30mm elevation

2.12 Summary

Three different tests were performed experimentally. The standard single point tests were used to validate the load-displacement data obtained from the modified single point tests. The standard unloading compliance test provided estimation of crack extension to target positions for replicas to be taken. CTOD measured on the cross section of the SRC represents the physical CTOD to which other CTOD estimation methods could be compared. Based on the experimental results, finite element modelling was used to predict the tests, described in Chapter 4.1.

Chapter 3

The effects of mid-test hold on test data

3.1 Modification of the standard testing method to accommodate silicone crack casting

In a standard single point fracture toughness test, the specimen is loaded continuously in displacement control rather than load control to the point of fracture, or end of test after maximum load has been passed. But in order to cast the crack replicas, it was necessary to pause the test at regular intervals. The silicone compound (Microset RF101) was originally present in a viscous fluid form, and takes about 5 minutes for the catalyst to fully solidify the silicone compound. To accommodate the casting process, the specimen needs to be held for at least 5 minutes for the silicone compound to solidify, and a reference value of load and clip gauge displacement is required to represent the point where the crack was replicated. The specimen can be held in either constant load or constant displacement control for silicone crack replication. The consequent differences in the load-displacement measurements, resulting from the two holding methods are described below.

3.2 The time dependent effects of different holding methods on the crack

Testing machines are capable of loading specimens in load and displacement control, i.e. incrementally increasing load and measuring displacement, or *vice versa*. In accordance with the fracture toughness testing standards (BSI 1991; ASTM 2015; ISO 2016), the specimens are required to be tested in displacement control to qualify for a valid result. This is because the specimen would break after maximum load is achieved in load control, whereas load would reduce with increasing displacement after the maximum load, allowing for plastic deformation.

A number of research papers describe work performed on cracked test specimens using displacement control, then interrupted the test by holding the specimen at different constant loads (Green & Knott 1975; Garwood 1986; Brenner et al. 1983; Schulze & Fuhlrott 1980; Tsuru & Garwood 1979). Generally, when the specimens were held at that constant load beyond the elastic loading region, the holding time required for the specimen to fracture at constant load reduces as the δ/δ_{max} increases (Figure 3.01). δ_{max} is based on the point of maximum load in the test, and therefore δ/δ_{max} would be representative of the holding load- maximum load ratio, P_{hold}/P_{max} in the test. Green & Knott (1975) also found that the trend for δ/δ_{max} relative to holding time decreases with the increase of specimen thickness, apart from very thin 5mm thick specimens. This is due to the increasing plane strain dominance across the crack for increasing thickness; contrary to the thin 5mm plane stress dominated specimen, with a larger plastic zone ahead of the crack tip.

Figure 1.21 shows the relative plastic zone size due to plane stress and plane strain dominance across the crack tip. Banerjee (1981) explained that as the plastic zone ahead of the crack tip increases in size, more energy is dissipated before the crack propagates and it is harder for unstable crack propagation to initiate. This generally results in higher fracture toughness in plane stress dominant specimens, and the opposite for plane strain dominant specimens.

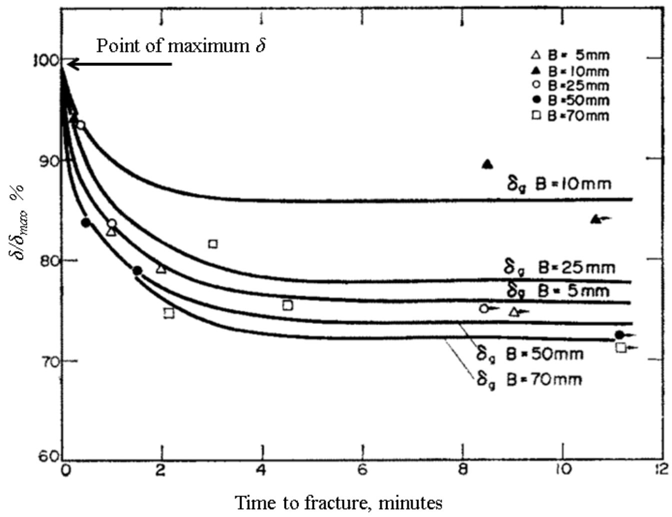

Figure 3.01Specimens of different thickness held in constant load (Green & Knott 1975)

In conditions where the specimen is held in constant load, the displacement and crack extension, Δa increase with time. The displacement/strain increase phenomenon is similar to that observed by Tagawa et al. (2011), where un-notched tensile specimens were held in constant load (Figure 3.02). However fracture did not occur in the constant load tensile tests, as strain appeared to converge after a certain period of hold time.

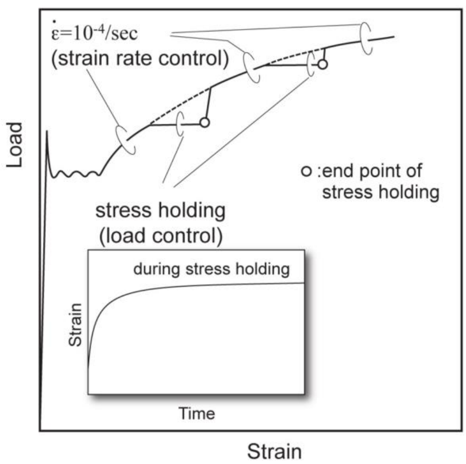

Figure 3.02 Load-strain data of tensile specimen held in constant load (Tagawa et al. 2011)

Based on several long term experiments conducted in TWI in the 1980's, Garwood (1986) found that time dependant fracture is expected only under fully yielded crack tip conditions, where the final fracture condition is dominated by plastic collapse. Based on the maximum displacement observed from the constant load tests, Garwood obtained an imaginary 'static' load-displacement curve, theoretically simulating a specimen loaded in an infinitesimally low rate. This imaginary curve is illustrated in Figure 3.03, showing the difference relative to a typical displacement controlled load-displacement curve from a standard monotonic displacement controlled fracture toughness test. The imaginary assumed 'static' load-displacement curve corresponds to a test where the specimen is loaded in a 'static' state (possibly attainable by loading the specimen in an infinitely low rate), giving slightly conservative fracture toughness estimations relative to a standard 'quasistatic' displacement controlled tests.

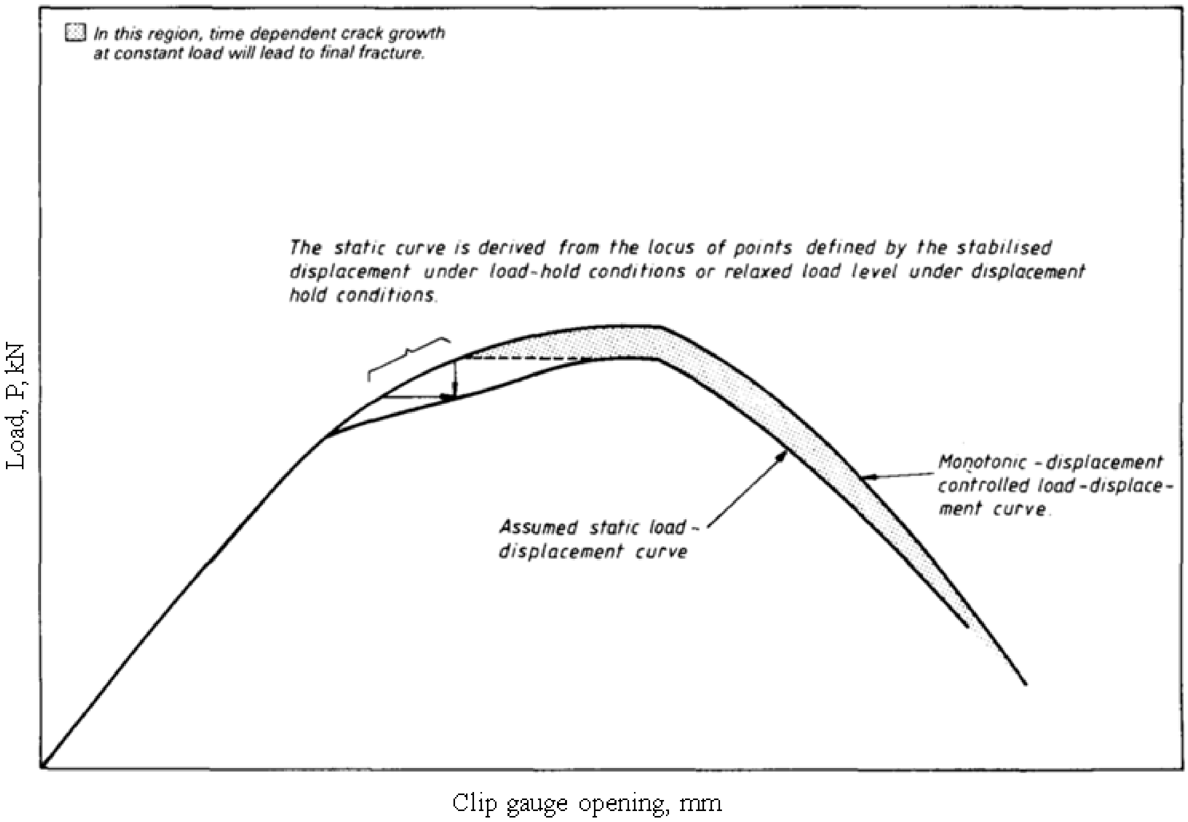

Figure 3.03A typical fracture toughness test load-displacement curve and an assumed static load-displacement curve based on observations of constant load hold tests (Garwood 1986)

In constant displacement tests, the effects due to time are different to that observed in constant load tests. In contrast to a crack growing while being held, it was reported that no time dependant crack growth was found in tests where the specimens were held in constant displacement (Garwood 1986; Tsuru & Garwood 1979). When the fracture toughness specimen is held in constant displacement, the load reduces exponentially and converges with the increase of time (Figure 3.04). A similar trend was observed by Tagawa et al. (2011) on tensile specimens held in constant displacement, shown in Figure 3.05. The load drop due to constant displacement is described as ‘load relaxation’.

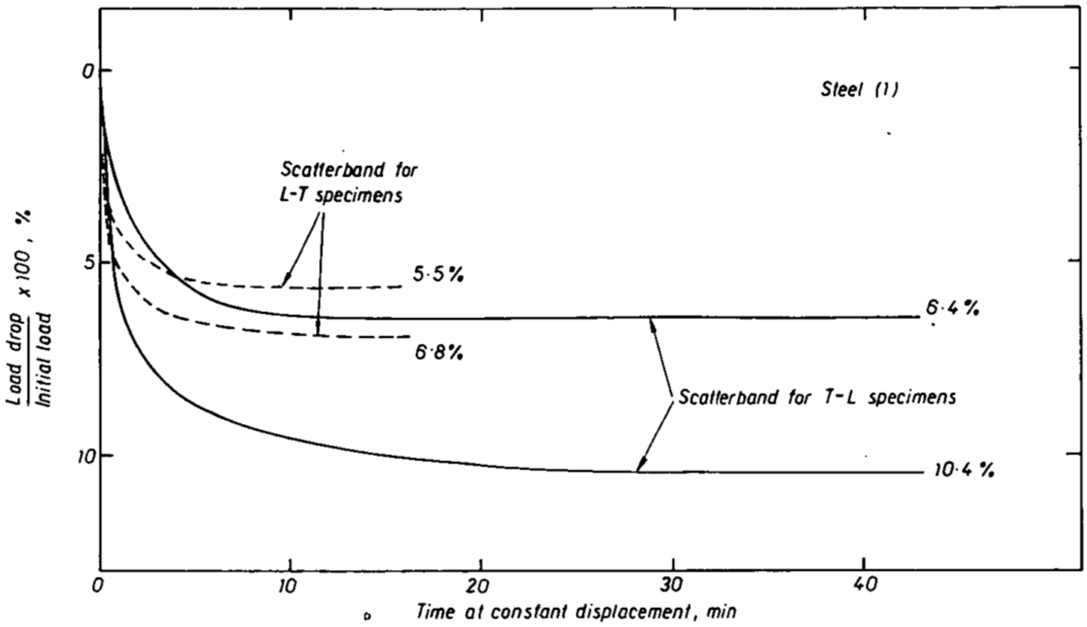

Figure 3.04 Load convergence when the specimen is held in constant displacement (Tsuru & Garwood 1979)

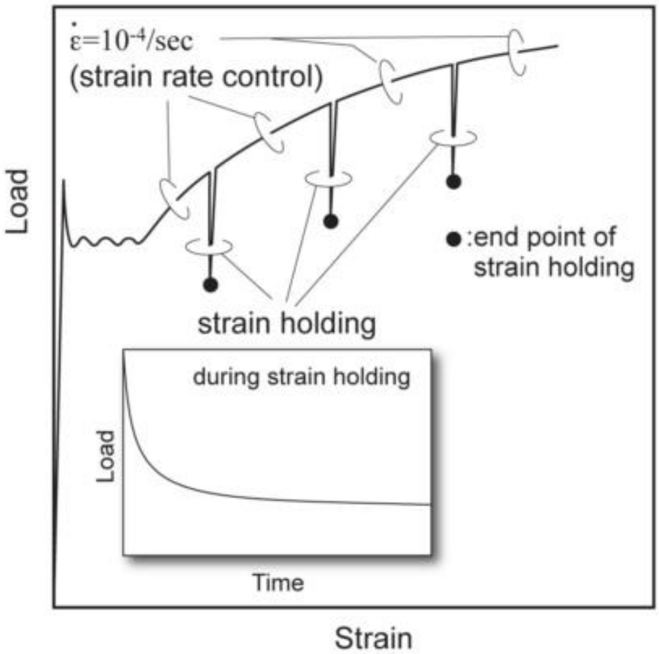

Figure 3.05 Load-strain data of tensile specimen held in constant displacement (Tagawa et al. 2011)

Tsuru & Garwood (1979) summarised the effects of constant displacement and constant load on fracture toughness specimens as shown in Figure 3.06. Based on this literature study, it can be concluded that fracture toughness specimens can retain the actual shape of the crack best when the specimen is held in constant displacement control while casting the silicone crack replicas.

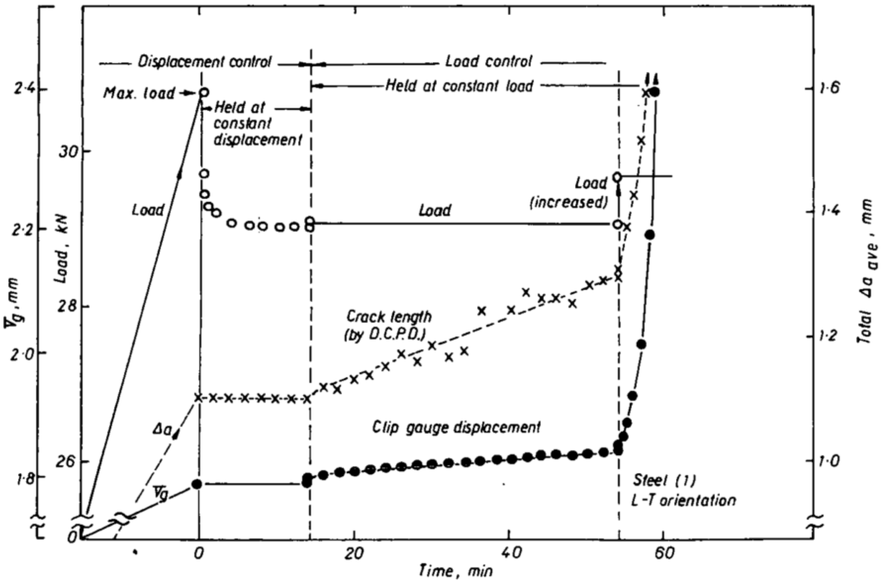

Figure 3.06 The effects of constant load and constant displacement on load, crack length and clip gauge displacement (Tsuru & Garwood 1979)

3.3 Results obtained from crack replication tests

To avoid the effects of time dependent constant load hold growth of the crack, the specimen was held under constant displacement (constant machine displacement) for the silicone crack replication tests. When the specimen was held in machine displacement for the injection of the silicone compound, the clip gauge readings were paused. The clip gauge readings were resumed only when the loading on the specimen was resumed. The load-CMOD data obtained from the silicone crack replication tests are shown in Figure 3.07.

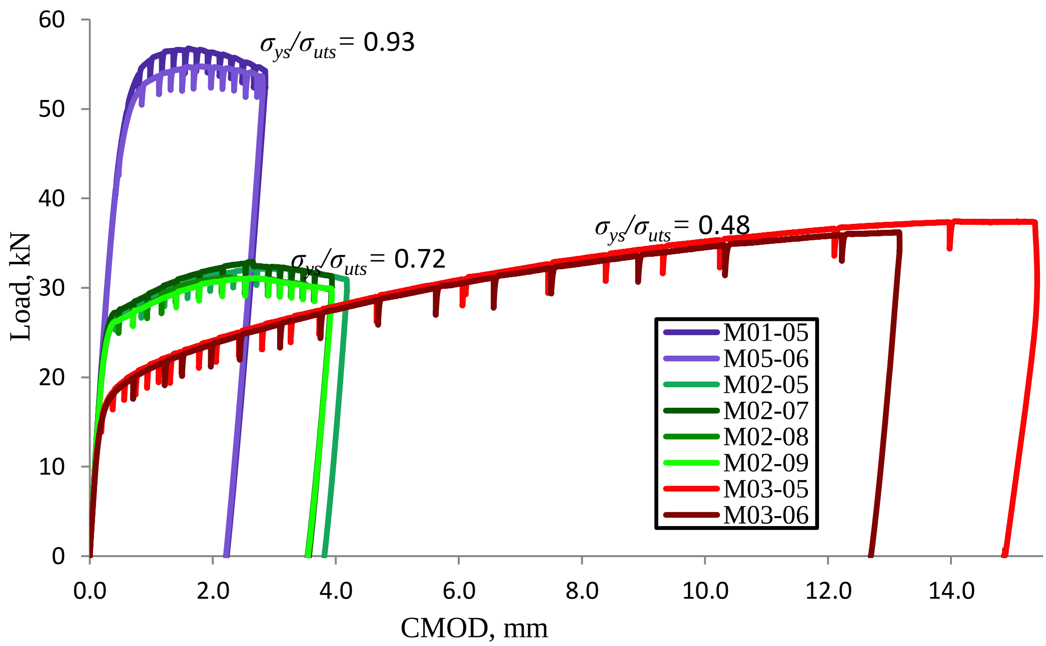

Figure 3.07 Load-CMOD data obtained from the silicone casting tests

The general shape of the load-CMOD curve in Figure 3.07 is similar to that obtained from a standard test, but with 'load drops' at points where the specimen was held in constant machine displacement. To confirm that the load drop observed in the test results were similar to that observed in literature (Figure 3.04), the load drop percentage, $(P_{drop}-P_{hold})/P_{hold}$ x100% was plotted to the hold time (Figure 3.08). By fitting a logarithmic trend line, it could be seen that the load drop percentages decrease and converges with the increase with time. Three points in the M01 (σ_{ys}/σ_{uts}= 0.93) were off trend, exhibiting less load drop percentage. Upon inspection, it was found that these points were held in the elastic dominated loading. This minimal load drop is explained in Tsuru & Garwood (1979) and Garwood's (1986) work, where the effect of load drop in constant displacement holding is relative to the plastic yielding of the specimen.

Figure 3.08 shows that the three different strain hardening material exhibited distinctively different load drop percentage. The general trend showed that the load drop percentage increased with the increase of material strain hardening. This is possibly due to the higher level of plasticity in higher strain hardening materials, leading to a higher load drop percentage.

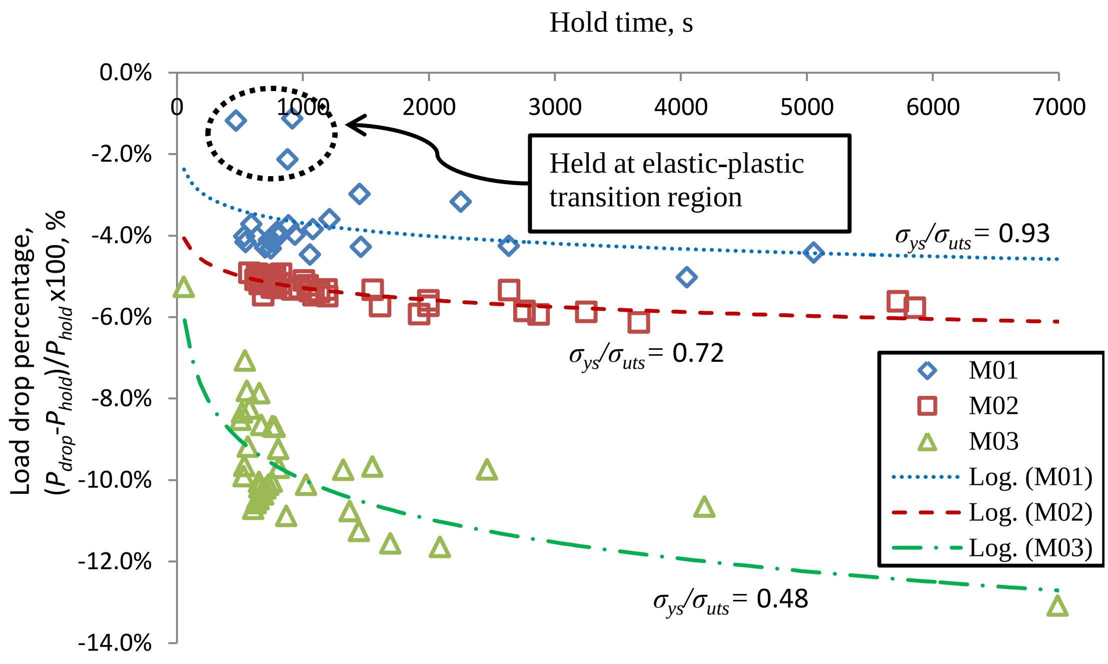

Figure 3.08 Load-drop experienced by the silicone casting specimens vs. hold time

During the silicone casting process where machine displacement was held constant, clip gauge feedback was paused. It was uncertain if there were any difference in the clip gauge displacement when the specimens experience load relaxation during constant machine displacement. This leads to the tests in the following subchapter, where feedback was recorded without being paused throughout the tests.

3.4 The effects of constant machine displacement on the clip gauge opening

Based on literature (Tsuru & Garwood 1979; Garwood 1986), it was found that there is no time dependent effect on the crack when the specimen is held in constant displacement. However, constant displacement can be performed on either maintaining machine displacement or clip gauge displacement. The effects of either measurements of constant displacement methods (machine displacement and clip gauge displacement) was not clearly investigated in literature, nor was explicitly shown in the silicone crack casting tests as the data feedback was paused during the hold period. The occurrence of the 'relaxation' effect could be due to the slacking of the machine, or redistribution of stress around the crack notch region.

To investigate the effects of constant machine displacement on the resultant load-displacement data, two three-point-bend tests were performed on 20mm×20mm×92mm solid rectangular bars, using M01 material (Figure 3.09). The tests were both performed in machine displacement control. Two clip gauges were mounted near the middle of the specimen (as shown on specimen M01-10) at different height to record continuous feedback throughout the test.

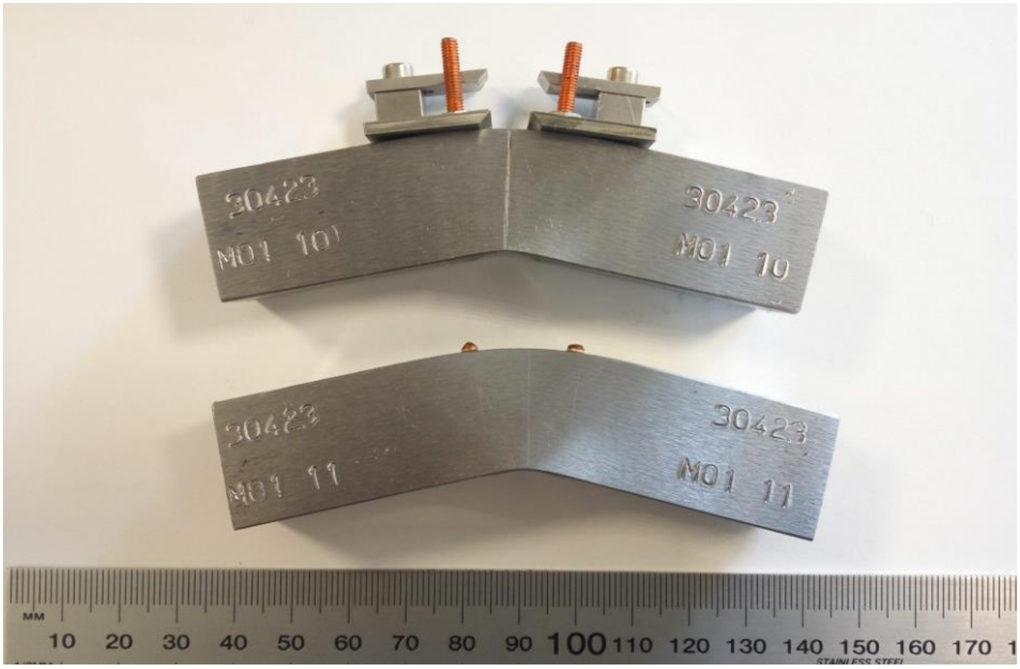

Figure 3.09 Plane bar specimens M01-10 (mounted with knife edges, hold test) and M01-11 (low loading rate test)

Assuming isotropic material properties and the absence of a crack, the test was intended to highlight the time effects of constant machine displacement and specimen loading rate. M01-10 was loaded at an approximate rate of 0.03mms^{-1}, held in constant machine displacement at selected clip gauge readings, similar to the procedure performed for the silicone crack replication tests but with continuous recording of the test feedback. This test was designed to investigate the effects of constant machine displacement on the load and clip gauge feedback during the hold. On the other hand, M01-11 was continuously loaded throughout the whole test at an approximate rate of 0.001mms^{-1}, in an attempt to produce the equivalent 'static' load-displacement curve shown in Figure 3.03. The load-displacement curve obtained from the solid bar tests are shown in Figure 3.10.

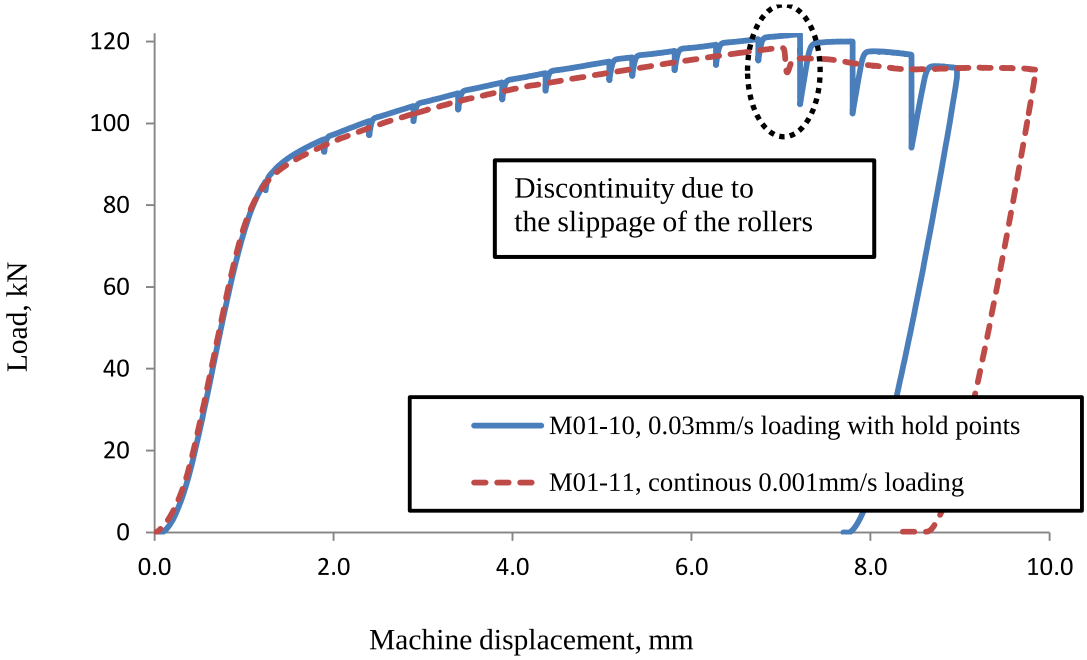

Figure 3.10 Load-machine displacement curve for M01-10 and M01-11

During both tests, the rollers slipped when the specimens experience a certain high level of deformation. The point of slippage of the rollers is shown in the discontinuity in the load-displacement data (Figure 3.10). Data after the point of roller slippage was not considered in subsequent analysis as the loading span of the specimen differs from the start of the test.

The load-displacement curve (Figure 3.10) showed results similar to that described by Garwood (1986) in Figure 3.03, where the specimen loaded at a lower displacement rate (M01-11) showed a lower load-displacement curve. Both M01-10 and M01-11 were tested in a rate which is significantly lower than the typical displacement control rate of 0.1mms^{-1}, and yet the difference in load-displacement feedback is noticeable. This shows that the loading rate, although within the allowable range described in the fracture toughness standards, could be one of the contributing factors to the scatter of fracture toughness results obtained from round robin tests.

To confirm that the specimens exhibit consistent load drop while held in constant machine displacement, the load drop percentage, $(P_{drop}\text{-}P_{hold})/P_{hold}$ x 100 was plotted to hold time, shown in Figure 3.11. The specimen was held between 300 to 340 seconds, or approximately between 5 to 6 minutes. Overall, it is seen that the load drop percentage decreases slowly, similar to the trend shown in Figure 3.05 and Figure 3.06 near the converged region. The point with the least load drop (≈340s) was held when the specimen is in the transition of elastic- fully plastic yielding (held at ≈85kN in Figure 3.10).

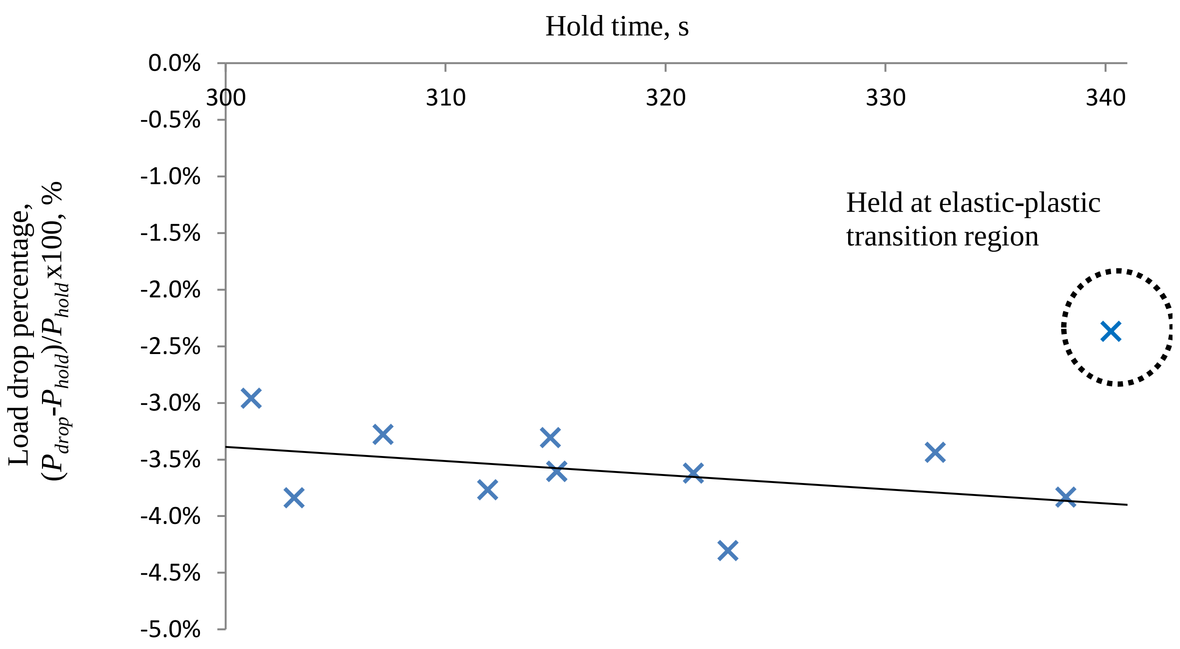

Figure 3.11 Load drop percentage relative to hold time observed in M01-10

To study the effects of constant machine displacement on the clip gauge displacement, the difference in the clip gauge displacements were plotted to the initial load when the specimen was held in constant machine displacement (Figure 3.12). Figure 3.12 shows that generally, the difference in the clip gauge reading while being held in constant machine displacement increase with load. This trend is suspected to be caused by the rotation of the crack flanks of the specimen due to bending. The variation between the upper and lower clip gauge differences due to a hold time at constant machine displacement increases with the higher load. This possibly implies that in a cracked specimen, holding the specimen in constant machine displacement leads to a small amount of crack opening. However, the magnitude of difference observed in the clip gauge displacement (maximum difference of 0.021mm) is small relative to the resultant fracture toughness.

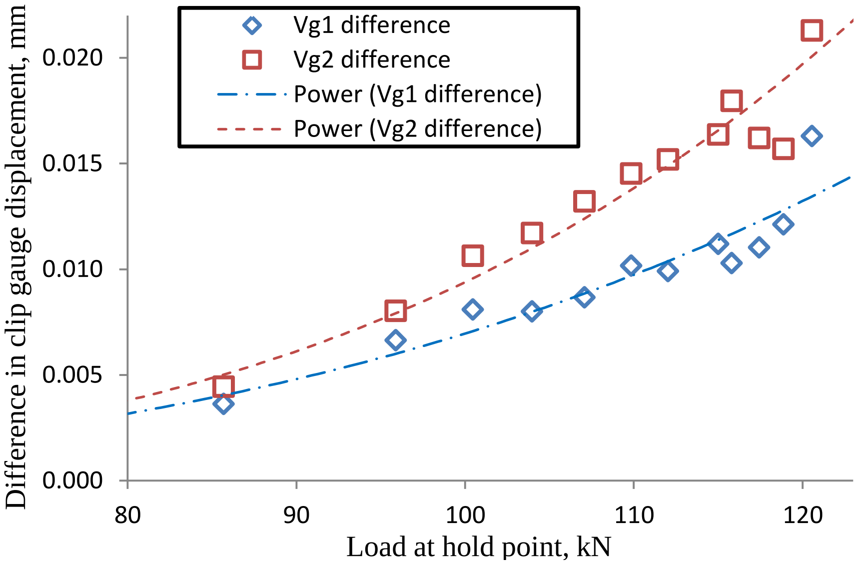

Figure 3.12 The difference in clip gauge opening vs. load at hold point

3.5 Discussion and conclusion

Based on the findings above, holding the specimen in constant clip gauge displacement is a better method to retain absolute crack shape while being held compared to holding the specimen in constant machine displacement. However, this method was not employed in this study due to the potential complications during the casting of the crack and extraction of the silicone replica with a clip gauge in-situ. It is predicted that if the specimen was held in constant clip gauge displacement, less load drop have occurred compared to when it was held in constant machine displacement.

To accommodate silicone crack casting, specimens can be held in constant machine displacement while the silicone compound cures in the crack to ensure constant crack condition. Holding the specimens in constant displacement, it was shown that the load drop percentage decrease with time in a logarithmic trend. It was also shown that load drop is relative to the plasticity level experienced in the specimen, where higher strength materials with lower strain hardening properties is less affected by the constant displacement hold.

The investigation verified that a lower loading rate would lead to an overall lower load-displacement feedback, potentially leading to lower processed fracture toughness results than under standard loading rates. The loading rate of the specimen is possibly one of the contributing factors of fracture toughness results in round robin tests.

When a dummy specimen (un-notched) was held in machine displacement, the test showed that clip gauge opening increases with the increasing initial holding load, indicating specimen deformation. However, the magnitude of the opening of the clip gauge while being held in constant machine displacement is small relative to the resultant fracture toughness result. Therefore, constant machine displacement is the best method to hold the specimens for the silicone crack casting tests.

3.6 Further work

The tests confirmed that the load drop experienced by the specimen is relative to the amount of plasticity in the specimen. However, the data obtained from the tests were not sufficient to draw an explicit relation between the load drop percentages to strain hardening or tensile ratio, and tests on a wider range of materials could develop this correlation. It could be useful to verify the condition of the crack length while holding the specimen in constant machine displacement, and use the Direct Current Potential Drop (DCPD) technique to monitor the crack to investigate the clip gauge opening while being held. The DCPD machine was unavailable during the time when the tests were performed, and thus not applied in this study.

The two dummy tests studied in this chapter were loaded below the typical rate used in a standard test, and yet differences in test results are noticeable. It would be interesting if fracture toughness tests are performed to the extremities of the loading rate described in the standards using different strain hardening steels. This would give a tolerance value to the scatter obtained in round robin tests due to different loading rate.

Chapter 4

Finite Element Modelling

4.1 Introduction

Finite Element (FE) modelling is a computational modelling method widely used to predict and analyse engineering problems. By modelling a real structure using FE, a solution can be obtained, predicting the reaction of the real structure based on the input properties and conditions defined in the model. FE modelling is able to show local effects, i.e. stress and strain distribution within a solid model, at locations where it could not be measured practically in a real structure. The method is well accepted in engineering, and further details may be found in texts (Zienkiewicz & Taylor 2000).

4.2 Model generation

In this study, commercial FE modelling software, ABAQUS 6.14-3 was used. ABAQUS is widely used in both universities and industry to solve engineering problems. This subchapter describe the procedure for the generation of the models used in this study.

4.2.1 Geometry

The B×2B SEN(B) specimen dimensions used in the experiments described in Chapter 2.1 were used as reference for modelling. Standard and Explicit settings were applied to the models. The specimens are symmetrical, and thus only quarter of the specimen was modelled. A 3-D deformable solid rectangular block, 92mm×40mm×10mm was generated to represent the quarter model. The block was partitioned as shown in Figure 4.01. This partitioning method allows the mesh density to be defined independently in different locations on the block. The partitions were extruded across the thickness in the z-direction.

The crack and the partitioning around the crack was generated separately using 3-D deformable shell setting. The dimensioning of the shell part is shown in Figure 4.02 and Figure 4.03. The shell part was extruded for 10mm.

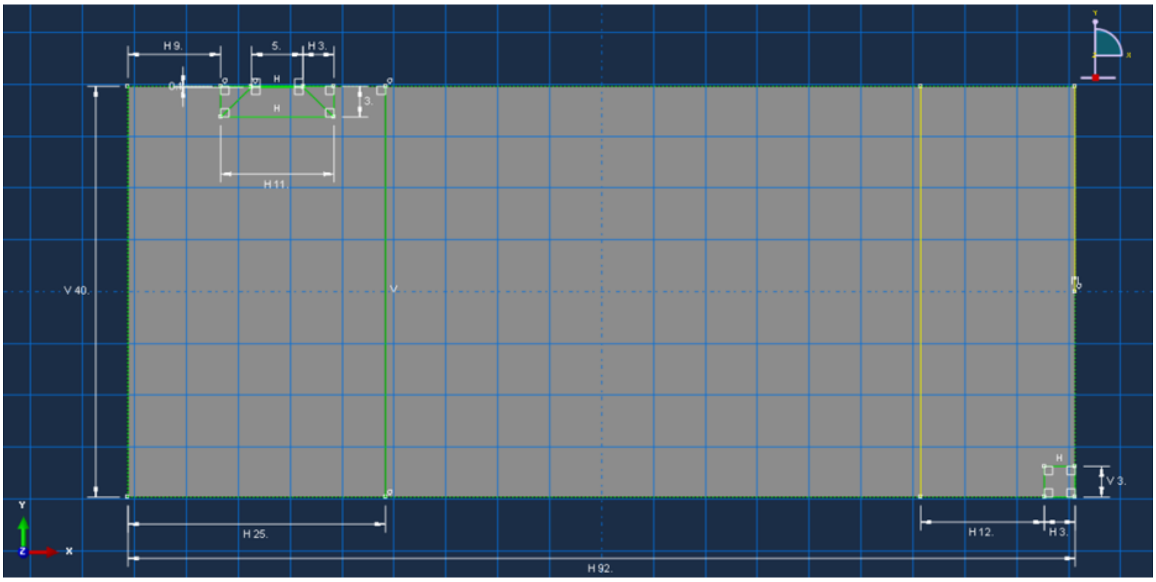

Figure 4.01 Partitioning on the quarter model

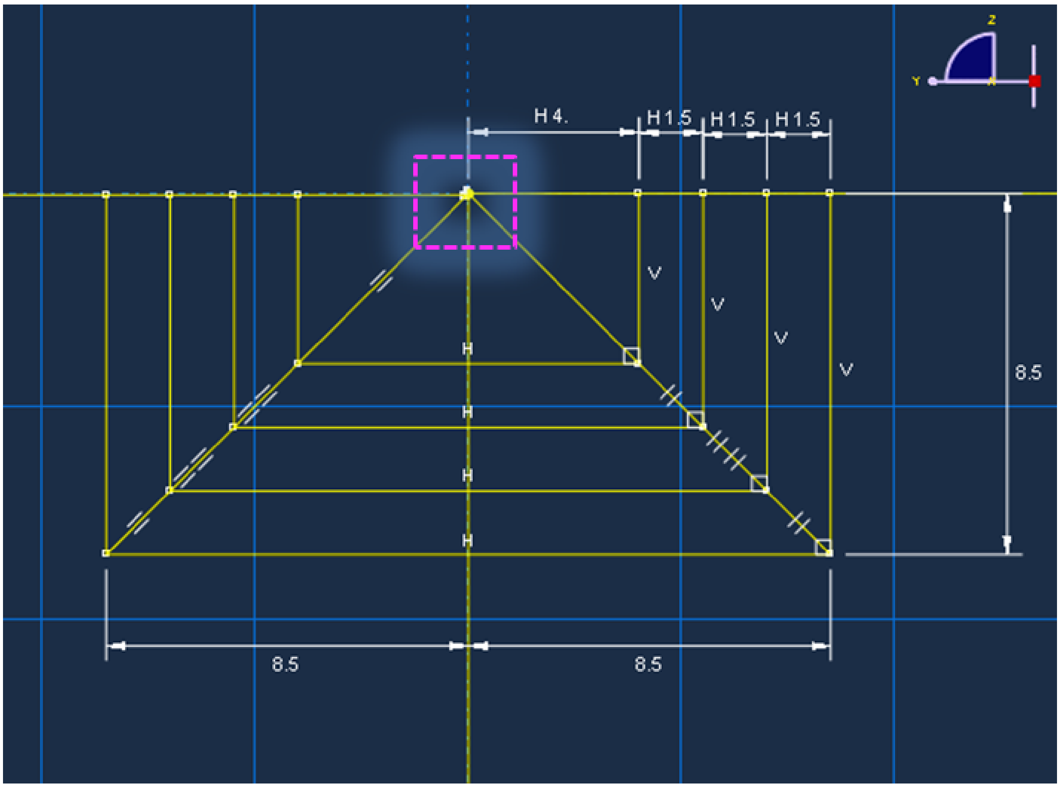

Figure 4.02 Sketch of crack shell (dotted box region shown in Figure 4.03)

The blunted crack tip (Figure 4.03) with a radius of 0.03mm was chosen to be applied to the models. Compared to a model with a perfectly sharp crack tip, this setting allows better deformation of the crack tip elements as the crack opens, and managed to closely represent the experimental specimen. Brick elements could be applied to a blunted crack tip, rather than triangular wedge elements on a sharp crack tip model. Although the blunted crack tip introduces a higher stress intensity factor compared to a sharp crack tip, the artificial increase of the overall fracture toughness is comparatively small at large deformation levels, and in this instance was considered to be acceptable, given the amount of specimen deformation in the experiments.

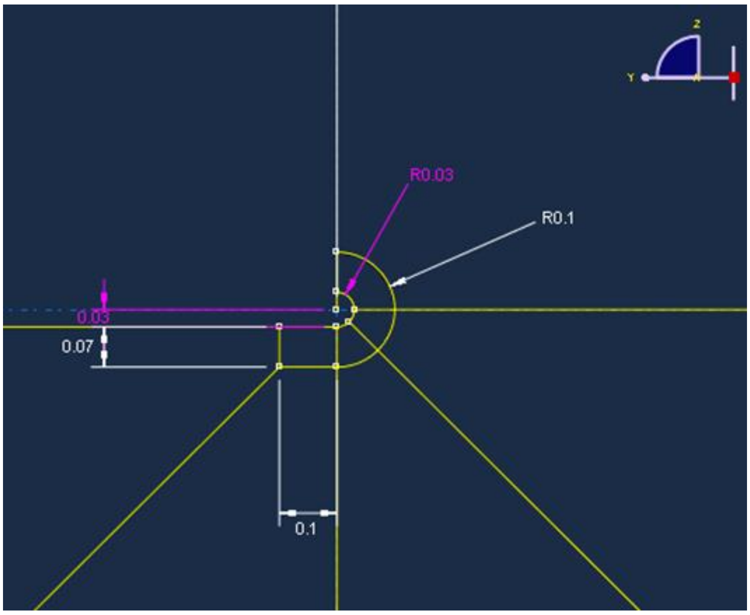

Figure 4.03 Expanded view of the crack tip region

Rollers were modelled for displacement application instead of theoretical line displacement. The rollers would ‘dent’ the loaded regions, and it was predicted that the stress distribution due to the loading technique on the loading point parallel to the crack line could affect the crack tip conditions at higher loading levels. Two analytically rigid ‘half circle’ shells of 20mm radius were generated to represent the rollers in the experimental tests. The sketches of the rollers were shown in Figure 4.04. The rollers were constrained to their respective reference points, RP.

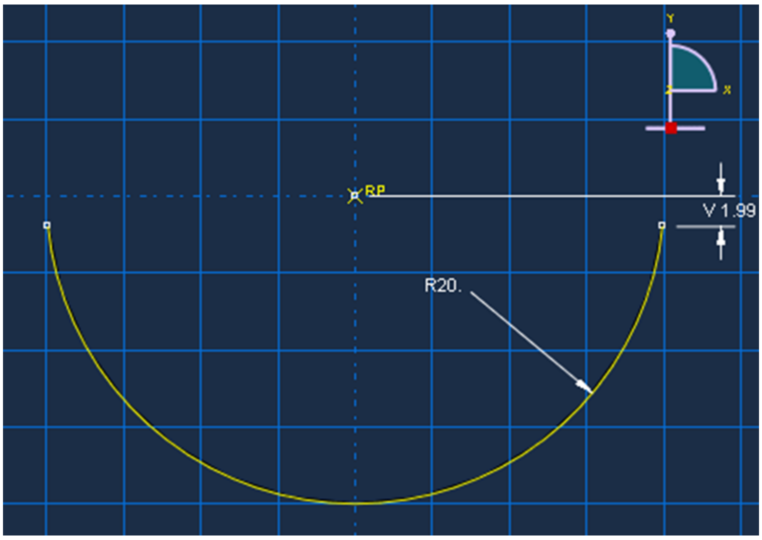

Figure 4.04 Sketch of the analytically rigid shell rollers

The crack shell and the block were merged in the assembly step, retaining the intersecting boundaries. The centre of the radius (Figure 4.03) was positioned at the point where the original crack length was defined. One of the rollers was positioned on the bottom right edge of the block; whereas the other roller was positioned at 12mm offset in the x-direction from the top left edge of the block. The final assembly of the rollers and quarter model is shown in Figure 4.05.

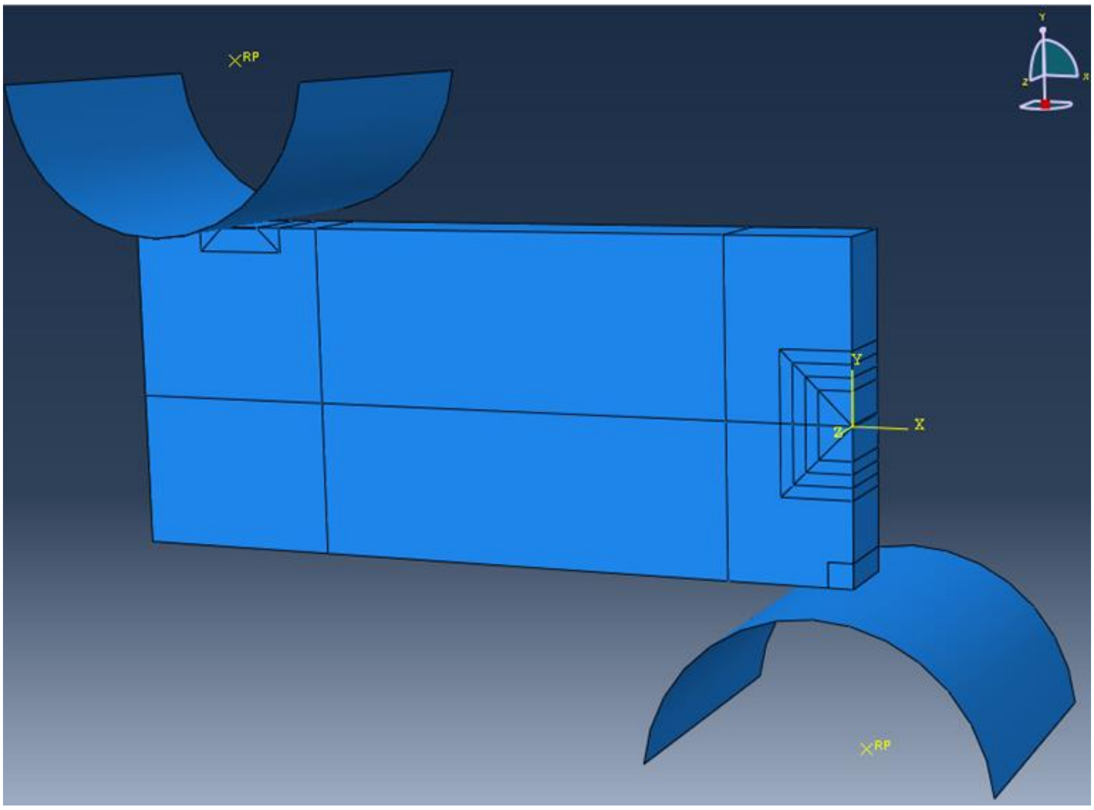

Figure 4.05 Partitioned quarter model with rollers

4.2.2 Defining material tensile properties

The FE model was intended to be a representation of the test specimens, and therefore tensile properties of the test specimens were used. To define the elastic properties, Young's Modulus of 207GPa was assumed for M01 and M02 (SA-543-GrB-Cl1 and 50D), whilst 200GPa was assumed for M03 (SS316) based on typical values for carbon steels and austenitic stainless steels. Engineering stress-strain data were obtained experimentally, and then converted to true stress-strain data using the Eq. 4.01 and Eq. 4.02.

$$\sigma_{true} = \sigma_{eng}\left(1 + \varepsilon_{eng}\right) \qquad \text{Eq. 4.01}$$

$$\varepsilon_{true} = \ln\left(1 + \varepsilon_{eng}\right) \qquad \text{Eq. 4.02}$$

The true stress-strain curve for M01, M02 and M03 is shown in Figure 2.05. For FE modelling, the true strain data were filtered for plastic true strain, and they were assigned to the models.

Additionally, a range of idealised tensile properties were generated based on the modified Ramberg-Osgood power law for 0.44≤ σ_{ys}/σ_{uts}≤ 0.98 to represent tensile properties not covered by the experimental materials (Ramberg & Osgood 1943; MacDonald et al. 2000). The equation is given as

$$\varepsilon = \frac{\sigma}{E} + \alpha\left(\frac{\sigma}{\sigma_{ys}}\right)^{n-1} \qquad \text{Eq. 4.03}$$

Where α= 0.002, E= 207GPa and σ_{ys}= 400MPa.The idealised true stress-strain data obtained using Eq.4.03 were shown in Figure 4.06.

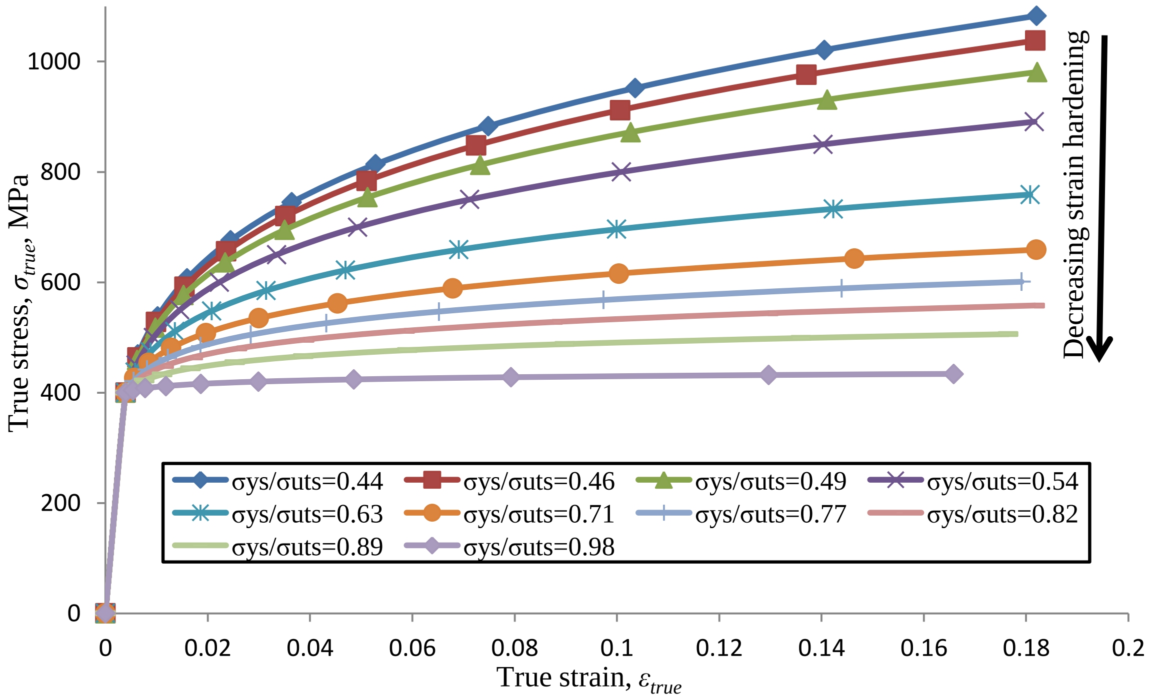

Figure 4.06 True stress-strain data calculated using Eq. 4.03

4.2.3 Meshing

A mesh defines the points where calculations are made. The 20-noded isoparametric brick element with reduced integration, C3D20R was used to mesh the model. Global element size of 2mm was specified for the model. Meshing was refined in the contact regions between the block and rollers (Figure 4.07). Higher mesh density was applied around the crack tip and contact regions to encourage higher calculation definition (Figure 4.08).

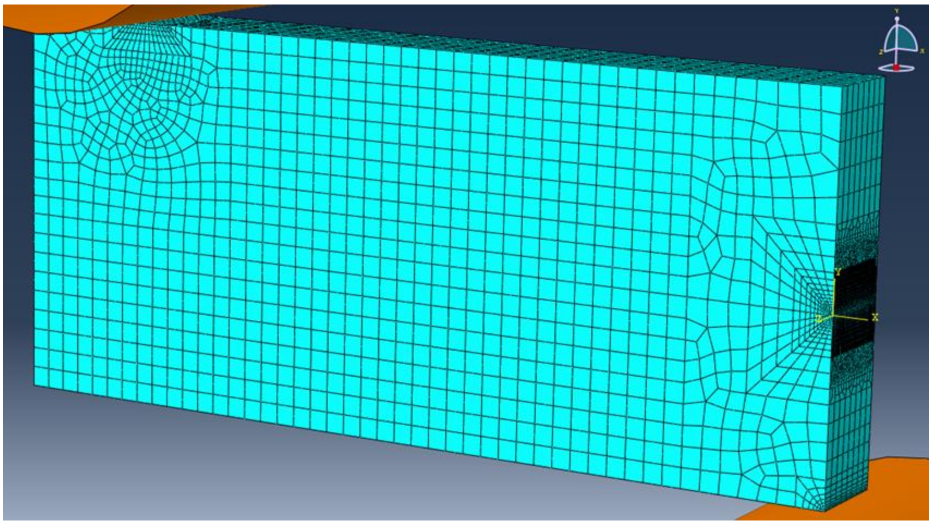

Figure 4.07 Mesh applied on the quarter model

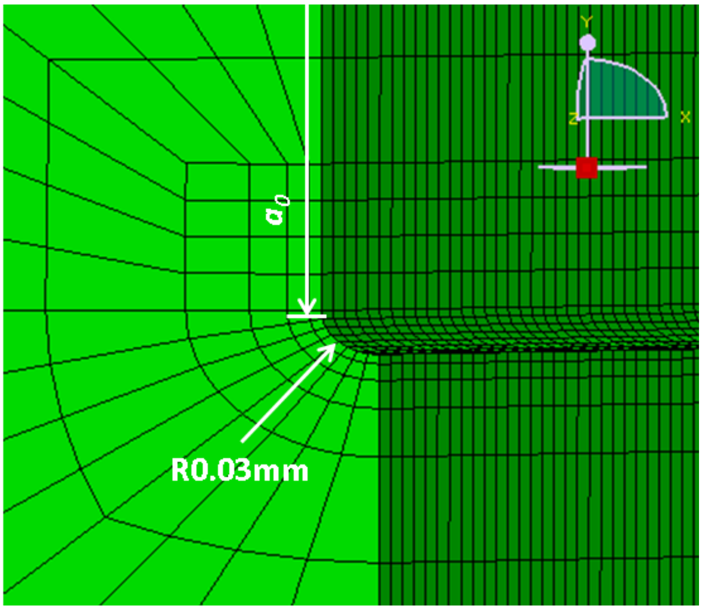

Figure 4.08 Close up of the meshed blunted crack tip

4.2.4 Interactions

'Contact' was selected for Interaction Properties, with 'Frictionless' Tangential Behaviour and 'Hard Contact' normal behaviour. On the 'Initial' step, contact properties were specified for the interaction between the rollers and the quarter model. Frictionless was set for tangential properties and "hard" contact for pressure-overclosure. The contact face on the roller was specified as the master surface, while the contact surface on the quarter model was specified as the slave surface. In the experimental tests, the rollers were able to move and rotate, and these settings were intended to replicate this.

A crack was assigned to the model for J calculation and to define the crack plane. The curved section near the crack tip in Figure 4.09 was set as the crack front (red highlighted surface), while the edge was set as the crack tip (pink line). This allows ABAQUS to calculate *J* based on the contours expanding from the first crack front, where the first contour would be on the first crack front itself. The direction of crack extension was defined as 0, -1, 0. The midside node was set at 0.5 with no degeneracy at the crack tip. Typically, degeneracy is applied on the crack tip elements when wedge elements are used around the crack tip region, where the midside node is moved closer to the edge node in the element.

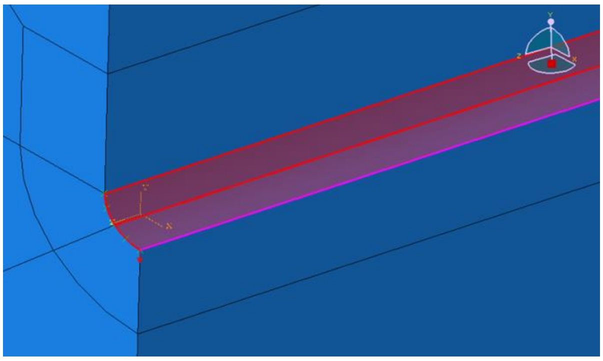

Figure 4.09 Crack face, tip and extension direction at crack tip

4.2.5 Boundary conditions

On the 'Initial' step, the bottom roller RP was set to 'ENCASTRE', while the top roller RP was constrained in all directions. The x-y plane on the block was set to z-symmetry, while the y-z plane on the block ahead of the crack was set to x-symmetry (refer Figure 4.10). The x and z symmetry would mirror the block on their respective planes, representing a full SEN(B) block. To model a three-point bend setup, displacement in the –y direction was applied to RP of the top roller in the 'Displacement' step.

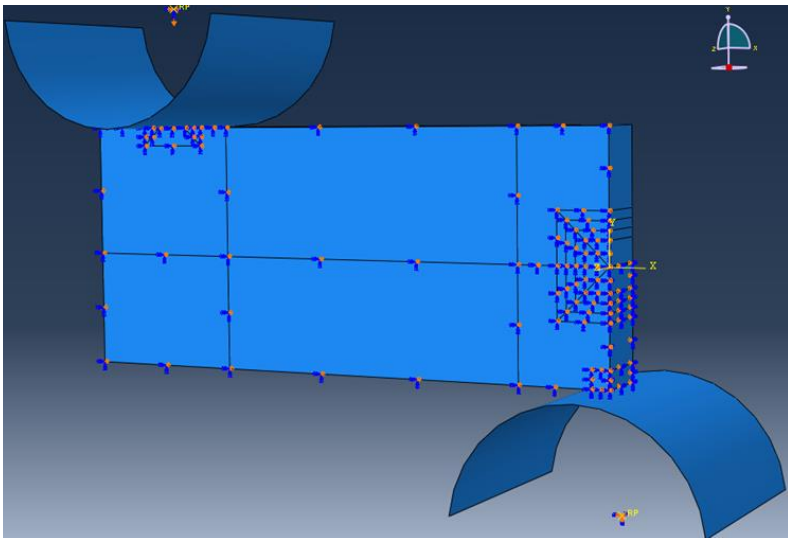

Figure 4.10 Boundary conditions applied to the quarter model

4.2.6 Job submission

A job was created for the model generated. It was then submitted to allow ABAQUS to solve the model. The computer that was used to process the models was running on Windows 7, Intel Xeon E5620 with a total of 16 CPUs, clocked at 2.40GHz and a total of 48GB RAM.

4.3 Element and mesh selection

Generally, two types of element were used to model cracked structures in 3-D: - 8-noded shell elements and 20-noded brick elements. Both types of elements have been successfully applied in FE modelling (Kawabata et al. 2016; Verstraete et al. 2014; Sarzosa et al. 2016; Kirk & Wang 1995; Kim et al. 2003; Huang & Zhou 2017; Souza & Ruggieri 2014; Pook 2003).

Specimen M03-05 was used for the mesh sensitivity validation test, as the M03 material deforms mainly in a plastic manner, similar to that exhibited in the FE model (further described in Chapter 6.3). Based on Model 00 (Figure 4.13(a)), both 8-noded shell element, C3D8R and 20-noded brick element, C3D20R were applied and the load-CMOD data were compared to that obtained experimentally (Figure 4.11).

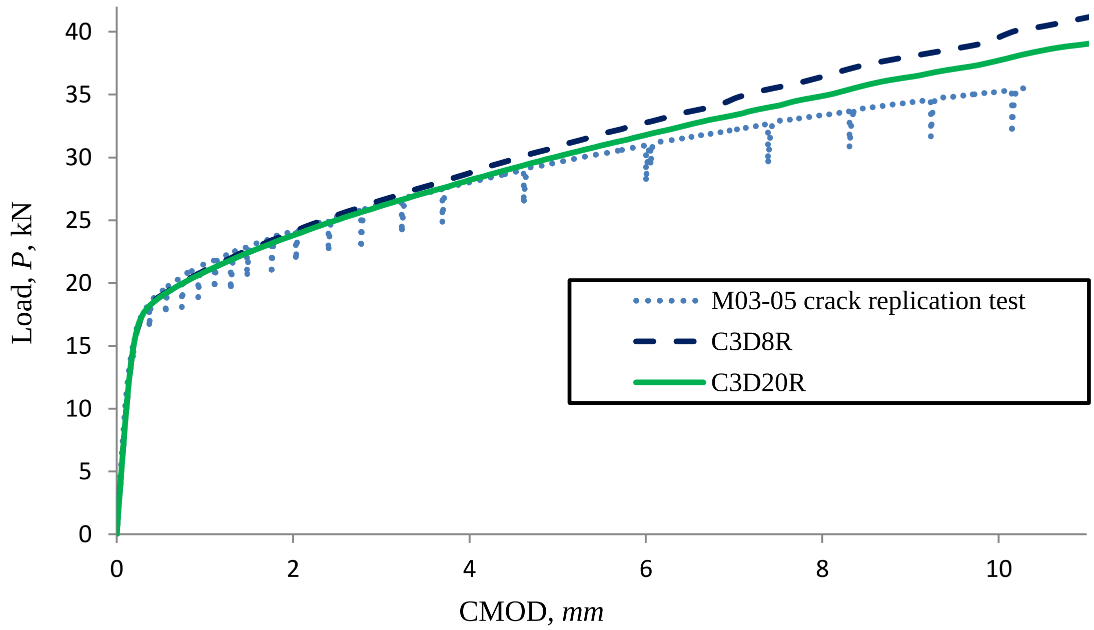

Figure 4.11 Load-CMOD data obtained from both C3D8R and C3D20R elements compared to experimental data

Table 4.01 shows that the 20-noded element model spent almost 7 times the time required to complete the 8-noded element model. The models based on both elements gave similar overall estimation, however C3D20R managed to predict the experimental results more accurately for a wider range of CMOD. If time and computational power is not a constraint, the C3D20R elements would provide prediction with better representation of the actual experiments. C3D20R elements were applied on the models used in this research.

Table 4.01 Total number of element, nodes and time spent in running the C3D8R and C3D20R models

Model	Elements	Nodes	Time, hour
C3D8R (8-noded)	104738	114333	24.5
C3D20R (20-noded)	104738	444794	169.6

For B×2B SEN(B) specimen setups complying with the relevant standards (BS 7448, ISO 12135 and ASTM E1820), the centre region across the crack tip would encounter the highest stress triaxiality, whereas the sides of the crack tip would be mostly plane stress, where stresses act in a 2-D plane. Using Model 00, the elastic strain in the z direction, *ee*33 and directional stresses, *s*11, *s*22 and *s*33 were extracted near the crack tip in the z-direction from Model 00 (Figure 4.13(a)). *ee*33 and the measure of stress triaxiality, *s*33/(*s*11+*s*22) were normalised to that extracted from the middle of the crack, where $z = 0$ (Figure 4.12). Figure 4.12 shows clearly that the middle of the crack ($z = 0$) is plane strain dominated, whereas the sides of the crack ($z = 10$) is plane stress.

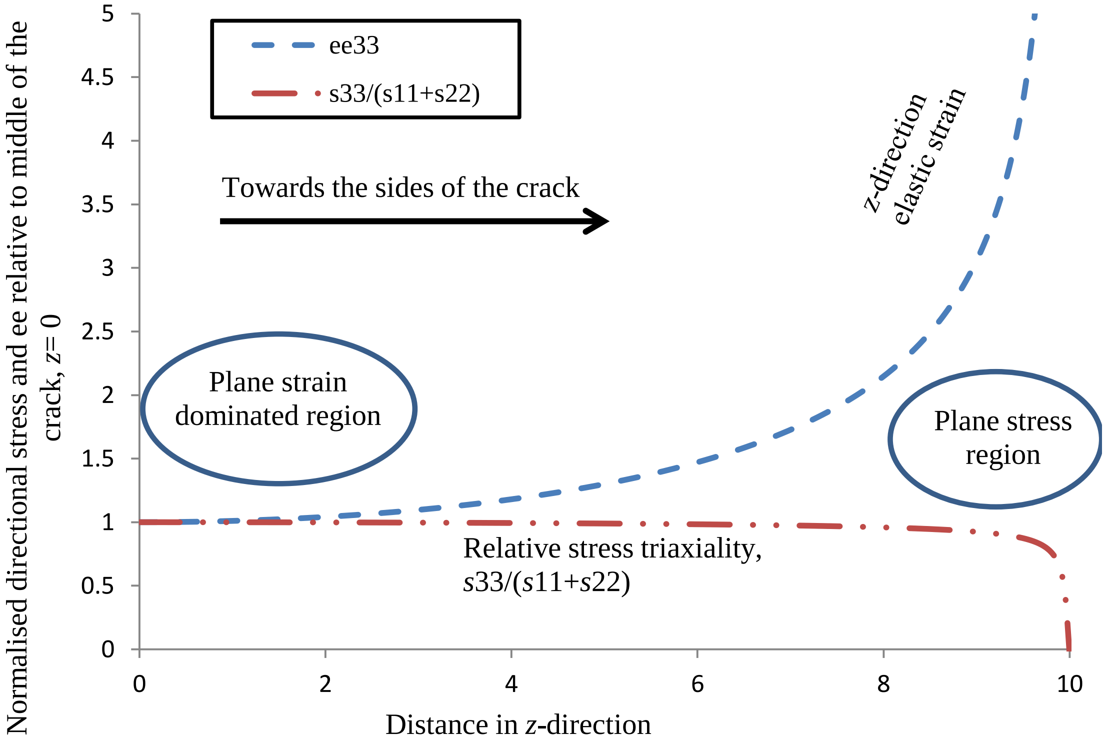

Figure 4.12 Normalised strain and stresses near the crack tip in the z-direction

The middle of the crack (position $z = 0$) is most plane strain and the main position of interest in this work, as the elastic CTOD and *J* equations assumes plane strain condition. Figure 4.12 showed that the magnitude of *ee*33 across the crack tip varies significantly, which might possibly affect the results obtained at the middle of the crack. To check the mesh dependency across the crack tip to the middle of the crack tip, various mesh density across the crack tip were used. The numbers of elements ranging from 16 elements to 256 elements were distributed across the crack tip in the models. The designated models with the corresponding crack tip mesh density are shown in Figure 4.13. The total amount of element and nodes in the models are listed in Table 4.02.

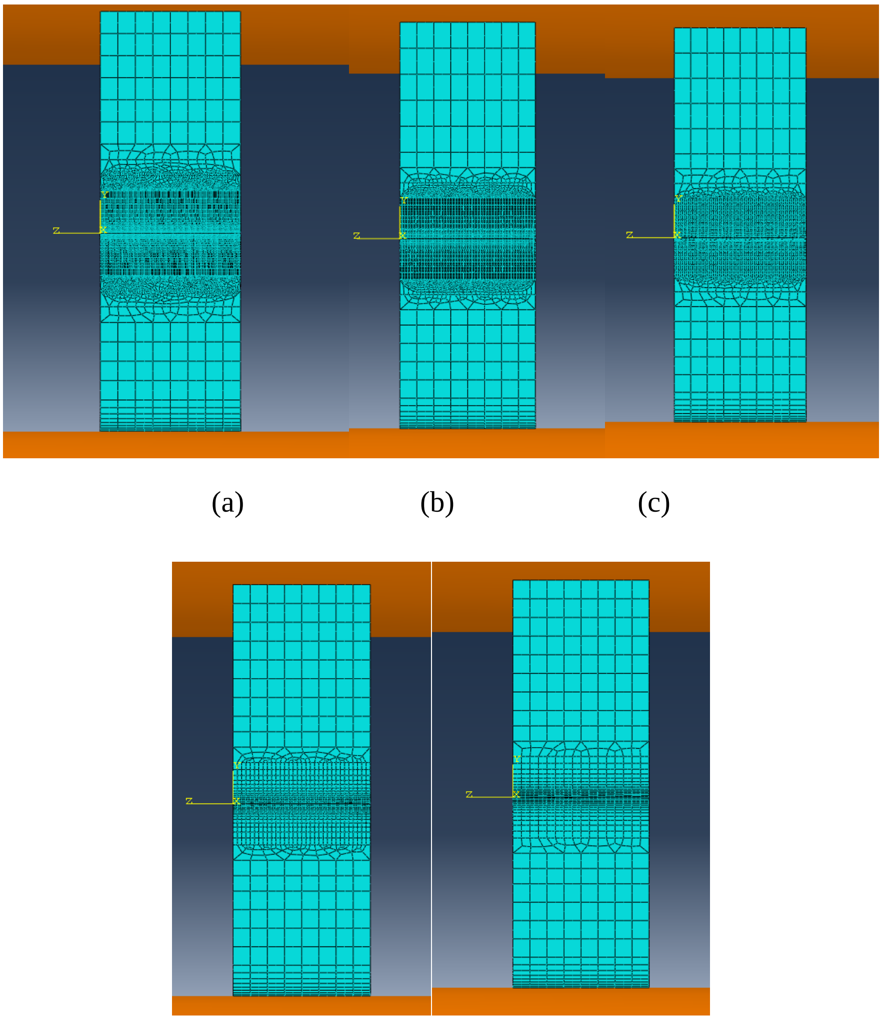

(a) (b) (c)

(d) (e)

Figure 4.13 Mesh density of Model 00 (a), 01 (b), 02 (c), 03 (d) and 04 (e) with 256, 128, 64, 32 and 16 elements distributed across the crack tip respectively

Load-CMOD data were extracted from all five models (Figure 4.14). The models gave similar predictions, despite the different mesh densities. The load and CMOD data are the main variables used in the calculation in fracture toughness, and based on the data shown in Figure 4.14, the change in mesh density in the thickness direction would give negligible difference in fracture toughness calculated between the models.

Table 4.02 Total number of element, nodes and time spent in running Models 00 to 04

Model	Elements	Nodes	Time, hour
00	100602	429585	1034.4
01	54402	234664	-
02	30498	133542	-
03	19402	86602	119.1
04	14522	65911	66.8

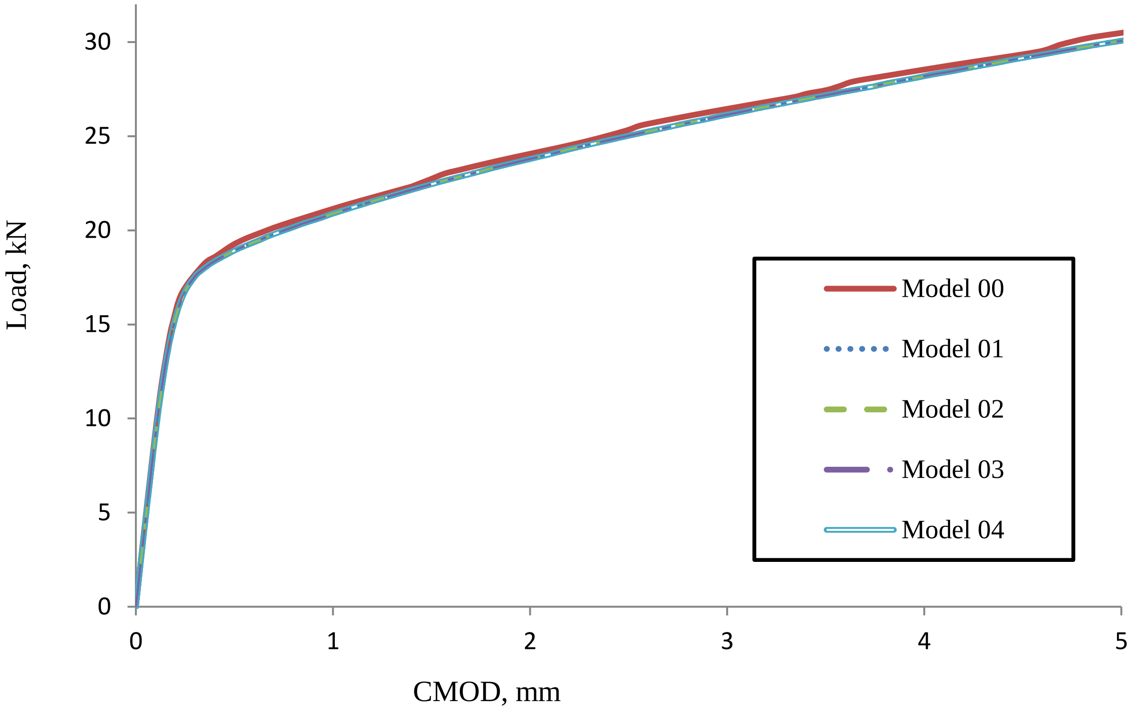

Figure 4.14 Load-CMOD data extracted from the models with different crack tip mesh density

The effect of the variation of mesh size across the crack tip was further checked in relation to fracture toughness. CTOD is the main parameter investigated in this study, but there are several different definitions used to describe CTOD. This might lead to biased or inconsistent comparison due to the different definition and data post processing technique. For elastic-plastic analysis, CTOD is directly proportional to *J* (Chapter 1.4.3), and therefore *J* was extracted from the models for comparison.

J is quantified as the strain energy density around the crack, calculated in ABAQUS based on the contours around the crack tip (Figure 4.15). The design of the model allows 18 valid contours around the crack tip for *J* calculation.

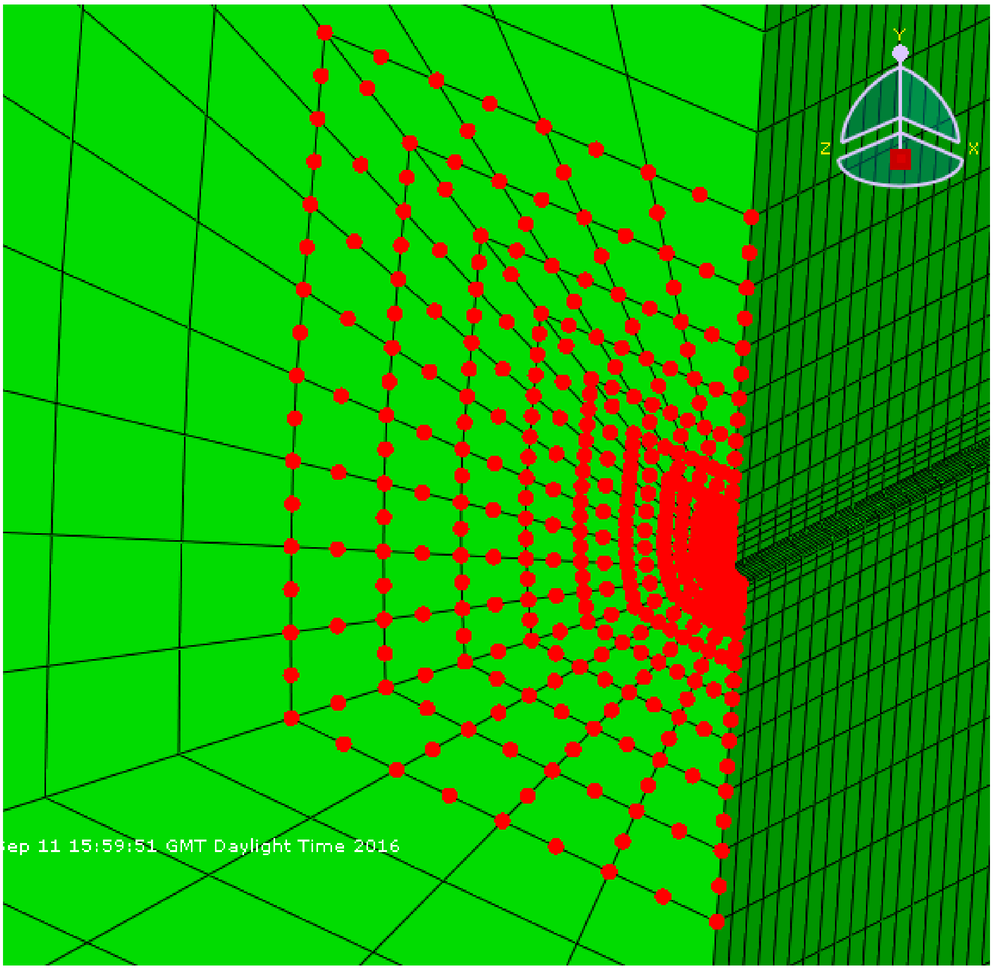

Figure 4.15 Contour 12 in the middle of Model 00 used for *J* calculation

The maximum amount of strain energy density calculated to *J* is limited by the area covered in the contour. The contours closer to the crack tip have lower *J* values compared to contours further away from the crack tip. With increasing deformation at the crack tip region, the difference between *J* calculated to the contour close to the crack tip and the contour further from the crack tip would increase. The contours from the middle of the model with *J* values within 10% difference relative to *J* from contour 18 are considered valid (Figure 4.16), and averaged. In fracture mechanics, *J* is path-independent, therefore only contours which are sufficiently similar could give the appropriate representative value of *J*.

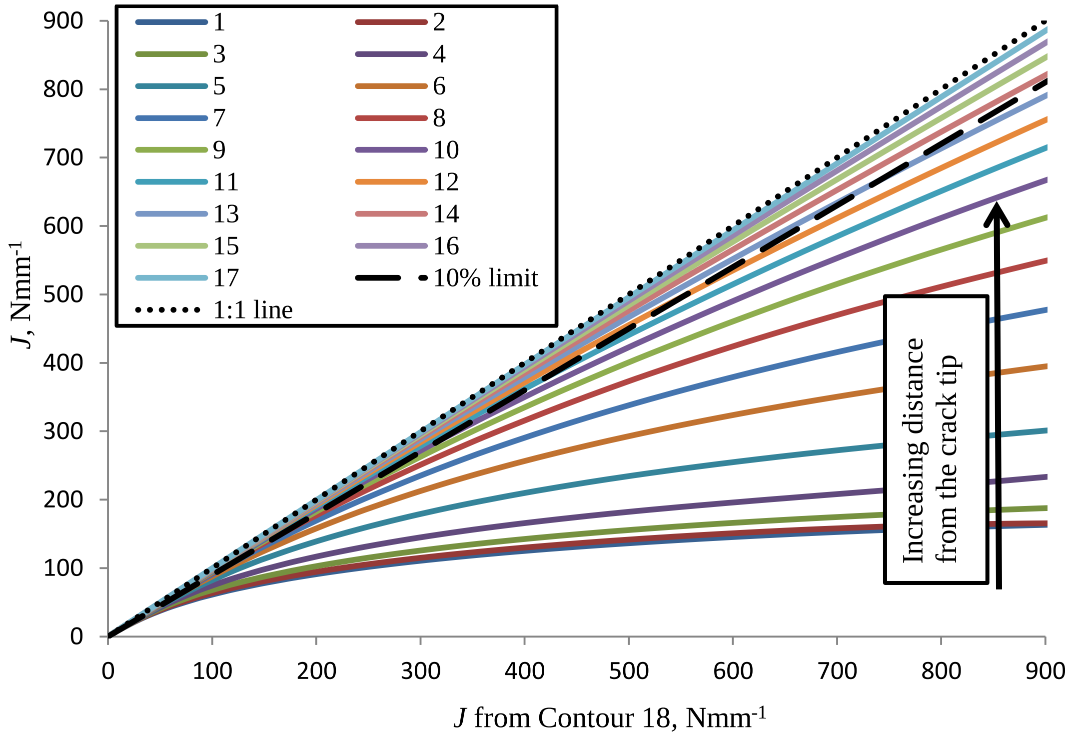

Figure 4.16 J extracted from different contours in Model 04

The average J values from the five different mesh models were plotted with increasing CMOD (Figure 4.17). The models showed comparable and consistent results. The difference due to the variation of mesh density across the crack tip was negligible.

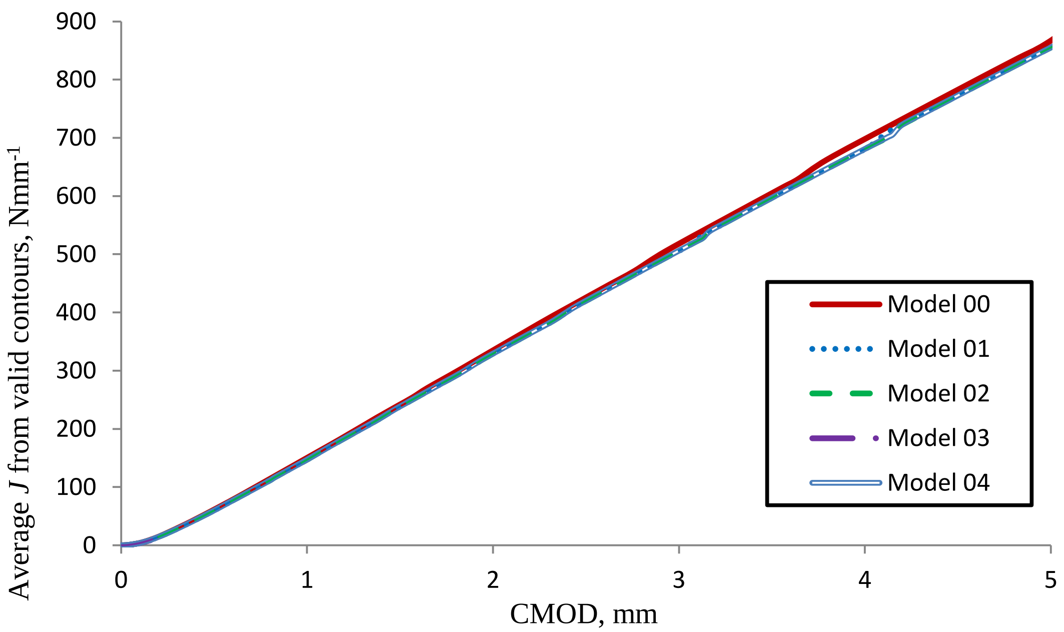

Figure 4.17 Average J extracted from the models with different crack tip mesh density

Based on the models, it is shown that 20-noded brick elements gave the best estimation and the mesh density across the crack tip does not affect *J* in the middle of the model. However, 8-noded brick elements gave comparable accuracy in the estimation (shown in Figure 4.11) and would be useful when time and computational power is limited.

4.4 CTOD post processing

CTOD is generally defined as the opening of the crack tip in the direction normal to the initial crack face. Various definitions have been proposed to describe CTOD within a numerical model. Two of the most established and popular definitions are the opening of the original crack tip, and the opening of the 45 degree intercept of the crack face, measured from the blunted crack tip, shown in Chapter 1.4.1. CTOD based on the opening of the original crack tip is analogous to the traditional definition of CTOD; whereas the 45 degree CTOD is generally applied on Finite Element models for CTOD measurements. In this study, CTOD was defined and measured based on the opening of the original crack tip. But to ensure the best approach was used, the 45 degree CTOD was also extracted from the models with idealised tensile properties from Chapter 4.2.2 for comparison.

4.4.1 CTOD based on the original crack tip

A simple method could be used to obtain an approximate evaluation of the CTOD based on the deformation of the original crack tip. The displacement in the x-direction of the node at the end of the original crack tip (Figure 4.18(a)) can be processed for CTOD. This method is dependent on the mesh density around the crack tip region. A finer mesh at the crack tip can increase the resolution of the crack tip nodes. However, a constant distance cannot be maintained between the node which was at the end of the original crack tip and the node at the crack mouth as the crack opens (Figure 4.18(b)). This leads to increased inaccuracy as the deformation at the crack tip increases.

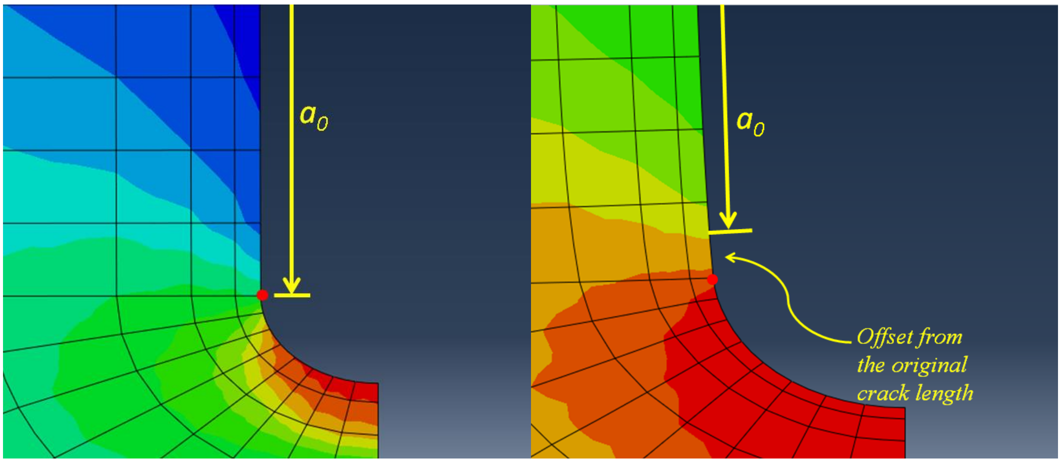

(a) **(b)**

Figure 4.18 Inconsistency of the determination of CTOD based on the same node

To refine the method to determine CTOD based on the opening of the original crack tip, an interpolation method was applied to obtain the relative opening of the original crack tip. The interpolation concept diagram was described in Figure 4.19.

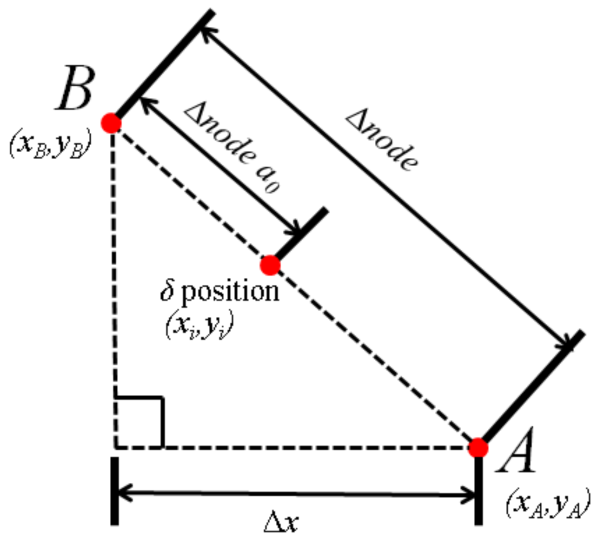

Figure 4.19 Diagram of the interpolation concept

This technique requires the position of the original crack tip to fall between node A and B. The relative ratio of the CTOD position from node B was first calculated using the following relation

$$R_{CTOD} = \frac{\Delta node\ a_0}{\Delta node} \quad \text{Eq. 4.04}$$

After the relative CTOD position is determined, R_{CTOD} used to determine the relative CTOD position based on node *B*. The equations following equations were used

$$R_{CTOD}\Delta x + x_B = x_i \quad \text{Eq. 4.05}$$

$$CTOD, \delta = (x_i + 0.03) \times -2 \quad \text{Eq. 4.06}$$

CTOD is calculated by doubling the value obtained in the symmetrical quarter model after allowing for the initial notch radius of 0.03mm. This technique allows the determination of CTOD independent of the mesh density influence at the crack tip region.

4.4.2 CTOD based on the 45 degree intercept method

This CTOD definition is measured at the 45 degree intercept of the crack faces from the blunted crack tip (refer Chapter 1.4.1). Ruggieri (2012), Huang & Zhou (2014) and Wang et al. (2014) determined the intersection points of the 45 degree at the blunted crack tip based on a linear regression line of the crack flanks. This method ignores the distorted elements at the crack tip, and an approximation can be obtained regardless of the condition of the crack tip. However the validity of this method for large deformation at the crack tip is less certain, as the 45 degree intercept method for CTOD was designed based on 2-D FE analysis, for small scale yielding crack tip conditions (Shih 1981).

In the FE model, no damage mechanism was specified, therefore the crack tip blunts continually as the crack opens without the occurrence of crack tip tearing. The 45 degree CTOD was determined based on the interception point of the 45 degree line from the blunted crack tip. The interpolation method was used, similar to that described in Figure 4.19. Instead of determining node A and B based on the original crack length from the CMOD position, it is determined based on the 45 degree intercept position on the crack face.

4.5 Comparison of the CTOD based on the opening of the original crack tip and the 45 degree intercept method

Both definitions of CTOD, the opening of the original crack tip and the opening based on the 45 degree intercept from the original crack tip were extracted from the FE models with idealised tensile properties. The FE models used in this investigation is based on $B\times2B$, thickness, B= 20mm, crack-specimen width ratio, a_0/W= 0.5, crack tip meshing based on Model 04 using C3D8R 8-noded shell elements.

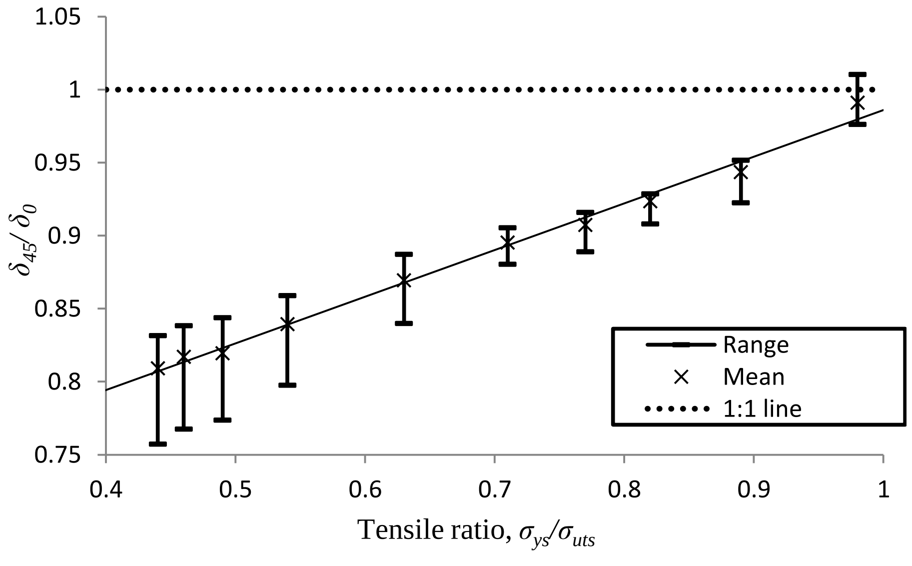

Figure 4.20 Comparison between the 45degree CTOD and the original tip CTOD for different tensile ratio in the range of 0.02mm< δ_0< 0.3mm

For the ease of identification, the opening of the original crack tip is described as δ_0 and the 45 degree CTOD as δ_{45} in Figure 4.20. As the crack opens in the FE model, the surface of the blunted crack tip and the crack face no longer connect smoothly after a certain deformation limit, which is dependent on strain hardening. Beyond this deformation limit, the 45 degree CTOD concept collapses and is no longer representative of CTOD. Comparatively, the deformation limit for the 45 degree CTOD increases with strain hardening. For a consistent comparison for all strain hardening models, both definitions of CTOD were extracted from the range of 0.02mm< δ_0< 0.3mm (which is below the deformation limit for the idealised models) and normalised, δ_{45}/δ_0. CTOD values below 0.02mm were not compared, as the differences in this CTOD range is dependent on the modelling technique and parameters used. The comparisons between the two CTOD definitions were shown in Figure 4.20.

Figure 4.20 shows that the difference between the 45 degree CTOD and the original tip CTOD is relatively constant for the same tensile ratio. Overall, the 45 degree CTOD underestimates the original tip CTOD, and the underestimation increases with the increase of strain hardening. The 45 degree CTOD was derived based on the HRR solution, and requires a blunted crack tip to determine the point of the 45 degree intercept (Shih 1981). Chapter 7.5.1 shows that crack extension is observed in the SRC, and raises difficulty for the measurement of the 45 degree CTOD. Therefore due to the obvious advantage and for consistency purposes, CTOD was defined based on the original crack tip in both the FE and experiments in the remaining of this research.

4.6 Further work

The set of models generated for this study were validated experimentally, and matched the measured CTOD with reasonable accuracy. However, the models were designed with a blunted crack tip, straight crack front and no damage mechanism specified. These settings were meant to predict CTOD more accurately at larger deformation levels, assuming plastic deformation at the crack tip. Nonetheless, these generalised setting could possibly have contributed to errors in the prediction of CTOD, as the crack tends to propagate in lower strain hardening material rather than causing major plastic deformation.

For a model with better representation of the actual experiments, several additional settings could be applied: -

- Curved crack front, to represent the ‘thumbnail’ shaped crack front obtained through fatigue cracking in the experimental specimens
- Damage mechanism, i.e. Gurson-Tvergaard-Needleman (GTN) yield criterion (Tvergaard 1981; Gurson 1977), to demonstrate crack propagation at the crack tip
- Reduced crack tip radius curvature, or straight sharp crack tip (if damage mechanisms are employed) to reduce the artificial increase of fracture toughness due to crack tip condition

Chapter 5

Comparison of CTOD formulae from national and international standards in relation to strain hardening

5.1 Fracture toughness testing Standards: - BS 7448-1, ISO 12135, ASTM E1820 and WES 1108

The British Standards Institution (BSI), International Organization for Standardization (ISO) and ASTM International (ASTM) defined methods for the determination of crack tip opening displacement (CTOD), δ in a fracture toughness test. Different assumptions are used in different standards, which lead to different values calculated.

All the current standards agree that CTOD (or δ) should be determined by the addition of two components; the elastic CTOD, δ_{el} and the plastic CTOD, δ_{pl}. (Wu 1981)

$$\delta = \delta_{el} + \delta_{pl} \qquad \text{Eq. 5.01}$$

BS 7448-1 and ISO 12135 use the same equation for the determination of CTOD. The elastic component is determined from the stress intensity factor, K, while the plastic component assumes a fixed plastic hinge in the ligament of the specimen ahead of the notch, and is calculated using the similar triangles method. The equation is given as (BSI 1991; ISO 2016)

$$\delta = K^2 \frac{(1-v^2)}{2\sigma_{ys}E} + \frac{0.4B_0V_p}{0.4W+0.6a_0+z} \qquad \text{Eq. 5.02}$$

Based on Lin et al. (1982) and Ingham et al. (1971) findings, the rotational factor was assumed to be 0.4. The BSI/ISO formula does not make any allowance for the strain hardening of the steel, and despite having been well validated for medium and high strength steels, the formula is less accurate for other steels with a lower yield to tensile ratio (Wei & Pisarski 2007; Khor et al. 2016).

ASTM E1820 uses a different approach for the determination of CTOD, where J is first calculated (by the summation of the elastic and plastic component) and then converted to CTOD using an 'm' factor, which includes the material yield and tensile properties in its calculation (ASTM 2014).

$$\delta = \frac{J}{m\sigma_y} \qquad \text{Eq. 5.03a}$$

Where $m= A_0- A_1(\sigma_{ys}/\sigma_{uts})+ A_2(\sigma_{ys}/\sigma_{uts})^2- A_3(\sigma_{ys}/\sigma_{uts})^3$

$A_0= 3.18- 0.22(a_0/W)$

$A_1= 4.32- 2.23(a_0/W)$

$A_2 = 4.44 - 2.29(a_0/W)$
$A_3 = 2.05 - 1.06(a_0/W)$

$$J = \frac{K^2(1-v^2)}{E} + \frac{\eta_{pl} A_p}{B_N B_o} \qquad \text{Eq. 5.03b}$$

Where $\eta_{pl} = 3.667 - 2.199(a_0/W) + 0.437(a_0/W)^2$

However, the ASTM method to determine CTOD is known to under-estimate CTOD significantly for many higher strength steels in comparison to the BSI/ISO method (Tagawa et al. 2010; Tagawa et al. 2014; Pisarski et al. 2010; Kayamori et al. 2008). In response to the need for an accurate method to determine CTOD, which also accounts for the materials strain hardening behaviour, the Japanese Welding Engineering Society, JWES developed a CTOD equation, based on the BSI/ISO approach but with a modified rotational factor and improved strain hardening factors calibrated using FEA and experiments (Kawabata et al. 2016). This equation is now being adopted by the Japanese national fracture toughness testing standard, WES1108 'Standard test method for crack-tip opening displacement (CTOD) fracture toughness measurement' (JWES 2014).

$$\delta = K^2 \frac{(1-v^2)}{m_{JWES}\sigma_{ys}E} + f_p \frac{0.43B_o V_p}{0.43B_o + a_0} \qquad \text{Eq. 5.04}$$

Where $m_{JWES} = 4.9 - 3.5(\sigma_{ys}/\sigma_{uts})$
$f_p = f(B) \times f(\sigma_{ys}/\sigma_{uts})$
$f(B) = 0.8 + 0.2 \exp\{-0.019\,(B - 25)\}$
$f(\sigma_{ys}/\sigma_{uts}) = -1.4(\sigma_{ys}/\sigma_{uts})^2 + 2.8(\sigma_{ys}/\sigma_{uts}) - 0.35$

This new equation has been developed for the avoidance of brittle fracture in steels for CTOD values up to 0.2mm. For the equation to be incorporated more widely into international standards, the equation has to be evaluated for more general applications over a larger range of CTOD. Hereafter, the BS 7448-1/ ISO 12135, ASTM E1820 and WES 1108 are described as BS/ISO, ASTM and JWES.

5.2 Evaluation of CTOD based on archived data

A total of 137 SEN(B) fracture toughness historical test data from steels has been compiled and evaluated for CTOD using BS/ISO, ASTM and the JWES methods. For the consistency of the comparison, only specimens with nominal crack ratio of $a_0/W= 0.5$ were evaluated. The data were based on tests within temperature range of -100°C to +290°C and specimen thickness in the range of 4.7mm to 58.6mm from TWI archives. Tensile property correction due to temperature was applied on the data (BSI 2014a). CTOD was calculated based on BS/ISO and plotted against tensile ratio (Figure 5.01). CTOD calculated using the standardised equations and testing conditions were shown in Table .

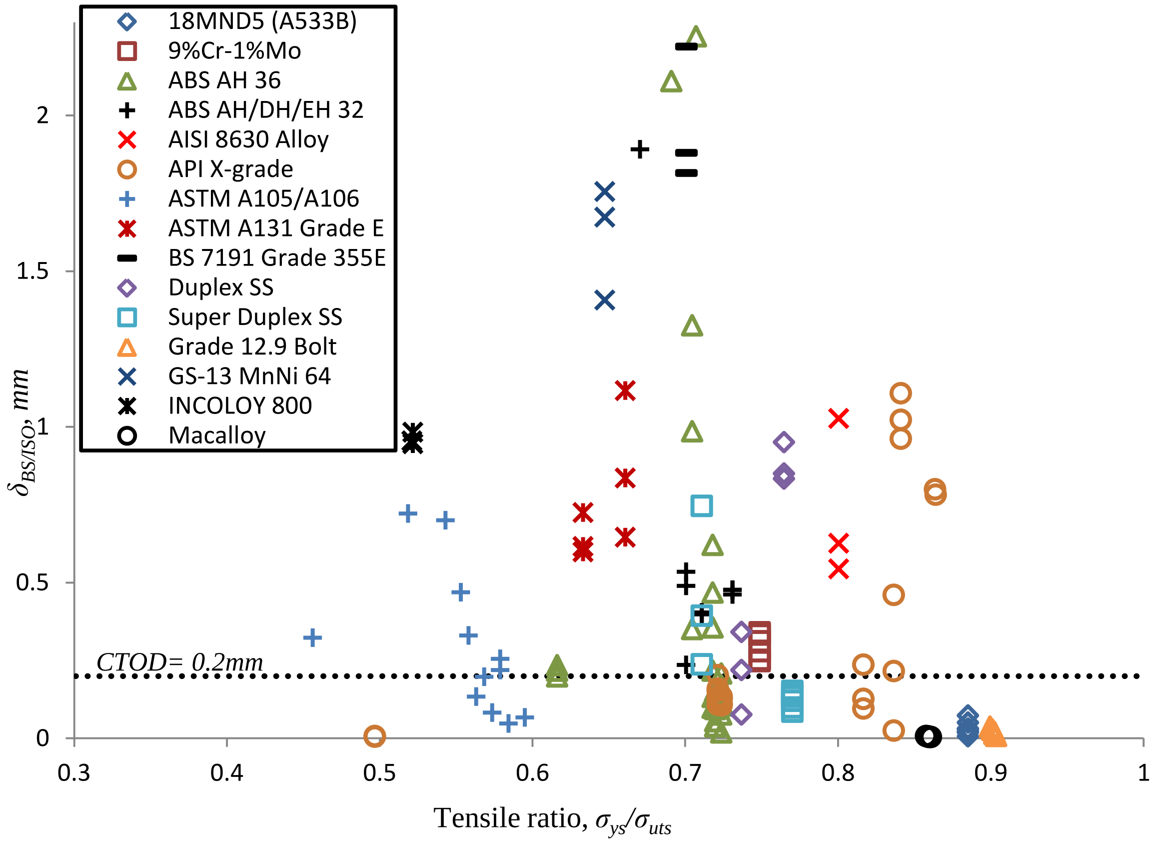

Figure 5.01 Compilation of CTOD calculated to BS/ISO

Table 5.01 Compilation of TWI CTOD data calculated to BS/ISO, JWES and ASTM

Material	Specimen thickness, mm	Test temperature, °c	Yield/ 0.2% proof strength, MPa	Tensile ratio	BS 7448-1/ ISO 12135 CTOD, mm	WES 1108 CTOD, mm	ASTM E1820 CTOD, mm
18MND5 (A533B)	24.9-25.1	-100	651	0.89	0.01 to 0.07	0.01 to 0.08	0.01 to 0.06
9%Cr-1%Mo	4.7	7	520	0.75	0.25 to 0.34	0.36 to 0.50	0.14 to 0.20
ABS AH 36	20.0-58.6	-70 to -10	341to 443	0.62 to 0.72	0.02 to 2.25	0.02 to 2.04	0.01 to 1.62
ABS AH/DH/EH 32	15.5-43.7	-10	317 to 402	0.67 to 0.73	0.24 to 1.89	0.28 to 1.78	0.14 to 1.64
API X-grade	8.0-30.0	-20 to 22	349to 540	0.5 to 0.86	0.01 to 1.11	0.00 to 1.34	0.00 to 1.10
ASTM A105/A106	23.0-23.1	0 to 290	216 to 339	0.46 to 0.60	0.05 to 0.72	0.04 to 0.59	0.03 to 0.49
ASTM A131 Grade E	20.0-28.0	-10	312 to 358	0.63 to 0.66	0.60 to 1.12	0.64 to 1.13	0.43 to 0.88
BS 7191 Grade 355E	45.2-25.3	-10	377	0.70	1.82 to 2.22	1.75 to 2.14	1.42 to 1.79
Duplex SS	25.0-35.1	-50 to -3	543 to 625	0.74 to 0.76	0.08 to 0.95	0.07 to 1.09	0.06 to 0.80
Grade 12.9 Bolt	27.0-27.2	0 to 100	1205 to 1231	0.90	0.01 to 0.04	0.01 to 0.04	0.01 to 0.02
GS-13 MnNi 64	45.0-45.1	-10	327	0.65	1.41 to 1.76	1.28 to 1.60	0.99 to 1.30
INCOLOY 800	5.7	20 to 22	381	0.52	0.95 to 0.98	1.01 to 1.06	0.48 to 0.50
Macalloy	10.0	-20 to 30	950 to 963	0.86	0.00 to 0.01	0.01 to 0.01	0.00 to 0.00
Super Duplex SS	28.0-53.1	-46 to 20	576 to 660	0.71 to 0.77	0.08 to 0.75	0.08 to 0.78	0.06 to 0.61

5.3 Comparison of CTOD determined using BS 7448-1/ISO 12135, ASTM E1820 and WES 1108

CTOD data shown in Table 5.01 were normalised to the respective elastic, plastic and total CTOD calculated to BS/ISO, giving $\delta_{el}/\delta_{el\ BS/ISO}$, $\delta_{pl}/\delta_{pl\ BS/ISO}$ and $\delta/\delta_{BS/ISO}$ (Figure 5.02). The BS/ISO CTOD was used as comparison as it was the most established, and the difference due to ASTM and JWES could be highlighted easily.

The BS/ISO equation does not consider the effects of strain hardening in the equation. In the elastic CTOD comparison, it is shown that the ASTM and JWES equations gave very similar estimations (Figure 5.02(a)). For low strain hardening, the ASTM and JWES gave higher elastic CTOD compared to BS/ISO, and gave lower elastic CTOD for tensile ratio, σ_{ys}/σ_{uts}< 0.84.

In the comparison of the plastic component of CTOD, the ASTM data is scattered and does not show any trend relative to BS/ISO. This is due to the different determinant variable used in the ASTM (plastic work, A_p rather than plastic displacement, V_p). The JWES plastic CTOD equation is based on the BS/ISO with strain hardening and specimen thickness correction, and therefore showed less scatter relative to the BS/ISO. JWES gives larger plastic CTOD for lower strain hardening properties; lower plastic CTOD for higher strain hardening. For the total CTOD determined based on the addition of the elastic and plastic CTOD, JWES and ASTM showed a trend due to strain hardening, with more scatter with the latter. Both JWES and ASTM showed increasing CTOD relative to BS/ISO for the increase of tensile ratio.

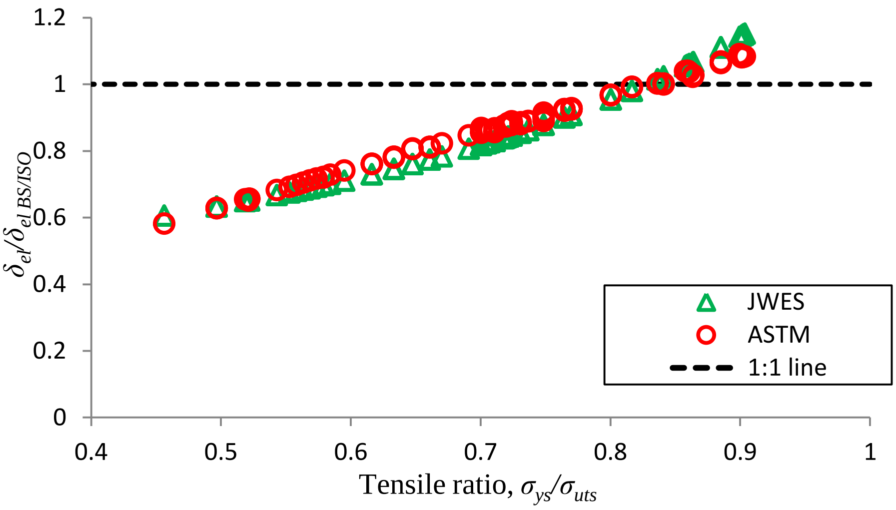

(a)

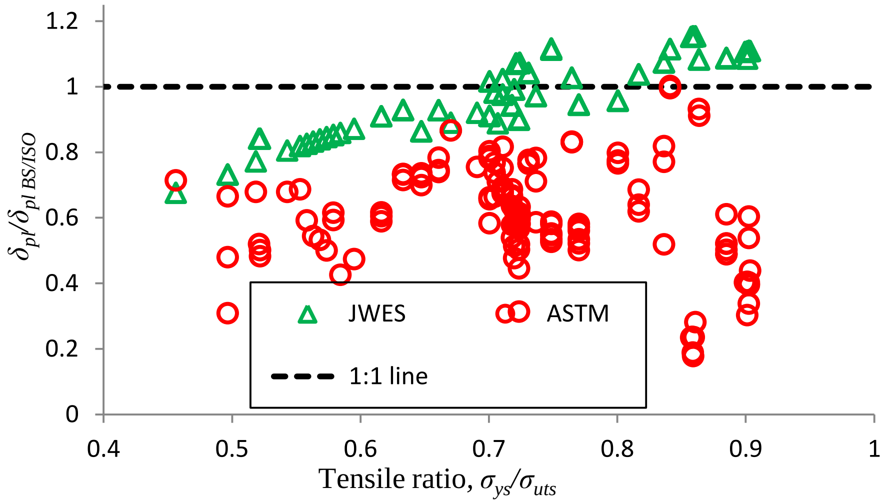

(b)

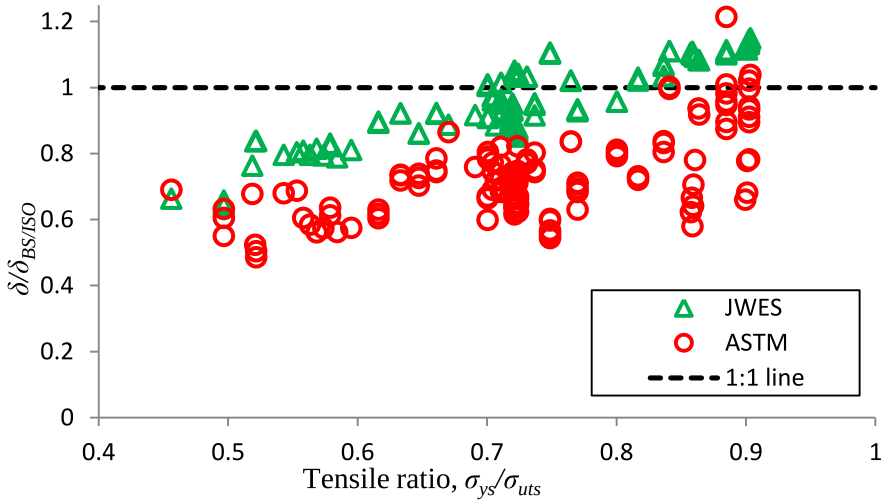

(c)

Figure 5.02Compilation of historic TWI CTOD data calculated using different methods, plotted normalised to the elastic (a), plastic (b) and total (c) CTOD determined from BSI/ISO

The ASTM method almost always underestimates the values of CTOD obtained using the methods in BSI/ISO, apart from several low strain hardening cases. This trend had been observed and noted by several research findings (Tagawa et al. 2010; Tagawa et al. 2014; Pisarski et al. 2010; Kayamori et al. 2008). Further study on the experimental and FE validation of the BS/ISO, JWES and ASTM CTOD is presented in Chapters 7.1 and 8.1.

5.4 The influence of the elastic and plastic component of CTOD

To investigate the effect of the elastic and plastic component in the overall determination of CTOD, the normalized CTOD component, δ_{el}/δ_{pl} was plotted for different σ_{ys}/σ_{uts}. The data were analysed to identify where failure had been by brittle cleavage fracture (δ_c), and fracture with ductile deformation or with stable ductile tearing (δ_u and δ_m). Calculation of CTOD and the determination of the mode of fracture were based on that described in BS 7448-1.

Data exhibiting δ_c were normalized (δ_{el}/δ_{pl}) and plotted for σ_{ys}/σ_{uts} (Figure 5.03). Specimens exhibiting δ_c fail in brittle cleavage fracture with little or no plastic deformation, or encountered pop-in when the crack extension, Δa is equal or less than 0.2mm (BSI 1991). Figure 5.03 showed that in extreme cases, the elastic CTOD can be up to 1340% the size of the plastic CTOD. Overall, the elastic CTOD were considerably larger than the plastic CTOD and is the main determinant of the overall CTOD for δ_c cases.

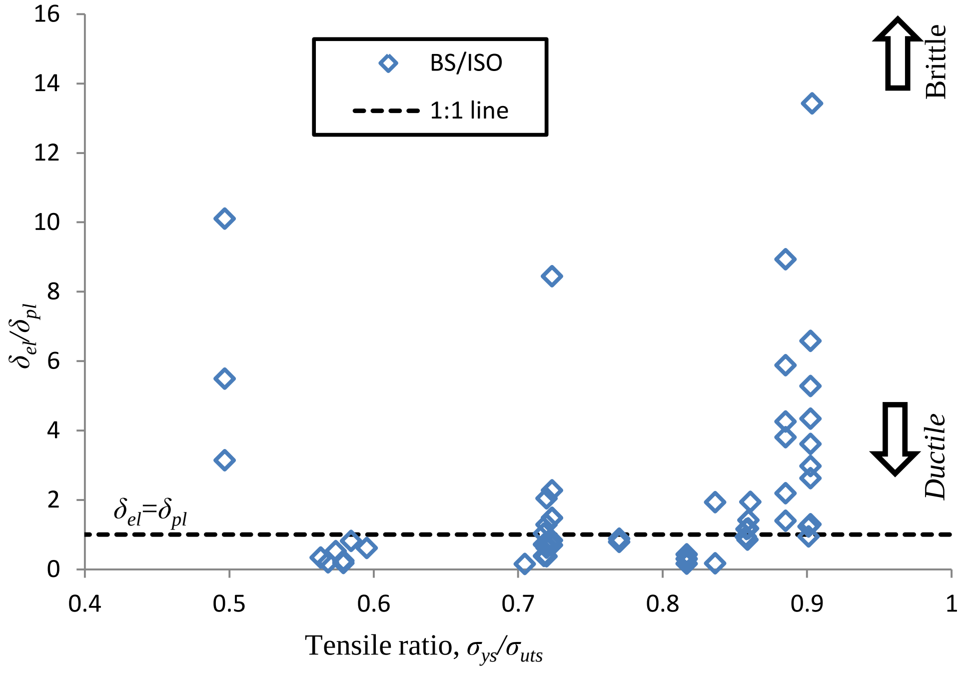

Figure 5.03 Normalized δ_c for different tensile ratio

It was expected that the elastic CTOD would be dominant in cases of δ_c. However, a significant scatter was observed in Figure 5.03, mainly due to the technique used to determine the plastic displacement, V_p. The linear regression method used in this study gave an elastic unloading line which is less steep compared to the loading line (Shown as line BD in Figure 5.04), rather than a perfect elastic unloading line parallel to OA, BC. The error due to this method increases as displacement decreases.

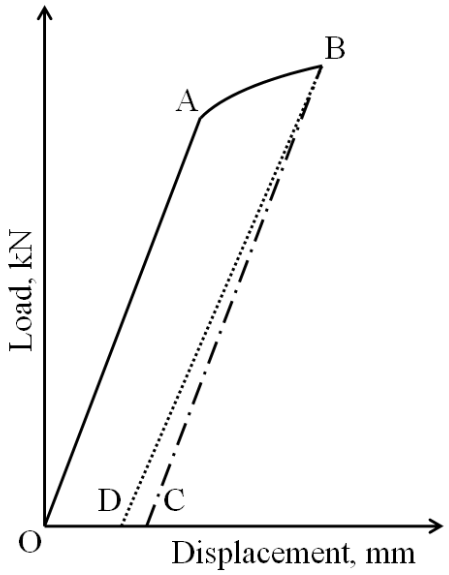

Figure 5.04 Analytical schematic of the loading and unloading line

The remaining normalized CTOD data exhibiting significant plastic deformation or stable ductile tearing (δ_u and δ_m) were shown in Figure 5.05 for 0.4≤ σ_{ys}/σ_{uts}≤ 1. Opposite to the distribution observed in Figure 5.03, none of the elastic CTOD were larger than the plastic CTOD. Majority of the elastic CTOD estimates less than 30% of the plastic CTOD, and therefore the plastic CTOD is generally very dominant in cases where considerable plastic deformation or stable ductile tearing is experienced at the crack tip.

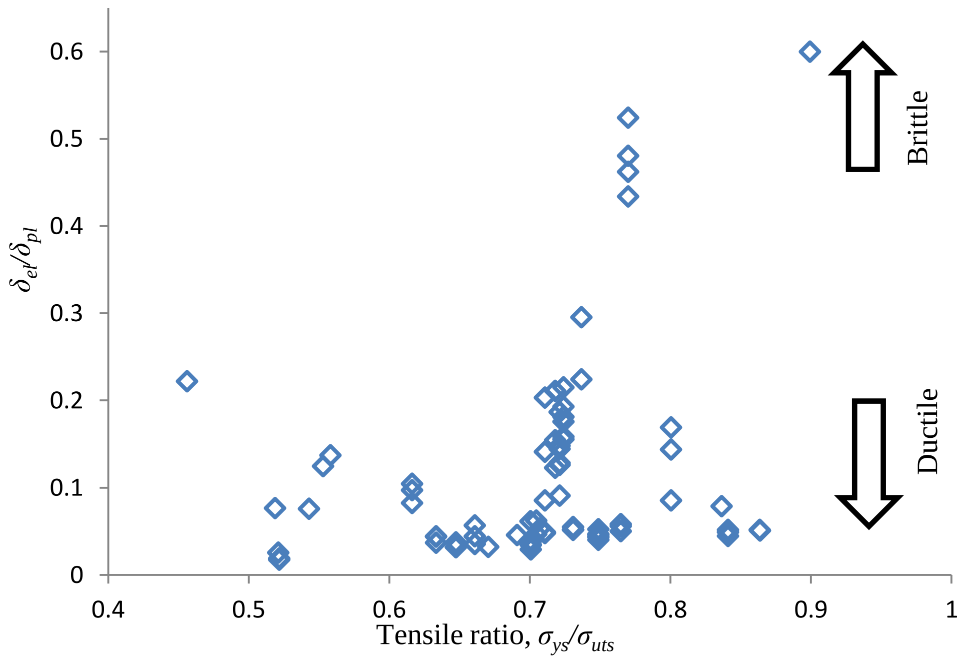

Figure 5.05 Normalized δ_u and δ_m for different tensile ratio

Based on the FE model with idealised tensile properties (Chapter 4.2.2), the elastic and plastic CTOD were calculated using the BS/ISO equation and plotted to the increasing CTOD based on the original crack tip. For visualisation purposes, only the lowest and highest strain hardening data (σ_{ys}/σ_{uts}= 0.98 and 0.44 respectively) were shown in Figure 5.06. It seems that initially, the CTOD ratio is very large, but it decreases exponentially and converges. The trend varies slightly for the two extremes of strain hardening. Therefore the accuracy in calculating δ_{el} has more influence for brittle materials, but for ductile materials, it's the accuracy in determining δ_{pl} which has the greatest effect.

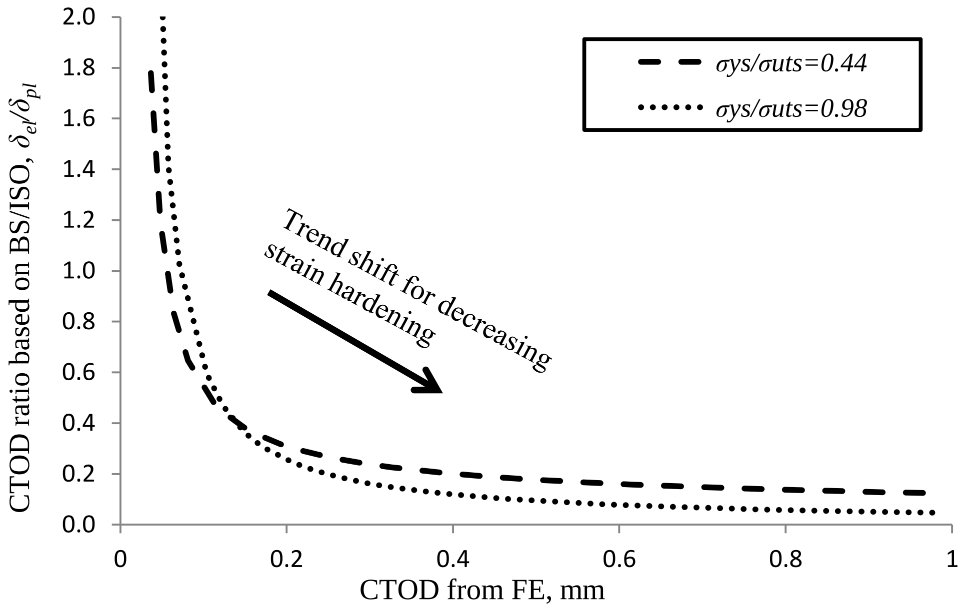

Figure 5.06 Trend of CTOD ratio for increasing CTOD from FE

5.5 Analytical comparison of the CTOD equations

All three equations (BS/ISO, ASTM and JWES) considered that CTOD is the addition of the elastic CTOD and plastic CTOD. Considering the elastic CTOD, all three equations used a similar approach, where the equation is based on the stress intensity factor, *K*. The major difference between the equations is the 'constraint' factor, *m*. BS/ISO adopted a constant value of *m*= 2, whereas ASTM and JWES calculates *m* as a function of tensile ratio (and a_0/W for ASTM).

The BS/ISO and JWES elastic CTOD is expressed in the form of

$$\delta_{el} = K^2 \frac{(1-v^2)}{mE\sigma_{ys}} \qquad \text{Eq. 5.05}$$

And rearranging the equation would give *m* as

$$m = K^2 \frac{(1-v^2)}{\delta_{el} E \sigma_{ys}} \quad \text{Eq. 5.06}$$

The ASTM used 'flow stress', $(\sigma_{ys}+\sigma_{uts})/2$ in the equation, which led to

$$\delta_{el} = K^2 \frac{(1-v^2)}{m_{ASTM} E \left(\frac{\sigma_{ys}+\sigma_{uts}}{2}\right)} \quad \text{Eq. 5.07}$$

Factoring the σ_{ys} gives

$$\delta_{el} = K^2 \frac{(1-v^2)}{\sigma_{ys} \frac{m_{ASTM}}{2} E \left(1+\frac{\sigma_{uts}}{\sigma_{ys}}\right)}$$

And rearranging the equation for the equivalent m in BS 7448-1 gives

$$\frac{m_{ASTM}}{2}\left(1+\frac{\sigma_{uts}}{\sigma_{ys}}\right) = K^2 \frac{(1-v^2)}{\delta_{el} E \sigma_{ys}} = m \quad \text{Eq. 5.08}$$

For SEN(B) specimens with crack length-specimen width ratio, a_0/W= 0.5, the inverse of m factor is calculated based on Eq. 5.04 and 5.08 for different tensile ratio, σ_{ys}/σ_{uts} (Figure 5.07). m is inversely proportional to the elastic CTOD, where higher m would lead to lower elastic CTOD calculated. Figure 5.07 showed that the ASTM m factor gave comparable values to the JWES m factor. This led to similar elastic CTOD estimated by the ASTM and JWES equations, shown in Figure 5.01(a).

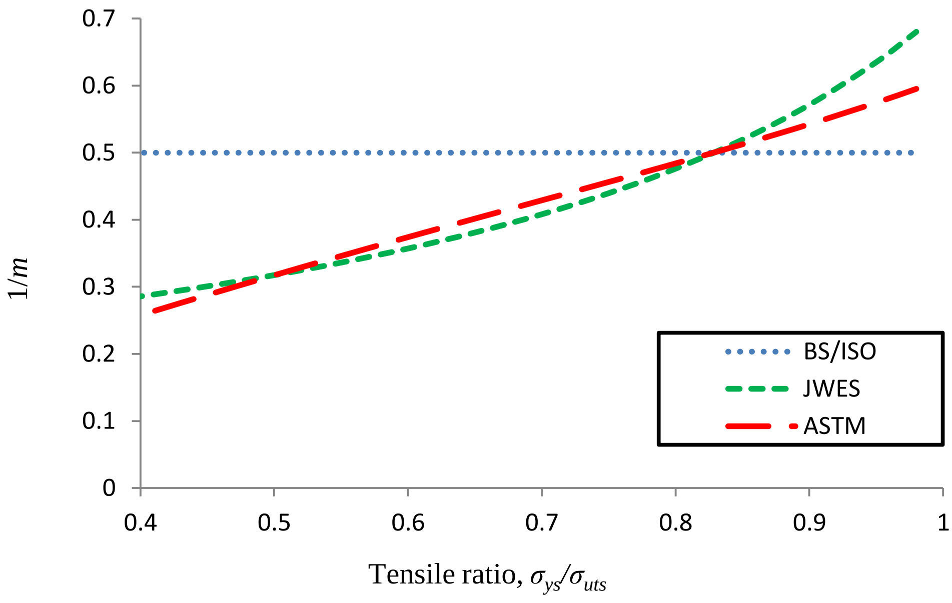

Figure 5.07 *m* factor considered in the equations for different tensile ratio for a_0/W= 0.5

The plastic component of CTOD is determined based on different variables in the standard equations. The plastic CTOD in BS/ISO and JWES is dependent on the analytically determined plastic displacement, V_p, whereas ASTM is based on the plastic work, A_p as described in Chapter 1.8.1. The BS/ISO and JWES method is direct and mainly geometrical, while ASTM calculates J, which is then converted to CTOD. Figure 5.08 shows two idealised cases, (a) and (b) to exhibit the different results obtained by V_p and A_p based equations.

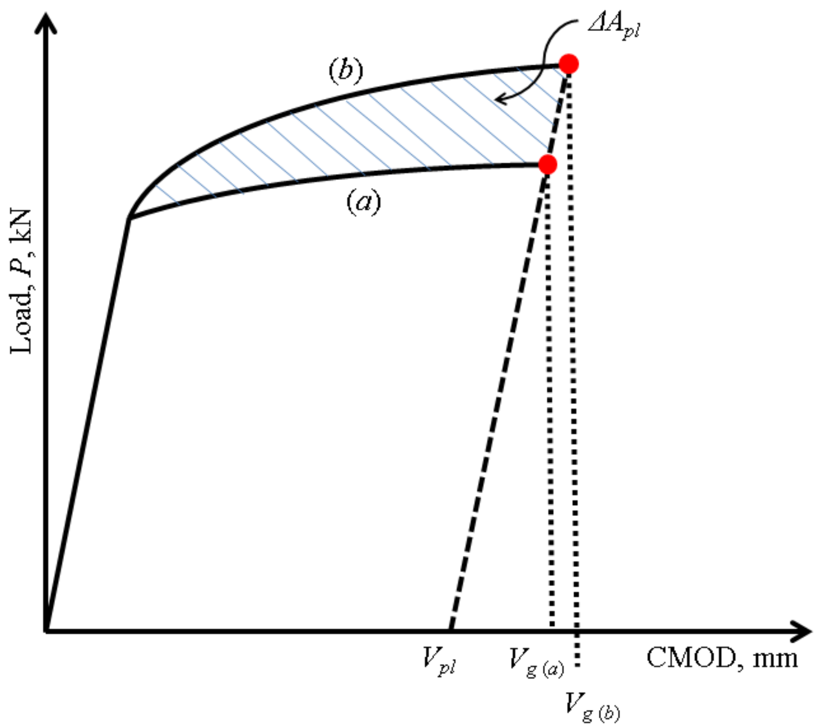

Figure 5.08 Different idealised loading cases, highlighting different A_p obtained

Assuming that the material exhibits the same tensile properties, both data (a) and (b) would result in the same V_p, despite the different post-elastic loading curve and V_g. This would lead to similar resultant CTOD calculated using the BS/ISO or JWES equation for both (a) and (b). However, data (a) and (b) gives different amount of plastic work, highlighted by the shaded region, ΔA_p in Figure 5.08. Based on the equation used in ASTM, different J values would be determined for (a) and (b) due to ΔA_p, which leads to different resultant CTOD. These different variables do not allow equivalent theoretical comparison of the plastic CTOD obtained from ASTM to the BS/ISO and JWES method.

The plastic CTOD used in the JWES equation is a modification of the BS/ISO equation with a different rotational factor, and two correction factors based on strain hardening (in terms of tensile ratio) and specimen thickness. Additionally, the JWES plastic CTOD is based on the plastic CMOD, different from the BS/ISO plastic CTOD which allows both plastic CMOD and plastic clip gauge measurements above the crack mouth (Figure 5.09).

CTOD was calculated based on the similar triangles principle using both r_p= 0.43 and 0.4, and normalised as $\delta_{BS\ rp=0.43}/\delta_{BS\ rp=0.4}$. The effect of the different rotational factor, and a typical clip gauge height (z= 2mm) used in JWES is shown in Figure 5.10. The higher rotational factor used in JWES gives increasing overestimation of the BS/ISO CTOD as the crack ratio, a_0/W increases, with a maximum overestimation of 7.4%. However, the maximum difference due to the different height above the crack mouth (z= 2mm) for the plastic opening displacement (CMOD or clip gauge opening above crack mouth) is ~0.05%. Therefore, in conventional tests, it could be safely assumed that

$$\frac{0.43(W-a_0)V_{p\ CMOD}}{0.43(W-a_0)+a_0} = \frac{0.43(W-a_0)V_{p\ clip\ gauge}}{0.43(W-a_0)+a_0+z} \quad \text{Eq. 5.09}$$

There are two advantages of measuring the opening displacement using a clip gauge above the crack mouth: - the simplification of the machining process without the integral knife edges, and the ease of the adjustment and positioning of the of the knife edges at the crack.

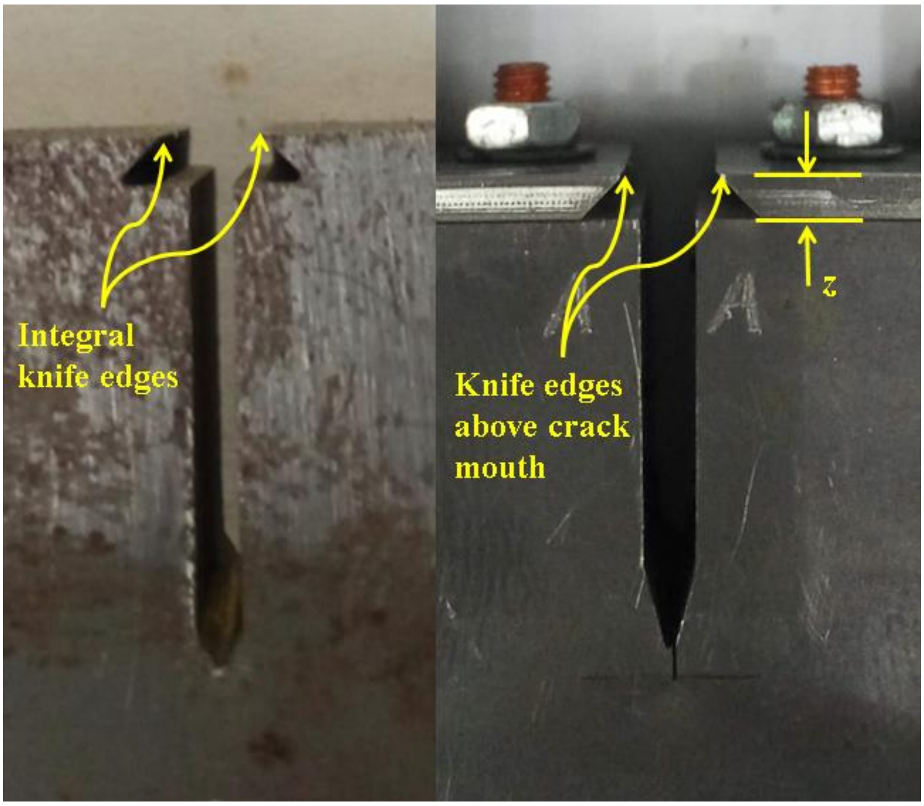

Figure 5.09 Integral knife edges and knife edge setup above the crack mouth for the measurement of the opening displacement

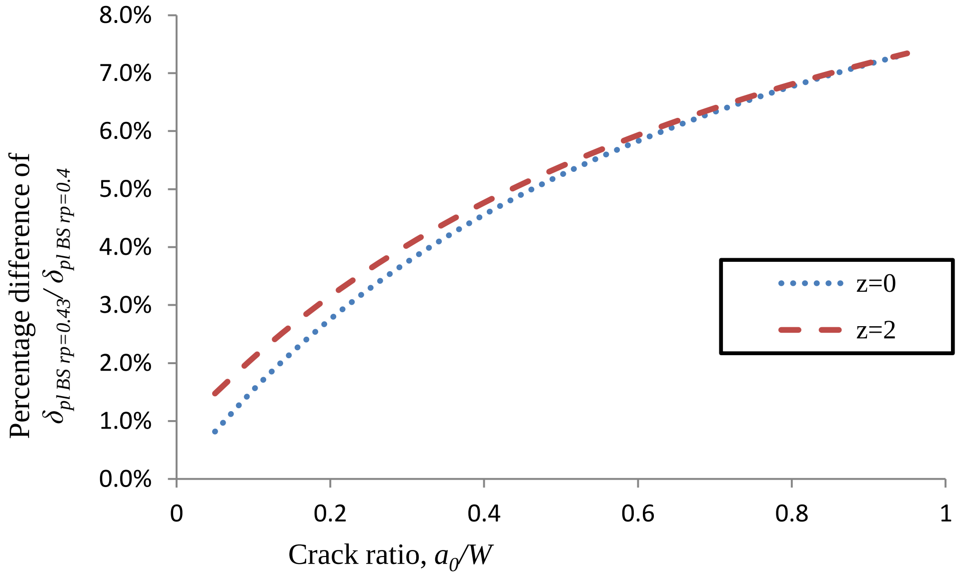

Figure 5.10 The effect of the different rotational factor and clip gauge height used in JWES

The influence of the strain hardening and specimen thickness correction factor used in JWES relative to BS/ISO is shown in Figure 5.11 and Figure 5.12 respectively. The strain hardening correction factor in Figure 5.11 showed a similar trend to that showed in Figure 5.07, where the resultant CTOD increases with the decrease of strain hardening (increasing tensile ratio). The JWES strain hardening correction factor would give similar estimation to that obtained from BS/ISO when $\sigma_{ys}/\sigma_{uts} \approx 0.85$.

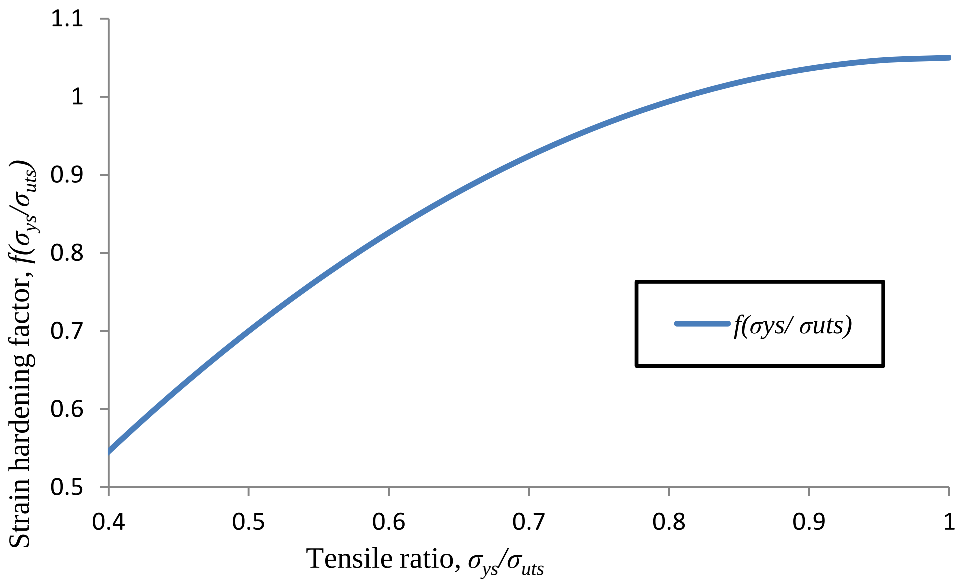

Figure 5.11 The effect of the strain hardening correction factor used in JWES

The calibration technique and method used for the specimen thickness correction factor is undisclosed, but it could be seen that thickness, B= 25mm was used as the baseline for the calibration of the equation. For *B*> 25mm, JWES would give lower CTOD; for *B*< 25mm, JWES gives larger CTOD than the BS/ISO formula. The trend of thickness correction for CTOD is similar to that fracture toughness obtained experimentally by Wallin (1985) and in FE modelling by Han et al. (2014).

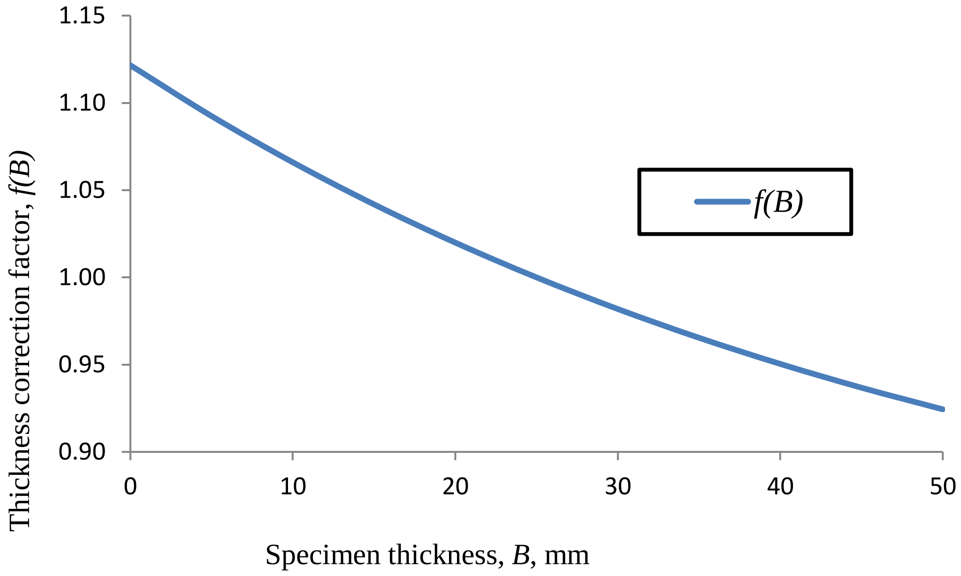

Figure 5.12 JWES thickness correction factor for increasing specimen thickness

5.6 Summary

The BS 7448-1/ ISO 12135 and ASTM E1820 have been the most commonly used for the determination of CTOD. Both standards approach the estimation of CTOD based on different assumption, which leads to different calculated CTOD. JWES (WES 1108) proposed a new CTOD equation which they validated against experimentally measured CTOD and numerical modelling.

CTOD was determined based on the addition of the elastic and plastic component of CTOD. Apart from cases where the specimen fails in brittle/cleavage fracture without stable ductile tearing, the plastic component of CTOD is generally the main determinant of the total CTOD. The elastic CTOD equation gave similar estimations based on both ASTM E1820 and WES 1108. The main difference between the equations lies on the determination of the plastic CTOD, which were based on different assumptions.

The BS 7448-1/ ISO 12135 equation does not consider the effects of strain hardening in the determination of CTOD. However, strain hardening factors are incorporated into both elastic and plastic component of CTOD for the ASTM E1820 and WES 1108 equations. Overall, the ASTM E1820 underestimates the BS 7448-1/ ISO 12135 CTOD; the JWES underestimates the

BS 7448-1/ ISO 12135 CTOD for high strain hardening properties, but overestimates them for low strain hardening properties.

The data suggests that the ASTM E1820 equation might possibly be over conservative for estimating CTOD. Based on the understanding of the trend of the different equations, further experimental and FE validation (Chapter 7.1 and 8.1) based on different strain hardening properties shall highlight the accuracy of the BS 7448-1/ISO 12135, ASTM E1820 and WES 1108 equations for CTOD.

Chapter 6

Variation of CTOD across the specimen thickness in 20mm thick austenitic stainless steel

6.1 Introduction

Several published research shown that fracture toughness is not constant but varies in the thickness direction at the crack tip (Pook 2013; Pook 2000; Pook 1994; Tagawa et al. 2014; Hutchison & Pisarski 2013). It is not well explained in the standardised equations (BSI 1991; ASTM 2015) the position where fracture toughness is addressed. This led to confusion when direct measurements of CTOD, i.e. δ_5 CTOD (Figure 6.01) and measurements on the silicone replicated crack (SRC) were performed. Surface measurements of CTOD can vary significantly from CTOD in the middle of the crack.

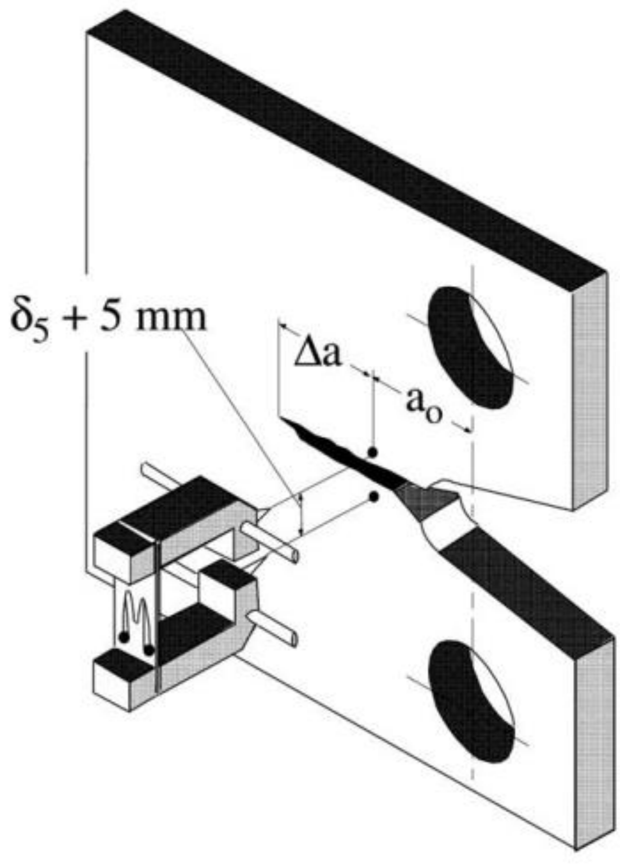

Figure 6.01 The direct CTOD measurement, δ_5 concept (Schwalbe et al. 2005; Schwalbe 1995)

Austenitic stainless steel, SS316 (material M03) was used in the tests. To investigate CTOD across the crack, the crack was replicated using silicone compound. The silicone replica enables direct measurement of the opening of the original crack tip. Additionally, an alternate direct measurement of CTOD on the specimen surface, δ_5 using the digital image correlation, DIC technique was obtained from a published work for analytical comparison purposes. A similar technique had been used and (Verstraete et al. 2013; Schwalbe 1995; Schwalbe et al. 2005). This enables comparison between the two different definitions of CTOD. A conservative relation was drawn for the estimation of CTOD in the middle of the crack using the δ_5 method.

The contents in this chapter were based on a published journal article (Khor et al. 2016), with improved SRC measurements and analysis.

6.2 Image measurements

The DIC is an optical surface measurement technique, enabling direct measurements of displacement. A commercial non-contact optical 3D deformation measuring system, GOM-ARAMIS v6.3 was used to process the images captured using the DIC system. Paint speckles were applied on the surface in a random manner, which enable the software to identify displacement of the speckles on the surface (Figure 6.02).

Utilising the DIC technique enables the direct measurement of δ_5 on the specimen surface. δ_5 is an alternative definition to CTOD originated from Germany, which is based on surface measurements at the crack tip (Schwalbe 1995; Schwalbe et al. 2005). δ_5 is the displacement between two points, positioned 5mm apart horizontally at the original crack tip (Figure 6.01). Typically, a special δ_5 clip gauge was used to measure δ_5 directly. The DIC technique enables the identification of the δ_5 points for displacement measurements when the specimen is loaded and the crack opens. Figure 6.02 shows the identification of the δ_5 points on the GOM-ARAMIS v6.3 software based on the paint speckles around the crack tip region.

DIC was used in seven SEN(B) specimens (M03-11 to M03-17) for δ_5 measurements. These DIC δ_5 data were provided by TWI (Khor et al. 2016).

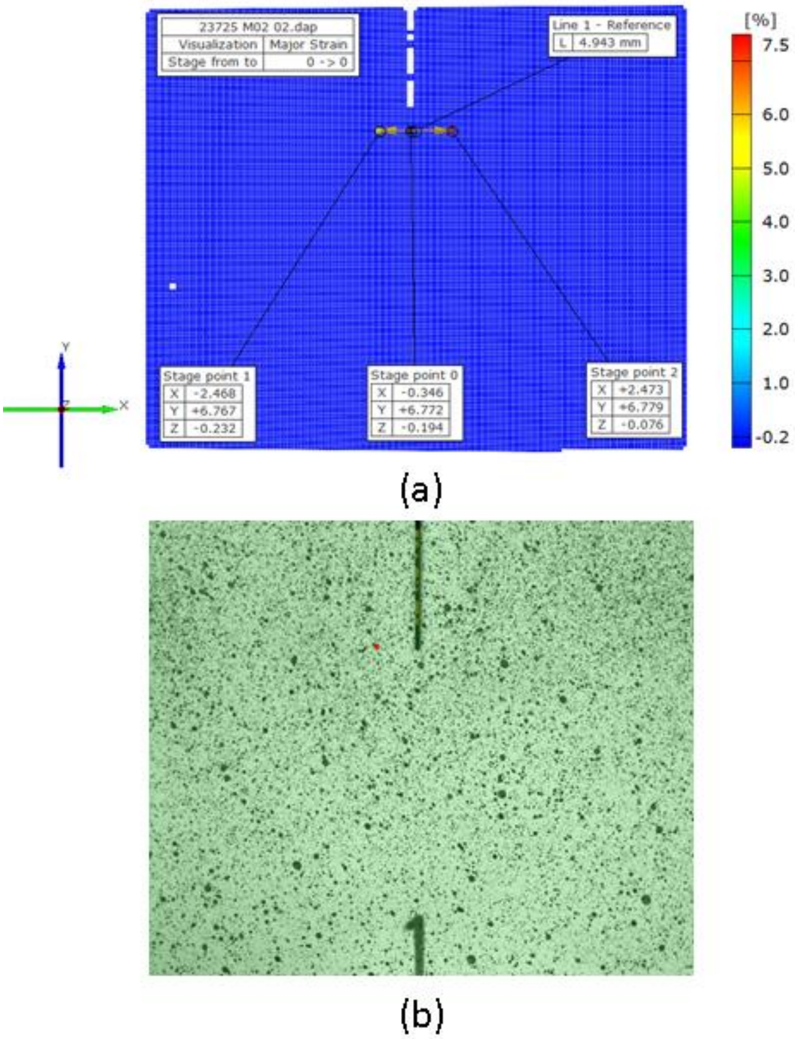

Figure 6.02 Determination of (a) δ_5 points based on (b) speckle pattern (Khor et al. 2016)

6.3 Results

CTOD measured on the silicone replicated crack is considered as the actual CTOD, and used to compare against the δ_5 CTOD measurements. For simplicity purposes, clip gauge displacement was converted to CMOD using Eq. 6.01, which was derived from ASTM E1290 (ASTM 2012).

$$CMOD = \frac{V_g}{1+\frac{z}{0.8a_0+0.2W}} \qquad \text{Eq. 6.01}$$

6.4 Experimental data

The load-displacement data obtained from a standard SEN(B) test (M03-03) and crack replication test (M03-05) was shown in Figure 6.03. No significant difference was observed between the overall load-displacement data obtained from the crack replication test and a standard test. The load-drop phenomenon due to constant displacement and implication on the validity of the silicone replica measurements are described in Chapter 3.4.

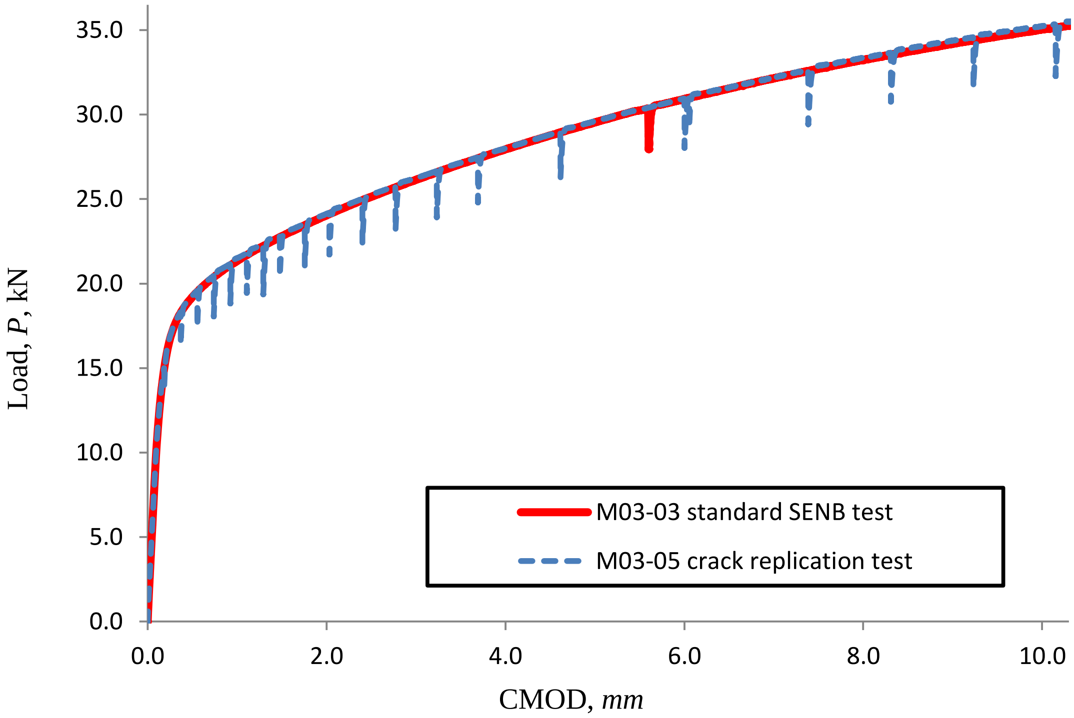

Figure 6.03 Load-displacement data obtained from the standard test and silicone crack replication test

The SRC extracted from the specimens were sliced on positions *b*= -0.5, 0 and 1 and CTOD was measured on the exposed cross section as described in Chapter 2.10 (Figure 6.04). The measurements on the SRC shows that CTOD on the *b*= ±0.5 position tend to show the lowest CTOD for all loading; the sides of the specimen (*b*= ±1) showing the highest CTOD throughout the crack front. The variation of CTOD across the crack tip is influenced by the crack tip shape, crack length and the plane strain-ness across the crack front, described later in the chapter.

The specimen was ductile and experienced large deformation in the test. Significant crack tip blunting and stretching before the initiation of stable ductile tearing was observed on the crack face, known as the stretch zone. The inclusion of the stretch zone in the measurement of the original crack length would lead to smaller CTOD measured on the SRC (Khor et al. 2016). To minimise the effect of stretch zone width, the original crack length was determined based on the SRC at CMOD= 0.62mm, where the silicone compound managed to fully cast the crack tip. This method give better accuracy compared to measuring the original crack length from the crack face, but slightly underestimates the actual measurements of CTOD, where the crack length measured from the SRC would be fractionally longer than the actual original crack length. This eliminates the concern about overestimating the actual CTOD due to under measuring the original crack length.

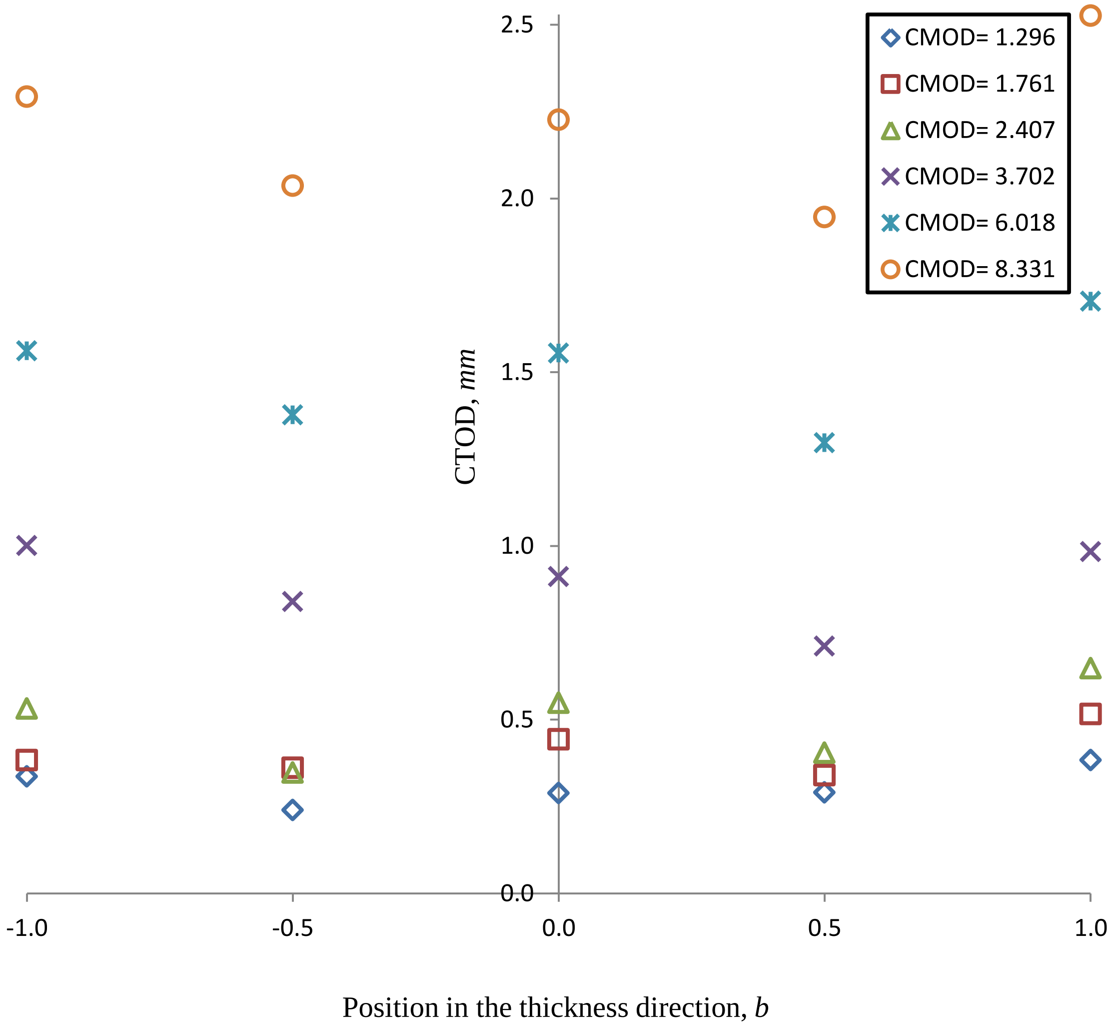

Figure 6.04 CTOD at different position across thickness for different CMOD (selected points for clarity)

6.5 DIC method for surface measurement

The DIC technique was applied to seven SEN(B) specimens for δ_5 measurement. The measurements of δ_5 were compiled for the following loads: - 10.0kN, 15.0kN, 20.0kN, 25.0kN and 27.5kN. Plotting the δ_5 measurements with the corresponding clip gauge opening for all seven specimens, the data shows that the measurements were very consistent with R^2= 0.9970 (Figure 6.05).

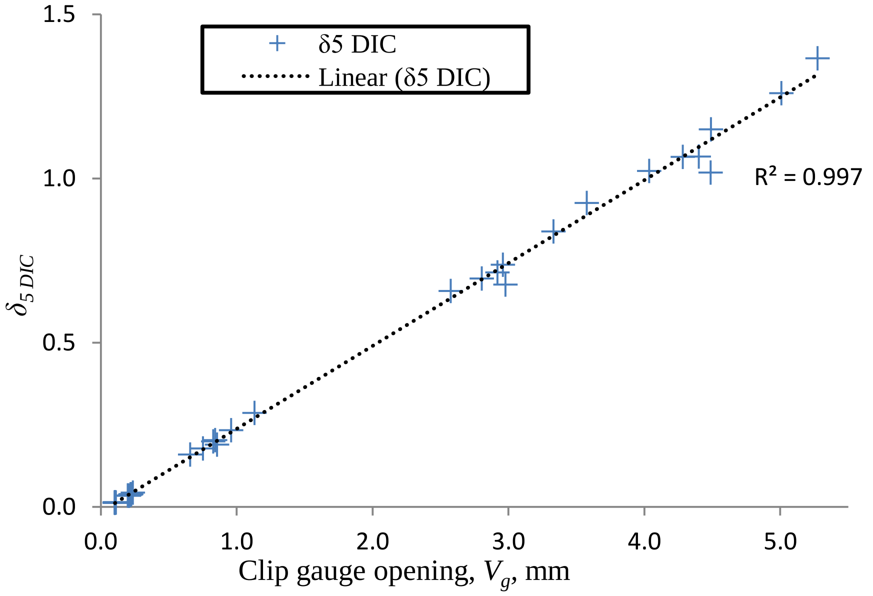

Figure 6.05 Clip gauge opening vs. δ_5 measured on the SS316 SEN(B) specimens tested using DIC (Khor et al. 2016)

6.6 Finite Element CTOD measurements

CTOD was extracted from the FE model from three positions in the thickness direction, where *b*= 0 (centre), 0.5, and *b*=1 (edge). The CTOD was shown with the increase of CMOD in Figure 6.06. Different from that observed in the CTOD extracted from the SRC, the FE model showed largest CTOD in the centre of the model (*b*= 0), followed by *b*= 0.5 and *b*= 1. This distribution of CTOD is similar to that observed by Hutchison & Pisarski (2013) for a straight crack front model.

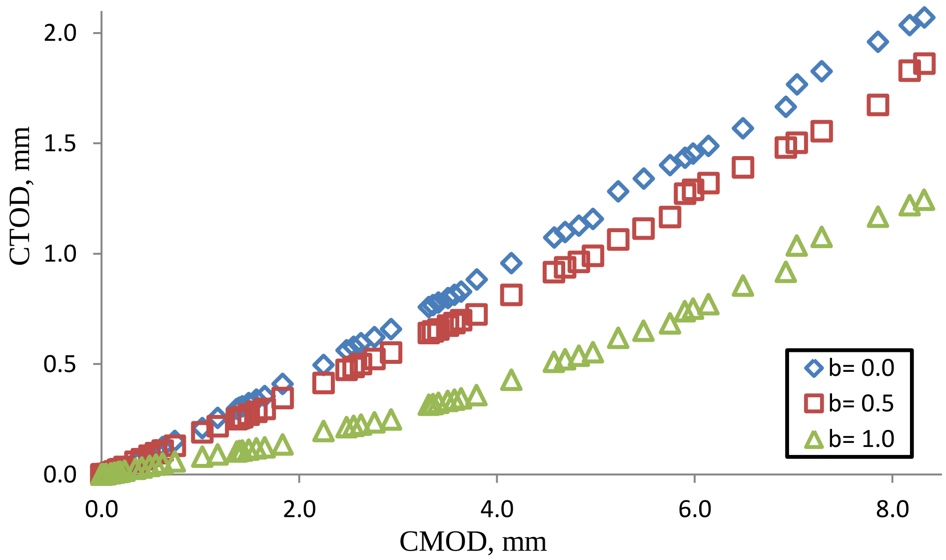

Figure 6.06 CMOD vs. CTOD at *b*= 0, 0.5 and 1.0 from the FE model

6.7 CTOD across the crack front

The δ_5 measured using DIC, $\delta_{5\ DIC}$ (surface measurement) was compared to CTOD measured on the surface (b= 1) and middle (b= 0) of the crack (Figure 6.07). Generally, $\delta_{5\ DIC}$ overestimate both CTOD measured from the side and middle of the specimen. Comparing CTOD measured on the side and middle of the specimen, the side of the specimen gave an average of 11.53% larger CTOD with standard deviation of 12.11%.

The CTOD equations in the standards (BS 7448-1, ISO 12135 and JWES) were formulated to estimate plane strain fracture toughness, which corresponds to the CTOD in the middle of the crack. Figure 6.07 showed a consistent relationship between $\delta_{5\ DIC}$ and $\delta_{SRC\ (b=0)}$, given as

$$\delta_{SRC\ (b=0)} = 0.742\delta_{5\ DIC} \qquad \text{Eq. 6.02}$$

The equation was able to give a conservative prediction of CTOD using δ_5. Eq. 6.02 is not suitable for prediction of CTOD below 0.2mm, where the elastic CTOD is dominant. Using DIC for the measurement of δ_5 gives an advantage where very large deformation at the crack tip could be measured without the need to consider the displacement measurement limitation of the δ_5 clip gauge.

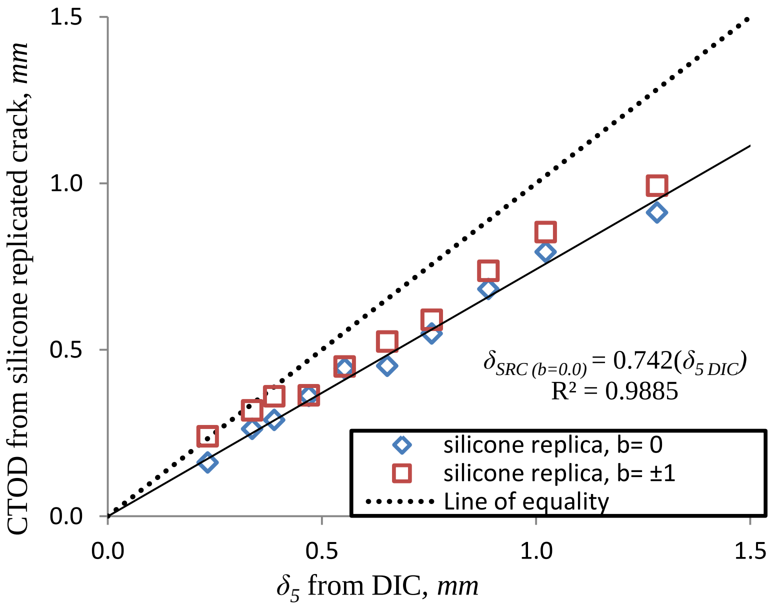

Figure 6.07 Comparison between $\delta_{5\ DIC}$, $\delta_{SRC\ (b=0)}$ (plane strain CTOD), and $\delta_{SRC\ (b=\pm1)}$ (surface CTOD)

The sides of the specimen (*b*= 1) showed the largest CTOD across the crack front (Figure 6.04). This effect is due to fatigue loading used to produce the crack tip, which led to a 'thumbnail' shaped crack front. Based on an idealised 'thumbnail' shaped crack front model, the crack length on the sides of the crack front is shorter than the crack length measured on the centre of the crack front (Figure 6.08). Based on the similar triangles assumption where the flanges of the SEN(B) specimen rotate about a rotational point ahead of the crack tip, a shorter crack length leads to higher CTOD compared to a longer crack length (Khor et al. 2016).

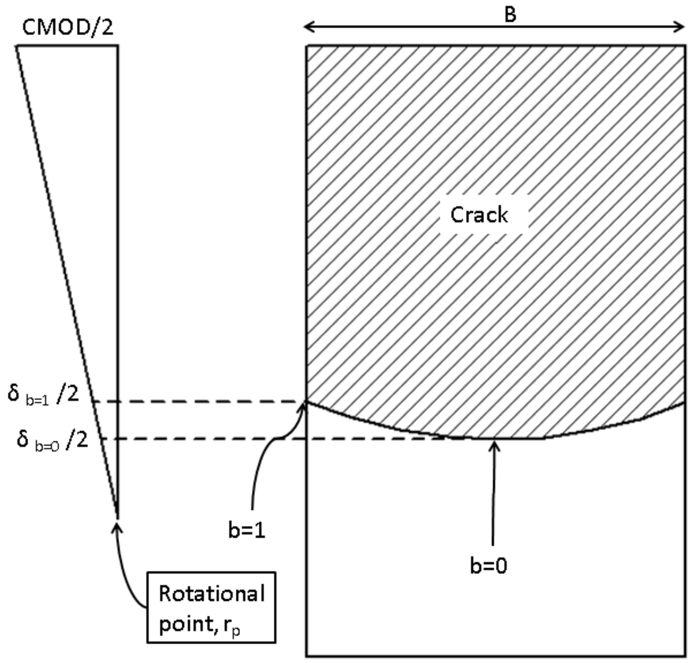

Figure 6.08 The effect of curved crack front on the determination of CTOD at the middle and side of the specimen (Khor et al. 2016)

The CTOD extracted from the FE model showed that the centre of the model showed the highest CTOD and lowest on the sides of the model (Figure 6.06). It should be noted that a straight crack front was used based on the average crack length, which conceptually gives similar cross section area ahead of the crack tip compared to a 'thumbnail' shaped crack front.

CTOD measured from the SRC showed a different distribution compared to the FE CTOD (Figure 6.04). A straight crack front was modelled in FE, and it shows that the plane strain region (middle of the model, b= 0) exhibited larger CTOD compared to the plane stress region (sides of the model, b= 1). This explains the larger CTOD observed in b= 0 compared to b= ±0.5 on the silicone replica, despite the slightly longer original crack length measured on b= 0.

Analytically, DIC measurements of δ_5 can give smaller values compared to the surface CTOD (b= 1) when rotation is prevalent on the specimen (Verstraete et al. 2013). This is due to the measurements being taken at an offset rather than directly at the crack tip (Figure 6.09) (Khor et al. 2016). However, Figure 6.07 showed otherwise, where δ_5 overestimates the surface CTOD for CTOD larger than 0.25mm. High strain levels on the surface of the specimen increased the original 5mm distance between the two measured points (Verstraete et al. 2013). The δ_5 gives an approximate estimate to the surface CTOD, but however the accuracy is dependent on the strain levels and rotation experienced by the specimen.

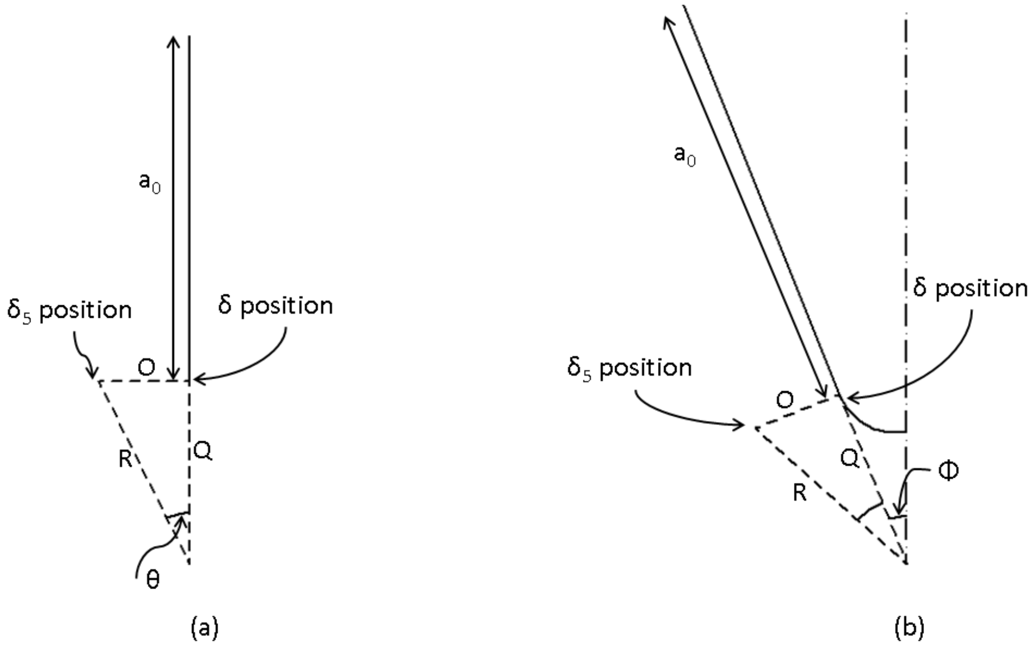

Figure 6.09 Geometrical analysis of δ and δ_5 on (a) an idealized initial crack and (b) an idealized blunted crack (Khor et al. 2016)

6.8 Conclusion

This chapter shows the variation of CTOD across the crack front in the thickness direction. A thumbnail shaped crack front with well distributed crack extension leads to higher CTOD measured on the sides of the specimen (*b*= ±1.0), followed by the middle of the specimen (*b*= 0.0), than the position between the sides and the middle (*b*= ±0.5).

DIC was applied on the specimen, which allows the measurement of δ_5 on the surface of the specimen. δ_5 is representative of the CTOD measured on the sides of the specimen. However, the accuracy of δ_5 is dependent on the strain and rotation level of the specimen.

Based on δ_5 measurements extracted using DIC, CTOD in the middle of the specimen (material CTOD, δ_{mat}) can be estimated using Eq. 6.02 for austenitic stainless steels. The equation provides conservative estimates of CTOD based on surface δ_5 measurements. This technique based on DIC is advantageous in situations where the displacement at the crack tip exceeds the measurement capabilities of the δ_5 clip gauge, and it reduces the human error on the placement of the δ_5 clip gauges at the crack tip.

Chapter 7

Validation of CTOD for different strain hardening materials

7.1 Introduction

The Crack Tip Opening Displacement (CTOD) is one of the three fracture toughness parameters, along with *J* and stress intensity factor, *K* (Zhu & Joyce 2012). CTOD as a material toughness parameter is defined as the opening of the crack tip in a standard fracture toughness specimen at the point of maximum load or unstable crack extension. CTOD is typically calculated using load and displacement data obtained from testing fracture toughness specimens (Chapter 1.8.1).

The current fracture toughness testing standards:- BS 7448-1, ISO 12135, and ASTM E1820 - specify methods to determine fracture toughness (BSI 1991; ISO 2002; ASTM 2014). The testing procedures and methodologies were well established and similar: - a clip gauge is used to extract displacement data from the opening of the crack mouth, whilst load feedback is obtained by the testing machine. The load-displacement data obtained from the tests would allow fracture toughness to be calculated based on equations provided in the standards.

BS 7448-1 and ISO 12135 use the same assumption to the determination of CTOD, while ASTM E1820 utilizes a *J*-CTOD conversion factor proposed by Shih (1981). Recently, researchers at the Japanese Welding Engineering Society (JWES) published a new equation with strain hardening consideration for CTOD based on the BS 7448-1 equation (Kawabata et al. 2016). The different assumptions used by BS 7448-1, ASTM E1820 and JWES can lead to different values of CTOD being estimated on the same fracture toughness specimen when assessed to different standards (Tagawa et al., 2014). This had sometimes caused significantly larger or smaller CTOD being estimated using the different equations, leading to different flaw acceptance criteria in ECA or material qualification pass or fails.

The current study addresses the validity of the BS 7448-1, ASTM E1820 and the JWES CTOD estimation on a range of different strain hardening steel. The silicone crack casting technique was used to produce a physical crack for direct measurement of CTOD, whilst Finite Element (FE) modelling was used to predict the experimental results.

7.2 Load-displacement data

From a typical SEN(B) test, load and displacement data is extracted for the fracture toughness estimation. The standard test was modified to accommodate casting of the crack (described in

Chapter 2.9). It is important that the modified tests were able to provide consistent data. Two crack replication tests were performed on low (M01-05 and M05-06) and high strain hardening material (M03-05 and M03-06), and four tests on medium strain hardening steel (M02-05, M02-07, M02-08 and M02-09). Load-CMOD data from the tests were displayed in Figure 7.01. Data obtained from the specimens of the same material were consistent with minimal difference. The difference is due to the fatigue method used to introduce the crack into the specimen. The fatigue method can produce a very sharp crack. However it would give a curved 'thumbnail' shaped crack front and it is difficult to reproduce the exact same crack tip on two separate specimens.

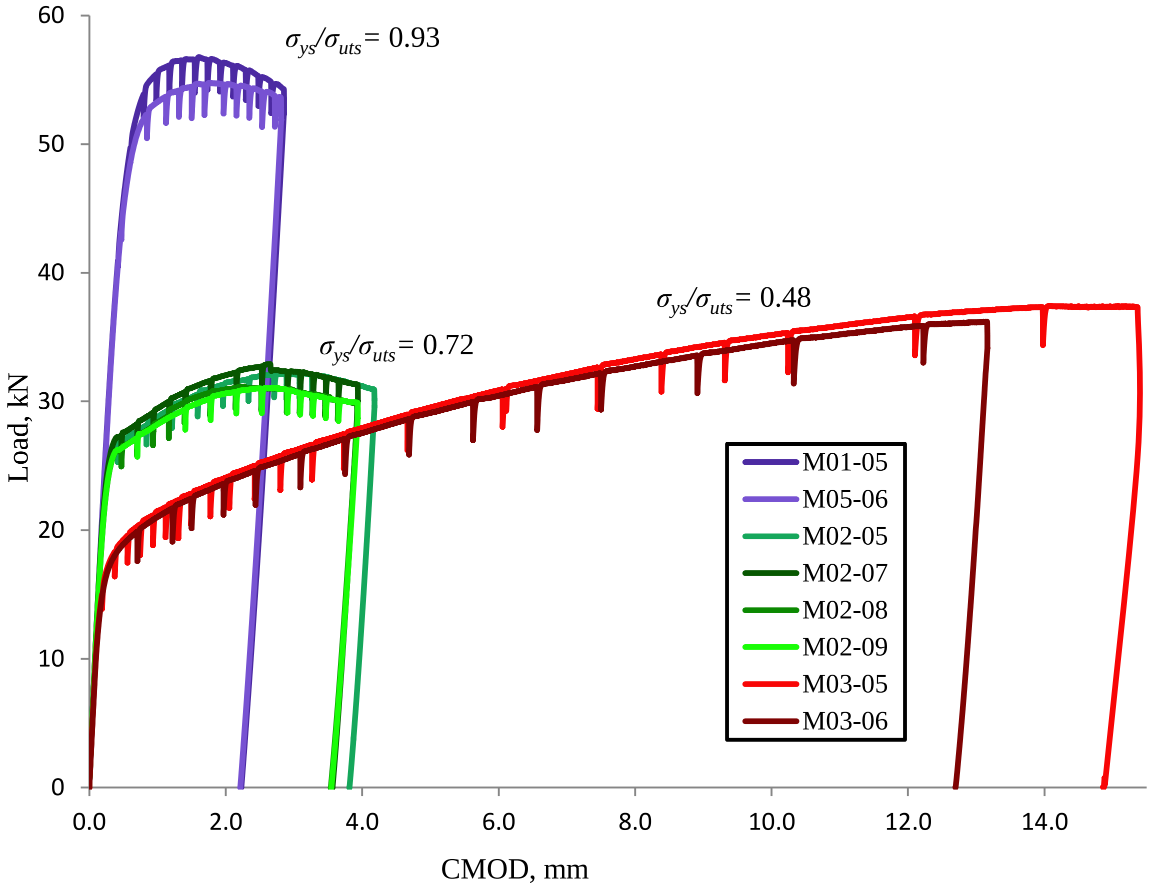

Figure 7.01 Load-displacement data from the standard and modified SEN(B) test

To justify the accuracy of the data obtained from the crack replication tests, three standard SEN(B) tests were performed in accordance to BS 7448-1 (M01-07, M02-03, M03-03). Additionally, three FE models were generated to predict CTOD based on the crack replication test specimens (M01-05, M02-05, M03-05). Load-displacement data obtained from the standard test, crack replication test and the FE model were shown in Figure 7.02. The standard test and crack replication test gave very consistent data. The FE data were consistent with the experimental data for the elastic loading region, but overestimate the plastic loading region. This effect is due to the properties used in the FE model, further discussed in Chapter 7.5. The load-CMOD data obtained from the SRC test showed load drops at positions where the crack casting procedures were performed. This load-drop phenomenon due to constant machine displacement is described in Chapter 3.1.

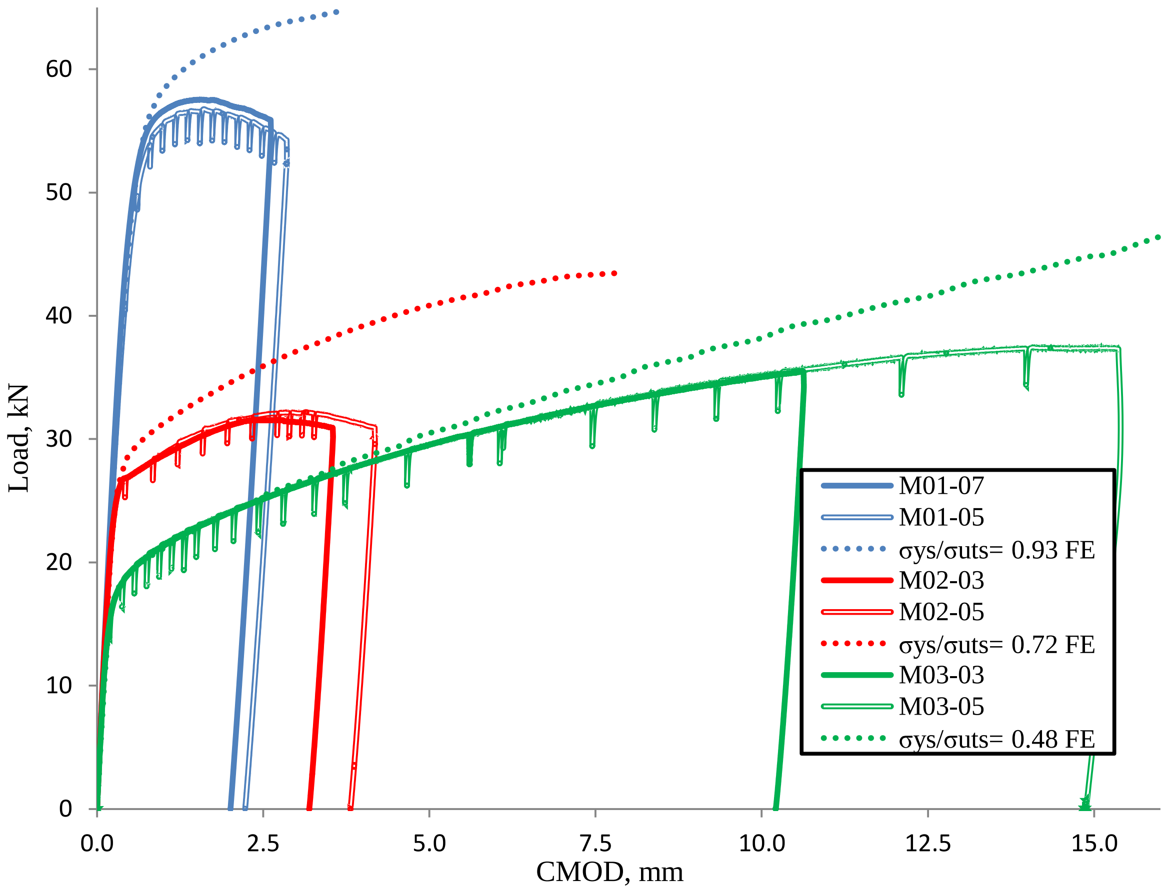

Figure 7.02 Load-CMOD data obtained from the experiment and FE models

In addition to the models based on the experimental specimens, 10 FE models were generated based on the idealised tensile properties described in Chapter 4.2.2, ranging from $0.44 \leq \sigma_{ys}/\sigma_{uts} \leq 0.98$. Similar modelling techniques were applied on models with the same specimen geometry: $B \times 2B$ SEN(B) setup, thickness, B= 20mm and crack ratio, a_0/W= 0.5. Figure 7.03 shows that for the idealised material properties with yield stress, σ_{ys}= 400MPa, increasing strain hardening gives a higher load-CMOD curve.

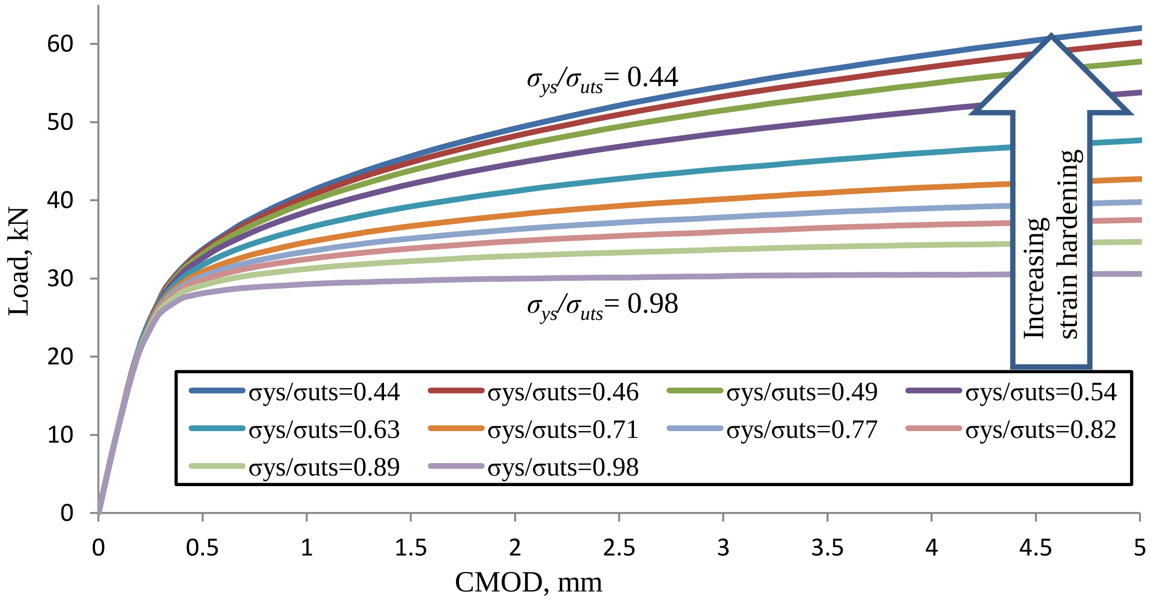

Figure 7.03 Load-CMOD obtained from the models with idealised tensile properties

7.3 CTOD measured from the silicone replicas

The SRC extracted from the test specimens were sliced in the middle and CTOD was measured using an optical microscope. CTOD measured from the SRC were plotted to their respective CMOD (Figure 7.04). There were minor scatter of CTOD measurements from different specimens of the same material. This shows that the silicone compound crack replication is a consistent and reliable method to obtain a physical crack. Generally, lower σ_{ys}/σ_{uts} would result in lower CTOD at the same CMOD.

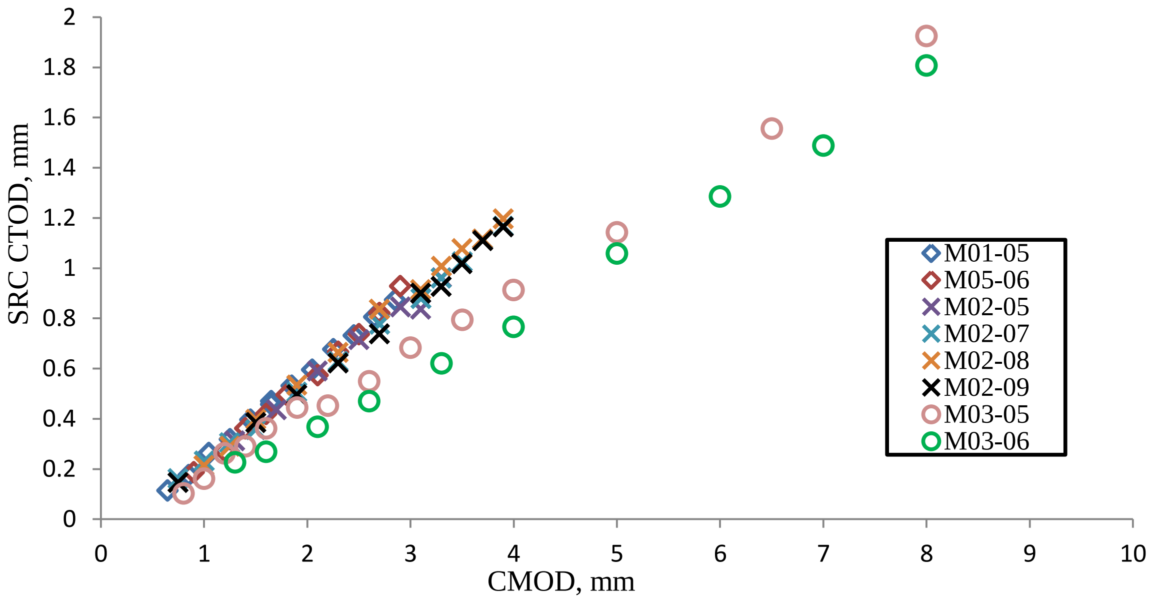

Figure 7.04CTOD measured from the SRC for the increase of CMOD

The crack length, a_0 is one of the parameters affecting the scatter of the measured CTOD from the same material. The validation of the FE models were based on specimens M01-05, M02-05 and M03-05 for the low, medium and high strain hardening material. CTOD from M01-05, M02-05 and M03-05 were shown in Figure 7.05 independent of the repeated test data. The measured CTOD, as well as the point where critical CTOD was determined in a single point test (CTOD based on the point of maximum load) were shown in the figure.

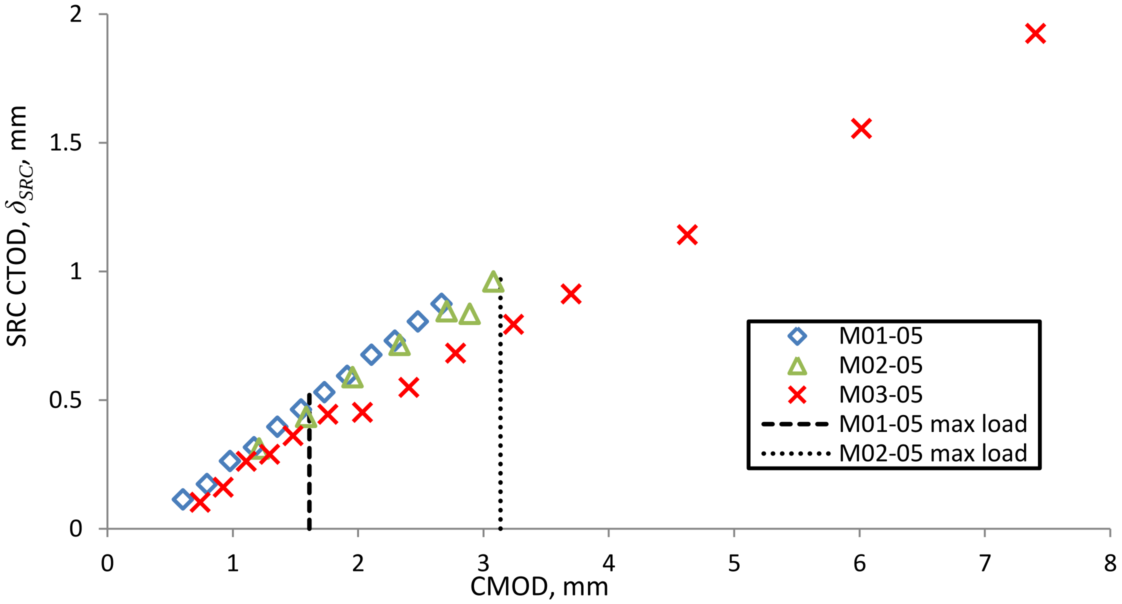

Figure 7.05 CTOD measured from M01-05, M02-05 and M03-05 (low, medium and high strain hardening respectively)

7.4 Results from the FE models

Three FE models (σ_{ys}/σ_{uts}= 0.93, 0.72 and 0.48) were generated based on the test specimens (M01-05, M02-05 and M03-05) to validate the modelling technique. CTOD was extracted from the FE models and plotted for increasing CMOD (Figure 7.06). The crack length used in the FE models were based on the average original crack length measured from M01-05, M02-05 and M03-05. For the range of CMOD> 2.0mm, the low strain hardening model showed the highest CTOD; whereas the high strain hardening model showed the lowest CTOD for the given CMOD.

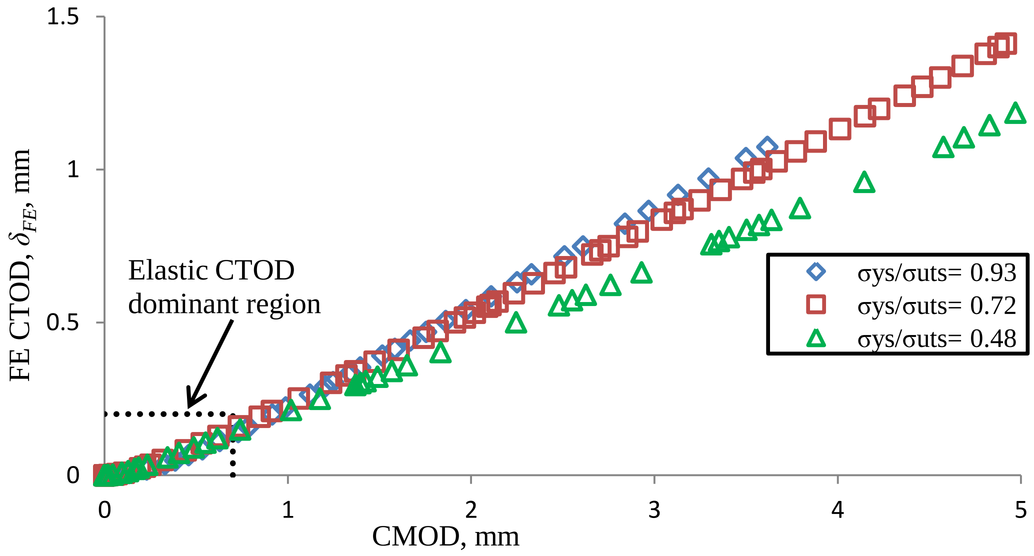

Figure 7.06 CTOD extracted from the FE model for low, medium and high strain hardening properties

In the low CTOD region, CTOD< 0.2mm, CTOD does not increase proportionally to the CMOD (seen in Figure 7.04, Figure 7.05 and Figure 7.06). FE CTOD in the range of CMOD< 0.5mm was shown in Figure 7.07 to highlight the curve during the early stages of loading. The elastic CTOD is dominant in this range (shown in Chapter 5.4) where crack blunting is assumed to occur instead of crack propagation. The non-linear increase of CTOD in this region is due to the transition from elastic dominance to plastic dominance of CTOD.

Observing the FE data for CMOD< 0.5mm, the low strain hardening model showed the highest load-CMOD curve, followed by the medium and high strain hardening model (Figure 7.07). However, the low strain hardening model showed the lowest CTOD-CMOD curve, followed by the medium and high strain hardening model. This is the opposite of that expected, and it was suspected that the odd trend is due to the different initial crack length and yield strength used in the models.

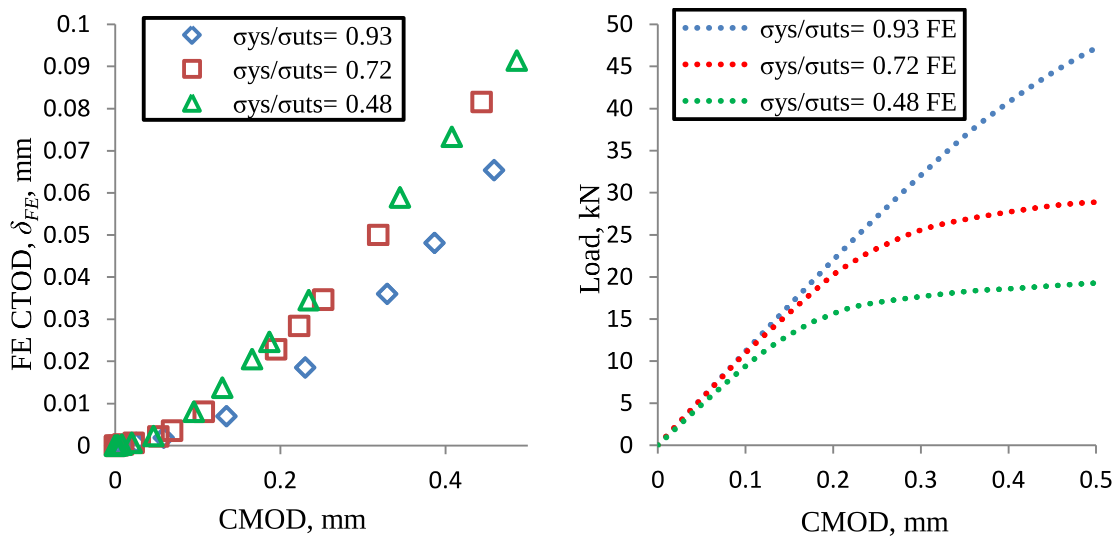

Figure 7.07 Expanded view of the CTOD-CMOD (left) and load-CMOD (right) from the FE model

Based on the FE models with idealised tensile properties, CTOD was extracted and plotted for CMOD (Figure 7.08). The models showed that the lowest strain hardening model, σ_{ys}/σ_{uts}= 0.98 gave the highest CTOD-CMOD curve, and the curve decreases with the increase of strain hardening. To exhibit the CTOD-CMOD and load-CMOD trend in the CMOD< 0.5mm region, the models with idealised tensile properties σ_{ys}/σ_{uts}= 0.44, 0.71 and 0.98 were used to represent high, medium and low strain hardening properties (Figure 7.09).

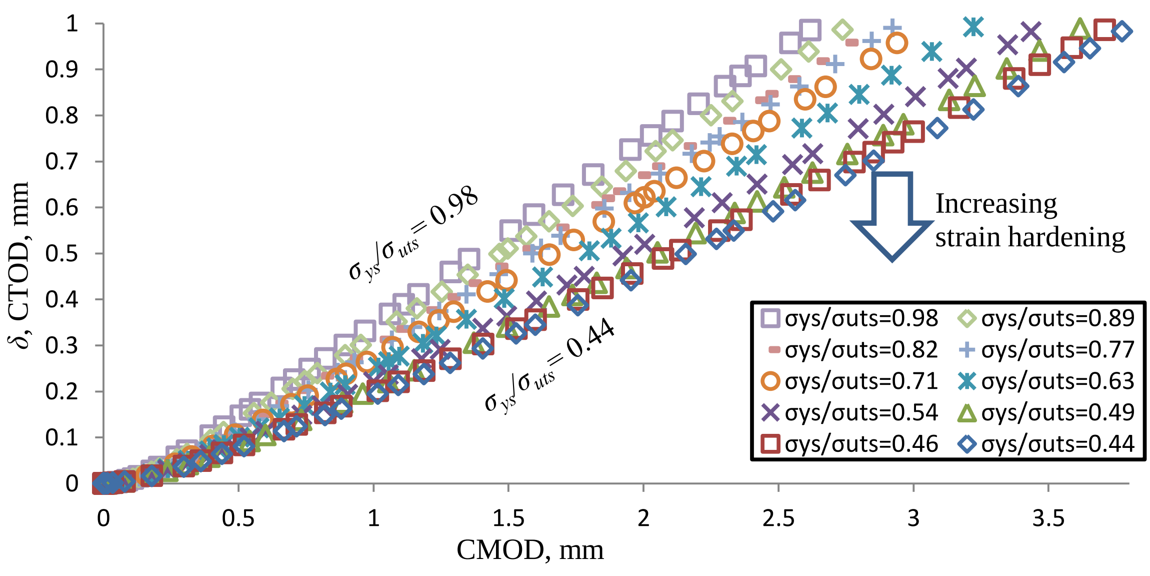

Figure 7.08 CTOD-CMOD curve from the FE models with idealised tensile properties

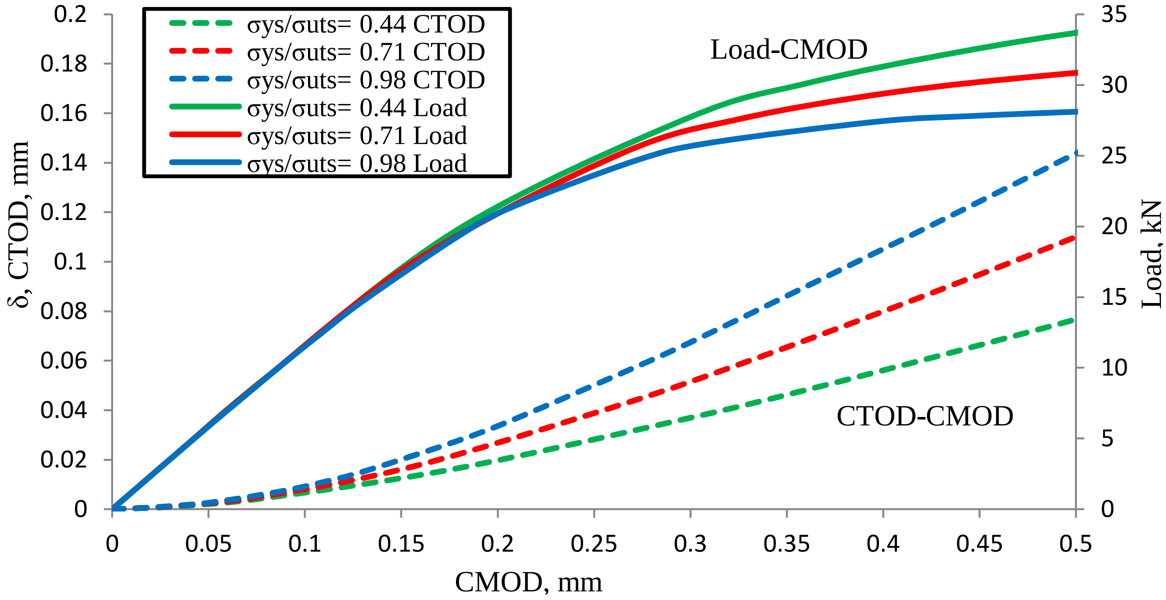

Figure 7.09CTOD-CMOD and load-CMOD curve for CMOD< 0.5mm (σ_{ys}/σ_{uts}= 0.44, 0.71 and 0.98)

Figure 7.09 shows that for different tensile ratio with the same yield strength, higher strain hardening properties would give higher load-CMOD curve, but lower CTOD-CMOD trend. CTOD< 0.2mm is highly affected by the elastic CTOD, and the trend of the CTOD-CMOD curve agrees to the *m* factor used in ASTM and JWES in Chapter 5.5, where decreasing strain hardening would give higher CTOD.

7.5 Discussion

The CTOD values obtained from the SRC tests were considered to be the actual physical CTOD, and thus the baseline as comparison to other methods. CTOD extracted from the FE model for different strain hardening were compared to the SRC CTOD, and a relation was found to improve the FE CTOD prediction. The BS 7448-1, ASTM E1820 and JWES methods were used to estimate SRC CTOD, and it was found that the equations gave different estimations for different material tensile ratios.

7.5.1 Differences between physical and FE CTOD

In a fracture toughness test, the load-displacement data is the primary feedback obtained for fracture toughness estimation. Observing Figure 7.02, it was shown that FE overestimates load for the low and medium strain hardening material. Measuring the crack extension, Δa on the middle of the specimen crack face and the FE model, major underestimation of crack extension was observed in the FE model for the low and medium strain hardening model (Table 7.01), which only accounts for blunting rather than tearing.

Table 7.01 Crack extension, Δa comparison at the CMOD where the specimen is unloaded

	σ_{ys}/σ_{uts}= 0.93	σ_{ys}/σ_{uts}= 0.72	σ_{ys}/σ_{uts}= 0.48
Δa from FE model, mm	0.975	1.11	2.702
Δa from specimen, mm	2.37	3.535	2.94
CMOD at point of specimen unloading, mm	2.855	4.177	15.339
FE Δa underestimation	58.86%	68.60%	8.10%

In a real specimen, stable ductile tearing initiates when the crack tip experiences large deformation; the crack tip continues deforming without tearing in the simple SEN(B) FE model, as this damage mechanism was not accounted for. The remaining intact cross-section area ahead of the crack tip was significantly larger in the FE model compared to the specimens in the low and medium strain hardening material, thus the overestimation of the load data.

To further understand the mode of crack deformation at the crack tip, images of the SRC for increasing CMOD were shown in Figure 7.10, Figure 7.11 and Figure 7.12. Figure 7.10 and Figure 7.11 showed that significant stable crack tearing occurs at the crack tip in the specimens with low and medium hardening properties, whereas more plastic crack tip deformation was observed in the specimen with high strain hardening property. Tearing occurs in the early stages of loading for the low and medium strain hardening material, which led to the FE overestimation of the experimental load-CMOD data in Figure 7.02. The crack tip deforms more plastically rather than tearing for the high strain hardening material (Figure 7.12), which explains the accuracy of the FE load-CMOD data for CMOD< 4mm.

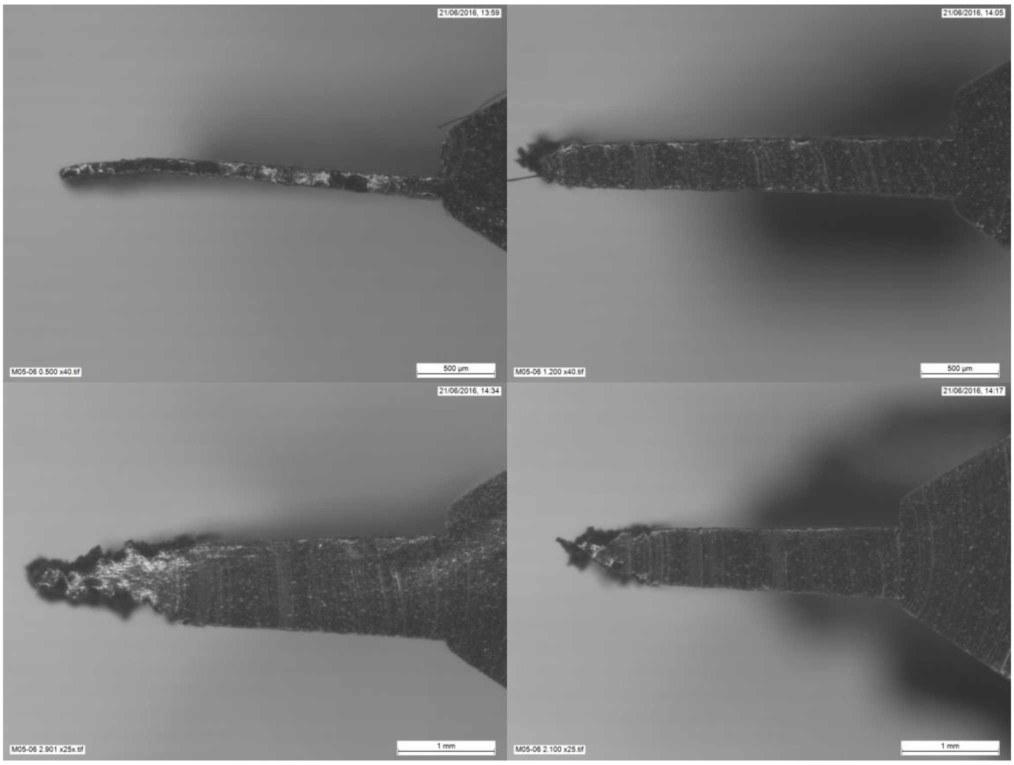

Figure 7.10 SRC from low strain hardening specimen M05-06, CMOD= 0.462, 1.108, 1.938, 2.678 (from top left, clockwise direction)

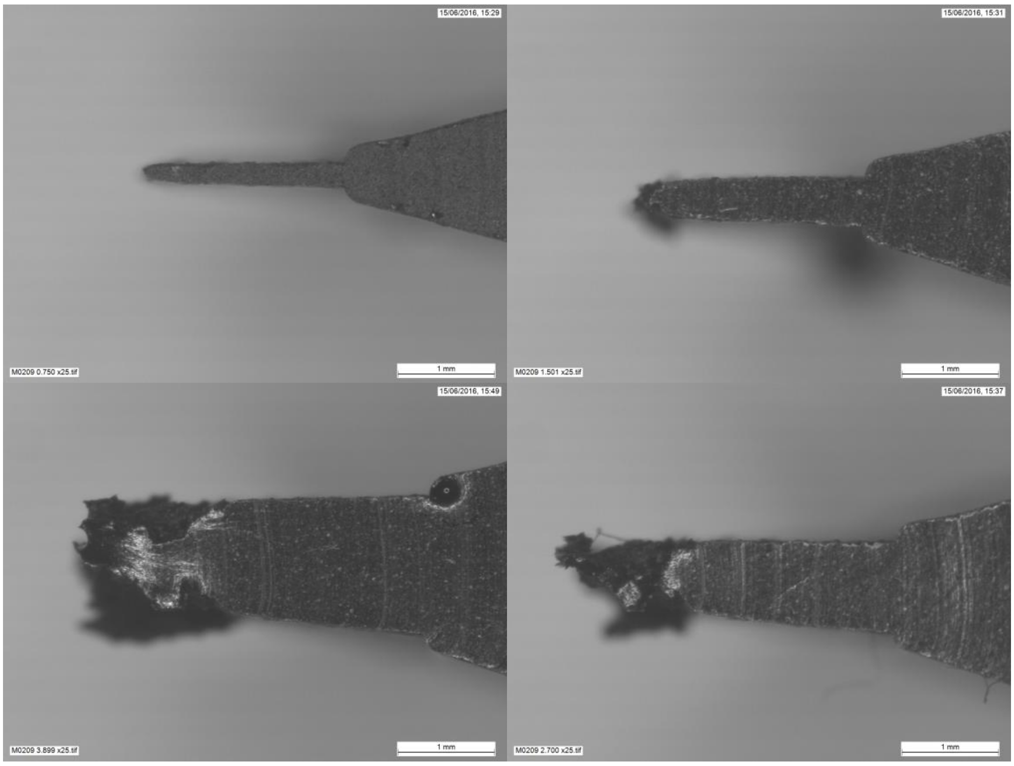

Figure 7.11 SRC from medium strain hardening specimen M02-09, CMOD= 0.692, 1.385, 2.492, 3.599 (from top left, clockwise direction)

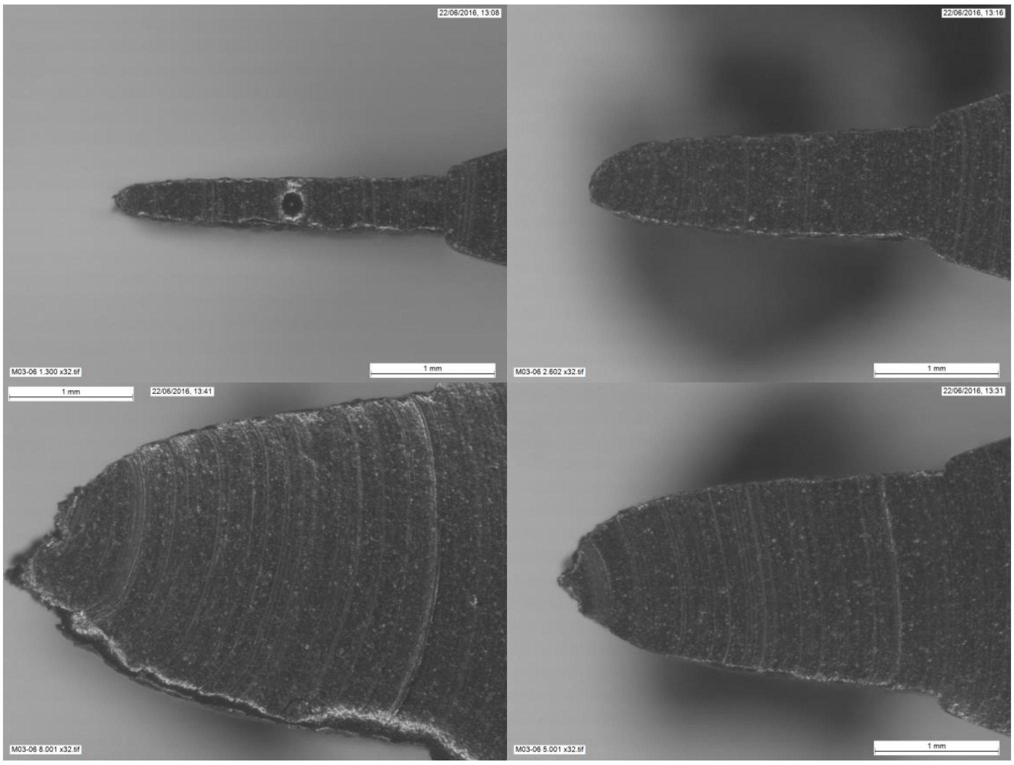

Figure 7.12 SRC from high strain hardening specimen M03-06, CMOD= 1.200, 2.402, 4.616, 7.386 (from top left, clockwise direction)

To investigate the accuracy of the FE model prediction, CTOD obtained from the SRC were compared to the CTOD obtained from the FE model (Figure 7.13). The results showed that FE consistently underestimated CTOD measured on the SRC. The FE model overestimated the low values of CTOD for the high strain hardening material, where CTOD< 0.2mm. This is due to the blunted initial crack tip used in the FE model, which leads to an increase of the stress intensity factor, resulting in higher overall CTOD estimated (Spink et al., 1973; Schindler et tal., 2014).

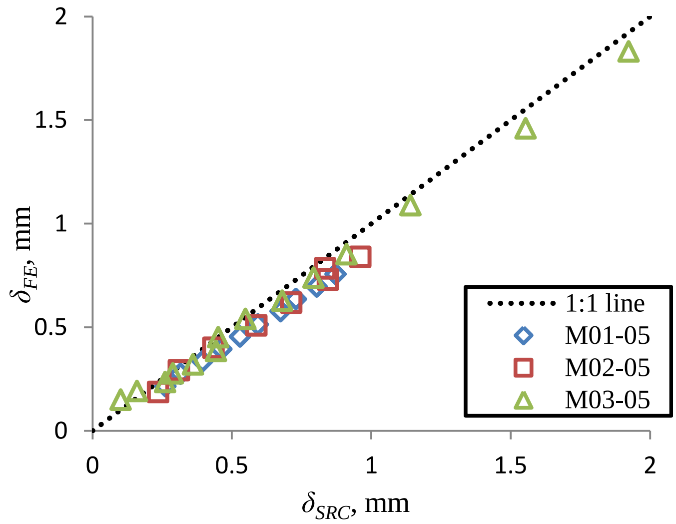

Figure 7.13 Comparison of CTOD extracted from the FE model to the CTOD measured from SRC

The underestimation of CTOD using FE for δ_{SRC}> 0.2mm was due to stable ductile tearing occurring ahead of the crack tip. A diagram comparing an idealized crack tip with and without crack propagation was shown in Figure 7.14. At the same displacement (CMOD), a crack tip with crack extension would result in a larger CTOD compared to a crack tip without crack extension.

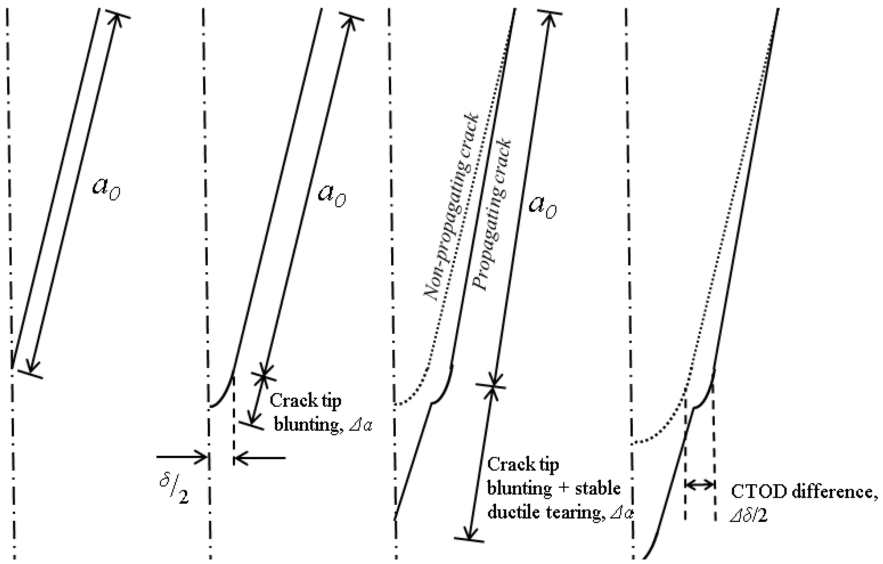

Figure 7.14CTOD on an idealized non-propagating crack (dotted line) and a propagating crack (solid line)

The percentage error of CTOD estimated by the FE model was calculated using

$$ERR_{FE} = \frac{\delta_{FE} - \delta_{SRC}}{\delta_{SRC}} \times 100\% \qquad \text{Eq. 7.01}$$

CTOD below 0.2mm was removed from the analysis due to the effect of the blunted crack tip and the artificial increase of stress intensity factor. Figure 7.15 shows the ERR_{FE} for different tensile ratio. The underestimation of CTOD increases in the FE model with the increase of CTOD. The mean error was -6.9%, -11.8%, and -14.5% for σ_{ys}/σ_{uts}= 0.48, 0.72 and 0.98 respectively.

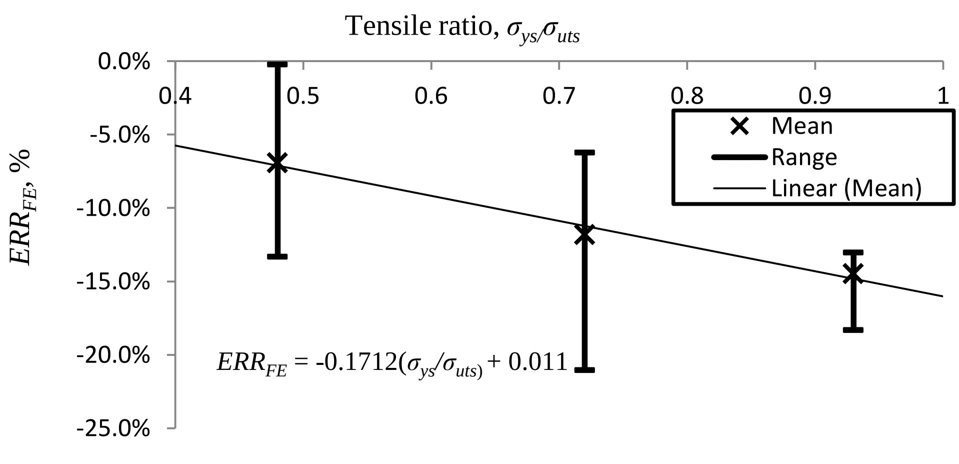

Figure 7.15 FE CTOD estimation error (%) for different tensile ratio

FE is a very powerful tool used in engineering prediction, but the result obtained is dependent on the defined properties and boundary conditions. The simple FE model with a blunted crack tip was able to provide a general estimation to predicting CTOD with limited material properties with good accuracy, whilst underestimating the actual CTOD. Based on the mean values, a linear relation was obtained based on the normalised CTOD for three tensile ratios (Figure 7.15).

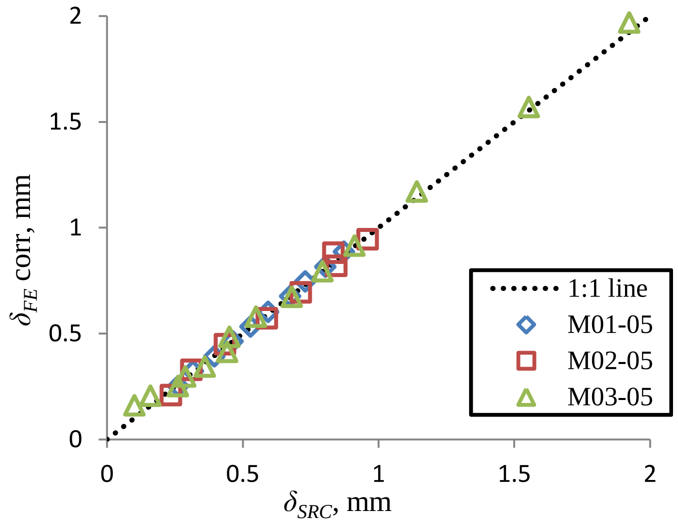

Figure 7.16 Corrected FE CTOD compared vs. the physical CTOD

CTOD extracted from the FE model was corrected using the linear relation obtained in Figure 7.15, $\delta_{FE\ corr}$, and compared to SRC CTOD, δ_{SRC} (Figure 7.16). The linear relation gives a correction to the FE model due to the lack of crack propagation mechanism. The corrected FE CTOD gave an increased accuracy in the prediction of the SRC CTOD, where majority error falls within -5.0%< ERR_{FE}< 5.0% (Figure 7.17).

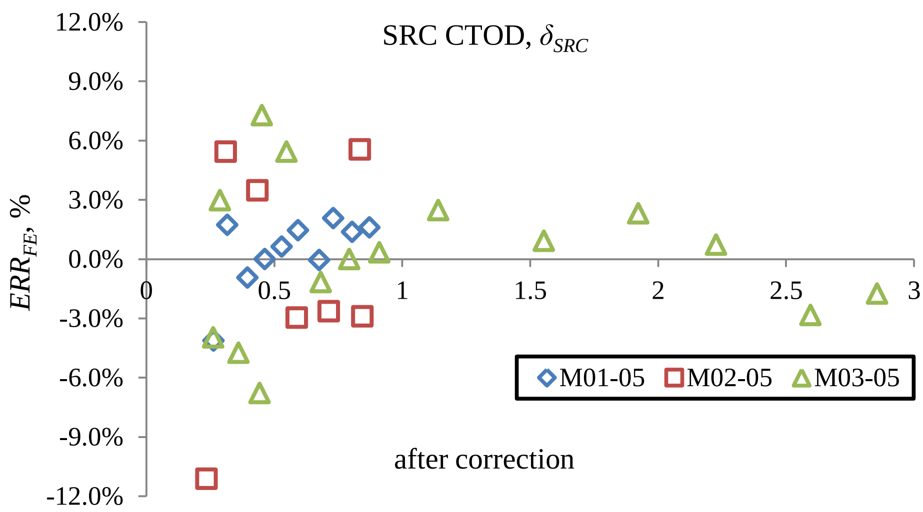

Figure 7.17 Corrected FE CTOD estimation errors, % for increasing SRC CTOD

The mean error obtained using the corrected CTOD was 0.08%, -0.7% and 0.4% for σ_{ys}/σ_{uts}= 0.48, 0.72 and 0.98 respectively. The maximum error was -11.1%. This shows that the corrected FE CTOD managed to improve the accuracy of the CTOD prediction.

Extracting and measuring the actual physical CTOD is not practical and is expensive for commercial fracture toughness estimation. A simple SEN(B) FE model with blunted crack tip is a reliable method to predict the actual CTOD using the modelling approach described in this study.

7.5.2 Validation of the standardized CTOD equations

The results for the different methods to determine CTOD plotted together against the values measured from silicone replicas are shown in Figure 7.18 (a), (b), (c) and (d) for M01, M02, M03 and an expanded view of M03 respectively.

ASTM converts CTOD from *J*, and recognises that *J* no longer characterises the crack tip conditions when high plastic deformation is experienced at the crack tip. The standard recommends a maximum value for δ, described as (ASTM 2014)

$$\delta_{max} = \frac{B_0}{10m} \qquad \text{Eq. 7.02}$$

m is defined in Eq. 5.03a. ASTM CTOD values not conforming to Eq. 7.02 are represented by dotted markers (Figure 7.18(c)).

In the low strain hardening material (M01), all three equations conservatively underestimate the CTOD from the silicone replica. The JWES estimation was most accurate compared to the silicone replicas, followed by ASTM then BS/ISO. JWES CTOD underestimated the SRC CTOD by a maximum of 17.5% at CTOD= 0.927mm.

Similarly, the equations also underestimate CTOD on the medium strain hardening material (M02, Figure 7.18(b)). For CTOD< 0.36mm, the BS/ISO and JWES equation gave very accurate CTOD estimations. BS/ISO and JWES gave very similar values, and were more accurate compared to ASTM. The BS/ISO and JWES equations underestimated the SRC CTOD by the SRC by a maximum of 21.1% and 21% respectively at CTOD= 0.836mm.

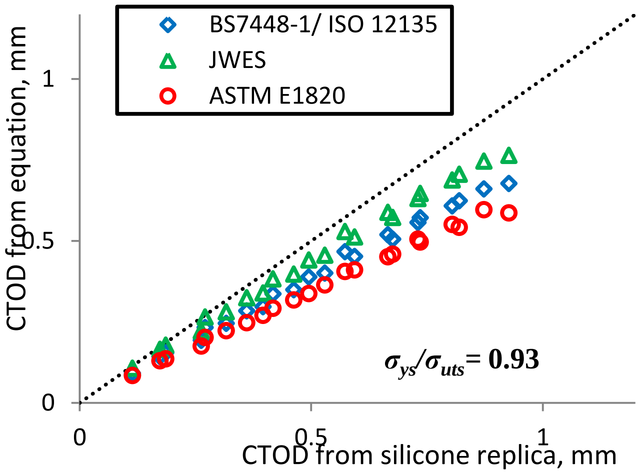
BS7448-1/ ISO 12135
JWES
ASTM E1820
CTOD from equation, mm
CTOD from silicone replica, mm
σ_{ys}/σ_{uts}= 0.93
0
0.5
1

(a)

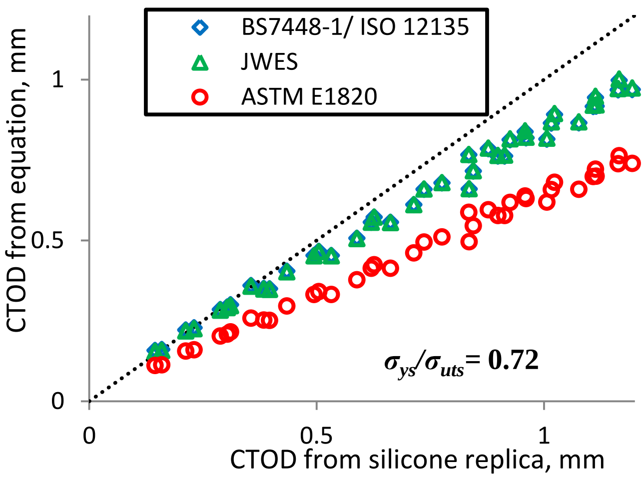
BS7448-1/ ISO 12135
JWES
ASTM E1820
CTOD from equation, mm
CTOD from silicone replica, mm
σ_{ys}/σ_{uts}= 0.72
0
0.5
1

(b)

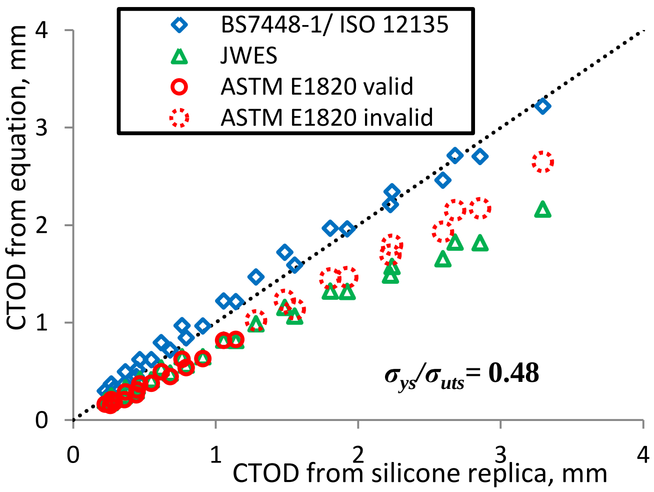
BS7448-1/ ISO 12135
JWES
ASTM E1820 valid
ASTM E1820 invalid
CTOD from equation, mm
CTOD from silicone replica, mm
σ_{ys}/σ_{uts}= 0.48
0
1
2
3
4

(c)

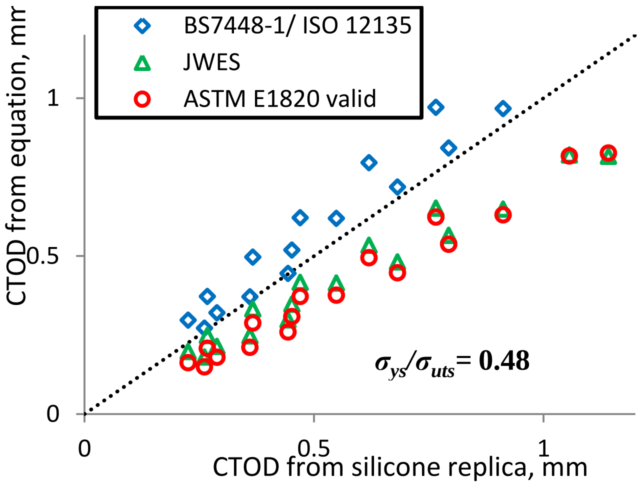

(d)

Figure 7.18 Comparison of CTOD methods for M01, M02, M03 and expanded view for M03 specimen (a, b, c and d [expanded view of c] respectively)

In contrast to the low and medium strain hardening material, CTOD estimated for the high strain hardening material (M03, Figure 7.18(c), (d)) was slightly overestimated with BS/ISO equation. The ASTM and JWES both gave conservative estimates of CTOD, with the JWES being fractionally closer to the SRC measurements at (Figure 7.18(d)).

The experimental results show that the JWES formula, despite being developed only for CTOD up to 0.2mm seems to be conservative for all the different strain hardening steel and most accurate for the low and medium strain hardening steel tested in this work. Even for the highest strain hardening materials, the JWES underestimated CTOD at CTOD> 0.2mm, which would be conservative for assessments of fitness-for-service or acceptance criteria.

The BS/ISO formula does not consider strain hardening, and this is demonstrated by a very different trend when this equation is used for high strain hardening material; a slight overestimation of CTOD. The error is not large, but the method shows reasonable accuracy over a wide range of materials. However, the risk with over-estimation of CTOD is that it predicts higher fracture toughness in a material than is actually the case, which can be potentially unsafe.

The ASTM method was able to adapt to prediction of CTOD in high strain hardening material, but was significantly over-conservative for low and medium strain hardening materials, with the commercial penalties that may potentially give rise to.

The optimum choice for a standard method to determine CTOD is one which gives accurate, but conservative estimates of CTOD for a wide range of materials, and from the comparison of standards shown here, the JWES equation seems to show great promise for inclusion into future international fracture toughness testing standards.

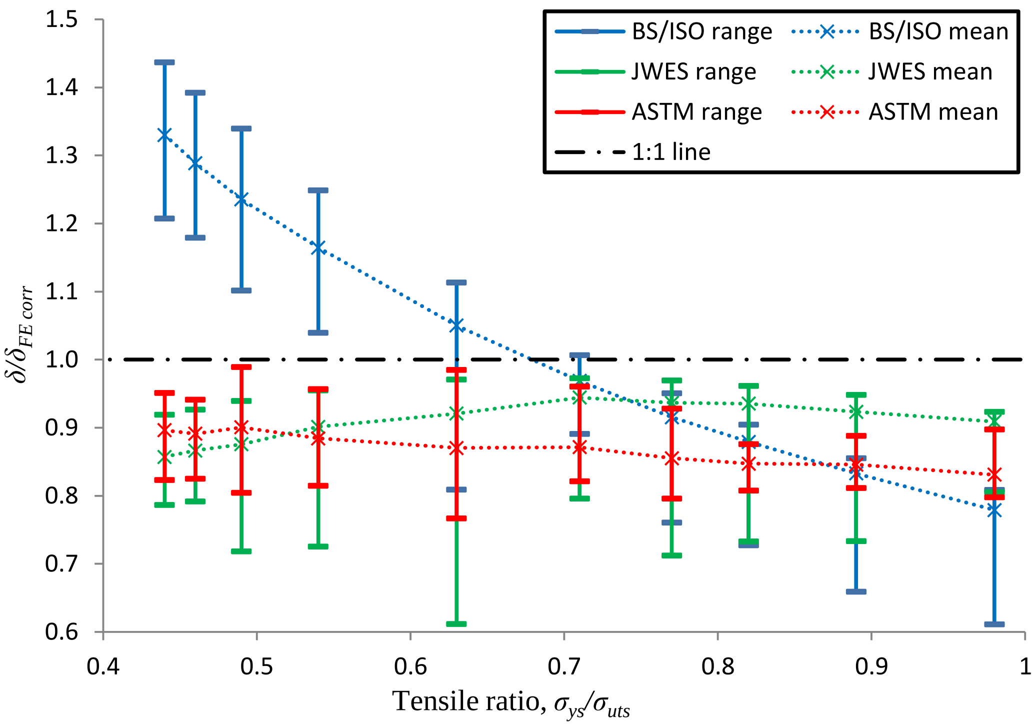

Figure 7.19 The trend of standardized equation prediction of CTOD for different strain hardening properties

Generally, the model gave a good agreement with experimental measurement over the range of CTOD and strain hardening materials, and was consistently closer to the silicone replica CTOD measurements than any of the standard formulae assessed (Figure 7.13 and Figure 7.18). Utilizing FE, CTOD could be estimated using different strain hardening properties, giving better resolution of the performance of the standardised equations. CTOD was extracted from the FE models with idealized material properties from Chapter 4.2.2, and corrected to the ERR_{FE} from Figure 7.15. The corrected FE CTOD, $\delta_{FE\ corr}$ was used to represent the actual CTOD. The standardised equations were used to calculate CTOD based on the load-CMOD data obtained from the FE model. CTOD from equations were normalised to the corrected FE CTOD for validation. Data were compiled for the range of 0.02mm$\leq \delta_{FE\ corr} \leq$ 1.00mm (Figure 7.19). CTOD below 0.02mm were not considered as differences of estimation in this range is too small and not representative of the actual error. The bar shows the upper and lower limit of the CTOD range and the crosses shows the mean value for the standardised CTOD equations. The dotted line connects the mean normalised CTOD to show the trend of CTOD difference for different strain hardening properties.

Similar to that predicted experimentally in Figure 7.18, the BS/ISO equation overestimated the corrected FE CTOD for the high strain hardening model, up to $\sigma_{ys}/\sigma_{uts} \approx$ 0.68. The JWES and ASTM CTOD underestimated the corrected FE CTOD by around 10%-15% regardless of strain hardening properties. The CTOD trend observed in Figure 7.19 is similar to that observed in Figure 7.18.

Apart from very high strain hardening cases, the JWES equation gave the most consistent accuracy in the prediction of the corrected FE CTOD.

7.6 Conclusions

The optimum choice for a standard method to determine CTOD is one which gives accurate, but does not risk overestimating CTOD for a wide range of strain hardening steels. From the comparison of standards shown here, the JWES equation seems to show great promise for inclusion into future international fracture toughness testing standards.

The assumption of a crack tip deforming by continued blunting in a FE model was generally accurate and conservative for the prediction of CTOD for the high strain hardening steel. However caution should be exercised when making predictions within the elastic-dominated CTOD region, where an initial blunt crack tip could lead to over-prediction of CTOD in the FE model. Nevertheless, the FE model used in this work managed to produce relatively accurate predictions of CTOD beyond the elastic dominated loading region.

CTODs calculated using the BS 7448-1/ISO 12135, JWES and ASTM E1820 equations were compared to results obtained experimentally by SRC and from FE modelling. The equations were generally conservative, apart from the BS/ISO equation overestimating CTOD for higher strain hardening materials. For $0.44 \leq \sigma_{ys}/\sigma_{uts} \leq 0.98$, the JWES equation gave a consistently better estimation of CTOD which was not overly conservative

The experiments revealed that the crack tip deformation mechanism in different steels vary, leading to some differences compared to the FE results. SEN(B) fracture toughness specimens in high strain hardening material such as 316 stainless steel deform at the crack tip by continued ‘blunting’ upon increased loading before tearing. This is different to the behaviour of medium and higher strength steels, where stable ductile tearing initiates after only a small amount of blunting at the crack tip during a fracture toughness test. The FE modelling method in this research does not consider tearing.

The equations used for the determination of critical CTOD does not consider the effect of crack extension/ ductile stable tearing, Δa. Based on the standard single point equations, BS 7448-1 gave good estimations of CTOD for the low and medium strain hardening material; whereas the ASTM E1820 and JWES gave better and conservative CTOD estimations for high strain hardening material. Equations considering the effects of crack extension are described in Chapter 8.1. It should also be noted that the rotational factor, r_p is not constant as assumed in BS 7448-1 and JWES, which could had led to inaccuracy in the estimation, further investigated in Chapter 9.1(Wells 1971; Wu 1983; Kolednik 1988).

Chapter 8

Comparison of CTOD formulae for the determination of tearing resistance curve (R-curves) in relation to strain hardening

8.1 Introduction

The tearing resistance curve (R-curve) gives the trend of fracture toughness relative to crack extension. Different to single point fracture toughness tests, where only the critical fracture toughness value is obtained, the R-curve enables the assessment of tearing resistivity of a crack relative to fracture toughness (Figure 8.01).

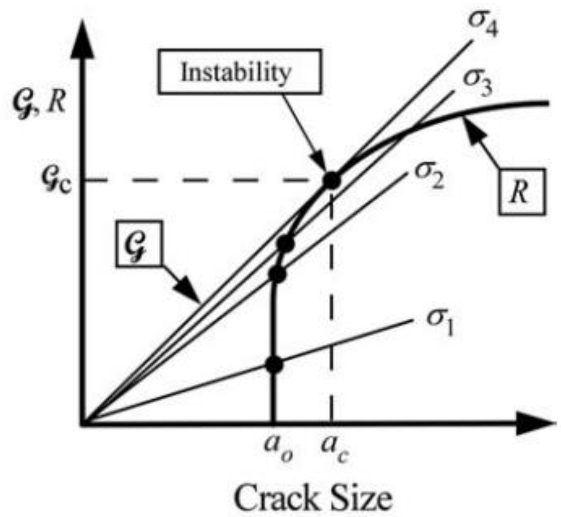

Figure 8.01 Illustration of an R-curve based on the Griffith energy release rate criterion (Anderson 2008, p.38)

Generally, there are two experimental methods to obtain data to generate an R-curve: - multiple specimen method, where multiple fracture toughness specimens were tested to different levels of tearing and evaluated independently, or the unloading compliance technique, where repeated partial loading-unloading cycle is applied on the specimen throughout the test and the crack length is estimated based on the elastic compliance during the loading-unloading cycle (Chapter 1.9.2).

For the data to qualify to the standards, they need to fall within several limits: - the offset line, maximum CTOD limit and maximum crack extension limit (Figure 8.02). To generate an R-curve fit to the data complying with the standards, a 0.2mm offset line is first built parallel to the construction line, which is also known as the blunting line. The construction line represents the blunting of the crack tip as it opens, and the 0.2mm offset line represents the limit of the stretch zone width at the crack tip, before the initiation of stable ductile tearing. The construction line is build based on the following equations,

$$\delta = 1.87\left(\frac{\sigma_{uts}}{\sigma_{ys}}\right)\Delta a$$

in BS 7448-4, and

$$\delta = 1.4\Delta a$$

in ASTM E1820. Both standards specify the limit for crack extension, Δa_{limit} as

$$\Delta a_{limit} = 0.25B_0$$

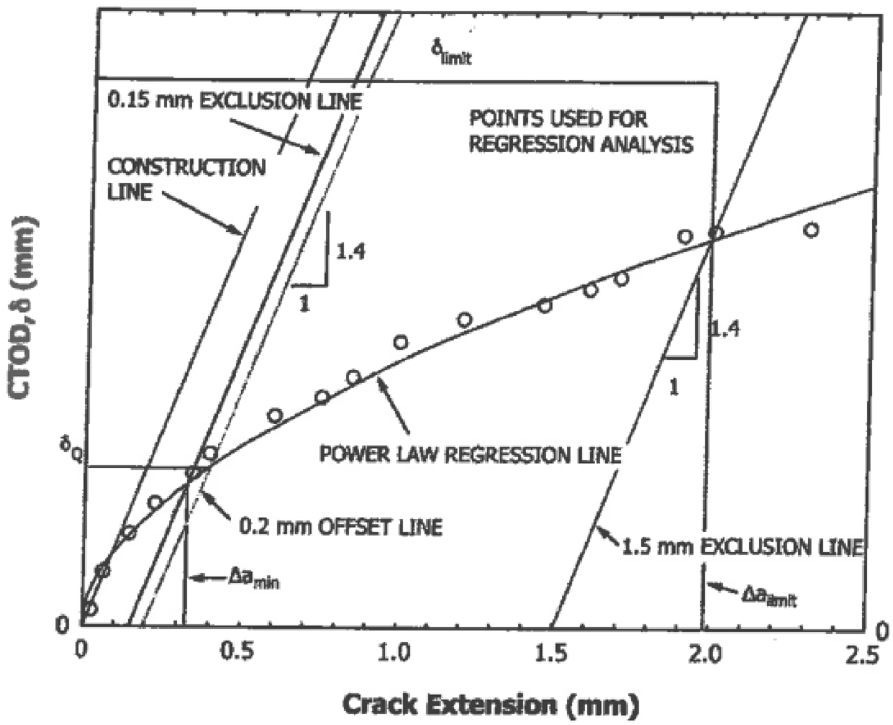

Figure 8.02 Diagram showing the method to extract valid data for R-curve fitting (ASTM 2015)

The limit of maximum CTOD, δ_{limit} is defined differently in BS and ASTM. BS utilizes the smaller of

$$\delta_{limit} = \frac{B_0}{30}$$

And

$$\delta_{limit} = \frac{B}{30}$$

Whereas, ASTM specify the CTOD limit as

$$\delta_{limit} = \frac{B_0}{10m}$$

m is described in Chapter 5.1 and is a function of σ_{ys}/σ_{uts}.

The points encapsulated in the area within the 0.2mm offset line, crack extension limit and maximum valid fracture toughness are fitted to a regression fit trend line. The standards specified recommends the power law regression curve to be fitted to the data, as it gives a better representation of fracture toughness at the initiation of tearing (Carlson & Williams 1981). Additionally, the offset power law regression curve gives a statistically improved representation of the material tearing resistance compared to a linear fit (Gibson & Druce 1985). The curve fitted to the data points would be representative of the R-curve for the given specimen.

8.2 Fracture toughness equations considering crack extension

The BS 7448-4, ASTM E1820 and ISO 12135 specify formulae for the determination of CTOD with the consideration of an extending crack. The equation used in BS 7448-4 does not consider strain hardening, and is primarily based on the fixed rotational point assumption, given as

$$\delta_{(i)} = \frac{K^2(1-v^2)}{2E\sigma_{ys}} + \frac{0.6\Delta a + 0.4(W-a_0)}{0.6(a_0+\Delta a)+0.4W+z} \times V_p \qquad \text{Eq. 8.01}$$

The ASTM E1820 converts CTOD from J for the tearing resistance curve, similar to the theory applied to the single point equation. The conversion is described as

$$\delta_{(i)} = \frac{J_{(i)}}{m\sigma_y}$$

Where $J_{(i)}$ is the addition of the instantaneous elastic and plastic J components,

$$J_{(i)} = J_{el(i)} + J_{pl(i)}$$

The instantaneous elastic J is similar to that used in the single point equation, described as

$$J_{el(i)} = \frac{{K_{(i)}}^2(1-v^2)}{E}$$

The crack extension correction is applied on the plastic J component (Zhu 2009)

$$J_{pl(i)} = \left[J_{pl(i-1)} + \left(\frac{\eta_{pl(i-1)}}{b_{(i-1)}}\right)\left(\frac{A_{pl(i)}-A_{pl(i-1)}}{B_N}\right)\right] \times \left[1 - \gamma_{pl(i-1)}\left(\frac{a_{(i)}-a_{(i-1)}}{B_{0(i-1)}}\right)\right] \qquad \text{Eq. 8.02}$$

Where γ_{pl}= 0.131+2.131($a_{(i-1)}/W$)-1.465($a_{(i-1)}/W)^2$. The concept of loading increment for loading point (i-1) and (i) is described in the diagram in Figure 8.03.

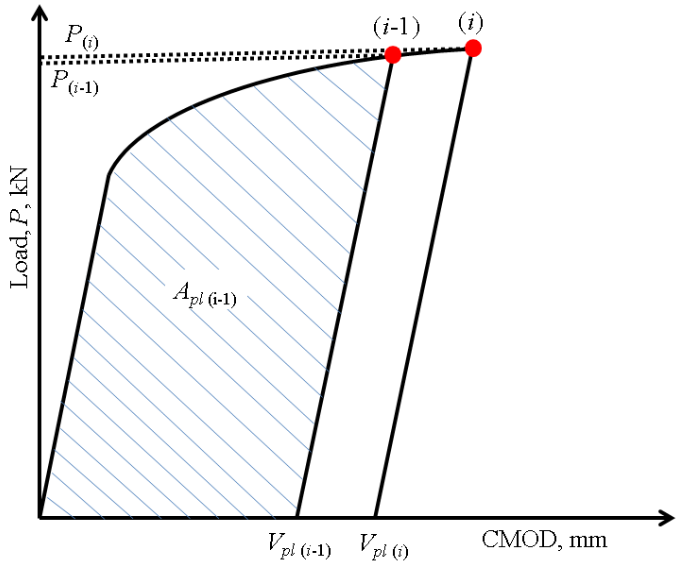

Figure 8.03 Definition of the loading increment concept used in ASTM E1820

ISO 12135 adopted the *J* conversion method for the determination of CTOD for tearing resistance curve (ISO 2016). The equation is the same as used in ASTM E1820, except the plastic component of *J*: ISO only allow the plastic work, U_p to be determined based on the load-line displacement, LLD, whereas ASTM allows plastic work to be determined from both CMOD and load-line displacement. ISO used a different crack extension factor compared to that in ASTM. The plastic *J* used in ISO is shown below

$$J_{pl(i)} = \frac{1.9U_p}{B_N B_0} \times \left(1 - \frac{\Delta a}{2B_0}\right) \quad \text{Eq. 8.03}$$

Experimentally, *J* can be described as

$$J = \frac{\eta A}{B_N B_0}$$

Where *A* is the work applied on the specimen, described as the area under the load-displacement curve. ISO 12135 allows the load-line displacement, *q* to be estimated using data from two clip gauges mounted above the crack mouth at different height based on the equation below (ISO 2016)

$$q = \frac{S}{2}\tan\left\{\sin^{-1}\left[\frac{V_2 - V_1}{2(z_2 - z_1)}\right]\right\} \quad \text{Eq. 8.04}$$

To highlight the difference between the different displacements, the plastic *J* component calculated using LLD and CMOD were normalised to the J values at the point of maximum load, $J_{pl\ LLD}/J_{pl\ LLD\ max\ load}$ and $J_{pl\ CMOD}/J_{pl\ CMOD\ max\ load}$ respectively. Data before 20% maximum load is not considered in the comparison, as the scatter of data in this range is mainly due to the stabilising of loading applied by the machine. Figure 8.04 shows that J_{pl} based on LLD gave a very good correlation to the J_{pl} based on CMOD.

Zhu derived a LLD estimation based on the following relationship, where for the same loading point, (Zhu et al. 2008; Zhu & Leis 2008)

$$\frac{V_{pl\,CMOD}}{V_{pl\,LLD}} = \lambda$$

Where λ is a function of the instantaneous crack length- specimen width ratio, $a_{(i)}/W$. Based on the relationship above, the plastic work between loading point (i-1) to (i) based on LLD can be calculated using plastic CMOD data, given below

$$A_{pl\,LLD}^{i-1,1} = \frac{1}{2}(P_i + P_{i-1})\left(\frac{V_{pl\,CMOD}^{i}}{\lambda_i} - \frac{V_{pl\,CMOD}^{i-1}}{\lambda_{i-1}}\right)$$

Although Eq. 8.04 is different to that derived by Zhu in his research (which is based on plastic work rather than geometrical evaluation), they both showed that J calculated based on CMOD and LLD gives a consistent minimal difference(Zhu et al. 2008; Zhu & Leis 2008). Zhu also showed that LLD calculated based on the CMOD conversion agrees well with the LLD measured. Therefore, in general conditions, it can be considered that J calculated using CMOD is representative and equivalent of J calculated using LLD.

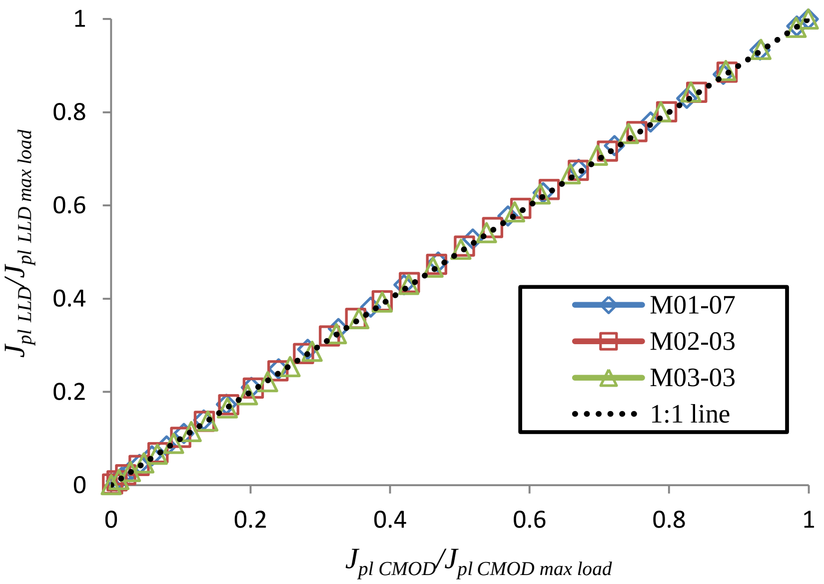

Figure 8.04 Comparison of the normalised plastic J's, $J_{pl\,LLD}/J_{pl\,LLD\,max\,load}$ and $J_{pl\,CMOD}/J_{pl\,CMOD\,max\,load}$

8.3 Effect of crack extension correction factor on the determination of *J*/CTOD

The main difference between the CTOD equations used for R-curve assessment and single point fracture toughness assessment is the consideration of crack extension, Δa. The standard methods determine R-curves by calculating the instantaneous CTOD (or J) based on the initial crack length and then apply a correction factor to account for crack extension. To highlight the effect of crack extension relative to the single point equations, the crack extension correction factors were evaluated independently for BS 7448-4, ASTM E1820 and ISO 12135.

The supporting evidence describing the crack correction component in the BS 7448-4 CTOD R-curve equation is unknown to the author. To isolate the crack correction component in the BS equations, the CTOD R-curve equation in BS 7448-4 is compared to its single point CTOD equation counterpart in BS 7448-1

$$\delta_{pl\ BS7448-4} = \delta_{pl\ BS7448-1} \times X$$

X is described as the crack extension correction factor for the BS equation. Expanding the terms gave

$$X \times V_p \frac{0.4B_0}{0.4B_0 + a_0 + z} = V_p \frac{0.6\Delta a + 0.4B_0}{0.6\Delta a + 0.4B_0 + a_0 + z}$$

Given that $a_0 + z = T$, $0.6\Delta a = U$, and $0.4B_0 = S$,

$$X \times \frac{S}{S + T} = \frac{U + S}{U + S + T}$$

Rearranging the terms,

$$X \times \frac{S}{U + S} = \frac{S + T}{U + S + T}$$

$$1 + \frac{U}{S + T} = \left(1 + \frac{U}{S}\right)\frac{1}{X}$$

$$X = \frac{\left(1 + \frac{U}{S}\right)}{\left(1 + \frac{U}{S + T}\right)}$$

Where X results in

$$X = \frac{1+\frac{0.6\Delta a}{0.4B_0}}{1+\frac{0.6\Delta a}{0.4B_0+a_0+z}} \quad \text{Eq. 8.05}$$

The ASTM and ISO crack correction factor is applied in J calculation, before being converted into CTOD. The basic concept of J correction for incremental crack growth is described in Figure 8.05. For a stationary non-growing crack where $a = a_i$, the amount of work experienced by the specimen for displacement Δ_{pl}^{i} to Δ_{pl}^{i+1} can be described by the shaded area under AB. However, for incremental crack growth, where $a = a_i+1$, the amount of work experienced by the specimen for displacement Δ_{pl}^{i} to Δ_{pl}^{i+1} can be described by the shaded area under AC. The area ABC can be described as the reduced work due to the extended crack length for the displacement increment, Δ_{pl}^{i} to Δ_{pl}^{i+1}.

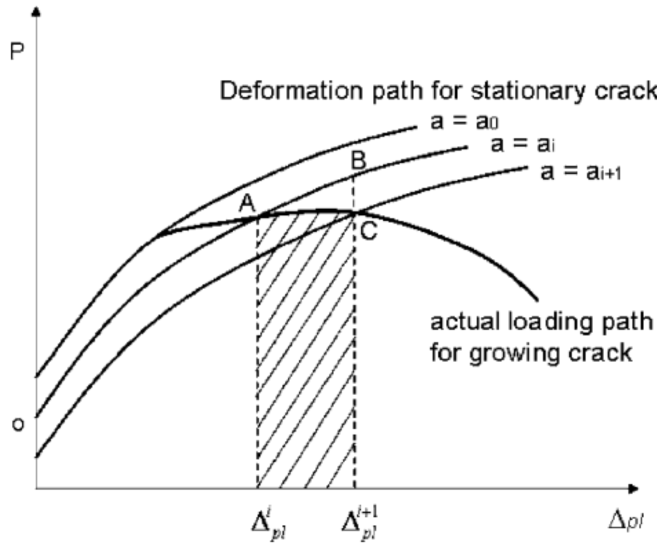

Figure 8.05 The concept of *J*-based crack correction for increasing crack length (Zhu et al. 2008)

The J based correction factor for incremental crack extension is described as Y. In ASTM E1820, the main J component is calculated for every crack increment. The incorporation of the ASTM crack correction factor, Y_{ASTM} is

$$J_{pl(i)} = \left[J_{pl(i-1)} + \left(\frac{\eta_{pl(i-1)}}{b_{(i-1)}}\right)\left(\frac{A_{pl(i)} - A_{pl(i-1)}}{B_N}\right)\right] \times Y_{ASTM}$$

$$Y_{ASTM} = \left[1 - \gamma_{pl(i-1)}\left(\frac{a_{(i)}-a_{(i-1)}}{B_{0(i-1)}}\right)\right] \quad \text{Eq. 8.06}$$

In ISO 12135, the effect of incremental crack growth is only applied on the ISO crack correction factor, Y_{ISO}

$$J_{pl(i)} = \frac{1.9U_p}{B_N B_0} \times Y_{ISO}$$

$$Y_{ISO} = \left(1 - \frac{\Delta a}{2B_0}\right) \quad \text{Eq. 8.07}$$

Based on the general specimen geometry used in the experiments (Bx$2B$, B=20mm, a_0/W= 0.45), the crack extension correction factors, X and Y are calculated. The crack extension factor used for the CTOD (BS 7448-4) and J (ASTM E1820 and ISO 12135) gives a different trend relative to the single point data. For an increasing crack length- the remaining ligament length ratio, $a_{(i)}/B_{0(i)}$ (increasing crack length), X gives an increasing value, whereas Y shows decreasing value (Figure 8.06 and Figure 8.07).

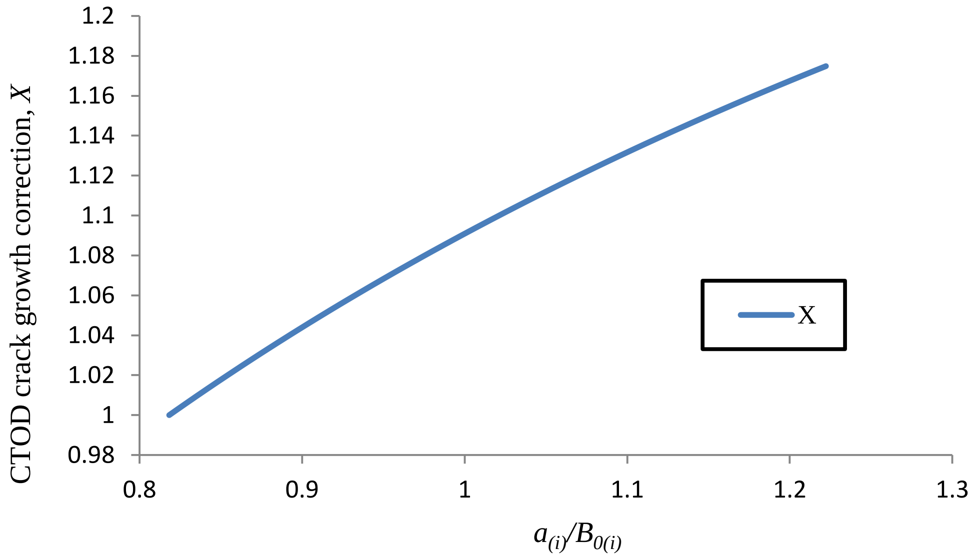

Figure 8.06The crack correction factor used in BS 7448-4 for increasing $a_{(i)}/B_{0(i)}$

The crack extension factors, Y_{ASTM} and Y_{ISO} decreases with increasing $a_{(i)}/B_{0(i)}$. However, Figure 8.07 showed that the main difference of Y_{ASTM} and Y_{ISO} is the magnitude. For the same specimen and crack parameter, Y_{ASTM} showed an approximate constant value of 0.998, whereas Y_{ISO} showed decrease from 1 to 0.91. Therefore comparatively, ISO would give lower values of J and CTOD for R-curves than ASTM.

For Y_{ASTM}, the instantaneous crack growth- remaining crack length ratio, $(a_{(i)}-a_{(i-1)})/B_{0(i-1)}$ is the determinant of the crack correction factor value. Figure 8.08 shows that for the same amount of total crack extension, the different rate of crack extension would result in different Y_{ASTM}. The figure shows that for increasing crack growth rate, Y_{ASTM} would give lower values and higher difference compared to a stationary non-growing crack. This suggests that in the case of a single specimen unloading compliance test, assuming the same specimen, the increase of the loading-unloading cycle would lead to a smaller decrease in Y_{ASTM}.

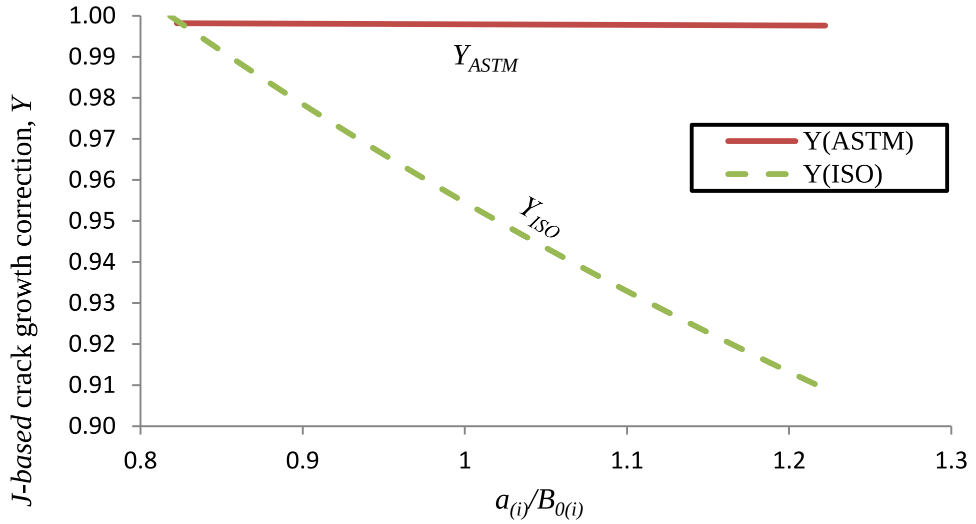

Figure 8.07Comparison of the ASTM E1820 and ISO 12135 crack correction factor for increasing $a_{(i)}/B_{0(i)}$

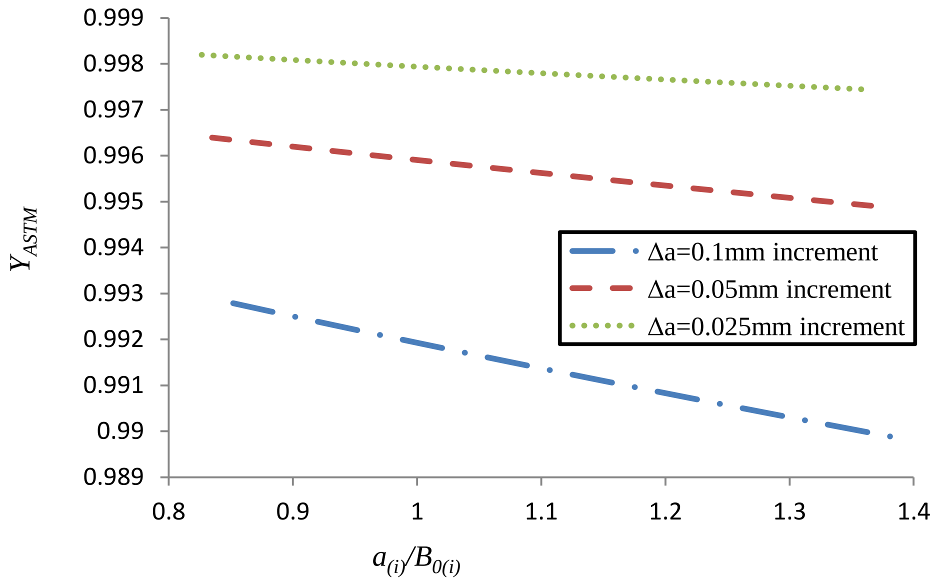

Figure 8.08 The effect of the crack extension rate to the crack correction factor in ASTM E1820

Chapter 5.3 showed that the *J*-based ASTM procedure almost always give lower CTOD compared to the other standards, and Chapter 7.5.2 showed that ASTM underestimate CTOD measured from the silicone replicas. Figure 8.08 showed that the Y_{ASTM} gives minimal difference to the plastic *J* component. The crack correction factor would lead to negligible difference to the resultant corrected plastic *J*, where Figure 8.08 showed that it would lead to a maximum of 1% decrease in *J*. The Y_{ASTM} does not improve the accuracy for CTOD, but yet increases the complication for calculation.

8.4 Experimental results and analysis

This experimental investigation into these different R-curve formulae is comprised by three main experimental investigations: -

- Observations on plane sided and side-grooved unloading compliance specimens
- R-curve obtained by from measuring the silicone replicated cracks
- Validation of the BS 7448-4, ASTM E1820, ISO 12135 and WES 1108 CTOD equations for R-curve

In this study, the single specimen unloading compliance method was used to obtain the R-curve data. The unloading compliance method evaluates the intermediate crack extension during the load-unloading cycle based on the elastic compliance (Willoughby 1981). Complete details and data obtained from the tests reports were compiled in Appendices.

The experimental data were fitted to the offset regression power law curve described in BS 7448-4. For the consistency of comparison of all three strain hardening materials, data points yielding negative crack extension were excluded from the curve fitting. The limit for the maximum valid CTOD limit and the maximum crack extension specified in the standards were ignored for the curve fitting, as this gives a better resolution of the curve.

The offset power law equation used for curve fitting of the data is described as

$$\delta = m + l(\Delta a)^x \qquad \text{Eq. 8.08}$$

The best fit correlation coefficient, r is calculated using x values from 0.01 up to 1.00, in steps of 0.01. The x value that gives the maximum correlation would provide the best fit for the data.

$$r = \left[\sum\{\delta_i(\Delta a_i)^x\} - \frac{\sum \Delta a_i{}^x \sum \delta_i}{k}\right]\left[\left\{\sum \delta_i{}^2 - \frac{(\sum \delta_i)^2}{k}\right\}\left\{\sum \Delta a_i{}^{2x} - \frac{(\sum a_i{}^x)^2}{k}\right\}\right]^{0.5}$$

The equations for coefficients l and m are given as

$$l = \left\{\sum \delta_i{}^2 - \frac{(\sum \delta_i)^2}{k}\right\}^{0.5}\left\{\sum \Delta a_i{}^{2x} - \frac{(\sum \Delta a_i{}^x)^2}{k}\right\}^{-0.5}$$

$$m = \frac{(\sum \delta_i - l \sum \Delta a_i{}^x)}{k}$$

The crack extension parameter used for R-curves is based on the predicted average crack extension across 9 points ahead of the fatigue crack tip, measured on the crack face (Figure 8.09). However, this approach is not practical for the silicone crack replicas, as it is difficult to slice 2.5mm thick portion consistently. For estimation purposes, the crack extension was measured from the middle thickness, and the crack length on the remaining 8 points across the crack tip were predicted based on the final crack length measured on the crack face.

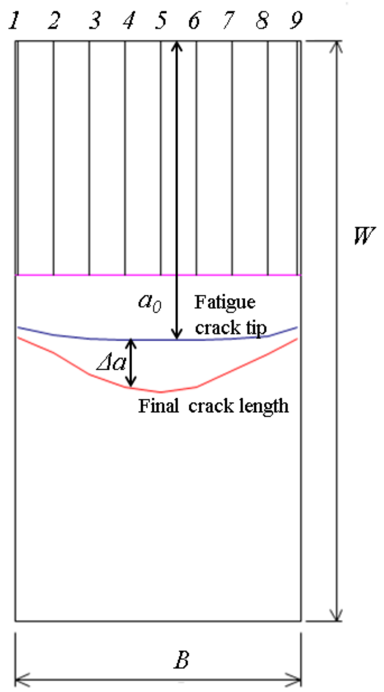

Figure 8.09 Sectioning of the crack face for the measurement of crack length and crack extension

For the average crack length prediction, Δa_{avg}, the crack was assumed to grow symmetrically. To obtain the relative positional crack ratio, R_{pos}, crack extension on the symmetrical position are averaged and normalized to the crack extension in the middle of the crack

$$\frac{\Delta a_{1,2,3,4} + \Delta a_{9,8,7,6}}{2 \times \Delta a_5} = R_{pos\ 1\&9,2\&8,3\&7,4\&6}$$

For calculation of Δa_{avg} based on the middle crack length,

$$\Delta a_{avg} = \frac{\Delta a_5 (1 + R_{pos\ 1\&9} + R_{pos\ 2\&8,} + R_{pos\ 3\&7} + R_{pos\ 4\&6})}{5} \qquad \text{Eq. 8.09}$$

The Δa_{avg} calculated using Eq. 8.09 was used as representation of the average crack extension for the silicone crack replicas.

8.4.1 The effects of material strain hardening properties on R-curves

Standard single specimen unloading compliance tests were performed on the three strain hardening materials used in this work, each on a plane sided and side grooved specimen. After processing the test data into CTOD based on BS 7448-4, the data was fitted to the offset power law described above, shown in Figure 8.10. The fitting data for crack extension below 0.2mm were not shown, as the crack extension in this region is mainly influenced by crack blunting, also described as the stretch zone. The unprocessed CTOD-crack extension data for the plane sided and side-grooved specimens are compiled in the Appendices.

Generally, it could be seen that the R-curve slope increases with strain hardening. The gradient of the slope exhibited by the R-curve reflects the level of crack tip constraint of the specimen, as well as a measure of tearing resistance. A highly constraint specimen would give a flatter slope; a lower constraint specimen gives a steeper slope (Zhou et al. 2009; Zhou 2011; Huang et al. 2014). In addition, a flatter curve implies lower resistance to tearing; a steeper curve suggests a higher resistance to tearing. The side groove removes some of the plane stress region on the sides of the crack, forcing the remaining thickness of the specimen, B_n to be plane strain dominant, and the tearing to progress in the same plane as the pre-crack, rather than to form shear lips. The plane strain region is more highly constrained, which generally results in a flatter R-curve slope (Turner & Etemad 1990). Additionally, higher constraint gives a lower tearing initiation fracture toughness value, which is loosely represented by CTOD values at Δa= 0.2mm (Vassilaros et al. 1980). However, this is not obvious on the low strain hardening material, most probably due to the limited number of specimens tested, high crack tip constraint and relatively low tearing resistance.

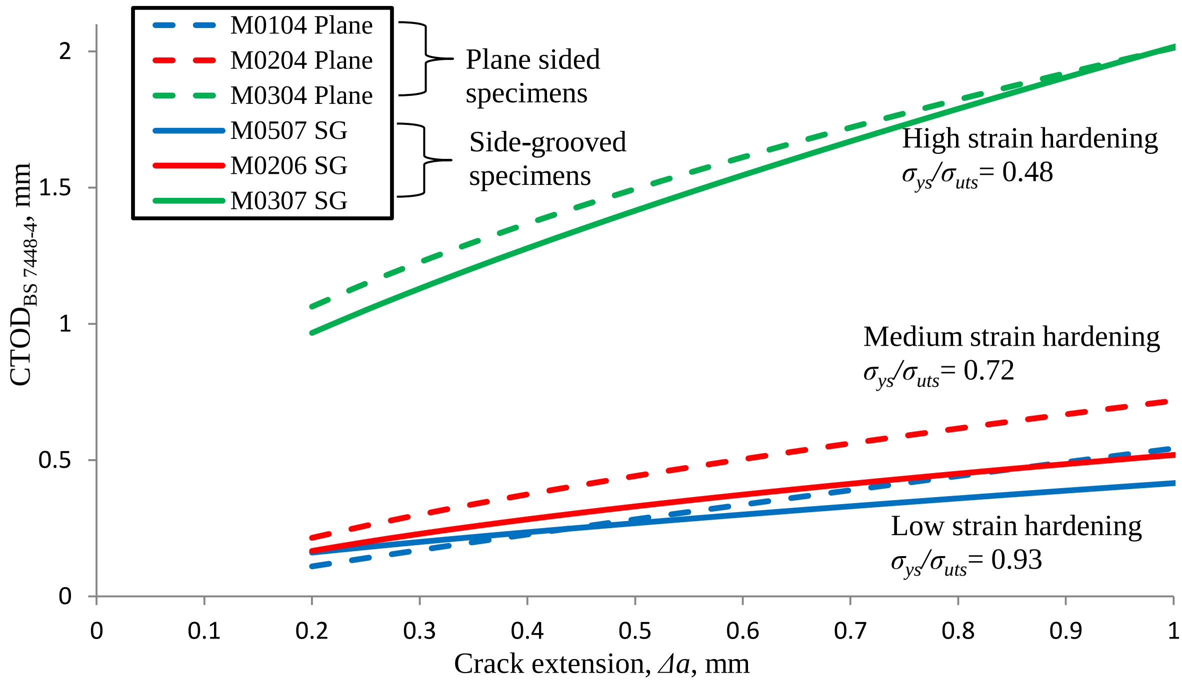

Figure 8.10 Plane sided and side grooved unloading compliance tests with fitted offset power law curve

8.4.2 R-curve based on silicone replica measurements

The silicone replicated cracks obtained from the modified standard tests were considered physical representation of the actual crack. CTOD and crack extension measurements were obtained from the silicone replicas, and curve fitted to obtain an R-curve (Figure 8.11, Figure 8.12 and Figure 8.13). The fitting coefficients were given in Table 8.01. The R-curves fitted to the measurements were fairly consistent for the same material, particularly for the high strain hardening material. Some scatter was observed on the R-curve for the medium and low strain hardening material. The inconsistency is mainly due to the material's lower resistance to crack extension.

To obtain a representative R-curve for each material, the R-curve data from the silicone replicas from the same material was averaged and plotted (Figure 8.14). Similar to that observed in Figure 8.10, the high strain hardening material showed the steepest slope (lowest crack tip constraint, higher tearing resistance), followed by the medium strain hardening material then the low strain hardening material (highest crack tip constraint, lower tearing resistance).

Table 8.01 Curve fitting coefficients for the silicone replica specimens

	x	*l*	*m*
M01-05	0.66	0.709326	0.026682
M05-06	0.63	0.92351	0.008924
M02-05	0.01	43.17085	-42.2108
M02-07	0.64	0.765718	-0.02991
M02-08	0.16	2.602425	-1.63739
M02-09	0.13	2.517419	-1.60263
M03-05	0.87	2.145926	-0.11897
M03-06	0.86	1.934779	-0.02571

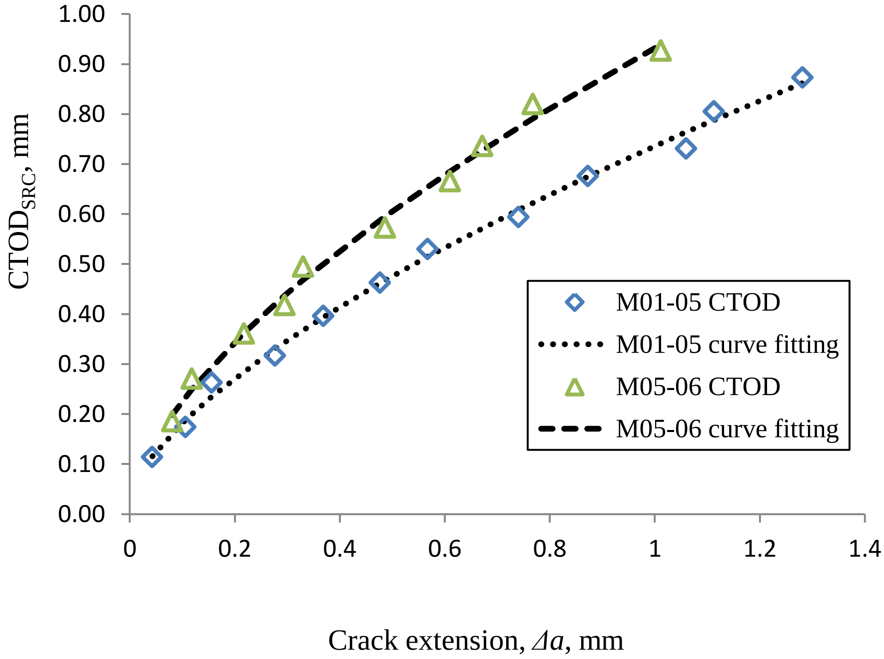

Figure 8.11 CTOD R-curve for low strain hardening material, σ_{ys}/σ_{uts}= 0.93

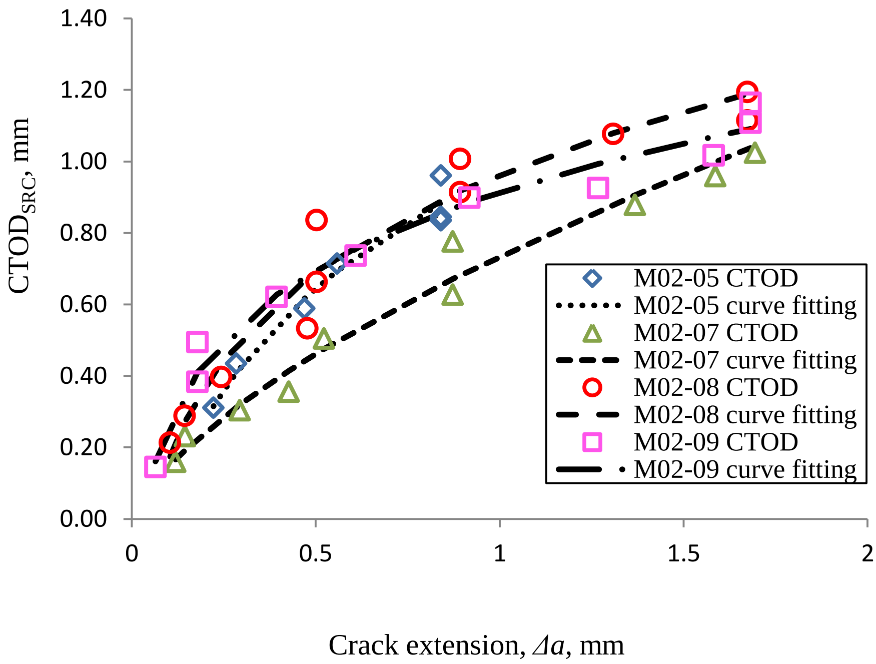

Figure 8.12 CTOD R-curve for medium strain hardening material, σ_{ys}/σ_{uts}= 0.72

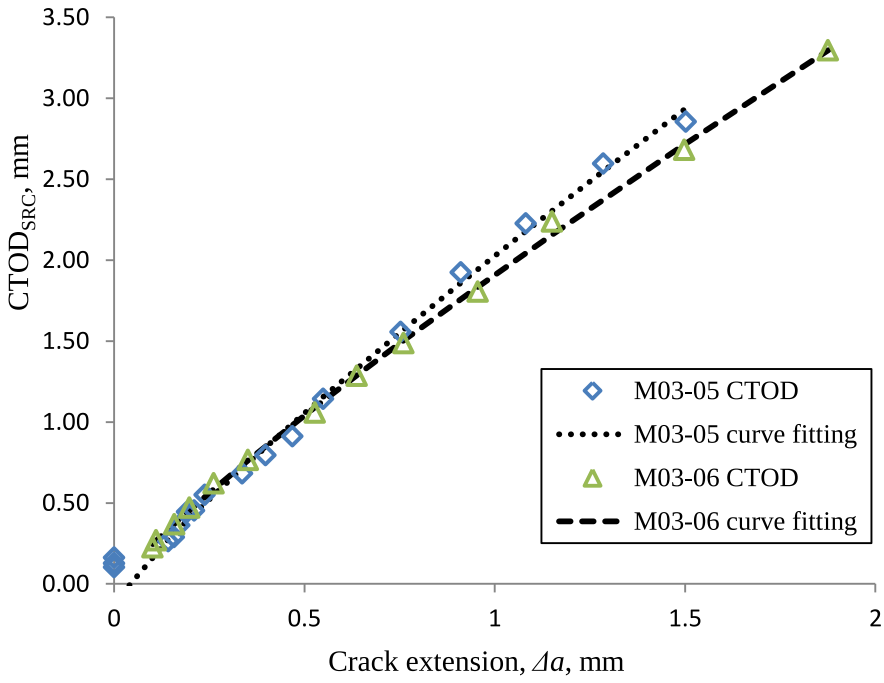

Figure 8.13 CTOD R-curve for high strain hardening material, σ_{ys}/σ_{uts}= 0.48

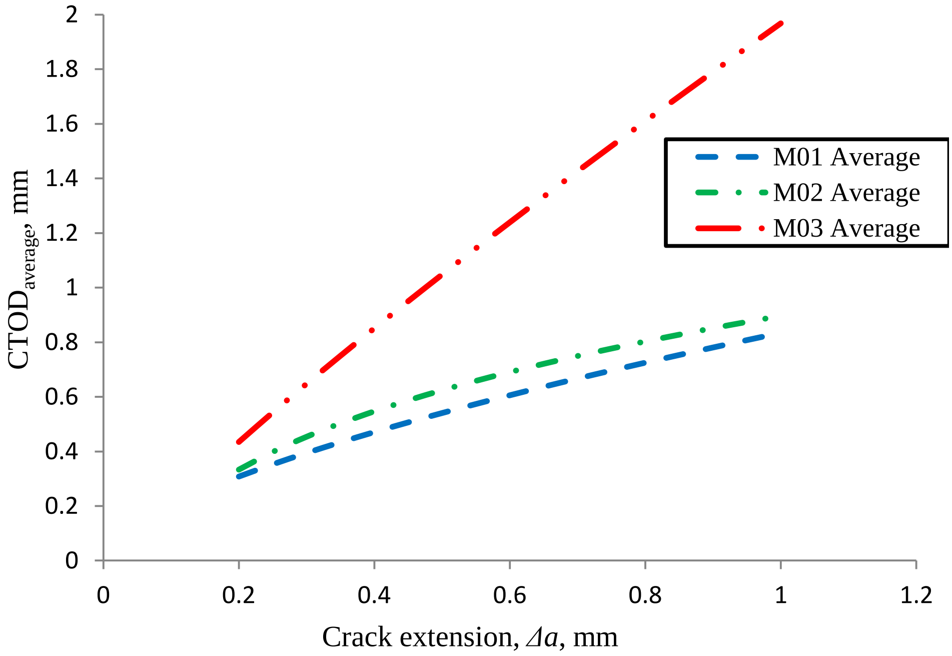

Figure 8.14 Averaged CTOD R-curve for the low, medium and high strain hardening material

8.4.3 Validation of the standardized R-curves

The crack correction factors on the standardized R-curve equations, *X* and *Y* either increase or decrease the value of CTOD relative to the single point equations. Chapter 7.5.2 shows that the standardized single point equations generally underestimate CTOD, apart from the BS equation for high strain hardening material. It would be useful to investigate if the crack correction factors improve the accuracy for the prediction of CTOD. The CTOD R-curves were obtained based on the standardized R-curve equations: - BS 7448-4, ASTM E1820 and ISO 12135. The single point equation from WES 1108 was included in the comparison to investigate its applicability for CTOD R-curves (Eq. 5.04 in Chapter 5.1).

The variability of crack extension on the specimens are dependent on several factors, including but not limited to crack tip constraint, fatigue crack tip shape, homogeneity of the material in the plane of crack extension and the crack tip plasticity due to fatigue pre-crack. A case-by-case qualitative study based on individual specimens could lead to biased observation rather than the general performance of the material. For each material, the R-curves obtained from each standard, plotted to the measured crack extension on the silicone replicas and averaged to obtain a representative R-curve. By normalizing the averaged CTOD R-curves from standards to the averaged CTOD R-curve from the silicone crack replica measurements, $\delta_{avg\ std}/\delta_{avg\ SRC}$, the accuracy of the standardized R-curve could be investigated.

The normalised R-curves were plotted for crack extension between 0.2 and 1mm. The observation in the low crack extension region, Δa< 0.2mm is not considered, because the offset of the fitted curve and minute difference in the R-curve slope is not representative of the actual crack condition. The initiation of tearing is assumed to be at Δa= 0.2mm, as this gives a consistent approach for the evaluation of the initiation of tearing independent of the material's strain hardening property. Additionally, this method gives a conservative evaluation of the tearing initiation CTOD compared to the methods described in the standards, where the tearing initiation CTOD is evaluated from a line parallel to the blunting/construction line at a 0.2mm offset.

Based on the observation, the ASTM and ISO R-curve gave identical estimation independent of the material strain hardening properties (Figure 8.15, Figure 8.16 and Figure 8.17). For simplicity purposes, the ASTM and ISO R-curve estimation shall be described as the *J*-based R-curve. In the low strain hardening material, all equations underestimate the actual CTOD (Figure 8.15). The JWES equation gave the best prediction of the actual R-curve despite being designed for single point estimation (i.e. without a correction factor for crack growth), followed by the BSI and *J*-based R-curve equation.

For the medium strain hardening material, the BS and JWES gave similar estimation. BS gave the best representative of the actual CTOD, followed by JWES and the *J*-based R-curves. Similar to the observation in Chapter 7.5.2, the BSI and JWES gave good representation of CTOD for low and medium strain hardening material, whereas the J-based R-curve severely underestimated the actual CTOD.

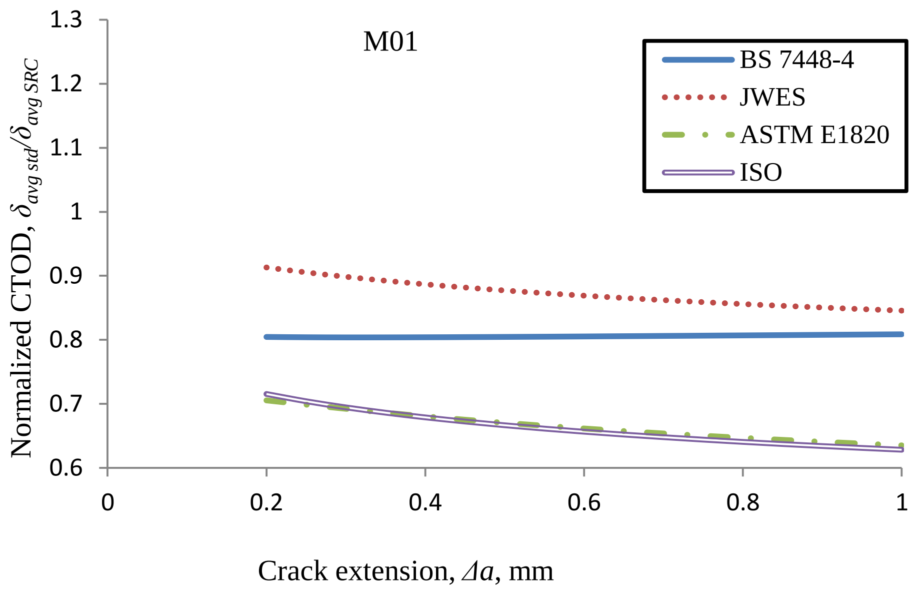

Figure 8.15 Normalized CTOD R-curve for the low strain hardening material, σ_{ys}/σ_{uts}= 0.93

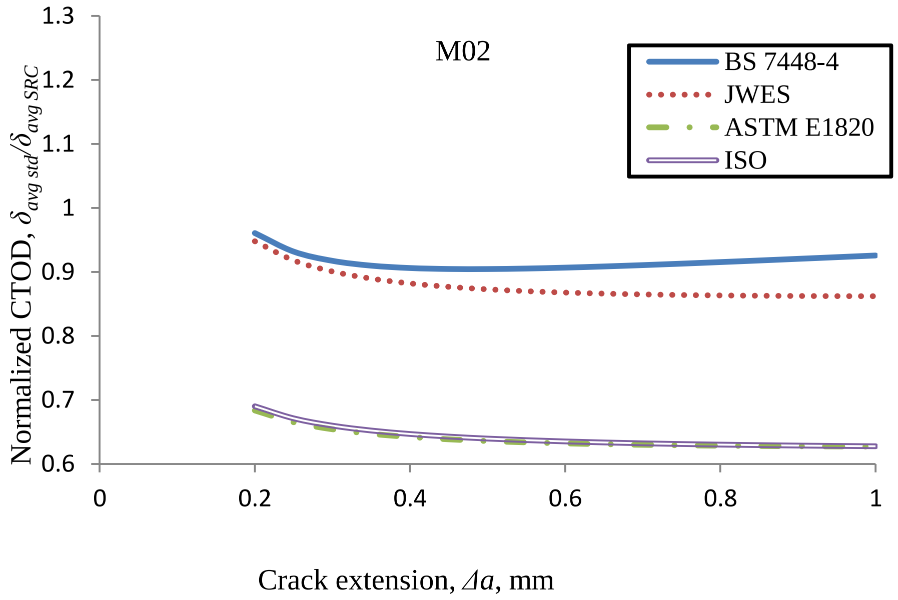

Figure 8.16 Normalized CTOD R-curve for the medium strain hardening material, σ_{ys}/σ_{uts}= 0.72

The standardized equations gave a different trend for the high strain hardening material. The BS equation overestimates the actual CTOD R-curve. The JWES and *J*-based R-curve underestimate the actual R-curve by up to 30%. The accuracy of the BS and *J*-based R-curves increases with increasing crack length, different to that decreasing accuracy from the JWES R-curve. The *J*-based R-curve gave a significantly lower prediction of the tearing initiation CTOD compared to the JWES R-curve.

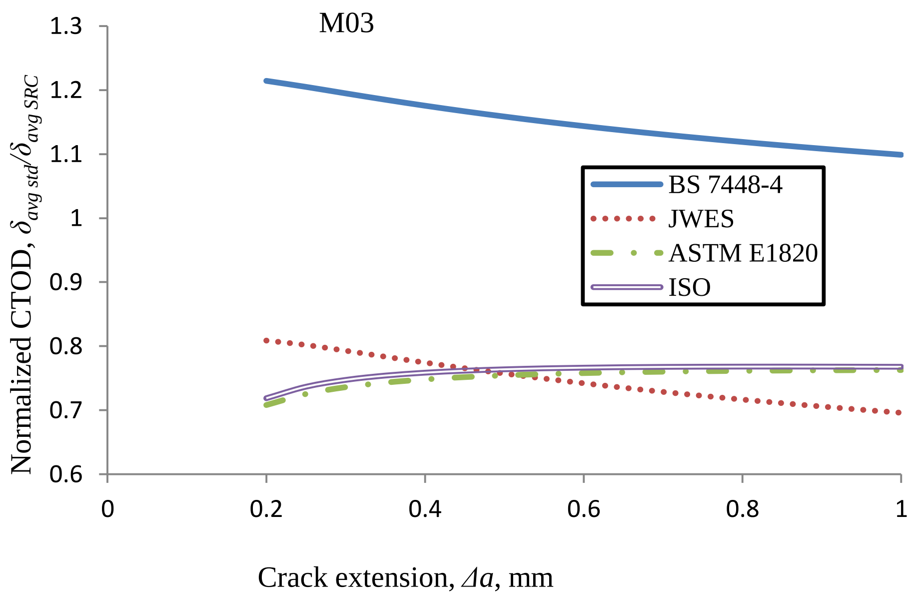

Figure 8.17 Normalized CTOD R-curve for the high strain hardening material, σ_{ys}/σ_{uts}= 0.48

8.5 Discussion

The different CTOD equations were formulated based on different assumptions: - geometrical estimation method in BS, geometrical estimation with strain hardening consideration in JWES, and *J*-based conversion in ASTM and ISO. It should also be noted that the BS definition of CTOD is the opening of the original crack tip, whereas CTOD is described as the opening at the 45-degree intercept from the crack tip for the *J*-based equations. The BS crack correction factor, X increases with crack extension, whereas the *J*-based crack correction factor, Y gives the opposite. This implies that the BS evaluates CTOD from a static location, whereas the *J*-based conversion method evaluates CTOD from on a moving crack tip. Based on the definition of CTOD adopted by the standards for the formulation of the equations, both X and Y is conceptually correct. The different definition for CTOD leads to different theoretical and practicality implications, further described in Chapter 10.1.

The *J*-based crack correction factors, Y_{ASTM} and Y_{ISO} used different equations and therefore gave different values. However, the Y_{ISO} gives a lower value regardless of the crack extension rate. Despite the differences, R-curves obtained from ASTM and ISO showed that the difference is negligible (Figure 8.15, Figure 8.16 and Figure 8.17). Considering that both Y_{ASTM} and Y_{ISO} led to similar CTOD values independent of strain hardening property, Y_{ISO} can be used as a representation of *J*-based crack correction factor, as it is simple and less complicated than Y_{ASTM}, simplifying the calculation without compromising precision.

For the experimental R-curve, it could be seen that the tearing initiation toughness (CTOD at Δa= 0.2mm) increases with the increase of the material strain hardening property (Figure 8.14). Additionally, the experimental R-curve showed that the crack tip constraint decreases and the tearing resistance of the material increase with the increase of material strain hardening (Figure 8.10 and Figure 8.14). This is related to the plasticity level of the material around the crack tip region.

The standardized R-curve equations gave a similar observation to that seen in Chapter 7.5.2. The standards generally underestimate CTOD for the low and medium strain hardening material. For engineering critical assessments, it is important that the estimated CTOD is as accurate as possible whilst being on the conservative side. The JWES equation, although does not consider crack extension in the equation, is most versatile and gave the best CTOD estimation. It is thought that possibly, the strain hardening property of the material affects the resultant CTOD more than the crack extension factor. This issue will be discussed in Chapter 10.5.

8.6 Summary

The CTOD R-curves are measures of the material’s resistivity to stable crack extension by ductile tearing. Crack extension correction factors were incorporated in the standard single point CTOD equations for the CTOD R-curve equations. The BS crack correction factor leads to increasing CTOD for increasing crack extension, whereas the opposite is observed for the ASTM and ISO crack correction factor. The apparent contradiction arising due to this opposite trend is explained in Chapter 10.3.

The ASTM and ISO equations were based on a *J*-CTOD conversion, but the ISO equation does not allow *J* to be calculated based on CMOD. Experimentally, *J* can be calculated using displacement from either CMOD and the load-line displacement. A conversion equation is provided in ISO to estimate the load-line displacement based on clip gauge displacement. Comparison showed that minimal difference is observed between the different methods, and that *J* calculated using CMOD is representative of *J* calculated using the load-line.

For the representation of the R-curve, an offset power law curve is fitted to the CTOD measured from the silicone crack replicas. The steepness of the R-curve slope indicates the level of crack tip constraint on the specimen and the material’s resistance to tearing. The high strain hardening material exhibited the lowest crack tip constraint and highest tearing initiation toughness (steepest curve), followed by the medium and low strain hardening material (flattest curve).

The CTOD R-curve was obtained based on the BS, ASTM, ISO and JWES equations and validated using the R-curves obtained from the silicone crack replicas. Generally, the standards underestimate the actual R-curve, apart from the BS R-curve for high strain hardening material, as it is the only equation not considering the effects of material strain hardening. The ASTM and ISO equations underestimate the CTOD R-curve regardless of strain hardening. The JWES equation, although was not designed for the CTOD R-curve, gave a relatively good estimate of the R-curves except for the high strain hardening steel, where accuracy decrease with increasing crack extension. The JWES equation is versatile, where it does not overestimate the high strain hardening material, nor does it severely underestimate the medium and low strain hardening material. This raises the concern if the crack correction factor is required for the estimation of CTOD, which will be discussed in Chapter 10.4.

8.7 Conclusion

Based on the investigation of the standard single point SEN(B) tests, it was found that *J* calculated using CMOD is equivalent to *J* calculated using LLD. The use of CMOD in fracture toughness tests is advantageous over LLD where they can be easily set-up at the crack mouth.

The *J*-based ASTM equation underestimates CTOD regardless of the material tensile property. The crack correction factor used in the ASTM equation, Y_{ASTM} gives negligible difference to the original value of CTOD without any correction.

The JWES equation, although does not consider the effects of crack extension, managed to give very good estimates of the low and medium strain hardening material, and decent prediction for the high strain hardening material. This argues the need to evaluate the effects of crack extension for R-curve assessments, and will be further discussed in Chapter 10.4.

Chapter 9

Rotational factors in SEN(B) specimens for the determination of CTOD

9.1 Introduction

In the early days of fracture toughness testing, SEN(B) and CT were the most commonly used specimen geometries. In deeply cracked specimens, i.e. specimens with crack ratio, $a_0/W \geq 0.5$, the deforming specimen ligament is assumed to behave like a plastic hinge, where the two opposite ends of the specimen rotate about a fixed 'rotational' point, which lies within the remaining un-cracked ligament ahead of the crack tip (refer Chapter 1.7.2).

Based on the plastic hinge assumption, CTOD is typically estimated by employing the similar triangles geometrical assumption, assuming a fixed location of the rotational point. By measuring the displacement at the crack mouth or a clip gauge at a given height above the crack mouth, the displacement at the crack tip can be determined. This CTOD estimation method had been employed in many fracture toughness testing standards, notably BS 7448-1, ISO 12135 and the now superseded early version of ASTM E1290 (BSI 1991; ISO 2002; ASTM 1999). BS 7448-1 and ISO 12135 use the same equation for the determination of CTOD. In reality, during the progression of the test, the rotational point typically starts from the crack tip on first load, then moves deeper into the un-cracked ligament as applied displacement on the specimen increases (Wells 1971; Ingham et al. 1971; Robinson & Tetelman 1974). However, BS 7448-1 and ASTM E1290 adopted a fixed value of rotational factor, r_p= 0.40 and 0.44 respectively for practical and simplicity purposes (Ingham et al. 1971).

The similar triangles assumption is the first order approximation of CTOD and it showed adequate accuracy at the maximum load position or at the onset of unstable crack extension (Ingham et al. 1971). The rotational factor is applied in the calculation of the plastic component of CTOD in the form of

$$\delta_{pl} = \frac{r_p B_o V_p}{r_p B_o + a_0 + z} \qquad \text{Eq. 9.01}$$

δ_{pl} is the plastic CTOD, a_0 is the original crack length, B_0 is the remaining ligament ahead of the crack tip (W- a_0), V_p is the plastic displacement and z is the height above the crack mouth where the crack mouth or clip gauge displacement is measured.

If the rotational factor is not constant as assumed, the use of a constant rotational factor could introduce unnecessary errors for the estimation of CTOD. The validity of the fixed rotational point assumption was investigated experimentally and using FE modelling based on three different strain hardening material properties (M01, M02 and M03).

9.2 Estimation errors of the fixed rotational point assumption with respect to the actual rotational point

The BS/ISO and ASTM CTOD equations used and assumed value of r_p= 0.4 and 0.44 respectively. This approach was further supported by Lin et al. (1982) and Wu's (1983) findings, where r_p is found to be generally larger than 0.46 for steel. However it should be noted that the research on the rotational point described above lacked data from high strain hardening, low tensile ratio steel, such as material M03 used in this work.

Eq. 9.01 was used to check the effect of varying r_p on the resultant CTOD. Assuming constant values for V_p= 1 and z= 0, the dimensionless plastic CTOD was calculated using Eq. 9.01 for $0.3 \leq r_p \leq 0.7$ for different crack ratio, a_0/W. If the actual rotational factor is less than 0.4, CTOD is actually lower than that predicted with r_p= 0.4 and the test BS/ISO equation overestimates the actual CTOD; if the actual rotational factor is greater than r_p= 0.4, the BS/ISO equation would give conservative estimations of CTOD.

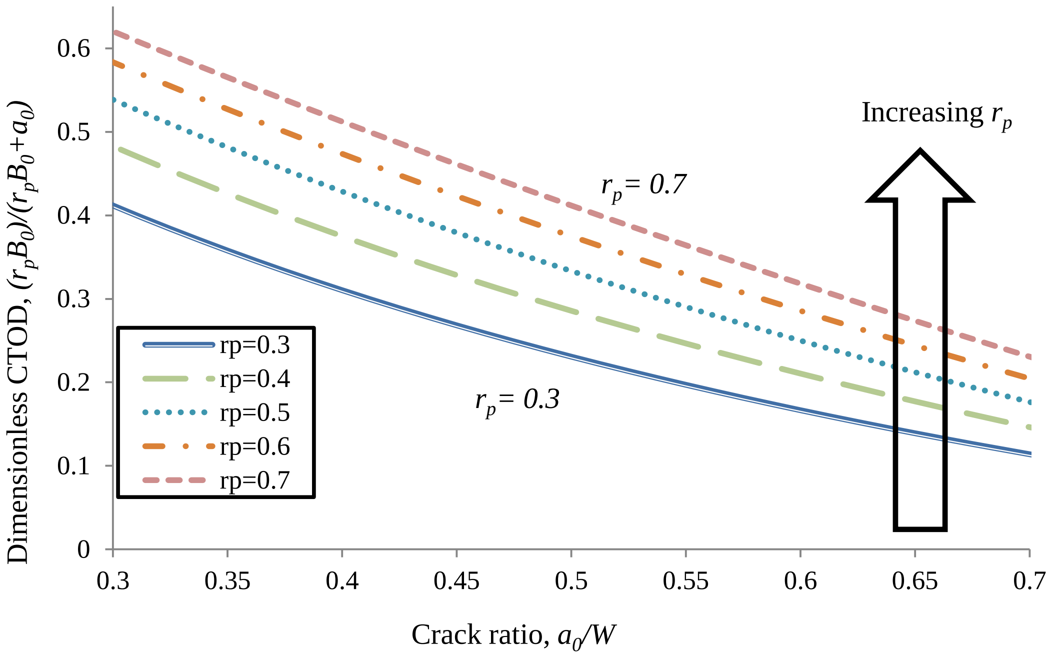

Figure 9.01 The effect of r_p on the plastic CTOD for different crack ratio, assuming constant V_p using Eq. 9.01

9.3 r_p based on crack face angle

9.3.1 r_p estimated using the double clip gauge method

Experimentally, by using two clip gauges positioned at different heights above the crack mouth position, the apex of the similar triangles can be determined and compared to the prediction based on a single clip gauge and fixed r_p assumption. This method extrapolates the crack face angles into the unbroken ligament ahead of the crack tip, where the intersection of the angles is described as the rotational point. A double clip gauge setup was employed on the specimen to extract displacement data by placing clip gauges on knife edges above the crack mouth at different heights (2mm and 12mm for $B\times 2B$, and 2.5mm and 8.5mm for BxB).

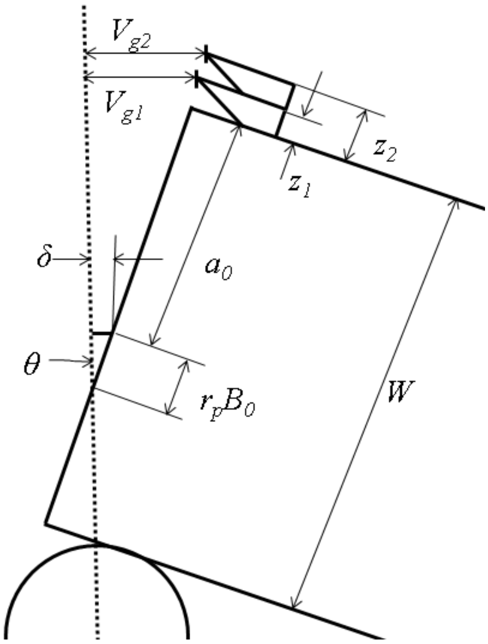

Figure 9.02Double clip gauge setup based on the similar triangles assumption

Figure 9.02 shows the analytical diagram for the determination of the r_p. A similar method had been used successfully by Robinson & Tetelman (1974) to determine the r_p. The following terms were used for simplicity purposes, $r_pB_0= Y$, $z_1+ a_0= C$, and $a_0+ z_2= D$. To relate the lower and upper clip gauge opening, V_{g1} and V_{g2} respectively to the point of rotation,

$$\sin\theta = \frac{V_{g1}}{C+Y} = \frac{V_{g2}}{D+Y}$$

Leading to

$$\frac{V_{g2}}{V_{g1}} = \frac{D+Y}{C+Y}$$

Expanding D and factoring $C+ Y$ gives

$$\frac{V_{g2}}{V_{g1}} = \frac{C + Y + (z_2 - z_1)}{C + Y} = 1 + \frac{(z_2 - z_1)}{C + Y}$$

Rearranging the equation leads to

$$Y = r_p B_0 = \left(\frac{z_2 - z_1}{V_{g2}/V_{g1} - 1} \right) - (z_1 + a_0)$$

Where the rotation factor, r_p based on V_{g1} and V_{g2} is given as

$$r_p = \left[\left(\frac{z_2 - z_1}{V_{g2}/V_{g1} - 1} \right) - (z_1 + a_0) \right] \times \frac{1}{B_0} \qquad \text{Eq. 9.02}$$

Eq. 9.02 allows the rotational factor to be calculated based on two clip gauges positioned at different heights above the crack mouth. Similarly, the rotational factor based on the plastic displacement can be obtained by simply replacing the lower and upper clip gauge displacement, V_{g1} and V_{g2} with the plastic lower and upper clip gauge displacement, V_{p1} and V_{p2}.

In the BS/ISO, the rotational factor is applied in the determination of the plastic CTOD. Based on data obtained from the single point specimen, M01-07, the rotational factor is calculated for both the actual and plastic clip gauge opening using Eq. 9.02 (Figure 9.03).

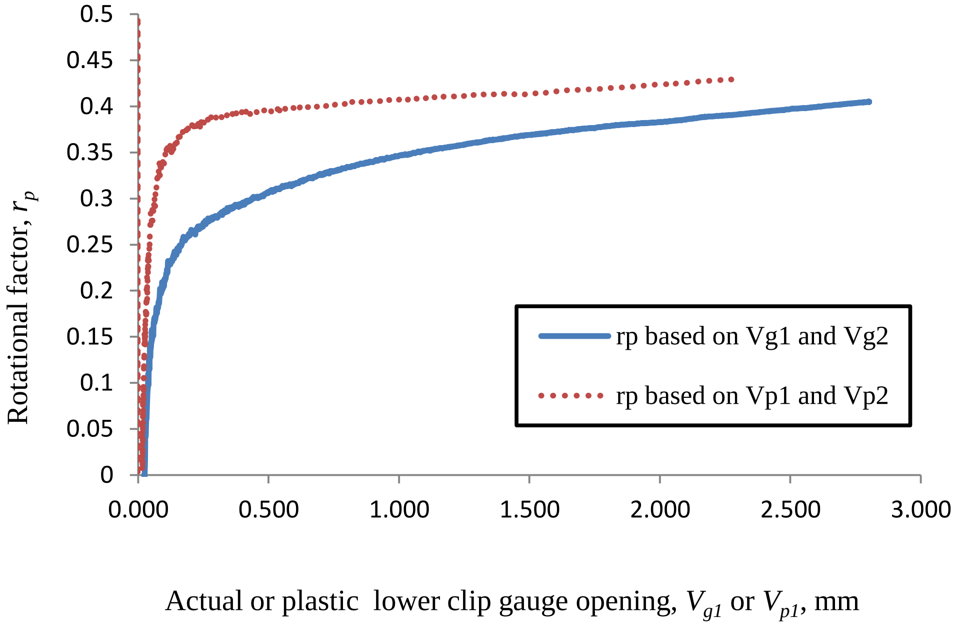

Figure 9.03 Rotational factor calculated based on specimen M01-07

r_p based on the actual clip gauge displacement is plotted to the actual lower clip gauge opening, whereas r_p based on the plastic clip gauge displacement is plotted to the plastic lower clip gauge opening. The overall trend between both r_p is similar, with r_p from plastic clip gauge displacement giving overall higher values throughout loading. r_p calculated using the actual and plastic clip gauge displacement for the remaining single point specimens (M02-03, M02-11 and M03-03) gave similar trend, and are shown in Appendices.

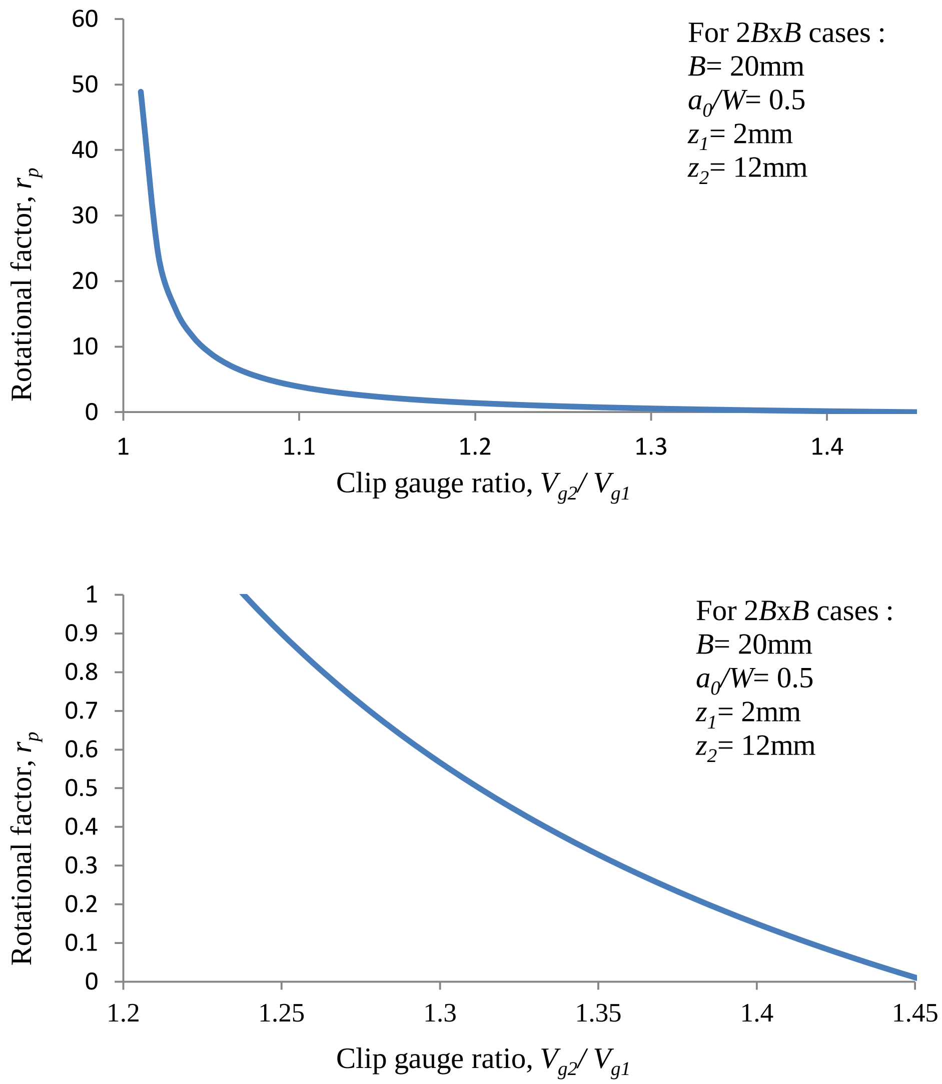

Figure 9.04 The relative rotational factor for increasing clip gauge ratio, (top), and the clip gauge ratio for 0< r_p< 1, (bottom)

Eq. 9.02 shows that the clip gauge ratio, V_{g2}/V_{g1} determines the resultant r_p. For the rotational point to fall ahead of the crack tip, V_{g2} must be larger than V_{g1} at all stages of loading. Figure 9.04 shows the effect of V_{g2}/V_{g1} on r_p. As V_{g2}/V_{g1} moves towards 1, r_p tends to move towards infinity (Figure 9.04 (top)). In real specimens, r_p lies in the unbroken ligament ahead of the crack tip, which falls between 0< r_p< 1. Figure 9.04 (bottom) shows that within the unbroken ligament, r_p decreases with the increase of the clip gauge ratio. Therefore in the early stages of loading, the extreme positive and negative r_p does not reflect the actual r_p of the specimen. Due to the additional inconsistency caused by the determination of the plastic clip gauge displacement, r_p in the following sections in this chapter is based on the actual clip gauge values.

The r_p is mainly used for the determination of the plastic CTOD. In Chapter 5.4, analytical data shows that for CTOD< 0.2mm, the elastic component is the dominant in the overall CTOD. To exhibit the r_p trend, the elastic dominated region (CTOD< 0.2mm) and highly deformed region (CTOD> 1.0mm) were excluded from the evaluation. The similar triangles assumption (Figure 9.02) was used to determine the r_p limits, assuming r_p = 0.4 and a_0/W= 0.5. The following relationship is derived to evaluate the limits of V_{g1} when CTOD= 0.2mm and 1.0mm.

$$\frac{V_{g1}}{z_1 + a_0 + r_p B_0} = \frac{\delta}{r_p B_0}$$

$$V_{g1} = \frac{\delta(z_1 + a_0 + r_p B_0)}{r_p B_0} \qquad \text{Eq. 9.03}$$

The actual clip gauge data from the standard single point tests were processed for the evaluation of r_p. The lower and upper limit for V_{g1} was filtered based on Eq. 9.03 (Figure 9.05).

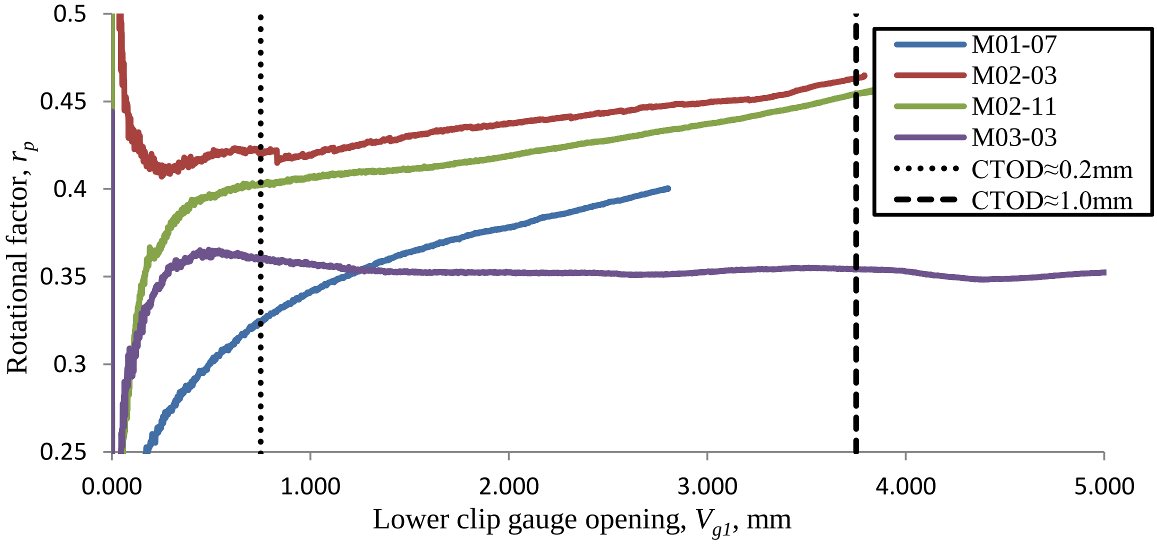

Figure 9.05 r_p extracted from the standard single point specimens

Figure 9.05 shows that the variation of r_p is minimal for the increasing clip gauge opening. The maximum difference of r_p is approximately 0.07, observed on specimen M01-07. For all specimens, r_p falls between 0.32 and 0.46. As r_p is a measure based on the global deformation of the specimen, the difference could be contributed by the crack front shape and the distribution of crack tearing across the crack front.

To allow direct comparison to the actual physical CTOD, data from the silicone replicated crack specimens were processed to obtain r_p (Figure 9.06). r_p obtained from the silicone replicated crack specimens showed fluctuations, which were due to opening of the crack mouth while the specimens were being held in constant machine displacement. The magnitude of the opening of the crack mouth is very small (described in Chapter 3.4), however r_p between 0 and 1 is very sensitive to the changes in the clip gauge ratio.

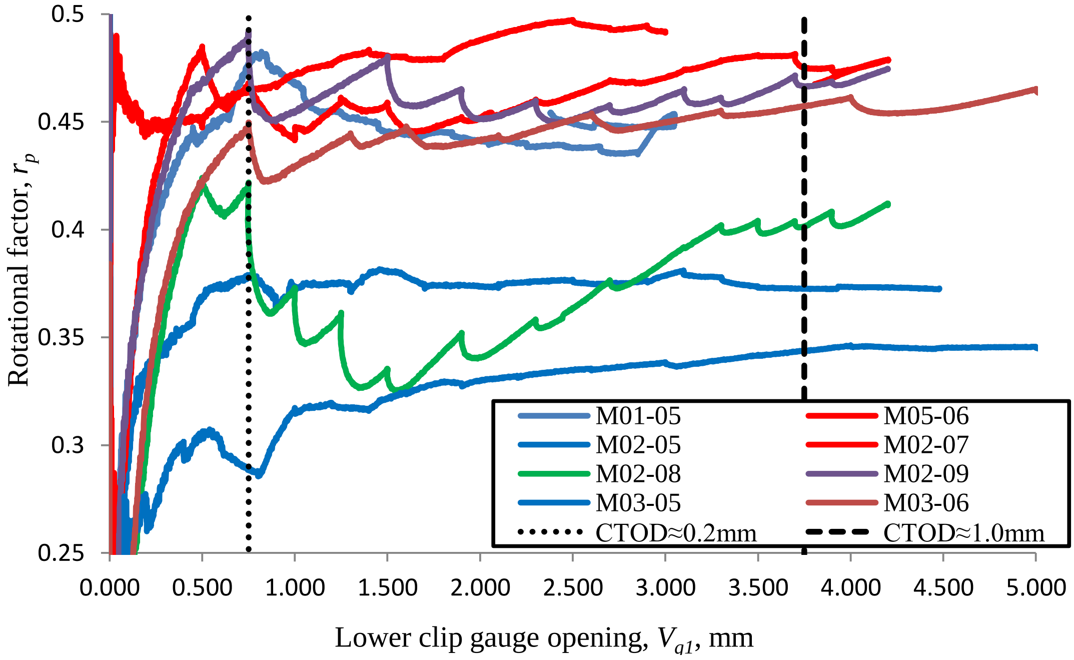

Figure 9.06 r_p extracted from the silicone crack replication specimens

The r_p extracted from the silicone crack replication tests were between 0.29 and 0.5, similar to that obtained from the standard single point specimens. The r_p from standard single point and silicone crack replication specimens suggests that the r_p used in BS/ISO might not give an accurate estimation of CTOD, but a good approximation of CTOD regardless of strain hardening.

9.3.2 r_p estimated using Finite Element modelling

r_p was investigated for the three material properties used in the experiments from the FE models generated in Chapter 4.1. The SEN(B) models were modelled under 3-point bend loading and the apex of the crack face opening was identified as the hinge location. Displacement values of the CMOD and the node below the CMOD, $CMOD_{-1}$ were extracted to evaluate r_p based on the similar triangles method (Figure 9.07). The distance between the two nodes, Δz was found to be constant throughout the loading, therefore the nodes CMOD and $CMOD_{-1}$ can be used to give a good representation of the crack face angle. Eq. 9.04 was modified based on Eq. 9.02 to accommodate the model geometry, given as

$$r_p = \left(\frac{\Delta z}{\left(\frac{CMOD}{CMOD_{-1}} - 1\right)} - (a_0 - \Delta z) \right) \times \frac{1}{B_0} \qquad \text{Eq. 9.04}$$

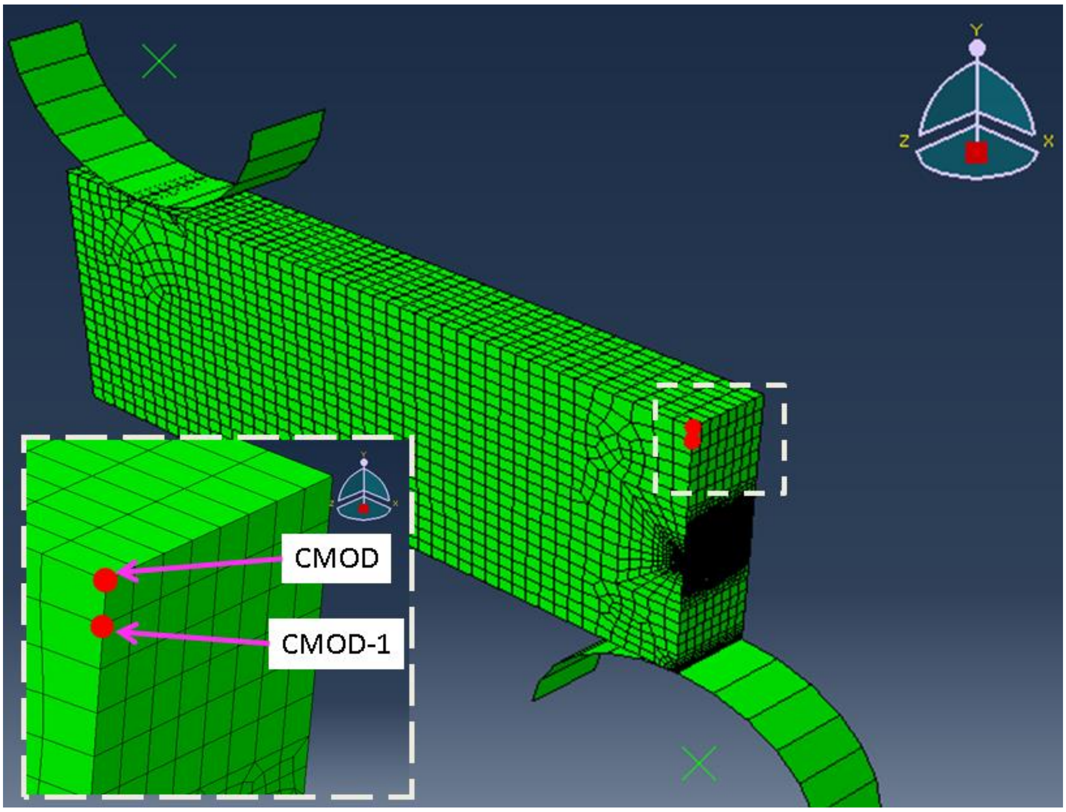

Figure 9.07 Nodes (CMOD and CMOD$_{-1}$) used for the calculation of r_p

r_p was calculated for both actual and plastic CMOD from the low, medium and high strain hardening model for increasing CMOD (Figure 9.08). r_p from the actual CMOD increased from near the crack tip into the remaining ligament ahead of the crack tip with increasing CMOD; r_p from the plastic CMOD moves towards the crack tip, converging at approximately r_p = 0.46. Similar to that applied on the experimental r_p, dotted lines are shows an approximate limit for CTOD≈ 0.2mm and 1.0mm. In contrast to that observed from the experimental results, r_p from CMOD were consistent, and less affected by the material strain hardening properties, where r_p is approximately 0.41.

The difference in r_p obtained from the experiments and FE models were mainly contributed by the crack tip shape and crack propagating mechanism. As shown in Figure 7.10 and Figure 7.11, the low and medium strain hardening specimens showed ‘tunnelling’ crack propagation ahead of the curved initial crack tip, where the crack extension in the middle of the crack grows at a higher rate than the sides of the crack. However, the FE model showed continuous blunting, where large crack extension or blunting was seen in the middle of the model, but minimal deformation on the sides of the model (Figure 9.09). The distribution of the un-cracked ligament is different between the experiments and FE model is different both before and after loading. The evaluation of r_p based on the crack face angle captures the overall specimen rotation, rather than any particular cross section in the specimen width-span plane.

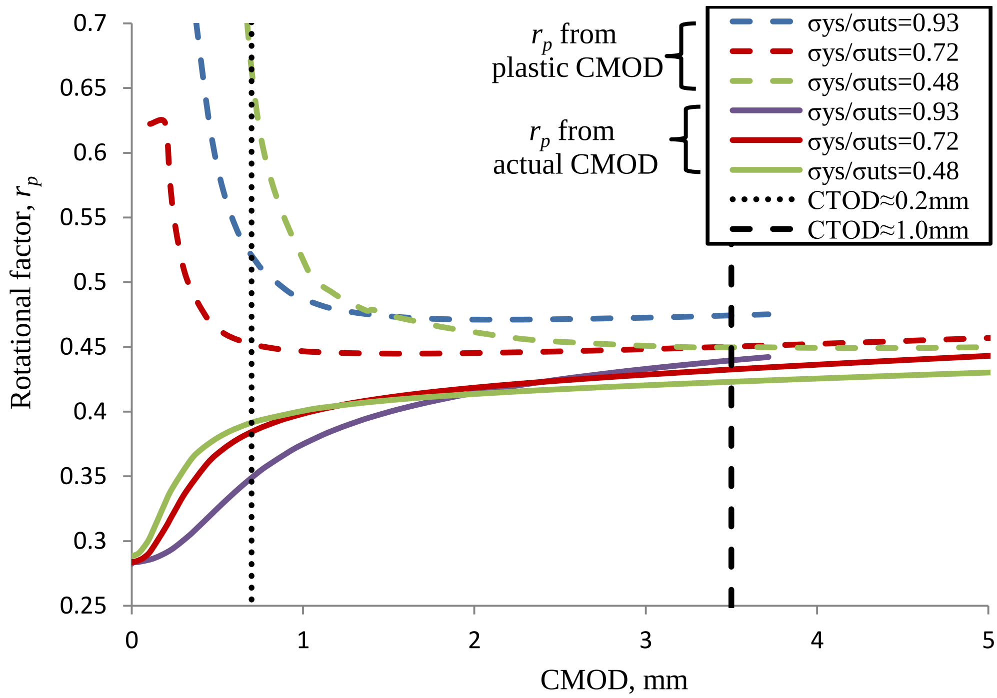

Figure 9.08 r_p from the FE model based on both CMOD and plastic CMOD

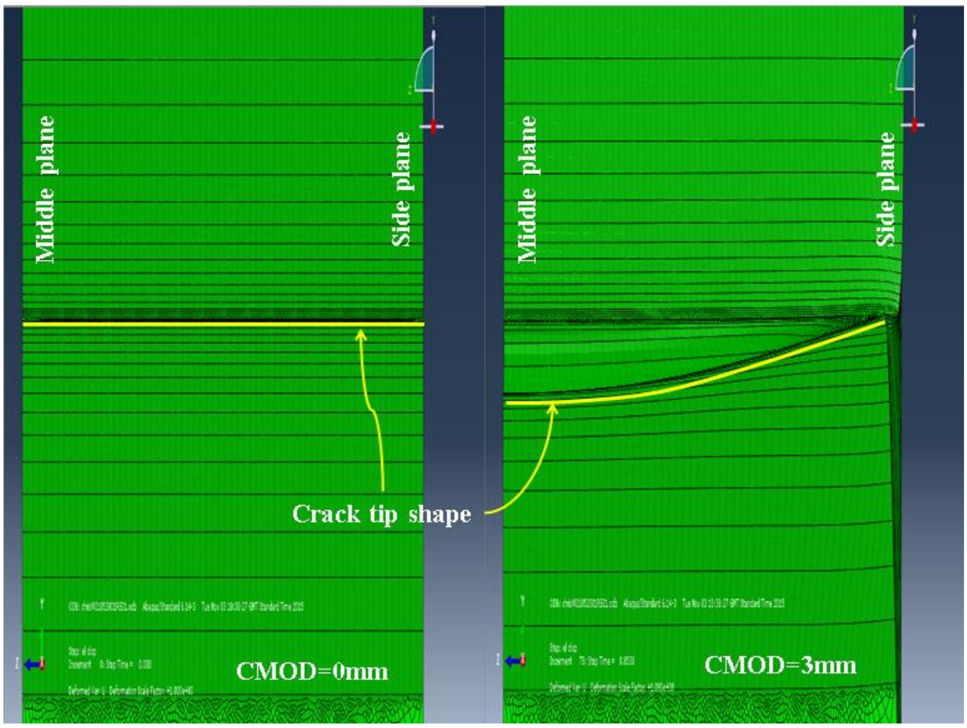

Figure 9.09 Crack tip shape at CMOD= 0mm (left) and CMOD= 3mm (right) for FE model with σ_{ys}/σ_{uts}=0.93

9.4 The effects of strain hardening on the determination of the geometrical based CTOD

The findings in Chapter 9.3 suggest that r_p evaluated based on the crack face angle might be independent of the effects of strain hardening. The scatter in experimental results did not allow valid comparison the FE model. Including the effects of strain hardening, r_p is extracted based on the intersection the line extrapolated from the lower clip gauge opening or CMOD and CTOD to the symmetry line (Figure 9.10). This r_p, thereafter described as $r_{p\ sh}$, gives lower r_p than that obtained from crack face angles.

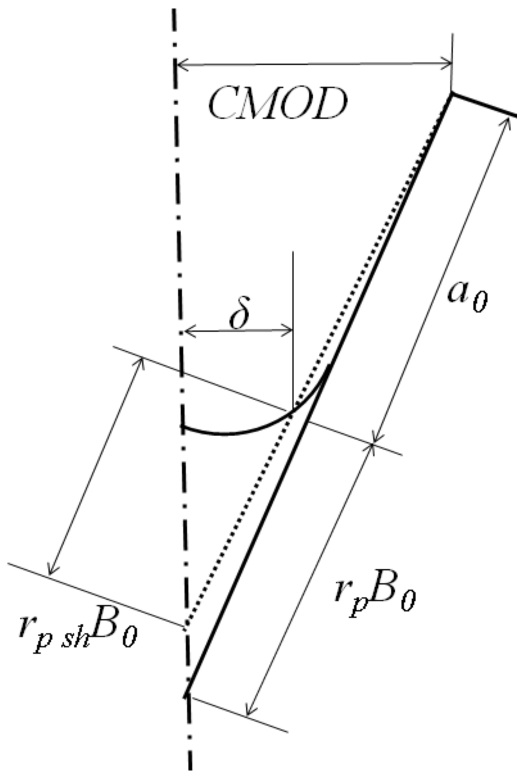

Figure 9.10 The effect of crack tip blunting due to strain hardening

To extract $r_{p\ sh}$ from the silicone replicated tests and FE models, Eq. 9.02 was modified based on the actual CTOD and CMOD, described as

$$r_{p\,sh} = \left[\left(\frac{z_1 + a_0}{{CMOD}/{\delta} - 1}\right)\right] \times \frac{1}{B_0} \qquad \text{Eq. 9.05}$$

Based on measurements from the silicone replicas, $r_{p\ sh}$ was calculated for all three strain hardening materials and plotted for the corresponding measured CTOD (Figure 9.11). For the data within the range of 0.2mm< SRC CTOD< 1.0mm, power law curve was fitted for data from material M01, M02 and M03 to show the distribution trend (σ_{ys}/σ_{uts}= 0.93, 0.72 and 0.48 respectively). The data distribution shows the overall data from the same material increases with increasing tensile ratio.

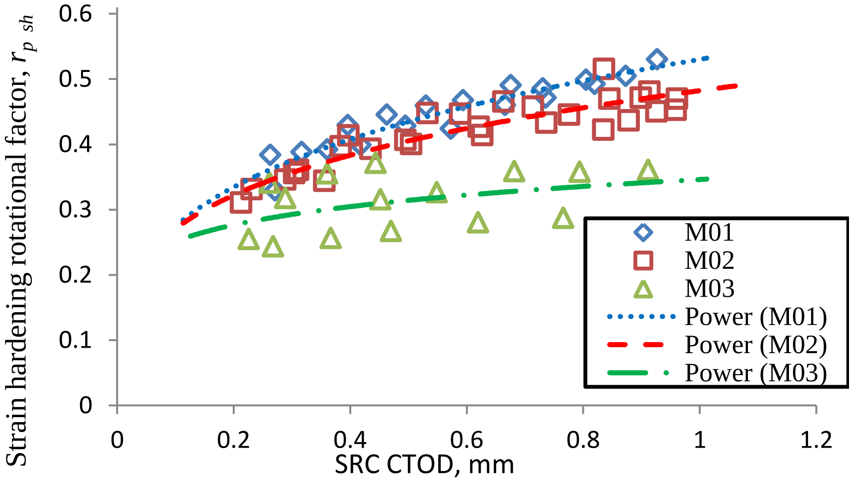

Figure 9.11 Strain hardening rotational factor vs. CTOD measured from the SRC

To obtain a better resolution of the $r_{p\ sh}$ distribution due to the effects of strain hardening, data were extracted from the FE models with idealised tensile properties (described in Chapter 4.2.2) and processed using Eq. 9.05. Data were extracted for 0.2mm< FE CTOD< 1.0mm to minimise the influence of the elastic CTOD and large deformation. Similar to that observed in Figure 9.11, $r_{p\ sh}$ increases with increasing tensile ratio.

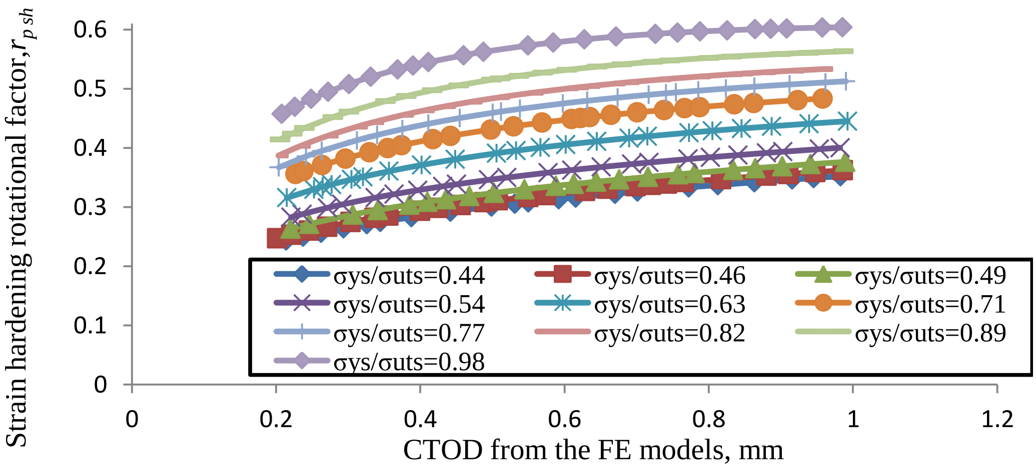

Figure 9.12 Strain hardening rotational factor vs. FE CTOD from the FE models with idealised tensile properties

Figure 9.11 and Figure 9.12 showed the dependency of $r_{p\ sh}$ on tensile ratio. $r_{p\ sh}$ extracted from the FE models were plotted for tensile ratio. For FE CTOD within the range of 0.2mm and 1.0mm, the maximum difference in $r_{p\ sh}$ is seen in σ_{ys}/σ_{uts} = 0.89, with a value of 0.15. Generally, the difference decrease with the decrease of tensile ratio, with the lowest difference of $r_{p\ sh} \approx 0.11$ seen in σ_{ys}/σ_{uts} = 0.44. Based on the average $r_{p\ sh}$ value, a linear relationship is observed due to tensile ratio. The relationship for $r_{p\ sh}$ and tensile ratio is described as

$$r_{p\ sh} = 0.4668\frac{\sigma_{ys}}{\sigma_{uts}} + 0.0996 \qquad \text{Eq. 9.06}$$

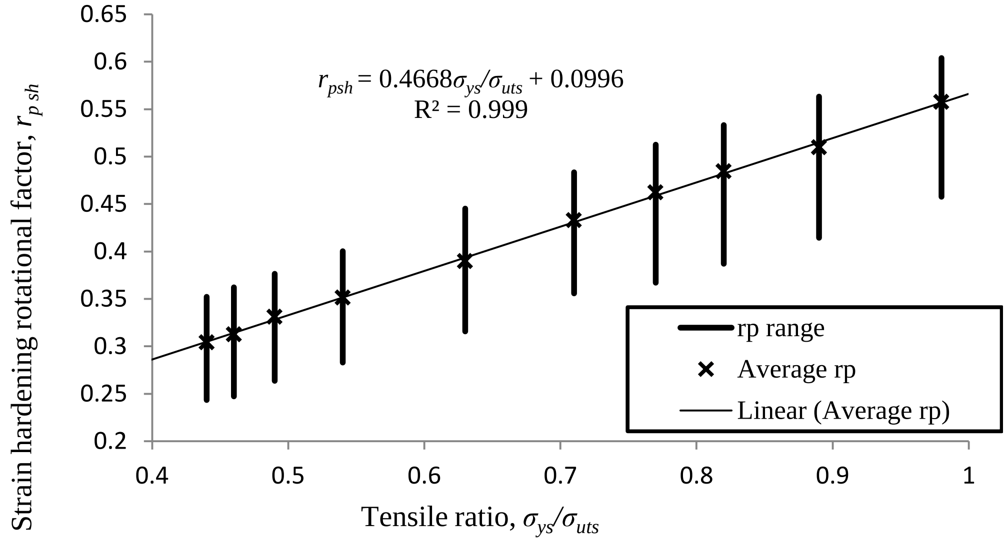

Figure 9.13 Relationship between the Strain hardening rotational factor and tensile ratio based on 0.2mm< FE CTOD< 1.0mm

Based on Eq. 9.06 obtained from Figure 9.13, $r_{p\,sh}$ was calculated based on the tensile ratio for M01, M02 and M03. Based on the average value of the power law trend in Figure 9.11 and linear relationship in Figure 9.13, the difference in the experimental and FE $r_{p\,sh}$, $\Delta r_{p\,sh} = r_{p\,sh\,FE} - r_{p\,sh\,SRC}$ could be highlighted for each of the material (Figure 9.14). Due to the similarity of deformation mechanism in the M03 material and the FE model, minimal difference ($\Delta r_{p\,sh} \approx 0.005$) is seen for $\sigma_{ys}/\sigma_{uts} = 0.48$. The difference increases exponentially, where $\sigma_{ys}/\sigma_{uts} = 0.93$ showed a maximum difference of $\Delta r_{p\,sh} \approx 0.08$. However, based on the observation in Figure 9.01, for $V_p = 1.0$mm, difference of 0.1 in r_p gives a maximum difference of approximately 0.05mm in the resultant CTOD. This shows that the $r_{p\,sh}$-tensile ratio relationship obtained from FE is representative of the experimental results.

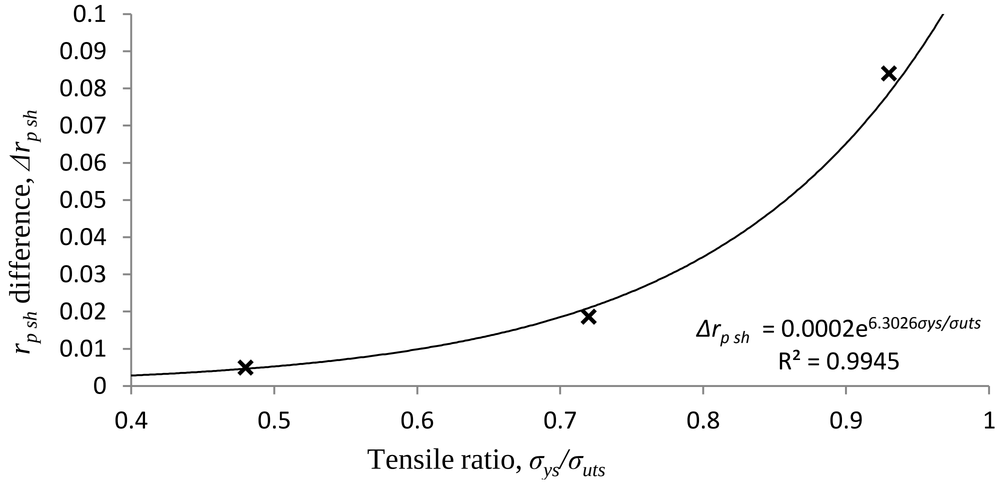

Figure 9.14 Difference in $r_{p\,sh}$ between FE and SRC specimens for different tensile ratio

The FE based $r_{p\,sh}$ from Eq. 9.06 was incorporated into a modified CTOD equation to be validated experimentally. Utilising the strain hardening corrected elastic component from the JWES equation and the plastic component from the BS 7448-1, replacing r_p with $r_{p\,sh}$ gives

$$\delta_{sh} = \delta_{el\,JWES} + \frac{r_{p\,sh} B_o V_p}{r_p B_o + a_0 + z} \qquad \text{Eq. 9.07}$$

Based on $r_{p\,sh}$ calculated using Eq. 9.06, CTOD was calculated using Eq. 9.07 and compared to CTOD measured from the silicone replicated cracks. The comparison for M01, M02 and M03 specimens up to SRC CTOD= 1.0mm were showed in Figure 9.15, Figure 9.16 and Figure 9.17 respectively. Generally, δ_{sh} was consistent with the SRC CTOD measurements, with most scatter observed in the M03 material. Based on the observation, the δ_{sh} gave better accuracy compared to all the standardized equations shown in Figure 7.18.

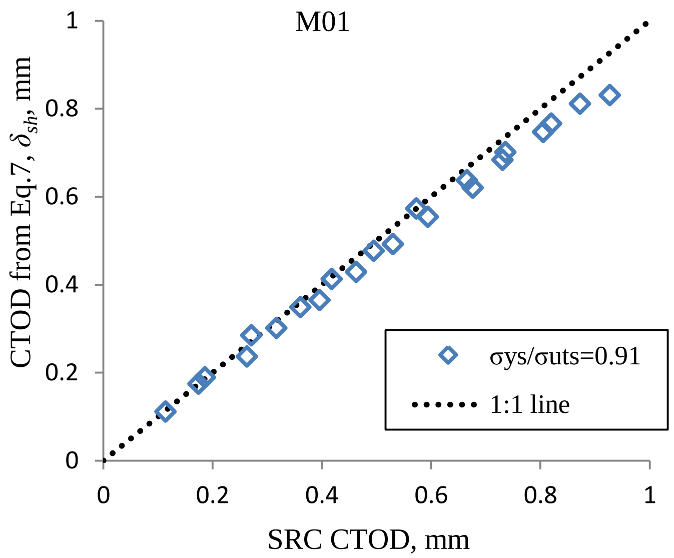

Figure 9.15 CTOD from Eq. 9.07 vs. SRC CTOD for M01

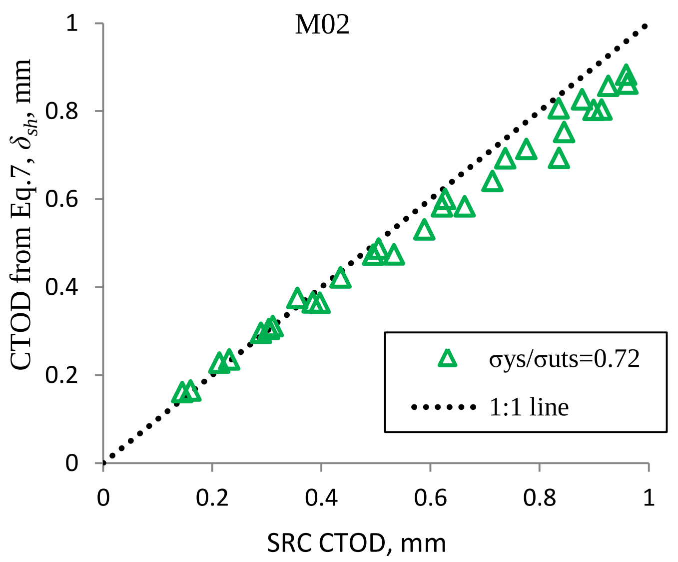

Figure 9.16 CTOD from Eq. 9.07 vs. SRC CTOD for M02

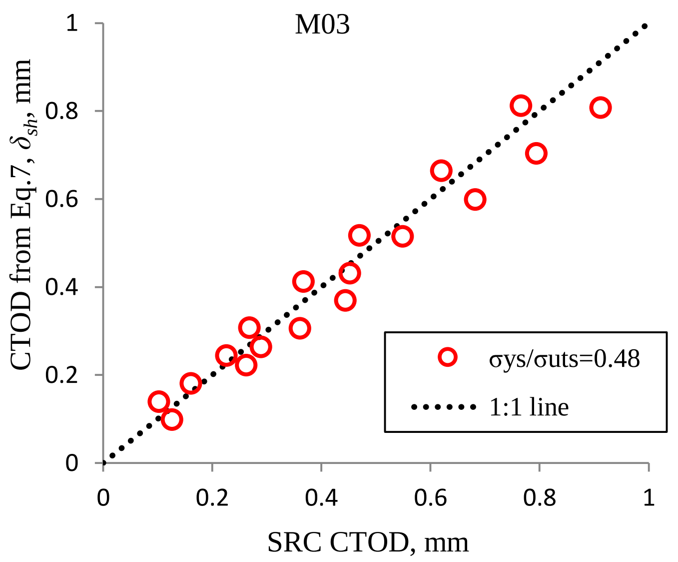

Figure 9.17 CTOD from Eq. 9.07 vs. SRC CTOD for M03

To highlight the difference, CTOD from Eq. 9.07, δ_{sh} was normalised to the SRC CTOD, $\delta_{sh}/\ \delta_{SRC}$ (Figure 9.18). The largest difference is seen in the range of SRC CTOD< 0.2mm, as values in this range are heavily influenced by elastic component of CTOD and small errors are magnified. Considering the range of SRC CTOD between 0.2mm and 1.0mm, M01, M02 and M03 gave R2 values of 0.700, 0.507 and 0.063 respectively relative to the 1:1 line. The maximum scatter of the normalized CTOD around the 1:1 line is 17.0%. The consistency in the normalized CTOD for 0.2mm< CTOD< 1.0mm shows that the similar triangle assumption with the inclusion of the effects of strain hardening is a valid and reliable method for the estimation of CTOD.

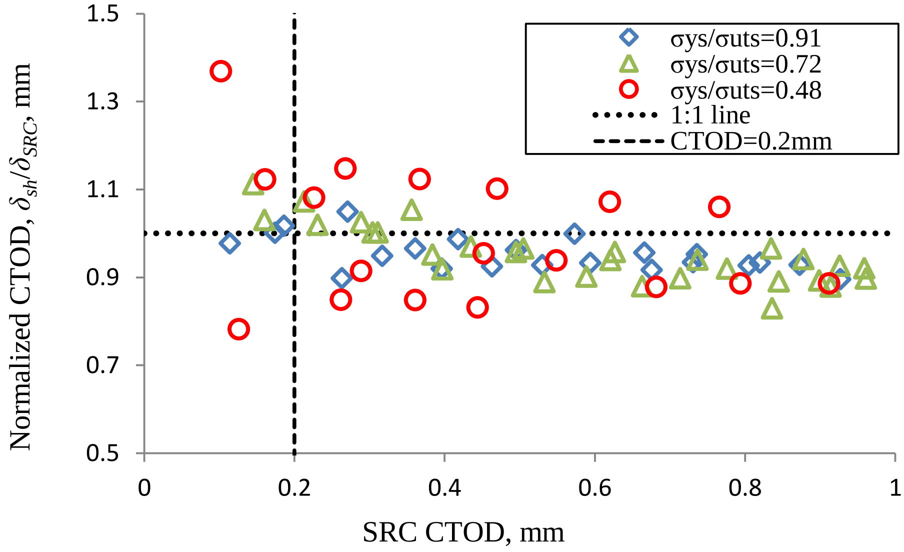

Figure 9.18 Normalized CTOD, $\delta_{sh}/\ \delta_{SRC}$ for increasing δ_{SRC}

9.5 Summary

The plastic hinge assumption for the determination of CTOD had been established in the BSI and ISO standards, assuming a constant rotational factor, r_p. The effect of the variation of r_p on the determination of plastic CTOD was investigated. Two different r_p was investigated: r_p based on the crack face angle, and r_p based on the line connected by CMOD and CTOD in the middle of the crack, $r_{p\ sh}$, which is effected by the material strain hardening properties.

r_p based on the crack face angle gave consistent values of approximately 0.41 from the FE model, whereas significant scatter and no obvious trend were observed in the experimental results. On the other hand, $r_{p\ sh}$ showed strain hardening dependency, where $r_{p\ sh}$ increase with increasing tensile ratio for both experimental and FE models. Based on the FE models, a linear relationship, Eq. 9.06 was obtained to relate $r_{p\ sh}$ based on the material tensile ratio

$$r_{p\ sh} = 0.4668\frac{\sigma_{ys}}{\sigma_{uts}} + 0.0996 \qquad \text{Eq. 9.06}$$

An equation was modified to include the effects of strain hardening, given as

$$\delta_{sh} = \delta_{el\ JWES} + \frac{r_{p\ sh}B_o V_p}{r_p B_o + a_0 + z} \qquad \text{Eq. 9.07}$$

Eq. 9.07 gave accurate and consistent estimations of the SRC CTOD. This proves that the similar triangles assumption used in BS/ISO and JWES is a valid method for the estimation of CTOD.

Chapter 10

Discussion

10.1 Introduction

This piece of work studied the equations used by BSI, ISO, ASTM and JWES for the determination of CTOD. To investigate the accuracy of the standard equations, a set of experiments, including a number of tests modified to accommodate silicone crack casting were performed. The silicone replicated cracks enable physical measurement of the actual CTOD. Additionally, a number of finite element models were generated to represent the experiments, enabling information to be extracted from different perspectives, i.e. stress and strain, CTOD across the crack tip, models with different strain hardening property.

10.2 Different definitions for CTOD and implications

There are a number of definitions used for CTOD. Two of the best known definitions are: - the opening of the original crack tip and the distance between the points of 45 degree intercept from the blunted crack tip (described in Chapter 1.4.1). CTOD based on the original crack tip was used on the experimental and FE models in this work.

CTOD based on the original crack tip is easily applicable to both cracks exhibiting continuous blunting and stable ductile tearing. The original tip CTOD was implemented based on the displacement due to stresses at the crack tip, derived in Chapter 1.4.1. As tearing occur at the crack tip, CTOD based on the crack tip would no longer represent the displacement at the original crack tip due to crack tip stresses.

CTOD based on the 45 degree intercept was correlated to the original crack tip CTOD using FE models. The study was based on small deformation, where CTOD was related to J based on the HRR solution at the crack tip (Shih 1981). Tearing ahead of the crack tip raises complications for the determination of the 45 degree CTOD, where the condition of a blunted crack tip is not always fulfilled.

For experimental evaluation of the 45 degree CTOD, Verstraete et al. (2013) utilized the method illustrated in Figure 10.01. The 45 degree intercept line was based on the original crack length, ignoring the effects of crack tip blunting and tearing ahead of the crack tip. This method could give comparable values to CTOD based on the opening of the original crack tip (Zhu et al. 2017). However, it should be noted that due to the offset of the origin of the 45 degree line is, the theoretical J-CTOD relationship due to the HRR solution is no longer valid. Therefore, defining

CTOD based on the original crack tip and rigid rotational point ahead of the crack tip gives a better representation of CTOD over a range of strain hardening properties.

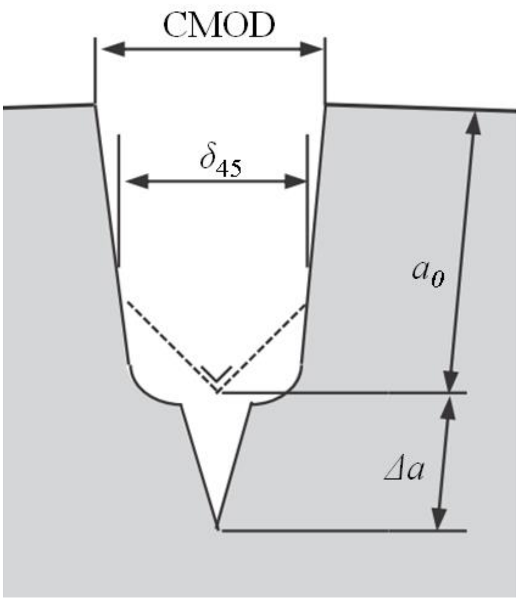

Figure 10.01 An alternative method for the evaluation of δ_{45} (Verstraete et al. 2013; Zhu et al. 2017)

10.3 Effects of ductile stable tearing on CTOD

The BS CTOD (based on the original crack tip) and ASTM CTOD (based on the 45 degree intercept) give contradicting trends for increasing crack tip tearing. For increasing crack length, BS will give larger CTOD compared to a constant crack length, and the opposite for ASTM (Chapter 8.3).

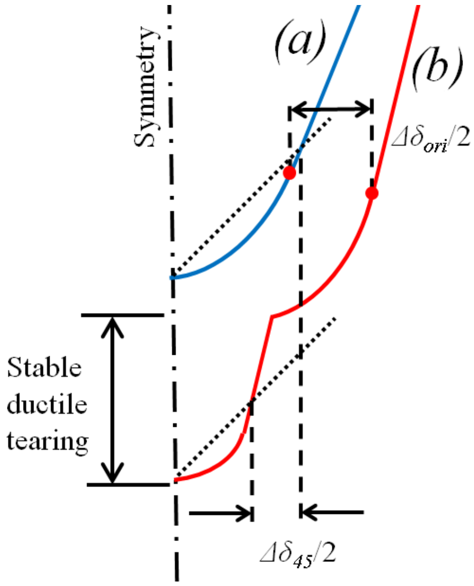

Figure 10.02 Difference in CTOD due to stable ductile tearing: crack tip with continuous blunting (a), and crack tip with stable ductile tearing (b)

Figure 10.02 shows the concept diagram of a half crack to illustrate the effect of tearing at the crack tip on the two different definitions of CTOD (based on the opening of the original crack tip and the 45 degree intercept method). The point of assessment for the CTOD based on the opening of the original crack tip is shown as red dots, and dotted lines were drawn from the blunted crack tips for the assessment of the 45 degree intercept CTOD. The difference of CTOD due to crack tearing is described as $\Delta\delta_{ori}/2$ for the CTOD from the original crack tip and $\Delta\delta_{45}/2$ for the 45 degree intercept CTOD.

Based on the illustration in Figure 10.02, it could be seen that with the occurrence of tearing, $\Delta\delta_{ori}/2$ would give positive value (larger CTOD), whereas $\Delta\delta_{45}/2$ gives negative value (smaller CTOD). The concept agrees to the trend of crack correction factors used by BS and ASTM (described in Chapter 8.3). When tearing occurs ahead of the crack tip, energy is released from the crack, leading to lower work experienced by the crack compared to one that deforms without tearing (Figure 8.05). This suggests that both CTOD used in BS and ASTM is correct based on the definition adopted. However, further work is required for the unification of *J* and CTOD in terms of physical and experimental significance.

10.4 Necessity of crack correction for single specimen unloading compliance R-curve

For the determination of CTOD for R-curves, BS, ASTM and ISO specified equations considering crack extension correction if the single specimen unloading compliance method was used. Apart from the BS estimation for the high strain hardening material, all three equations underestimate the physical CTOD from the silicone replicas (Chapter 8.4.3).

For the BS equation, assuming similar load-displacement data, the standard single point equation (used for multiple specimen R-curve) would give lower values compared to the equation with crack extension correction. Increasing crack length applied on the standard single point equation would give reducing CTOD (Figure 6.08), *vice versa* for equation with crack correction (Figure 10.02).

The *J*-based equations considering crack correction (ASTM and ISO) underestimate CTOD regardless of the material strain hardening. Both *J*-based standard single point equation and equation considering crack correction give reducing CTOD with increasing crack length.

Chapter 7.5.2 and 8.4.3 showed that both standard single point equation and equation considering crack extension correction underestimate CTOD, apart from BS for high strain hardening material. Additionally, the FE models showed that apart from the BS estimation for σ_{ys}/σ_{uts}< 0.68, all standard single point equations (BS, ASTM and JWES) underestimate CTOD (Figure 7.19). This suggests that for specimen thickness of B=20mm, the single point equations generally underestimate CTOD, therefore the crack extension correction is not necessary for the CTOD R-curve, as it raises additional complication in the calculation. However, it should be noted that the crack extension correction factor might improve the CTOD estimations for large specimen sizes, where more crack extension is encountered.

10.5 The geometrical and strain hardening effects on CTOD

The BS equations does not consider the effects of strain hardening, and issues arise when it overestimates CTOD from both the silicone replica and the FE model for higher strain hardening material properties (Chapter 7.5.2 and 8.4.3). ASTM considers strain hardening in the *m* factor used in the *J*-CTOD conversion, whereas JWES corrects for strain hardening using its own (and different) *m* factor in the elastic CTOD equation and f(σ_{ys}/σ_{uts}), a tensile ratio based function for the plastic CTOD equation (Figure 5.07 and Figure 5.11).

Both the JWES *m* factor and f(σ_{ys}/σ_{uts}) corrects the equations to give lower CTOD for higher strain hardening properties, and *vice versa* for lower strain hardening properties. The ASTM and JWES equation consistently underestimate CTOD from the FE models with idealised tensile properties by about 12%, showing a similar trend for the models exhibiting continuous crack tip blunting.

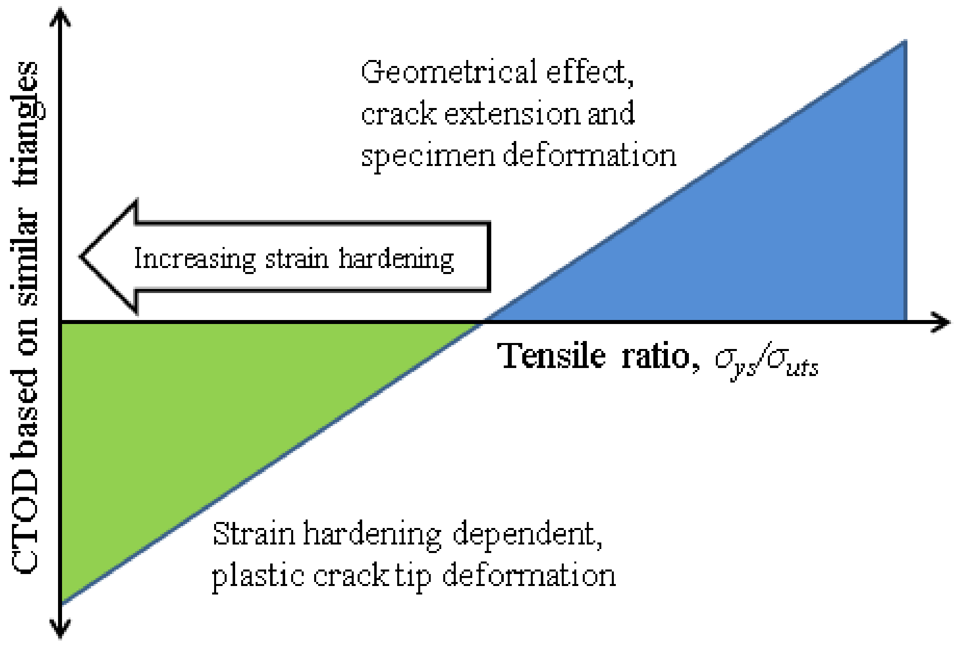

Figure 10.03 The relative influence of strain hardening and geometrical effect on CTOD based on similar triangles

The FE models replicating the experiments showed a consistent rotational factor, r_p of approximately 0.4 (Figure 9.08), whilst the strain hardening corrected rotational factor, $r_{p\ sh}$ range from 0.33 to 0.55 for $0.44 \leq \sigma_{ys}/\sigma_{uts} \leq 0.98$ (Figure 9.13). This suggests that for low tensile ratio, the plastic crack tip deformation at the crack tip leads to lower CTOD than that estimated from the similar triangles method; for high tensile ratio, crack extension and specimen bending would give larger CTOD than that estimated using the similar triangles method (Figure 10.03). The ASTM, JWES and Eq. 9.07 from Chapter 9.4 showed that strain hardening correction are necessary for the estimation of CTOD for different strain hardening material.

10.6 The implication of different CTOD values in flaw assessment

CTOD as a fracture parameter is commonly used in applications such as in defect assessment procedures, material characterisation in the steel industry as well as in the additive manufacturing industry. The experimental and finite element modelling results (Figure 4.12) show that the equations in national and international code and standards for CTOD gives different values between these Standards, particularly for materials with lower yield to tensile ratios.

These differences were considered in relation to the assumptions about the loading on the crack, and in particular across the crack front. In a through-thickness crack, the middle of the crack is considered to be plane strain dominant, whereas the sides of the crack on the surface of the specimen would be plane stress dominant (Figure 4.12). Based on the theoretical derivation of CTOD in Small Scale Yielding (SSY) conditions (Eq. 1.15), the plane strain region (where $E'=E/(1-v^2)$) should give lower CTOD compared to the plane stress region (where $E'=E$). Therefore it is expected that CTOD will be lower in the middle of the specimen, than at the surface.

Upon reviewing the studies which led to the implementation in Standards (Chapter 1.7), particularly in ASTM E1820, it was found that the equations were calibrated to the average of CTOD across the crack in the thickness direction. In Chapter 6.4, it was shown that CTOD in the middle of the crack is an approximation of the average CTOD across the thickness, which was assumed to be representative of the CTOD estimated by the standards, based on clip gauge measurements.

The effect of variation in the assumption about CTOD on the expected structural integrity of a structure can be quantified using fracture mechanics methods. In BS 7910 (BSI 2014a), CTOD is applied in Failure Assessment Diagrams, FAD in terms of dimensionless parameter, K_r, where (Ozawa et al. 2014; Minami et al. 2006)

$$K_r = \frac{K_{assessed}}{K_{mat}} \quad \text{Eq. 10.01}$$

BS 7910 converts the material toughness in terms of CTOD, δ_{mat}, to K_{mat} using the following equation

$$K_{mat} = \sqrt{\frac{m\sigma_{ys}\delta_{mat}E}{1-v^2}} \quad \text{Eq. 10.02}$$

where for 0.3≤ σ_{ys}/σ_{uts}≤ 0.98, i.e. for the full range of materials from high strain hardening to extremely brittle materials.

$$m = 1.517\left(\frac{\sigma_{ys}}{\sigma_{uts}}\right)^{0.3188}$$

Figure 10.04 shows a generic FAD used in defect assessment. The L_r, load ratio and assessment line are described in BS 7910 based on material stress and strain properties. If the assessment points fall within the acceptable region of the assessment line, the assessed defect is considered safe, and *vice versa* if the assessment point falls outside the acceptable region.

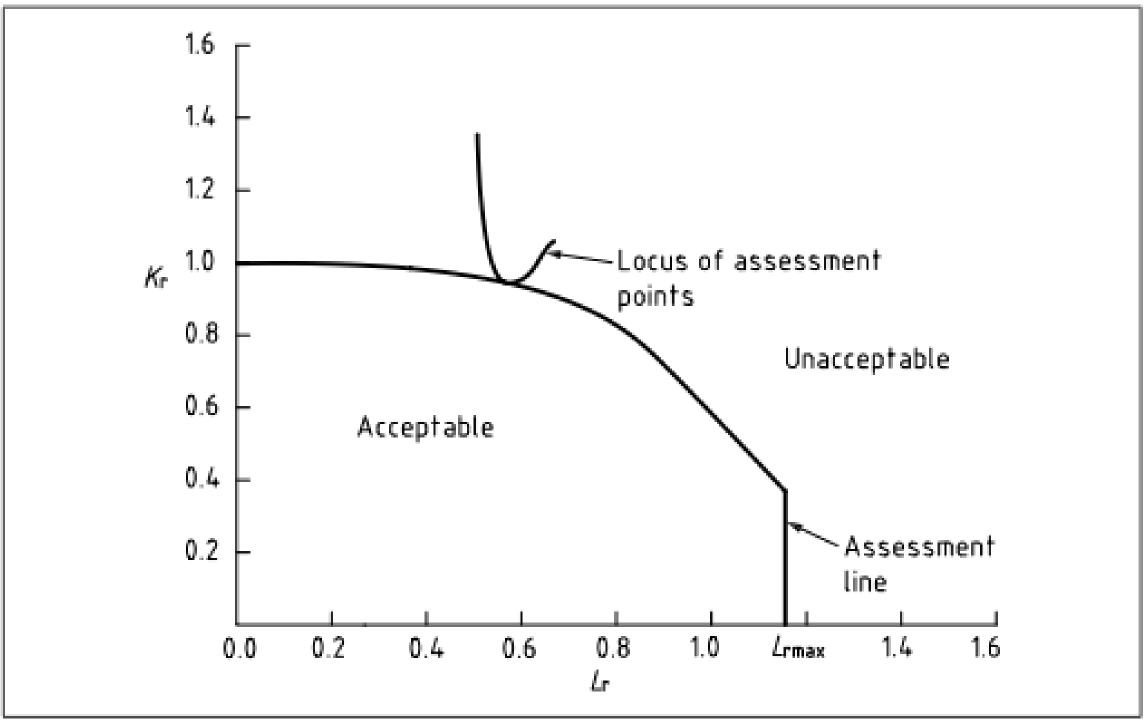

Figure 10.04 FAD diagram based on BS 7910 (BSI 2014a)

To exhibit the importance of the accuracy of CTOD in terms of flaw assessment, a hypothetical case was assessed using BS 7910 procedures within TWI's CrackWISE5 software, and using R-curve data from M02-08. Three different CTOD R-curve cases were used to represent fracture toughness, based on ASTM E1820, BS 7448-4 and the silicone replica (Figure 10.05). Figure 10.05 shows that the silicone replica gave the highest toughness CTOD R-curve, followed by BS 7448-4 and ASTM E1820.

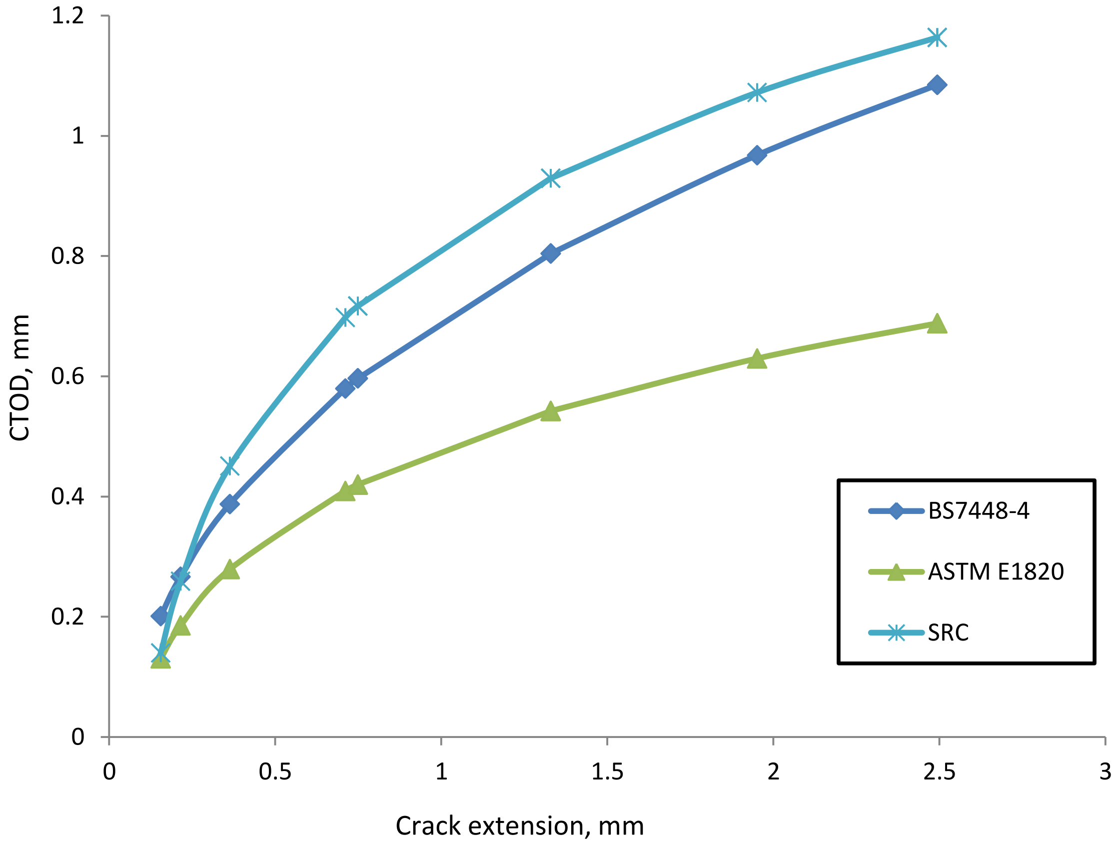

Figure 10.05 CTOD R-curves from M02-08

A flat plate case with surface flaw was investigated (B= 20mm), containing a surface flaw of dimensions 10mm by 20mm, under a membrane stress of 280MPa, and assuming the tensile properties of material M02. Full details of the assessment case are attached in appendices. Figure 10.06 shows the failure assessment diagram (FAD) with assessments based on the three CTOD R-curves in Figure 10.05. The results illustrate that the ASTM based CTOD gave the highest overall K_r, and gives an unsafe assessment for this scenario. The BS and silicone replica CTOD R-curves are lower, and partially inside the FAD, indicating that this flaw would be safe with these properties. Relating the output to the CTOD R-curve input, it could be determined that a comparatively lower CTOD would lead to higher K_r in FADs, contributing to the possibility of a flaw assessment procedure predicting that a flaw is unsafe when the actual properties (as represented by the silicone replica data) show that it would have been acceptable.

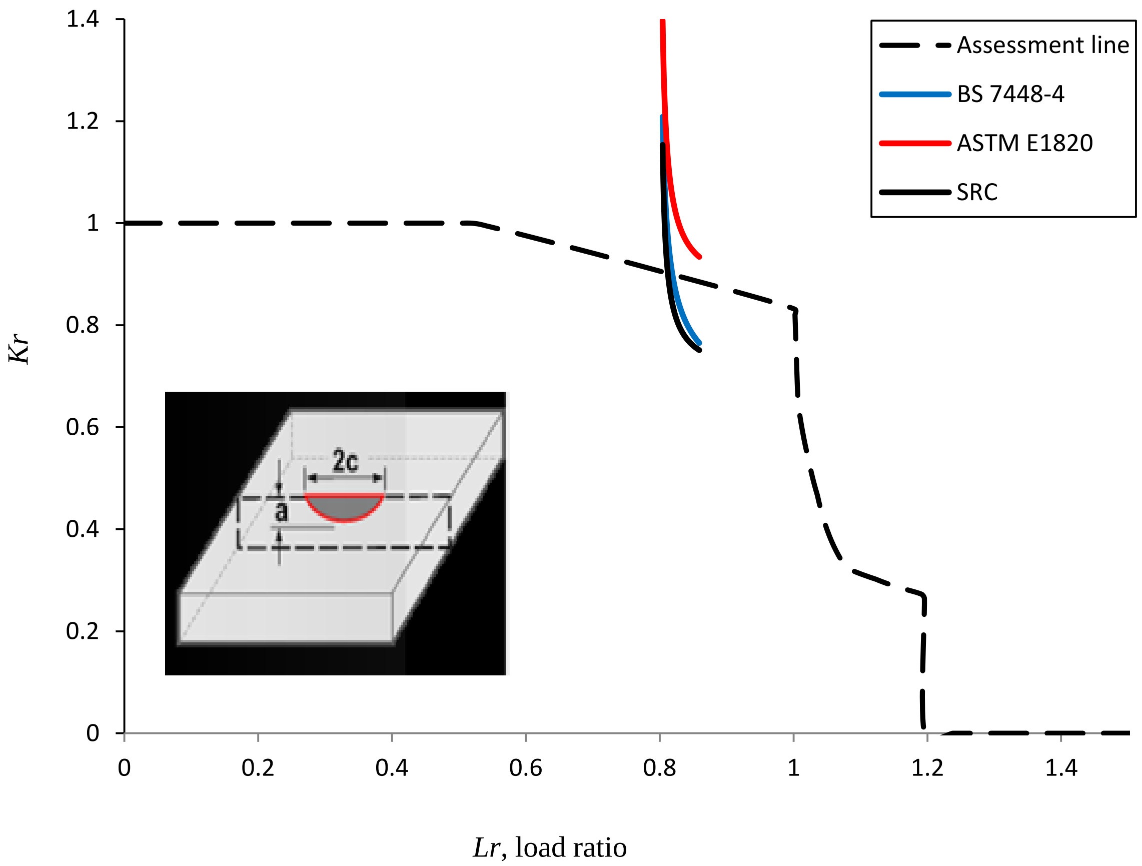

Figure 10.06 FAD based on CTOD from M02-08, calculated using BS 7448-4 , ASTM E1820 and silicone replica measurements

The analyses presented here show that for a postulated case, the difference in CTOD determined from different standard methods could be the difference between assessments being wrongly considered potentially unsafe. This is a particular concern for tearing resistance curves (R-curves) where the standards show a large discrepancy. Being over-conservative in the determination of fracture toughness might sometimes contribute to failures of flaw assessment procedures, leading to potential unnecessary financial and time penalty due to repairs and replacements. It is tedious and expensive if special methods, i.e. measurement of silicone replicas and digital image correlation techniques were used for the determination of CTOD for fracture toughness data, and therefore it is important that the CTOD equations in the standards give accurate representation of CTOD without being over-conservative.

Chapter 11

General conclusion, recommendation and further work

11.1 General conclusion

This piece of work provides a study on the CTOD equations from BS 7448, ISO 12135, ASTM E1820 and WES 1108 based on physical measurements of the crack replica and FE models. The ideal equation should estimate CTOD with the best accuracy, but yet does not overestimate the actual value of CTOD to ensure conservatism when used in fitness-for-service applications.

Based on analysis of archived single point fracture toughness data, it could be concluded that the ASTM E1820 will almost always underestimate BS 7448 regardless of material strain hardening properties. Generally, the elastic CTOD would be the main determinant of the resultant CTOD if CTOD< 0.2mm; and plastic CTOD most significant for CTOD> 0.2mm. It should be noted that the magnitude of elastic CTOD values are small despite being the main factor in low CTOD values. The accuracy of the plastic component of CTOD would be more important in cases where high plastic deformation is encountered.

Upon measuring the silicone crack replicas from the SS316 specimen, it was confirmed that CTOD is not constant across the crack front. The sides of the crack showed the highest CTOD, followed by the middle of the crack. The difference is not as obvious because the tearing across the crack tip was distributed, somewhat correcting for the difference when driving the crack extension. This would mean that for fatigue pre-cracked specimens, if crack tip ‘tunnelling’ is experienced at the fatigue crack tip, measurements of CTOD based on the side surfaces of the specimen would not be suitable as they would overestimate CTOD in the middle.

The single point CTOD equations were validated to the measurements from the silicone replicas. BS 7448 gave good estimation for CTOD but overestimates higher strain hardening, lower tensile ratio materials. Both ASTM E1820 and WES 1108 underestimate CTOD regardless of material strain hardening, and thus should give a safe prediction of CTOD for ECA and FFS purposes. A series of FE models showed that the WES 1108 gives more consistent accuracy than ASTM E1820 for the range of tensile ratio, $0.44 \leq \sigma_{ys}/\sigma_{uts} \leq 0.98$.

The BS 7448 and the *J*-based CTOD equations (ASTM E1820 and ISO 12135) gave opposing trend for the R-curve CTOD equations. Based on CTOD measured from the silicone replicas, similar to that observed in the single point CTOD validation, BS 7448 overestimates the high strain hardening material, and ASTM E1820 showed the lowest CTOD R-curve for most cases. The WES 1108 equation, despite not corrected for crack growth, gave a good estimation of the CTOD

R-curve for the low, medium and high strain hardening material.

r_p was extracted experimentally from the double clip gauge data for approximate CTOD values between 0.2mm to 1.0mm. Different from that assumed in BS 7448 and WES 1108, r_p scatters between 0.3 and 0.5. Analysing r_p determined from the FE model based on the CMOD and CTOD, it was shown that r_p is 0.56 for σ_{ys}/σ_{uts}= 0.98, decreasing linearly to 0.30 for σ_{ys}/σ_{uts}= 0.44. This shows that the rotational factor concept for the estimation of CTOD is valid, but correction is required based on the material tensile properties. Based on the FE modelling in this work, an improved CTOD equation was obtained, which gives good correlation to the SRC CTOD based on the opening of the original crack tip. The equation is given as

$$\delta_{sh} = \delta_{el\ JWES} + \frac{r_{p\ sh} B_o V_p}{r_p B_o + a_0 + z} \qquad \text{Eq. 9.07}$$

Where

$$r_{p\ sh} = 0.4668 \frac{\sigma_{ys}}{\sigma_{uts}} + 0.0996 \qquad \text{Eq. 9.06}$$

The equation would be suitable for instances where the standard equations are less suitable, e.g. BS 7448 in high strain hardening materials.

11.2 Recommendation

An ideal estimation for CTOD is being as accurate as possible, but yet not overestimates the physical representation of CTOD. Based on the findings from the silicone replica and FE models, it was shown that the BS 7448-1, ASTM E1820 and WES 1108 are all fit for estimating CTOD for tensile ratio 0.7≤ σ_{ys}/σ_{uts}≤ 1.0. For tensile ratio, σ_{ys}/σ_{uts}≤0.7, the ASTM E1820 and WES 1108 gave good estimates of CTOD, whereas the BS 7448 overestimates CTOD due to the assumptions used in the equation. As result, the WES 1108 equation would give a better estimate of CTOD for 0.44≤ σ_{ys}/σ_{uts}≤ 1.0, as it is slightly more versatile and accurate than ASTM E1820. This is true for both single point CTOD values and CTOD R-curves. It should be noted that the ISO 12135 uses the same equation as the BS 7448 for single point values, but a *J*-based equation similar to ASTM E1820 for CTOD R-curves.

For the SEN(B) setup, it was found that the crack correction factor does not give any significant improvement in the accuracy for estimating the CTOD R-curve. The WES 1108 equation does not include a crack correction factor in the equation, but it still manages to give equivalent, if not more accurate estimation of CTOD R-curves.

11.3 Further work

The author is aware that the CTOD definition used in BS 7448 and ASTM E1820 is different due to the assumption used. The crack extension correction applied by both standards for CTOD R-curves gives the opposite trend, the diagram in Chapter 10.1 showed that both definitions are conceptually correct, which leaves a quandary when defining CTOD for R-curves. The *J*-CTOD association was initially formulated without the consideration of crack tip tearing. This suggests that more work is required for the *J*-CTOD unification in general conditions where tearing is expected.

The crack tip from the FE models in this work deforms plastically and does not involve crack tearing. By applying crack tip tearing boundary conditions in the model by using the GTN criterion or similar, the change of CTOD and *J* due to crack tip tearing could be investigated directly. This would be useful in validating the crack tearing correction factors used in BS 7448-4 and ASTM E1820.

The position in the middle of the crack is chosen as the representative location for the assessment of CTOD from the silicone replicas and FE models. This decision was based on the analysis of the elastic component of the CTOD equations, where a plane strain correction was used. However, it should be noted that none of the standards specify the exact location for the assessment of fracture toughness, and the *J* equation in ASTM E1820 is calibrated using data from the middle and average of the crack. The fracture toughness values across the crack tip would be more consistent is the crack tip constraint across the crack front is similar (plane strain dominated), possible if side grooves are used. This assumption has yet to be validated in this work.

Additionally, it is difficult to model the curved crack front manufactured by fatigue loading in a real specimen. The curved crack front increases the complexity of the meshing around the crack tip, especially if the *J*-contours are required. It would be convenient if a correlation could be made between a FE model with a blunted crack tip vs. actual specimen with blunted crack tip vs. actual specimen with fatigue pre-cracked tip. This could give an estimate of correction required if a blunted crack tip is used in FE, which is ideal for the formation of *J* contours around the crack tip.

References

Anderson, T.L., 1984. Effect of Crack-tip Region Constraint on Fracture in the Ductile-to-Brittle Transition. *National Bureau of Standards*.

Anderson, T.L., 2008. *Fracture Mechanics: Fundamentals and application* 3rd ed., Taylor & Francis Group. Available at: http://medcontent.metapress.com/index/A65RM03P4874243N.pdf [Accessed February 6, 2014].

Anderson, T.L., McHenry, H.I. & Dawes, M.G., 1985. Elastic-Plastic Fracture Toughness Tests with Single-Edge Notched Bend Specimens. *ASTM STP 856*, pp.210–229.

Anderson, T.L. & Osage, D.A., 2000. API 579: a comprehensive fitness-for-service guide. *International Journal of Pressure Vessels and Piping*, 77(14–15), pp.953–963. Available at: http://www.sciencedirect.com/science/article/pii/S0308016101000187 [Accessed March 4, 2015].

API, 2007. API 579- Fitness-For-Service. *American Petroleum Institute*.

ASTM, 2012. ASTM E1290-08e1 - Standard Test Method for Crack-Tip Opening Displacement (CTOD) Fracture toughness measurement. *ASTM*, pp.1–15.

ASTM, 1999. ASTM E1290-99 - Standard Test Method for Crack-Tip Opening Displacement (CTOD) Fracture toughness measurement. *ASTM*.

ASTM, 2014. ASTM E1820-13 - Standard Measurement of Fracture Toughness. *ASTM*, pp.1–54.

ASTM, 2015. ASTM E1820-15a - Standard Measurement of Fracture Toughness. *ASTM*.

Banerjee, S., 1981. Influence of specimen size and configuration on the plastic zone size, toughness and crack growth. *Engineering Fracture Mechanics*, 15(3–4), pp.343–390. Available at: http://www.sciencedirect.com/science/article/pii/0013794481900655 [Accessed March 6, 2014].

Begley, J.A. & Landes, J.D., 1972. The J integral as a fracture criterion. *ASTM STP 514*, pp.1–20.

Brenner, U., Schulze, H.D. & Gnirß, G., 1983. Fracture mechanics analysis of stable crack growth under sustained load and instability of circumferential cracks in straight water-steam pipes. *International Journal of Pressure Vessels and Piping*, 11(2), pp.65–79.

BSI, 1991. BS 7448-1:1991 - Fracture mechanics toughness tests — Part 1: Method for determination of KIc, critical CTOD and critical J values of metallic materials. *BSI*, ((R 2007)).

BSI, 1997. BS 7448-4:1997 - Fracture mechanics toughness tests — Part 4: Method for determination of fracture resistance curves and initiation values for stable crack extension in metallic materials. *BSI*, (1).

BSI, 2014a. BS 7910:2013 - Guide to methods for assessing the acceptability of flaws in metallic structures. *BSI*.

BSI, 2014b. BSI 8571 - Method of test for determination of fracture toughness in metallic materials using single edge notched tension (SENT) specimens (draft). *BSI*, (March), pp.1–24.

Carlson, K.W. & Williams, J.A., 1981. A more basic approach to the analysis of multiple-specimen R-curves for determination of Jc. *ASTM STP 743*, pp.503–524.

Cotterell, B., 2002. The past, present, and future of fracture mechanics. *Engineering Fracture Mechanics*, 69, pp.533–553.

Dawes, M.G., 1979. Elastic-Plastic Fracture Toughness Based on the COD and J-Contour Integral Concepts. *ASTM STP 668*, pp.307–333.

Dawes, M.G. et al., 1992. Shallow crack test methods for the determination of Kic, CTOD and J fracture toughness.

DNV, 2006. DNV-RP-F108 - Fracture Control for Pipeline Installation Methods Introducing Cyclic Plastic Strain. *Det Norske Veritas*, (January).

Donato, G.H.B. & Ruggieri, C., 2006. Estimation Procedures for J and CTOD Fracture Parameters Using Three-Point Bend Specimens. In *6th International Pipeline Conference*. Calgary, Alberta, Canada: ASME, pp. 1–9. Available at: http://proceedings.asmedigitalcollection.asme.org/proceeding.aspx?articleid=1597148 [Accessed April 23, 2014].

Garwood, S.J., 1986. Time dependent ductile crack extension in A533B Class I steel. *Nuclear Engineering and Design*, 91, pp.179–206.

Gere, J.M., 2004. *Mechanics of Materials* 6th ed., Thomson Learning Inc.

Gibson, G.P. & Druce, S.G., 1985. Some Observations on J-R Curves. *ASTM STP 856*, pp.166–182.

Gordon, J.R., Keith, G. & Gordon, N.C., 2013. Defect and Strain Tolerance of Girth Welds in High Strength Pipelines. In *International Seminar on Welding High Strength Pipeline Steels*. CBMM and TMS.

Green, A.P., 1956. The plastic yielding of shallow notched bars due to bending. *Journal of the Mechanics and Physics of Solids*, 4(4), pp.259–268. Available at: http://www.sciencedirect.com/science/article/pii/0022509656900357 [Accessed September 3, 2014].

Green, A.P. & Hundy, B.B., 1956. Initial plastic yielding in notch bend tests. *Journal of the Mechanics and Physics of Solids*, 4(2), pp.128–144. Available at: http://www.sciencedirect.com/science/article/pii/0022509656900850 [Accessed February 17, 2014].

Green, G. & Knott, J.F., 1975. On effects of thickness on ductile crack growth in mild steel. *Journal of the Mechanics and Physics of Solids*, 23(3), pp.167–183.

Griffith, A.A., 1921. The Phenomena of Rupture and Flow in Solids. *Philosophical Transactions of the Royal Society of London*, 221, pp.163–198.

Gurson, A.L., 1977. Continuum theory of ductile rupture by void nucleation and growth: Part 1 - yield criteria and flow rules for porous ductile media. *Journal of Engineering Materials and Technology*, 99(1), pp.2–15.

Han, K. et al., 2014. The effect of constraint on CTOD fracture toughness of API X65 steel. *Engineering Fracture Mechanics*, 124–125, pp.167–181. Available at: http://dx.doi.org/10.1016/j.engfracmech.2014.04.014.

Haslett, M., Yang, Y. & Eren, E., 2015. Report 23725/1/15: Investigation of CTOD Fracture Toughness Analysis Methods. *TWI Report*, 44(March).

Higdon, A. et al., 1978. *Mechanics of Materials* 3rd ed., New York: John Wiley & Sons Inc.

Hosford, W.F., 2010. *Solid Mechanics*, Cambridge University Press.

Huang, Y. & Zhou, W., 2017. Effective Thickness of Side-Grooved Clamped SE(T) Specimens for J-R Curve Testing. *Journal of Testing and Evaluation*, 45(2), p.20150274. Available at: http://www.astm.org/doiLink.cgi?JTE20150274.

Huang, Y. & Zhou, W., 2014. J-CTOD relationship for clamped SE(T) specimens based on three-dimensional finite element analyses. *Engineering Fracture Mechanics*, 131(April 2016), pp.643–655. Available at: http://www.sciencedirect.com/science/article/pii/S0013794414003294 [Accessed August 18, 2015].

Huang, Y., Zhou, W. & Wang, E., 2014. Constraint-corrected J-R curve based on three-dimensional finite element analyses. *Fatigue & Fracture of Engineering Materials & Structures*, 37(10), pp.1101–1115.

Hunt, R.A. & McCartney, L.N., 1979. A new approach to Weibull's statistical theory of brittle fracture. *International Journal of Fracture*, 15(4), pp.365–375.

Hutchison, E. & Pisarski, H.G., 2013. Effects of Crack Front Curvature on J and CTOD determination in Fracture Toughness Specimens by FEA. In *Proceedings of the ASME 2013 32nd International Conference on Ocean, Offshore and Arctic Engineering OMAE 2013*. pp. 1–8.

Ingham, T. et al., 1971. The effect of geometry on the interpretation of COD test data. In *Practical application of fracture mechanics to pressure-vessel technology, Institution of Electrical Engineers*. Savoy Place, London: Institution of Mechanical Engineers, pp. 200–208.

Inglis, C.E., 1913. Stresses in a Plate due to the presence of Cracks and Sharp Corners. *Trans. I.N.A.*

Irwin, G.R., 1968. Linear fracture mechanics, fracture transition, and fracture control. *Engineering Fracture Mechanics*, 1(2), pp.241–257. Available at: http://www.sciencedirect.com/science/article/pii/0013794468900015 [Accessed June 9, 2014].

ISO, 2002. ISO 12135 - 02 Metallic materials - Unified method of test for the determination of quasistatic fracture toughness.

ISO, 2016. ISO 12135 - 16 Metallic materials - Unified method of test for the determination of quasistatic fracture toughness.

Janssen, M., Zuidema, J. & Wanhill, R., 2004. *Fracture Mechanics* 2nd ed., Spon Press.

JWES, 1995. WES 1108: 1995 Standard test method for Crack-Tip Opening Displacement (CTOD). *The Japan Welding Engineering Society*.

JWES, 2014. WES 1108: 2014 Standard test method for Crack-Tip Opening Displacement (CTOD) fracture toughness measurement *draft. *The Japan Welding Engineering Society*, 1(1).

Kawabata, T. et al., 2016. Proposal for a new CTOD calculation formula. *Engineering Fracture Mechanics*, 159, pp.16–34. Available at: http://linkinghub.elsevier.com/retrieve/pii/S0013794416301096.

Kayamori, Y., Inoue, T. & Tagawa, T., 2008. Transformation of BS7448-CTOD to ASTM E1290-

CTOD. *ASME Pressure Vessels and Piping Division Conference*, 1, pp.1–8.

Khor, W. et al., 2016. Measurement and prediction of CTOD in austenitic stainless steel. *Fatigue & Fracture of Engineering Materials & Structures*, 39, pp.1433–1442. Available at: http://doi.wiley.com/10.1111/ffe.12487.

Kim, Y., Chao, Y.J. & Zhu, X.K., 2003. Effect of specimen size and crack depth on 3D crack-front constraint for SENB specimens. *International Journal of Solids and Structures*, 40(23), pp.6267–6284. Available at: http://www.sciencedirect.com/science/article/pii/S0020768303003925 [Accessed March 6, 2014].

Kim, Y.-J. et al., 2004. 3-D constraint effects on J testing and crack tip constraint in M(T), SE(B), SE(T) and C(T) specimens: numerical study. *Engineering Fracture Mechanics*, 71, pp.1203–1218. Available at: http://www.sciencedirect.com/science/article/pii/S001379440300211X [Accessed April 22, 2014].

Kirk, M.T. & Dodds Jr., R.H., 1993. J and CTOD Estimation Equations for Shallow Cracks in Single Edge Notch Bend Specimens. *Journal of Testing and Evaluation*, 21(4), pp.228–238.

Kirk, M.T. & Wang, Y.-Y., 1995. Wide range CTOD estimation formulae for SE(B) specimens. *ASTM STP 1256*, pp.126–141.

Kobayashi, H. & Onoue, H., 1943. Brittle Fracture of Liberty Ships. *Failure Knowledge Database 100 Selected Cases*, (April), pp.1–7. Available at: http://www.sozogaku.com/fkd/en/hfen/HB1011020.pdf.

Kolednik, O., 1988. On the calculation of COD from the clip-gauge displacement in CT and bend specimens. *Engineering Fracture Mechanics*, 29(2), pp.173–188. Available at: http://www.sciencedirect.com/science/article/pii/0013794488900458 [Accessed February 17, 2014].

Kumar, V., German, M.D. & Shih, C.F., 1981. *An Engineering Approach for Elastic-Plastic Fracture Analysis*, New York.

Landes, J.D. & Begley, J.A., 1972. The effect of specimen geometry on Jic. *ASTM STP 514*, pp.24–39.

Lin, I.H. et al., 1982. Displacements and rotational factors in Single Edge Notched Bend specimens. *International Journal of Fracture*, 20, pp.R3–R7.

MacDonald, M., Rhodes, J. & Taylor, G.T., 2000. Mechanical properties of stainless steel lipped channels. *Fifteenth International Specialty Conference on Cold-Formed Steel Structures*, pp.673–686.

Meshii, T., Lu, K. & Fujiwara, Y., 2016. Extended investigation of the test specimen thickness (TST) effect on the fracture toughness (Jc) of a material in the ductile-to-brittle transition temperature region as a difference in the crack tip constraint ? What is the loss of constraint in the TST. *Engineering Fracture Mechanics*, 135(July), pp.286–294.

Minami, F. et al., 2006. Method of constraint loss correction of CTOD fracture toughness for fracture assessment of steel components. *Engineering Fracture Mechanics*, 73(14), pp.1996–2020. Available at: http://www.sciencedirect.com/science/article/pii/S0013794406001202 [Accessed March 1, 2014].

Moore, P. & Nicholas, J., 2013. The effect of Inclusions on the Fracture Toughness of Loacl Brittle Zones in the HAZ of Girth Welded Line Pipe. In *Proceedings of the ASME 2013 32nd*

International Conference on Ocean, Offshore and Arctic Engineering OMAE13. pp. 1–10.

Moskovic, R., 1993. Statistical analysis of censored fracture toughness data in the ductile to brittle transition temperature region. *Engineering Fracture Mechanics*, 44(1), pp.21–41. Available at: http://www.sciencedirect.com/science/article/pii/0013794493900798 [Accessed January 28, 2015].

Nevalainen, M. & Dodds Jr., R.H., 1995. Numerical investigation of 3-D constraint effects on brittle fracture SE(B) and C(T) specimens. *International Journal of Fracture*, 74, pp.131–161.

Nowak-Coventry, M., Pisarski, H.G. & Moore, P.L., 2015. The effect of fatigue pre-cracking forces on fracture toughness. *Fatigue & Fracture of Engineering Materials & Structures*, 0, pp.1–14. Available at: http://doi.wiley.com/10.1111/ffe.12339.

Ozawa, T., Yoshinari, H. & Aihara, S., 2014. Study on CTOD-FAD (first report) -Fracture strength assessment for through thickness crack- CTOD-FAD の検討 （ 第一報 ）. , (December), pp.127–135.

Pisarski, H. et al., 2010. Experimental Comparison of CTOD Estimated According to BS7448 & ASTM E1820. *ASTM workshop on Critical Evaluation of Calculation Methods for Crack-Tip Opening Displacement (CTOD), San Antonio, TX*, (November).

Pisarski, H.G., 1987. Measurement of Heat Affected Zone Fracture Toughness. In *Steel in Marine Structures*.

Pook, L.P., 2013. A 50-year retrospective review of three-dimensional effects at cracks and sharp notches. *Fatigue & Fracture of Engineering Materials & Structures*, 36(8), pp.699–723.

Pook, L.P., 2003. A finite element analysis of cracked square plates and bars under antiplane loading. *Fatigue & Fracture of Engineering Materials & Structures*, 26(6), pp.533–541.

Pook, L.P., 2000. Finite element analysis of corner point displacements and stress intensity factors for narrow notches in square sheets and plates. *Fatigue & Fracture of Engineering Materials & Structures*, 23(12), pp.979–992.

Pook, L.P., 1994. Some implications of corner point singularities. *Engineering Fracture Mechanics*, 48(3), pp.367–378.

Ramberg, W. & Osgood, W.R., 1943. Description of stress-strain curves by three parameters.

Rice, J.R., 1968. A Path Independent Integral and the Approximate Analysis of Strain Concentration by Notches and Cracks. *Journal of Applied Mechanics*, 35(2), pp.379–386. Available at: http://appliedmechanics.asmedigitalcollection.asme.org/article.aspx?articleid=1398618.

Rice, J.R., Paris, P.C. & Merkle, J.G., 1973. Some further results of J-Integral analysis and estimates. *ASTM STP 536*, pp.231–245.

Robinson, J.N. & Tetelman, A.S., 1976. Comparison of various methods of measuring kic on small precracked bend specimens that fracture after general yield. *Engineering Fracture Mechanics*, 8(2), pp.301–313.

Robinson, J.N. & Tetelman, A.S., 1974. Measurement of KIC on small specimens using Critical Crack Tip Opening Displacement. *ASTM STP 559*, pp.139–158.

Robinson, J.N. & Tetelman, A.S., 1975. The relationship between crack tip opening displacement, local strain and specimen geometry. *International Journal of Fracture*, 11(3), pp.453–468. Available at: http://link.springer.com/article/10.1007/BF00033532 [Accessed September 1, 2014].

Ruggieri, C., 2012. Further results in J and CTOD estimation procedures for SE(T) fracture specimens – Part I: Homogeneous materials. *Engineering Fracture Mechanics*, 79, pp.245–265. Available at: http://www.sciencedirect.com/science/article/pii/S0013794411004115 [Accessed January 29, 2014].

Sarzosa, D.F.B. et al., 2016. Numerical simulation of ductile crack growth in medium wide plate specimens using 3-D computational cells. *Engineering Fracture Mechanics*, 168, pp.26–45. Available at: http://dx.doi.org/10.1016/j.engfracmech.2016.09.008.

Sarzosa, D.F.B., Souza, R.F. & Ruggieri, C., 2015. J–CTOD relations in clamped SE(T) fracture specimens including 3-D stationary and growth analysis. *Engineering Fracture Mechanics*. Available at: http://www.sciencedirect.com/science/article/pii/S0013794415002118 [Accessed June 4, 2015].

Schindler, H.J., Kalkhof, D. & Viehrig, H.W., 2014. Effect of notch acuity on the apparent fracture toughness. *Engineering Fracture Mechanics*, 129, pp.26–37. Available at: http://dx.doi.org/10.1016/j.engfracmech.2014.07.022.

Schulze, H.D. & Fuhlrott, H., 1980. Stable crack growth and variation of crack opening displacement of pre-cracked specimens under sustained load. *International Journal of Pressure Vessels and Piping*, 8(2), pp.131–142.

Schwalbe, K., 1995. Introduction of δ5 as an Operational Definition of the CTOD and its Practical Use. *ASTM STP 1256*, pp.763–778.

Schwalbe, K.-H., Newman, J.C. & Shannon, J.L., 2005. Fracture mechanics testing on specimens with low constraint—standardisation activities within ISO and ASTM. *Engineering Fracture Mechanics*, 72(4), pp.557–576. Available at: http://www.sciencedirect.com/science/article/pii/S0013794404001067 [Accessed March 28, 2014].

Selva, R., 2012. Living with Defects : Replace / Repair or prove Fitness-For-Service (FFS)? *13th International Conference on Pressure Vessel & Piping Technology*, (May), pp.20–23.

Shen, G. et al., 2004. Fracture Toughness Testing of Pipeline Girth Welds. In *International Pipeline Conference*. Calgary, Alberta, Canada: Minister of Natural Resources, Canada.

Shih, C.F., 1981. Relationships between the J-integral and the crack opening displacement for stationary and extending cracks. *Journal of the Mechanics and Physics of Solids*, 29(4), pp.305–326. Available at: http://www.sciencedirect.com/science/article/pii/002250968190003X [Accessed March 31, 2014].

Souza, R.F. De & Ruggieri, C., 2014. Revised η-factors for 3P SE(B) fracture specimens incorporating 3-D effects. In *Proceedings of the ASME 2014 Pressure Vessels & Piping Conference*. Anaheim, California, USA: ASME, pp. 1–10.

Spink, G.M., Worthington, P.J. & Heald, P.T., 1973. The Effect of Notch Acuity on Fracture Toughness Testing. *Materials Science and Engineering*, 11, pp.113–117.

SSC, RMS Titanic casestudy. *Ship Structure Committee*, pp.1–11. Available at: http://shipstructure.org/case_studies/RMSTitanic.pdf.

Tagawa, T. et al., 2010. Difference between ASTM E1290 and BS 7448 CTOD Estimation Procedures. *Welding in the World*, 54(7–8), pp.R182–R188. Available at: http://dx.doi.org/10.1007/BF03263504.

Tagawa, T. et al., 2014. Experimental measurements of deformed crack tips in different yield-to-tensile ratio steels. *Engineering Fracture Mechanics*, 128, pp.157–170. Available at: http://www.sciencedirect.com/science/article/pii/S0013794414002227 [Accessed August 12, 2014].

Tagawa, T., Haramishi, Y. & Minami, F., 2011. Stress Relaxation Behavior of Low Carbon Structural Steels. *Quarterly Journal of the Japan Welding Society*, 29(1), pp.48–54.

Taggart, R., Wahi, K.K. & Beeuwkes Jr., R., 1976. Relationship between the fracture toughness and the crack tip radius. *ASTM STP 605*, pp.62–71.

Tanguy, B. et al., 2007. Ductile to brittle transition of an A508 steel characterized by Charpy impact test , part I ., experimental results e Pineau To cite this version : Ductile to brittle transition of an A508 steel characterized by Charpy impact test . Part — I : experimenta.

Tsuru, S. & Garwood, S.J., 1979. Some aspects of the time dependent ductile fracturee of line pipe steels. *TWI Research Report 92/1979*.

Turner, C.E. & Etemad, M.R., 1990. Scaling of curves for side grooved pieces. *International Journal of Pressure Vessels and Piping*, 41(1), pp.43–58. Available at: http://www.sciencedirect.com/science/article/pii/030801619090076T [Accessed February 17, 2014].

Tvergaard, V., 1981. Influence of voids on shear band instabilities under plane strain conditions. *International Journal of Fracture*, 17(4), pp.389–407.

Vassilaros, M.G., Joyce, J.A. & Gudas, J.P., 1980. Effects of specimen geometry on the JI-R curve for ASTM A533B steel. *ASTM STP 700*, pp.251–270.

Verstraete, M.A. et al., 2013. Determination of CTOD resistance curves in side-grooved Single-Edge Notched Tensile specimens using full field deformation measurements. *Engineering Fracture Mechanics*, 110, pp.12–22. Available at: http://linkinghub.elsevier.com/retrieve/pii/S0013794413002609 [Accessed February 7, 2014].

Verstraete, M.A. et al., 2014. Evaluation and interpretation of ductile crack extension in SENT specimens using unloading compliance technique. *Engineering Fracture Mechanics*, 115, pp.190–203. Available at: http://www.sciencedirect.com/science/article/pii/S0013794413003585 [Accessed January 14, 2015].

Wallin, K., 2002. Master curve analysis of the "Euro" fracture toughness dataset. *Engineering Fracture Mechanics*, 69(4), pp.451–481. Available at: http://www.sciencedirect.com/science/article/pii/S0013794401000716 [Accessed July 22, 2014].

Wallin, K., 1985. The size effect in KIC results. *Engineering Fracture Mechanics*, 22(1), pp.149–163. Available at: http://www.sciencedirect.com/science/article/pii/0013794485901675 [Accessed July 22, 2014].

Wang, E., Zhou, W. & Shen, G., 2014. Three-dimensional finite element analysis of crack-tip fields of clamped single-edge tension specimens – Part I: Crack-tip stress fields. *Engineering Fracture Mechanics*, 116, pp.122–143. Available at: http://linkinghub.elsevier.com/retrieve/pii/S0013794413003883 [Accessed February 7, 2014].

Wang, Y.-Y., Reemsnyder, H.S. & Kirk, M.T., 1997. Inference Equations for Fracture Toughness Testing: Numerical analysis and Experimental verification. *ASTM STP 1321*, pp.469–484.

Wanhill, R.J.H., 2002. Milestone Case Histories in Aircraft Structural integrity. *National Aerospace Laboratory NLR*, (NLR-TP-2002-521), pp.1–25.

Wei, L. & Pisarski, H.G., 2007. FEA investigations into the effects of geometry and tensile properties on J and CTOD in standard fracture specimens. In *ESIA9 - 9th International Conference on Engineering Structural Integrity Assessment*,. Beijing, China.: EMAS.

Wells, A.A., 1969. Crack opening displacements from elastic-plastic analyses of externally notched tension bars. *Engineering Fracture Mechanics*, 1(3), pp.399–410. Available at: http://www.sciencedirect.com/science/article/pii/0013794469900010 [Accessed July 9, 2014].

Wells, A.A., 1971. The status of COD in Fracture Mechancis. In P. G. Glockner, ed. *Thirs Canadian Congress of Applied Mechanics*. The University of Calgary, pp. 59–77.

Wells, A.A., 1961. Unstable Crack Propagation in Metals: Cleavage and Fast Fracture. In *Proceedings of the Crack Propagation Symposium*. Cranfield, pp. 210–230.

Westergaard, H.M., 1939. Bearing pressures and cracks. *Journal of Applied Mechanics*, 61, pp.A49–A53.

Willoughby, A.A., 1981. On the Unloading Compliance Method of deriving Single-specimen R-Curves in Three-point Bending. *TWI Research Report*, August(153/1981).

Wu, S.-X., 1989. Evaluations of CTOD and J-integral for Three-point Bend Specimens with Shallow Cracks. In *Advances in Fracture Research: Proceedings of the 7th International Conference on Fracture (ICF7)*. Houston, Texas, pp. 517–524.

Wu, S.-X., 1983. Plastic rotational factor and J-COD relationship of three point bend specimen. *Engineering Fracture Mechanics*, 18(1), pp.83–95. Available at: http://www.sciencedirect.com/science/article/pii/001379448390098X [Accessed February 17, 2014].

Wu, S.-X., 1981. Relationship between the J-integral and crack opening displacement for pure power hardening material. *International Journal of Fracture*, 17, pp.R63–R66.

Zhou, D.W., 2011. Measurement and modelling of R-curves for low-constraint specimens. *Engineering Fracture Mechanics*, 78(3), pp.605–622. Available at: http://linkinghub.elsevier.com/retrieve/pii/S0013794410003887 [Accessed February 7, 2014].

Zhou, D.W., Xu, W.G. & Smith, S.D., 2009. R-Curve Modelling with Constraint Effect. In *12th International Conference on Fracture*. Ottawa, Canada.

Zhu, X., 2009. J-integral resistance curve testing and evaluation. *Journal of Zhejiang University SCIENCE A*, 10(11), pp.1541–1560. Available at: http://www.springerlink.com/index/10.1631/jzus.A0930004 [Accessed March 12, 2014].

Zhu, X.-K. & Joyce, J.A., 2012. Review of fracture toughness (G, K, J, CTOD, CTOA) testing and standardization. *Engineering Fracture Mechanics*, 85, pp.1–46. Available at: http://www.sciencedirect.com/science/article/pii/S001379441200063X [Accessed February 7, 2014].

Zhu, X.-K. & Leis, B.N., 2008. Experimental Determination of J-R Curves Using SENB Specimens and P-CMOD Data. In *ASME Pressure Vessels and Piping Division Conference*. July 27-31, 2008, Chicago, Illinois, USA: Asme, pp. 61–68. Available at:

http://proceedings.asmedigitalcollection.asme.org/proceeding.aspx?doi=10.1115/PVP2008-61219.

Zhu, X.-K., Leis, B.N. & Joyce, J. a., 2008. Experimental Estimation of J-R curves from Load-CMOD Record for SE(B) Specimens. *ASTM STP 1508*, 5(5), pp.66–86.

Zhu, X.-K., Zelenak, P. & McGaughy, T., 2017. Comparative study of CTOD-resistance curve test methods for SENT specimens. *Engineering Fracture Mechanics*, 172, pp.17–38. Available at: http://linkinghub.elsevier.com/retrieve/pii/S0013794416304647.

Zienkiewicz, O.C. & Taylor, R.L., 2000. *The Finite Element Method Volume 1 : The Basis*,

Appendices

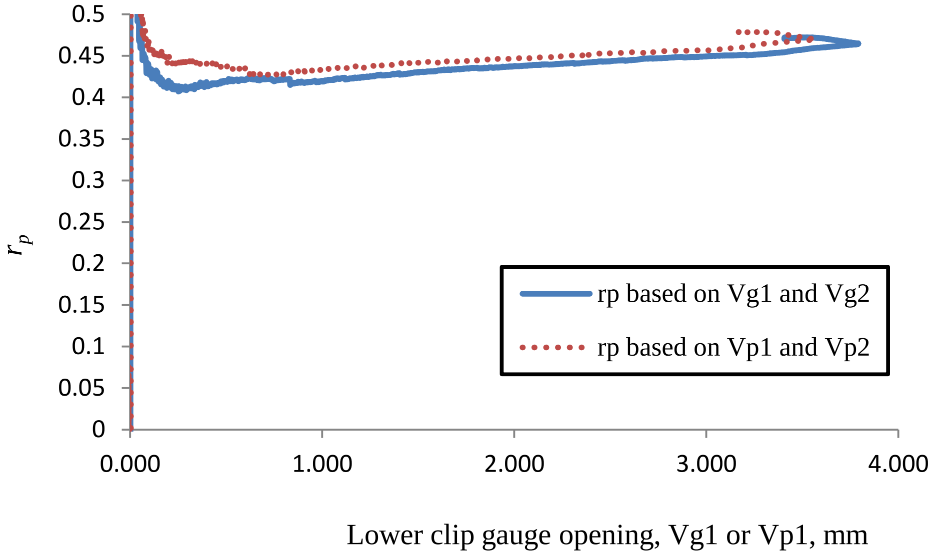

Figure A.01 A Rotational factor calculated based on specimen M02-03

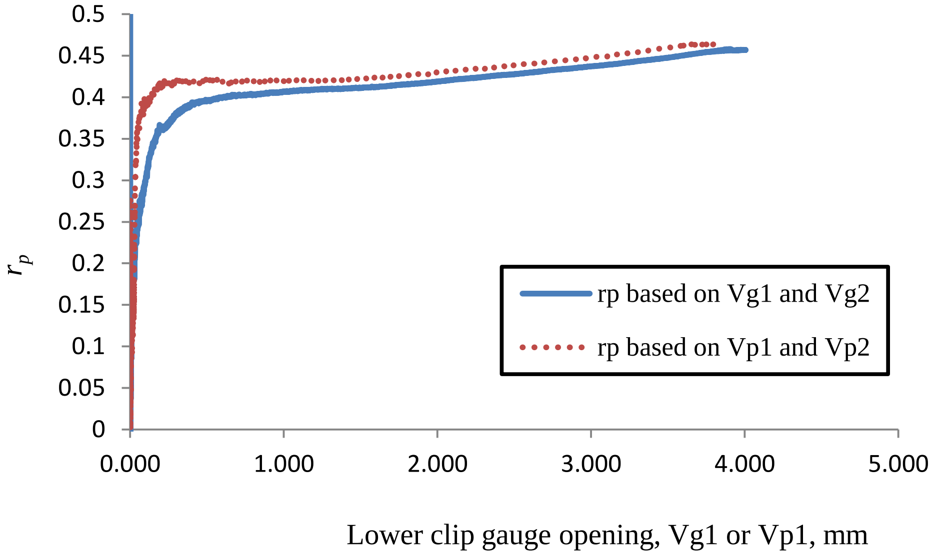

Figure A.02 Rotational factor calculated based on specimen M02-11

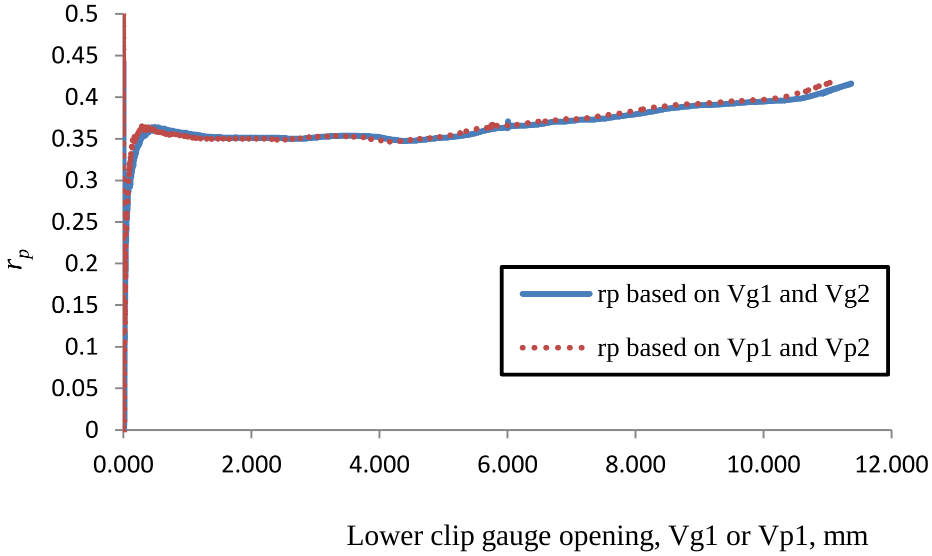

Figure A.03 Rotational factor calculated based on specimen M03-03

SENB R-CURVE TEST 24624 M01 04

0088

Client	CRP		
Project leader	WeeLiam Khor		Signed:

R-Curve data source

Data logging program	LVRCURVE V 1.31 03 Sep 2013
Program used to calculate R-curve data	LVRCALC V 1.16 17-Nov-2014
Calculation date of R-curve data	22 Sep 2015

Specimen details

Material	SS316	
Specimen type	SENB, Sub-size	
Crack plane orientation	Y-X	
Type of notch tip	Fatigue	
Notch tip location	Parent material	
Specimen side grooved	No	
Specimen width	39.97	mm
Specimen thickness	19.98	mm
Initial crack length, a0	20.16	mm
Estimated final crack length, ap	22.19	mm

Test details

Test standard	BS7448 Prt 4:1997		
Test method	Unloading compliance		
Test date	21/09/2015		
Test time	16:03:34		
Test technician	Phillip Cossey		Signed:
Test machine	Instron B107		
Test environment	Air		
Test temperature	21.0	°C	
Soak time @ Test temperature	NA	minutes	
Knife edge heights	2.000, 12.000	mm	
Initial K-Rate	24.31	$N/mm^{3/2}/sec$	
Loading span	160.0	mm	
Double roller diameter	25.00	mm	
Single roller diameter	25.00	mm	

Material properties

Yield strength @ Fatigue temperature	850.0	N/mm^2
Tensile strength @ Fatigue temperature	914.0	N/mm^2
Yield strength @ Test temperature	850.0	N/mm^2
Tensile strength @ Test temperature	914.0	N/mm^2
Poisson's ratio	0.3	
Youngs modulus	192422	N/mm^2

Fatigue details

Stress ratio	0.100		
Final load	9.50	kN	
Loading span	160.0	mm	

Test procedure

Number of elastic unloadings	10		
Load relaxation limit	5.00	%	of elastic loading rate
1st Increment size	0.05	mm	
1st Maximum displacement	1.00	mm	
2nd Increment size	0.10	mm	
2nd Maximum displacement	4.00	mm	

Analysis details

Yield strength temperature correction	No
Young's modulus temperature correction	No
Method of determining J	DOUBLE CLIP
Young's modulus adjusted for crack agreement	Yes
Clip gauge used for crack length calculations	Clip 1

Compiled by: Phillip Cossey **Signed:** ____________

UKAS TESTING
0088

TWI

SENB R-CURVE TEST 24624 M01 04

Qualification checks to BS7448 Prt 4:1997

(6.1.2)	
Knife edge spacing	**Pass**
(8.4.1)	
Single roller diameter	**Pass**
Double roller diameter	**Pass**
(9.3.1)	
Loading span	**Pass**
(9.6)	
Intitial K-rate between 0.5 $MPa.m^{0.5}s^{-1}$ to 3.0 $MPa.m^{0.5}s^{-1}$	**Pass**
(9.9.3)	
Was there a defect on fracture surface	**No**
(10.3.2)	
Estimated initial crack length a_o within 2% of measured a_o	**Pass**
(10.3.3)	
Estimated final crack growth within +/- 15% Δa	**Pass**
(14.2.3)	
Minimum surface crack length (a)	**Pass**
Minimum crack extension at surface (b)	**Pass**
Difference in surface crack measurements (c)	**Pass**
Surface crack measurements (d)	**Pass**
(14.2.4)	
Multiplane cracking (a)	**Pass**
a_0/W check 0.45-0.7 (b)	**Pass**
Crack shape (c)	**Pass**
Minimum crack length (d)	**Pass**
Crack within envelope (e)	**Pass**
(14.3.1)	
The specimen did not fracture or pop-in (a)	**No**
The final fatigue precracking force was < F_f (b)	**Pass**
The stress ratio < 0.1 (c)	**Pass**

0088

SENB R-CURVE TEST 24624 M01 04

ELASTIC UNLOADINGS

No.	Coeff	Comp'nce	Load	Vgo	Vpo	Q	Ram	Total Uarea	Plastic Uarea	Estimated a	Corrected a	Estimated Δa	Corrected Δa	CTOD	CTOD Corrected	K	K Corrected	Jdef	J Corrected	CMOD	CMOD Parea	First Rec	Last Rec
		mm/kN	kN	mm	mm	mm	mm	kNmm	kNmm	mm	mm	mm	mm	mm	mm	$N/mm^{3/2}$	$N/mm^{3/2}$	N/mm	N/mm	mm	kNmm		
1	0.99994	0.009369	9.60	0.089	-0.001	0.115	0.222	0.57	-0.05	20.15	20.16	0.00	0.01	0.002	0.002	820.7	821.1	2.9	2.9	0.085	0.38	998	1097
2	0.99993	0.009435	9.62	0.089	-0.001	0.115	0.223	0.57	-0.06	20.20	20.21	0.05	0.06	0.002	0.002	822.3	826.0	2.9	2.9	0.085	0.38	1250	1350
3	0.99994	0.009340	9.62	0.089	-0.002	0.115	0.222	0.57	-0.06	20.13	20.14	-0.02	-0.02	0.001	0.001	823.1	821.9	2.9	2.9	0.085	0.38	1503	1603
4	0.99994	0.009385	9.64	0.089	-0.002	0.115	0.223	0.57	-0.06	20.17	20.17	0.01	0.02	0.001	0.001	824.3	825.4	2.9	2.9	0.085	0.38	1756	1855
5	0.99994	0.009409	9.64	0.089	-0.002	0.115	0.223	0.57	-0.06	20.18	20.19	0.03	0.04	0.001	0.001	824.7	827.1	2.9	2.9	0.085	0.38	2010	2110
6	0.99992	0.009358	9.62	0.088	-0.002	0.115	0.223	0.57	-0.06	20.14	20.15	-0.01	0.00	0.001	0.001	822.9	822.7	2.9	2.9	0.085	0.38	2263	2362
7	0.99993	0.009343	9.62	0.088	-0.002	0.115	0.222	0.57	-0.06	20.13	20.14	-0.02	-0.01	0.001	0.001	823.1	822.2	2.9	2.9	0.085	0.38	2514	2614
8	0.99994	0.009395	9.63	0.088	-0.003	0.115	0.223	0.57	-0.06	20.17	20.18	0.02	0.03	0.001	0.001	823.4	825.1	2.9	2.9	0.085	0.38	2766	2866
9	0.99992	0.009326	9.60	0.087	-0.003	0.115	0.222	0.57	-0.06	20.12	20.13	-0.03	-0.03	0.001	0.001	821.1	819.3	2.9	2.9	0.085	0.38	3018	3118
10	0.99996	0.009339	9.63	0.087	-0.003	0.115	0.223	0.57	-0.06	20.13	20.14	-0.02	-0.02	0.001	0.001	823.9	822.8	2.9	2.9	0.085	0.38	3270	3370

0088

SENB R-CURVE TEST 24624 M01 04

PLASTIC UNLOADINGS

No.	Coeff	Comp'nce	Load	Vgo	Vpo	Q	Ram	Total Uarea	Plastic Uarea	Estimated a	Corrected a	Estimated Δa	Corrected Δa	CTOD	CTOD Corrected	K	K Corrected	Jdef	J Corrected	CMOD	CMOD Parea	First Rec	Last Rec
		mm/kN	kN	mm	mm	mm	mm	kNmm	kNmm	mm	mm	mm	mm	mm	mm	$N/mm^{3/2}$	$N/mm^{3/2}$	N/mm	N/mm	mm	kNmm		
11	0.99992	0.009426	11.12	0.101	-0.003	0.131	0.252	0.73	-0.10	20.20	20.20	0.04	0.05	0.002	0.002	950.9	954.6	3.8	3.8	0.095	0.48	3582	3682
12	0.99995	0.009495	16.19	0.151	-0.001	0.194	0.349	1.59	-0.18	20.25	20.26	0.09	0.11	0.005	0.005	1384.6	1396.3	8.2	8.1	0.142	1.10	4032	4132
13	0.99997	0.009364	21.15	0.201	0.003	0.256	0.443	2.76	-0.27	20.15	20.17	-0.01	0.01	0.010	0.010	1809.0	1810.5	14.1	14.1	0.189	1.96	4549	4649
14	0.99997	0.009413	25.82	0.251	0.009	0.318	0.533	4.21	-0.30	20.19	20.21	0.03	0.05	0.016	0.016	2208.1	2217.1	21.6	21.5	0.236	3.04	5074	5174
15	0.99998	0.009425	30.29	0.301	0.017	0.379	0.623	5.94	-0.26	20.20	20.22	0.04	0.06	0.023	0.023	2590.4	2603.7	30.4	30.4	0.283	4.34	5642	5742
16	0.99998	0.009493	34.40	0.351	0.029	0.440	0.710	7.91	-0.09	20.25	20.27	0.09	0.12	0.032	0.032	2942.4	2970.4	40.5	40.4	0.330	5.85	6243	6343
17	0.99996	0.009503	38.11	0.401	0.044	0.500	0.794	10.10	0.28	20.25	20.28	0.10	0.13	0.041	0.041	3259.0	3293.0	51.6	51.5	0.377	7.54	6877	6977
18	0.99999	0.009434	41.41	0.452	0.064	0.561	0.877	12.54	0.95	20.20	20.24	0.05	0.08	0.052	0.052	3541.6	3564.7	64.1	64.0	0.424	9.42	7538	7638
19	0.99999	0.009457	44.12	0.501	0.088	0.622	0.955	15.12	1.96	20.22	20.26	0.07	0.10	0.063	0.063	3773.0	3804.1	77.2	77.0	0.471	11.39	8210	8310
20	0.99999	0.009495	46.43	0.551	0.116	0.684	1.031	17.95	3.38	20.25	20.29	0.09	0.13	0.075	0.075	3970.8	4014.0	91.6	91.3	0.518	13.54	8909	9009
21	0.99997	0.009512	48.30	0.602	0.149	0.745	1.105	20.83	5.06	20.26	20.31	0.11	0.15	0.087	0.087	4131.1	4181.5	106.3	105.9	0.565	15.75	9625	9725
22	0.99998	0.009531	49.83	0.651	0.184	0.807	1.175	23.87	7.08	20.28	20.32	0.12	0.17	0.099	0.099	4262.1	4320.2	121.7	121.2	0.612	18.04	10353	10453
23	0.99999	0.009570	51.05	0.701	0.223	0.868	1.243	26.98	9.37	20.30	20.36	0.15	0.20	0.112	0.112	4365.8	4437.0	137.5	136.8	0.659	20.41	11088	11188
24	0.99999	0.009595	52.01	0.752	0.264	0.931	1.310	30.19	11.90	20.32	20.38	0.17	0.22	0.125	0.125	4447.8	4528.4	153.7	152.8	0.706	22.84	11836	11936
25	0.99998	0.009605	52.78	0.802	0.307	0.993	1.379	33.44	14.61	20.33	20.39	0.18	0.23	0.138	0.138	4513.6	4599.6	170.2	169.1	0.753	25.31	12586	12686
26	0.99998	0.009654	53.37	0.852	0.352	1.055	1.446	36.73	17.47	20.37	20.43	0.21	0.27	0.151	0.152	4564.7	4666.8	186.8	185.5	0.800	27.80	13336	13436
27	0.99998	0.009667	53.81	0.902	0.398	1.117	1.511	40.04	20.47	20.38	20.44	0.22	0.29	0.164	0.165	4601.8	4709.6	203.6	202.1	0.847	30.30	14092	14192
28	0.99997	0.009700	54.15	0.952	0.445	1.179	1.576	43.37	23.55	20.40	20.47	0.25	0.32	0.177	0.178	4631.4	4750.5	220.4	218.7	0.894	32.84	14849	14949
29	0.99997	0.009713	54.42	1.001	0.491	1.238	1.640	46.61	26.59	20.41	20.48	0.26	0.33	0.190	0.191	4654.2	4779.1	236.8	234.8	0.940	35.34	15606	15706
30	0.99997	0.009775	54.78	1.102	0.588	1.362	1.766	53.38	33.09	20.46	20.54	0.30	0.38	0.216	0.218	4685.4	4831.6	271.0	268.4	1.035	40.48	16494	16594
31	0.99996	0.009840	55.12	1.202	0.686	1.484	1.893	60.09	39.55	20.50	20.59	0.35	0.44	0.242	0.245	4713.8	4882.4	304.9	301.5	1.129	45.65	17387	17487
32	0.99997	0.009894	55.39	1.302	0.783	1.608	2.018	66.88	46.14	20.54	20.64	0.39	0.48	0.269	0.272	4737.1	4925.0	339.2	335.1	1.223	50.84	18279	18379
33	0.99996	0.009957	55.51	1.402	0.882	1.731	2.143	73.72	52.90	20.59	20.69	0.43	0.53	0.295	0.299	4747.3	4956.7	373.8	368.8	1.317	56.05	19172	19272
34	0.99996	0.010035	55.62	1.502	0.981	1.852	2.267	80.45	59.54	20.64	20.75	0.49	0.60	0.321	0.326	4756.9	4992.1	407.8	401.7	1.410	61.23	20063	20163
35	0.99996	0.010067	55.69	1.602	1.080	1.975	2.390	87.27	66.31	20.66	20.78	0.51	0.63	0.348	0.354	4762.6	5010.4	442.3	435.3	1.504	66.47	20961	21061
36	0.99995	0.010130	55.76	1.702	1.180	2.096	2.511	94.00	72.99	20.71	20.83	0.55	0.68	0.374	0.381	4768.8	5038.1	476.3	468.1	1.599	71.71	21857	21957
37	0.99996	0.010179	55.80	1.802	1.279	2.217	2.635	100.77	79.73	20.74	20.87	0.59	0.72	0.400	0.408	4772.0	5058.5	510.4	501.2	1.692	76.92	22756	22856
38	0.99995	0.010268	55.76	1.901	1.379	2.339	2.754	107.53	86.52	20.80	20.94	0.65	0.79	0.427	0.436	4769.2	5084.0	544.6	533.8	1.786	82.14	23651	23751
39	0.99996	0.010342	55.74	2.002	1.479	2.460	2.873	114.30	93.30	20.85	21.00	0.70	0.84	0.453	0.463	4767.1	5106.0	578.8	566.5	1.880	87.39	24545	24645
40	0.99995	0.010396	55.67	2.102	1.580	2.582	2.992	121.09	100.15	20.89	21.04	0.74	0.89	0.479	0.491	4761.2	5118.4	613.1	599.4	1.974	92.63	25440	25540
41	0.99996	0.010486	55.53	2.202	1.682	2.703	3.111	127.79	106.94	20.95	21.11	0.80	0.95	0.506	0.519	4749.5	5134.4	646.9	631.3	2.068	97.85	26334	26434
42	0.99995	0.010569	55.38	2.302	1.783	2.823	3.230	134.43	113.70	21.01	21.17	0.85	1.02	0.532	0.547	4736.3	5146.8	680.5	663.0	2.162	103.06	27229	27329
43	0.99996	0.010619	55.25	2.402	1.885	2.944	3.349	141.15	120.51	21.04	21.21	0.88	1.06	0.559	0.575	4725.4	5152.3	714.4	695.3	2.256	108.23	28125	28225
44	0.99996	0.010696	55.14	2.502	1.986	3.064	3.469	147.76	127.21	21.09	21.27	0.94	1.12	0.585	0.603	4715.6	5166.5	747.8	726.7	2.350	113.42	29022	29122
45	0.99995	0.010773	54.99	2.602	2.086	3.184	3.584	154.33	133.89	21.14	21.33	0.99	1.17	0.611	0.631	4703.1	5177.3	781.0	757.9	2.444	118.57	29915	30015
46	0.99997	0.010843	54.80	2.702	2.189	3.305	3.702	160.94	140.65	21.18	21.38	1.03	1.22	0.638	0.659	4686.4	5181.5	814.4	789.2	2.538	123.73	30808	30908
47	0.99995	0.010948	54.43	2.802	2.292	3.424	3.816	167.46	147.43	21.25	21.45	1.10	1.30	0.664	0.687	4655.0	5179.0	847.3	819.5	2.632	128.85	31699	31799
48	0.99995	0.011023	54.23	2.901	2.393	3.542	3.931	173.87	153.99	21.30	21.51	1.14	1.35	0.690	0.715	4637.7	5183.6	879.6	849.6	2.726	133.94	32586	32686
49	0.99997	0.011098	54.05	3.002	2.496	3.660	4.049	180.25	160.51	21.35	21.56	1.19	1.41	0.717	0.744	4622.3	5190.1	911.9	879.5	2.821	139.08	33476	33576
50	0.99995	0.011222	53.73	3.102	2.599	3.779	4.161	186.67	167.16	21.42	21.64	1.27	1.49	0.744	0.773	4595.2	5196.3	944.3	908.8	2.914	144.13	34360	34460
51	0.99997	0.011301	53.42	3.202	2.701	3.898	4.277	193.00	173.71	21.47	21.70	1.32	1.54	0.770	0.801	4569.1	5191.1	976.3	938.2	3.008	149.16	35246	35346
52	0.99996	0.011392	53.22	3.302	2.803	4.016	4.389	199.29	180.15	21.53	21.76	1.37	1.61	0.796	0.830	4551.7	5199.0	1008.0	967.2	3.102	154.17	36129	36229
53	0.99996	0.011489	52.97	3.402	2.905	4.133	4.502	205.50	186.53	21.59	21.83	1.43	1.67	0.823	0.859	4530.1	5203.2	1039.4	995.5	3.196	159.14	37015	37115
54	0.99996	0.011554	52.74	3.502	3.008	4.252	4.613	211.78	192.98	21.63	21.87	1.47	1.72	0.849	0.888	4510.3	5201.1	1071.1	1024.7	3.291	164.12	37899	37999
55	0.99997	0.011633	52.49	3.602	3.110	4.370	4.728	217.99	199.37	21.67	21.92	1.52	1.77	0.875	0.917	4488.9	5200.2	1102.5	1053.2	3.385	169.07	38782	38882
56	0.99997	0.011731	52.12	3.702	3.214	4.487	4.839	224.09	205.73	21.73	21.99	1.57	1.83	0.902	0.946	4457.4	5192.4	1133.3	1080.8	3.479	173.97	39662	39762
57	0.99997	0.011852	51.82	3.802	3.316	4.604	4.952	230.16	212.01	21.80	22.07	1.64	1.91	0.928	0.975	4431.5	5196.8	1163.9	1107.8	3.573	178.86	40545	40645
58	0.99998	0.011931	51.45	3.902	3.420	4.719	5.063	236.09	218.20	21.85	22.12	1.69	1.96	0.955	1.005	4400.0	5183.4	1193.9	1134.7	3.667	183.72	41422	41522
59	0.99997	0.012050	51.13	4.002	3.523	4.836	5.173	242.07	224.40	21.91	22.19	1.76	2.04	0.982	1.034	4372.9	5184.8	1224.0	1161.2	3.761	188.55	42300	42400

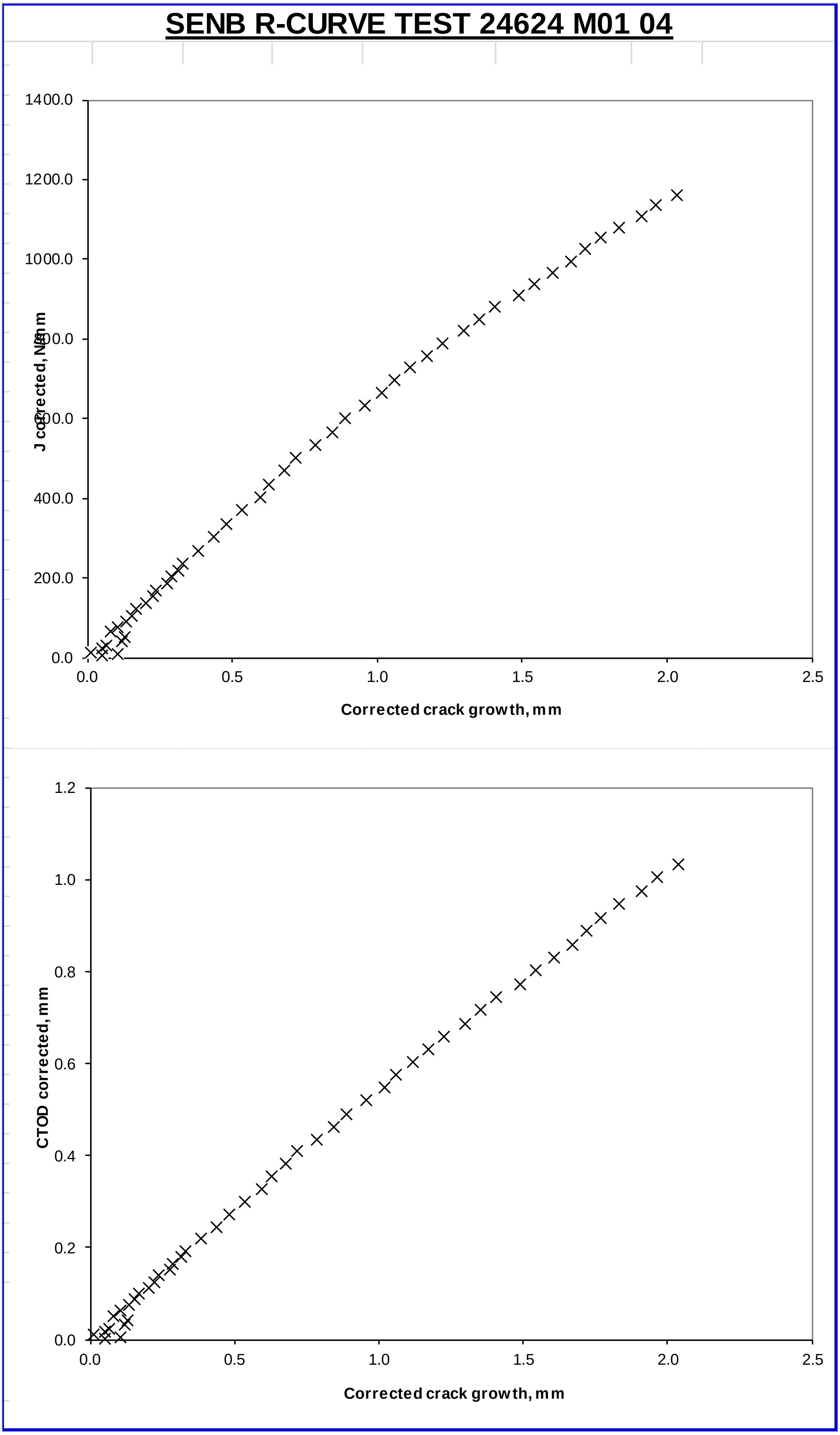
SENB R-CURVE TEST 24624 M01 04
J corrected, N/mm
Corrected crack growth, mm
0.0
200.0
400.0
600.0
800.0
1000.0
1200.0
1400.0
0.0
0.5
1.0
1.5
2.0
2.5
CTOD corrected, mm
Corrected crack growth, mm
0.0
0.2
0.4
0.6
0.8
1.0
1.2

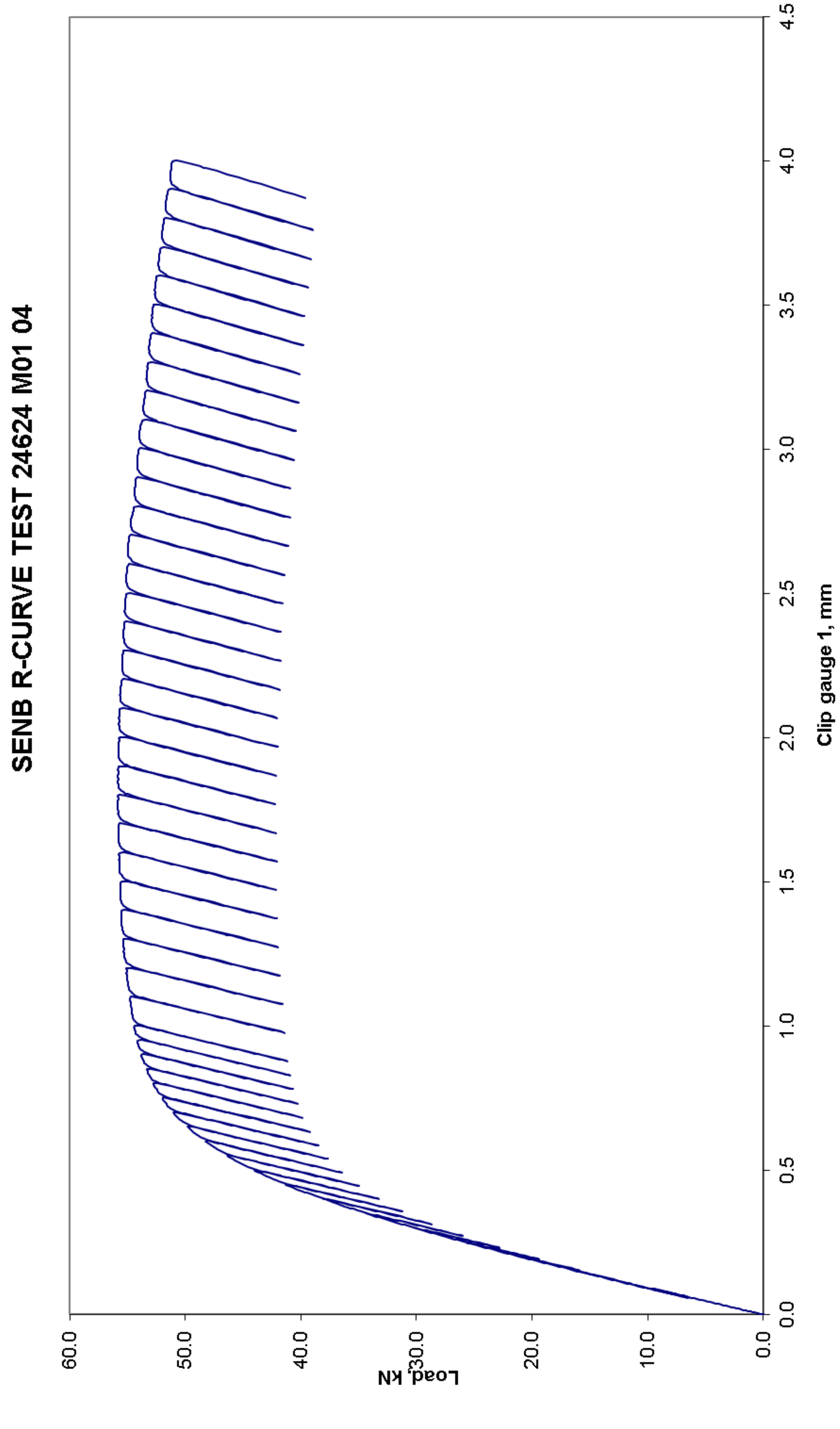
SENB R-CURVE TEST 24624 M01 04
Load, kN
0.0
10.0
20.0
30.0
40.0
50.0
60.0
Clip gauge 1, mm
0.0
0.5
1.0
1.5
2.0
2.5
3.0
3.5
4.0
4.5

SENB R-CURVE TEST 24624 M01 04

Specimen width, W	39.970	mm
Specimen Thickness, B	19.980	mm
Machined notch depth, M	16.200	mm
Surface crack length, a_{S1}	19.440	mm
Surface crack length, a_{S2}	19.360	mm
Net section thickness, B_N	19.980	mm
a_{max}	20.370	mm
a_{min}	19.500	mm

Diagram of fracture face

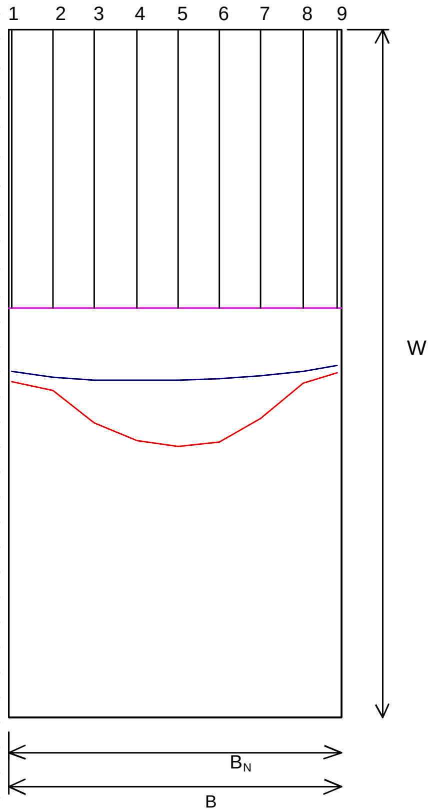

Measured by: Phillip Cossey

Signed:

Measurement Line	Fatigue crack length a0, mm	Slow stable crack extension Fatigue crack ap, mm	Slow stable crack extension including stretch zone, deltaa, mm
1	19.860	20.500	0.640
2	20.200	21.010	0.810
3	20.350	22.880	2.530
4	20.370	23.920	3.550
5	20.350	24.240	3.890
6	20.280	23.990	3.710
7	20.110	22.590	2.480
8	19.900	20.590	0.690
9	19.500	19.950	0.450
Weighted Average	**20.155**	**22.431**	**2.276**

UKAS TESTING
0088

TWI

SENB FRACTURE TEST 24624 M01-05

Client	CRP	
Project leader	Weeliam Khor	Signed:

Data source

Data logging program	LVGENLOG V 1.29 19-Nov-2013
Program used to calculate CTOD/J	LVGENPLOT V 1.28 30-Jan-2015
Calculation date of CTOD/J	24 Mar 2015

Specimen details

Material	SA-543-GrB-Cl1	
Specimen type	Subsize, SENB	
Crack plane orientation	Y-X	
Type of notch tip	Fatigue	
Notch tip location	Parent material	
Specimen width	39.970	mm
Specimen thickness	19.970	mm
Initial crack length	20.393	mm
Original PM 1 thickness	50.00	mm

Test details

Test standard(s)	BS 7448: Part 1: 1991	
Test date	23/03/2015	
Test time	09:55:00	
Test technician	Phillip Cossey	Signed:
Test machine	INSTRON 8500 B107	
Test environment	AIR	
Test temperature	21.0	°C
Soak time @ test temperature	0.0	minutes
Knife edge heights	2.000, 12.000	mm
Knife edge spacing	14.00	mm
Initial K-rate	1.4	$MPa.m^{1/2}/s$
Loading span	160.0	mm
Double roller diameter	25.00	mm
Single roller diameter	25.00	mm

SENB FRACTURE TEST 24624 M01-05

Qualification checks to **BS 7448: Part 1: 1991**

(5.1.3)	
Knife edge attachment spacing	**Pass**
(6.4.5,6.4.6)	
The final fatigue precracking force <= F_f (a)	**Pass**
ΔK/E below limit (b)	**Pass**
(6.4.7)	
Initial/Final K ratio during precracking < 1.3 (a)	**Pass**
(7.5.1)	
Single roller diameter	**Pass**
Double roller diameter	**Pass**
Loading span	**Pass**
(8.5)	
Initial K-rate between 0.5 MPa.$m^{0.5}s^{-1}$ and 3.0 MPa.$m^{0.5}s^{-1}$	**Pass**
(10.2.2)	
Minimum surface crack length (a)	**Pass**
Minimum crack extension at surface (b)	**Pass**
Difference in surface crack measurements (c)	**Pass**
Surface fatigue cracks in envelope (d)	**Pass**
Crack plane within 10° (e)	**Pass**
(10.2.3)	
Multiplane cracking (a)	**Pass**
a_0/W check 0.45-0.55 (b)	**Pass**
Crack shape (c)	**Fail**
Minimum crack length (d)	**Pass**
(10.3)	
The stress ratio <= 0.1 (c)	**Pass**

0088

SENB FRACTURE TEST 24624 M01-05

Test date	23/03/2015	Client	CRP
Technician	Phillip Cossey	Project leader	Weeliam Khor
Test machine	INSTRON 8500 B107	Investigator's signature	
Control mode	Displacement	Compiled by	Dan Bloom

SPECIMEN DETAILS

Force, F	56.77	kN
Width, W	39.970	mm
Thickness, B	19.970	mm
Crack length, a_0	20.393	mm
Loading span, S	160.00	mm
Yield strength	850	MPa
Young's modulus	207	GPa
Poisson's ratio	0.300	
Test temperature	21.0	°C

RESULTS

δ	0.367	mm
K @ calculation point	156.6	$MPa.m^{1/2}$
F_{max}/F_Q	1.91	
K_Q	81.80	$MPa.m^{1/2}$
Total area under Force v q	100.66	kNmm
J0 from q from DOUBLE CLIP	516.54	kJ/m² (N/mm)
Plastic area Force v CMOD	58.85	kNmm
Type of result	δ/J_m	
Test standard(s)	BS 7448: Part 1: 1991	
Result qualified to standard(s)	NO	

LOWER CLIP GAUGE VALUES

Knife edge height	2.00	mm
Vg	1.721	mm
Vp	1.173	mm

UPPER CLIP GAUGE VALUES

Knife edge height	12.00	mm
Vg	2.275	mm
Vp	1.547	mm

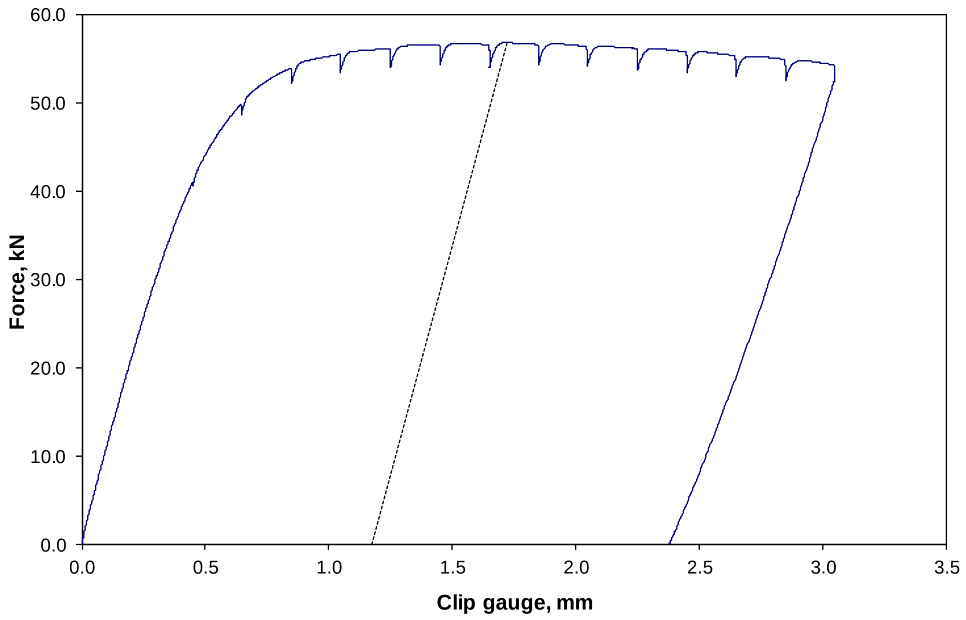

SENB FRACTURE TEST 24624 M01-05

Diagram of fracture face

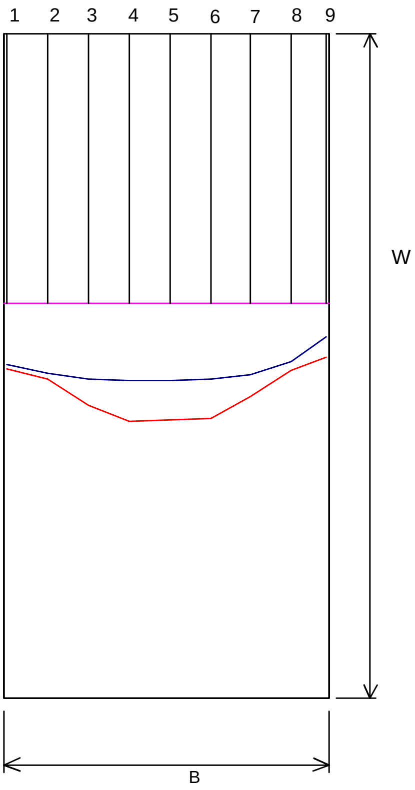

Specimen width, W	39.970	mm
Specimen thickness, B	19.970	mm
Machined notch depth, M	16.200	mm
Surface crack length, a_{S1}	19.460	mm
Surface crack length, a_{S2}	17.980	mm
a_{max}	20.915	mm
a_{min}	18.290	mm

Comments

Measurement Line	Fatigue crack length a_0, mm	Slow stable crack extension + fatigue crack a_p, mm	Slow stable crack extension including stretch zone, Δ_a, mm
1	19.940	20.190	0.250
2	20.415	20.765	0.350
3	20.765	22.390	1.625
4	20.875	23.325	2.450
5	20.915	23.285	2.370
6	20.795	23.120	2.325
7	20.495	21.875	1.380
8	19.770	20.250	0.480
9	18.290	19.455	1.165
Weighted Average	**20.393**	**21.854**	**1.461**

Measured by: Dan Bloom **Signed:**

UKAS TESTING 0088

TWI

SENB FRACTURE TEST 24624 M01-07

Client	CRP	
Project leader	WeeLiam Khor	Signed:

Data source

Data logging program	LVGENLOG V 1.29 19-Nov-2013
Program used to calculate CTOD/J	LVGENPLOT V 1.28 30-Jan-2015
Calculation date of CTOD/J	19 Mar 2015

Specimen details

Material	SA-543-GrB-CL1	
Specimen type	Subsize, SENB	
Crack plane orientation	Y-X	
Type of notch tip	Fatigue	
Notch tip location	Parent material	
Specimen width	39.980	mm
Specimen thickness	19.980	mm
Initial crack length	20.138	mm
Original PM 1 thickness	50.00	mm

Test details

Test standard(s)	BS 7448: Part 1: 1991	
Test date	17/03/2015	
Test time	13:51:00	
Test technician	Phillip Cossey	Signed:
Test machine	INSTRON 8500 B107	
Test environment	AIR	
Test temperature	23.0	°C
Soak time @ test temperature	0.0	minutes
Knife edge heights	2.000, 12.000	mm
Knife edge spacing	14.00	mm
Initial K-rate	1.4	$MPa.m^{1/2}/s$
Loading span	160.0	mm
Double roller diameter	25.00	mm
Single roller diameter	25.00	mm

Material properties

Yield strength for pre-cracking	850.0	MPa	Assumed from material specification
Tensile strength for pre-cracking	914.0	MPa	Assumed from material specification
Yield strength for testing	850.0	MPa	Assumed from material specification
Tensile strength for testing	914.0	MPa	Assumed from material specification
Poisson's ratio	0.3		Assumed
Young's modulus	207	GPa	Assumed

Fatigue details

Stress ratio, R	0.100	
Final force, F_f	9.50	kN
Final K	25.6	$MPa.m^{1/2}$
Fatigue temperature	21.0	°C
Loading span, S	160.0	mm

Analysis details

Method of determining Load Point Displacement, q	DOUBLE CLIP
Lower knife edge height check	OK

Compiled by: Dan Bloom **Signed:** ____________

SENB FRACTURE TEST 24624 M01-07

Qualification checks to **BS 7448: Part 1: 1991**

(5.1.3)	
Knife edge attachment spacing	**Pass**
(6.4.5,6.4.6)	
The final fatigue precracking force <= F_f (a)	**Pass**
$\Delta K/E$ below limit (b)	**Pass**
(6.4.7)	
Initial/Final K ratio during precracking < 1.3 (a)	**Pass**
(7.5.1)	
Single roller diameter	**Pass**
Double roller diameter	**Pass**
Loading span	**Pass**
(8.5)	
Initial K-rate between 0.5 MPa.$m^{0.5}s^{-1}$ and 3.0 MPa.$m^{0.5}s^{-1}$	**Pass**
(10.2.2)	
Minimum surface crack length (a)	**Pass**
Minimum crack extension at surface (b)	**Pass**
Difference in surface crack measurements (c)	**Pass**
Surface fatigue cracks in envelope (d)	**Pass**
Crack plane within 10° (e)	**Pass**
(10.2.3)	
Multiplane cracking (a)	**Pass**
a_0/W check 0.45-0.55 (b)	**Pass**
Crack shape (c)	**Pass**
Minimum crack length (d)	**Pass**
(10.3)	
The stress ratio <= 0.1 (c)	**Pass**

UKAS TESTING 0088

TWI

SENB FRACTURE TEST 24624 M01-07

Test date	17/03/2015	Client	CRP
Technician	Phillip Cossey	Project leader	WeeLiam Khor
Test machine	INSTRON 8500 B107	Investigator's signature	
Control mode	Displacement	Compiled by	Dan Bloom

SPECIMEN DETAILS

Force, F	57.54	kN
Width, W	39.980	mm
Thickness, B	19.980	mm
Crack length, a_0	20.138	mm
Loading span, S	160.00	mm
Yield strength	850	MPa
Young's modulus	207	GPa
Poisson's ratio	0.300	
Test temperature	23.0	°C

RESULTS

δ	0.362	mm
K @ calculation point	155.3	$MPa.m^{1/2}$
F_{max}/F_Q	1.73	
K_Q	89.57	$MPa.m^{1/2}$
Total area under Force v q	103.68	kNmm
J0 from q from DOUBLE CLIP	524.41	kJ/m² (N/mm)
Plastic area Force v CMOD	58.10	kNmm
Type of result	δ/J_m	
Test standard(s)	BS 7448: Part 1: 1991	
Result qualified to standard(s)	YES	

LOWER CLIP GAUGE VALUES

Knife edge height	2.00	mm
Vg	1.664	mm
Vp	1.135	mm

UPPER CLIP GAUGE VALUES

Knife edge height	12.00	mm
Vg	2.228	mm
Vp	1.511	mm

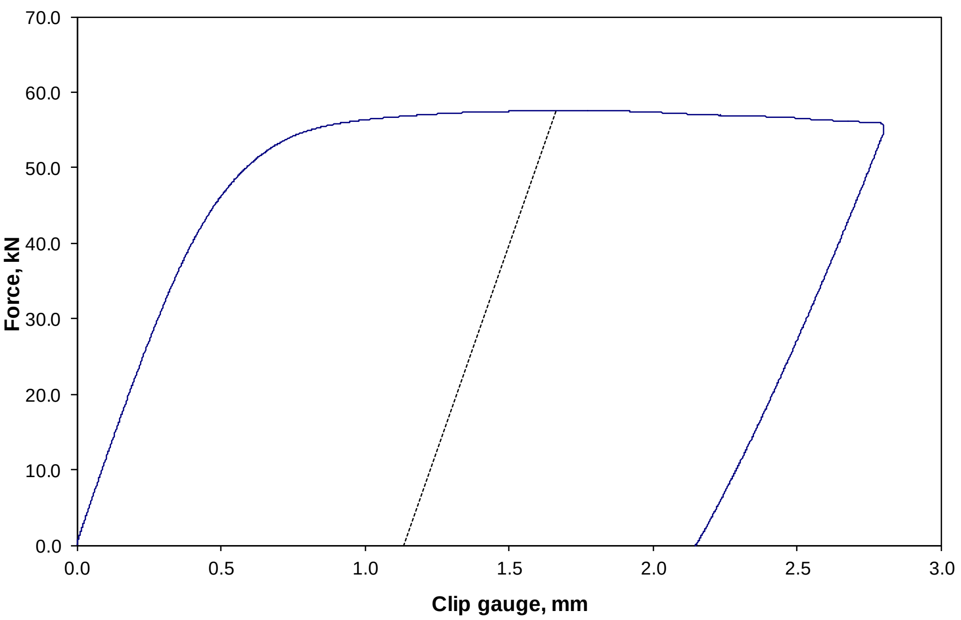

SENB FRACTURE TEST 24624 M01-07

Diagram of fracture face

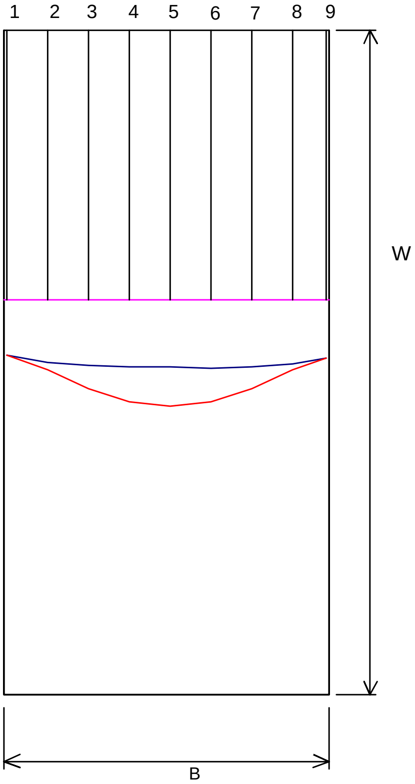

Specimen width, W	39.980	mm
Specimen thickness, B	19.980	mm
Machined notch depth, M	16.200	mm
Surface crack length, a_{S1}	19.450	mm
Surface crack length, a_{S2}	19.420	mm
a_{max}	20.320	mm
a_{min}	19.595	mm

Comments

Measurement Line	Fatigue crack length a_0, mm	Slow stable crack extension + fatigue crack a_p, mm	Slow stable crack extension including stretch zone, Δ_a, mm
1	19.595	19.595	0.000
2	20.015	20.465	0.450
3	20.185	21.575	1.390
4	20.305	22.360	2.055
5	20.315	22.595	2.280
6	20.320	22.375	2.055
7	20.240	21.590	1.350
8	20.060	20.435	0.375
9	19.730	19.730	0.000
Weighted Average	**20.138**	**21.382**	**1.244**

Measured by: Dan Bloom **Signed:** ____________

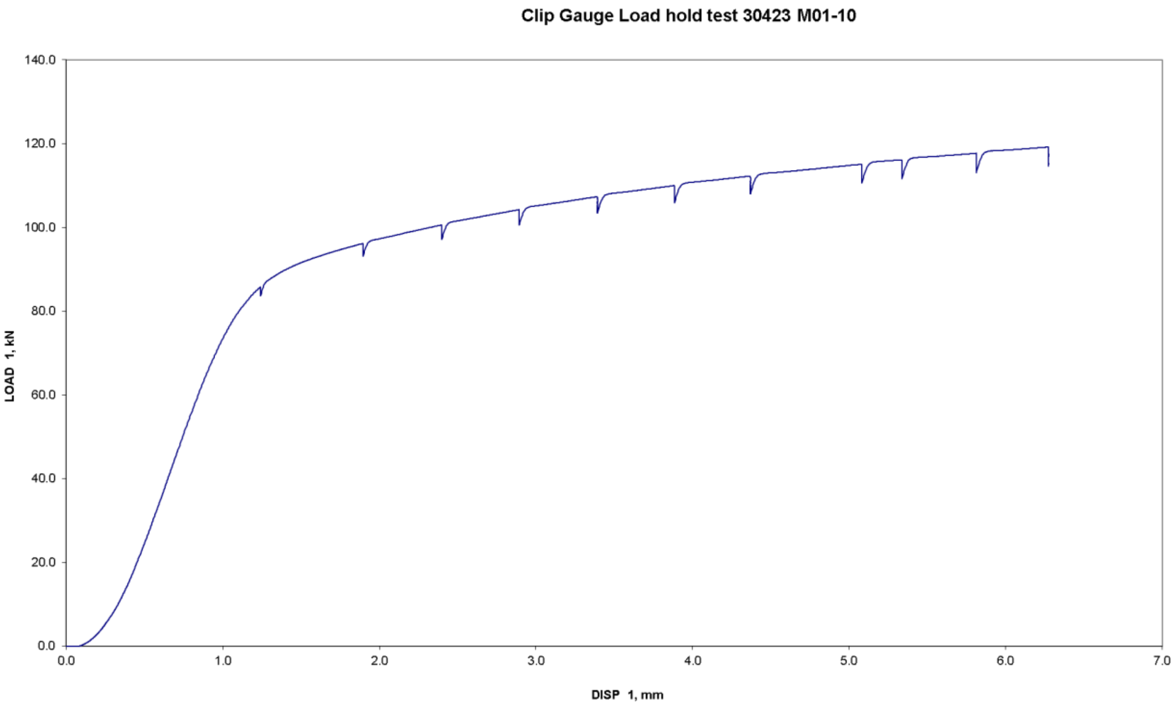
Clip Gauge Load hold test 30423 M01-10
LOAD 1, kN
0.0
20.0
40.0
60.0
80.0
100.0
120.0
140.0
0.0
1.0
2.0
3.0
4.0
5.0
6.0
7.0
DISP 1, mm

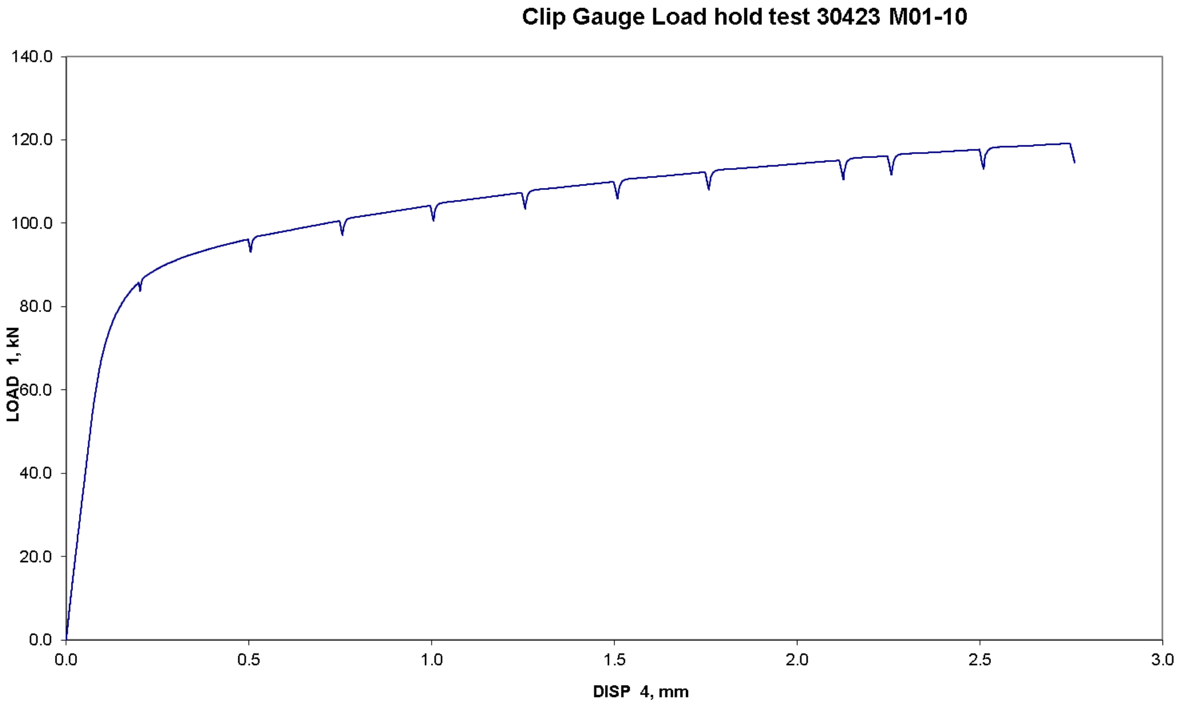
Clip Gauge Load hold test 30423 M01-10
LOAD 1, kN
0.0
20.0
40.0
60.0
80.0
100.0
120.0
140.0
0.0
0.5
1.0
1.5
2.0
2.5
3.0
DISP 4, mm

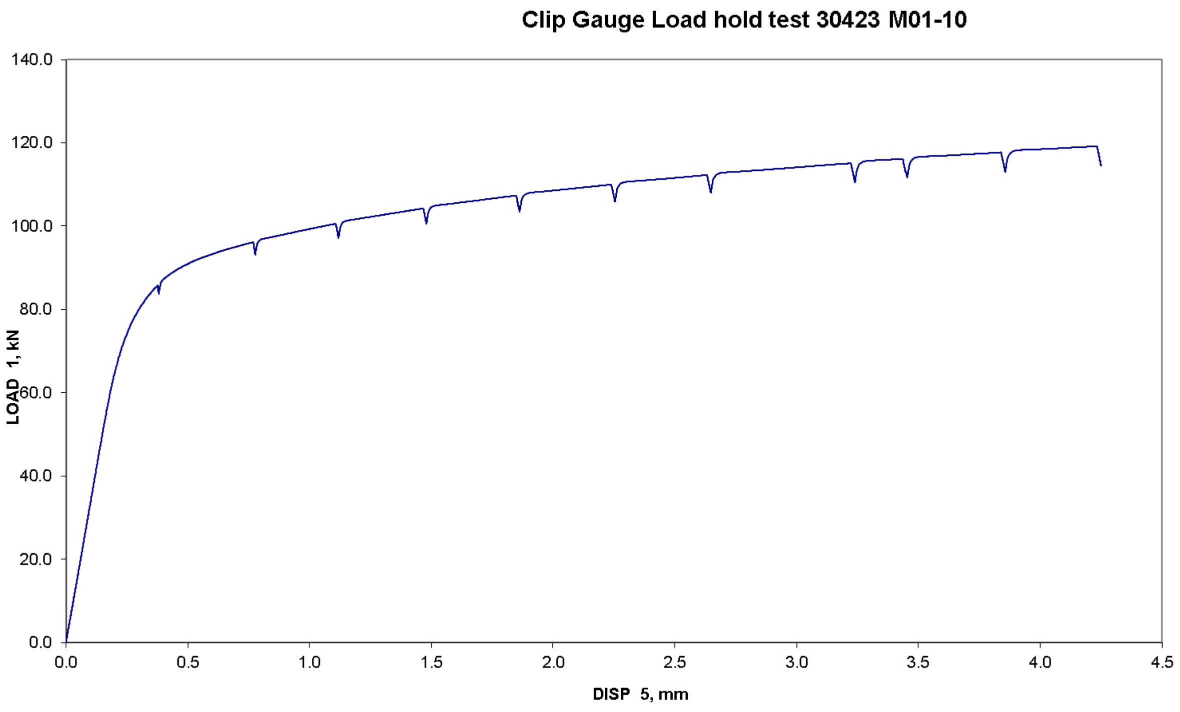
Clip Gauge Load hold test 30423 M01-10
LOAD 1, kN
DISP 5, mm
140.0
120.0
100.0
80.0
60.0
40.0
20.0
0.0
0.0
0.5
1.0
1.5
2.0
2.5
3.0
3.5
4.0
4.5

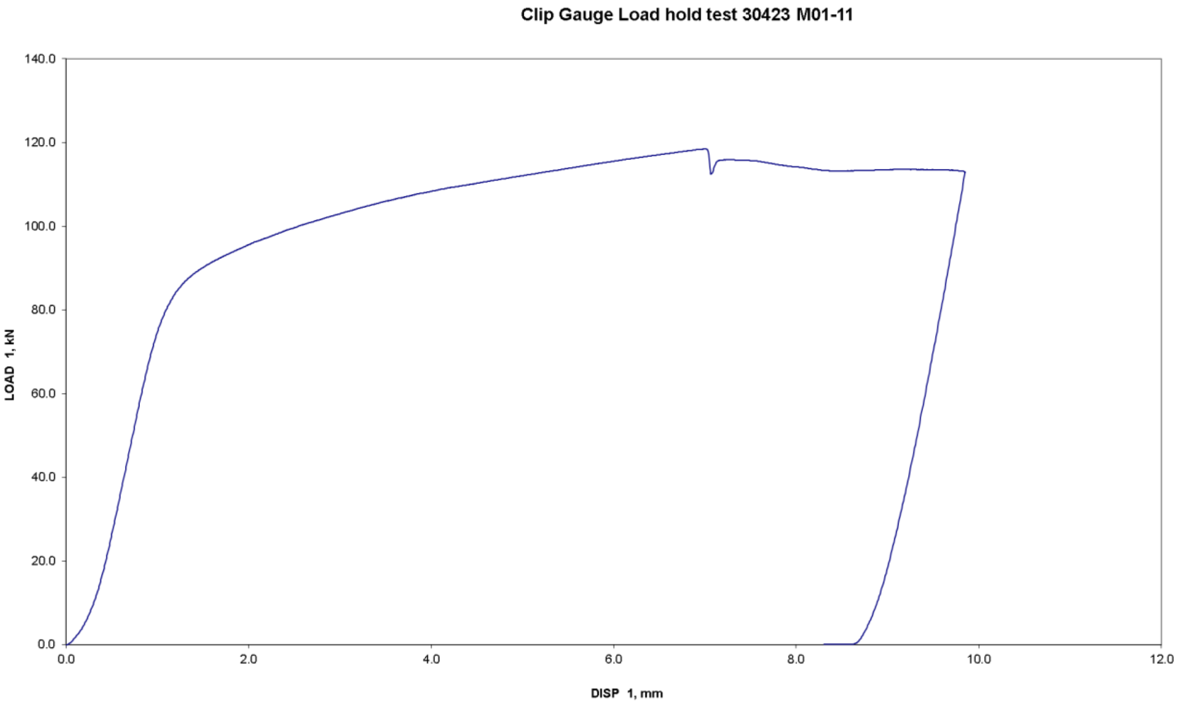
Clip Gauge Load hold test 30423 M01-11
LOAD 1, kN
DISP 1, mm
140.0
120.0
100.0
80.0
60.0
40.0
20.0
0.0
0.0
2.0
4.0
6.0
8.0
10.0
12.0

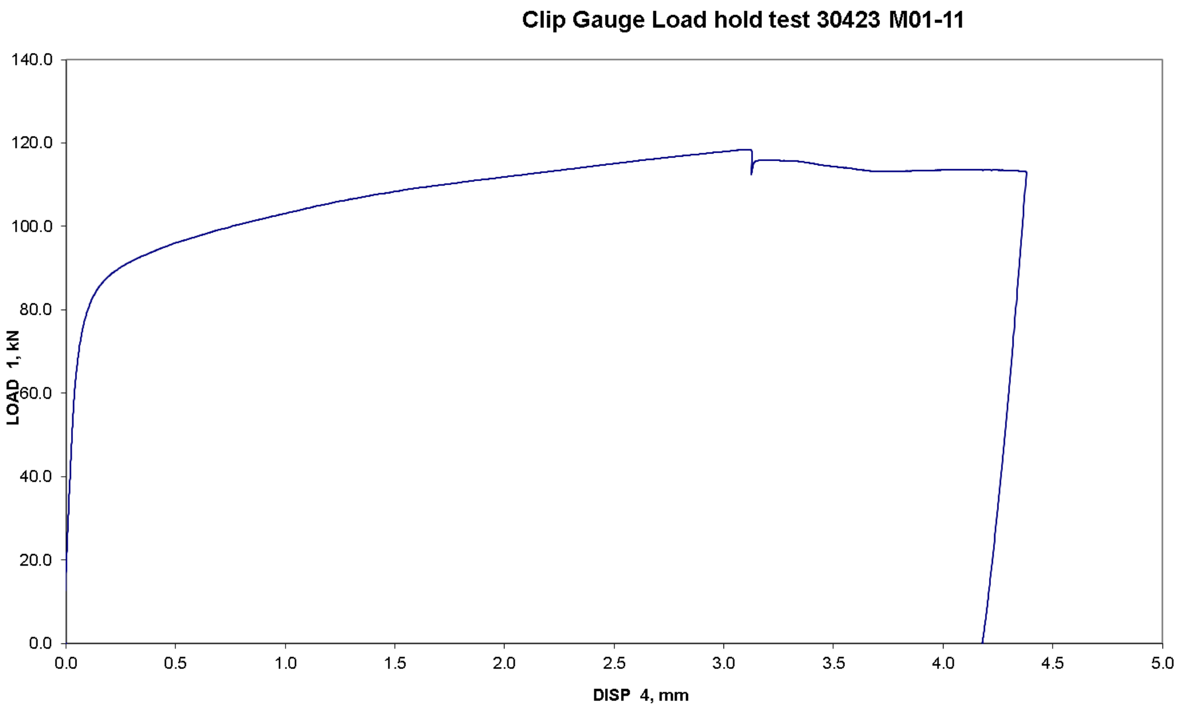
Clip Gauge Load hold test 30423 M01-11
140.0
120.0
100.0
80.0
60.0
40.0
20.0
0.0
LOAD 1, kN
0.0
0.5
1.0
1.5
2.0
2.5
3.0
3.5
4.0
4.5
5.0
DISP 4, mm

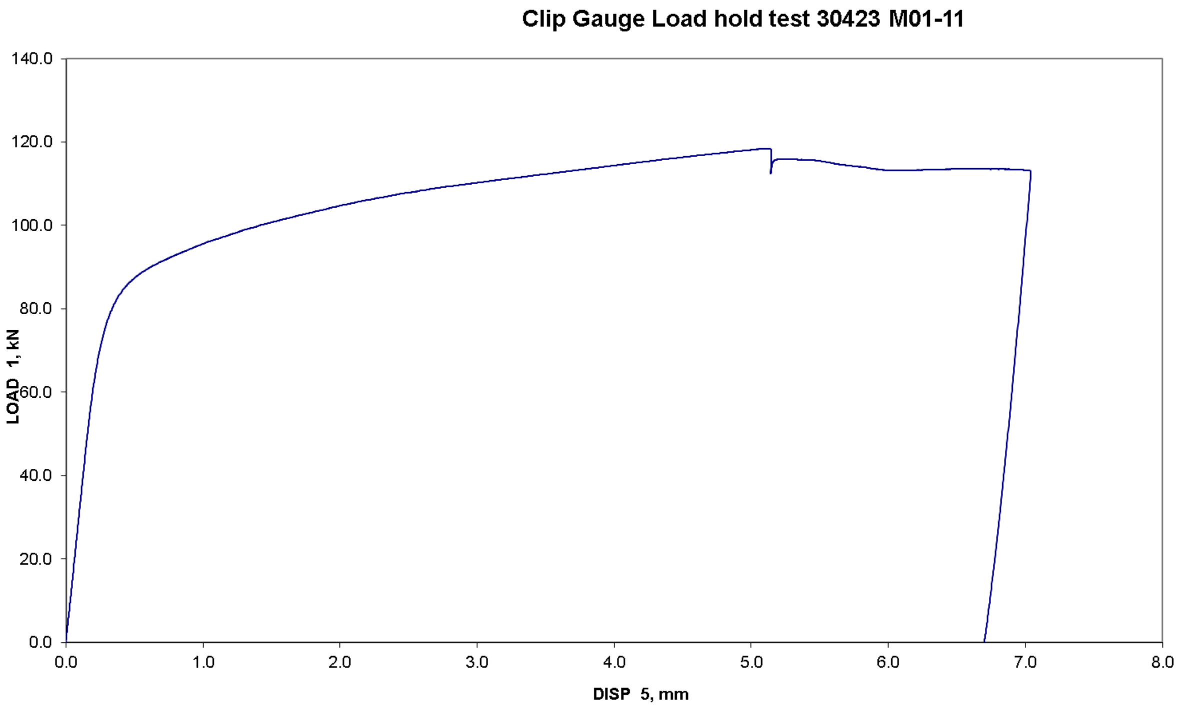
Clip Gauge Load hold test 30423 M01-11
140.0
120.0
100.0
80.0
60.0
40.0
20.0
0.0
LOAD 1, kN
0.0
1.0
2.0
3.0
4.0
5.0
6.0
7.0
8.0
DISP 5, mm

UKAS TESTING
0088

TWI

SENB FRACTURE TEST 24624 M02-03

Client	CRP		
Project leader	W Khor		Signed:

Data source

Data logging program	LVGENLOG V 1.29 19-Nov-2013
Program used to calculate CTOD/J	LVGENPLOT V 1.28 30-Jan-2015
Calculation date of CTOD/J	11 Mar 2015

Specimen details

Material		
Specimen type	Subsize, SENB	
Crack plane orientation	Y-X	
Type of notch tip	Fatigue	
Notch tip location	Parent material	
Specimen width	40.000	mm
Specimen thickness	19.980	mm
Initial crack length	20.304	mm
Original PM 1 thickness	42.00	mm

Test details

Test standard(s)	BS 7448: Part 1: 1991		
Test date	11/03/2015		
Test time	11:55:00		
Test technician	J Godden		Signed:
Test machine	INSTRON 8500 B107		
Test environment	AIR		
Test temperature	24.0	°C	
Soak time @ test temperature	0.0	minutes	
Knife edge heights	2.000, 12.000	mm	
Knife edge spacing	14.00	mm	
Initial K-rate	1.1	$MPa.m^{1/2}/s$	
Loading span	160.0	mm	
Double roller diameter	25.00	mm	
Single roller diameter	25.00	mm	

Material properties

Yield strength for pre-cracking	421.0	MPa	Measured at RT
Tensile strength for pre-cracking	585.0	MPa	Measured at RT
Yield strength for testing	421.0	MPa	Measured at RT
Tensile strength for testing	585.0	MPa	Measured at RT
Poisson's ratio	0.3		Assumed
Young's modulus	207	GPa	Assumed

Fatigue details

Stress ratio, R	0.100	
Final force, F_f	9.00	kN
Final K	24.6	$MPa.m^{1/2}$
Fatigue temperature	20.0	°C
Loading span, S	160.0	mm

Analysis details

Method of determining Load Point Displacement, q	DOUBLE CLIP
Lower knife edge height check	OK

Compiled by: J Godden **Signed:** ____________

SENB FRACTURE TEST 24624 M02-03

Qualification checks to **BS 7448: Part 1: 1991**

(5.1.3)	
Knife edge attachment spacing	**Pass**
(6.4.5,6.4.6)	
The final fatigue precracking force <= F_f (a)	**Pass**
$\Delta K/E$ below limit (b)	**Pass**
(6.4.7)	
Initial/Final K ratio during precracking < 1.3 (a)	**Pass**
(7.5.1)	
Single roller diameter	**Pass**
Double roller diameter	**Pass**
Loading span	**Pass**
(8.5)	
Initial K-rate between 0.5 $MPa.m^{0.5}s^{-1}$ and 3.0 $MPa.m^{0.5}s^{-1}$	**Pass**
(10.2.2)	
Minimum surface crack length (a)	**Pass**
Minimum crack extension at surface (b)	**Pass**
Difference in surface crack measurements (c)	**Pass**
Surface fatigue cracks in envelope (d)	**Pass**
Crack plane within 10° (e)	**Pass**
(10.2.3)	
Multiplane cracking (a)	**Pass**
a_0/W check 0.45-0.55 (b)	**Pass**
Crack shape (c)	**Pass**
Minimum crack length (d)	**Pass**
(10.3)	
The stress ratio <= 0.1 (c)	**Pass**

UKAS TESTING
0088

TWI

SENB FRACTURE TEST 24624 M02-03

Test date	11/03/2015
Technician	J Godden
Test machine	INSTRON 8500 B107
Control mode	Displacement

Client	CRP
Project leader	W Khor
Investigator's signature	
Compiled by	J Godden

SPECIMEN DETAILS

Force, F	31.56	kN
Width, W	40.000	mm
Thickness, B	19.980	mm
Crack length, a_0	20.304	mm
Loading span, S	160.00	mm
Yield strength	421	MPa
Young's modulus	207	GPa
Poisson's ratio	0.300	
Test temperature	24.0	°C

RESULTS

δ	0.714	mm
K @ calculation point	86.2	$MPa.m^{1/2}$
F_{max}/F_Q	1.90	
K_Q	45.40	$MPa.m^{1/2}$
Total area under Force v q	103.77	kNmm
J0 from q from DOUBLE CLIP	527.83	kJ/m² (N/mm)
Plastic area Force v CMOD	71.37	kNmm
Type of result	δ/J_m	
Test standard(s)	BS 7448: Part 1: 1991	
Result qualified to standard(s)	YES	

LOWER CLIP GAUGE VALUES

Knife edge height	2.00	mm
Vg	2.881	mm
Vp	2.587	mm

UPPER CLIP GAUGE VALUES

Knife edge height	12.00	mm
Vg	3.806	mm
Vp	3.413	mm

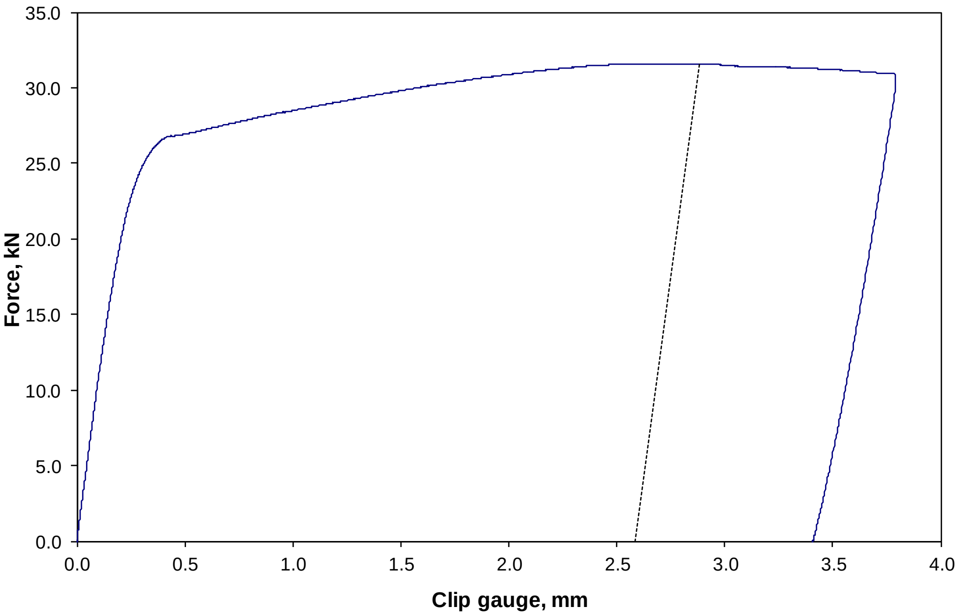

SENB FRACTURE TEST 24624 M02-03

Specimen width, W	40.000	mm
Specimen thickness, B	19.980	mm
Machined notch depth, M	16.200	mm
Surface crack length, a_{S1}	19.410	mm
Surface crack length, a_{S2}	19.270	mm
a_{max}	20.590	mm
a_{min}	19.535	mm

Diagram of fracture face

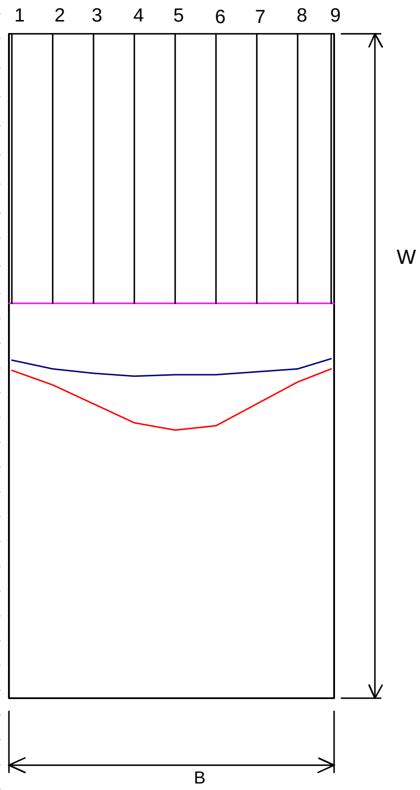

Comments

Measurement Line	Fatigue crack length a_0, mm	Slow stable crack extension + fatigue crack a_p, mm	Slow stable crack extension including stretch zone, Δ_a, mm
1	19.680	20.235	0.555
2	20.215	21.140	0.925
3	20.440	22.250	1.810
4	20.590	23.460	2.870
5	20.505	23.825	3.320
6	20.520	23.610	3.090
7	20.395	22.255	1.860
8	20.160	21.000	0.840
9	19.535	20.185	0.650
Weighted Average	**20.304**	**22.219**	**1.915**

Measured by: Jerry Godden **Signed:**

UKAS TESTING 0088

TWI

SENB R-CURVE TEST 24624 M02 04

Client	CRP		
Project leader	WeeLiam Khor		Signed:

R-Curve data source

Data logging program	LVRCURVE V 1.31 03 Sep 2013
Program used to calculate R-curve data	LVRCALC V 1.16 17-Nov-2014
Calculation date of R-curve data	19 Mar 2015

Specimen details

Material	S355J2	
Specimen type	SENB, Sub-size	
Crack plane orientation	Y-X	
Type of notch tip	Fatigue	
Notch tip location	Parent material	
Specimen side grooved	No	
Specimen width	40.00	mm
Specimen thickness	19.98	mm
Initial crack length, a0	20.38	mm
Estimated final crack length, ap	22.80	mm

Test details

Test standard	BS7448 Prt 4:1997	
Test method	Unloading compliance	
Test date	16/03/2015	
Test time	15:28:18	
Test technician	Phillip Cossey	Signed:
Test machine	Instron B107	
Test environment	Air	
Test temperature	23.0	°C
Soak time @ Test temperature	NA	minutes
Knife edge heights	2.000, 12.000	mm
Initial K-Rate	19.93	$N/mm^{3/2}/sec$
Loading span	160.0	mm
Double roller diameter	25.00	mm
Single roller diameter	25.00	mm

Material properties

Yield strength @ Fatigue temperature	421.0	N/mm^2
Tensile strength @ Fatigue temperature	585.0	N/mm^2
Yield strength @ Test temperature	421.0	N/mm^2
Tensile strength @ Test temperature	585.0	N/mm^2
Poisson's ratio	0.3	
Youngs modulus	201744	N/mm^2

Fatigue details

Stress ratio	0.100		
Final load	9.00	kN	
Loading span	160.0	mm	

Test procedure

Number of elastic unloadings	10		
Load relaxation limit	5.00	%	of elastic loading rate
1st Increment size	0.05	mm	
1st Maximum displacement	1.00	mm	
2nd Increment size	0.10	mm	
2nd Maximum displacement	10.00	mm	

Analysis details

Yield strength temperature correction	No
Young's modulus temperature correction	No
Method of determining J	DOUBLE CLIP
Young's modulus adjusted for crack agreement	Yes
Clip gauge used for crack length calculations	Clip 1

Compiled by: Dan Bloom **Signed:** ____________

UKAS TESTING 0088

TWI

SENB R-CURVE TEST 24624 M02 04

Qualification checks to BS7448 Prt 4:1997

(6.1.2)	
Knife edge spacing	**Pass**
(8.4.1)	
Single roller diameter	**Pass**
Double roller diameter	**Pass**
(9.3.1)	
Loading span	**Pass**
(9.6)	
Intitial K-rate between 0.5 MPa.$m^{0.5}s^{-1}$ to 3.0 MPa.$m^{0.5}s^{-1}$	**Pass**
(9.9.3)	
Was there a defect on fracture surface	**Yes**
(10.3.2)	
Estimated initial crack length a_o within 2% of measured a_o	**Pass**
(10.3.3)	
Estimated final crack growth within +/- 15% Δa	**Pass**
(14.2.3)	
Minimum surface crack length (a)	**Pass**
Minimum crack extension at surface (b)	**Pass**
Difference in surface crack measurements (c)	**Pass**
Surface crack measurements (d)	**Pass**
(14.2.4)	
Multiplane cracking (a)	**Pass**
a_0/W check 0.45-0.7 (b)	**Pass**
Crack shape (c)	**Pass**
Minimum crack length (d)	**Pass**
Crack within envelope (e)	**Pass**
(14.3.1)	
The specimen did not fracture or pop-in (a)	**Yes**
The final fatigue precracking force was < F_f (b)	**Pass**
The stress ratio < 0.1 (c)	**Pass**

UKAS TESTING 0088 — TWI

SENB R-CURVE TEST 24624 M02 04

ELASTIC UNLOADINGS

No.	Coeff	Comp'nce	Load	Vgo	Vpo	Q	Ram	Total Uarea	Plastic Uarea	Estimated a	Corrected a	Estimated Δa	Corrected Δa	CTOD	CTOD Corrected	K	K Corrected	Jdef	J Corrected	CMOD	CMOD Parea	First Rec	Last Rec			
		mm/kN	kN	mm	mm	mm	mm	kNmm	kNmm	mm	mm	mm	mm	mm	mm	$N/mm^{3/2}$	$N/mm^{3/2}$	N/mm	N/mm	mm	kNmm					
1	0.99998	0.009168	9.09	0.081	-0.002	0.113	0.406	0.51	-0.03	20.36	20.37	-0.02	-0.01	0.003	0.003	790.1	789.1	2.7	2.7	0.076	0.32	1396	1496	0	0	0
2	0.99998	0.009190	9.10	0.082	-0.002	0.113	0.406	0.51	-0.03	20.38	20.38	0.00	0.00	0.003	0.003	790.4	790.6	2.7	2.7	0.076	0.32	1664	1763	0	0	0
3	0.99999	0.009243	9.09	0.082	-0.002	0.113	0.406	0.51	-0.03	20.42	20.43	0.04	0.04	0.003	0.003	789.6	792.3	2.7	2.7	0.076	0.32	1930	2030	0	0	0
4	0.99998	0.009189	9.08	0.081	-0.002	0.113	0.406	0.51	-0.03	20.38	20.38	0.00	0.00	0.003	0.003	789.1	789.2	2.7	2.7	0.076	0.32	2196	2296	0	0	0
5	0.99998	0.009155	9.09	0.081	-0.002	0.113	0.406	0.51	-0.03	20.35	20.36	-0.03	-0.03	0.003	0.003	790.1	788.6	2.7	2.7	0.076	0.32	2462	2562	0	0	0
6	0.99999	0.009190	9.10	0.082	-0.002	0.113	0.406	0.51	-0.03	20.38	20.38	0.00	0.00	0.003	0.003	790.4	790.6	2.7	2.7	0.076	0.32	2727	2827	0	0	0
7	0.99998	0.009225	9.09	0.081	-0.002	0.113	0.406	0.51	-0.03	20.41	20.41	0.02	0.03	0.003	0.003	790.0	791.9	2.7	2.7	0.076	0.32	2993	3093	0	0	0
8	0.99998	0.009216	9.09	0.081	-0.002	0.114	0.407	0.52	-0.02	20.40	20.41	0.02	0.02	0.003	0.003	790.3	791.8	2.7	2.7	0.076	0.32	3259	3359	0	0	0
9	0.99999	0.009191	9.09	0.081	-0.002	0.114	0.406	0.52	-0.02	20.38	20.39	0.00	0.00	0.003	0.003	789.5	789.7	2.7	2.7	0.076	0.32	3523	3623	0	0	0
10	0.99998	0.009180	9.09	0.081	-0.002	0.114	0.406	0.52	-0.02	20.37	20.38	-0.01	-0.01	0.003	0.003	789.9	789.6	2.7	2.7	0.076	0.32	3787	3887	0	0	0

UKAS TESTING 0088 — TWI

SENB R-CURVE TEST 24624 M02 04

PLASTIC UNLOADINGS

No.	Coeff	Comp'nce	Load	Vgo	Vpo	Q	Ram	Total Uarea	Plastic Uarea	Estimated a	Corrected a	Estimated Δa	Corrected Δa	CTOD	CTOD Corrected	K	K Corrected	Jdef	J Corrected	CMOD	CMOD Parea	First Rec	Last Rec			
		mm/kN	kN	mm	mm	mm	mm	kNmm	kNmm	mm	mm	mm	mm	mm	mm	$N/mm^{3/2}$	$N/mm^{3/2}$	N/mm	N/mm	mm	kNmm					
11	0.99997	0.009171	11.17	0.101	-0.002	0.140	0.454	0.79	-0.04	20.36	20.37	-0.02	-0.01	0.005	0.005	970.7	969.9	4.1	4.1	0.094	0.50	4148	4248	0	0	0
12	0.99999	0.009201	15.90	0.151	0.005	0.206	0.562	1.69	0.02	20.39	20.40	0.00	0.02	0.011	0.011	1381.6	1383.5	8.7	8.7	0.141	1.11	4627	4727	0	0	0
13	0.99999	0.009209	19.90	0.201	0.018	0.272	0.660	2.88	0.27	20.39	20.41	0.01	0.03	0.021	0.021	1729.1	1732.8	14.9	14.9	0.188	1.94	5162	5262	0	0	0
14	0.99999	0.009207	22.78	0.251	0.042	0.339	0.749	4.30	0.89	20.39	20.41	0.01	0.03	0.032	0.032	1979.1	1983.7	22.2	22.2	0.235	2.94	5678	5778	0	0	0
15	0.99999	0.009248	24.61	0.302	0.075	0.403	0.829	5.84	1.85	20.42	20.45	0.04	0.06	0.044	0.044	2138.7	2149.8	30.1	30.0	0.282	4.05	6202	6302	0	0	0
16	0.99999	0.009277	25.78	0.352	0.115	0.468	0.901	7.47	3.09	20.45	20.47	0.06	0.09	0.057	0.057	2240.2	2256.6	38.4	38.3	0.329	5.24	6731	6831	0	0	0
17	0.99999	0.009268	26.37	0.401	0.159	0.531	0.971	9.12	4.54	20.44	20.47	0.06	0.09	0.069	0.070	2291.6	2307.9	46.9	46.8	0.375	6.44	7256	7356	0	0	0
18	0.99999	0.009281	26.49	0.452	0.208	0.597	1.038	10.86	6.24	20.45	20.48	0.07	0.10	0.082	0.083	2302.1	2321.1	55.8	55.6	0.423	7.69	7782	7882	0	0	0
19	0.99999	0.009277	26.66	0.501	0.256	0.662	1.105	12.60	7.93	20.45	20.48	0.06	0.10	0.095	0.096	2316.6	2335.8	64.7	64.5	0.469	8.93	8307	8407	0	0	0
20	0.99999	0.009298	26.81	0.552	0.305	0.727	1.173	14.33	9.60	20.46	20.50	0.08	0.12	0.108	0.109	2330.1	2353.1	73.5	73.3	0.516	10.17	8835	8935	0	0	0
21	0.99998	0.009288	27.00	0.602	0.353	0.792	1.240	16.07	11.28	20.45	20.50	0.07	0.12	0.121	0.122	2345.9	2368.4	82.4	82.1	0.563	11.43	9365	9465	0	0	0
22	0.99998	0.009286	27.14	0.652	0.402	0.856	1.306	17.79	12.95	20.45	20.50	0.07	0.12	0.134	0.135	2358.0	2381.0	91.2	90.9	0.609	12.70	9892	9992	0	0	0
23	0.99998	0.009296	27.31	0.702	0.451	0.921	1.373	19.57	14.66	20.46	20.51	0.08	0.13	0.147	0.148	2373.6	2398.9	100.2	99.9	0.657	13.97	10423	10523	0	0	0
24	0.99999	0.009305	27.49	0.752	0.499	0.986	1.440	21.35	16.38	20.47	20.53	0.08	0.14	0.160	0.161	2388.8	2416.5	109.3	108.9	0.703	15.26	10953	11053	0	0	0
25	0.99998	0.009325	27.64	0.801	0.547	1.051	1.505	23.13	18.10	20.48	20.54	0.10	0.16	0.173	0.174	2401.6	2433.2	118.4	117.9	0.750	16.53	11481	11581	0	0	0
26	0.99998	0.009341	27.83	0.851	0.595	1.115	1.572	24.91	19.82	20.49	20.56	0.11	0.18	0.186	0.187	2418.2	2453.2	127.5	126.9	0.797	17.83	12013	12113	0	0	0
27	0.99998	0.009328	27.97	0.902	0.644	1.181	1.637	26.75	21.60	20.48	20.55	0.10	0.17	0.199	0.200	2430.8	2464.8	136.9	136.3	0.844	19.14	12545	12645	0	0	0
28	0.99998	0.009343	28.15	0.952	0.693	1.245	1.703	28.54	23.33	20.50	20.57	0.11	0.19	0.212	0.213	2446.3	2483.6	146.0	145.3	0.890	20.45	13080	13180	0	0	0
29	0.99997	0.009352	28.30	1.001	0.740	1.308	1.766	30.31	25.04	20.50	20.58	0.12	0.20	0.225	0.226	2458.9	2498.5	155.1	154.3	0.936	21.74	13612	13712	0	0	0
30	0.99998	0.009377	28.46	1.051	0.790	1.374	1.833	32.19	26.86	20.52	20.60	0.14	0.22	0.238	0.239	2473.0	2517.4	164.6	163.7	0.983	23.07	14151	14251	0	0	0
31	0.99999	0.009356	28.62	1.101	0.838	1.439	1.899	34.04	28.65	20.51	20.59	0.12	0.21	0.251	0.252	2487.0	2529.3	174.1	173.2	1.030	24.41	14691	14791	0	0	0
32	0.99998	0.009405	28.75	1.152	0.887	1.503	1.965	35.87	30.43	20.54	20.63	0.16	0.25	0.264	0.266	2498.7	2549.7	183.5	182.3	1.077	25.76	15232	15332	0	0	0
33	0.99998	0.009425	28.90	1.202	0.936	1.567	2.029	37.73	32.23	20.56	20.65	0.17	0.27	0.277	0.279	2511.8	2566.9	192.9	191.6	1.124	27.12	15772	15872	0	0	0
34	0.99996	0.009467	29.03	1.251	0.985	1.630	2.093	39.55	34.01	20.59	20.69	0.21	0.30	0.290	0.292	2522.6	2585.5	202.2	200.7	1.170	28.45	16313	16413	0	0	0
35	0.99997	0.009475	29.18	1.301	1.033	1.695	2.158	41.43	35.82	20.59	20.70	0.21	0.31	0.303	0.305	2535.7	2600.9	211.8	210.1	1.217	29.81	16859	16959	0	0	0
36	0.99998	0.009500	29.32	1.352	1.082	1.760	2.222	43.34	37.68	20.61	20.72	0.23	0.34	0.316	0.318	2547.8	2618.1	221.6	219.7	1.265	31.20	17406	17506	0	0	0
37	0.99998	0.009505	29.45	1.402	1.131	1.824	2.287	45.20	39.49	20.62	20.73	0.23	0.34	0.329	0.332	2559.2	2631.4	231.0	229.0	1.311	32.56	17950	18050	0	0	0
38	0.99998	0.009537	29.59	1.452	1.180	1.888	2.352	47.10	41.35	20.64	20.75	0.26	0.37	0.342	0.345	2570.9	2649.6	240.8	238.5	1.358	33.95	18498	18598	0	0	0
39	0.99998	0.009541	29.73	1.502	1.229	1.952	2.416	48.99	43.18	20.64	20.76	0.26	0.38	0.355	0.358	2583.3	2663.8	250.4	248.0	1.405	35.33	19047	19147	0	0	0
40	0.99998	0.009563	29.86	1.552	1.277	2.015	2.481	50.85	44.99	20.66	20.78	0.28	0.40	0.368	0.371	2594.9	2680.0	259.9	257.3	1.452	36.72	19595	19695	0	0	0
41	0.99998	0.009594	29.97	1.602	1.326	2.078	2.540	52.74	46.83	20.68	20.81	0.30	0.42	0.381	0.385	2604.5	2696.0	269.6	266.7	1.499	38.11	20145	20245	0	0	0
42	0.99997	0.009594	30.08	1.652	1.375	2.142	2.603	54.66	48.71	20.68	20.81	0.30	0.43	0.394	0.398	2613.5	2706.0	279.4	276.3	1.545	39.50	20696	20796	0	0	0
43	0.99999	0.009634	30.22	1.701	1.424	2.206	2.666	56.59	50.59	20.71	20.84	0.33	0.46	0.406	0.411	2625.6	2726.0	289.2	285.8	1.592	40.92	21250	21350	0	0	0
44	0.99997	0.009636	30.33	1.752	1.473	2.271	2.732	58.55	52.49	20.71	20.85	0.33	0.47	0.420	0.425	2635.9	2737.9	299.2	295.6	1.639	42.34	21801	21901	0	0	0
45	0.99997	0.009661	30.42	1.802	1.522	2.335	2.794	60.48	54.40	20.73	20.87	0.35	0.49	0.432	0.438	2643.1	2750.4	309.1	305.2	1.686	43.75	22353	22453	0	0	0
46	0.99998	0.009686	30.51	1.852	1.572	2.399	2.857	62.43	56.31	20.75	20.89	0.37	0.51	0.446	0.451	2651.2	2763.8	319.0	314.9	1.733	45.19	22909	23009	0	0	0
47	0.99997	0.009712	30.59	1.902	1.621	2.463	2.921	64.38	58.22	20.77	20.92	0.39	0.53	0.459	0.465	2658.3	2776.4	329.0	324.5	1.780	46.62	23465	23565	0	0	0
48	0.99997	0.009749	30.62	1.952	1.670	2.526	2.983	66.31	60.14	20.80	20.95	0.41	0.56	0.472	0.478	2660.6	2785.8	338.8	334.0	1.826	48.04	24020	24120	0	0	0
49	0.99998	0.009786	30.71	2.002	1.719	2.590	3.045	68.26	62.05	20.82	20.98	0.44	0.59	0.484	0.491	2668.4	2801.0	348.8	343.5	1.873	49.47	24576	24676	0	0	0
50	0.99998	0.009806	30.77	2.052	1.769	2.653	3.108	70.22	63.99	20.84	20.99	0.45	0.61	0.497	0.505	2674.2	2811.1	358.8	353.2	1.920	50.91	25132	25232	0	0	0
51	0.99998	0.009821	30.86	2.102	1.818	2.716	3.172	72.15	65.88	20.85	21.01	0.47	0.63	0.511	0.518	2681.7	2822.4	368.6	362.7	1.967	52.35	25689	25789	0	0	0
52	0.99997	0.009857	30.92	2.151	1.867	2.780	3.232	74.10	67.81	20.87	21.04	0.49	0.66	0.523	0.532	2687.1	2835.1	378.6	372.2	2.014	53.79	26249	26349	0	0	0
53	0.99997	0.009877	31.00	2.202	1.917	2.845	3.297	76.11	69.78	20.89	21.06	0.51	0.67	0.536	0.545	2693.9	2846.4	388.8	382.1	2.061	55.24	26811	26911	0	0	0
54	0.99998	0.009898	31.06	2.252	1.967	2.907	3.357	78.05	71.70	20.90	21.08	0.52	0.69	0.550	0.559	2698.8	2856.1	398.7	391.7	2.108	56.69	27373	27473	0	0	0
55	0.99998	0.009912	31.11	2.302	2.016	2.971	3.419	80.01	73.64	20.91	21.09	0.53	0.71	0.563	0.572	2703.8	2864.6	408.7	401.4	2.154	58.15	27935	28035	0	0	0
56	0.99997	0.009942	31.21	2.352	2.065	3.034	3.482	81.99	75.58	20.93	21.11	0.55	0.73	0.575	0.586	2712.2	2879.4	418.9	411.1	2.201	59.60	28497	28597	0	0	0
57	0.99998	0.009978	31.26	2.402	2.115	3.097	3.544	83.96	77.53	20.96	21.14	0.58	0.76	0.589	0.599	2716.4	2891.0	428.9	420.6	2.248	61.07	29060	29160	0	0	0
58	0.99998	0.010014	31.26	2.452	2.164	3.159	3.604	85.88	79.44	20.99	21.17	0.60	0.79	0.601	0.613	2716.6	2898.1	438.7	429.8	2.294	62.51	29622	29722	0	0	0
59	0.99997	0.010041	31.31	2.502	2.214	3.221	3.666	87.82	81.37	21.00	21.19	0.62	0.81	0.614	0.626	2720.4	2907.6	448.6	439.3	2.342	63.98	30186	30286	0	0	0
60	0.99997	0.010080	31.37	2.552	2.263	3.283	3.728	89.76	83.29	21.03	21.22	0.65	0.84	0.627	0.640	2726.2	2921.2	458.5	448.7	2.388	65.44	30750	30850	0	0	0
61	0.99997	0.010137	31.41	2.602	2.313	3.345	3.790	91.71	85.22	21.07	21.27	0.69	0.88	0.640	0.654	2729.1	2934.8	468.4	457.9	2.435	66.91	31316	31416	0	0	0
62	0.99997	0.010162	31.42	2.651	2.363	3.407	3.849	93.65	87.16	21.09	21.29	0.71	0.91	0.653	0.667	2730.2	2941.2	478.4	467.3	2.482	68.38	31882	31982	0	0	0
63	0.99997	0.010193	31.43	2.702	2.413	3.469	3.909	95.58	89.08	21.11	21.31	0.73	0.93	0.666	0.681	2731.3	2948.6	488.2	476.6	2.529	69.84	32448	32548	0	0	0
64	0.99997	0.010235	31.43	2.752	2.463	3.531	3.971	97.53	91.03	21.14	21.35	0.76	0.96	0.679	0.695	2731.1	2956.4	498.1	485.9	2.576	71.32	33017	33117	0	0	0
65	0.99997	0.010280	31.42	2.802	2.513	3.594	4.031	99.50	93.00	21.17	21.38	0.79	1.00	0.692	0.708	2730.6	2964.3	508.2	495.3	2.623	72.80	33582	33682	0	0	0
66	0.99996	0.010334	31.45	2.902	2.612	3.718	4.150	103.38	96.88	21.21	21.42	0.82	1.04	0.718	0.736	2733.2	2978.1	528.0	514.0	2.717	75.73	34269	34369	0	0	0
67	0.99997	0.010416	31.47	3.002	2.713	3.842	4.272	107.28	100.77	21.26	21.49	0.88	1.10	0.744	0.763	2734.4	2995.0	547.9	532.5	2.811	78.69	34956	35056	0	0	0
68	0.99997	0.010453	31.50	3.102	2.812	3.963	4.392	111.11	104.58	21.28	21.52	0.90	1.13	0.770	0.791	2736.9	3005.9	567.4	551.0	2.905	81.65	35645	35745	0	0	0
69	0.99996	0.010514	31.54	3.202	2.912	4.088	4.514	115.03	108.48	21.33	21.56	0.94	1.18	0.796	0.819	2741.1	3022.6	587.4	569.7	2.999	84.61	36335	36435	0	0	0
70	0.99997	0.010584	31.54	3.302	3.012	4.210	4.631	118.87	112.32	21.37	21.62	0.99	1.24	0.822	0.846	2740.6	3035.8	607.0	587.9	3.092	87.56	37022	37122	0	0	0
71	0.99997	0.010656	31.54	3.402	3.112	4.332	4.754	122.73	116.19	21.42	21.67	1.04	1.29	0.848	0.874	2740.7	3049.8	626.7	606.2	3.186	90.52	37710	37810	0	0	0
72	0.99997	0.010753	31.52	3.502	3.212	4.453	4.870	126.54	120.00	21.48	21.74	1.10	1.36	0.874	0.902	2739.2	3066.3	646.2	623.8	3.280	93.46	38400	38500	0	0	0
73	0.99996	0.010834	30.98	3.602	3.317	4.574	4.985	130.32	124.00	21.53	21.80	1.15	1.42	0.900	0.930	2692.0	3028.7	665.4	641.4	3.374	96.41	39081	39181	0	0	0
74	0.99996	0.010939	30.83	3.702	3.418	4.696	5.099	134.10	127.84	21.60	21.87	1.22	1.49	0.926	0.958	2678.7	3032.8	684.7	658.7	3.468	99.30	39761	39861	0	0	0
75	0.99996	0.011104	30.64	3.802	3.520	4.818	5.214	137.83	131.65	21.70	21.98	1.32	1.60	0.952	0.986	2662.9	3043.3	703.8	675.1	3.562	102.19	40442	40542	0	0	0
76	0.99996	0.011223	30.52	3.902	3.622	4.939	5.331	141.54	135.41	21.78	22.06	1.39	1.68	0.978	1.015	2651.8	3051.7	722.7	691.7	3.656	105.08	41125	41225	0	0	0
77	0.99997	0.011378	30.34	4.002	3.723	5.058	5.445	145.15	139.10	21.87	22.16	1.49	1.78	1.004	1.043	2636.2	3060.5	741.1	707.5	3.750	107.92	41801	41901	0	0	0
78	0.99996	0.011507	30.06	4.102	3.826	5.176	5.557	148.70	142.76	21.95	22.25	1.56	1.86	1.030	1.072	2611.8	3054.2	759.2	723.2	3.844	110.78	42479	42579	0	0	0
79	0.99997	0.011608	30.00	4.202	3.926	5.296	5.671	152.28	146.36	22.01	22.31	1.62	1.93	1.056	1.101	2606.9	3066.2	777.5	739.3	3.938	113.59	43159	43259	0	0	0
80	0.99997	0.011722	29.93	4.302	4.026	5.414	5.789	155.84	149.95	22.07	22.38	1.69	2.00	1.081	1.129	2600.5	3078.3	795.6	755.1	4.032	116.41	43839	43939	0	0	0
81	0.99997	0.011838	29.83	4.402	4.127	5.531	5.903	159.32	153.46	22.14	22.46	1.76	2.07	1.107	1.158	2592.4	3088.6	813.4	770.4	4.126	119.20	44516	44616	0	0	0
82	0.99998	0.011988	29.71	4.502	4.229	5.648	6.015	162.81	157.00	22.22	22.55	1.84	2.17	1.133	1.187	2581.7	3101.0	831.2	785.3	4.221	122.01	45197	45297	0	0	0
83	0.99997	0.012117	29.59	4.602	4.330	5.777	6.131	166.63	160.87	22.30	22.63	1.91	2.24	1.159	1.216	2571.4	3110.4	850.7	802.0	4.314	124.78	45878	45978	0	0	0
84	0.99997	0.012256	29.44	4.702	4.431	5.895	6.243	170.08	164.38	22.37	22.71	1.99	2.33	1.185	1.246	2557.8	3117.1	868.3	816.8	4.408	127.54	46558	46658	0	0	0
85	0.99999	0.012416	29.26	4.802	4.533	6.015	6.355	173.60	167.96	22.46	22.80	2.08	2.42	1.211	1.275	2542.7	3124.7	886.2	831.5	4.502	130.31	47241	47341	0	0	0

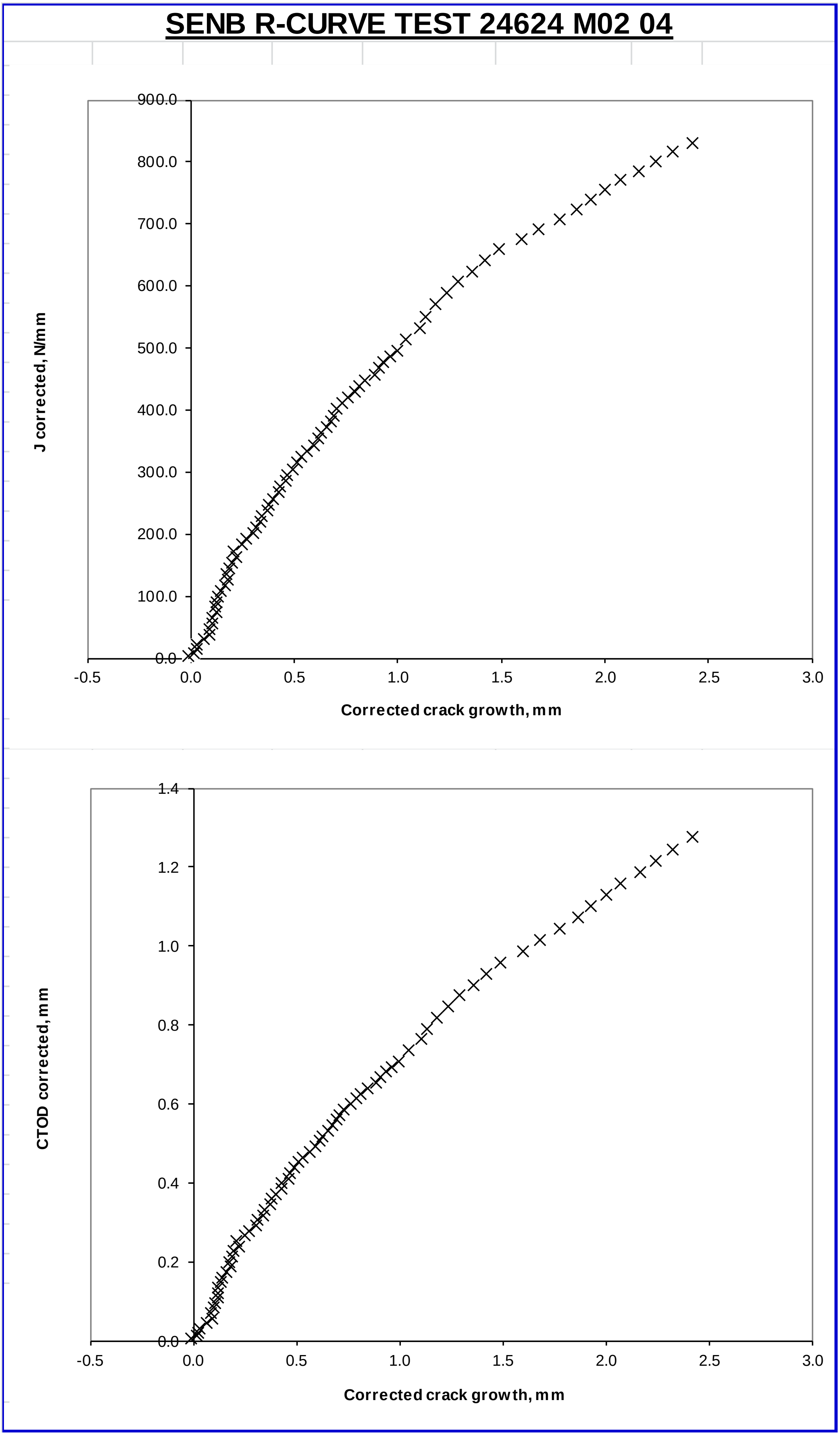
SENB R-CURVE TEST 24624 M02 04
J corrected, N/mm
Corrected crack growth, mm
CTOD corrected, mm
Corrected crack growth, mm

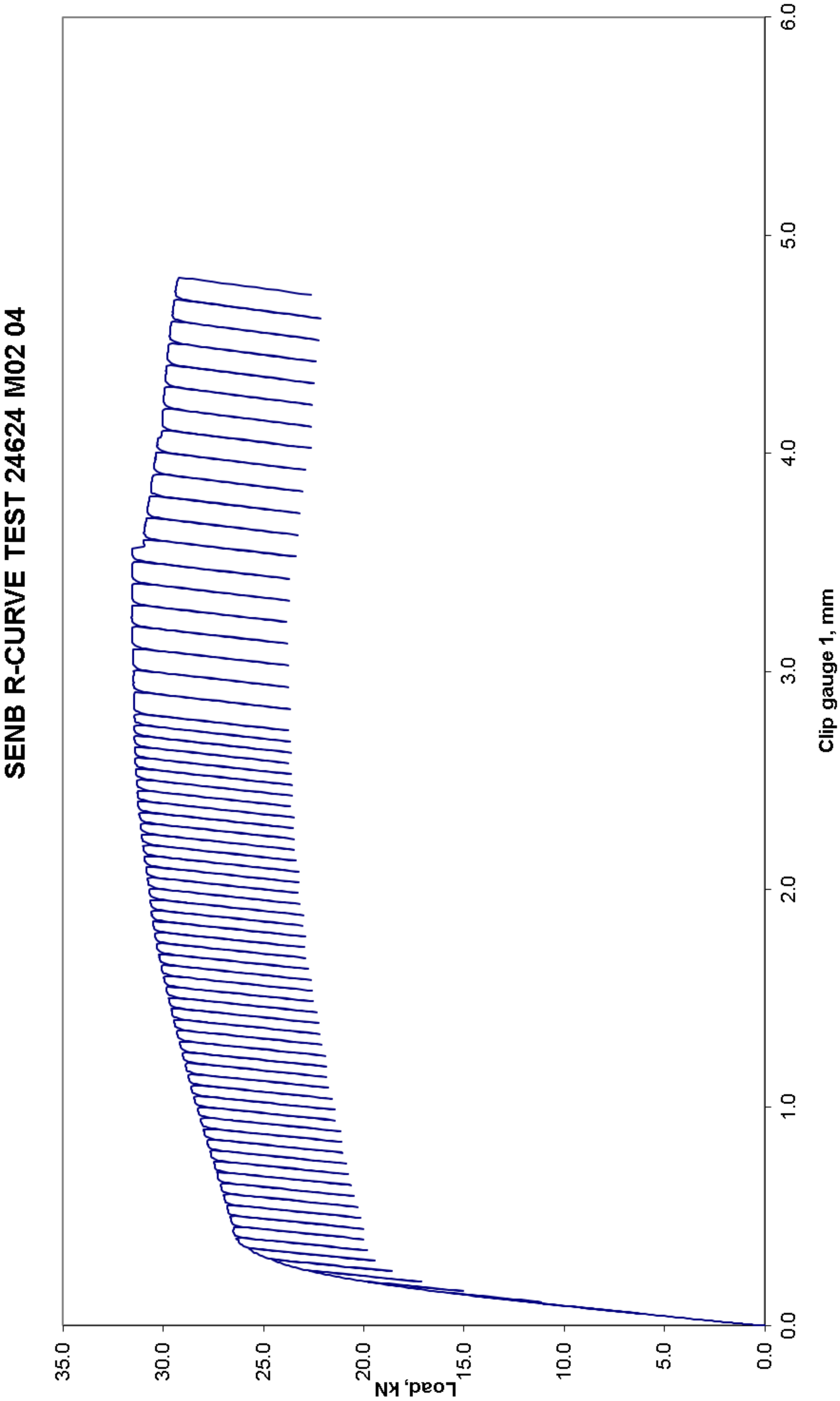
SENB R-CURVE TEST 24624 M02 04
Load, kN
Clip gauge 1, mm
0.0
5.0
10.0
15.0
20.0
25.0
30.0
35.0
0.0
1.0
2.0
3.0
4.0
5.0
6.0

SENB R-CURVE TEST 24624 M02 04

Specimen width, W	40.000	mm
Specimen Thickness, B	19.980	mm
Machined notch depth, M	16.200	mm
Surface crack length, a_{S1}	19.400	mm
Surface crack length, a_{S2}	19.390	mm
Net section thickness, B_N	19.980	mm
a_{max}	20.600	mm
a_{min}	19.770	mm

Diagram of fracture face

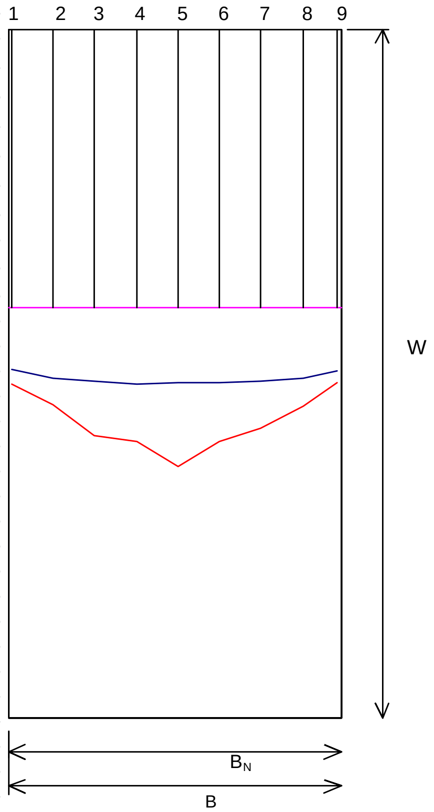

Measured by:

Signed:

Measurement Line	Fatigue crack length a0, mm	Slow stable crack extension Fatigue crack ap, mm	Slow stable crack extension including stretch zone, deltaa, mm
1	19.770	20.620	0.850
2	20.290	21.840	1.550
3	20.470	23.630	3.160
4	20.600	23.960	3.360
5	20.570	25.390	4.820
6	20.530	23.980	3.450
7	20.510	23.240	2.730
8	20.290	21.890	1.600
9	19.830	20.550	0.720
Weighted Average	**20.383**	**23.064**	**2.682**

UKAS TESTING
0088

TWI

SENB FRACTURE TEST 24624 M02-05

Client	CRP		
Project leader	Weeliam Khor	Signed:	

Data source

Data logging program	LVGENLOG V 1.29 19-Nov-2013
Program used to calculate CTOD/J	LVGENPLOT V 1.28 30-Jan-2015
Calculation date of CTOD/J	24 Mar 2015

Specimen details

Material	S355J2	
Specimen type	Subsize, SENB	
Crack plane orientation	Y-X	
Type of notch tip	Fatigue	
Notch tip location	Parent material	
Specimen width	40.000	mm
Specimen thickness	20.000	mm
Initial crack length	20.423	mm
Original PM 1 thickness	50.00	mm

Test details

Test standard(s)	BS 7448: Part 1: 1991		
Test date	20/03/2015		
Test time	11:12:00		
Test technician	Phillip Cossey		Signed:
Test machine	INSTRON 8500 B107		
Test environment	AIR		
Test temperature	21.0	°C	
Soak time @ test temperature	0.0	minutes	
Knife edge heights	2.000, 12.000	mm	
Knife edge spacing	14.00	mm	
Initial K-rate	1.3	$MPa.m^{1/2}/s$	
Loading span	160.0	mm	
Double roller diameter	25.00	mm	
Single roller diameter	25.00	mm	

Material properties

Yield strength for pre-cracking	421.0	MPa	Assumed from material specification
Tensile strength for pre-cracking	585.0	MPa	Assumed from material specification
Yield strength for testing	421.0	MPa	Assumed from material specification
Tensile strength for testing	585.0	MPa	Assumed from material specification
Poisson's ratio	0.3		Assumed
Young's modulus	207	GPa	Assumed

Fatigue details

Stress ratio, R	0.100	
Final force, F_f	9.00	kN
Final K	24.8	$MPa.m^{1/2}$
Fatigue temperature	21.0	°C
Loading span, S	160.0	mm

Analysis details

Method of determining Load Point Displacement, q	DOUBLE CLIP
Lower knife edge height check	OK

Compiled by: Dan Bloom **Signed:** ________________

SENB FRACTURE TEST 24624 M02-05

Qualification checks to **BS 7448: Part 1: 1991**

(5.1.3)	
Knife edge attachment spacing	**Pass**
(6.4.5,6.4.6)	
The final fatigue precracking force <= F_f (a)	**Pass**
ΔK/E below limit (b)	**Pass**
(6.4.7)	
Initial/Final K ratio during precracking < 1.3 (a)	**Pass**
(7.5.1)	
Single roller diameter	**Pass**
Double roller diameter	**Pass**
Loading span	**Pass**
(8.5)	
Initial K-rate between 0.5 $MPa.m^{0.5}s^{-1}$ and 3.0 $MPa.m^{0.5}s^{-1}$	**Pass**
(10.2.2)	
Minimum surface crack length (a)	**Pass**
Minimum crack extension at surface (b)	**Pass**
Difference in surface crack measurements (c)	**Pass**
Surface fatigue cracks in envelope (d)	**Pass**
Crack plane within 10° (e)	**Pass**
(10.2.3)	
Multiplane cracking (a)	**Pass**
a_0/W check 0.45-0.55 (b)	**Pass**
Crack shape (c)	**Pass**
Minimum crack length (d)	**Pass**
(10.3)	
The stress ratio <= 0.1 (c)	**Pass**

0088

SENB FRACTURE TEST 24624 M02-05

Test date	20/03/2015
Technician	Phillip Cossey
Test machine	INSTRON 8500 B107
Control mode	Displacement

Client	CRP
Project leader	Weeliam Khor
Investigator's signature	
Compiled by	Dan Bloom

SPECIMEN DETAILS

Force, F	32.19	kN
Width, W	40.000	mm
Thickness, B	20.000	mm
Crack length, a_0	20.423	mm
Loading span, S	160.00	mm
Yield strength	421	MPa
Young's modulus	207	GPa
Poisson's ratio	0.300	
Test temperature	21.0	°C

RESULTS

δ	0.834	mm
K @ calculation point	88.7	$MPa.m^{1/2}$
F_{max}/F_Q	1.97	
K_Q	44.90	$MPa.m^{1/2}$
Total area under Force v q	129.85	kNmm
J0 from q from DOUBLE CLIP	663.77	kJ/m² (N/mm)
Plastic area Force v CMOD	85.79	kNmm
Type of result	δ/J_m	
Test standard(s)	BS 7448: Part 1: 1991	
Result qualified to standard(s)	YES	

LOWER CLIP GAUGE VALUES

Knife edge height	2.00	mm
Vg	3.361	mm
Vp	3.062	mm

UPPER CLIP GAUGE VALUES

Knife edge height	12.00	mm
Vg	4.491	mm
Vp	4.090	mm

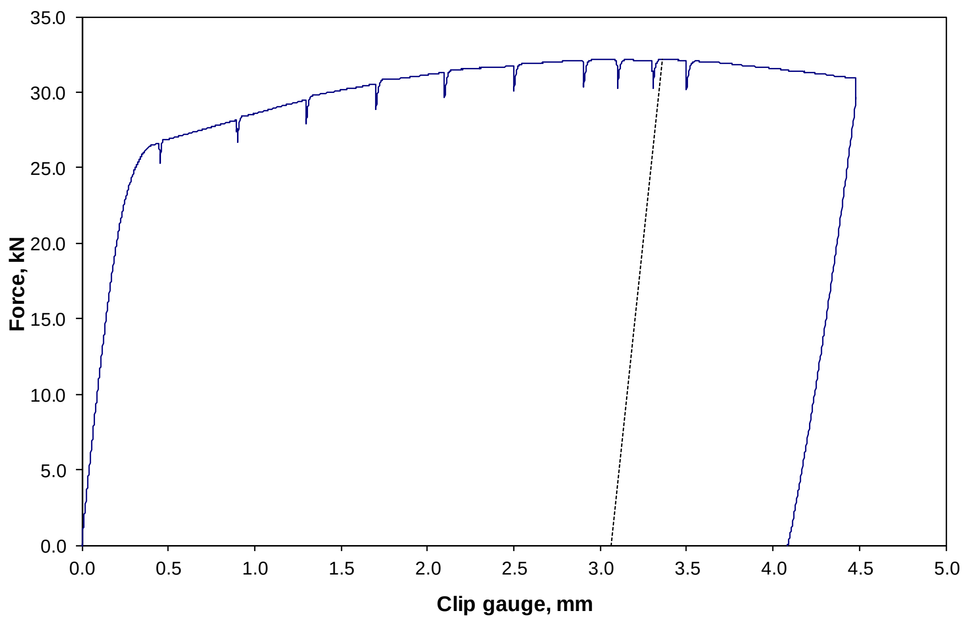

SENB FRACTURE TEST 24624 M02-05

Specimen width, W	40.000	mm
Specimen thickness, B	20.000	mm
Machined notch depth, M	16.150	mm
Surface crack length, a_{S1}	19.400	mm
Surface crack length, a_{S2}	19.550	mm
a_{max}	20.660	mm
a_{min}	19.740	mm

Diagram of fracture face

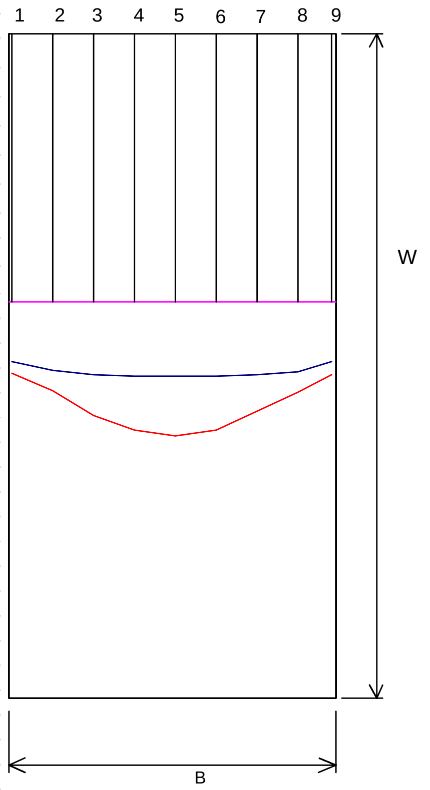

Comments

Measurement Line	Fatigue crack length a_0, mm	Slow stable crack extension + fatigue crack a_p, mm	Slow stable crack extension including stretch zone, Δ_a, mm
1	19.740	20.430	0.690
2	20.315	21.515	1.200
3	20.515	22.965	2.450
4	20.600	23.875	3.275
5	20.660	24.195	3.535
6	20.640	23.840	3.200
7	20.540	22.715	2.175
8	20.350	21.585	1.235
9	19.785	20.535	0.750
Weighted Average	**20.423**	**22.647**	**2.224**

Measured by: Dan Bloom **Signed:**

UKAS TESTING 0088

TWI

SENB R-CURVE TEST 24624 M02 06

Client	CRP		
Project leader	WeeLiam Khor		Signed:

R-Curve data source

Data logging program	LVRCURVE V 1.31 03 Sep 2013
Program used to calculate R-curve data	LVRCALC V 1.20 01-Jul-2016
Calculation date of R-curve data	04 Jul 2016

Specimen details

Material	S355J2	
Specimen type	SENB, Sub-size	
Crack plane orientation	Y-X	
Type of notch tip	Fatigue	
Notch tip location	Parent material	
Specimen side grooved	Yes	
Specimen width	40.00	mm
Specimen thickness	20.00	mm
Initial crack length, a0	20.32	mm
Estimated final crack length, ap	22.63	mm

Test details

Test standard	BS7448 Prt 4:1997		
Test method	Unloading compliance		
Test date	16/03/2015		
Test time	13:45:09		
Test technician	Phillip Cossey		Signed:
Test machine			
Test environment	Air		
Test temperature	23.0	°C	
Soak time @ Test temperature	NA	minutes	
Knife edge heights	2.000, 12.000	mm	
Initial K-Rate	18.71	$N/mm^{3/2}/sec$	
Loading span	160.0	mm	
Double roller diameter	25.00	mm	
Single roller diameter	25.00	mm	

Material properties

Yield strength @ Fatigue temperature	421.0	N/mm^2
Tensile strength @ Fatigue temperature	585.0	N/mm^2
Yield strength @ Test temperature	421.0	N/mm^2
Tensile strength @ Test temperature	585.0	N/mm^2
Poisson's ratio	0.3	
Youngs modulus	204745	N/mm^2

Fatigue details

Stress ratio	0.100	
Final load	9.00	kN
Loading span	160.0	mm

Test procedure

Number of elastic unloadings	5		
Load relaxation limit	5.00	%	of elastic loading rate
1st Increment size	0.05	mm	
1st Maximum displacement	1.00	mm	
2nd Increment size	0.05	mm	
2nd Maximum displacement	10.00	mm	

Analysis details

Yield strength temperature correction	No
Young's modulus temperature correction	No
Method of determining J	DOUBLE CLIP
Young's modulus adjusted for crack agreement	No
Clip gauge used for crack length calculations	Clip 1

Compiled by: J.Bradford **Signed:**

UKAS TESTING 0088

TWI

SENB R-CURVE TEST 24624 M02 06

Qualification checks to BS7448 Prt 4:1997

(6.1.2)	
Knife edge spacing	**Pass**
(8.4.1)	
Single roller diameter	**Pass**
Double roller diameter	**Pass**
(9.3.1)	
Loading span	**Pass**
(9.6)	
Intitial K-rate between 0.5 $MPa.m^{0.5}s^{-1}$ to 3.0 $MPa.m^{0.5}s^{-1}$	**Pass**
(9.9.3)	
Was there a defect on fracture surface	**Yes**
(10.3.2)	
Estimated initial crack length a_o within 2% of measured a_o	**Pass**
(10.3.3)	
Estimated final crack growth within +/- 15% Δa	**Fail**
(14.2.3)	
Minimum surface crack length (a)	**Pass**
Minimum crack extension at surface (b)	**Pass**
Difference in surface crack measurements (c)	**Pass**
Surface crack measurements (d)	**Pass**
(14.2.4)	
Multiplane cracking (a)	**Fail**
a_0/W check 0.45-0.7 (b)	**Pass**
Crack shape (c)	**Pass**
Minimum crack length (d)	**Pass**
Crack within envelope (e)	**Pass**
(14.3.1)	
The specimen did not fracture or pop-in (a)	**Yes**
The final fatigue precracking force was < F_f (b)	**Pass**
The stress ratio < 0.1 (c)	**Pass**

SENB R-CURVE TEST 24624 M02 06

ELASTIC UNLOADINGS

0088

No.	Coeff	Comp'nce	Load	Vgo	Vpo	Q	Ram	Total Uarea	Plastic Uarea	Estimated a	Corrected a	Estimated Δa	Corrected Δa	CTOD	CTOD Corrected	K	K Corrected	Jdef	J Corrected	CMOD	CMOD Parea	First Rec	Last Rec
		mm/kN	kN	mm	mm	mm	mm	kNmm	kNmm	mm	mm	mm	mm	mm	mm	$N/mm^{3/2}$	$N/mm^{3/2}$	N/mm	N/mm	mm	kNmm		
1	0.99998	0.009745	7.28	0.069	0.002	0.100	0.332	0.34	0.02	20.64	20.65	0.32	0.33	0.003	0.003	699.0	717.9	2.3	2.3	0.064	0.00	1200	1300
2	0.99998	0.009803	7.28	0.069	0.002	0.101	0.332	0.35	0.02	20.69	20.69	0.36	0.37	0.003	0.003	698.6	719.9	2.3	2.3	0.064	0.00	1444	1544
3	0.99997	0.009756	7.28	0.069	0.002	0.101	0.332	0.35	0.02	20.65	20.66	0.33	0.34	0.003	0.003	698.6	717.8	2.3	2.3	0.064	0.00	1691	1791
4	0.99998	0.009758	7.29	0.069	0.002	0.101	0.332	0.35	0.02	20.65	20.66	0.33	0.34	0.003	0.003	699.4	718.8	2.3	2.3	0.064	0.00	1937	2037
5	0.99998	0.009763	7.29	0.069	0.002	0.101	0.332	0.35	0.02	20.66	20.66	0.34	0.34	0.003	0.003	699.9	719.5	2.3	2.3	0.064	0.00	2183	2283

SENB R-CURVE TEST 24624 M02 06

PLASTIC UNLOADINGS

0088

No.	Coeff	Comp'nce	Load	Vgo	Vpo	Q	Ram	Total Uarea	Plastic Uarea	Estimated a	Corrected a	Estimated Δa	Corrected Δa	CTOD	CTOD Corrected	K	K Corrected	Jdef	J Corrected	CMOD	CMOD Parea	First Rec	Last Rec
		mm/kN	kN	mm	mm	mm	mm	kNmm	kNmm	mm	mm	mm	mm	mm	mm	$N/mm^{3/2}$	$N/mm^{3/2}$	N/mm	N/mm	mm	kNmm		
6	0.99998	0.009741	10.34	0.101	0.004	0.142	0.405	0.71	0.06	20.64	20.65	0.32	0.33	0.006	0.006	992.9	1019.6	4.8	4.7	0.094	0.02	2579	2679
7	0.99999	0.009782	14.77	0.151	0.014	0.208	0.512	1.55	0.21	20.67	20.68	0.35	0.36	0.014	0.014	1418.1	1460.3	10.3	10.2	0.141	0.10	3049	3149
8	0.99999	0.009818	18.33	0.201	0.030	0.273	0.606	2.62	0.58	20.70	20.71	0.38	0.39	0.024	0.024	1759.5	1816.2	17.4	17.2	0.188	0.34	3568	3668
9	0.99999	0.009798	20.85	0.251	0.057	0.339	0.693	3.91	1.26	20.68	20.70	0.36	0.38	0.036	0.036	2001.4	2064.1	25.7	25.4	0.234	0.81	4071	4171
10	0.99999	0.009828	22.49	0.301	0.092	0.403	0.770	5.31	2.22	20.70	20.73	0.38	0.41	0.049	0.049	2158.9	2231.2	34.7	34.3	0.281	1.51	4580	4680
11	0.99999	0.009816	23.63	0.352	0.131	0.467	0.844	6.78	3.37	20.69	20.72	0.37	0.40	0.061	0.062	2268.4	2343.3	44.0	43.6	0.328	2.35	5097	5197
12	0.99999	0.009849	24.19	0.402	0.176	0.532	0.910	8.33	4.76	20.72	20.75	0.40	0.43	0.074	0.075	2322.6	2404.8	53.9	53.3	0.375	3.35	5611	5711
13	0.99999	0.009868	24.61	0.452	0.222	0.596	0.977	9.90	6.21	20.73	20.77	0.41	0.45	0.087	0.089	2362.0	2449.1	63.8	63.0	0.422	4.40	6129	6229
14	0.99999	0.009883	24.96	0.502	0.270	0.660	1.045	11.48	7.68	20.74	20.78	0.42	0.46	0.101	0.102	2395.8	2487.1	73.7	72.8	0.469	5.48	6647	6747
15	0.99999	0.009926	25.24	0.552	0.317	0.723	1.112	13.06	9.17	20.77	20.82	0.45	0.50	0.114	0.116	2423.0	2522.4	83.7	82.6	0.516	6.59	7168	7268
16	0.99999	0.009922	25.54	0.602	0.364	0.786	1.179	14.68	10.70	20.77	20.82	0.45	0.50	0.127	0.129	2451.4	2552.2	93.8	92.7	0.562	7.70	7691	7791
17	0.99998	0.009932	25.75	0.652	0.412	0.851	1.246	16.33	12.29	20.78	20.83	0.46	0.51	0.140	0.142	2472.1	2576.0	104.3	102.9	0.610	8.86	8216	8316
18	0.99998	0.009961	25.97	0.701	0.460	0.915	1.311	17.97	13.86	20.80	20.85	0.48	0.53	0.153	0.156	2492.6	2602.5	114.6	113.1	0.656	10.01	8742	8842
19	0.99998	0.009968	26.16	0.752	0.508	0.979	1.376	19.64	15.47	20.80	20.86	0.48	0.54	0.166	0.169	2511.6	2624.3	125.1	123.4	0.703	11.18	9270	9370
20	0.99997	0.009988	26.34	0.801	0.556	1.042	1.442	21.29	17.05	20.82	20.88	0.50	0.56	0.179	0.183	2528.7	2646.0	135.4	133.5	0.749	12.36	9797	9897
21	0.99999	0.010022	26.49	0.852	0.605	1.105	1.508	22.95	18.67	20.84	20.91	0.52	0.59	0.192	0.196	2542.9	2666.9	145.9	143.7	0.796	13.56	10326	10426
22	0.99998	0.010022	26.66	0.902	0.654	1.169	1.573	24.65	20.31	20.84	20.91	0.52	0.59	0.205	0.210	2559.2	2684.8	156.6	154.3	0.843	14.77	10857	10957
23	0.99998	0.010064	26.81	0.952	0.702	1.232	1.638	26.34	21.96	20.87	20.94	0.55	0.62	0.218	0.223	2573.9	2707.6	167.3	164.6	0.890	15.99	11390	11490
24	0.99998	0.010071	26.95	1.001	0.750	1.294	1.701	28.00	23.57	20.88	20.95	0.55	0.63	0.231	0.236	2586.7	2723.0	177.7	174.8	0.936	17.19	11919	12019
25	0.99998	0.010108	27.06	1.052	0.800	1.358	1.766	29.72	25.26	20.90	20.98	0.58	0.66	0.244	0.250	2598.0	2741.6	188.5	185.3	0.984	18.44	12458	12558
26	0.99998	0.010128	27.18	1.102	0.849	1.421	1.831	31.43	26.93	20.92	21.00	0.59	0.68	0.257	0.264	2609.4	2757.7	199.2	195.8	1.031	19.68	12992	13092
27	0.99998	0.010164	27.29	1.152	0.898	1.485	1.895	33.16	28.62	20.94	21.03	0.62	0.71	0.270	0.277	2620.1	2775.6	210.1	206.3	1.077	20.92	13529	13629
28	0.99998	0.010196	27.40	1.202	0.947	1.548	1.958	34.89	30.31	20.96	21.05	0.64	0.73	0.283	0.291	2630.5	2792.6	220.9	216.8	1.124	22.17	14065	14165
29	0.99998	0.010218	27.51	1.252	0.996	1.613	2.022	36.66	32.05	20.98	21.07	0.66	0.75	0.296	0.304	2640.4	2807.4	232.1	227.7	1.171	23.43	14604	14704
30	0.99998	0.010245	27.59	1.301	1.045	1.676	2.085	38.39	33.75	21.00	21.09	0.68	0.77	0.309	0.318	2648.9	2821.7	243.0	238.2	1.218	24.69	15145	15245
31	0.99998	0.010274	27.69	1.352	1.094	1.741	2.150	40.20	35.52	21.02	21.12	0.69	0.80	0.323	0.332	2658.1	2837.0	254.3	249.2	1.265	25.98	15687	15787
32	0.99998	0.010321	27.78	1.402	1.143	1.804	2.213	41.94	37.23	21.05	21.15	0.73	0.83	0.336	0.345	2666.7	2854.6	265.3	259.7	1.312	27.24	16230	16330
33	0.99998	0.010338	27.86	1.451	1.192	1.867	2.276	43.68	38.95	21.06	21.17	0.74	0.85	0.349	0.359	2674.4	2866.5	276.2	270.3	1.358	28.50	16769	16869
34	0.99998	0.010374	27.93	1.502	1.242	1.931	2.340	45.47	40.71	21.08	21.20	0.76	0.88	0.362	0.373	2681.7	2881.1	287.4	281.0	1.405	29.80	17313	17413
35	0.99998	0.010436	28.01	1.552	1.291	1.995	2.402	47.24	42.46	21.13	21.24	0.80	0.92	0.375	0.386	2688.7	2899.5	298.6	291.6	1.452	31.09	17857	17957
36	0.99998	0.010467	28.05	1.602	1.340	2.057	2.463	48.99	44.20	21.15	21.27	0.82	0.94	0.388	0.400	2692.7	2909.8	309.6	302.1	1.499	32.38	18399	18499
37	0.99998	0.010518	28.09	1.651	1.390	2.121	2.523	50.77	45.96	21.18	21.30	0.86	0.98	0.401	0.414	2696.5	2923.0	320.7	312.7	1.545	33.67	18939	19039
38	0.99997	0.010560	28.14	1.702	1.440	2.184	2.585	52.55	47.72	21.21	21.33	0.89	1.01	0.414	0.428	2701.4	2936.1	331.9	323.4	1.592	34.98	19481	19581
39	0.99997	0.010613	28.16	1.752	1.489	2.248	2.647	54.34	49.50	21.24	21.37	0.92	1.05	0.427	0.441	2702.9	2947.2	343.1	334.0	1.639	36.29	20027	20127
40	0.99998	0.010703	28.15	1.802	1.540	2.312	2.709	56.14	51.30	21.30	21.44	0.98	1.12	0.440	0.455	2702.1	2962.0	354.4	344.4	1.686	37.61	20575	20675
41	0.99998	0.010749	28.15	1.852	1.589	2.375	2.771	57.91	53.08	21.33	21.47	1.01	1.15	0.453	0.469	2702.4	2970.7	365.6	354.9	1.733	38.92	21120	21220
42	0.99997	0.010825	28.14	1.902	1.640	2.438	2.833	59.68	54.85	21.38	21.52	1.06	1.20	0.466	0.483	2701.3	2982.6	376.7	365.2	1.780	40.26	21669	21769
43	0.99997	0.010888	28.10	1.952	1.690	2.501	2.892	61.43	56.62	21.42	21.57	1.10	1.24	0.479	0.497	2697.0	2989.0	387.6	375.4	1.827	41.57	22217	22317
44	0.99997	0.010955	28.13	2.002	1.740	2.564	2.955	63.22	58.40	21.46	21.61	1.14	1.29	0.492	0.511	2700.0	3004.0	398.9	385.8	1.873	42.88	22764	22864
45	0.99997	0.011023	28.12	2.052	1.790	2.627	3.016	64.98	60.16	21.51	21.66	1.18	1.34	0.505	0.525	2699.2	3014.9	409.9	396.0	1.921	44.21	23314	23414
46	0.99997	0.011098	28.11	2.102	1.840	2.689	3.076	66.71	61.89	21.55	21.71	1.23	1.39	0.518	0.539	2698.0	3026.5	420.8	405.9	1.967	45.51	23863	23963
47	0.99998	0.011167	28.12	2.152	1.890	2.750	3.138	68.44	63.61	21.60	21.75	1.27	1.43	0.531	0.553	2699.8	3040.5	431.6	415.9	2.014	46.82	24415	24515
48	0.99997	0.011242	28.08	2.202	1.941	2.813	3.198	70.20	65.39	21.64	21.80	1.32	1.48	0.544	0.567	2695.5	3048.6	442.7	426.0	2.061	48.16	24968	25068
49	0.99997	0.011320	28.02	2.252	1.991	2.876	3.258	71.95	67.16	21.69	21.85	1.37	1.53	0.557	0.581	2689.7	3055.5	453.6	436.0	2.108	49.48	25518	25618
50	0.99996	0.011399	27.99	2.302	2.041	2.939	3.318	73.71	68.93	21.74	21.91	1.42	1.58	0.570	0.595	2686.9	3065.8	464.7	446.0	2.155	50.80	26066	26166
51	0.99998	0.011465	27.94	2.352	2.092	3.000	3.376	75.42	70.66	21.78	21.95	1.45	1.63	0.583	0.609	2681.7	3071.2	475.4	455.7	2.202	52.11	26616	26716
52	0.99997	0.011542	27.93	2.402	2.142	3.062	3.438	77.15	72.39	21.82	22.00	1.50	1.68	0.596	0.624	2681.5	3084.1	486.3	465.5	2.249	53.43	27168	27268
53	0.99997	0.011612	27.93	2.452	2.192	3.123	3.496	78.85	74.09	21.86	22.04	1.54	1.72	0.609	0.638	2681.2	3095.7	496.9	475.2	2.295	54.73	27722	27822
54	0.99997	0.011667	27.95	2.502	2.242	3.186	3.559	80.59	75.82	21.90	22.08	1.57	1.76	0.622	0.652	2682.7	3107.1	507.8	485.2	2.343	56.04	28276	28376
55	0.99997	0.011738	27.92	2.552	2.292	3.248	3.617	82.33	77.58	21.94	22.12	1.62	1.80	0.635	0.667	2679.8	3115.8	518.8	495.0	2.389	57.34	28832	28932
56	0.99996	0.011822	27.87	2.602	2.342	3.312	3.679	84.10	79.36	21.99	22.18	1.66	1.85	0.648	0.681	2675.8	3125.3	529.8	504.9	2.436	58.66	29387	29487
57	0.99995	0.011963	26.72	2.652	2.403	3.372	3.728	85.74	81.38	22.07	22.26	1.74	1.94	0.661	0.695	2564.6	3017.5	540.0	513.4	2.483	60.21	29920	30020
58	0.99996	0.011983	26.81	2.701	2.452	3.436	3.784	87.43	83.05	22.08	22.27	1.76	1.95	0.674	0.710	2573.2	3031.6	550.6	523.3	2.530	61.44	30468	30568
59	0.99994	0.011960	26.83	2.752	2.502	3.503	3.844	89.23	84.84	22.06	22.26	1.74	1.94	0.687	0.724	2575.4	3031.8	561.9	534.1	2.577	62.70	31018	31118
60	0.99996	0.011983	26.76	2.802	2.552	3.568	3.903	90.97	86.60	22.08	22.28	1.76	1.96	0.700	0.739	2569.2	3028.9	572.8	544.3	2.623	63.95	31563	31663
61	0.99996	0.012127	26.66	2.852	2.604	3.636	3.963	92.77	88.43	22.16	22.37	1.84	2.04	0.713	0.753	2559.5	3040.0	584.1	553.7	2.670	65.22	32111	32211
62	0.99995	0.012247	26.59	2.902	2.654	3.698	4.019	94.43	90.12	22.23	22.44	1.90	2.11	0.726	0.768	2552.8	3050.8	594.5	562.6	2.717	66.48	32658	32758
63	0.99996	0.012382	26.47	2.952	2.705	3.763	4.075	96.14	91.86	22.30	22.51	1.98	2.19	0.739	0.782	2541.2	3057.9	605.2	571.5	2.764	67.75	33203	33303
64	0.99997	0.012592	26.07	3.003	2.760	3.826	4.128	97.80	93.66	22.41	22.63	2.09	2.31	0.753	0.797	2502.5	3042.7	615.6	579.5	2.811	69.10	33744	33844

SENB R-CURVE TEST 24624 M02 06

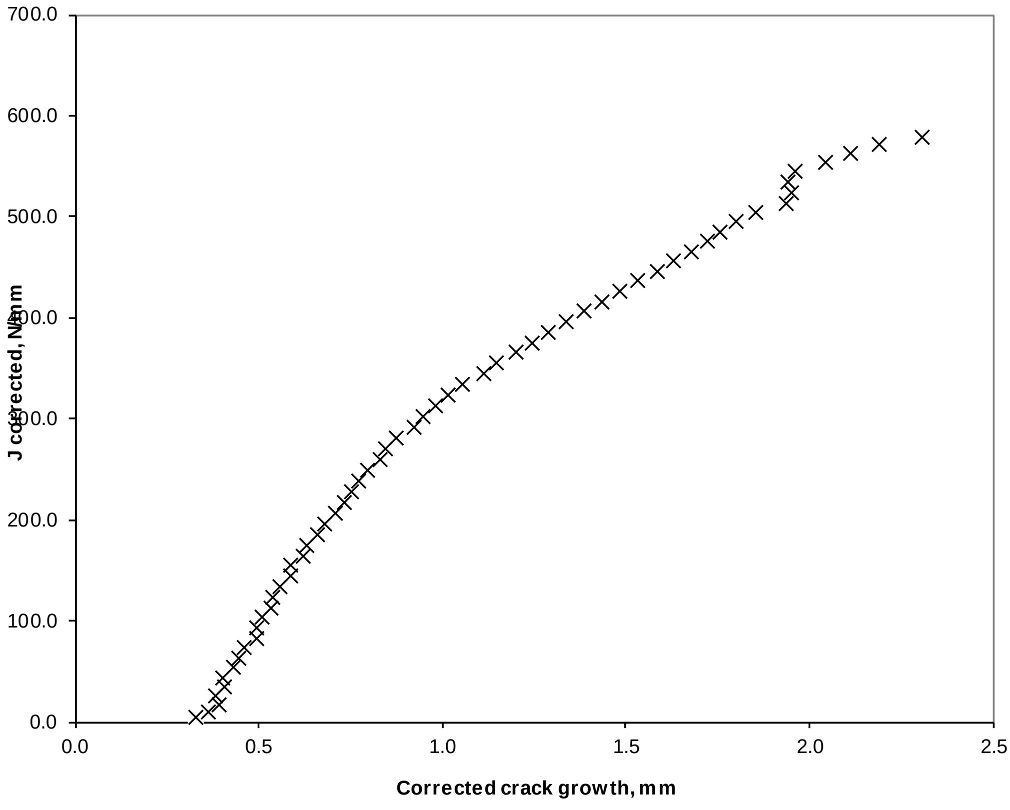

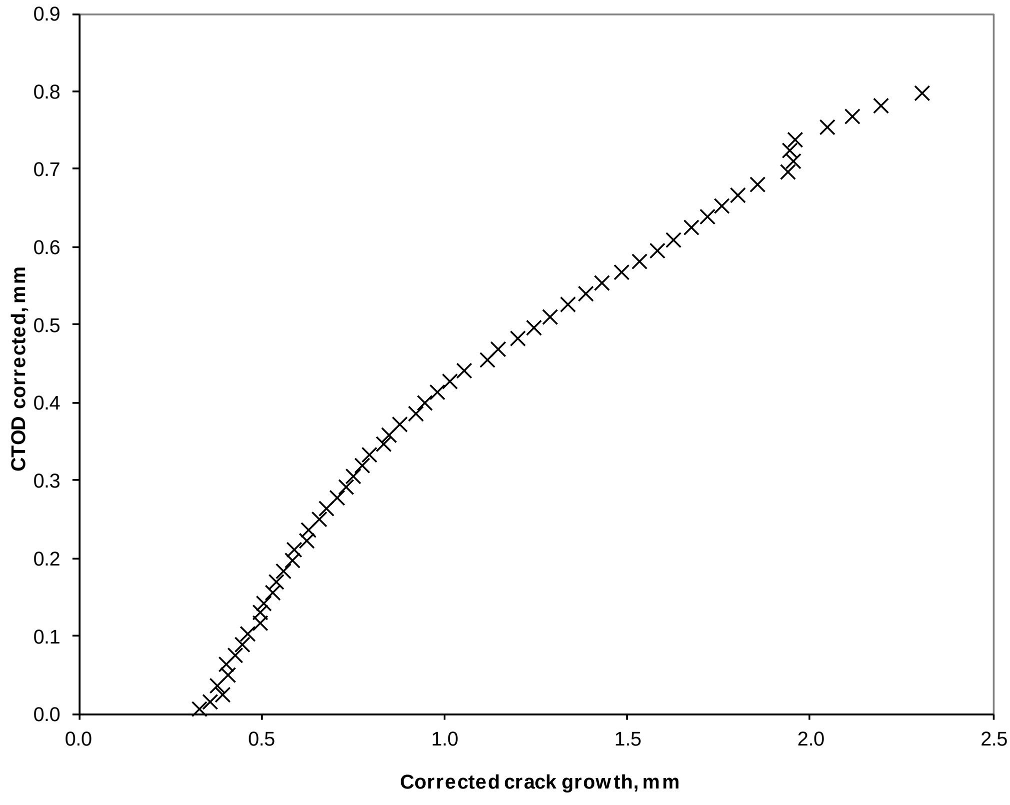

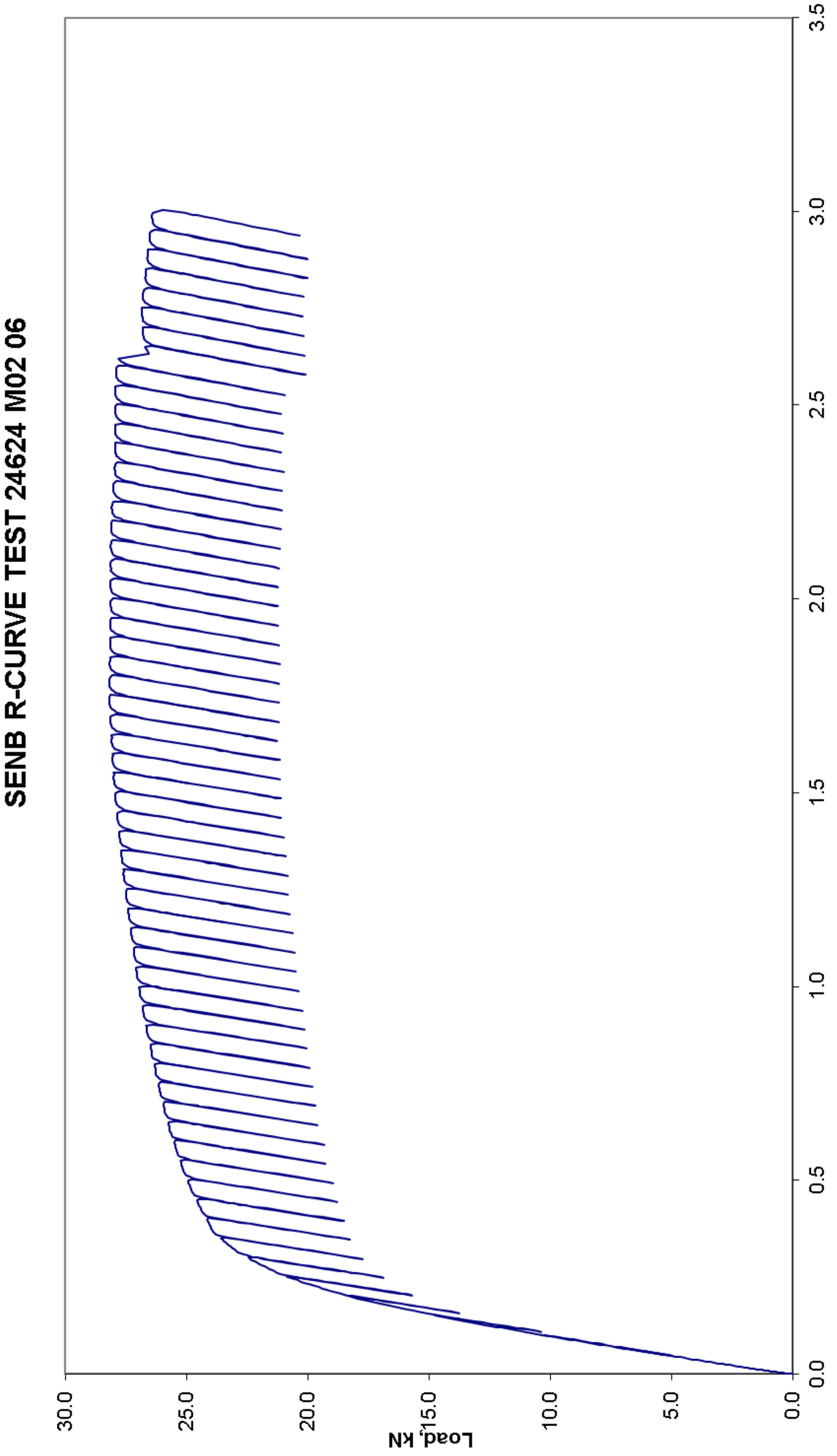
SENB R-CURVE TEST 24624 M02 06
Load, kN
0.0
5.0
10.0
15.0
20.0
25.0
30.0
Clip gauge 1, mm
0.0
0.5
1.0
1.5
2.0
2.5
3.0
3.5

SENB R-CURVE TEST 24624 M02 06

Diagram of fracture face

Specimen width, W	40.000	mm
Specimen Thickness, B	20.000	mm
Machined notch depth, M	16.190	mm
Surface crack length, a_{S1}	19.340	mm
Surface crack length, a_{S2}	19.330	mm
Net section thickness, B_N	16.195	mm
a_{max}	20.430	mm
a_{min}	20.050	mm

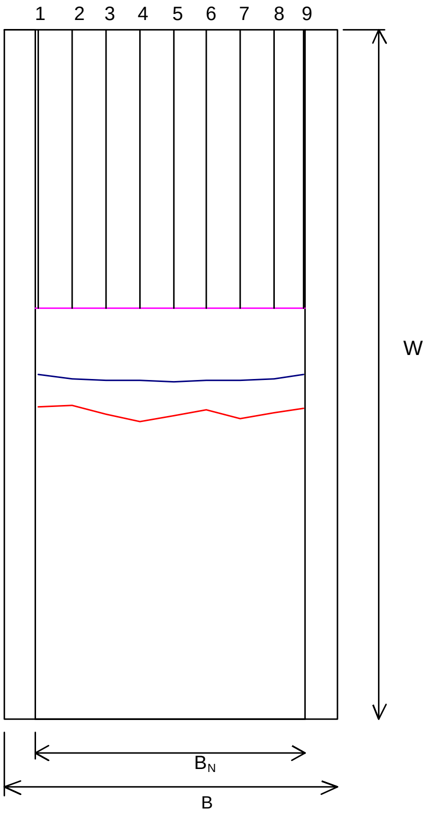

Measured by: Phillip Cossey

Signed: ____________

Measurement Line	Fatigue crack length a0, mm	Slow stable crack extension Fatigue crack ap, mm	Slow stable crack extension including stretch zone, deltaa, mm
1	20.050	21.960	1.910
2	20.280	21.870	1.590
3	20.390	22.390	2.000
4	20.400	22.780	2.380
5	20.430	22.410	1.980
6	20.400	22.130	1.730
7	20.360	22.580	2.220
8	20.260	22.290	2.030
9	20.050	21.980	1.930
Weighted Average	**20.321**	**22.303**	**1.981**

UKAS TESTING 0088

TWI

SENB FRACTURE TEST 24624 M02-07

Client	CRP	
Project leader	Weeliam Khor	Signed:

Data source

Data logging program	LVGENLOG V 1.29 19-Nov-2013
Program used to calculate CTOD/J	LVGENPLOT V 1.30 04-Aug-2015
Calculation date of CTOD/J	29 Sep 2015

Specimen details

Material	S355J2	
Specimen type	Subsize, SENB	
Crack plane orientation	Y-Z	
Type of notch tip	Fatigue	
Notch tip location	Parent material	
Specimen width	40.000	mm
Specimen thickness	19.990	mm
Initial crack length	20.054	mm
Original PM 1 thickness	40.00	mm

Test details

Test standard(s)	BS 7448: Part 1: 1991	
Test date	24/09/2015	
Test time	11:14:00	
Test technician	Phillip Cossey	Signed:
Test machine	INSTRON 8500 B107	
Test environment	AIR	
Test temperature	21.0	°C
Soak time @ test temperature	0.0	minutes
Knife edge heights	2.000, 12.000	mm
Knife edge spacing	14.00	mm
Initial K-rate	1.0	$MPa.m^{1/2}/s$
Loading span	160.0	mm
Double roller diameter	25.00	mm
Single roller diameter	25.00	mm

Material properties

Yield strength for pre-cracking	421.0	MPa	Assumed from material specification
Tensile strength for pre-cracking	585.0	MPa	Assumed from material specification
Yield strength for testing	421.0	MPa	Assumed from material specification
Tensile strength for testing	585.0	MPa	Assumed from material specification
Poisson's ratio	0.3		Assumed
Young's modulus	207	GPa	Assumed

Fatigue details

Stress ratio, R	0.100	
Final force, F_f	9.00	kN
Final K	24.1	$MPa.m^{1/2}$
Fatigue temperature	21.0	°C
Loading span, S	160.0	mm

Analysis details

Method of determining Load Point Displacement, q	DOUBLE CLIP
Lower knife edge height check	OK

Compiled by: Phillip Cossey **Signed:** ____________

SENB FRACTURE TEST 24624 M02-07

Qualification checks to **BS 7448: Part 1: 1991**

(5.1.3)	
Knife edge attachment spacing	**Pass**
(6.4.5,6.4.6)	
The final fatigue precracking force <= F_f (a)	**Pass**
ΔK/E below limit (b)	**Pass**
(6.4.7)	
Initial/Final K ratio during precracking < 1.3 (a)	**Pass**
(7.5.1)	
Single roller diameter	**Pass**
Double roller diameter	**Pass**
Loading span	**Pass**
(8.5)	
Initial K-rate between 0.5 MPa.$m^{0.5}s^{-1}$ and 3.0 MPa.$m^{0.5}s^{-1}$	**Pass**
(10.2.2)	
Minimum surface crack length (a)	**Pass**
Minimum crack extension at surface (b)	**Pass**
Difference in surface crack measurements (c)	**Pass**
Surface fatigue cracks in envelope (d)	**Pass**
Crack plane within 10° (e)	**Pass**
(10.2.3)	
Multiplane cracking (a)	**Pass**
a_0/W check 0.45-0.55 (b)	**Pass**
Crack shape (c)	**Pass**
Minimum crack length (d)	**Pass**
(10.3)	
The stress ratio <= 0.1 (c)	**Pass**

0088

SENB FRACTURE TEST 24624 M02-07

Test date	24/09/2015
Technician	Phillip Cossey
Test machine	INSTRON 8500 B107
Control mode	Displacement

Client	CRP
Project leader	Weeliam Khor
Investigator's signature	
Compiled by	Phillip Cossey

SPECIMEN DETAILS

Force, F	32.91	kN
Width, W	40.000	mm
Thickness, B	19.990	mm
Crack length, a_0	20.054	mm
Loading span, S	160.00	mm
Yield strength	421	MPa
Young's modulus	207	GPa
Poisson's ratio	0.300	
Test temperature	21.0	°C

RESULTS

δ	0.714	mm
K @ calculation point	88.0	$MPa.m^{1/2}$
F_{max}/F_Q	1.98	
K_Q	44.44	$MPa.m^{1/2}$
Total area under Force v q	103.59	kNmm
J0 from q from DOUBLE CLIP	520.01	kJ/m² (N/mm)
Plastic area Force v CMOD	71.86	kNmm
Type of result	δ/J_m	
Test standard(s)	BS 7448: Part 1: 1991	
Result qualified to standard(s)	YES	

LOWER CLIP GAUGE VALUES

Knife edge height	2.00	mm
Vg	2.834	mm
Vp	2.536	mm

UPPER CLIP GAUGE VALUES

Knife edge height	12.00	mm
Vg	3.737	mm
Vp	3.334	mm

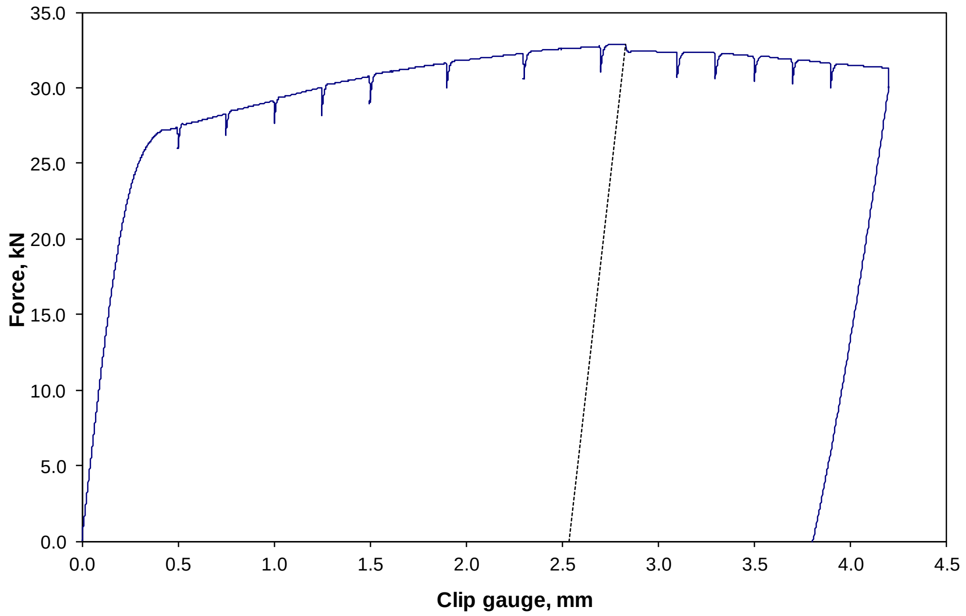

SENB FRACTURE TEST 24624 M02-07

Specimen width, W	40.000	mm
Specimen thickness, B	19.990	mm
Machined notch depth, M	16.210	mm
Surface crack length, a_{S1}	19.170	mm
Surface crack length, a_{S2}	19.470	mm
a_{max}	20.260	mm
a_{min}	19.400	mm

Diagram of fracture face

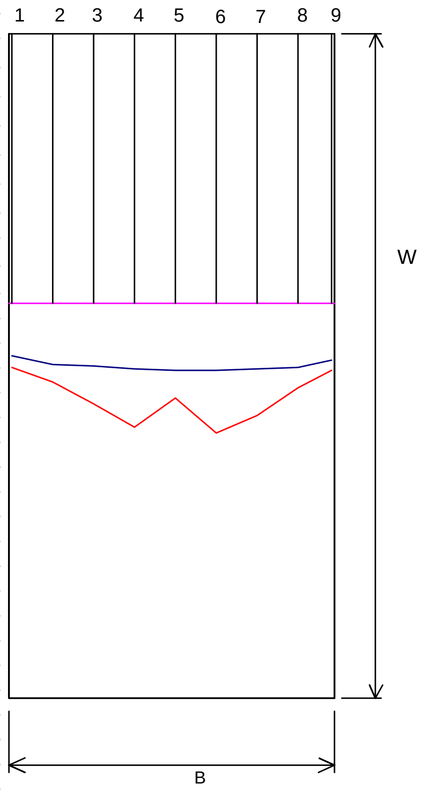

Comments

Measurement Line	Fatigue crack length a_0, mm	Slow stable crack extension + fatigue crack a_p, mm	Slow stable crack extension including stretch zone, Δ_a, mm
1	19.400	20.140	0.740
2	19.910	21.010	1.100
3	20.040	22.300	2.260
4	20.150	23.660	3.510
5	20.250	21.960	1.710
6	20.260	24.010	3.750
7	20.220	23.020	2.800
8	20.080	21.290	1.210
9	19.640	20.230	0.590
Weighted Average	**20.054**	**22.179**	**2.126**

Measured by: Phillip Cossey **Signed:**

UKAS TESTING
0088

TWI

SENB FRACTURE TEST 24624 M02-08

Client	CRP		
Project leader	Weeliam Khor		Signed:

Data source

Data logging program	LVGENLOG V 1.29 19-Nov-2013
Program used to calculate CTOD/J	LVGENPLOT V 1.30 04-Aug-2015
Calculation date of CTOD/J	29 Sep 2015

Specimen details

Material	S355J2	
Specimen type	Subsize, SENB	
Crack plane orientation	Y-Z	
Type of notch tip	Fatigue	
Notch tip location	Parent material	
Specimen width	40.000	mm
Specimen thickness	19.990	mm
Initial crack length	20.465	mm
Original PM 1 thickness	40.00	mm

Test details

Test standard(s)	BS 7448: Part 1: 1991		
Test date	25/09/2015		
Test time	08:38:00		
Test technician	Phillip Cossey		Signed:
Test machine	INSTRON 8500 B107		
Test environment	AIR		
Test temperature	21.0	°C	
Soak time @ test temperature	0.0	minutes	
Knife edge heights	2.000, 12.000	mm	
Knife edge spacing	14.00	mm	
Initial K-rate	1.0	$MPa.m^{1/2}/s$	
Loading span	160.0	mm	
Double roller diameter	25.00	mm	
Single roller diameter	25.00	mm	

Material properties

Yield strength for pre-cracking	421.0	MPa	Assumed from material specification
Tensile strength for pre-cracking	585.0	MPa	Assumed from material specification
Yield strength for testing	421.0	MPa	Assumed from material specification
Tensile strength for testing	585.0	MPa	Assumed from material specification
Poisson's ratio	0.3		Assumed
Young's modulus	207	GPa	Assumed

Fatigue details

Stress ratio, R	0.100	
Final force, F_f	9.00	kN
Final K	24.9	$MPa.m^{1/2}$
Fatigue temperature	21.0	°C
Loading span, S	160.0	mm

Analysis details

Method of determining Load Point Displacement, q	DOUBLE CLIP
Lower knife edge height check	OK

Compiled by: Phillip Cossey **Signed:** ________________

SENB FRACTURE TEST 24624 M02-08

Qualification checks to **BS 7448: Part 1: 1991**

(5.1.3)	
Knife edge attachment spacing	**Pass**
(6.4.5,6.4.6)	
The final fatigue precracking force <= F_f (a)	**Pass**
ΔK/E below limit (b)	**Pass**
(6.4.7)	
Initial/Final K ratio during precracking < 1.3 (a)	**Pass**
(7.5.1)	
Single roller diameter	**Pass**
Double roller diameter	**Pass**
Loading span	**Pass**
(8.5)	
Initial K-rate between 0.5 MPa.$m^{0.5}s^{-1}$ and 3.0 MPa.$m^{0.5}s^{-1}$	**Pass**
(10.2.2)	
Minimum surface crack length (a)	**Pass**
Minimum crack extension at surface (b)	**Pass**
Difference in surface crack measurements (c)	**Pass**
Surface fatigue cracks in envelope (d)	**Pass**
Crack plane within 10° (e)	**Pass**
(10.2.3)	
Multiplane cracking (a)	**Pass**
a_0/W check 0.45-0.55 (b)	**Pass**
Crack shape (c)	**Pass**
Minimum crack length (d)	**Pass**
(10.3)	
The stress ratio <= 0.1 (c)	**Pass**

UKAS TESTING
0088

TWI

SENB FRACTURE TEST 24624 M02-08

Test date	25/09/2015
Technician	Phillip Cossey
Test machine	INSTRON 8500 B107
Control mode	Displacement

Client	CRP
Project leader	Weeliam Khor
Investigator's signature	
Compiled by	Phillip Cossey

SPECIMEN DETAILS

Force, F	31.17	kN
Width, W	40.000	mm
Thickness, B	19.990	mm
Crack length, a_0	20.465	mm
Loading span, S	160.00	mm
Yield strength	421	MPa
Young's modulus	207	GPa
Poisson's ratio	0.300	
Test temperature	21.0	°C

RESULTS

δ	0.576	mm
K @ calculation point	86.2	$MPa.m^{1/2}$
F_{max}/F_Q	1.93	
K_Q	44.59	$MPa.m^{1/2}$
Total area under Force v q	87.29	kNmm
J0 from q from DOUBLE CLIP	447.54	kJ/m² (N/mm)
Plastic area Force v CMOD	55.78	kNmm
Type of result	δ/J_m	
Test standard(s)	BS 7448: Part 1: 1991	
Result qualified to standard(s)	YES	

LOWER CLIP GAUGE VALUES

Knife edge height	2.00	mm
Vg	2.377	mm
Vp	2.081	mm

UPPER CLIP GAUGE VALUES

Knife edge height	12.00	mm
Vg	3.185	mm
Vp	2.780	mm

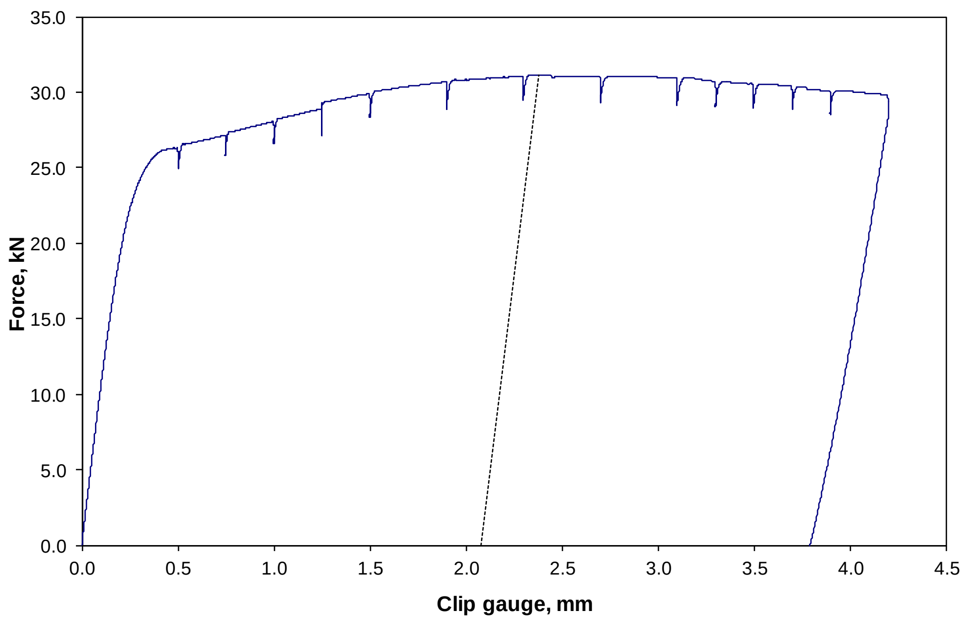

SENB FRACTURE TEST 24624 M02-08

Diagram of fracture face

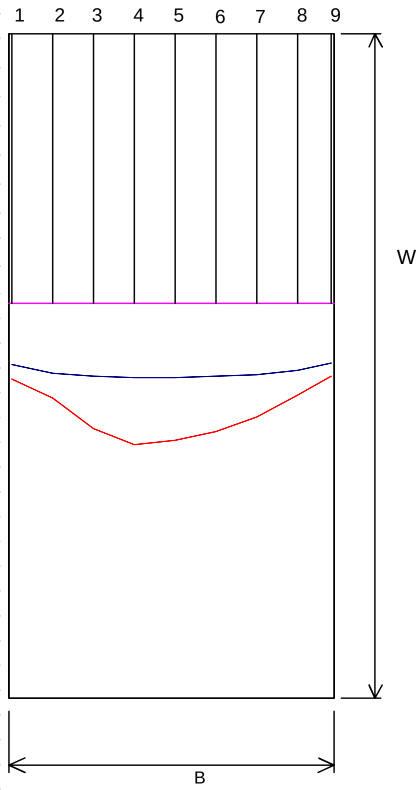

Specimen width, W	40.000	mm
Specimen thickness, B	19.990	mm
Machined notch depth, M	16.210	mm
Surface crack length, a_{S1}	19.390	mm
Surface crack length, a_{S2}	19.380	mm
a_{max}	20.680	mm
a_{min}	19.830	mm

Comments

Measurement Line	Fatigue crack length a_0, mm	Slow stable crack extension + fatigue crack a_p, mm	Slow stable crack extension including stretch zone, Δ_a, mm
1	19.910	20.810	0.900
2	20.420	21.940	1.520
3	20.610	23.770	3.160
4	20.670	24.770	4.100
5	20.680	24.460	3.780
6	20.630	23.930	3.300
7	20.540	23.100	2.560
8	20.300	21.730	1.430
9	19.830	20.660	0.830
Weighted Average	**20.465**	**23.054**	**2.589**

Measured by: Phillip Cossey **Signed:** ____________

UKAS TESTING 0088

TWI

SENB FRACTURE TEST 24624 M02-09

Client	CRP		
Project leader	Weeliam Khor		Signed:

Data source

Data logging program	LVGENLOG V 1.29 19-Nov-2013
Program used to calculate CTOD/J	LVGENPLOT V 1.30 04-Aug-2015
Calculation date of CTOD/J	29 Sep 2015

Specimen details

Material	S355J2	
Specimen type	Subsize, SENB	
Crack plane orientation	Y-Z	
Type of notch tip	Fatigue	
Notch tip location	Parent material	
Specimen width	40.000	mm
Specimen thickness	19.990	mm
Initial crack length	20.504	mm
Original PM 1 thickness	40.00	mm

Test details

Test standard(s)	BS 7448: Part 1: 1991		
Test date	28/09/2015		
Test time	10:21:00		
Test technician	Phillip Cossey		Signed:
Test machine	INSTRON 8500 B107		
Test environment	AIR		
Test temperature	21.0	°C	
Soak time @ test temperature	0.0	minutes	
Knife edge heights	2.000, 12.000	mm	
Knife edge spacing	14.00	mm	
Initial K-rate	1.0	$MPa.m^{1/2}/s$	
Loading span	160.0	mm	
Double roller diameter	25.00	mm	
Single roller diameter	25.00	mm	

Material properties

Yield strength for pre-cracking	421.0	MPa	Assumed from material specification
Tensile strength for pre-cracking	585.0	MPa	Assumed from material specification
Yield strength for testing	421.0	MPa	Assumed from material specification
Tensile strength for testing	585.0	MPa	Assumed from material specification
Poisson's ratio	0.3		Assumed
Young's modulus	207	GPa	Assumed

Fatigue details

Stress ratio, R	0.100	
Final force, F_f	9.00	kN
Final K	25.0	$MPa.m^{1/2}$
Fatigue temperature	21.0	°C
Loading span, S	160.0	mm

Analysis details

Method of determining Load Point Displacement, q	DOUBLE CLIP
Lower knife edge height check	OK

Compiled by: Phillip Cossey **Signed:** ____________

SENB FRACTURE TEST 24624 M02-09

Qualification checks to **BS 7448: Part 1: 1991**

(5.1.3)	
Knife edge attachment spacing	**Pass**
(6.4.5,6.4.6)	
The final fatigue precracking force <= F_f (a)	**Pass**
$\Delta K/E$ below limit (b)	**Pass**
(6.4.7)	
Initial/Final K ratio during precracking < 1.3 (a)	**Pass**
(7.5.1)	
Single roller diameter	**Pass**
Double roller diameter	**Pass**
Loading span	**Pass**
(8.5)	
Initial K-rate between 0.5 $MPa.m^{0.5}s^{-1}$ and 3.0 $MPa.m^{0.5}s^{-1}$	**Pass**
(10.2.2)	
Minimum surface crack length (a)	**Pass**
Minimum crack extension at surface (b)	**Pass**
Difference in surface crack measurements (c)	**Pass**
Surface fatigue cracks in envelope (d)	**Pass**
Crack plane within 10° (e)	**Pass**
(10.2.3)	
Multiplane cracking (a)	**Pass**
a_0/W check 0.45-0.55 (b)	**Pass**
Crack shape (c)	**Pass**
Minimum crack length (d)	**Pass**
(10.3)	
The stress ratio <= 0.1 (c)	**Pass**

TWI

0088

SENB FRACTURE TEST 24624 M02-09

Test date	28/09/2015	Client	CRP
Technician	Phillip Cossey	Project leader	Weeliam Khor
Test machine	INSTRON 8500 B107	Investigator's signature	
Control mode	Displacement	Compiled by	Phillip Cossey

SPECIMEN DETAILS

Force, F	31.08	kN
Width, W	40.000	mm
Thickness, B	19.990	mm
Crack length, a_0	20.504	mm
Loading span, S	160.00	mm
Yield strength	421	MPa
Young's modulus	207	GPa
Poisson's ratio	0.300	
Test temperature	21.0	°C

RESULTS

δ	0.723	mm
K @ calculation point	86.2	$MPa.m^{1/2}$
F_{max}/F_Q	1.95	
K_Q	44.13	$MPa.m^{1/2}$
Total area under Force v q	103.55	kNmm
J0 from q from DOUBLE CLIP	531.89	kJ/m² (N/mm)
Plastic area Force v CMOD	72.27	kNmm
Type of result	δ/J_m	
Test standard(s)	BS 7448: Part 1: 1991	
Result qualified to standard(s)	YES	

LOWER CLIP GAUGE VALUES

Knife edge height	2.00	mm
Vg	2.949	mm
Vp	2.659	mm

UPPER CLIP GAUGE VALUES

Knife edge height	12.00	mm
Vg	3.887	mm
Vp	3.500	mm

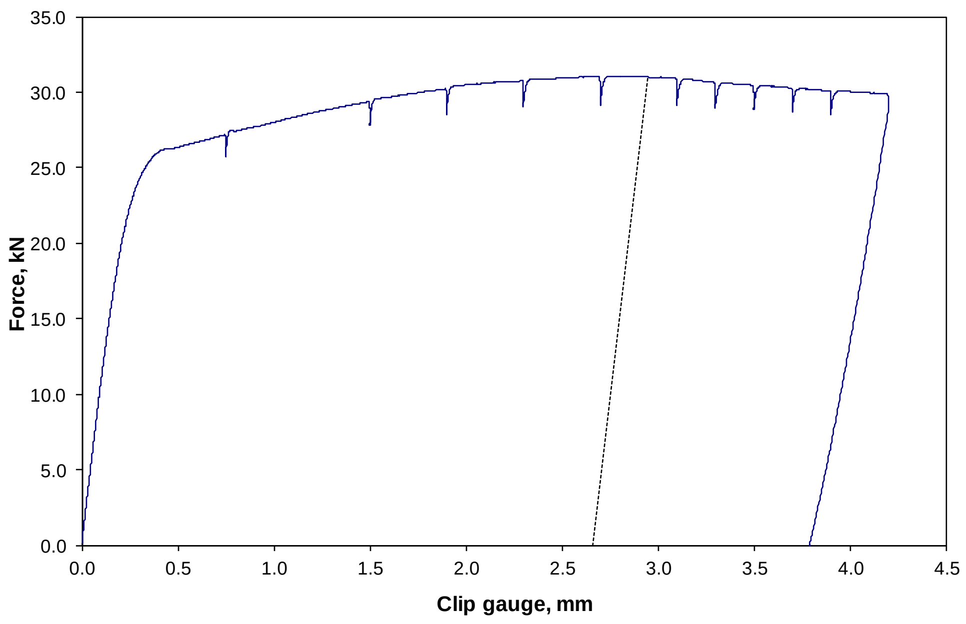

SENB FRACTURE TEST 24624 M02-09

Diagram of fracture face

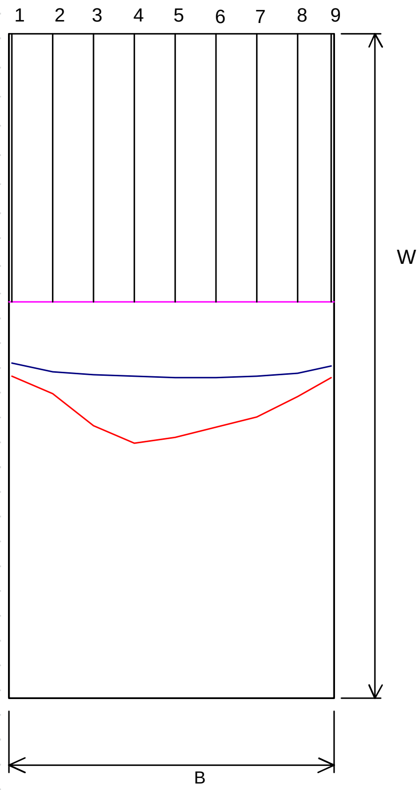

Specimen width, W	40.000	mm
Specimen thickness, B	19.990	mm
Machined notch depth, M	16.180	mm
Surface crack length, a_{S1}	19.390	mm
Surface crack length, a_{S2}	19.400	mm
a_{max}	20.720	mm
a_{min}	19.830	mm

Comments

Measurement Line	Fatigue crack length a_0, mm	Slow stable crack extension + fatigue crack a_p, mm	Slow stable crack extension including stretch zone, Δ_a, mm
1	19.830	20.620	0.790
2	20.350	21.690	1.340
3	20.550	23.620	3.070
4	20.640	24.640	4.000
5	20.720	24.300	3.580
6	20.720	23.720	3.000
7	20.660	23.090	2.430
8	20.480	21.860	1.380
9	20.000	20.690	0.690
Weighted Average	**20.504**	**22.947**	**2.443**

Measured by: Phillip Cossey **Signed:** ____________

UKAS TESTING
0088

TWI

SENB FRACTURE TEST 24624 M03-03

Client	CRP		
Project leader	WeeLiam Khor		Signed:

Data source

Data logging program	LVGENLOG V 1.29 19-Nov-2013
Program used to calculate CTOD/J	LVGENPLOT V 1.28 30-Jan-2015
Calculation date of CTOD/J	19 Mar 2015

Specimen details

Material	SS316	
Specimen type	Subsize, SENB	
Crack plane orientation	Y-X	
Type of notch tip	Fatigue	
Notch tip location	Parent material	
Specimen width	40.060	mm
Specimen thickness	20.040	mm
Initial crack length	20.968	mm
Original PM 1 thickness	50.00	mm

Test details

Test standard(s)	BS 7448: Part 1: 1991		
Test date	17/03/2015		
Test time	14:33:00		
Test technician	Phillip Cossey		Signed:
Test machine	INSTRON 8500 B107		
Test environment	AIR		
Test temperature	21.0	°C	
Soak time @ test temperature	0.0	minutes	
Knife edge heights	2.000, 12.000	mm	
Knife edge spacing	14.00	mm	
Initial K-rate	1.2	$MPa.m^{1/2}/s$	
Loading span	160.0	mm	
Double roller diameter	25.00	mm	
Single roller diameter	25.00	mm	

Material properties

Yield strength for pre-cracking	268.0	MPa	Assumed from material specification
Tensile strength for pre-cracking	595.0	MPa	Assumed from material specification
Yield strength for testing	268.0	MPa	Assumed from material specification
Tensile strength for testing	595.0	MPa	Assumed from material specification
Poisson's ratio	0.3		Assumed
Young's modulus	200	GPa	Assumed

Fatigue details

Stress ratio, R	0.100	
Final force, F_f	9.50	kN
Final K	27.2	$MPa.m^{1/2}$
Fatigue temperature	21.0	°C
Loading span, S	160.0	mm

Analysis details

Method of determining Load Point Displacement, q	DOUBLE CLIP
Lower knife edge height check	OK

Compiled by: Dan Bloom **Signed:** ________

SENB FRACTURE TEST 24624 M03-03

Qualification checks to **BS 7448: Part 1: 1991**

(5.1.3)	
Knife edge attachment spacing	**Pass**
(6.4.5,6.4.6)	
The final fatigue precracking force <= F_f (a)	**Pass**
ΔK/E below limit (b)	**Pass**
(6.4.7)	
Initial/Final K ratio during precracking < 1.3 (a)	**Pass**
(7.5.1)	
Single roller diameter	**Pass**
Double roller diameter	**Pass**
Loading span	**Pass**
(8.5)	
Initial K-rate between 0.5 $MPa.m^{0.5}s^{-1}$ and 3.0 $MPa.m^{0.5}s^{-1}$	**Pass**
(10.2.2)	
Minimum surface crack length (a)	**Pass**
Minimum crack extension at surface (b)	**Pass**
Difference in surface crack measurements (c)	**Pass**
Surface fatigue cracks in envelope (d)	**Pass**
Crack plane within 10° (e)	**Pass**
(10.2.3)	
Multiplane cracking (a)	**Pass**
a_0/W check 0.45-0.55 (b)	**Pass**
Crack shape (c)	**Pass**
Minimum crack length (d)	**Pass**
(10.3)	
The stress ratio <= 0.1 (c)	**Pass**

UKAS TESTING 0088

TWI

SENB FRACTURE TEST 24624 M03-03

Test date	17/03/2015	Client	CRP
Technician	Phillip Cossey	Project leader	WeeLiam Khor
Test machine	INSTRON 8500 B107	Investigator's signature	
Control mode	Displacement	Compiled by	Dan Bloom

SPECIMEN DETAILS

Force, F	35.50	kN
Width, W	40.060	mm
Thickness, B	20.040	mm
Crack length, a_0	20.968	mm
Loading span, S	160.00	mm
Yield strength	268	MPa
Young's modulus	200	GPa
Poisson's ratio	0.300	
Test temperature	21.0	°C

RESULTS

δ	2.825	mm
K @ calculation point	101.5	$MPa.m^{1/2}$
F_{max}/F_Q	3.08	
K_Q	32.94	$MPa.m^{1/2}$
Total area under Force v q	419.81	kNmm
J0 from q from DOUBLE CLIP	2195.37	kJ/m² (N/mm)
Plastic area Force v CMOD	299.38	kNmm
Type of result	Unloading	
Test standard(s)	BS 7448: Part 1: 1991	
Result qualified to standard(s)	YES	

LOWER CLIP GAUGE VALUES

Knife edge height	2.00	mm
Vg	11.349	mm
Vp	10.973	mm

UPPER CLIP GAUGE VALUES

Knife edge height	12.00	mm
Vg	15.021	mm
Vp	14.518	mm

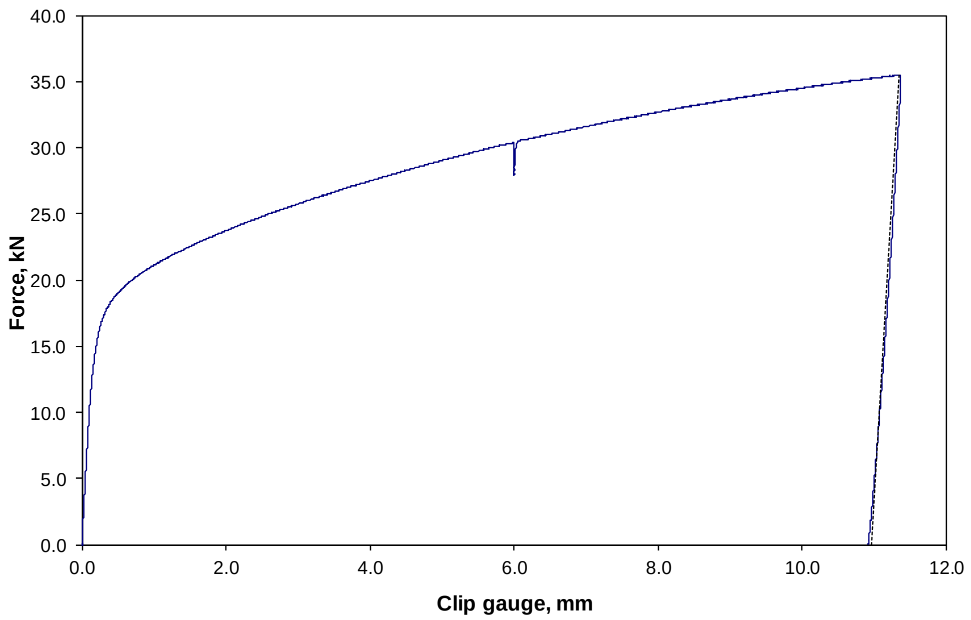

SENB FRACTURE TEST 24624 M03-03

Specimen width, W	40.060	mm
Specimen thickness, B	20.040	mm
Machined notch depth, M	16.230	mm
Surface crack length, a_{S1}	19.410	mm
Surface crack length, a_{S2}	19.450	mm
a_{max}	21.255	mm
a_{min}	20.200	mm

Comments

Diagram of fracture face

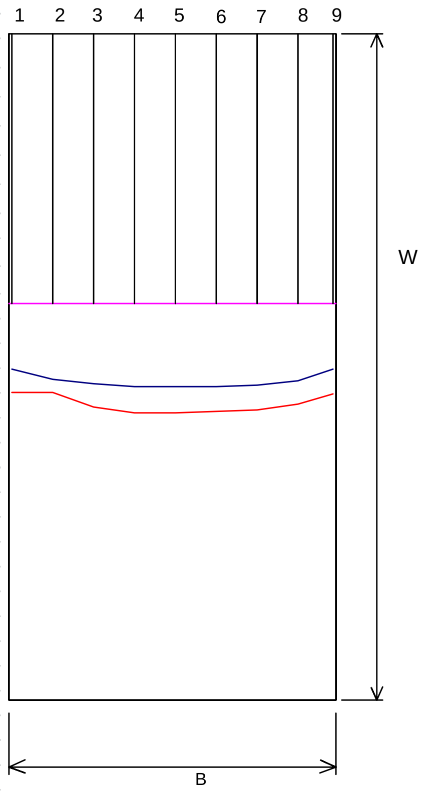

Measurement Line	Fatigue crack length a_0, mm	Slow stable crack extension + fatigue crack a_p, mm	Slow stable crack extension including stretch zone, Δ_a, mm
1	20.205	21.620	1.415
2	20.795	21.605	0.810
3	21.035	22.475	1.440
4	21.220	22.780	1.560
5	21.255	22.820	1.565
6	21.225	22.690	1.465
7	21.110	22.625	1.515
8	20.905	22.245	1.340
9	20.200	21.685	1.485
Weighted Average	**20.968**	**22.362**	**1.393**

Measured by: Dan Bloom **Signed:** ____________

UKAS TESTING 0088

TWI

SENB R-CURVE TEST 24624 M03 04

Client	CRP		
Project leader	WeeLiam Khor		Signed:

R-Curve data source

Data logging program	LVRCURVE V 1.31 03 Sep 2013
Program used to calculate R-curve data	LVRCALC V 1.16 17-Nov-2014
Calculation date of R-curve data	22 Sep 2015

Specimen details

Material	SS316	
Specimen type	SENB, Sub-size	
Crack plane orientation	Y-X	
Type of notch tip	Fatigue	
Notch tip location	Parent material	
Specimen side grooved	No	
Specimen width	40.05	mm
Specimen thickness	20.04	mm
Initial crack length, a0	20.84	mm
Estimated final crack length, ap	21.86	mm

Test details

Test standard	BS7448 Prt 4:1997		
Test method	Unloading compliance		
Test date	21/09/2015		
Test time	14:00:20		
Test technician	Phillip Cossey		Signed:
Test machine	Instron B107		
Test environment	Air		
Test temperature	21.0	°C	
Soak time @ Test temperature	NA	minutes	
Knife edge heights	2.000, 12.000	mm	
Initial K-Rate	24.27	$N/mm^{3/2}/sec$	
Loading span	160.0	mm	
Double roller diameter	25.00	mm	
Single roller diameter	25.00	mm	

Material properties

Yield strength @ Fatigue temperature	268.0	N/mm^2
Tensile strength @ Fatigue temperature	595.0	N/mm^2
Yield strength @ Test temperature	268.0	N/mm^2
Tensile strength @ Test temperature	595.0	N/mm^2
Poisson's ratio	0.3	
Youngs modulus	190591	N/mm^2

Fatigue details

Stress ratio	0.100		
Final load	9.50	kN	
Loading span	160.0	mm	

Test procedure

Number of elastic unloadings	10		
Load relaxation limit	5.00	%	of elastic loading rate
1st Increment size	0.05	mm	
1st Maximum displacement	1.00	mm	
2nd Increment size	0.20	mm	
2nd Maximum displacement	8.10	mm	

Analysis details

Yield strength temperature correction	No
Young's modulus temperature correction	No
Method of determining J	DOUBLE CLIP
Young's modulus adjusted for crack agreement	Yes
Clip gauge used for crack length calculations	Clip 1

Compiled by: Phillip Cossey **Signed:** ____________

UKAS TESTING
0088

TWI

SENB R-CURVE TEST 24624 M03 04

Qualification checks to BS7448 Prt 4:1997

(6.1.2)	
Knife edge spacing	**Pass**
(8.4.1)	
Single roller diameter	**Pass**
Double roller diameter	**Pass**
(9.3.1)	
Loading span	**Pass**
(9.6)	
Intitial K-rate between 0.5 $MPa.m^{0.5}s^{-1}$ to 3.0 $MPa.m^{0.5}s^{-1}$	**Pass**
(9.9.3)	
Was there a defect on fracture surface	**No**
(10.3.2)	
Estimated initial crack length a_o within 2% of measured a_o	**Pass**
(10.3.3)	
Estimated final crack growth within +/- 15% Δa	**Pass**
(14.2.3)	
Minimum surface crack length (a)	**Pass**
Minimum crack extension at surface (b)	**Pass**
Difference in surface crack measurements (c)	**Pass**
Surface crack measurements (d)	**Pass**
(14.2.4)	
Multiplane cracking (a)	**Pass**
a_0/W check 0.45-0.7 (b)	**Pass**
Crack shape (c)	**Pass**
Minimum crack length (d)	**Pass**
Crack within envelope (e)	**Pass**
(14.3.1)	
The specimen did not fracture or pop-in (a)	**No**
The final fatigue precracking force was < F_f (b)	**Pass**
The stress ratio < 0.1 (c)	**Pass**

UKAS TESTING 0088

TWI

SENB R-CURVE TEST 24624 M03 0

ELASTIC UNLOADINGS

No.	Coeff	Comp'nce	Load	Vgo	Vpo	Q	Ram	Total Uarea	Plastic Uarea	Estimated a	Corrected a	Estimated Δa	Corrected Δa	CTOD	CTOD Corrected	K	K Corrected	Jdef	J Corrected	CMOD	CMOD Parea	First Rec	Last Rec			
		mm/kN	kN	mm	mm	mm	mm	kNmm	kNmm	mm	mm	mm	mm	mm	mm	$N/mm^{3/2}$	$N/mm^{3/2}$	N/mm	N/mm	mm	kNmm					
1	0.99993	0.010298	9.60	0.095	-0.004	0.158	0.230	0.80	0.13	20.85	20.86	0.01	0.01	0.006	0.006	860.0	861.0	4.2	4.2	0.090	0.41	994	1094	0	0	0
2	0.99992	0.010340	9.61	0.095	-0.004	0.160	0.229	0.82	0.15	20.87	20.88	0.03	0.04	0.006	0.006	860.4	863.5	4.3	4.3	0.090	0.41	1253	1353	0	0	0
3	0.99994	0.010317	9.62	0.094	-0.005	0.162	0.230	0.84	0.17	20.86	20.87	0.02	0.03	0.005	0.005	861.5	863.4	4.4	4.4	0.090	0.41	1510	1610	0	0	0
4	0.99995	0.010331	9.62	0.094	-0.005	0.165	0.230	0.87	0.20	20.87	20.88	0.03	0.04	0.005	0.005	861.5	864.2	4.6	4.6	0.090	0.41	1767	1867	0	0	0
5	0.99996	0.010336	9.61	0.093	-0.006	0.167	0.230	0.89	0.22	20.87	20.88	0.03	0.04	0.005	0.005	860.8	863.8	4.7	4.7	0.090	0.41	2023	2123	0	0	0
6	0.99994	0.010255	9.62	0.092	-0.007	0.168	0.231	0.90	0.22	20.82	20.83	-0.02	-0.01	0.005	0.005	861.6	860.6	4.7	4.7	0.090	0.41	2280	2380	0	0	0
7	0.99993	0.010266	9.60	0.092	-0.007	0.169	0.231	0.91	0.24	20.82	20.83	-0.02	-0.01	0.005	0.005	859.7	859.3	4.8	4.8	0.090	0.41	2539	2638	0	0	0
8	0.99994	0.010249	9.61	0.092	-0.007	0.170	0.231	0.91	0.24	20.81	20.82	-0.03	-0.02	0.005	0.005	860.7	859.4	4.8	4.8	0.090	0.41	2795	2895	0	0	0
9	0.99995	0.010274	9.63	0.092	-0.007	0.171	0.231	0.93	0.26	20.83	20.84	-0.01	0.00	0.005	0.005	862.4	862.3	4.9	4.9	0.090	0.41	3054	3153	0	0	0
10	0.99995	0.010235	9.60	0.091	-0.008	0.172	0.230	0.93	0.27	20.80	20.81	-0.04	-0.03	0.005	0.005	859.5	857.5	4.9	4.9	0.090	0.41	3308	3408	0	0	0

UKAS TESTING 0088

TWI

SENB R-CURVE TEST 24624 M03 0

PLASTIC UNLOADINGS

No.	Coeff	Comp'nce	Load	Vgo	Vpo	Q	Ram	Total Uarea	Plastic Uarea	Estimated a	Corrected a	Estimated Δa	Corrected Δa	CTOD	CTOD Corrected	K	K Corrected	Jdef	J Corrected	CMOD	CMOD Parea	First Rec	Last Rec			
		mm/kN	kN	mm	mm	mm	mm	kNmm	kNmm	mm	mm	mm	mm	mm	mm	$N/mm^{3/2}$	$N/mm^{3/2}$	N/mm	N/mm	mm	kNmm					
11	0.99991	0.010309	10.47	0.101	-0.007	0.187	0.249	1.09	0.29	20.85	20.86	0.01	0.02	0.006	0.006	937.8	939.7	5.7	5.7	0.092	0.43	3601	3701	0	0	0
12	0.99996	0.010289	13.36	0.151	0.014	0.251	0.335	1.85	0.56	20.84	20.85	0.00	0.01	0.016	0.016	1196.9	1198.3	9.8	9.8	0.139	0.98	4014	4114	0	0	0
13	0.99995	0.010322	15.22	0.202	0.045	0.313	0.413	2.75	1.07	20.86	20.88	0.02	0.04	0.028	0.028	1363.3	1367.7	14.5	14.4	0.187	1.65	4464	4564	0	0	0
14	0.99990	0.010387	16.40	0.251	0.082	0.375	0.485	3.73	1.78	20.91	20.93	0.07	0.09	0.040	0.040	1469.0	1479.7	19.6	19.5	0.233	2.39	4889	4989	0	0	0
15	0.99986	0.010372	17.17	0.302	0.125	0.438	0.554	4.79	2.65	20.90	20.92	0.06	0.08	0.053	0.053	1538.2	1548.5	25.1	25.0	0.281	3.18	5319	5419	0	0	0
16	0.99991	0.010335	17.74	0.352	0.170	0.502	0.623	5.89	3.61	20.87	20.90	0.03	0.06	0.065	0.065	1589.0	1596.9	30.8	30.8	0.328	4.00	5752	5852	0	0	0
17	0.99981	0.010248	18.15	0.402	0.215	0.564	0.690	7.00	4.62	20.81	20.84	-0.03	0.00	0.078	0.078	1625.7	1626.2	36.6	36.6	0.374	4.83	6187	6287	0	0	0
18	0.99992	0.010233	18.52	0.452	0.261	0.626	0.757	8.15	5.66	20.80	20.84	-0.04	0.00	0.090	0.090	1658.8	1658.5	42.5	42.5	0.421	5.68	6628	6728	0	0	0
19	0.99996	0.010195	18.82	0.501	0.308	0.690	0.823	9.33	6.76	20.78	20.82	-0.07	-0.03	0.103	0.103	1685.7	1682.3	48.7	48.7	0.468	6.55	7070	7170	0	0	0
20	0.99996	0.010193	19.08	0.552	0.355	0.752	0.890	10.50	7.86	20.77	20.82	-0.07	-0.02	0.115	0.116	1709.4	1706.2	54.8	54.8	0.515	7.44	7512	7612	0	0	0
21	0.99993	0.010091	19.33	0.602	0.403	0.815	0.955	11.71	9.00	20.70	20.75	-0.14	-0.09	0.128	0.128	1731.0	1718.2	61.1	61.2	0.562	8.34	7952	8052	0	0	0
22	0.99996	0.010129	19.56	0.651	0.450	0.877	1.020	12.91	10.14	20.73	20.78	-0.11	-0.06	0.141	0.141	1751.6	1743.0	67.3	67.4	0.609	9.24	8396	8496	0	0	0
23	0.99996	0.010189	19.78	0.702	0.498	0.939	1.086	14.13	11.29	20.77	20.83	-0.07	-0.01	0.153	0.153	1771.7	1769.6	73.7	73.7	0.656	10.16	8840	8940	0	0	0
24	0.99996	0.010080	19.98	0.752	0.547	1.004	1.153	15.41	12.51	20.70	20.75	-0.15	-0.09	0.166	0.166	1790.0	1777.4	80.3	80.5	0.703	11.09	9291	9391	0	0	0
25	0.99995	0.010089	20.18	0.802	0.594	1.066	1.216	16.64	13.69	20.70	20.76	-0.14	-0.08	0.179	0.179	1807.2	1795.9	86.7	86.9	0.749	12.02	9741	9841	0	0	0
26	0.99995	0.010148	20.35	0.852	0.642	1.128	1.278	17.89	14.89	20.74	20.81	-0.10	-0.03	0.191	0.191	1823.1	1818.3	93.2	93.3	0.796	12.97	10187	10287	0	0	0
27	0.99997	0.010104	20.53	0.902	0.690	1.192	1.343	19.18	16.13	20.71	20.78	-0.13	-0.06	0.204	0.204	1838.9	1830.1	100.0	100.1	0.844	13.92	10636	10736	0	0	0
28	0.99995	0.010054	20.69	0.952	0.739	1.254	1.407	20.47	17.37	20.68	20.75	-0.16	-0.09	0.217	0.216	1853.5	1839.9	106.6	106.9	0.890	14.88	11086	11186	0	0	0
29	0.99997	0.010088	20.84	1.001	0.786	1.315	1.469	21.71	18.57	20.70	20.78	-0.14	-0.06	0.229	0.229	1866.8	1857.2	113.1	113.3	0.936	15.82	11534	11634	0	0	0
30	0.99996	0.010079	21.14	1.101	0.884	1.441	1.599	24.36	21.12	20.69	20.78	-0.15	-0.06	0.254	0.254	1893.3	1883.7	126.9	127.1	1.030	17.80	12120	12220	0	0	0
31	0.99995	0.010076	21.43	1.201	0.981	1.565	1.727	27.00	23.67	20.69	20.78	-0.15	-0.06	0.280	0.279	1919.2	1910.5	140.6	140.8	1.124	19.79	12701	12801	0	0	0
32	0.99993	0.010126	21.70	1.301	1.078	1.690	1.855	29.68	26.27	20.73	20.83	-0.11	-0.01	0.305	0.305	1943.3	1941.2	154.5	154.5	1.218	21.81	13289	13389	0	0	0
33	0.99994	0.010081	21.97	1.402	1.176	1.815	1.983	32.42	28.92	20.70	20.80	-0.15	-0.04	0.330	0.330	1968.3	1962.1	168.7	168.9	1.312	23.86	13876	13976	0	0	0
34	0.99994	0.010043	22.22	1.502	1.273	1.942	2.109	35.20	31.63	20.67	20.78	-0.17	-0.06	0.356	0.355	1990.1	1980.9	183.2	183.5	1.406	25.93	14464	14564	0	0	0
35	0.99994	0.010011	22.46	1.601	1.370	2.067	2.235	37.98	34.33	20.65	20.77	-0.19	-0.07	0.381	0.380	2011.6	1999.9	197.7	198.0	1.499	28.01	15050	15150	0	0	0
36	0.99994	0.010048	22.69	1.702	1.468	2.192	2.362	40.80	37.07	20.67	20.80	-0.17	-0.04	0.406	0.406	2032.6	2026.2	212.3	212.5	1.593	30.12	15641	15741	0	0	0
37	0.99996	0.010027	22.94	1.802	1.566	2.318	2.489	43.66	39.85	20.66	20.79	-0.18	-0.05	0.432	0.431	2054.7	2047.0	227.2	227.5	1.687	32.25	16233	16333	0	0	0
38	0.99995	0.010025	23.16	1.902	1.664	2.444	2.616	46.57	42.68	20.66	20.80	-0.18	-0.04	0.457	0.456	2074.4	2067.6	242.3	242.5	1.781	34.41	16824	16924	0	0	0
39	0.99996	0.010005	23.38	2.002	1.761	2.568	2.743	49.46	45.50	20.64	20.79	-0.20	-0.05	0.482	0.481	2094.0	2086.2	257.3	257.6	1.874	36.58	17416	17516	0	0	0
40	0.99995	0.010010	23.57	2.102	1.860	2.694	2.866	52.40	48.37	20.65	20.81	-0.19	-0.03	0.508	0.507	2111.3	2105.2	272.6	272.8	1.968	38.78	18008	18108	0	0	0
41	0.99996	0.010010	23.79	2.202	1.957	2.819	2.989	55.36	51.26	20.65	20.81	-0.20	-0.03	0.533	0.532	2130.6	2125.7	288.0	288.2	2.062	40.99	18603	18703	0	0	0
42	0.99995	0.010027	24.00	2.302	2.055	2.946	3.116	58.38	54.21	20.66	20.83	-0.18	-0.01	0.559	0.557	2149.9	2148.5	303.7	303.8	2.156	43.23	19200	19300	0	0	0
43	0.99996	0.010040	24.19	2.401	2.153	3.070	3.239	61.36	57.12	20.67	20.85	-0.17	0.01	0.584	0.583	2166.7	2168.2	319.2	319.1	2.249	45.47	19801	19901	0	0	0
44	0.99997	0.010035	24.40	2.501	2.250	3.194	3.365	64.38	60.06	20.66	20.85	-0.18	0.01	0.609	0.608	2185.7	2188.0	334.9	334.8	2.343	47.74	20398	20498	0	0	0
45	0.99996	0.010041	24.60	2.602	2.349	3.320	3.488	67.45	63.07	20.67	20.86	-0.17	0.02	0.634	0.633	2203.5	2207.8	350.8	350.6	2.437	50.05	21000	21100	0	0	0
46	0.99996	0.010047	24.79	2.701	2.446	3.445	3.613	70.53	66.08	20.67	20.88	-0.17	0.04	0.660	0.659	2220.2	2226.7	366.8	366.5	2.530	52.35	21604	21704	0	0	0
47	0.99996	0.010061	24.97	2.802	2.545	3.570	3.737	73.62	69.10	20.68	20.89	-0.16	0.05	0.685	0.684	2236.9	2246.6	382.9	382.4	2.624	54.67	22204	22304	0	0	0
48	0.99997	0.010058	25.18	2.901	2.642	3.696	3.861	76.78	72.19	20.68	20.90	-0.16	0.06	0.710	0.710	2255.2	2266.0	399.3	398.7	2.718	57.02	22810	22910	0	0	0
49	0.99996	0.010048	25.34	3.002	2.741	3.821	3.985	79.93	75.27	20.67	20.90	-0.17	0.06	0.736	0.735	2269.8	2280.9	415.7	415.0	2.812	59.40	23417	23517	0	0	0
50	0.99997	0.010043	25.51	3.101	2.839	3.944	4.108	83.06	78.34	20.67	20.90	-0.17	0.06	0.761	0.761	2284.5	2296.4	431.9	431.2	2.905	61.75	24022	24122	0	0	0
51	0.99997	0.010068	25.69	3.202	2.937	4.069	4.233	86.25	81.46	20.69	20.93	-0.15	0.09	0.787	0.786	2301.1	2317.9	448.5	447.5	2.999	64.15	24632	24732	0	0	0
52	0.99995	0.010047	25.87	3.302	3.035	4.195	4.357	89.48	84.63	20.67	20.92	-0.17	0.08	0.812	0.812	2317.3	2332.9	465.3	464.3	3.093	66.57	25244	25344	0	0	0
53	0.99996	0.010062	26.05	3.402	3.134	4.319	4.479	92.68	87.76	20.68	20.94	-0.16	0.10	0.837	0.837	2333.5	2352.5	482.0	480.7	3.187	68.99	25852	25952	0	0	0
54	0.99995	0.010056	26.22	3.502	3.232	4.444	4.600	95.95	90.97	20.68	20.94	-0.16	0.10	0.863	0.863	2348.2	2368.1	498.9	497.6	3.281	71.44	26463	26563	0	0	0
55	0.99994	0.010052	26.38	3.602	3.331	4.568	4.726	99.21	94.16	20.67	20.95	-0.17	0.11	0.888	0.888	2363.3	2384.2	515.9	514.5	3.375	73.90	27076	27176	0	0	0
56	0.99994	0.010078	26.54	3.701	3.428	4.693	4.848	102.49	97.38	20.69	20.97	-0.15	0.13	0.913	0.914	2377.2	2403.3	532.9	531.1	3.468	76.37	27688	27788	0	0	0
57	0.99992	0.010065	26.69	3.801	3.527	4.817	4.972	105.78	100.62	20.68	20.97	-0.16	0.13	0.939	0.939	2390.8	2416.8	550.1	548.2	3.562	78.85	28300	28400	0	0	0
58	0.99993	0.010070	26.85	3.902	3.625	4.941	5.094	109.11	103.88	20.69	20.98	-0.15	0.14	0.964	0.965	2405.0	2433.4	567.3	565.2	3.656	81.36	28922	29022	0	0	0
59	0.99992	0.010086	27.03	4.001	3.723	5.065	5.217	112.43	107.14	20.70	21.00	-0.14	0.16	0.989	0.990	2420.8	2453.1	584.6	582.2	3.749	83.88	29539	29639	0	0	0
60	0.99994	0.010065	27.17	4.102	3.823	5.191	5.338	115.83	110.48	20.68	21.00	-0.16	0.15	1.015	1.016	2433.8	2465.0	602.3	599.9	3.844	86.43	30163	30263	0	0	0
61	0.99992	0.010085	27.33	4.202	3.921	5.314	5.462	119.17	113.76	20.70	21.02	-0.14	0.18	1.040	1.042	2447.8	2483.6	619.6	616.8	3.937	88.97	30780	30880	0	0	0
62	0.99993	0.010095	27.48	4.302	4.019	5.439	5.582	122.61	117.14	20.71	21.03	-0.14	0.19	1.066	1.067	2461.0	2499.8	637.5	634.3	4.031	91.54	31408	31508	0	0	0
63	0.99991	0.010092	27.64	4.402	4.117	5.562	5.706	125.97	120.44	20.70	21.04	-0.14	0.20	1.091	1.093	2475.8	2516.1	655.0	651.7	4.125	94.12	32029	32129	0	0	0
64	0.99993	0.010094	27.78	4.502	4.216	5.685	5.826	129.37	123.77	20.70	21.05	-0.14	0.20	1.116	1.119	2488.4	2530.8	672.6	669.0	4.218	96.69	32655	32755	0	0	0
65	0.99991	0.010067	27.93	4.602	4.314	5.809	5.951	132.81	127.16	20.69	21.03	-0.15	0.19	1.142	1.144	2501.8	2542.0	690.5	687.1	4.312	99.31	33283	33383	0	0	0
66	0.99996	0.010101	28.10	4.702	4.413	5.930	6.073	136.22	130.50	20.71	21.07	-0.13	0.22	1.167	1.170	2516.7	2563.7	708.2	704.1	4.407	101.95	33912	34012	0	0	0
67	0.99995	0.010033	28.14	4.740	4.450	5.978	6.119	137.53	131.80	20.66	21.02	-0.18	0.18	1.177	1.180	2520.4	2558.1	715.1	711.7	4.443	102.94	34391	34491	0	0	0
68	0.99996	0.010067	26.78	4.738	4.462	5.978	6.107	137.53	132.34	20.69	21.04	-0.15	0.20	1.174	1.177	2398.7	2439.3	715.0	711.2	4.443	102.95	34757	34857	0	0	0
69	0.99996	0.010627	28.28	4.802	4.511	6.110	6.216	141.19	135.40	21.07	21.43	0.23	0.59	1.193	1.196	2533.2	2660.4	734.1	722.8	4.498	104.50	35361	35461	0	0	0
70	0.99994	0.010367	28.40	4.902	4.609	6.245	6.344	144.99	139.15	20.89	21.27	0.05	0.43	1.218	1.222	2543.6	2634.7	753.8	745.5	4.591	107.14	36003	36103	0	0	0
71	0.99992	0.010323	28.53	5.002	4.708	6.370	6.468	148.55	142.65	20.86	21.24	0.02	0.40	1.243	1.248	2555.1	2641.9	772.3	764.2	4.685	109.80	36637	36737	0	0	0
72	0.99994	0.010275	28.67	5.102	4.807	6.491	6.591	152.00	146.05	20.83	21.22	-0.01	0.38	1.269	1.274	2568.0	2649.6	790.3	782.5	4.778	112.48	37267	37367	0	0	0
73	0.99994	0.010282	28.91	5.302	5.004	6.732	6.834	158.92	152.86	20.83	21.24	-0.01	0.40	1.319	1.326	2589.5	2676.1	826.2	817.6	4.966	117.88	38145	38245	0	0	0
74	0.99995	0.010276	29.19	5.502	5.201	6.971	7.076	165.88	159.70	20.83	21.25	-0.01	0.41	1.370	1.378	2614.7	2704.6	862.4	853.2	5.155	123.35	39022	39122	0	0	0
75	0.99996	0.010290	29.44	5.702	5.399	7.209	7.315	172.83	166.55	20.84	21.27	0.00	0.43	1.421	1.430	2636.6	2732.8	898.5	888.4	5.343	128.86	39901	40001	0	0	0
76	0.99996	0.010317	29.70	5.902	5.597	7.447	7.557	179.86	173.47	20.86	21.31	0.02	0.47	1.472	1.482	2660.3	2764.9	935.0	923.7	5.531	134.43	40780	40880	0	0	0
77	0.99997	0.010327	29.96	6.102	5.794	7.683	7.794	186.91	180.41	20.87	21.33	0.03	0.49	1.523	1.534	2683.1	2793.6	971.7	959.3	5.719	140.02	41661	41761	0	0	0
78	0.99997	0.010395	30.22	6.302	5.991	7.920	8.036	194.01	187.39	20.91	21.39	0.07	0.55	1.573	1.586	2707.1	2832.8	1008.6	994.2	5.907	145.67	42545	42645	0	0	0
79	0.99996	0.010470	30.41	6.501	6.189	8.152	8.277	201.05	194.35	20.96	21.45	0.12	0.61	1.624	1.639	2723.9	2866.0	1045.1	1028.5	6.095	151.36	43427	43527	0	0	0
80	0.99997	0.010443	30.66	6.702	6.387	8.384	8.520	208.12	201.31	20.94	21.45	0.10	0.61	1.675	1.691	2746.4	2888.7	1081.9	1064.8	6.284	157.14	44319	44419	0	0	0
81	0.99997	0.010525	30.88	6.902	6.584	8.613	8.760	215.15	208.24	21.00	21.52	0.16	0.68	1.726	1.744	2765.9	2926.1	1118.4	1098.7	6.473	162.93	45210	45310	0	0	0
82	0.99997	0.010631	31.10	7.102	6.782	8.841	8.998	222.21	215.21	21.07	21.60	0.23	0.76	1.776	1.797	2785.4	2967.7	1155.1	1132.3	6.661	168.76	46105	46205	0	0	0
83	0.99997	0.010739	31.32	7.302	6.980	9.070	9.240	229.34	222.23	21.14	21.68	0.30	0.84	1.827	1.850	2805.6	3010.5	1192.1	1166.0	6.850	174.64	47002	47102	0	0	0
84	0.99998	0.010810	31.51	7.502	7.178	9.298	9.475	236.49	229.30	21.19	21.74	0.35	0.90	1.878	1.903	2822.3	3043.7	1229.3	1200.4	7.038	180.56	47902	48002	0	0	0
85	0.99997	0.010898	31.67	7.631	7.305	9.448	9.631	241.21	233.94	21.24	21.81	0.40	0.97	1.911	1.938	2837.0	3076.7	1253.8	1222.2	7.160	184.39	48638	48738	0	0	0
86	0.99997	0.010962	31.77	7.702	7.375	9.568	9.739	244.99	237.67	21.28	21.86	0.44	1.02	1.929	1.957	2845.8	3099.0	1273.5	1239.8	7.225	186.46	49281	49381	0	0	0
87	0.99995	0.010735	31.96	7.902	7.573	9.788	9.986	251.99	244.58	21.14	21.73	0.30	0.89	1.979	2.010	2862.8	3082.9	1309.8	1279.7	7.414	192.49	50199	50299	0	0	0
88	0.99996	0.010748	30.13	7.915	7.605	9.806	9.994	252.54	245.96	21.15	21.74	0.31	0.90	1.979	2.011	2698.9	2908.8	1312.6	1282.1	7.425	192.83	51794	51894	0	0	0

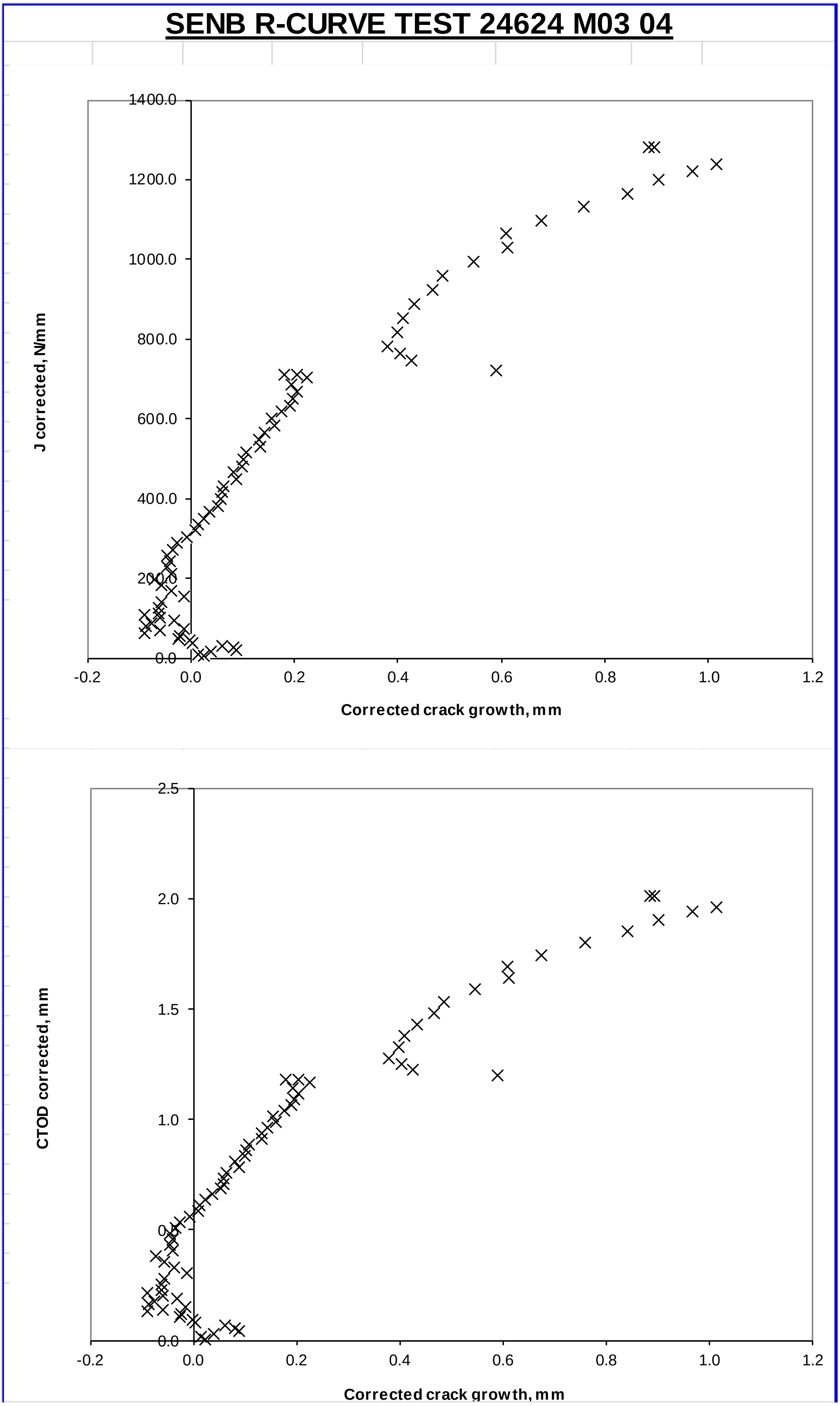
SENB R-CURVE TEST 24624 M03 04
J corrected, N/mm
1400.0
1200.0
1000.0
800.0
600.0
400.0
200.0
0.0
-0.2
0.0
0.2
0.4
0.6
0.8
1.0
1.2
Corrected crack growth, mm
CTOD corrected, mm
2.5
2.0
1.5
1.0
0.5
0.0
Corrected crack growth, mm

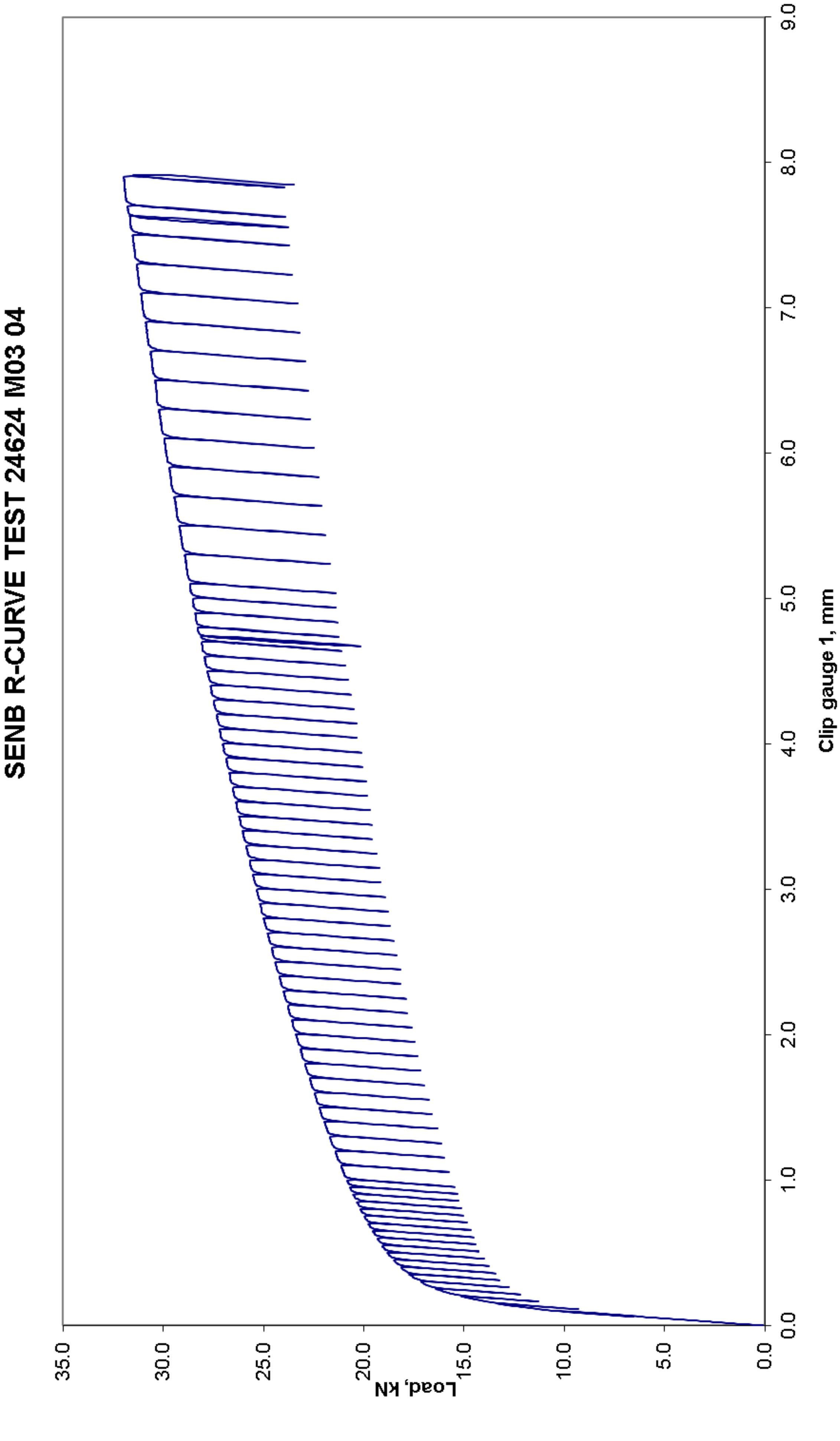
SENB R-CURVE TEST 24624 M03 04
Load, kN
0.0
5.0
10.0
15.0
20.0
25.0
30.0
35.0
Clip gauge 1, mm
0.0
1.0
2.0
3.0
4.0
5.0
6.0
7.0
8.0
9.0

SENB R-CURVE TEST 24624 M03 04

Diagram of fracture face

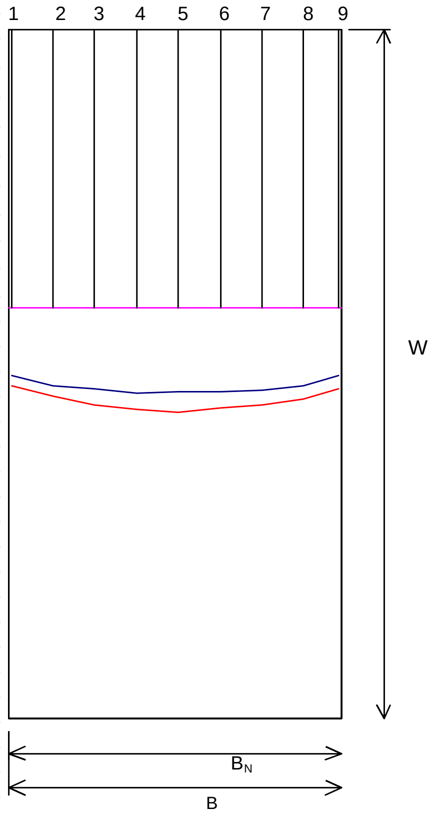

Specimen width, W	40.050	mm
Specimen Thickness, B	20.040	mm
Machined notch depth, M	16.200	mm
Surface crack length, a_{S1}	19.430	mm
Surface crack length, a_{S2}	19.400	mm
Net section thickness, B_N	20.040	mm
a_{max}	21.130	mm
a_{min}	20.110	mm

Measured by: Phillip Cossey

Signed: ____________

Measurement Line	Fatigue crack length a0, mm	Slow stable crack extension Fatigue crack ap, mm	Slow stable crack extension including stretch zone, deltaa, mm
1	20.120	20.750	0.630
2	20.720	21.360	0.640
3	20.890	21.880	0.990
4	21.130	22.120	0.990
5	21.070	22.300	1.230
6	21.030	22.030	1.000
7	21.010	21.850	0.840
8	20.760	21.520	0.760
9	20.110	20.940	0.830
Weighted Average	**20.841**	**21.738**	**0.898**

UKAS TESTING
0088

TWI

SENB FRACTURE TEST 24624 M03-05

Client	???		
Project leader	???	Signed:	

Data source

Data logging program	LVGENLOG V 1.29 19-Nov-2013
Program used to calculate CTOD/J	LVGENPLOT V 1.31 18-Jan-2016
Calculation date of CTOD/J	18 Feb 2016

Specimen details

Material	SS316	
Specimen type	Subsize, SENB	
Crack plane orientation	Y-X	
Type of notch tip	Fatigue	
Notch tip location	Parent material	
Specimen width	40.050	mm
Specimen thickness	20.030	mm
Initial crack length	21.118	mm
Original PM 1 thickness	50.00	mm

Test details

Test standard(s)	BS 7448: Part 1: 1991		
Test date	25/03/2015		
Test time	10:16:00		
Test technician	Phillip Cossey		Signed:
Test machine	INSTRON 8500 B107		
Test environment	AIR		
Test temperature	21.0	°C	
Soak time @ test temperature	0.0	minutes	
Knife edge heights	2.000, 12.000	mm	
Knife edge spacing	14.00	mm	
Initial K-rate	1.2	$MPa.m^{1/2}/s$	
Loading span	160.0	mm	
Double roller diameter	25.00	mm	
Single roller diameter	25.00	mm	

Material properties

Yield strength for pre-cracking	268.0	MPa	Assumed from material specification
Tensile strength for pre-cracking	595.0	MPa	Assumed from material specification
Yield strength for testing	268.0	MPa	Assumed from material specification
Tensile strength for testing	595.0	MPa	Assumed from material specification
Poisson's ratio	0.3		Assumed
Young's modulus	200	GPa	Assumed

Fatigue details

Stress ratio, R	0.100	
Final force, F_f	9.50	kN
Final K	27.5	$MPa.m^{1/2}$
Fatigue temperature	21.0	°C
Loading span, S	160.0	mm

Analysis details

Method of determining Load Point Displacement, q	DOUBLE CLIP
Lower knife edge height check	OK

Compiled by: Phillip Cossey **Signed:** ____________

SENB FRACTURE TEST 24624 M03-05

Qualification checks to **BS 7448: Part 1: 1991**

(5.1.3)	
Knife edge attachment spacing	**Pass**
(6.4.5,6.4.6)	
The final fatigue precracking force <= F_f (a)	**Pass**
$\Delta K/E$ below limit (b)	**Pass**
(6.4.7)	
Initial/Final K ratio during precracking < 1.3 (a)	**Pass**
(7.5.1)	
Single roller diameter	**Pass**
Double roller diameter	**Pass**
Loading span	**Pass**
(8.5)	
Initial K-rate between 0.5 $MPa.m^{0.5}s^{-1}$ and 3.0 $MPa.m^{0.5}s^{-1}$	**Pass**
(10.2.2)	
Minimum surface crack length (a)	**Pass**
Minimum crack extension at surface (b)	**Pass**
Difference in surface crack measurements (c)	**Pass**
Surface fatigue cracks in envelope (d)	**Pass**
Crack plane within 10° (e)	**Pass**
(10.2.3)	
Multiplane cracking (a)	**Pass**
a_0/W check 0.45-0.55 (b)	**Pass**
Crack shape (c)	**Pass**
Minimum crack length (d)	**Pass**
(10.3)	
The stress ratio <= 0.1 (c)	**Pass**

UKAS TESTING 0088

TWI

SENB FRACTURE TEST 24624 M03-05

Test date	25/03/2015	Client	???
Technician	Phillip Cossey	Project leader	???
Test machine	INSTRON 8500 B107	Investigator's signature	
Control mode	Displacement	Compiled by	Phillip Cossey

SPECIMEN DETAILS

Force, F	37.45	kN
Width, W	40.050	mm
Thickness, B	20.030	mm
Crack length, a_0	21.118	mm
Loading span, S	160.00	mm
Yield strength	268	MPa
Young's modulus	200	GPa
Poisson's ratio	0.300	
Test temperature	21.0	°C

RESULTS

δ	3.990	mm
K @ calculation point	108.6	$MPa.m^{1/2}$
F_{max}/F_Q	3.14	
K_Q	34.60	$MPa.m^{1/2}$
Total area under Force v q	680.46	kNmm
J0 from q from DOUBLE CLIP	3589.75	kJ/m² (N/mm)
Plastic area Force v CMOD	462.51	kNmm
Type of result	δ/J_m	
Test standard(s)	BS 7448: Part 1: 1991	
Result qualified to standard(s)	YES	

DRAFT

LOWER CLIP GAUGE VALUES

Knife edge height	2.00	mm
Vg	16.172	mm
Vp	15.766	mm

UPPER CLIP GAUGE VALUES

Knife edge height	12.00	mm
Vg	21.647	mm
Vp	21.102	mm

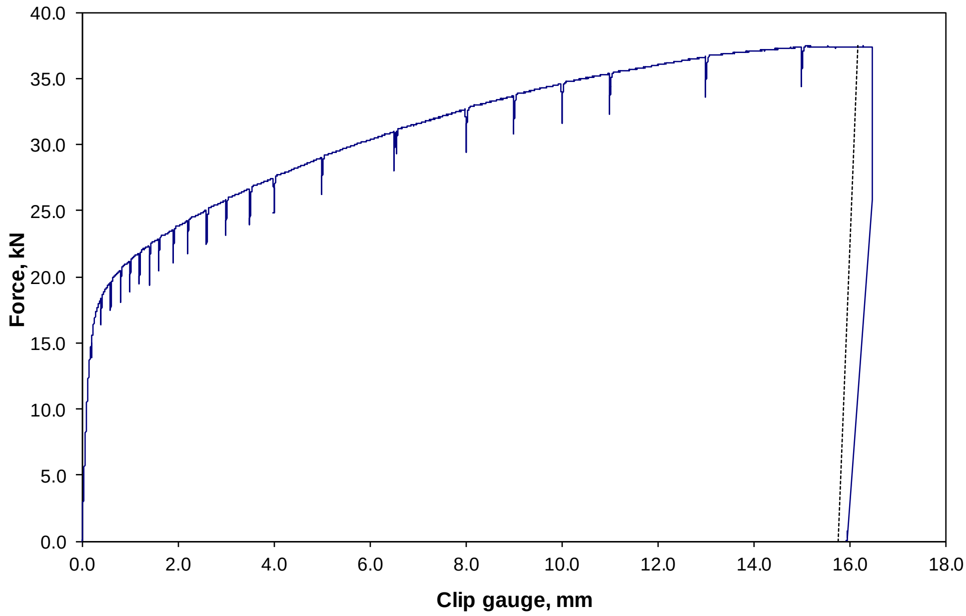

SENB FRACTURE TEST 24624 M03-05

Specimen width, W	40.050	mm
Specimen thickness, B	20.030	mm
Machined notch depth, M	16.200	mm
Surface crack length, a_{S1}	19.450	mm
Surface crack length, a_{S2}	19.470	mm
a_{max}	21.400	mm
a_{min}	20.460	mm

Diagram of fracture face

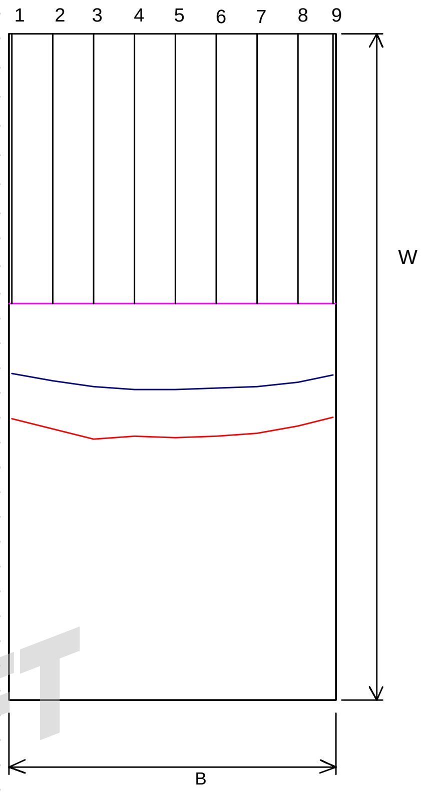

Comments

Measurement Line	Fatigue crack length a_0, mm	Slow stable crack extension + fatigue crack a_p, mm	Slow stable crack extension including stretch zone, Δ_a, mm
1	20.460	23.120	2.660
2	20.890	23.770	2.880
3	21.250	24.400	3.150
4	21.400	24.250	2.850
5	21.370	24.310	2.940
6	21.300	24.230	2.930
7	21.270	24.020	2.750
8	20.960	23.620	2.660
9	20.540	23.060	2.520
Weighted Average	**21.118**	**23.961**	**2.844**

Measured by: Phillip Cossey **Signed:**

UKAS TESTING
0088

TWI

SENB FRACTURE TEST 24624 M03-06

Client	CRP		
Project leader	WeeLiam Khor		Signed:

Data source

Data logging program	LVGENLOG V 1.29 19-Nov-2013
Program used to calculate CTOD/J	LVGENPLOT V 1.31 18-Jan-2016
Calculation date of CTOD/J	25 Jan 2016

Specimen details

Material	SS316	
Specimen type	Subsize, SENB	
Crack plane orientation	Y-Z	
Type of notch tip	Fatigue	
Notch tip location	Parent material	
Specimen width	40.060	mm
Specimen thickness	20.030	mm
Initial crack length	21.053	mm
Original PM 1 thickness	41.00	mm

Test details

Test standard(s)	BS 7448: Part 1: 1991		
Test date	06/10/2015		
Test time	09:05:00		
Test technician	Phillip Cossey		Signed:
Test machine	INSTRON 8500 B107		
Test environment	AIR		
Test temperature	21.0	°C	
Soak time @ test temperature	0.0	minutes	
Knife edge heights	2.000, 12.000	mm	
Knife edge spacing	14.00	mm	
Initial K-rate	1.1	$MPa.m^{1/2}/s$	
Loading span	160.0	mm	
Double roller diameter	25.00	mm	
Single roller diameter	25.00	mm	

Material properties

Yield strength for pre-cracking	286.0	MPa	Assumed from material specification
Tensile strength for pre-cracking	595.0	MPa	Assumed from material specification
Yield strength for testing	286.0	MPa	Assumed from material specification
Tensile strength for testing	595.0	MPa	Assumed from material specification
Poisson's ratio	0.3		Assumed
Young's modulus	207	GPa	Assumed

Fatigue details

Stress ratio, R	0.100	
Final force, F_f	9.50	kN
Final K	27.4	$MPa.m^{1/2}$
Fatigue temperature	21.0	°C
Loading span, S	160.0	mm

Analysis details

Method of determining Load Point Displacement, q	DOUBLE CLIP
Lower knife edge height check	OK

Compiled by: Phillip Cossey **Signed:** ______________

SENB FRACTURE TEST 24624 M03-06

Qualification checks to **BS 7448: Part 1: 1991**

(5.1.3)	
Knife edge attachment spacing	**Pass**
(6.4.5,6.4.6)	
The final fatigue precracking force <= F_f (a)	**Pass**
$\Delta K/E$ below limit (b)	**Pass**
(6.4.7)	
Initial/Final K ratio during precracking < 1.3 (a)	**Pass**
(7.5.1)	
Single roller diameter	**Pass**
Double roller diameter	**Pass**
Loading span	**Pass**
(8.5)	
Initial K-rate between 0.5 $MPa.m^{0.5}s^{-1}$ and 3.0 $MPa.m^{0.5}s^{-1}$	**Pass**
(10.2.2)	
Minimum surface crack length (a)	**Pass**
Minimum crack extension at surface (b)	**Pass**
Difference in surface crack measurements (c)	**Pass**
Surface fatigue cracks in envelope (d)	**Pass**
Crack plane within 10° (e)	**Pass**
(10.2.3)	
Multiplane cracking (a)	**Pass**
a_0/W check 0.45-0.55 (b)	**Pass**
Crack shape (c)	**Pass**
Minimum crack length (d)	**Pass**
(10.3)	
The stress ratio <= 0.1 (c)	**Pass**

TWI

0088

SENB FRACTURE TEST 24624 M03-06

Test date	06/10/2015
Technician	Phillip Cossey
Test machine	INSTRON 8500 B107
Control mode	Displacement

Client	CRP
Project leader	WeeLiam Khor
Investigator's signature	
Compiled by	Phillip Cossey

SPECIMEN DETAILS

Force, F	36.21	kN
Width, W	40.060	mm
Thickness, B	20.030	mm
Crack length, a_0	21.053	mm
Loading span, S	160.00	mm
Yield strength	286	MPa
Young's modulus	207	GPa
Poisson's ratio	0.300	
Test temperature	21.0	°C

RESULTS

δ	3.458	mm
K @ calculation point	104.3	MPa.m$^{1/2}$
F_{max}/F_Q	3.13	
K_Q	33.31	MPa.m$^{1/2}$
Total area under Force v q	495.23	kNmm
J0 from q from DOUBLE CLIP	2602.43	kJ/m² (N/mm)
Plastic area Force v CMOD	384.77	kNmm
Type of result	δ/J_m	
Test standard(s)	BS 7448: Part 1: 1991	
Result qualified to standard(s)	YES	

LOWER CLIP GAUGE VALUES

Knife edge height	2.00	mm
Vg	13.999	mm
Vp	13.606	mm

UPPER CLIP GAUGE VALUES

Knife edge height	12.00	mm
Vg	18.199	mm
Vp	17.670	mm

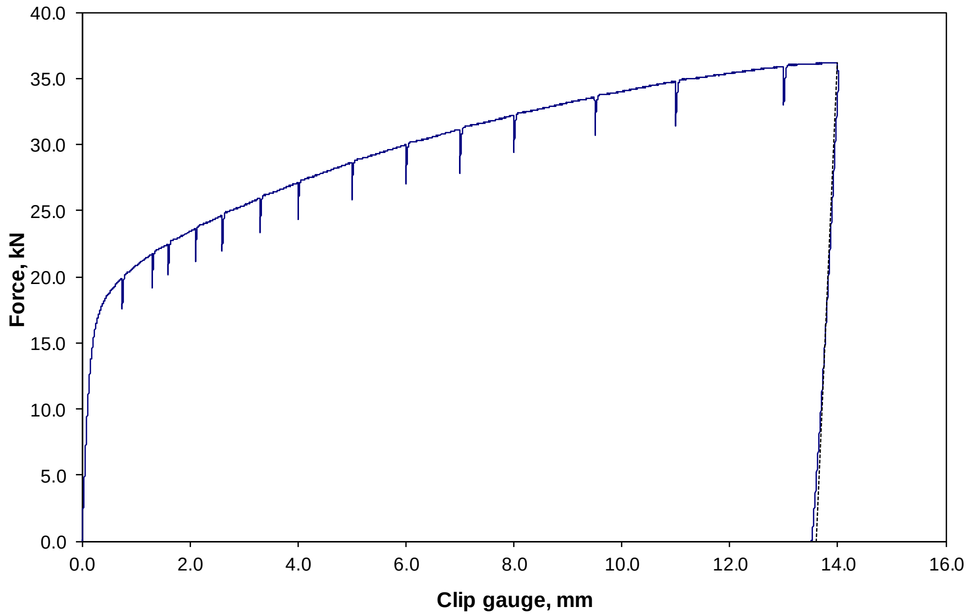

SENB FRACTURE TEST 24624 M03-06

Specimen width, W	40.060	mm
Specimen thickness, B	20.030	mm
Machined notch depth, M	16.220	mm
Surface crack length, a_{S1}	19.490	mm
Surface crack length, a_{S2}	19.400	mm
a_{max}	21.390	mm
a_{min}	20.240	mm

Diagram of fracture face

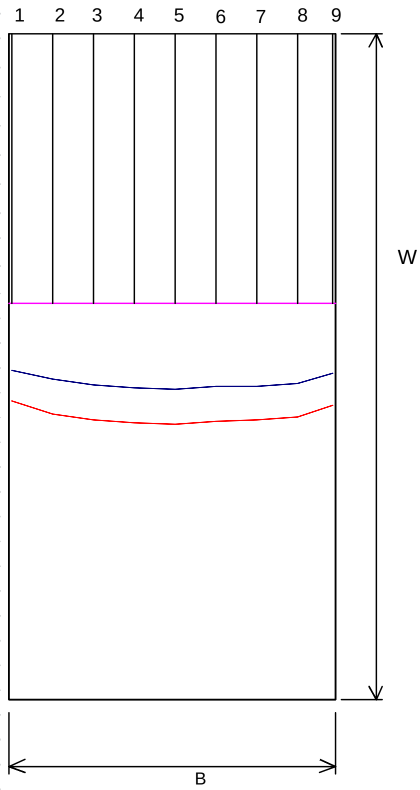

Comments

Measurement Line	Fatigue crack length a_0, mm	Slow stable crack extension + fatigue crack a_p, mm	Slow stable crack extension including stretch zone, Δ_a, mm
1	20.240	22.150	1.910
2	20.760	22.880	2.120
3	21.110	23.280	2.170
4	21.280	23.390	2.110
5	21.390	23.510	2.120
6	21.210	23.340	2.130
7	21.240	23.240	2.000
8	21.080	23.040	1.960
9	20.460	22.360	1.900
Weighted Average	**21.053**	**23.117**	**2.064**

Measured by: Phillip Cossey **Signed:**

UKAS TESTING 0088

TWI

SENB R-CURVE TEST 24624 M03 07

Client	CRP		
Project leader	WeeLiam Khor		Signed:

R-Curve data source

Data logging program	LVRCURVE V 1.39 08 Feb 2016
Program used to calculate R-curve data	LVRCALC V 1.20 01-Jul-2016
Calculation date of R-curve data	08 Aug 2016

Specimen details

Material	SS316	
Specimen type	SENB, Sub-size	
Crack plane orientation	Y-X	
Type of notch tip	Fatigue	
Notch tip location	Parent material	
Specimen side grooved	Yes	
Specimen width	40.01	mm
Specimen thickness	20.00	mm
Initial crack length, a0	20.97	mm
Estimated final crack length, ap	21.69	mm

Test details

Test standard	BS7448 Prt 4:1997		
Test method	Unloading compliance		
Test date	28/07/2016		
Test time	09:41:09		
Test technician	Phillip Cossey		Signed:
Test machine			
Test environment	Air		
Test temperature	24.0	°C	
Soak time @ Test temperature	NA	minutes	
Knife edge heights	2.000, 12.000	mm	
Initial K-Rate	19.34	$N/mm^{3/2}/sec$	
Loading span	160.0	mm	
Double roller diameter	25.00	mm	
Single roller diameter	25.00	mm	

Material properties

Yield strength @ Fatigue temperature	286.0	N/mm^2
Tensile strength @ Fatigue temperature	595.0	N/mm^2
Yield strength @ Test temperature	286.0	N/mm^2
Tensile strength @ Test temperature	595.0	N/mm^2
Poisson's ratio	0.3	
Youngs modulus	180742	N/mm^2

Fatigue details

Stress ratio	0.100		
Final load	9.50	kN	
Loading span	160.0	mm	

Test procedure

Number of elastic unloadings	10		
Load relaxation limit	5.00	%	of elastic loading rate
1st Increment size	0.05	mm	
1st Maximum displacement	1.00	mm	
2nd Increment size	0.20	mm	
2nd Maximum displacement	20.00	mm	

Analysis details

Yield strength temperature correction	No
Young's modulus temperature correction	No
Method of determining J	DOUBLE CLIP
Young's modulus adjusted for crack agreement	Yes
Clip gauge used for crack length calculations	Clip 1

Compiled by: Phillip Cossey **Signed:**

UKAS TESTING 0088

TWI

SENB R-CURVE TEST 24624 M03 07

Qualification checks to BS7448 Prt 4:1997

(6.1.2)	
Knife edge spacing	**Pass**
(8.4.1)	
Single roller diameter	**Pass**
Double roller diameter	**Pass**
(9.3.1)	
Loading span	**Pass**
(9.6)	
Intitial K-rate between 0.5 $MPa.m^{0.5}s^{-1}$ to 3.0 $MPa.m^{0.5}s^{-1}$	**Pass**
(9.9.3)	
Was there a defect on fracture surface	**No**
(10.3.2)	
Estimated initial crack length a_o within 2% of measured a_o	**Pass**
(10.3.3)	
Estimated final crack growth within +/- 15% Δa	**Pass**
(14.2.3)	
Minimum surface crack length (a)	**Pass**
Minimum crack extension at surface (b)	**Pass**
Difference in surface crack measurements (c)	**Pass**
Surface crack measurements (d)	**Pass**
(14.2.4)	
Multiplane cracking (a)	**Pass**
a_0/W check 0.45-0.7 (b)	**Pass**
Crack shape (c)	**Pass**
Minimum crack length (d)	**Pass**
Crack within envelope (e)	**Pass**
(14.3.1)	
The specimen did not fracture or pop-in (a)	**No**
The final fatigue precracking force was < F_f (b)	**Pass**
The stress ratio < 0.1 (c)	**Pass**

UKAS TESTING 0088

SENB R-CURVE TEST 24624 M03 07

ELASTIC UNLOADINGS

No.	Coeff	Comp'nce	Load	Vgo	Vpo	Q	Ram	Total Uarea	Plastic Uarea	Estimated a	Corrected a	Estimated Δa	Corrected Δa	CTOD	CTOD Corrected	K	K Corrected	Jdef	J Corrected	CMOD	CMOD Parea	First Rec	Last Rec
		mm/kN	kN	mm	mm	mm	mm	kNmm	kNmm	mm	mm	mm	mm	mm	mm	$N/mm^{3/2}$	$N/mm^{3/2}$	N/mm	N/mm	mm	kNmm		
1	0.99989	0.011696	7.68	0.083	-0.005	0.108	0.312	0.44	0.10	21.08	21.09	0.12	0.12	0.004	0.004	773.5	781.3	3.6	3.6	0.078	-0.02	1159	1258
2	0.99988	0.011427	7.67	0.083	-0.006	0.111	0.311	0.47	0.12	20.92	20.93	-0.05	-0.04	0.004	0.004	773.4	770.8	3.8	3.8	0.078	-0.02	1417	1517
3	0.99993	0.011541	7.67	0.082	-0.006	0.111	0.312	0.47	0.12	20.99	21.00	0.02	0.03	0.004	0.004	773.0	774.8	3.8	3.8	0.078	-0.02	1676	1775
4	0.99984	0.011466	7.70	0.082	-0.007	0.112	0.312	0.48	0.13	20.94	20.95	-0.02	-0.02	0.004	0.004	775.6	774.5	3.9	3.9	0.078	-0.02	1933	2033
5	0.99991	0.011480	7.69	0.082	-0.007	0.113	0.313	0.48	0.14	20.95	20.96	-0.02	-0.01	0.004	0.004	774.8	774.2	3.9	3.9	0.078	-0.02	2194	2294
6	0.99989	0.011565	7.68	0.081	-0.007	0.114	0.313	0.49	0.14	21.00	21.01	0.04	0.04	0.004	0.004	774.0	776.8	3.9	3.9	0.078	-0.02	2453	2552
7	0.99984	0.011403	7.71	0.081	-0.007	0.115	0.313	0.50	0.15	20.90	20.91	-0.06	-0.06	0.003	0.003	777.3	773.7	4.0	4.0	0.078	-0.02	2709	2808
8	0.99995	0.011600	7.69	0.081	-0.008	0.116	0.313	0.50	0.16	21.03	21.03	0.06	0.06	0.003	0.003	775.0	779.2	4.0	4.0	0.078	-0.02	2967	3067
9	0.99987	0.011457	7.72	0.081	-0.008	0.118	0.314	0.52	0.17	20.94	20.95	-0.03	-0.02	0.003	0.003	778.0	776.6	4.1	4.1	0.078	-0.03	3226	3326
10	0.99984	0.011414	7.69	0.080	-0.008	0.118	0.313	0.52	0.17	20.91	20.92	-0.06	-0.05	0.003	0.003	775.4	772.3	4.2	4.2	0.078	-0.02	3485	3585

UKAS TESTING 0088

SENB R-CURVE TEST 24624 M03 07

PLASTIC UNLOADINGS

No.	Coeff	Comp'nce	Load	Vgo	Vpo	Q	Ram	Total Uarea	Plastic Uarea	Estimated a	Corrected a	Estimated Δa	Corrected Δa	CTOD	CTOD Corrected	K	K Corrected	Jdef	J Corrected	CMOD	CMOD Parea	First Rec	Last Rec
		mm/kN	kN	mm	mm	mm	mm	kNmm	kNmm	mm	mm	mm	mm	mm	mm	$N/mm^{3/2}$	$N/mm^{3/2}$	N/mm	N/mm	mm	kNmm		
11	0.99982	0.011404	9.31	0.101	-0.006	0.145	0.359	0.75	0.24	20.91	20.91	-0.06	-0.05	0.006	0.006	938.1	934.0	6.0	6.0	0.094	-0.04	3838	3937
12	0.99993	0.011378	11.79	0.152	0.016	0.206	0.452	1.40	0.59	20.89	20.90	-0.08	-0.07	0.016	0.016	1188.4	1181.9	10.9	10.9	0.141	0.17	4275	4375
13	0.99990	0.011263	13.35	0.201	0.048	0.268	0.531	2.18	1.13	20.82	20.83	-0.15	-0.13	0.028	0.028	1345.6	1330.9	16.4	16.5	0.188	0.55	4737	4837
14	0.99995	0.011332	14.38	0.252	0.086	0.330	0.606	3.04	1.83	20.86	20.88	-0.11	-0.09	0.040	0.040	1448.9	1438.5	22.4	22.4	0.235	1.04	5173	5273
15	0.99994	0.011247	15.05	0.302	0.128	0.393	0.676	3.96	2.63	20.81	20.83	-0.16	-0.14	0.052	0.052	1516.7	1499.7	28.5	28.6	0.282	1.62	5607	5707
16	0.99992	0.011279	15.56	0.351	0.172	0.455	0.744	4.90	3.48	20.83	20.85	-0.14	-0.11	0.065	0.064	1568.6	1554.1	34.8	34.9	0.329	2.24	6046	6146
17	0.99994	0.011335	15.98	0.401	0.217	0.518	0.814	5.89	4.39	20.86	20.89	-0.10	-0.07	0.077	0.077	1610.5	1600.7	41.3	41.4	0.375	2.90	6486	6586
18	0.99994	0.011399	16.32	0.451	0.264	0.581	0.880	6.90	5.34	20.90	20.94	-0.06	-0.03	0.089	0.089	1644.8	1640.6	48.0	48.1	0.422	3.60	6931	7031
19	0.99991	0.011308	16.64	0.501	0.310	0.645	0.946	7.96	6.34	20.85	20.88	-0.12	-0.08	0.102	0.102	1676.6	1665.1	55.0	55.1	0.469	4.31	7373	7473
20	0.99990	0.011355	16.91	0.551	0.357	0.708	1.012	9.00	7.33	20.88	20.92	-0.09	-0.05	0.114	0.114	1704.0	1696.8	61.8	61.9	0.516	5.04	7822	7922
21	0.99989	0.011344	17.15	0.602	0.405	0.771	1.080	10.07	8.35	20.87	20.91	-0.10	-0.05	0.127	0.127	1728.8	1721.2	68.8	68.9	0.564	5.80	8273	8373
22	0.99992	0.011326	17.38	0.652	0.452	0.833	1.144	11.14	9.37	20.86	20.91	-0.11	-0.06	0.140	0.139	1751.7	1742.8	75.8	75.9	0.610	6.56	8722	8822
23	0.99993	0.011319	17.57	0.702	0.499	0.896	1.210	12.23	10.42	20.85	20.91	-0.11	-0.06	0.152	0.151	1771.1	1762.1	82.9	83.1	0.657	7.33	9173	9273
24	0.99992	0.011256	17.79	0.752	0.548	0.960	1.276	13.37	11.51	20.81	20.87	-0.15	-0.10	0.165	0.164	1792.5	1778.1	90.3	90.6	0.704	8.12	9629	9729
25	0.99988	0.011209	17.98	0.802	0.595	1.022	1.340	14.47	12.57	20.78	20.84	-0.18	-0.12	0.177	0.176	1812.0	1793.7	97.5	97.9	0.750	8.90	10084	10184
26	0.99987	0.011196	18.16	0.851	0.642	1.086	1.405	15.61	13.68	20.78	20.84	-0.19	-0.13	0.189	0.189	1830.5	1811.3	105.0	105.3	0.797	9.71	10547	10647
27	0.99988	0.011189	18.34	0.902	0.691	1.149	1.471	16.77	14.79	20.77	20.84	-0.20	-0.13	0.202	0.201	1848.3	1828.8	112.5	112.9	0.844	10.53	11001	11101
28	0.99986	0.011204	18.50	0.952	0.739	1.212	1.536	17.92	15.91	20.78	20.85	-0.19	-0.11	0.215	0.214	1864.9	1847.3	120.0	120.4	0.891	11.35	11462	11562
29	0.99991	0.011134	18.65	1.000	0.786	1.274	1.598	19.06	17.02	20.74	20.81	-0.23	-0.16	0.227	0.226	1879.3	1855.3	127.5	128.0	0.937	12.16	11916	12016
30	0.99992	0.011151	18.96	1.102	0.884	1.403	1.726	21.47	19.36	20.75	20.83	-0.22	-0.14	0.252	0.251	1910.9	1889.3	143.2	143.7	1.032	13.88	12504	12604
31	0.99993	0.011092	19.22	1.202	0.980	1.529	1.854	23.88	21.71	20.71	20.80	-0.26	-0.17	0.277	0.276	1937.5	1911.0	158.8	159.5	1.125	15.60	13095	13195
32	0.99994	0.011073	19.50	1.302	1.078	1.655	1.982	26.32	24.09	20.70	20.80	-0.27	-0.17	0.302	0.301	1965.1	1937.5	174.7	175.5	1.219	17.36	13687	13787
33	0.99995	0.011093	19.76	1.402	1.174	1.781	2.110	28.78	26.49	20.71	20.82	-0.26	-0.15	0.327	0.325	1991.9	1967.2	190.7	191.4	1.313	19.14	14280	14380
34	0.99995	0.011050	20.00	1.502	1.272	1.908	2.237	31.30	28.95	20.68	20.80	-0.28	-0.17	0.353	0.350	2016.1	1987.8	207.0	208.0	1.407	20.95	14873	14973
35	0.99995	0.011057	20.26	1.601	1.368	2.032	2.362	33.80	31.39	20.69	20.81	-0.28	-0.16	0.377	0.375	2042.0	2015.4	223.2	224.2	1.500	22.76	15467	15567
36	0.99995	0.011104	20.50	1.701	1.466	2.158	2.489	36.35	33.88	20.72	20.84	-0.25	-0.12	0.403	0.400	2065.7	2044.9	239.8	240.6	1.594	24.62	16069	16169
37	0.99995	0.011069	20.72	1.802	1.564	2.284	2.615	38.95	36.43	20.70	20.83	-0.27	-0.14	0.428	0.425	2088.6	2065.1	256.7	257.6	1.688	26.50	16663	16763
38	0.99996	0.011083	20.93	1.902	1.661	2.409	2.742	41.54	38.97	20.70	20.85	-0.26	-0.12	0.453	0.450	2109.6	2088.7	273.5	274.4	1.781	28.39	17262	17362
39	0.99994	0.011055	21.15	2.002	1.758	2.535	2.867	44.18	41.56	20.69	20.84	-0.28	-0.13	0.478	0.475	2131.9	2109.1	290.7	291.7	1.875	30.30	17859	17959
40	0.99995	0.011091	21.36	2.102	1.857	2.660	2.995	46.83	44.16	20.71	20.87	-0.26	-0.10	0.503	0.500	2153.0	2135.2	307.8	308.7	1.969	32.25	18465	18565
41	0.99996	0.011067	21.56	2.202	1.954	2.785	3.119	49.52	46.79	20.69	20.86	-0.27	-0.11	0.528	0.525	2173.1	2153.8	325.3	326.2	2.063	34.21	19071	19171
42	0.99996	0.011093	21.74	2.302	2.052	2.910	3.243	52.20	49.42	20.71	20.88	-0.26	-0.08	0.553	0.550	2190.8	2175.6	342.6	343.4	2.156	36.17	19668	19768
43	0.99996	0.011093	21.93	2.401	2.149	3.035	3.366	54.92	52.10	20.71	20.89	-0.26	-0.08	0.578	0.574	2210.5	2196.6	360.3	361.0	2.250	38.16	20277	20377
44	0.99995	0.011093	22.13	2.502	2.247	3.160	3.492	57.67	54.80	20.71	20.90	-0.26	-0.07	0.603	0.600	2230.3	2217.6	378.1	378.8	2.343	40.18	20884	20984
45	0.99995	0.011089	22.31	2.602	2.345	3.285	3.615	60.45	57.53	20.71	20.90	-0.26	-0.06	0.628	0.625	2248.3	2236.3	396.1	396.8	2.437	42.21	21494	21594
46	0.99995	0.011092	22.50	2.702	2.443	3.411	3.741	63.24	60.28	20.71	20.91	-0.26	-0.05	0.654	0.650	2267.3	2257.1	414.3	414.9	2.531	44.26	22104	22204
47	0.99993	0.011063	22.67	2.801	2.541	3.535	3.864	66.05	63.03	20.69	20.90	-0.28	-0.07	0.679	0.675	2284.9	2272.5	432.4	433.2	2.625	46.32	22716	22816
48	0.99994	0.011065	22.82	2.902	2.639	3.659	3.988	68.86	65.80	20.69	20.91	-0.27	-0.06	0.704	0.700	2300.3	2289.5	450.7	451.3	2.719	48.42	23326	23426
49	0.99995	0.011069	23.01	3.002	2.737	3.784	4.111	71.72	68.61	20.70	20.92	-0.27	-0.05	0.729	0.725	2319.3	2310.3	469.2	469.8	2.813	50.51	23940	24040
50	0.99995	0.011095	23.19	3.102	2.835	3.908	4.234	74.57	71.41	20.71	20.94	-0.26	-0.02	0.754	0.750	2336.6	2332.2	487.6	487.9	2.906	52.62	24550	24650
51	0.99996	0.011092	23.35	3.202	2.933	4.033	4.357	77.46	74.27	20.71	20.95	-0.26	-0.02	0.779	0.775	2353.1	2349.7	506.4	506.6	3.000	54.76	25165	25265
52	0.99995	0.011139	23.49	3.302	3.032	4.157	4.479	80.37	77.13	20.74	20.99	-0.23	0.02	0.804	0.800	2367.5	2371.4	525.2	524.9	3.094	56.91	25779	25879
53	0.99996	0.011152	23.81	3.502	3.228	4.405	4.726	86.22	82.90	20.75	21.01	-0.22	0.04	0.855	0.850	2399.3	2407.8	563.1	562.5	3.282	61.27	26643	26743
54	0.99997	0.011429	24.12	3.702	3.424	4.647	4.969	92.01	88.60	20.92	21.20	-0.05	0.23	0.905	0.901	2430.6	2477.4	600.6	597.0	3.469	65.67	27506	27606
55	0.99997	0.011622	24.41	3.901	3.621	4.886	5.211	97.81	94.31	21.04	21.33	0.07	0.36	0.955	0.952	2459.8	2534.8	638.1	632.1	3.657	70.14	28369	28469
56	0.99996	0.011678	24.60	4.024	3.741	5.036	5.359	101.47	97.92	21.07	21.37	0.10	0.40	0.986	0.984	2478.8	2563.4	661.9	654.9	3.772	72.91	29050	29150
57	0.99996	0.011525	24.72	4.102	3.817	5.165	5.464	104.63	101.05	20.98	21.29	0.01	0.32	1.005	1.004	2491.1	2558.0	682.3	676.6	3.843	74.62	29638	29738
58	0.99995	0.011455	24.98	4.302	4.015	5.425	5.708	111.07	107.41	20.94	21.26	-0.03	0.29	1.056	1.055	2517.8	2579.7	724.0	718.4	4.031	79.21	30511	30611
59	0.99995	0.011477	25.26	4.502	4.211	5.671	5.954	117.24	113.50	20.95	21.29	-0.02	0.32	1.106	1.106	2545.8	2614.5	763.9	757.5	4.218	83.83	31386	31486
60	0.99996	0.011466	25.51	4.701	4.408	5.915	6.193	123.44	119.62	20.94	21.30	-0.02	0.33	1.156	1.157	2570.6	2641.8	804.0	797.1	4.406	88.52	32255	32355
61	0.99995	0.011470	25.77	4.901	4.605	6.162	6.439	129.75	125.86	20.95	21.31	-0.02	0.35	1.206	1.208	2597.0	2672.9	844.9	837.3	4.593	93.24	33126	33226
62	0.99996	0.011484	26.01	5.101	4.802	6.404	6.680	136.00	132.03	20.95	21.34	-0.01	0.37	1.256	1.260	2621.4	2703.2	885.4	876.8	4.781	98.04	34006	34106
63	0.99996	0.011515	26.27	5.302	5.000	6.643	6.923	142.25	138.20	20.97	21.37	0.01	0.40	1.307	1.311	2647.7	2738.0	925.8	916.0	4.970	102.88	34888	34988
64	0.99996	0.011557	26.50	5.502	5.197	6.880	7.165	148.49	144.37	21.00	21.41	0.03	0.44	1.357	1.363	2670.7	2771.1	966.2	955.0	5.158	107.76	35769	35869
65	0.99993	0.011526	26.73	5.702	5.394	7.118	7.405	154.81	150.62	20.98	21.41	0.01	0.44	1.407	1.414	2693.7	2793.9	1007.1	995.5	5.346	112.70	36655	36755
66	0.99994	0.011600	26.94	5.902	5.592	7.354	7.645	161.15	156.89	21.03	21.46	0.06	0.50	1.458	1.466	2715.4	2830.5	1048.0	1034.4	5.534	117.68	37536	37636
67	0.99996	0.011645	27.17	6.102	5.789	7.587	7.886	167.44	163.11	21.05	21.51	0.08	0.54	1.508	1.518	2738.4	2864.3	1088.7	1073.4	5.722	122.70	38418	38518
68	0.99998	0.011781	27.39	6.302	5.987	7.817	8.125	173.71	169.31	21.13	21.60	0.17	0.63	1.558	1.570	2760.3	2910.5	1129.3	1110.5	5.911	127.77	39304	39404
69	0.99998	0.012038	27.60	6.502	6.184	8.054	8.362	180.24	175.77	21.28	21.76	0.32	0.80	1.608	1.622	2781.3	2973.7	1171.5	1147.0	6.099	132.87	40190	40290
70	0.99998	0.012350	27.78	6.702	6.382	8.278	8.599	186.42	181.90	21.46	21.95	0.49	0.98	1.658	1.675	2799.4	3042.0	1211.5	1180.2	6.288	138.05	41081	41181
71	0.99998	0.012513	27.99	6.902	6.580	8.509	8.842	192.84	188.25	21.55	22.05	0.58	1.09	1.709	1.729	2820.4	3092.4	1253.0	1217.2	6.476	143.22	41982	42082
72	0.99996	0.012017	27.58	6.901	6.584	8.571	8.852	194.54	190.07	21.27	21.78	0.30	0.81	1.708	1.728	2779.9	2977.2	1263.6	1236.6	6.476	143.35	42418	42518
73	0.99994	0.011595	28.16	7.102	6.778	8.846	9.100	202.24	197.59	21.02	21.55	0.05	0.59	1.759	1.781	2838.4	2981.0	1313.7	1293.5	6.660	148.32	43337	43437
74	0.99995	0.011615	28.34	7.302	6.976	9.102	9.345	209.46	204.75	21.03	21.58	0.07	0.61	1.809	1.833	2856.2	3006.9	1360.4	1338.5	6.846	153.53	44237	44337
75	0.99994	0.011986	28.51	7.502	7.174	9.340	9.585	216.23	211.46	21.25	21.81	0.29	0.84	1.859	1.885	2873.7	3085.5	1404.1	1373.0	7.035	158.82	45137	45237
76	0.99995	0.011571	28.70	7.702	7.371	9.583	9.819	223.15	218.32	21.01	21.58	0.04	0.62	1.909	1.937	2892.0	3045.5	1448.9	1425.4	7.222	164.13	46041	46141
77	0.99996	0.011723	26.55	7.863	7.558	9.784	9.998	228.92	224.78	21.10	21.69	0.13	0.72	1.945	1.975	2675.9	2842.7	1484.4	1456.4	7.374	169.13	52256	52356

SENB R-CURVE TEST 24624 M03 07

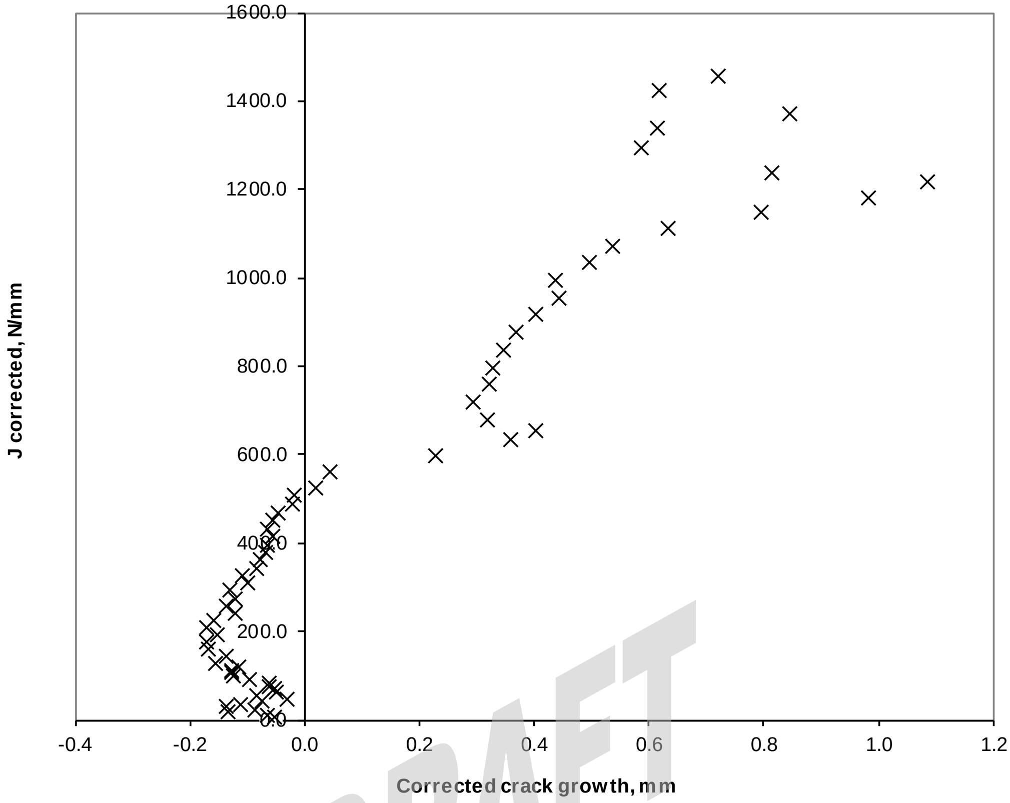

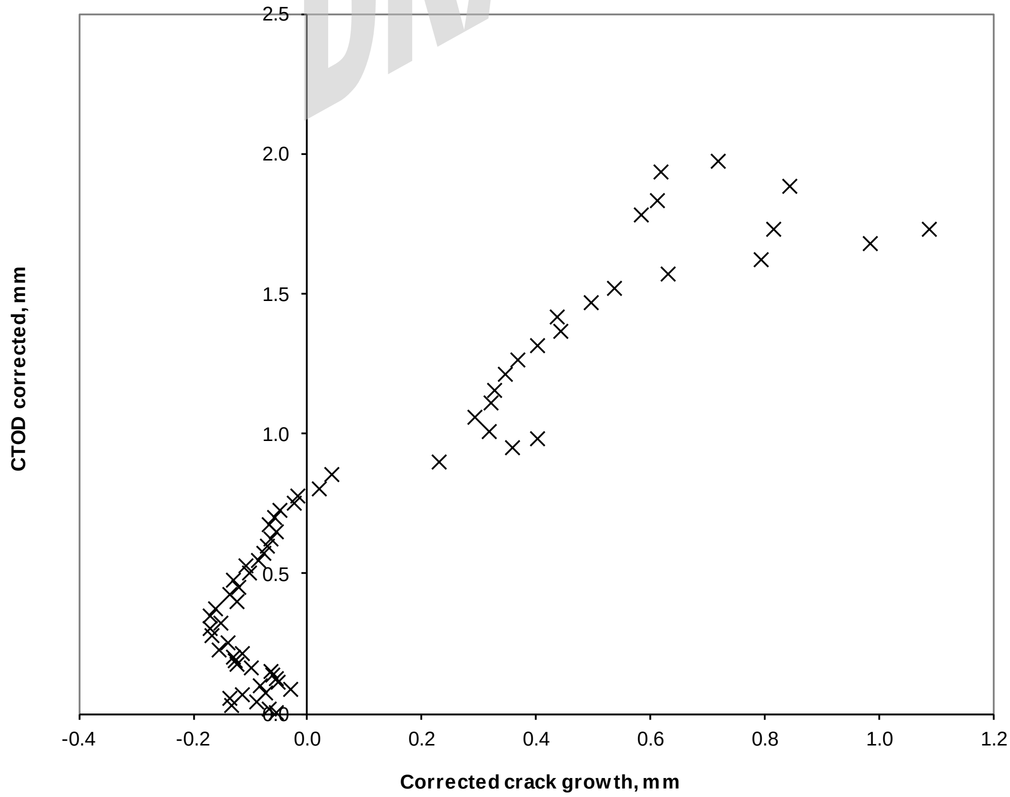

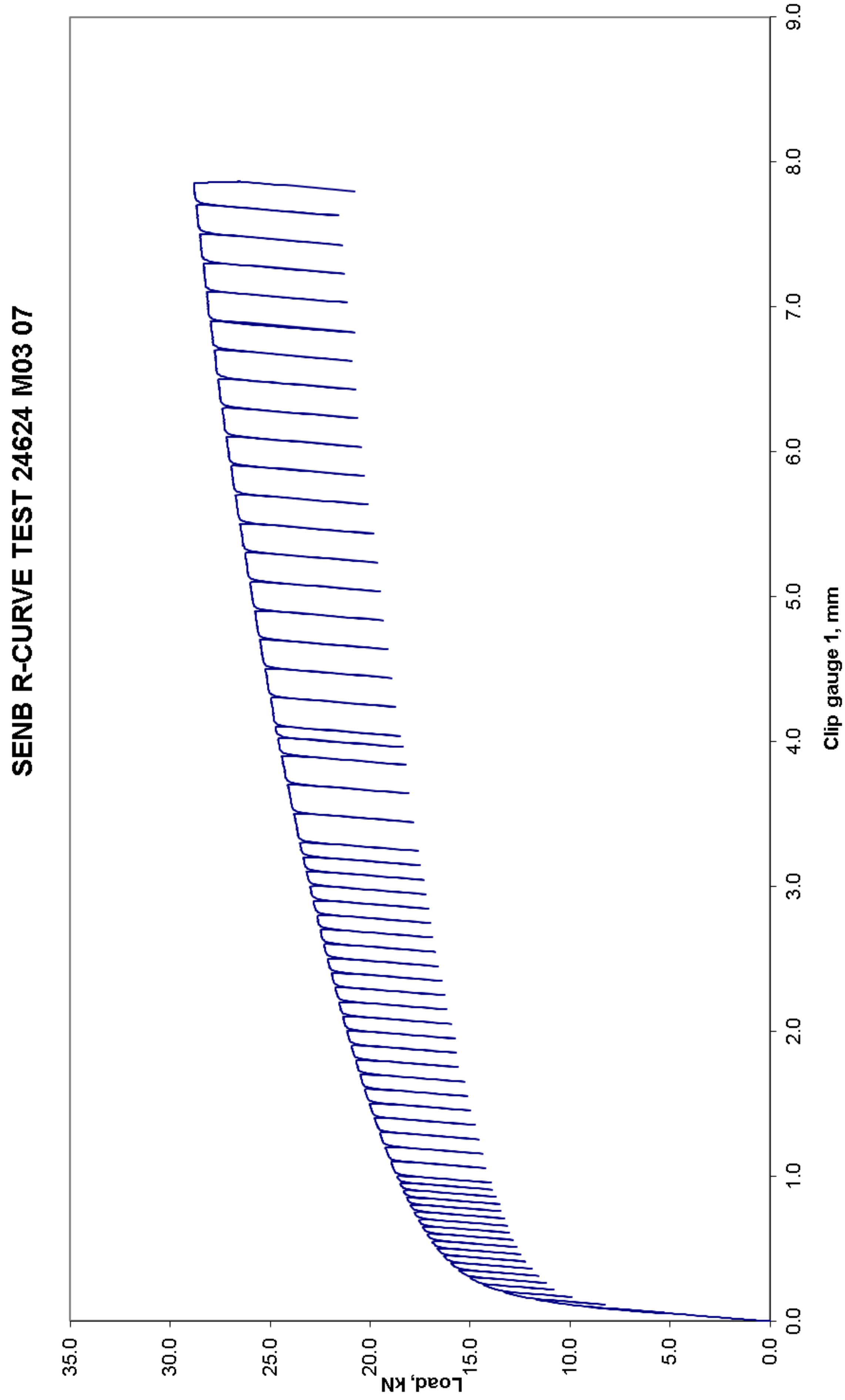
SENB R-CURVE TEST 24624 M03 07
Load, kN
Clip gauge 1, mm
0.0
5.0
10.0
15.0
20.0
25.0
30.0
35.0
0.0
1.0
2.0
3.0
4.0
5.0
6.0
7.0
8.0
9.0

SENB R-CURVE TEST 24624 M03 07

Diagram of fracture face

Specimen width, W	40.010	mm
Specimen Thickness, B	20.000	mm
Machined notch depth, M	16.210	mm
Surface crack length, a_{S1}	19.420	mm
Surface crack length, a_{S2}	19.450	mm
Net section thickness, B_N	16.300	mm
a_{max}	21.180	mm
a_{min}	20.560	mm

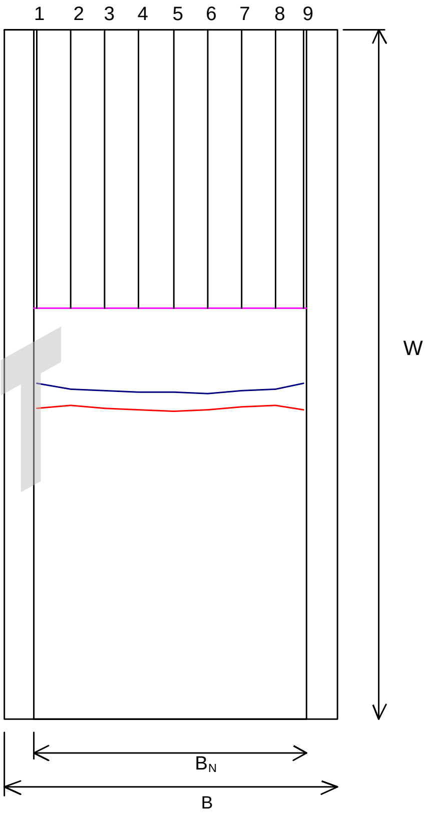

Measured by: Phillip Cossey

Signed:

Measurement Line	Fatigue crack length a0, mm	Slow stable crack extension Fatigue crack ap, mm	Slow stable crack extension including stretch zone, deltaa, mm
1	20.580	22.050	1.470
2	20.890	21.880	0.990
3	20.970	21.980	1.010
4	21.110	22.070	0.960
5	21.100	22.200	1.100
6	21.180	22.110	0.930
7	21.020	21.920	0.900
8	20.900	21.810	0.910
9	20.560	22.120	1.560
Weighted Average	**20.967**	**22.007**	**1.039**

UKAS TESTING
0088

TWI

SENB FRACTURE TEST 24624 M05-06

Client	CRP		
Project leader	WeeLiam Khor	Signed:	

Data source

Data logging program	LVGENLOG V 1.29 19-Nov-2013
Program used to calculate CTOD/J	LVGENPLOT V 1.31 18-Jan-2016
Calculation date of CTOD/J	25 Jan 2016

Specimen details

Material	SA-543-GrB-Cl1	
Specimen type	Subsize, SENB	
Crack plane orientation	Y-X	
Type of notch tip	Fatigue	
Notch tip location	Parent material	
Specimen width	40.000	mm
Specimen thickness	20.000	mm
Initial crack length	20.277	mm
Original PM 1 thickness	25.00	mm

Test details

Test standard(s)	BS 7448: Part 1: 1991		
Test date	20/01/2016		
Test time	09:13:00		
Test technician	Phillip Cossey		Signed:
Test machine	INSTRON 8500 B107		
Test environment	AIR		
Test temperature	21.0	°C	
Soak time @ test temperature	0.0	minutes	
Knife edge heights	2.000, 12.000	mm	
Knife edge spacing	14.00	mm	
Initial K-rate	1.1	$MPa.m^{1/2}/s$	
Loading span	160.0	mm	
Double roller diameter	25.00	mm	
Single roller diameter	25.00	mm	

Material properties

Yield strength for pre-cracking	850.0	MPa	Assumed from material specification
Tensile strength for pre-cracking	914.0	MPa	Assumed from material specification
Yield strength for testing	850.0	MPa	Assumed from material specification
Tensile strength for testing	915.0	MPa	Assumed from material specification
Poisson's ratio	0.3		Assumed
Young's modulus	207	GPa	Assumed

Fatigue details

Stress ratio, R	0.100	
Final force, F_f	8.00	kN
Final K	21.8	$MPa.m^{1/2}$
Fatigue temperature	21.0	°C
Loading span, S	160.0	mm

Analysis details

Method of determining Load Point Displacement, q	DOUBLE CLIP
Lower knife edge height check	OK

Compiled by: Phillip Cossey **Signed:** ____________

SENB FRACTURE TEST 24624 M05-06

Qualification checks to BS 7448: Part 1: 1991

(5.1.3)	
Knife edge attachment spacing	**Pass**
(6.4.5,6.4.6)	
The final fatigue precracking force <= F_f (a)	**Pass**
$\Delta K/E$ below limit (b)	**Pass**
(6.4.7)	
Initial/Final K ratio during precracking < 1.3 (a)	**Pass**
(7.5.1)	
Single roller diameter	**Pass**
Double roller diameter	**Pass**
Loading span	**Pass**
(8.5)	
Initial K-rate between 0.5 $MPa.m^{0.5}s^{-1}$ and 3.0 $MPa.m^{0.5}s^{-1}$	**Pass**
(10.2.2)	
Minimum surface crack length (a)	**Pass**
Minimum crack extension at surface (b)	**Pass**
Difference in surface crack measurements (c)	**Pass**
Surface fatigue cracks in envelope (d)	**Pass**
Crack plane within 10° (e)	**Pass**
(10.2.3)	
Multiplane cracking (a)	**Pass**
a_0/W check 0.45-0.55 (b)	**Pass**
Crack shape (c)	**Pass**
Minimum crack length (d)	**Pass**
(10.3)	
The stress ratio <= 0.1 (c)	**Pass**

0088

TWI

SENB FRACTURE TEST 24624 M05-06

Test date	20/01/2016	Client	CRP
Technician	Phillip Cossey	Project leader	WeeLiam Khor
Test machine	INSTRON 8500 B107	Investigator's signature	
Control mode	Displacement	Compiled by	Phillip Cossey

SPECIMEN DETAILS

Force, F	54.76	kN
Width, W	40.000	mm
Thickness, B	20.000	mm
Crack length, a_0	20.277	mm
Loading span, S	160.00	mm
Yield strength	850	MPa
Young's modulus	207	GPa
Poisson's ratio	0.300	
Test temperature	21.0	°C

RESULTS

δ	0.413	mm
K @ calculation point	149.1	$MPa.m^{1/2}$
F_{max}/F_Q	1.73	
K_Q	85.94	$MPa.m^{1/2}$
Total area under Force v q	106.72	kNmm
J0 from q from DOUBLE CLIP	542.42	kJ/m² (N/mm)
Plastic area Force v CMOD	66.20	kNmm
Type of result	δ/J_m	
Test standard(s)	BS 7448: Part 1: 1991	
Result qualified to standard(s)	YES	

LOWER CLIP GAUGE VALUES

Knife edge height	2.00	mm
Vg	1.893	mm
Vp	1.359	mm

UPPER CLIP GAUGE VALUES

Knife edge height	12.00	mm
Vg	2.488	mm
Vp	1.781	mm

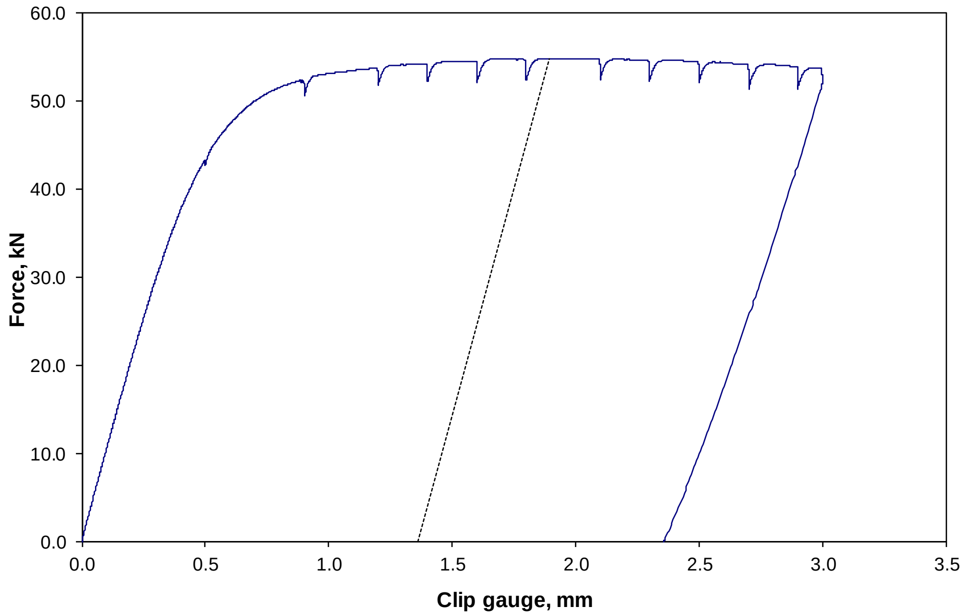

SENB FRACTURE TEST 24624 M05-06

Diagram of fracture face

Specimen width, W	40.000	mm
Specimen thickness, B	20.000	mm
Machined notch depth, M	16.190	mm
Surface crack length, a_{S1}	19.530	mm
Surface crack length, a_{S2}	19.570	mm
a_{max}	20.490	mm
a_{min}	19.690	mm

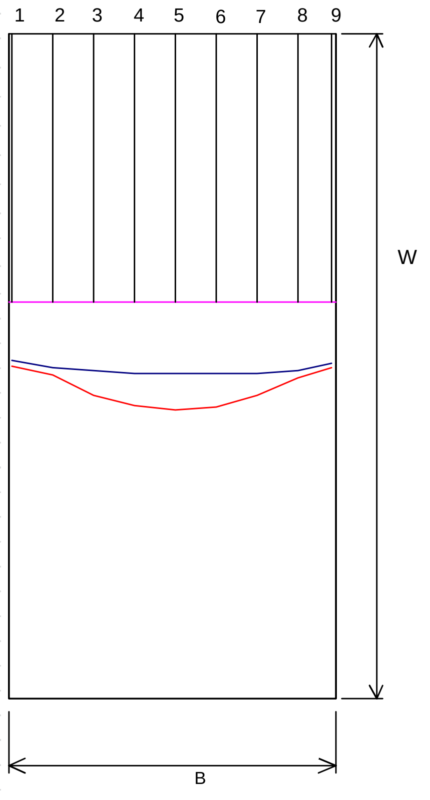

Comments

Measurement Line	Fatigue crack length a_0, mm	Slow stable crack extension + fatigue crack a_p, mm	Slow stable crack extension including stretch zone, Δ_a, mm
1	19.690	20.050	0.360
2	20.100	20.570	0.470
3	20.310	21.740	1.430
4	20.420	22.350	1.930
5	20.480	22.650	2.170
6	20.490	22.450	1.960
7	20.420	21.780	1.360
8	20.250	20.740	0.490
9	19.800	20.080	0.280
Weighted Average	**20.277**	**21.543**	**1.266**

Measured by: Phillip Cossey **Signed:**

UKAS TESTING
0088

TWI

SENB R-CURVE TEST 24624 M05 07

Client	CRP		
Project leader	WeeLiam Khor		Signed:

R-Curve data source

Data logging program	LVRCURVE V 1.39 08 Feb 2016
Program used to calculate R-curve data	LVRCALC V 1.20 01-Jul-2016
Calculation date of R-curve data	08 Aug 2016

Specimen details

Material	SS316	
Specimen type	SENB, Sub-size	
Crack plane orientation	Y-X	
Type of notch tip	Fatigue	
Notch tip location	Parent material	
Specimen side grooved	Yes	
Specimen width	40.00	mm
Specimen thickness	20.00	mm
Initial crack length, a0	20.20	mm
Estimated final crack length, ap	22.38	mm

Test details

Test standard	BS7448 Prt 4:1997		
Test method	Unloading compliance		
Test date	28/07/2016		
Test time	12:03:34		
Test technician	Phillip Cossey		Signed:
Test machine			
Test environment	Air		
Test temperature	24.0	°C	
Soak time @ Test temperature	NA	minutes	
Knife edge heights	2.000, 12.000	mm	
Initial K-Rate	19.07	$N/mm^{3/2}/sec$	
Loading span	160.0	mm	
Double roller diameter	25.00	mm	
Single roller diameter	25.00	mm	

Material properties

Yield strength @ Fatigue temperature	850.0	N/mm^2
Tensile strength @ Fatigue temperature	914.0	N/mm^2
Yield strength @ Test temperature	850.0	N/mm^2
Tensile strength @ Test temperature	914.0	N/mm^2
Poisson's ratio	0.3	
Youngs modulus	183774	N/mm^2

 SI/FRA/F/26 Rev 0.0 Jun 2016

Fatigue details

Stress ratio	0.100	
Final load	8.00	kN
Loading span	160.0	mm

Test procedure

Number of elastic unloadings	10		
Load relaxation limit	5.00	%	of elastic loading rate
1st Increment size	0.05	mm	
1st Maximum displacement	1.00	mm	
2nd Increment size	0.10	mm	
2nd Maximum displacement	50.00	mm	

Analysis details

Yield strength temperature correction	No
Young's modulus temperature correction	No
Method of determining J	DOUBLE CLIP
Young's modulus adjusted for crack agreement	Yes
Clip gauge used for crack length calculations	Clip 1

Compiled by:	Phillip Cossey	**Signed:**

UKAS TESTING 0088

TWI

SENB R-CURVE TEST 24624 M05 07

Qualification checks to BS7448 Prt 4:1997

(6.1.2)	
Knife edge spacing	**Pass**
(8.4.1)	
Single roller diameter	**Pass**
Double roller diameter	**Pass**
(9.3.1)	
Loading span	**Pass**
(9.6)	
Intitial K-rate between 0.5 $MPa.m^{0.5}s^{-1}$ to 3.0 $MPa.m^{0.5}s^{-1}$	**Pass**
(9.9.3)	
Was there a defect on fracture surface	**No**
(10.3.2)	
Estimated initial crack length a_o within 2% of measured a_o	**Pass**
(10.3.3)	
Estimated final crack growth within +/- 15% Δa	**Pass**
(14.2.3)	
Minimum surface crack length (a)	**Pass**
Minimum crack extension at surface (b)	**Pass**
Difference in surface crack measurements (c)	**Pass**
Surface crack measurements (d)	**Pass**
(14.2.4)	
Multiplane cracking (a)	**Pass**
a_0/W check 0.45-0.7 (b)	**Pass**
Crack shape (c)	**Pass**
Minimum crack length (d)	**Pass**
Crack within envelope (e)	**Pass**
(14.3.1)	
The specimen did not fracture or pop-in (a)	**No**
The final fatigue precracking force was < F_f (b)	**Pass**
The stress ratio < 0.1 (c)	**Pass**

0088

SENB R-CURVE TEST 24624 M05 07

ELASTIC UNLOADINGS

No.	Coeff	Comp'nce	Load	Vgo	Vpo	Q	Ram	Total Uarea	Plastic Uarea	Estimated a	Corrected a	Estimated Δa	Corrected Δa	CTOD	CTOD Corrected	K	K Corrected	Jdef	J Corrected	CMOD	CMOD Parea	First Rec	Last Rec
		mm/kN	kN	mm	mm	mm	mm	kNmm	kNmm	mm	mm	mm	mm	mm	mm	$N/mm^{3/2}$	$N/mm^{3/2}$	N/mm	N/mm	mm	kNmm		
1	0.99990	0.010219	6.49	0.063	-0.003	0.081	0.270	0.28	0.03	20.24	20.25	0.04	0.04	0.000	0.000	613.2	615.3	2.0	2.0	0.059	-0.01	1055	1155
2	0.99982	0.010187	6.49	0.062	-0.004	0.083	0.270	0.29	0.04	20.22	20.22	0.02	0.02	0.000	0.000	612.4	613.4	2.1	2.1	0.059	-0.01	1294	1394
3	0.99988	0.010196	6.50	0.062	-0.004	0.083	0.270	0.29	0.04	20.23	20.23	0.02	0.03	0.000	0.000	613.6	614.9	2.1	2.1	0.059	-0.01	1533	1632
4	0.99989	0.010183	6.47	0.062	-0.004	0.083	0.270	0.29	0.04	20.22	20.22	0.01	0.02	0.000	0.000	611.2	612.1	2.1	2.1	0.059	-0.01	1772	1872
5	0.99987	0.010201	6.49	0.062	-0.004	0.083	0.270	0.29	0.04	20.23	20.23	0.03	0.03	0.000	0.000	613.0	614.5	2.1	2.1	0.059	-0.01	2011	2111
6	0.99984	0.010132	6.47	0.061	-0.005	0.084	0.269	0.30	0.05	20.18	20.19	-0.02	-0.02	0.000	0.000	611.2	610.4	2.2	2.2	0.059	-0.01	2248	2347
7	0.99983	0.010095	6.50	0.061	-0.005	0.084	0.270	0.30	0.05	20.15	20.16	-0.05	-0.04	0.000	0.000	613.5	611.4	2.2	2.2	0.059	-0.01	2484	2584
8	0.99981	0.010113	6.47	0.061	-0.005	0.084	0.269	0.30	0.05	20.17	20.17	-0.04	-0.03	0.000	0.000	611.0	609.6	2.2	2.2	0.059	-0.01	2722	2822
9	0.99984	0.010192	6.48	0.061	-0.005	0.085	0.270	0.30	0.05	20.22	20.23	0.02	0.02	0.000	0.000	611.4	612.6	2.2	2.2	0.059	-0.01	2958	3058
10	0.99981	0.010104	6.49	0.061	-0.005	0.086	0.270	0.31	0.06	20.16	20.17	-0.04	-0.04	0.000	0.000	612.8	611.0	2.2	2.2	0.059	-0.01	3195	3294

0088

SENB R-CURVE TEST 24624 M05 07

PLASTIC UNLOADINGS

No.	Coeff	Comp'nce	Load	Vgo	Vpo	Q	Ram	Total Uarea	Plastic Uarea	Estimated a	Corrected a	Estimated Δa	Corrected Δa	CTOD	CTOD Corrected	K	K Corrected	Jdef	J Corrected	CMOD	CMOD Parea	First Rec	Last Rec
		mm/kN	kN	mm	mm	mm	mm	kNmm	kNmm	mm	mm	mm	mm	mm	mm	$N/mm^{3/2}$	$N/mm^{3/2}$	N/mm	N/mm	mm	kNmm		
11	0.99987	0.010082	10.44	0.101	-0.005	0.135	0.369	0.72	0.08	20.15	20.15	-0.06	-0.05	0.001	0.001	985.4	981.4	5.3	5.3	0.094	-0.03	3633	3733
12	0.99997	0.010101	15.21	0.151	-0.004	0.195	0.480	1.49	0.13	20.16	20.17	-0.04	-0.03	0.005	0.005	1436.5	1432.7	11.0	11.0	0.141	-0.01	4119	4219
13	0.99996	0.010058	19.81	0.201	0.000	0.254	0.579	2.54	0.22	20.13	20.14	-0.07	-0.06	0.010	0.010	1870.5	1861.6	18.7	18.7	0.188	0.04	4659	4759
14	0.99997	0.010068	24.23	0.251	0.005	0.315	0.676	3.88	0.41	20.14	20.15	-0.07	-0.05	0.017	0.017	2287.9	2279.0	28.4	28.5	0.235	0.14	5200	5300
15	0.99998	0.010105	28.37	0.301	0.013	0.376	0.765	5.48	0.72	20.16	20.18	-0.04	-0.02	0.024	0.024	2679.1	2675.1	40.0	40.0	0.282	0.33	5772	5872
16	0.99999	0.010088	32.09	0.352	0.025	0.439	0.852	7.37	1.28	20.15	20.18	-0.05	-0.03	0.033	0.033	3029.9	3023.4	53.4	53.4	0.330	0.68	6379	6479
17	0.99997	0.010162	35.31	0.401	0.042	0.501	0.935	9.48	2.11	20.20	20.23	0.00	0.03	0.044	0.044	3334.2	3342.0	68.0	68.0	0.376	1.19	7010	7110
18	0.99996	0.010144	38.03	0.451	0.065	0.563	1.015	11.75	3.20	20.19	20.22	-0.01	0.02	0.055	0.055	3590.5	3596.2	83.5	83.5	0.423	1.96	7662	7762
19	0.99997	0.010147	40.31	0.501	0.092	0.625	1.094	14.19	4.59	20.19	20.23	-0.01	0.03	0.066	0.066	3806.2	3814.1	100.0	99.9	0.470	2.95	8337	8437
20	0.99999	0.010121	42.27	0.552	0.122	0.688	1.170	16.78	6.21	20.17	20.21	-0.03	0.01	0.079	0.079	3991.7	3995.2	117.1	117.1	0.517	4.11	9026	9126
21	0.99999	0.010145	43.86	0.601	0.156	0.749	1.242	19.43	8.06	20.19	20.23	-0.01	0.03	0.091	0.091	4141.5	4152.0	134.5	134.4	0.564	5.46	9723	9823
22	0.99998	0.010177	45.21	0.651	0.192	0.812	1.313	22.23	10.15	20.21	20.26	0.01	0.06	0.104	0.104	4269.1	4289.0	152.7	152.4	0.611	6.97	10431	10531
23	0.99998	0.010228	46.30	0.701	0.231	0.874	1.384	25.06	12.39	20.25	20.30	0.04	0.10	0.116	0.116	4371.7	4405.8	170.9	170.5	0.658	8.64	11151	11251
24	0.99998	0.010268	47.20	0.752	0.272	0.938	1.453	28.01	14.85	20.28	20.33	0.07	0.13	0.129	0.130	4457.2	4503.6	189.7	189.1	0.705	10.43	11881	11981
25	0.99998	0.010281	47.92	0.801	0.314	1.000	1.520	31.00	17.43	20.29	20.35	0.08	0.14	0.142	0.143	4524.4	4576.2	208.6	207.8	0.751	12.32	12614	12714
26	0.99998	0.010311	48.43	0.852	0.360	1.062	1.587	33.98	20.12	20.31	20.37	0.10	0.17	0.155	0.156	4573.3	4634.6	227.3	226.4	0.799	14.35	13349	13449
27	0.99997	0.010353	48.90	0.902	0.405	1.124	1.649	36.97	22.84	20.34	20.40	0.13	0.20	0.168	0.169	4617.4	4691.8	246.1	244.8	0.845	16.41	14087	14187
28	0.99998	0.010398	49.25	0.951	0.451	1.186	1.713	40.02	25.69	20.37	20.44	0.16	0.23	0.182	0.182	4650.6	4738.7	265.1	263.5	0.892	18.54	14831	14931
29	0.99997	0.010436	49.49	1.001	0.498	1.248	1.776	43.08	28.61	20.39	20.47	0.19	0.26	0.195	0.195	4672.9	4772.7	284.1	282.2	0.938	20.70	15575	15675
30	0.99997	0.010528	49.87	1.102	0.595	1.376	1.905	49.41	34.71	20.45	20.54	0.25	0.33	0.221	0.222	4709.3	4837.1	323.3	320.6	1.033	25.22	16454	16554
31	0.99998	0.010669	50.08	1.202	0.693	1.498	2.031	55.53	40.71	20.55	20.64	0.35	0.43	0.247	0.249	4728.6	4897.3	361.1	357.2	1.127	29.79	17329	17429
32	0.99998	0.010853	50.21	1.302	0.791	1.620	2.157	61.64	46.74	20.67	20.77	0.47	0.56	0.274	0.276	4740.8	4961.8	398.8	393.1	1.221	34.44	18209	18309
33	0.99998	0.010975	50.29	1.402	0.891	1.743	2.281	67.79	52.84	20.75	20.85	0.55	0.65	0.300	0.303	4748.3	5004.7	436.7	429.5	1.314	39.11	19092	19192
34	0.99997	0.011123	50.32	1.502	0.990	1.863	2.403	73.84	58.87	20.84	20.95	0.64	0.75	0.326	0.331	4751.3	5049.9	473.9	464.9	1.409	43.83	19978	20078
35	0.99997	0.011230	50.27	1.602	1.091	1.984	2.523	79.91	64.98	20.91	21.03	0.71	0.82	0.352	0.358	4746.2	5075.5	511.2	500.6	1.502	48.57	20861	20961
36	0.99997	0.011355	50.13	1.701	1.192	2.104	2.644	85.95	71.10	20.99	21.11	0.79	0.91	0.379	0.386	4733.4	5097.6	548.2	535.7	1.596	53.34	21745	21845
37	0.99996	0.011472	50.00	1.802	1.294	2.224	2.764	91.93	77.16	21.06	21.19	0.86	0.99	0.405	0.414	4721.4	5118.1	584.9	570.4	1.691	58.13	22629	22729
38	0.99996	0.011649	49.69	1.902	1.397	2.344	2.885	97.90	83.31	21.17	21.30	0.96	1.10	0.431	0.442	4691.5	5134.3	621.4	604.1	1.784	62.94	23509	23609
39	0.99996	0.011818	49.45	2.002	1.499	2.464	3.003	103.85	89.40	21.27	21.41	1.06	1.21	0.458	0.470	4669.0	5155.9	657.8	637.8	1.878	67.71	24395	24495
40	0.99996	0.011948	49.31	2.102	1.601	2.585	3.121	109.83	95.46	21.34	21.49	1.14	1.29	0.484	0.498	4656.2	5177.9	694.5	671.9	1.972	72.41	25285	25385
41	0.99996	0.012183	48.87	2.202	1.705	2.704	3.236	115.67	101.55	21.48	21.64	1.28	1.43	0.510	0.526	4614.8	5193.7	730.1	703.7	2.067	77.24	26169	26269
42	0.99996	0.012369	48.51	2.302	1.809	2.824	3.350	121.50	107.59	21.58	21.75	1.38	1.54	0.537	0.555	4580.1	5204.0	765.7	735.8	2.161	81.98	27055	27155
43	0.99996	0.012577	48.10	2.402	1.913	2.944	3.468	127.26	113.59	21.70	21.87	1.50	1.66	0.563	0.584	4541.9	5214.6	800.8	767.1	2.255	86.71	27935	28035
44	0.99996	0.012786	47.70	2.502	2.017	3.061	3.581	132.88	119.44	21.81	21.99	1.61	1.78	0.589	0.613	4503.8	5224.4	835.1	797.4	2.349	91.38	28818	28918
45	0.99996	0.013026	47.23	2.602	2.122	3.181	3.695	138.58	125.40	21.94	22.12	1.74	1.92	0.616	0.642	4459.5	5233.3	869.8	827.7	2.443	96.05	29698	29798
46	0.99995	0.013256	46.77	2.702	2.227	3.299	3.809	144.10	131.17	22.06	22.25	1.85	2.04	0.642	0.672	4416.2	5239.7	903.4	856.8	2.537	100.69	30581	30681
47	0.99997	0.013509	46.30	2.802	2.331	3.416	3.921	149.55	136.89	22.19	22.38	1.98	2.18	0.669	0.701	4371.3	5247.9	936.6	885.1	2.631	105.26	31459	31559

DRAFT

SENB R-CURVE TEST 24624 M05 07

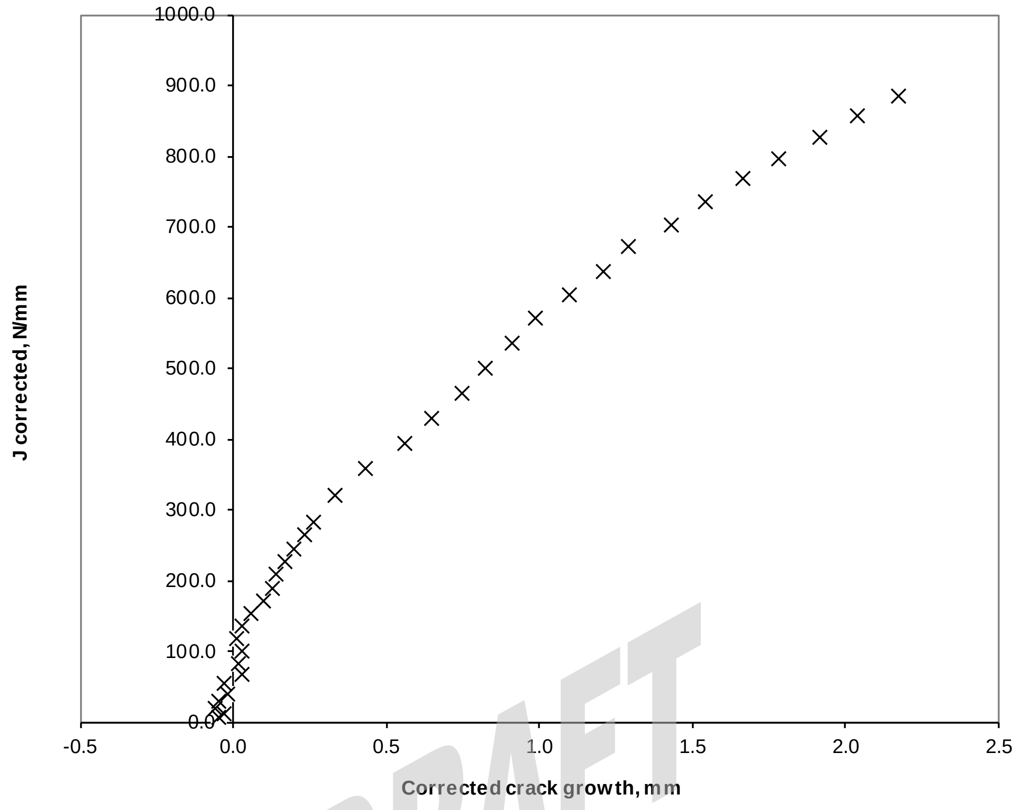

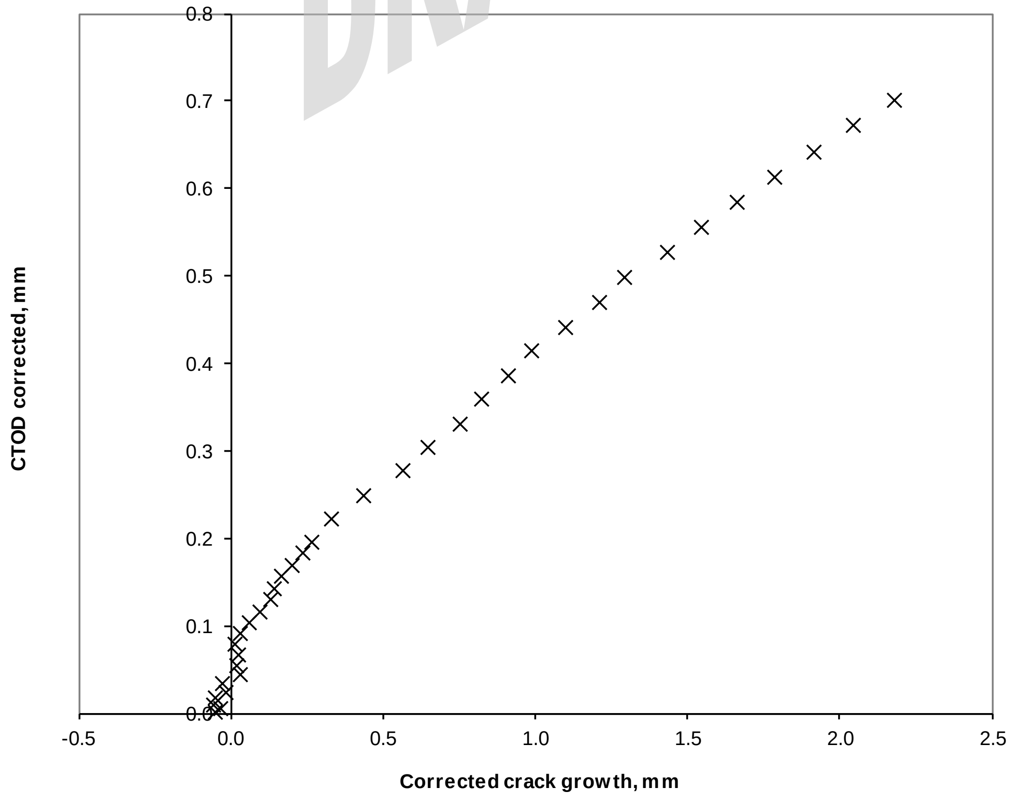

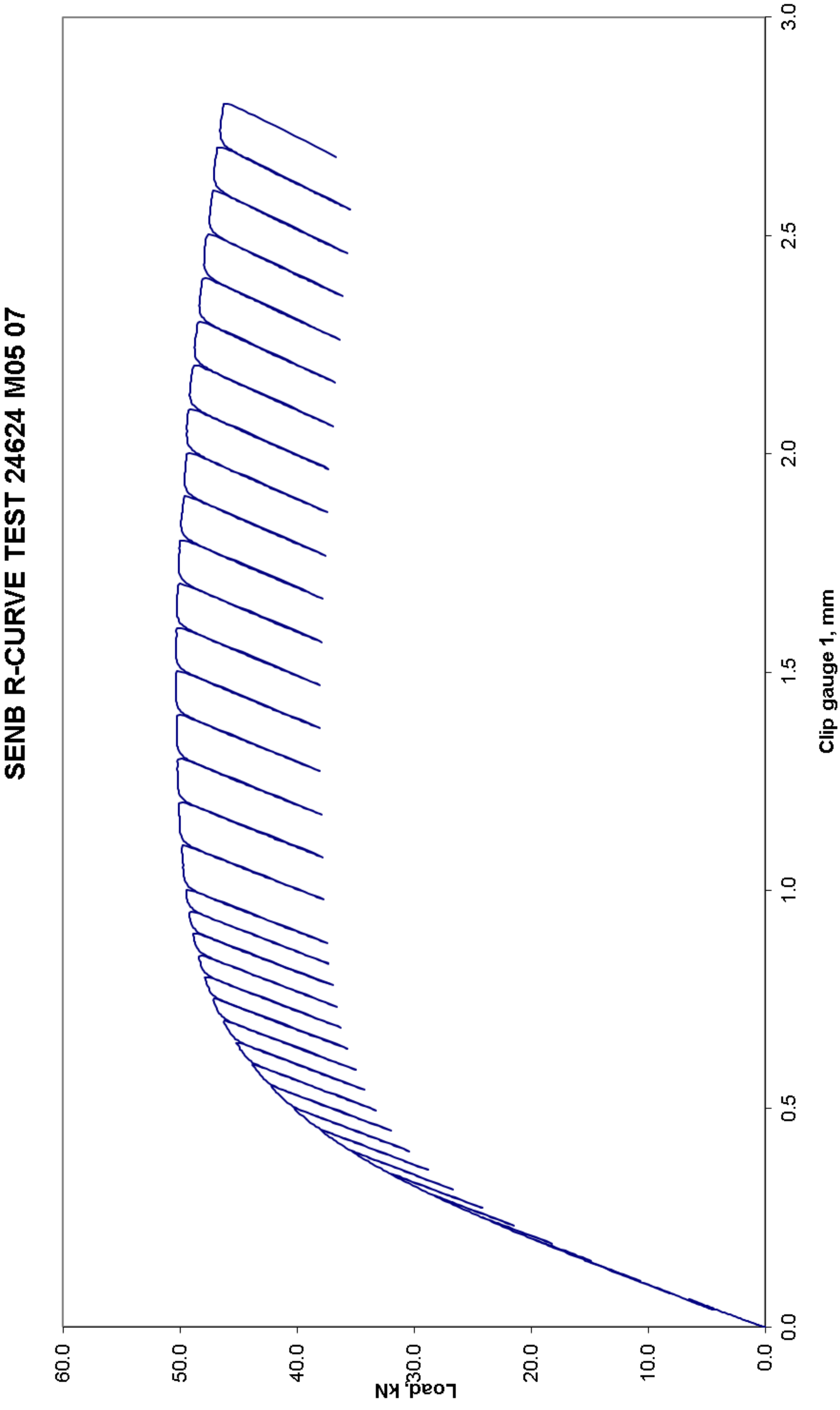
SENB R-CURVE TEST 24624 M05 07
Load, kN
60.0
50.0
40.0
30.0
20.0
10.0
0.0
Clip gauge 1, mm
0.0
0.5
1.0
1.5
2.0
2.5
3.0

SENB R-CURVE TEST 24624 M05 07

Specimen width, W	40.000	mm
Specimen Thickness, B	20.000	mm
Machined notch depth, M	16.170	mm
Surface crack length, a_{S1}	19.360	mm
Surface crack length, a_{S2}	19.560	mm
Net section thickness, B_N	16.425	mm
a_{max}	20.290	mm
a_{min}	19.980	mm

Diagram of fracture face

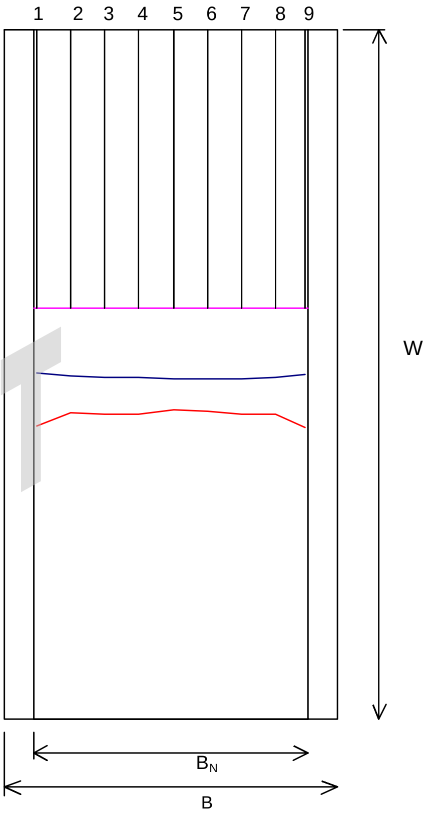

Measured by: Phillip Cossey

Signed:

Measurement Line	Fatigue crack length a0, mm	Slow stable crack extension Fatigue crack ap, mm	Slow stable crack extension including stretch zone, deltaa, mm
1	19.980	23.070	3.090
2	20.110	22.300	2.190
3	20.220	22.310	2.090
4	20.230	22.320	2.090
5	20.290	22.100	1.810
6	20.290	22.140	1.850
7	20.270	22.320	2.050
8	20.190	22.320	2.130
9	20.070	23.090	3.020
Weighted Average	**20.203**	**22.361**	**2.158**

Fatigue & Fracture of Engineering Materials & Structures
ORIGINAL CONTRIBUTION
doi: 10.1111/ffe.12487

Measurement and prediction of CTOD in austenitic stainless steel

W. KHOR[1,2], P. L. MOORE[3], H. G. PISARSKI[3], M. HASLETT[3] and C. J. BROWN[1]
[1]*Brunel University London, Uxbridge UB8 3PH, UK,* [2]*NSIRC, Granta Park CB21 6AL, UK,* [3]*TWI, Granta Park CB21 6AL, UK*

Received Date: 10 March 2016; Accepted Date: 16 May 2016; Published Online: 2016

ABSTRACT Variation of Crack Tip Opening Displacement (CTOD) test values can have a significant effect on the Engineering Critical Assessment of a structure. This paper examines the development of CTOD with increasing load in an austenitic stainless steel. The silicone replication method giving variation of CTOD across the specimen thickness, and Digital Image Correlation (DIC) are compared to each other, and in turn to clip gauge measurements from tests. Results from Finite Element models are also presented. Estimations of CTOD from BS 7448-1, ISO 12135 and ASTM E1820, and a proposed modification from JWES are compared to the experimental data from the crack cast in silicone compound – assumed to be the actual CTOD. The DIC measurement showed consistency with crack replicas, and a formula is given to estimate CTOD using DIC. For high strain hardening austenitic stainless steel, both the JWES and ASTM E1820 estimations provide adequate accuracy for CTOD.

NOMENCLATURE

A_p = plastic area under P versus V_p
a_0 = initial crack length
B = specimen thickness
B_0 = remaining ligament, $W - a_0$
b = position on section as a ratio of $B/2$
E = modulus of elasticity
J = strain energy around the crack
K = stress intensity factor
K_I = stress intensity factor in mode I loading
m = plane strain function used in JWES
m_{ASTM} = function relating J to CTOD
n = strain hardening exponent
P = load
r_p = rotational factor for plastic hinge assumption
V_g = clip gauge opening displacement
V_p = plastic component of clip gauge opening displacement
W = specimen width
z = knife edge height
δ = crack tip opening displacement (CTOD)
δ_5 = direct CTOD measurement from two points at the specimen surface 5 mm apart, placed directly at the crack tip
$\delta_{5\ DIC}$ = δ_5 measured using the DIC technique
δ_{SRC} = CTOD measured on the silicone replicas
δ_{FE} = CTOD obtained from the FE model
v = Poisson's ratio
σ_{ys} = 0.2% proof strength at test temperature
σ_{uts} = ultimate tensile strength at test temperature
σ_y = flow stress at test temperature, $(\sigma_{ys} + \sigma_{uts})/2$
ε = strain
η = geometrical based calibration function for J

Correspondence: C. J. Brown. E-mail: chris.brown@brunel.ac.uk

INTRODUCTION

Fracture toughness is used in Engineering Critical Assessment (ECA) to assess the fitness-for-service of engineering structures with respect to avoidance of fracture.[1–5] Differences in the values of fracture toughness measurements on the same specimen using different methods could result in a structure being considered safe or not. It is therefore important that the estimation of failure criteria, such as critical flaw size, does not result in over-conservative design, while still ensuring structural integrity.[6]

Crack Tip Opening Displacement (CTOD) is a measure of the physical opening of an original crack tip in a standard fracture toughness test specimen at the point of stable or unstable crack extension. The CTOD concept was proposed by Wells[7] using notched tension bars. In the early days, a 'COD meter' had been used to measure CTOD.[8] It was placed at the bottom of a sawn notch and the opening of the crack could be measured directly. Modern techniques introduce a fatigue precrack in fracture toughness specimens to mimic an actual crack. Displacement data are obtained by measuring the displacement of the load or the opening of the crack mouth (CMOD) from which CTOD is inferred.[9,10]

Current standards-based procedures – such as BS 7448-1,[9] ISO 12135[11] and ASTM E1820[10] – specify methods to determine fracture toughness, including determination of the critical CTOD for the material under the application of slowly increasing loading on the specimen. The fracture test procedure and methodology are well established and are similar between standards. A clip gauge is often used to measure the displacement data from the opening of the crack mouth because of its consistency[12] and simplicity. However, despite the similar testing methods, different standards give different CTOD estimation equations.[13] Figure 1a shows an SENB specimen with the clip gauge attached prior to testing, while Fig. 1b shows the same specimen after testing.

BS 7448-1 and ISO 12135 use the same equation for CTOD based on the assumption of the development of a plastic hinge, while ASTM E1820 calculates CTOD based on a different fracture toughness parameter, J.[14–16] J is defined as the path-independent strain energy around the crack.[17] Recently, researchers at the Japanese Welding Engineering Society (JWES) have suggested a modification to include a strain hardening consideration in the calculation used in BS 7448-1.[18]

A potential application for the JWES strain hardening modification can occur when stainless steel is used. Austenitic stainless steel is often used in harsh environments because of its corrosion resistance properties.[19–22] When compared to typical structural and high strength steel, austenitic stainless steel can have significantly higher strain hardening, which is a result of its high ductility. This ductility usually implies better fracture toughness properties, which in turn leads to reduced engineering safety concerns, but it is still important that this design criterion is assessed. Grade 300 austenitic stainless steel typically contains 18% Chromium, 10% Nickel and 1% Manganese with the balance being made up by Iron.[23]

The current study was carried out to examine the validity of the available standard equations when applied to austenitic stainless steel. In a standard Single Edge Notched Bend (SENB) test, the crack width was estimated using standard clip gauges. Silicone casting and Digital Image Correlation (DIC) were used to measure CTOD directly, and a Finite Element (FE) model was used to simulate the experimental results. The CTOD measurements were not limited to low CTOD values.

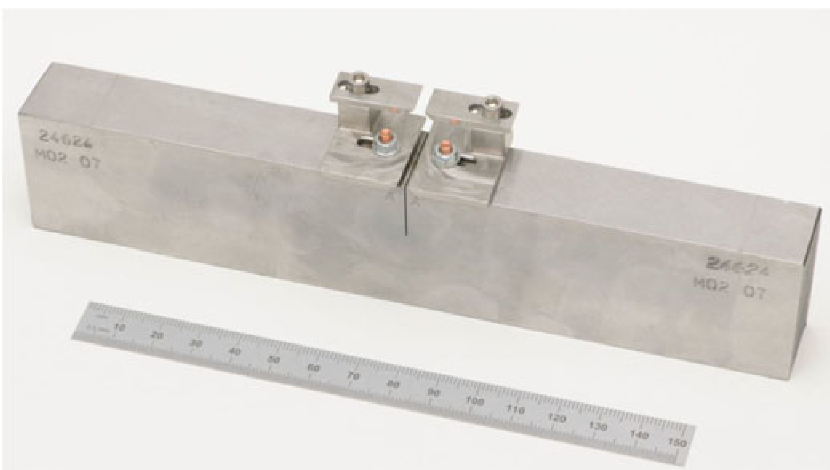

Fig. 1 (a). SENB specimen with double clip gauge attached before loading, (b) SENB specimen after loading without clip gauges.

MATERIAL AND METHODS

Experiments were carried out using standard SENB testing procedures, in accordance with BS 7448-1 (Fig. 1). SS316 plate was used as the austenitic stainless steel for experimental testing. Mechanical and chemical properties are given in Tables 1 and 2 respectively. Strain hardening, n, was estimated by fitting an offset power law equation to the tensile data obtained from a standard tensile test. Twenty-one-millimetre thick plate was machined to nine standard $B \times 2B$ SENB specimens, where $B = 20$ mm. All SENB specimens are fatigue pre-cracked to a nominal initial crack length of $a_0/W = 0.5$. A full list of all the tests carried out is given in Table 3.

Physical crack casting

Physical crack measurement has been a challenge. It is clear from others[24] that a section can be sectioned to measure CTOD – with the consequence that only one measurement per specimen may be made. More recently Tagawa *et al.*[13] and Kawabata *et al.*[18] have used the silicone compound method to replicate the physical crack. However the castings were limited to one per specimen and confined to CTOD ≤ 0.2 mm. A more extensive process is described here.

One of the $B \times 2B$ SENB specimens, labelled M03-05, was used for the physical crack replication test. The crack replication test was similar to a standard test, except that the specimen was held at constant displacement at chosen loads, while a two-part silicone compound (Microset RF-101) was used to make a cast of the crack (Fig. 2a). After the silicone compound had cured (approximately 5 min for each casting), the specimen was further loaded and held at the next chosen load (Fig. 2b), when it was possible to remove the cured crack replica (Fig. 2c), and the casting procedure was then repeated.

Table 1 Tensile properties tested in accordance to BS EN ISO 6892-1:2009 B

Material	SS316
Strain hardening, n[a]	0.53
Plate thickness, mm	21
Yield to tensile ratio, σ_{ys}/σ_{uts}	0.48
0.2% offset proof strength, MPa	285.5
Tensile strength, MPa	595.3
Elongation, %	67.5

[a]Strain hardening measurement is based on curve fitting using offset power law equation.

Table 3 Specimen numbering and description

Specimen number	Description	Setup
M03-03	Single point SENB test	
M03-05	Interrupted SENB test with silicone crack replication	
M03-11		Nominally 20 mm × 40 mm B × 2B SENB specimen
M03-12		
M03-13		
M03-14	Single point SENB test with DIC measurement	
M03-15		
M03-16		
M03-17		

Image measurements

Image measurements are becoming more viable to measure crack development. The δ_5 method was first devised in the 1980s in Germany.[25] δ_5 is the displacement between two fixed measurement points set initially 5 mm apart on the specimen surface at both sides of the crack tip. For a standard δ_5 test, a special instrument called a δ_5 clip is used to measure the CTOD directly, and the displacement is recorded as the increasing loading is applied. Others adopted the technique and report initial work on thin specimens.[26] More recently Ktari *et al.*[27] have used DIC effectively for crack opening measurement.

DIC measurement was applied on seven different fracture toughness specimens (M03-11 to M03-17), which were tested in a single point SENB setup. A commercial non-contact optical 3D deformation measuring system, GOM-ARAMIS v6.3, was used during these tests to determine δ_5.

By using GOM-ARAMIS, the software is able to recognize the surface structure of the measured object in digital camera images and allocates coordinates to the image pixels. Hence, instead of using δ_5 clips, two stage points with a distance of 5 mm can be defined directly on the recorded images, the displacements of the two points can be obtained from the recorded series of testing images, and δ_5 can be calculated throughout the test. Figure 3 shows the two points recognized on the surface of the specimen for δ_5 measurement, and the displacement of the respective points after the specimen is

Table 2 Chemical composition of SS316 by weigh percentage, measured using electrical discharge method

C	Si	Mn	P	S	Cr	Mo	Ni	Al	As
0.021	0.26	1.76	0.037	0.003	17.4	1.94	10.1	<0.01	<0.01
B	**Co**	**Cu**	**Nb**	**Pb**	**Sn**	**Ti**	**V**	**W**	**Ca**
<0.001	0.19	0.37	<0.01	<0.002	0.01	<0.005	0.06	0.07	<0.001

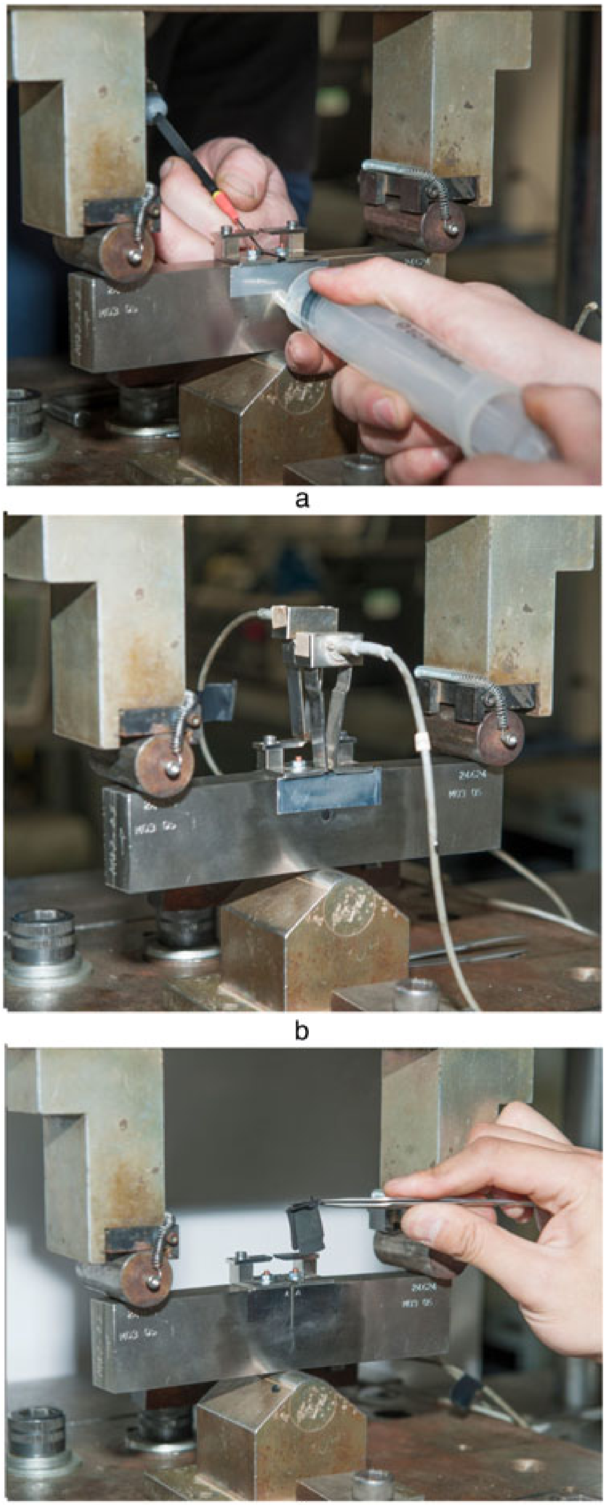

Fig. 2 (a) Crack casting process—filling the crack with silicone compound, (b) crack casting process—specimen further loaded after silicone compound cures, (c) crack casting process—cured crack replica removed from the crack.

loaded. The δ_5 is considered to give an alternative estimation of crack displacement to the CTOD values determined from the standard tests. It provides a direct measurement of CTOD at the surface which may differ from CTOD within the interior of the specimen.

Austenitic stainless steels exhibit high strain hardening and are capable of large plastic deformation. In a three-point-bend test, it was found that the displacement measuring clip gauge often achieved its limit mid-test and required adjustment to continue measurement. DIC, however, measures displacement based on the speckle patterns it recognizes on the surface, which can provide continuous surface displacement measurement.

Finite element models

The FE method has often been applied to investigate fracture toughness estimation equations.[13,18,24,28–30] A Geometrically and Materially Non-linear Analysis (GMNA) FE model was used to predict CTOD in an SENB setup. A fully three-dimensional quarter SENB model was simulated using commercially available software (ABAQUS v6.14) with a blunted crack tip of 0.03 mm radius. The blunted crack tip allows better deformation of the crack tip at larger deformation level. Symmetry was defined on the x–y plane on the side of the specimen facing in the z-direction and the y-z plane on the unbroken ligament facing the x-direction. Figure 4 shows the outline geometry of the SENB specimen investigated and the detail of the mesh adjacent to the crack. Both 8-noded elements (C3D8R) and 20-noded elements (C3D20R) were used to model the SENB specimen. The 20-noded elements gave a better representation of the actual specimen and thus were used in the subsequent sections.

A modulus of elasticity of 200 GPa and Poisson's ratio of 0.3 was used to define the elastic properties, and the experimentally determined true stress–strain properties used for post-elastic material definition are shown in Fig. 5. Displacement in the negative y-direction was applied on the upper roller, whereas the lower roller was fixed. A total of 104 736 elements were generated for the model, and a standard convergence test was performed based on varying the element size distributed across the crack tip. CTOD was measured based on opening of the original crack tip.

RESULTS

The CTOD measured on the Silicone Replica Crack (SRC) was considered as representative of the actual physical crack at the particular loading, and used to compare against the other CTOD measurements, finite element predictions and CTOD estimation equations.

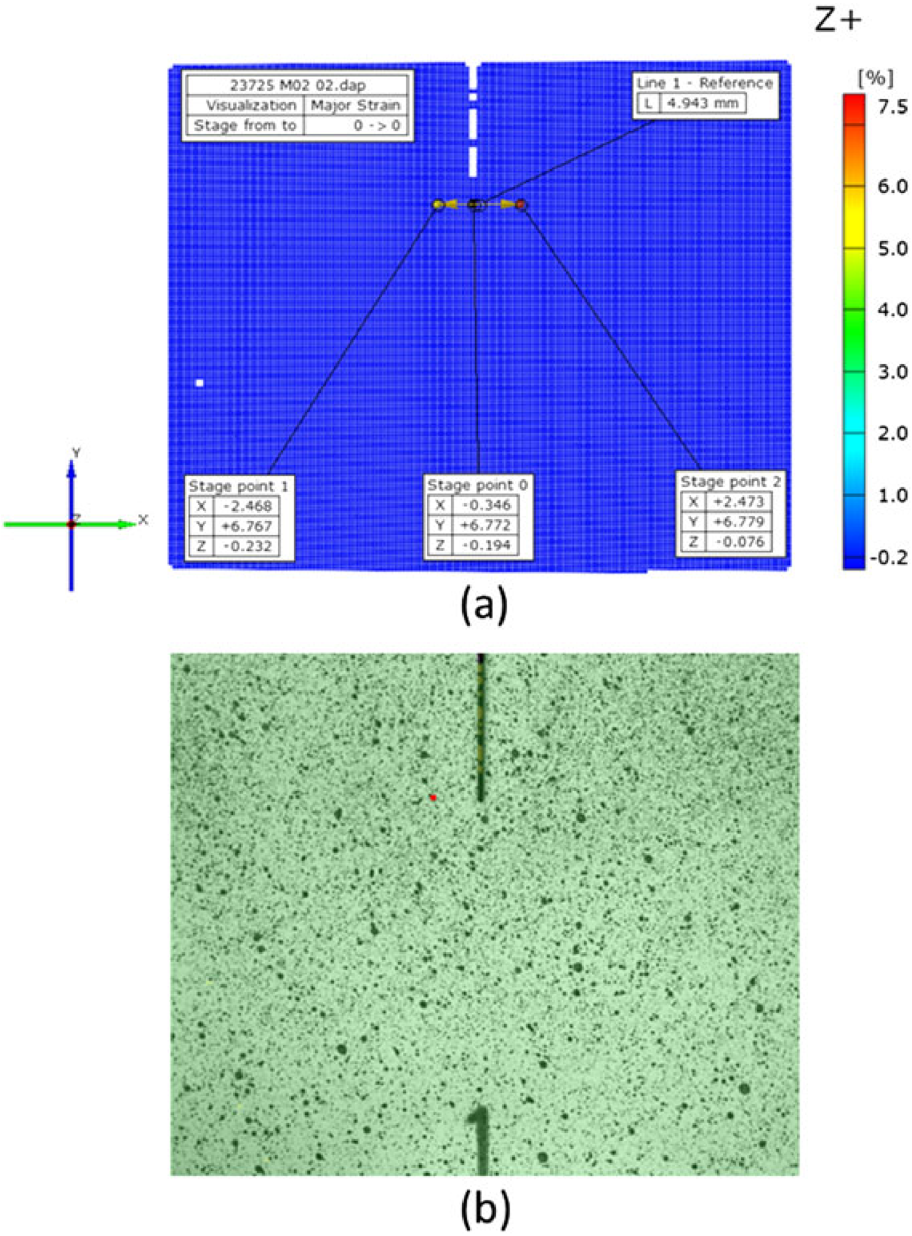

Fig. 3 Determination of (a) δ5 points based on (b) speckle pattern.

In order to compare experimental and FE results, the lower clip gauge opening is converted to CMOD using Equation (1), which is derived from ASTM E1290.[31]

$$CMOD = \frac{Vg}{1 + \frac{z}{0.8a_0 + 0.2W}} \tag{1}$$

Experimental CTOD measurements

Once removed, the silicone replicas were sliced at $b = -0.5$, 0 and 0.5, giving five sections across the replica (Fig. 6). CTOD was then measured on the sliced crack replicas using an optical microscope (Fig. 7). The values of CTOD obtained from the silicone replicas are plotted in Fig. 8 for increasing loads, represented by increasing CMOD.

The specimen was ductile and experienced large deformation in the test. A significant crack tip deformation before tearing, known as the stretch zone, was expected. However the stretch zone width was included in the measurement of original crack length, a_0, because of difficulties in isolating the start and end of the stretch zone width accurately under the microscope. Hence it might be expected that the CTOD measured on the silicone replicas could be fractionally smaller than the actual CTOD.

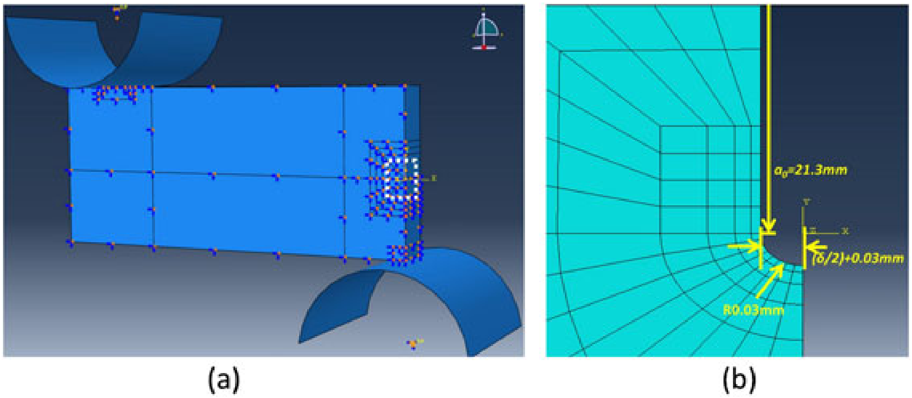

Fig. 4 Quarter SENB model showing boundary conditions, crack shape and mesh near the crack tip.

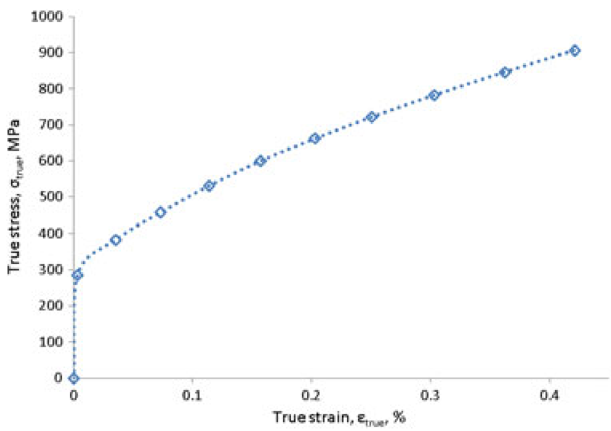

Fig. 5 True stress–strain properties used in the FE model.

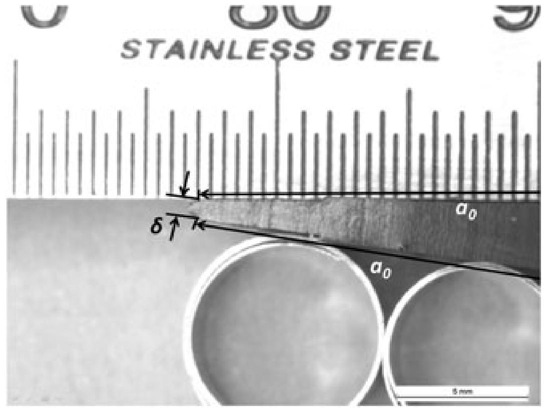

Fig. 7 Definition of CTOD measured on the silicone replica (CMOD = 2.771 mm, b = 0).

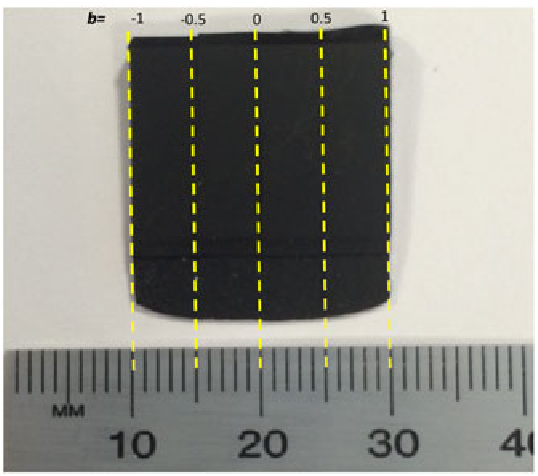

Fig. 6 Silicone crack replica from M03-05, taken at CMOD = 2.031 mm, showing the five equally spaced cross sections for CTOD measurement, described in terms of b, where b = 0 is the middle of the specimen.

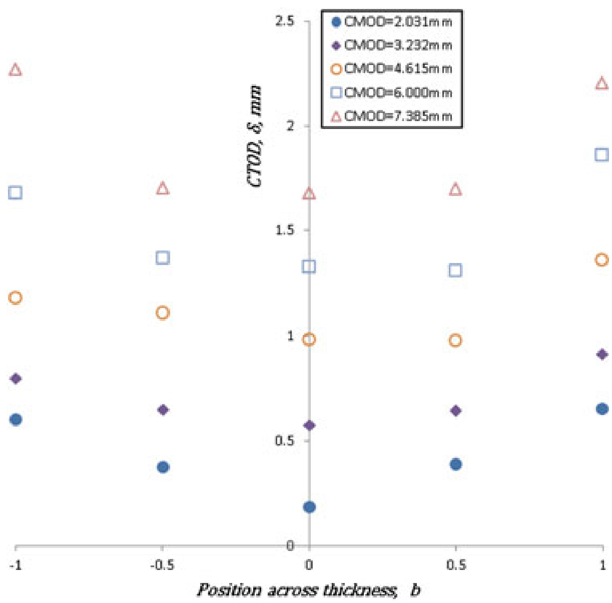

Fig. 8 CTOD at different position across thickness for different CMOD (selected points for clarity).

The load–displacement plot (Fig. 9) for the crack replication test shows load reductions at loads where the crack is replicated by insertion of silicone. This phenomenon is because of load relaxation when the specimen is held at constant displacement.[32] However this phenomenon does not appear to have any significant effect on the overall load–displacement plot and differences between this and a standard test, also shown in Fig. 9 are negligible. The non-linear nature of CMOD with increasing load can be observed.

DIC method for surface measurement

Seven specimens (M03-11 to M03-17) were tested in the SENB configuration. Compiling δ_{5DIC} measurements for each of the seven specimens at loads 10.0 kN, 15.0 kN, 20.0 kN, 25.0 kN and 27.5 kN, and comparing to the clip gauge readings taken at the same load, it was found (Fig. 10) that the $\delta_{5\ DIC}$ measurements were highly correlated to their equivalent clip gauge displacement data ($R^2 = 0.9970$).

Finite element CTOD measurements

The load–displacement relation obtained from the FE model is also shown in Fig. 9. From the FE model, CTOD was determined at three points across the section, $b = 0$ (centre), 0.5 and $b = 1$ (edge). Because of symmetry of the model, these points would also correspond to $b = 0$, -0.5 and -1 in a complete model. Figure 11 shows the relation between CTOD and CMOD, both determined from the FE model. Figure 9 has shown the close agreement between measured and FE modelled CMOD up to a value of about 5 mm; discrepancies that occur after 5 mm are discussed further below.

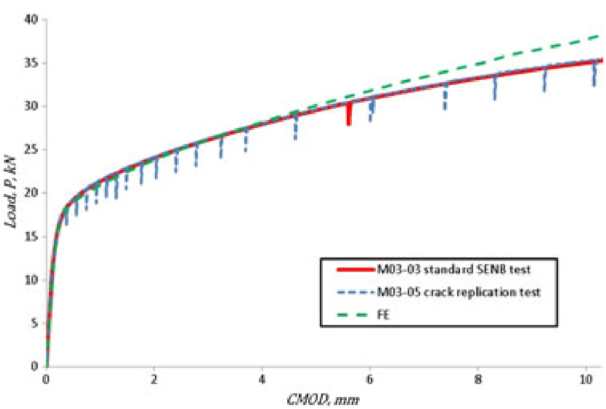

Fig. 9 Load–displacement data obtained from the experiment and FE model.

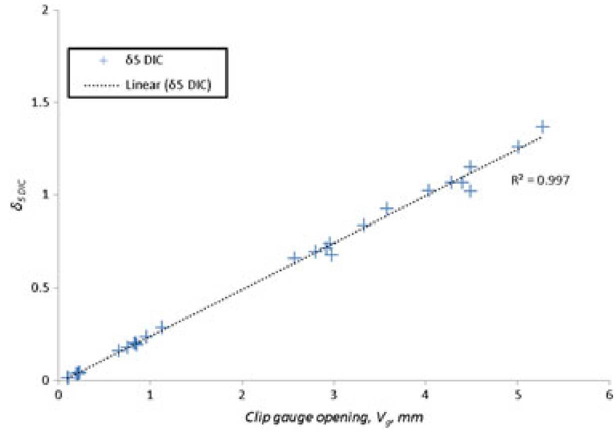

Fig. 10 Clip gauge opening versus δ5 measured on the SS316 SENB specimens tested using DIC.

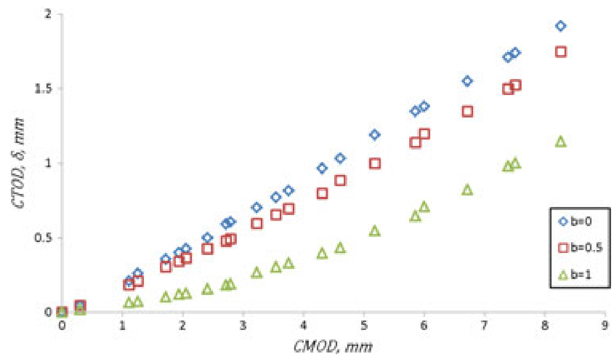

Fig. 11 CMOD versus CTOD at b = 0, 0.5 and 1 obtained from the FE model.

DISCUSSION

The CTOD estimation equations used in the standards (BS 7448-1, ISO 12135 and JWES) were based on research which did not cover material with high strain hardening properties.[33,34] Figure 12 shows CTOD measured from the SRC specimens at the centre ($b = 0$), and the average of the two edge values ($b = \pm 1$), plotted against the value measured using DIC for austenitic stainless steel. The measurements at the surface are both the same estimate of CTOD, and it can be seen that very good agreement is obtained using a linear relation[35] with $R^2 = 0.9974$. DIC measurements might be more conservative than the surface CTOD from SRC at large displacement. This is because the measurements are taken at an offset rather than directly at the crack tip (Fig. 13).[36] However, this not thought to be a problem here.

From Fig. 6 it can be seen that the line defining the crack tip front is curved. The straight crack front FE model (Fig. 11) shows that the CTOD is greater at the

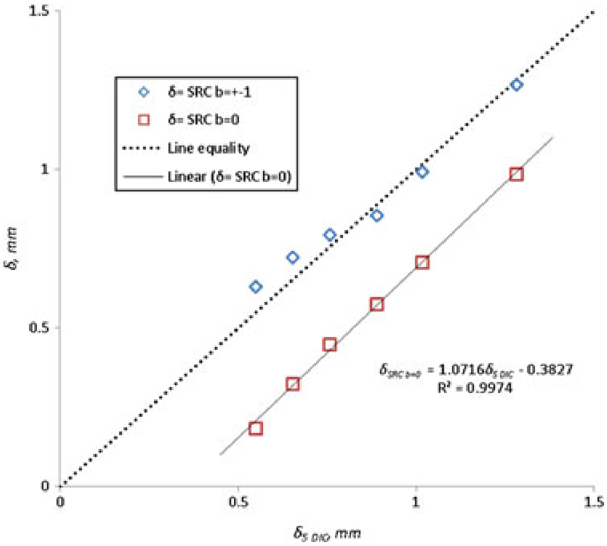

Fig. 12 Comparison between δ5 DIC, δ SRC (b = 0) (plane strain CTOD), and δ SRC (b = ±1) (surface CTOD).

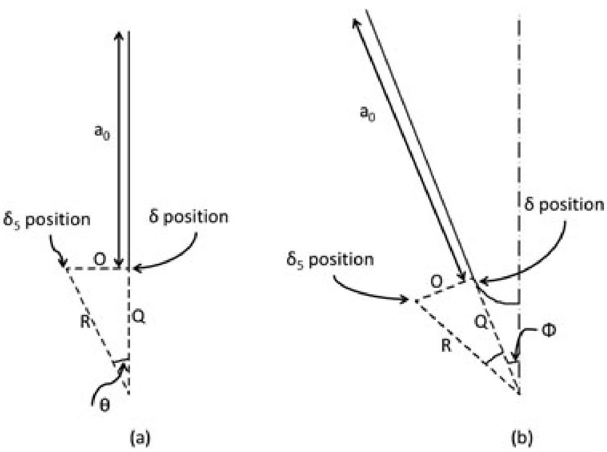

Fig. 13 Geometrical analysis of δ and δ5 on (a) an idealized initial crack and (b) an idealized blunted crack.

crack centre than at the outside surfaces but Fig. 12 shows that the value of δ_{SRC} at the sides is greater than that at the centre. However, from Fig. 14 it can be seen that the geometry and the assumption of a constant point of specimen rotation dictate otherwise, and the curved crack front means a lower value of δ_{SRC} is found at the centre.

A consistent relationship between $\delta_{5\ DIC}$ and $\delta_{SRC\ (b=0)}$ is observed (Fig. 12) for $\delta_{5\ DIC} > 0.5$ mm, indicating a little-changing difference between the crack width at the centre of the specimen and that at the outer edges. CTOD at the centre of the specimen is approximately 0.34 mm lower than at the surface CTOD for the crack front curvature present in this specimen. Equation (2) shows the relation of $\delta_{5\ DIC}$ to $\delta_{SRC\ (b=0)}$.

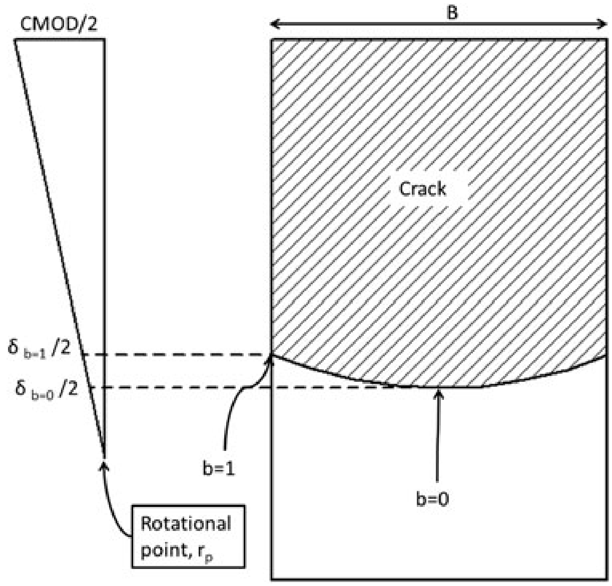

Fig. 14 The effect of curved crack front on the determination of CTOD at the middle and side of the specimen.

$$\delta_{SRC\ (b\ =\ 0)} = 1.0716\delta_{5\ DIC} - 0.3827 \quad (2)$$

The elastic CTOD equations in BS 7448-1, ASTM E1820 and in the JWES equation assume plane strain conditions for the estimation of CTOD. By investigating the strain data across the crack tip obtained from the FE model, it is found that conditions approximating plane strain are achieved across much of the thickness. CTOD at $b = 0$ is considered the ‘plane strain’ CTOD estimated by the standardized equations; this is discussed further later in the paper.

A straight crack front model was simulated in FE as an idealized test specimen. Pook has provided a useful retrospective[37] of the importance of 3-D effects on the crack front, and in particular, the importance of understanding the consequences of a curved crack front. A linear elastic analysis[38] shows similarities between the FE and stress intensity factor models.

The measured initial crack length of the sides of the specimen tested is shorter than the initial crack length on the middle of the specimen. This phenomenon is a result of the fatigue loading on the specimen, which is used to induce a crack. Figure 11 shows the CTOD obtained at different positions across the crack front, which shows an opposite trend when compared to the CTOD measured from the silicone replicas in Fig. 8. These findings are consistent with Hutchison & Pisarski’s[29] FE predictions, where straight crack front models give larger CTOD in the middle of the crack front while a curved crack front model gives larger CTOD in the sides of the crack. Analysing the effect of crack length using the similar triangles principle used in BS 7448-1, a lower a_0/W ratio (shorter crack length) would result in higher CTOD, as described above for the experimental results.

The CTOD obtained from FE and standardized estimation equations were compared to that measured on the silicone replica (Fig. 15). The FE model and BS 7448-1 overestimate the silicone replica CTOD for all values of CTOD, while ASTM E1820 and JWES overestimate low values of CTOD, but underestimate towards larger CTOD values. Experimentally, stable ductile tearing initiates under large deformation at the crack tip; in the FE model, the crack tip continues deforming under increasing load, as damage mechanisms and crack extension were not accounted for in the model. Figure 15 shows that the FE estimations become close to the SRC measurements at larger CTOD values ($\delta_{SRC\ (b=0)} > 1$ mm). The larger difference observed in lower CTOD values in the FE model is because of the blunted crack tip used which might result in an increase in CTOD when compared to a fatigue pre-cracked notch.[39]

If an underestimation of CTOD up to 15% is considered acceptable, both the JWES equation and ASTM E1820 estimation can be considered to be acceptable predictors of $\delta_{SRC(b=0)}$. Based on CTOD measured in the $\delta_{SRC\ (b=0)} > 1$ mm region, JWES gives a very good estimation of $\delta_{SRC\ (b=0)}$. In the range $\delta_{SRC\ (b=0)} > 0.5$ mm, ASTM E1820 gives a lower value of CTOD, but generally within the 15% limit. The overestimation of the lower values of CTOD is because of the underestimation of the physical CTOD, a result of the inclusion of stretch zone width in the determination of the original crack length, a_0,resulting in the overestimation being more obvious in the lower CTOD region, e.g. $\delta_{SRC\ (b=0)} <$ 0.5 mm. The results suggest that the JWES and ASTM

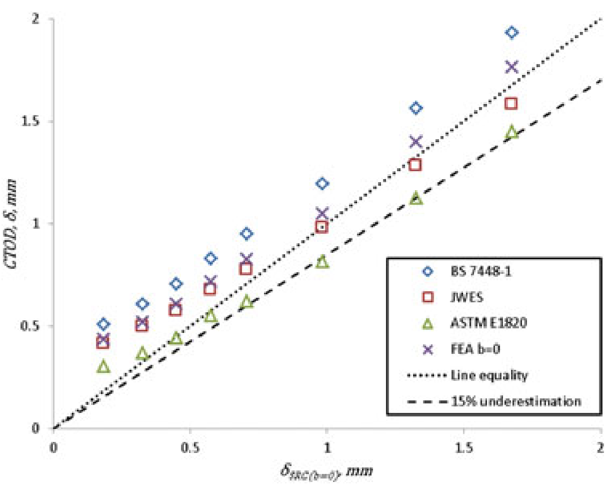

Fig. 15 Comparison of the silicone replica CTOD, δ SRC (b = 0) to FE CTOD, δ FE (b = 0) and standard CTOD estimations.

E1820 methods are better alternatives than BS 7448-1 to estimate CTOD in high strain hardening austenitic stainless steels.

Based on the results obtained from the silicone replicas and FE, it was found that the Japanese modification to the BS 7448-1 and ISO 12165 equation, and the ASTM E1820 estimation are both recommended for determining CTOD for austenitic stainless steel and high strain hardening materials. The JWES CTOD equation for SENB specimens is given by[18]

$$\delta = K^2 \frac{(1 - v^2)}{m\sigma_{ys}E} + f\left(B, \frac{\sigma_{ys}}{\sigma_{uts}}\right) \frac{0.43B_o V_p}{0.43B_o + a_0 + z}$$

where the correction factors are:

$$m = 4.9 - 3.5\left(\frac{\sigma_{ys}}{\sigma_{uts}}\right)$$

$$f(B) = 0.8 + 0.2exp\{-0.019(B - 25)\}$$

$$f\left(\frac{\sigma_{ys}}{\sigma_{uts}}\right) = -1.4\left(\frac{\sigma_{ys}}{\sigma_{uts}}\right)^2 + 2.8\frac{\sigma_{ys}}{\sigma_{uts}} - 0.35.$$

CONCLUSIONS

This paper has shown the measurement of CTOD using silicone replicas. δ_5 DIC measurements have been validated using the silicone replica CTOD data. An FE model has been used to generate predictions of the experimental data.

For austenitic stainless steel and high strain hardening materials, CTOD measured on the silicone replica suggest that JWES give good estimates of CTOD for $\delta_{SRC\ (b=0)} > 1$ mm. The ASTM E1820 estimation is an alternative for measuring $\delta_{SRC\ (b=0)} < 1$ mm.

For high strain hardening materials, direct measurement of δ_5 at the specimen surface using the DIC approach can estimate CTOD for 0.5 mm < $\delta_{5\ DIC}$ using Equation (2). This equation provides a good estimate of CTOD for research applications; however, the use of DIC would not necessarily be practical for commercial test houses.

Acknowledgements

The authors wish to acknowledge the funding and facility provided by TWI and NSIRC for this work. The authors also wish to thank Philip Cossey and Dan Bloom for assistance in the crack replication tests, Mark Tinkler for the setup of the DIC equipment and Prof. Tetsuya Tagawa for the updates and discussion on the silicone crack replication method.

REFERENCES

1 Shen, G., Gianetto, J. A., Bouchard, R., Bowker, J. T., and Tyson, W. R. (2004) Fracture toughness testing of pipeline girth welds. *International Pipeline Conference*. Minister of Natural Resources, Canada, Calgary.

2 Gordon, J. R., Keith, G. and Gordon, N. C. (2013) Defect and strain tolerance of girth welds in high strength pipelines. In: *International Seminar on Welding High Strength Pipeline Steels*, CBMM and TMS: USA, pp. 365–394.

3 Sarzosa, D. F. B., Souza, R. F. and Ruggieri, C. (2015) J–CTOD relations in clamped SE(T) fracture specimens including 3-D stationary and growth analysis. *Eng. Fract. Mech.*, **147**, 331–354.

4 BSI (2014) BS 7910:2013—guide to methods for assessing the acceptability of flaws in metallic structures. BSI.

5 API (2007) API 579—fitness-for-service.

6 Anderson, T. L. and Osage, D. A. (2000) API 579: a comprehensive fitness-for-service guide. *Int. J. Pres. Ves. Pip.*, **77**, 953–963.

7 Wells, A. A. (1969) Crack opening displacements from elastic–plastic analyses of externally notched tension bars. *Eng. Fract. Mech.*, **1**, 399–410.

8 Burdekin, F. M. and Stone, D. E. W. (1966) The crack opening displacement approach to fracture mechanics in yielding materials. *J. Strain. Anal. Eng. Des.*, **1**, 145–153.

9 BSI (1991) BS 7448-1:1991—Fracture mechanics toughness tests — Part 1: Method for determination of KIc, critical CTOD and critical J values of metallic materials. BSI.

10 ASTM (2014) ASTM E1820-13—standard measurement of fracture toughness. ASTM, 1–54.

11 ISO (2002) ISO 12135—02 metallic materials—unified method of test for the determination of quasistatic fracture toughness. ISO.

12 Kirk, M. T. and Dodds, R. H. Jr. (1993) J and CTOD estimation equations for shallow cracks in single edge notch bend specimens. *J. Test. Eval.*, **21**, 228–238.

13 Tagawa, T., Kawabata, T., Sakimoto, T., Kayamoi, Y., Ohata, M., Yamashita, Y., Tamura, E., Yoshinari, H., Aihara, S., Minami, F., Mimura, H. and Hagihara, Y. (2014) Experimental measurements of deformed crack tips in different yield-to-tensile ratio steels. *Eng. Fract. Mech.*, **128**, 157–170.

14 Shih, C. F. (1981) Relationships between the J-integral and the crack opening displacement for stationary and extending cracks. *J. Mech. Phys. Solids*, **29**, 305–326.

15 Kumar, V., German, M. D. and Shih, C. F. (1981) An Engineering Approach for Elastic–Plastic Fracture Analysis. *Electric Power Research Institute Report NP-1931*. General Electric Company, Palo Alto, California.

16 Zhu, X.-K. and Joyce, J. A. (2012) Review of fracture toughness (G, K, J, CTOD, CTOA) testing and standardization. *Eng. Fract. Mech.*, **85**, 1–46.

17 Rice, J. R. (1968) A path independent integral and the approximate analysis of strain concentration by notches and cracks. *J. Appl. Mech.*, **35**, 379–386.

18 Kawabata, T., Tagawa, T., Sakimoto, T., Kayamoi, Y., Ohata, M., Yamashita, Y., Tamura, E., Yoshinari, H., Aihara, S., Minami, F., Mimura, H. and Hagihara, Y. (2016) Proposal for a new CTOD calculation formula. *Eng. Fract. Mech.*, **159**, 16–34.

19 Ebara, R. (2002) Long-term corrosion fatigue behaviour of structural materials. *Fatigue Fract. Eng. Mater. Struct.*, **25**, 855–859.

20 Spindler, M. W. (2004) The multiaxial creep ductility of austenitic stainless steels. *Fatigue Fract. Eng. Mater. Struct.*, **27**, 273–281.

21 Colin, J. and Fatemi, A. (2010) Variable amplitude cyclic deformation and fatigue behaviour of stainless steel 304 L including step, periodic, and random loadings. *Fatigue Fract. Eng. Mater. Struct.*, **33**, 205–220.

22 Rahimi, S. and Marrow, T. J. (2012) Effects of orientation, stress and exposure time on short intergranular stress corrosion crack behaviour in sensitised type 304 austenitic stainless steel. *Fatigue Fract. Eng. Mater. Struct.*, **35**, 359–373.

23 ASTM (2006) ASTM A276-06—standard specification for stainless steel bars and shapes. ASTM, 1–7.

24 Wang, Y.-Y., Reemsnyder, H. S., and Kirk, M. T. (1997) Inference equations for fracture toughness testing: numerical analysis and experimental verification. *ASTM STP 1321*. 469–484.

25 Schwalbe, K.-H. (1995) Introduction of δ_5 as an operational definition of the CTOD and its practical use. *ASTM STP 1256*. 763–778.

26 Ipina, J. E. P. (1997) CTOD with slow stable crack growth: analysis of the elastic component. *Fatigue Fract. Eng. Mater. Struct.*, **20**, 1075–1082.

27 Ktari, A., Baccar, M., Shah, M., Haddar, N., Ayedi, H. F. and Rezai-Aria, F. (2014) A crack propagation criterion based on ΔCTOD measured with 2D-digital image correlation technique. *Fatigue Fract. Eng. Mater. Struct.*, **37**, 682–694.

28 Tagawa, T., Kawabata, T., Sakimoto, T., Kayamoi, Y., Ohata, M., Yamashita, T., Tamura, E., Yoshinari, H., Aihara, S., Minami, F., Mimura, H. and Hagihara, Y. (2014) A new CTOD calculation formula, considering strain-hardening property. *Procedia Mate. Sci.*, **3**, 772–777.

29 Hutchison, E., and Pisarski, H. G. (2013) Effects of crack front curvature on J and CTOD determination in fracture toughness specimens by FEA. *Proceedings of the ASME 2013 32nd International Conference on Ocean, Offshore and Arctic Engineering OMAE 2013*, Nantes, France.

30 Hutchison, E., London, T. (2015) Simulation of stable ductile tearing using re-mesh techniques coupled with nodal release incorporating constraint. *NAFEMS World Congress 2015*, San Diego, USA.

31 ASTM (2008) ASTM E 1290-08—standard test method for crack-tip opening displacement (CTOD) fracture toughness measurement. ASTM, 1–15.

32 Tagawa, T., Haramishi, Y. and Minami, F. (2011) Stress relaxation behavior of low carbon structural steels. *Q. J. Jpn. Weld. Soc.*, **29**, 48–54.

33 Lin, I. H., Anderson, T. L., Derit, R., Dawes, M. G., DeWit, R. and Dawes, M. G. (1982) Displacements and rotational factors in single edge notched bend specimens. *Int. J. Fract.*, **20**, R3–R7.

34 Wu, S.-X. (1983) Plastic rotational factor and J-COD relationship of three point bend specimen. *Eng. Fract. Mech.*, **18**, 83–95.

35 Microsoft (2010) Microsoft Excel.

36 Verstraete, M. A., Denys, R. M., Van Minnebruggen, K., Hertelé, S. and De Waele, W. (2013) Determination of CTOD resistance curves in side-grooved Single-Edge Notched Tensile specimens using full field deformation measurements. *Eng. Fract. Mech.*, **110**, 12–22.

37 Pook, L. P. (2013) A 50-year retrospective review of three-dimensional effects at cracks and sharp notches. *Fatigue Fract. Eng. Mater. Struct.*, **36**, 699–723.

38 Pook, L. P. (2000) Finite element analysis of corner point displacements and stress intensity factors for narrow notches in square sheets and plates. *Fatigue Fract. Eng. Mater. Struct.*, **23**, 979–992.

39 Spink, G. M., Worthington, P. J. and Heald, P. T. (1973) The effect of notch acuity on fracture toughness testing. *Mater. Sci. Eng.*, **11**, 113–117.

Received: 12 January 2017 | Revised: 21 August 2017 | Accepted: 24 August 2017

DOI: 10.1111/ffe.12718

ORIGINAL CONTRIBUTION

WILEY

Comparison of methods to determine CTOD for SENB specimens in different strain hardening steels

W.L. Khor[1,2] | P. Moore[3] | H. Pisarski[3] | C. Brown[1]

[1] Brunel University London, Uxbridge UB8 3PH, UK

[2] NSIRC, Granta Park, Cambridge CB21 6AL, UK

[3] TWI, Granta Park, Cambridge CB21 6AL, UK

Correspondence
Wee Liam Khor, Brunel University London, Uxbridge, UB8 3PH, UK.
Email: weeliam.khor@gmail.com

Abstract

Methods for determining crack tip opening displacement (CTOD) given in national and international standards are compared for steels with a range of strain hardening characteristics.

Crack tip opening displacement measurements were made from single-edge notched bend notches using a silicone rubber casting method. The finite element model produced good agreements with predictions of these CTOD measurements. The versatility of the finite element model enabled CTOD from the original crack tip and the 45° intercept method to be compared. The 45° CTOD generally underestimates the original crack tip CTOD, and is less useful for conditions with stable crack extension.

Apart from the high strain hardening material, CTOD calculated using BS 7448-1, WES 1108 (JWES), and ASTM E1820 was slightly lower than the values determined from silicone measurements and modelling, which is conservative. ASTM E1820 gave the largest underestimation of CTOD, whilst BS 7448-1 may be unsuitable for higher strain hardening steels, where the standard predicts higher CTOD than measured from the replica. JWES gives the most consistent estimation of CTOD for steels with a wide range of strain hardening values.

KEYWORDS

ASTM E1820, BS 7448-1, CTOD, strain hardening, WES 1108

Nomenclature: A_p, Plastic work, area under P vs V_p, Nmm; a_0, Original crack length, mm; a_0/W, Crack length- specimen width ratio; B, Specimen thickness, mm; B_0, Remaining ligament ahead of the crack tip, W-a_0, mm; B_N, Net specimen thickness in the remaining ligament ahead of the crack tip, mm; CMOD, Crack mouth opening displacement, mm; E, Modulus of elasticity, MPa; FE, Finite element; J, Path independent strain energy around the crack, also called J-integral, Nmm^{-1}; K, Stress intensity factor, Nmm$^{-3/2}$; m, Factor relating CTOD to J or K (sometimes referred to as a "constraint" factor); SENB, Single-edge notched bend; V_p, Plastic component of the clip gauge opening displacement, mm; W, Specimen width, mm; z, Vertical height above the crack mouth where displacement is measured, mm; δ, Crack tip opening displacement, CTOD, mm; δ_0, CTOD based on the opening of the original crack tip, mm; δ_{45}, CTOD measured based on the 45° intercept from the blunted crack tip in FE, mm; δ_{el}, Elastic component of CTOD, mm; δ_{FE}, CTOD measured from the middle thickness of the FE model based on the opening of the original crack tip, mm; $\delta_{FE\ corr}$, δ_{FE} with applied correction factor validated to experimental results, mm; δ_{pl}, Plastic component of CTOD, mm; δ_{SRC}, CTOD measured from the middle thickness of the silicone replica based on the original crack tip, mm; σ_{uts}, Ultimate tensile stress, MPa; σ_y, "Flow" stress defined in ASTM E1820, $(\sigma_{ys} + \sigma_{uts})/2$, MPa; σ_{ys}, 0.2% yield/ proof stress, MPa; σ_{ys}/σ_{uts}, Tensile ratio; η_{pl}, Geometrical based calibration factor for J; ν, Poisson's ratio

1 | INTRODUCTION

Crack tip opening displacement (or CTOD) has been the most widely used fracture toughness parameter within the oil and gas industry for nearly 50 years. Originally developed from research at TWI in the UK during the 1960s,[1] CTOD is a versatile fracture parameter for both ductile and brittle materials, making it suitable for characterising the fracture toughness of medium strength carbon manganese steels commonly used in applications such as pressure vessels, offshore platforms, and pipelines where the application of linear elastic fracture mechanics was insufficient to account for their ductility. Today, CTOD is used to define the fracture toughness for a wide range of engineering alloys.

Crack tip opening displacement as a material toughness parameter is defined as the opening of the crack tip in a standard fracture toughness specimen at the point of maximum load, initiation for stable crack extension, or unstable crack extension. Crack tip opening displacement is typically determined using load and displacement data obtained from testing deeply-notched fracture toughness specimens, often single-edge notched bend (SENB) specimens.

Fracture toughness testing became standardised in the 1970s and is currently represented in a number of standards including BS 7448, ISO 12135, ASTM E1820, and WES1108.[2-5] Different assumptions about the determination of CTOD are used in each, which can give different values of CTOD. Ideally, all standards would give methods, which result in the same accurate value of CTOD being determined. However, in practise, they each have different levels of conservatism to ensure CTOD is not overestimated. The challenge is to define the value of CTOD with accuracy, particularly when CTOD is being used as an acceptance criterion in material characterisation. However, overestimating CTOD when using the results to determine tolerable flaw sizes for the assessment of the structural integrity might lead to potentially unsafe structures being assessed as fit-for-service.

2 | CTOD FORMULAE IN FRACTURE TOUGHNESS TESTING STANDARDS

All the current standards agree that CTOD (or δ) should be determined by the addition of 2 components; the elastic CTOD, δ_{el}, and the plastic CTOD, δ_{pl}.[6]

$$\delta = \delta_{el} + \delta_{pl}. \tag{1}$$

BS 7448-1 and ISO 12135 use the same equation for the determination of CTOD. The elastic component is determined from the stress intensity factor, K, while the plastic component assumes a fixed plastic hinge in the ligament of the specimen ahead of the notch and is calculated from the displacement measured from a clip gauge, V_p, fixed to the specimen at a knife edge height, z, using the similar triangles method. The equation is given as[2,3]

$$\delta = K^2\frac{(1-\nu^2)}{2\sigma_{ys}E} + \frac{0.4B_oV_p}{0.4W + 0.6a_0 + z}. \tag{2}$$

Based on Lin[7] and Ingham's[8] findings, the rotational factor is taken to be 0.4, ie, the specimen rotates about a fixed point ahead of the crack at a distance of 0.4 of the remaining ligament. The BSI/ISO formula does not make any allowance for the strain hardening of the material, and despite having been well validated for medium and high strength steels,[9,10] the formula is less accurate for other materials with a lower yield to tensile ratio.[11]

ASTM E1820 uses a different approach for the determination of CTOD, where J is first calculated (by the summation of the elastic and plastic components) and then converted to CTOD using an "m" factor, which includes the material yield and tensile properties in its calculation.[4] The determination of J is originally from numerical modelling, and the subsequent definition of CTOD based on the 45° intercept method was derived using the HRR field.[12]

$$\delta = \frac{J}{m\sigma_y}, \tag{3a}$$

where $m = A_0 - A_1(\sigma_{ys}/\sigma_{uts}) + A_2(\sigma_{ys}/\sigma_{uts})^2 - A_3(\sigma_{ys}/\sigma_{uts})^3$

$$A_0 = 3.18 - 0.22(a_0/W)$$
$$A_1 = 4.32 - 2.23(a_0/W)$$
$$A_2 = 4.44 - 2.29(a_0/W)$$
$$A_3 = 2.05 - 1.06(a_0/W)$$

$$J = \frac{K^2(1-\nu^2)}{E} + \frac{\eta_{pl}A_p}{B_NB_o}, \tag{3b}$$

where $\eta_{pl} = 3.667 - 2.199(a_0/W) + 0.437(a_0/W)^2$.

As a consequence of these different approaches to the definition of CTOD, the ASTM method to determine CTOD is known to underestimate CTOD significantly for many higher strength steels in comparison to the BSI/ISO method.[13-16] In response to the need for an accurate method to determine CTOD, which also accounts for the materials strain hardening behaviour, the Japanese Welding Engineering Society, JWES, have developed a

CTOD equation, based on the BSI/ISO approach but with a modified rotational factor and strain hardening factors calibrated using FE modelling and experiments.[17] This equation is now being adopted by the Japanese national fracture toughness testing standard, WES1108 "Standard test method for crack-tip opening displacement (CTOD) fracture toughness measurement."[5]

$$\delta = K^2 \frac{(1-\nu^2)}{m_{JWES}\sigma_{ys}E} + f_p \frac{0.43B_o V_p}{0.43B_o + a_0}, \tag{4}$$

where $m_{JWES} = 4.9 - 3.5(\sigma_{ys}/\sigma_{uts})$

$$f_p = f(B) \times f(\sigma_{ys}/\sigma_{uts})$$
$$f(B) = 0.8 + 0.2 \exp\{-0.019\ (B - 25)\}$$
$$f(\sigma_{ys}/\sigma_{uts}) = -1.4(\sigma_{ys}/\sigma_{uts})^2 + 2.8(\sigma_{ys}/\sigma_{uts}) - 0.35.$$

This new equation has been developed for the avoidance of brittle fracture in steels for CTOD values up to 0.2 mm. For the equation to be incorporated more widely into international standards, further evaluation over a larger range of CTOD is needed. Hereafter, the BS 7448-1/ISO 12135, ASTM E1820, and WES 1108 are described as BS/ISO, ASTM, and JWES.

To illustrate the difference in CTOD that can be obtained from the different standards, the results from a total of 137 SENB historical fracture toughness tests in steel materials were compiled from TWI's archive of test data and evaluated to BS/ISO, to ASTM and to the JWES method (Table 1). The data were based on tests within the temperature range of −100°C to +290°C and specimen thickness in the range of 4.7 mm to 58.6 mm, all with nominal crack ratio of $a_0/W = 0.5$.

The elastic, plastic, and total CTOD calculated to the equations were normalised to the respective BS/ISO CTOD components, $\delta_{el}/\delta_{el\ BS/ISO}$, $\delta_{pl}/\delta_{pl\ BS/ISO}$, and $\delta/\delta_{BS/ISO}$ (Figure 1). The BS/ISO CTOD was used as comparison as it is most established, and the differences from ASTM and JWES could be highlighted easily.

The BS/ISO equation does not consider the effects of strain hardening. In the elastic CTOD comparison, it is shown that the ASTM and JWES equations gave very similar estimations (Figure 1A). At high yield to tensile ratio (σ_{ys}/σ_{uts}), the ASTM and JWES gave higher elastic CTOD compared to BS/ISO and lower elastic CTOD for tensile ratio below 0.84.

In the comparison of the plastic component of CTOD, the ASTM data are scattered and do not show any trend relative to BS/ISO with tensile properties, but are always lower than the BS/ISO plastic component of CTOD. The JWES plastic CTOD equation is based on the BS/ISO modified for strain hardening and specimen thickness correction. The JWES gives larger plastic CTOD for material with higher yield to tensile ratios.

For the total CTOD determined based on the addition of the elastic and plastic CTOD, JWES and ASTM showed a

TABLE 1 Compilation of TWI crack tip opening displacement (CTOD) data calculated to BS/ISO, JWES, and ASTM

Material	Specimen Thickness, mm	Test Temperature, °C	Yield/ 0.2% Proof Strength, MPa	Tensile Ratio	BS 7448–1/ ISO 12135 CTOD, mm	WES 1108 CTOD, mm	ASTM E1820 CTOD, mm
18MND5 (A533B)	24.9-25.1	−100	651	0.89	0.01 to 0.07	0.01 to 0.08	0.01 to 0.06
9%Cr-1%Mo	4.7	7	520	0.75	0.25 to 0.34	0.36 to 0.50	0.14 to 0.20
ABS AH 36	20.0-58.6	70 to −10	341 to 443	0.62 to 0.72	0.02 to 2.25	0.02 to 2.04	0.01 to 1.62
ABS AH/DH/EH 32	15.5-43.7	−10	317 to 402	0.67 to 0.73	0.24 to 1.89	0.28 to 1.78	0.14 to 1.64
API X-grade	8.0-30.0	−20 to 22	349 to 540	0.5 to 0.86	0.01 to 1.11	0.00 to 1.34	0.00 to 1.10
ASTM A105/A106	23.0-23.1	0 to 290	216 to 339	0.46 to 0.60	0.05 to 0.72	0.04 to 0.59	0.03 to 0.49
ASTM A131 grade E	20.0-28.0	−10	312 to 358	0.63 to 0.66	0.60 to 1.12	0.64 to 1.13	0.43 to 0.88
BS 7191 grade 355E	45.2-25.3	−10	377	0.70	1.82 to 2.22	1.75 to 2.14	1.42 to 1.79
Duplex SS	25.0-35.1	−50 to −3	543 to 625	0.74 to 0.76	0.08 to 0.95	0.07 to 1.09	0.06 to 0.80
Grade 12.9 bolt	27.0-27.2	0 to 100	1205 to 1231	0.90	0.01 to 0.04	0.01 to 0.04	0.01 to 0.02
GS-13 MnNi 64	45.0-45.1	−10	327	0.65	1.41 to 1.76	1.28 to 1.60	0.99 to 1.30
INCOLOY 800	5.7	20 to 22	381	0.52	0.95 to 0.98	1.01 to 1.06	0.48 to 0.50
Macalloy	10.0	−20 to 30	950 to 963	0.86	0.00 to 0.01	0.01 to 0.01	0.00 to 0.00
Super duplex SS	28.0-53.1	−46 to 20	576 to 660	0.71 to 0.77	0.08 to 0.75	0.08 to 0.78	0.06 to 0.61

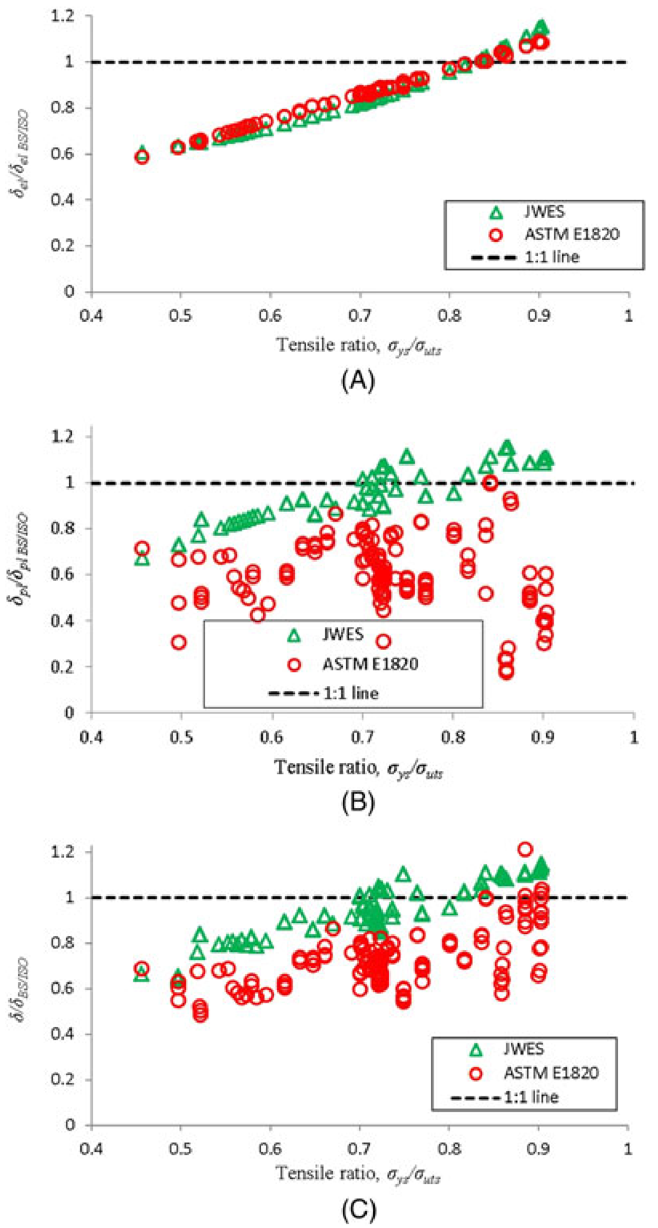

FIGURE 1 Compilation of historic TWI crack tip opening displacement (CTOD) data calculated using different methods, plotted normalised to the elastic CTOD (A), plastic CTOD (B), and total CTOD (C) determined from BSI/ISO [Colour figure can be viewed at wileyonlinelibrary.com]

trend due to strain hardening, more scatter with the latter. Both JWES and ASTM showed increasing estimation of CTOD relative to BS/ISO for the increase of tensile ratio.

The ASTM method almost always underestimates the values of CTOD obtained using the methods in BSI/ISO, apart from some several low strain hardening cases. This trend had been observed and noted by several research findings.[13-16]

To determine which method gives the most consistent accuracy for different strain hardening steels without overestimating the value of CTOD, these 3 formulae were compared to the value of CTOD measured from the actual displacement at the crack tip. This was determined from sectioning cast silicone replicas of the original crack and measuring the CTOD. A numerical model provided further comparison.

3 | SILICONE CRACK REPLICATION FROM SENB SPECIMENS

Three different steels were chosen for the experimental work to cover a range of strain hardening behaviour (Figure 2):

- M01 was a grade SA-543-GrB-Cl1 high strength steel with yield strength of 850 MPa. It had low strain hardening with a tensile ratio of 0.93.
- M02 was a grade S355J2 structural steel with yield strength of 421 MPa. It had medium strain hardening with a tensile ratio of 0.72.
- M03 was grade SS316 austenitic stainless steels. Its yield strength was 286 MPa and had high strain hardening with a tensile ratio of 0.48.

Single-edge notched bend specimens of cross-section 20 mm × 40 mm were machined from the steel plates, notched, and fatigue pre-cracked to give a nominal a_0/W ratio of 0.5. One specimen from each material was tested in a standard way to BS 7448-1, and the load versus clip gauge displacement data was plotted. For subsequent specimens, the test procedure was modified to allow for the crack casting process. Initially, the specimens were loaded in the same manner as the standard test. At selected displacement points based on the clip gauge opening, the machine loading was paused, and the specimens were held in displacement control. While held, the clip gauge data logging was paused and the clip gauges

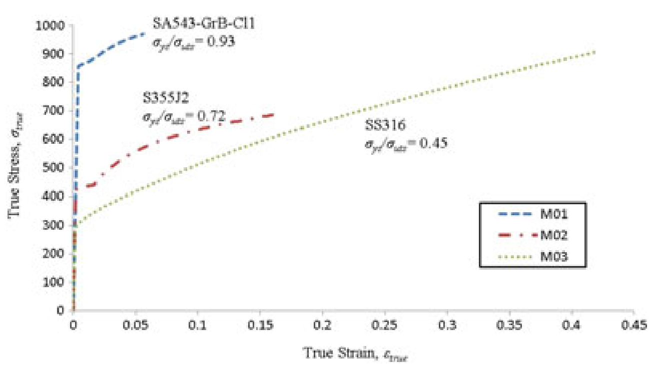

FIGURE 2 True stress-strain properties of the low, medium and high strain hardening material [Colour figure can be viewed at wileyonlinelibrary.com]

removed. The sides of the crack were sealed using tape, while a tiny "exhaust" hole was made at the crack tip, which allowed air to vent. The silicone compound was slowly injected into the crack from one side of the specimen, allowing the silicone compound to completely fill the void. A syringe was used to induce vacuum on the "exhaust' holes, removing a minimal amount of silicone compound along with any air bubbles near the sides of the crack tip (Figure 3). The crack was fully filled with the silicone compound and left to cure. After 5 minutes curing time, the clip gauges were replaced, and the displacement logging was resumed. The specimen was loaded to the next specified displacement, and then held in displacement control. The replica was removed, and the procedure was repeated casting a new crack replica. Typically, around 10 replicas were cast at different displacement levels for each test. The overall load-crack mouth opening displacement (CMOD) traces from these paused tests were plotted against the standard results to demonstrate that the replicas were representative of standard test behaviour (Figure 4). The overall match was good, but small load drops could be seen at the points where replicas were taken as the specimen relaxed slightly when held in displacement control.[18] The specimen descriptions were shown in Table 2.

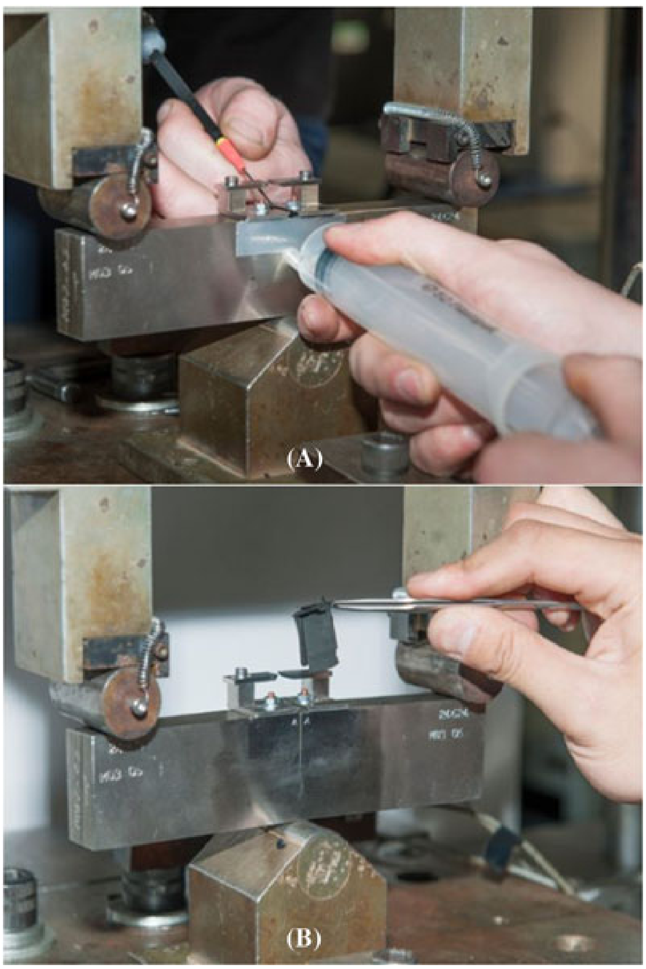

FIGURE 3 The silicone replication process with the injection of the silicone (A) and the extraction of the cured replica (B) (courtesy of TWI Ltd) [Colour figure can be viewed at wileyonlinelibrary.com]

4 | PHYSICAL MEASUREMENTS OF CTOD

Crack tip opening displacement values obtained from the silicone replica cast (SRC) tests were treated as the baseline for comparison to other methods. The location of the initial fatigue crack tip was identified as the initial crack length, and the width of the silicone replica at that point was measured to give the value of CTOD from the replica. Replicas from M03 were sliced at mid and quarter thickness into 4 equal portions and measured for CTOD at each cut location and the outer surfaces. It was found that the CTOD in the middle of the specimen gave similar values compared to that averaged between the 5measured points across the crack front. Therefore, the other replicas were sectioned in the middle for determination of CTOD. The silicone casting beyond the original fatigue crack tip shows where stable ductile crack extension has occurred (Figure 5). The measurements taken from the middle of the SRCs were compared to the instantaneous values of CTOD that were determined using different standards and from numerical model predictions.

5 | FINITE ELEMENT MODELLING METHODS

A geometrically and materially non-linear analysis finite element (FE) model was used to predict CTOD in SENB

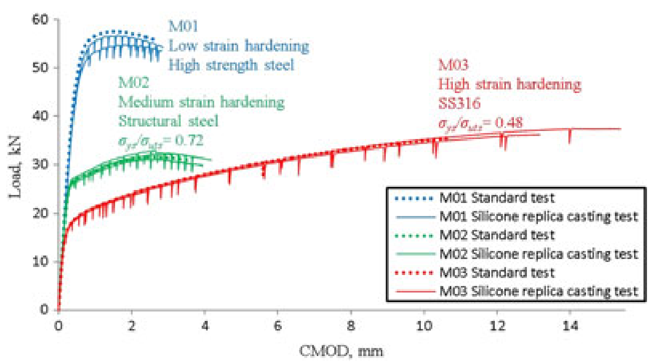

FIGURE 4 Load–crack mouth opening displacement (CMOD) traces from standard single-edge notched bend tests (dotted line) and from tests held for intermittent replication of the notch cavity, in 3 different steels [Colour figure can be viewed at wileyonlinelibrary.com]

TABLE 2 Specimen numbering and description

Specimen Number	Description	Set-up
M01-06		
M02-03	Standard single point SENB test	
M03-03		
M01-05		
M01-07		
M02-05		Nominally 20 mm × 40 mm B × 2B SENB specimen
M02-07	Interrupted SENB test with silicone crack replication	
M02-08		
M02-09		
M03-05		
M03-06		

Abbreviation: SENB, single-edge notched bend.

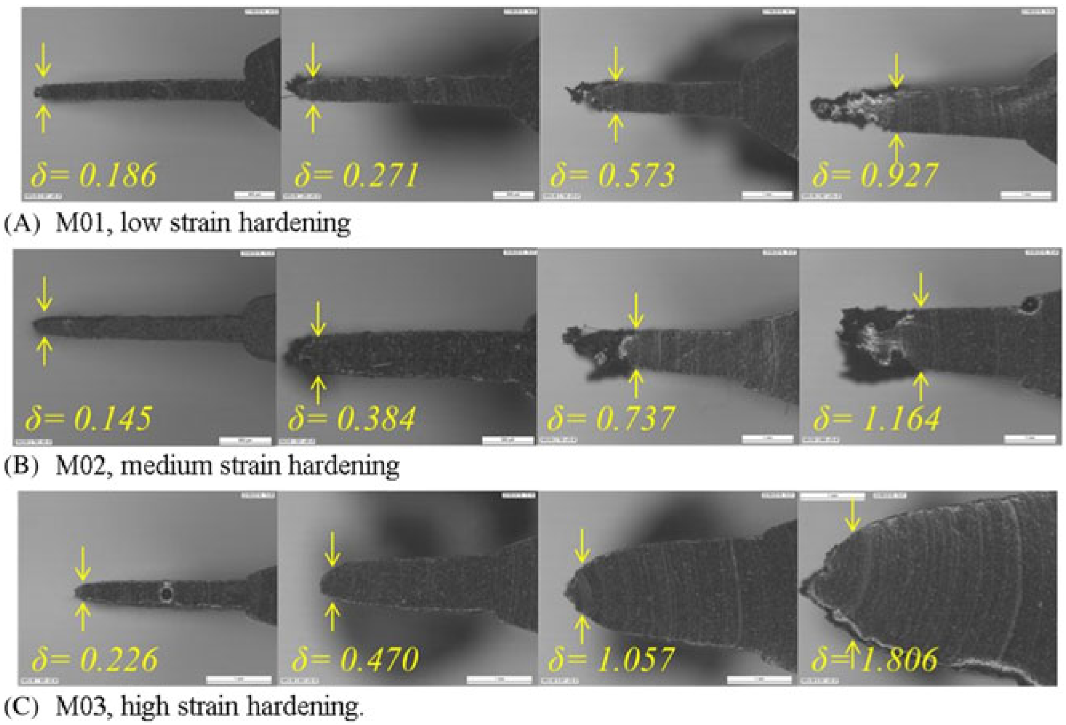

FIGURE 5 Sections through silicone replica casting taken at incremental stages through a fracture toughness test, for 3 different strain hardening materials (courtesy of TWI Ltd) [Colour figure can be viewed at wileyonlinelibrary.com]

specimens with the same geometry and material properties as the experimental tests. Fully 3-dimensional quarter SENB models were simulated using commercially available software (ABAQUS v6.14). Figure 6A shows the meshing of the model. Twenty-noded quadratic brick elements (C3D20R) were used in the models. Symmetry was defined on the marked surfaces to simulate a full specimen. Figure 6B shows an expended view of the crack tip region, where a blunted cracks tip of 0.03-mm radius was applied. The blunted crack tip is an artefact of the model to allow better deformation of the crack tip at larger deformation levels, rather than theoretically accurate prediction of the small-scale yielding, elastic dominated region using a sharp crack tip.[19,20] The roller ahead of the crack tip was fixed, whereas the displacement was set in the negative y-direction for the roller on the top of the model to simulate 3-point bending.

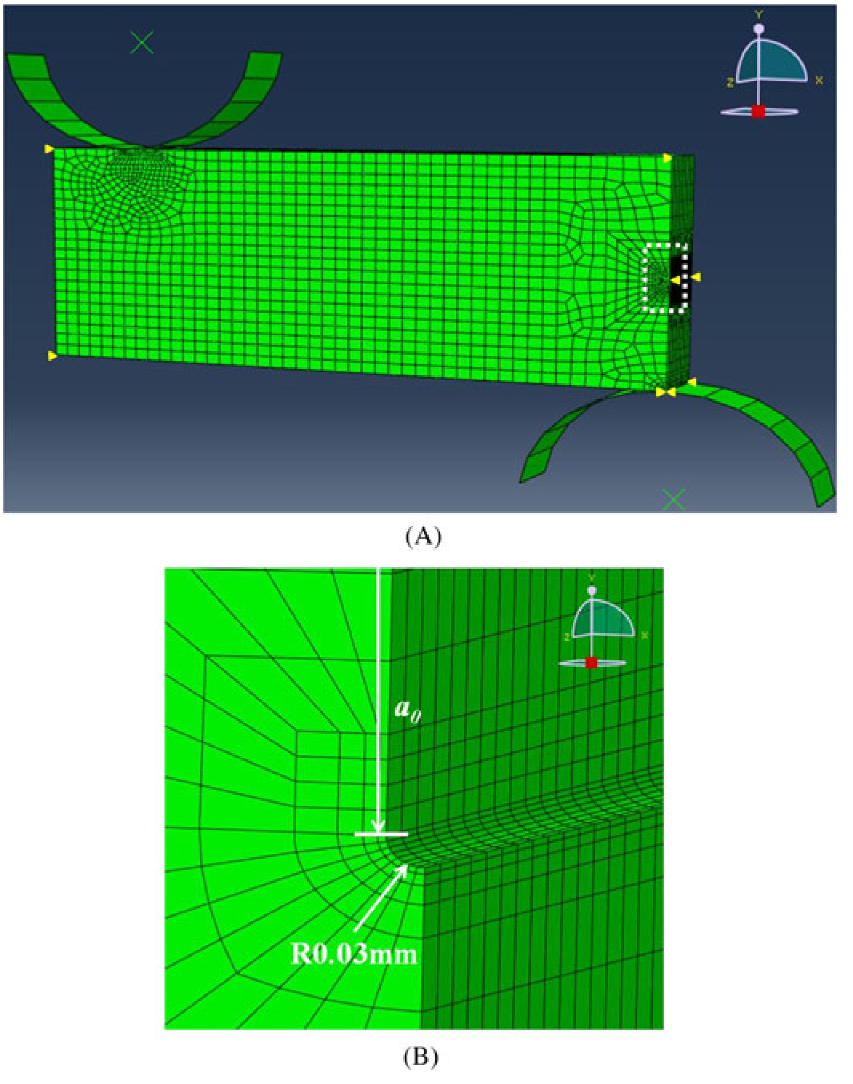

FIGURE 6 Quarter single-edge notched bend model showing mesh and boundary conditions (A), and expanded view of the crack tip region (B) [Colour figure can be viewed at wileyonlinelibrary.com]

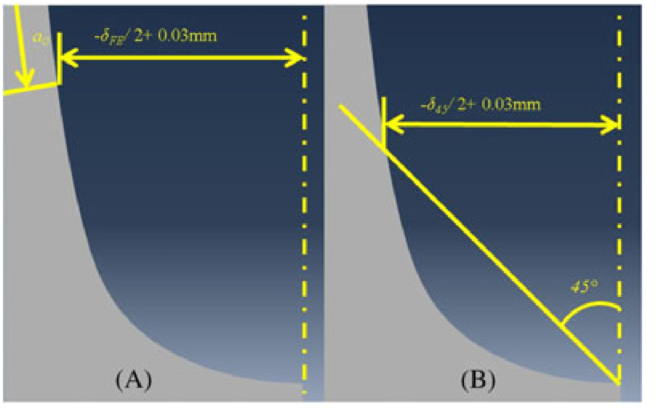

FIGURE 7 Definition of crack tip opening displacement from the numerical model, based on (A) the displacement at the tip of the original crack, δ_{FE} and (B) the 45° intercept method, δ_{45}, adjusted for the 0.03 mm crack radius used in the models [Colour figure can be viewed at wileyonlinelibrary.com]

The experimentally determined tensile properties were used as the basis for the true stress-strain behaviour for post-elastic material definition. A standard convergence test was performed based on varying the element size distributed across the crack tip when the models were set up. Crack tip opening displacement was determined from the numerical model based on both the opening of the original crack tip (Figure 7A), which is the traditional concept of CTOD and equivalent to the replica measurement, and the opening of the 45° angle from the blunted crack tip (Figure 7B).

The numerical models were generated based on geometry and material properties of specimens M01-05, M02-05, and M03-05, representing low, medium, and high strain hardening, respectively. The load-displacement data obtained from the numerical models were compared to those obtained experimentally to validate the model (Figure 8).

The FE data were consistent with the experimental data for the elastic loading region, but overestimate the loads in the plastic loading region, particularly for the low and medium strain hardening materials. This is due to assumptions about the crack tip deformation made in

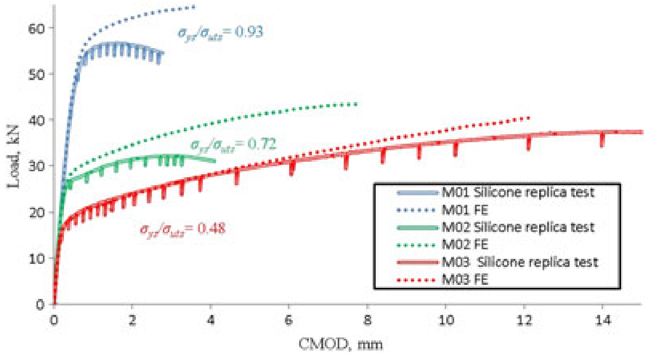

FIGURE 8 Load–crack mouth opening displacement (CMOD) curves generated experimentally, and from finite element (FE) representing M01, M02, and M03 [Colour figure can be viewed at wileyonlinelibrary.com]

the FE model, which allows the elements to deform in a manner where the crack continually "blunts" as loading is increased. However, in these steels, after a period of initial blunting, stable ductile crack extension, often described as "tearing," takes place under increasing load (see Figure 5). These numerical models do not account for tearing in the prediction of CTOD. Instead, the cross section of the remaining ligament directly ahead of the crack tip deforms and moves in the direction away from the crack tip, rather than crack propagation. This is the cause of the significantly larger loads predicted in the FE model at higher crack mouth displacement. However, this modelling assumption was considered to be sufficiently representative of the crack deformation in the high strain hardening SS316 (M03) to give more accurate load-CMOD predictions.

Additional FE analyses were undertaken using the same specimen geometry as before but with idealised tensile properties generated using the modified Ramberg-Osgood power law for $0.44 \leq \sigma_{ys}/\sigma_{uts} \leq 0.98$. The equation used is given in Equation 5[21,22]

$$\varepsilon = \frac{\sigma}{E} + \alpha\left(\frac{\sigma}{\sigma_{ys}}\right)^{n-1}, \tag{5}$$

where $\alpha = 0.002$, $E = 207$GPa, and $\sigma_{ys} = 400$ MPa. The results were converted to engineering stress-strain curve, and the maximum ultimate tensile strain was set to 0.2. Relatively, decreasing n would lead to the increase of strain hardening (decreasing tensile ratio). The true stress-strain curve obtained based on Equation 5 was shown in Figure 9.

6 | RESULTS AND DISCUSSION

6.1 | Fracture toughness variation across the crack front

To compare the physical measurement of CTOD at the centre of the replica to a CTOD parameter determined from clip gauge data and standard formulae, it is necessary to consider whether the CTOD at the middle of the specimen is equivalent to the average CTOD across the crack front. This is not necessarily the case,[10,11,14] but Hutchison and Pisarski found that the curvature of the crack front greatly influences the resultant fracture toughness across the crack tip in the thickness direction.[23] For a straight crack front, the middle of the crack is most plane strain and gives the highest CTOD across the crack tip in the thickness direction.[11,23] However, where there is curvature of the crack (for example, as a consequence of fatigue pre-cracking), the opposite may be true. Therefore, the actual curvature of the fatigue pre-crack in real specimens can mitigate somewhat the CTOD variation through thickness. The measured crack curvature from the fracture faces of these test specimens was around 5% of the average crack length in all but one of the M01 specimens (which had 12%), and these levels are expected

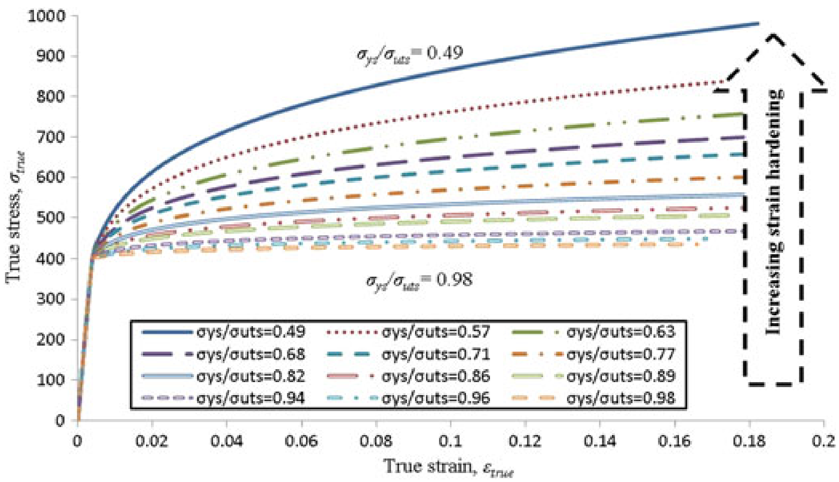

FIGURE 9 Idealised true stress-strain curve based on the modified Ramberg-Osgood power law [Colour figure can be viewed at wileyonlinelibrary.com]

to give a CTOD at the mid-thickness location less than 10% different to the average CTOD.[23] For the silicone replicas therefore, the effect of the location of sectioning was not considered to have a strong effect on the values of CTOD determined. The model cases used a straight crack front, but the results extracted from the centre of the model specimen are predicted to match more closely to results from a curved crack front in experimental specimens. Averaging the CTOD across the straight crack front model would underestimate the CTOD expected for an experimental specimen. The ASTM method is based on straight crack front models, which partly explains the lower plastic component of CTOD determined using the ASTM method in comparison to BS/ISO methods.

The elastic CTOD equation in BS/ISO, ASTM, and JWES suggest that plane strain CTOD was assessed in the equations. Green and Knott's observation on Charpy specimens and Kawabata et al size correction factor in WES 1108 suggest the specimen thickness used in this study (B = 20 mm) falls in the "plane stress-plane strain transition zone," where the specimen is not sufficiently thick to give a converged plane strain CTOD value.[17,24] Therefore, if an average CTOD across the crack tip is used as a representation of the plane strain CTOD, it would give conservative values if the crack front is straight, but overestimate a curved crack front. Although the elastic component is often only a small part of the total CTOD, this raises the question whether in sufficiently thin specimens the elastic component should be based on the plane stress elastic modulus instead. Nonetheless, in this study, CTOD in the middle of the crack is used as the definition of CTOD from both the silicone replicas and FE models, as this position is most plane strain, which corresponds to the equations with best accuracy.

6.2 | Definition of CTOD based on the opening of the original crack tip and the 45° intercept method

Two of the most well-known definitions of CTOD, the opening of the original crack tip and the opening based on the 45° intercept from the original crack tip, were extracted from the FE models with idealised tensile properties. For the ease of identification, the opening of the original crack tip is described as δ_0 and the 45° CTOD as δ_{45} in Figure 10. As the crack opens in the FE model, the surface of the blunted crack tip and the crack face no longer connect smoothly after a certain deformation limit, which is dependent on strain hardening. Beyond this deformation limit, the 45° CTOD concept collapses and is no longer representative of CTOD. Comparatively, the deformation limit for the 45° CTOD increases with strain hardening. For a consistent comparison for all strain hardening models, both definitions of CTOD were extracted from the range of 0.02 mm $< \delta_0 <$ 0.3 mm (which is below the deformation limit for the 3 steels) and normalised, δ_{45}/δ_0. Crack tip opening displacement values below 0.02 mm were not compared, as the differences in this CTOD range is dependent on the modelling technique used. The comparisons between the 2 CTOD definitions were shown in Figure 10.

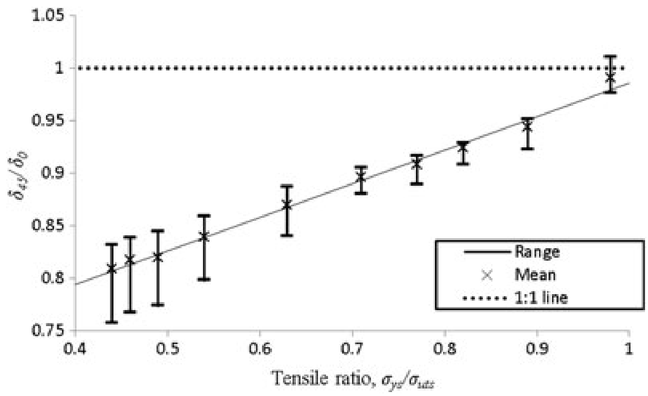

FIGURE 10 Comparison between the 45° crack tip opening displacement and the original tip crack tip opening displacement for different tensile ratio

Figure 10 shows that the difference between the 45° CTOD and the original tip CTOD is relatively constant for the same tensile ratio. Overall, the 45° CTOD underestimates the original tip CTOD, and the underestimation increases with the increase of strain hardening. The 45° CTOD was derived based on the HRR solution and requires a blunted crack tip to determine the point of the 45° intercept.[10] Figure 5 shows that crack extension is observed in the SRC, and raises difficulty for the measurement of the 45° CTOD. Therefore for consistency purposes, CTOD was defined based on the original crack tip in both the FE and experiments in the following study.

6.3 | Results of finite element modelling of CTOD

To investigate the accuracy of the FE model with respect to prediction of CTOD, the values obtained from the silicone replicas were compared to the CTOD (at the original crack tip) obtained from the FE model for the same CMOD (Figure 11). Crack tip opening displacement was defined from the original crack tip for both the FE model and silicone replicas. The results show that the FE consistently underestimated the CTOD measured on the silicone replica, except for low values of CTOD for the high strain hardening material, where the model overestimated the CTOD < 0.2 mm. The latter was due to the initial blunted crack tip assumed in the FE model,

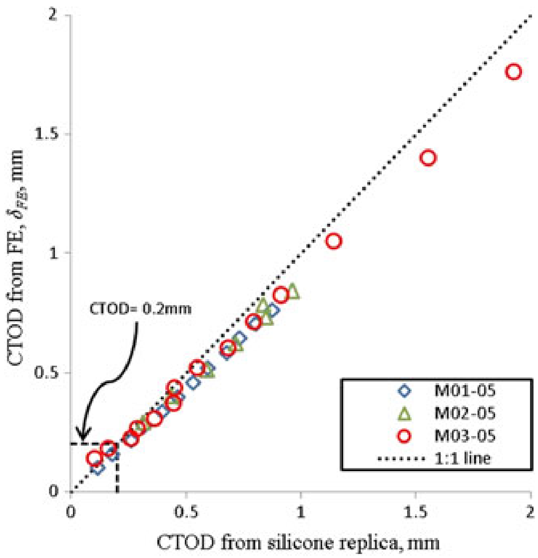

FIGURE 11 Prediction of crack tip opening displacement (CTOD) from finite element (FE) model compared to experimentally measured silicone replica data for three different strain hardening materials [Colour figure can be viewed at wileyonlinelibrary.com]

which predicted an artificially higher initial stress intensity factor compared to the experimental sharp fatigue pre-crack.[19,20]

To check the accuracy of the FE CTOD, percentage error of CTOD estimated by the FE model was calculated using

$$ERR_{FE} = \frac{\delta_{FE} - \delta_{SRC}}{\delta_{SRC}} \times 100\%. \tag{7}$$

Crack tip opening displacement below 0.2 mm was removed from the analysis, as the effect of the blunted crack tip is not representative of the experimentally sharp crack tip in the elastic dominated small scale yielding region. Figure 12 shows the ERR_{FE} for different

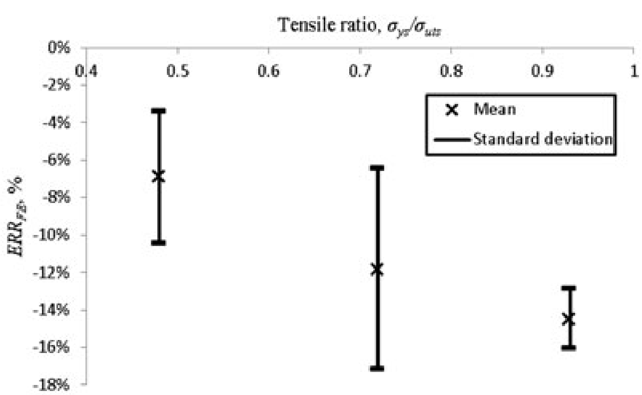

FIGURE 12 Finite element crack tip opening displacement estimation error (%) for different tensile ratio

tensile ratio. The underestimation of FE CTOD based on the SRC CTOD is fairly consistent for the same strain hardening material. The mean error was −6.92%, −11.81%, and −14.48% for σ_{ys}/σ_{uts} = 0.48, 0.72, and 0.93, respectively (M03, M02, and M01). Although there is a limited number of experimental strain hardening materials here to compare, the lowest error was observed on the high strain hardening material (σ_{ys}/σ_{uts} = 0.48), as the crack tip deformed mainly in a plastic manner rather than experiencing crack tearing, which is similar to the deformation mechanism in the FE model (Figure 5C).

6.4 | Results of SENB tests to different standard equations in a range of strain hardening materials

The results for the different methods to determine CTOD plotted together against the values measured from silicone replicas are shown in Figure 13A-D for M01, M02, M03, and an expanded view of M03, respectively.

In the low strain hardening material (M01), all 3 equations underestimate the CTOD from the silicone replica. The JWES estimation was most accurate compared to the silicone replicas, followed by ASTM then BS/ISO. JWES CTOD underestimated the SRC CTOD by a maximum of 17.5% at CTOD = 0.927 mm.

Similarly, the equations also underestimate CTOD for medium strain hardening material (M02, Figure 13B). For CTOD < 0.36 mm, the BS/ISO and JWES equations gave good CTOD estimations compared to the replicas. The BS/ISO and JWES equations underestimated the SRC CTOD by a maximum of 21% at CTOD = 0.836 mm.

In contrast to the low and medium strain hardening material, CTOD estimated for the high strain hardening material (M03, Figure 13C,D) was slightly overestimated with BS/ISO equation. The ASTM and JWES both gave conservative estimates of CTOD, with the JWES being fractionally closer to the SRC values of CTOD (Figure 13D).

The crack tip replicas in Figure 5 show that significant stable crack tearing occurs at the crack tip in the specimens with low and medium strain hardening properties (M01 and M02), whereas more plastic crack tip deformation and blunting was observed in the specimen with high strain hardening (M03). Tearing initiates in the early stages of loading for the low and medium strain hardening material (CTOD < 0.2 mm in Figure 5A,B), but has hardly initiated in the high strain hardening material even at a CTOD of 1 mm. This explains why the numerical model (which does not include tearing) was a more accurate predictor of the higher strain hardening

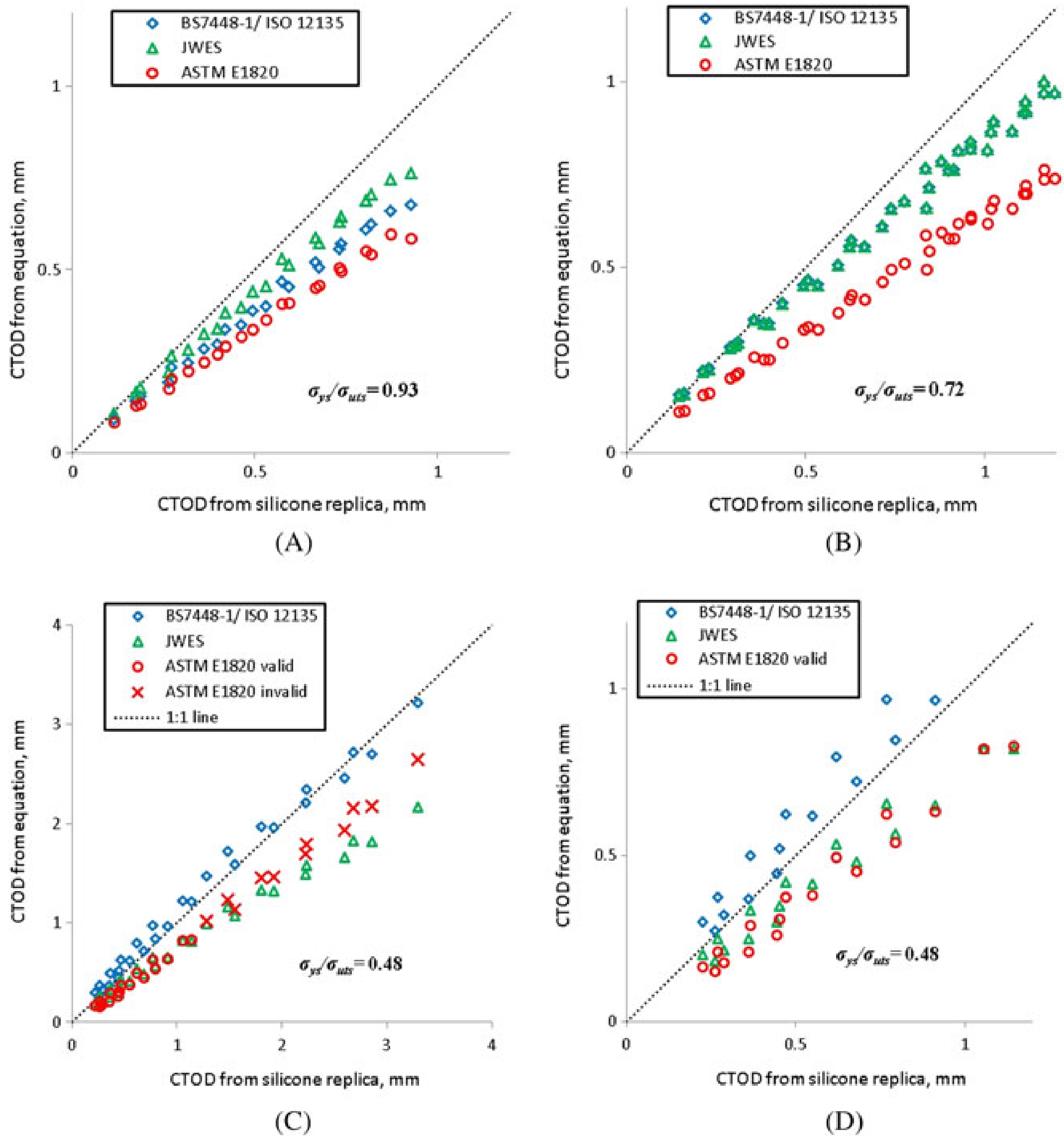

FIGURE 13 Comparison of crack tip opening displacement (CTOD) methods for M01, M02, M03, and expanded view for M03 specimen (A, B, C, and D [expanded view of C] respectively) [Colour figure can be viewed at wileyonlinelibrary.com]

material, which deformed by continual blunting. Generally, the FE model was consistently closer to the silicone replica CTOD measurements than any of the standard formulae assessed (Figures 11 and 13) over the range of CTOD and strain hardening materials studied. Crack tip opening displacement was extracted from the FE models with idealized material properties (Figure 9) and corrected to the ERR_{FE} (Figure 12) based on the linear fitting to the mean error. The corrected FE CTOD, $\delta_{FE\ corr}$, was used as the baseline CTOD. The standardised equations were used to calculate CTOD based on the load-CMOD data obtained from the FE model. Crack tip opening displacement from equations were normalised to the corrected FE CTOD for validation. Data were compiled for the range of 0.02 mm $\leq \delta_{FE\ corr} \leq$ 1.00 mm (Figure 14). Crack tip opening displacement below 0.02 mm were not considered. The bar shows the upper and lower limit of the CTOD range, and the crosses show the mean value for the standardised CTOD equations. The dotted line connects the mean normalised CTOD to show the trend of CTOD difference for different strain hardening properties.

Similar to that predicted experimentally in Figure 13, the BS/ISO equation overestimated the corrected FE CTOD for the strain hardening materials up to $\sigma_{ys}/\sigma_{uts} \approx 0.68$. However, the JWES and ASTM CTOD consistently underestimated the corrected FE CTOD by around 10% to 15% regardless of strain hardening properties, and this may be more useful for design purposes. The ASTM equation showed a

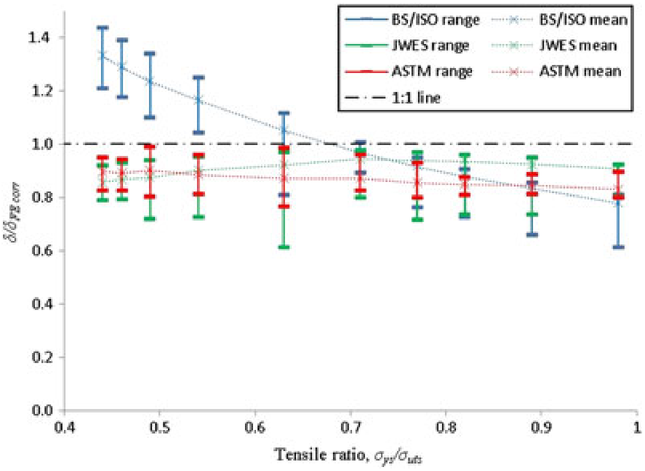

FIGURE 14 The trend of standardized equation prediction of crack tip opening displacement for different strain hardening properties [Colour figure can be viewed at wileyonlinelibrary.com]

narrower range of results across the CTOD range, but the JWES gave average results closer to the model predictions.

6.5 | Discussion of the different standard equations

ASTM converts CTOD from J and recognises that J no longer characterises the crack tip conditions when high plastic deformation is experienced at the crack tip. The standard defines the criterion for the maximum value of δ by[4]

$$\delta_{max} = \frac{B_0}{10m}. \tag{6}$$

m is defined in Equation 3a. ASTM CTOD values not conforming to Equation 6 are represented by cross markers (Figure 13C).

Conversely, the experimental results show that the JWES formula, despite being developed only for CTOD up to 0.2 mm, seems to underestimate measurements for all the different strain hardening steel and most accurate for the low and medium strain hardening steel tested in this work. Even for the highest strain hardening materials, the JWES underestimated CTOD at CTOD > 0.2 mm, which would be conservative for assessments of fitness-for-service or acceptance criteria. This approach allows CTOD to be determined using a method based on rigid rotation and displacement of the crack flanks, while ensuring reasonable accuracy across a wide range of strain hardening behaviour.

The BS/ISO formula does not consider strain hardening, and this is demonstrated by a very different trend when this equation is used for high strain hardening material; a slight overestimation of CTOD. The difference is not large, but otherwise the method shows reasonable agreement. However, the risk with overestimation of CTOD is that it predicts higher fracture toughness in a material than is actually the case, which can be potentially unsafe.

The ASTM method was able to adapt to prediction of CTOD in high strain hardening material, but somewhat underestimated CTOD for low and medium strain hardening materials. For applications where the use of clip gauges are challenging for SENB specimens (for example, high temperature or environmental tests), the ASTM approach offers a method to determine CTOD from J without necessarily needing to measure the crack mouth displacement, while also ensuring reasonable accuracy across a range of strain hardening materials.

The optimum choice for a standard method to determine CTOD is one which gives accurate, but conservative estimates of CTOD for a wide range of materials. From the comparison of standards shown here, the JWES equation seems to show promise as an improved rigid rotation approach to determine CTOD for inclusion into future international fracture toughness testing standards.

7 | SUMMARY AND CONCLUSIONS

The experiments were performed to evaluate CTOD in test specimens and revealed that the crack tip deformation mechanism in different steels vary, leading to some differences when compared to the FE results. Single-edge notched bend fracture toughness specimens in high strain hardening material such as 316 stainless steel deform at the crack tip by continued "blunting" upon increased loading before tearing. This is different to the behaviour of medium and higher strength steels, where stable ductile tearing initiates after only a small amount of blunting at the crack tip during a fracture toughness test. The assumption of a crack tip deforming by continued blunting in a FE model was accurate and conservative for the prediction of CTOD for the high strain hardening steel. However, caution should be exercised when making predictions within the elastic-dominated CTOD region, where an initial blunt crack tip could lead to overprediction of CTOD in the FE model. Nevertheless, the FE model used in this work managed to produce relatively accurate predictions of CTOD beyond the elastic dominated loading region.

Crack tip opening displacements calculated using the BS 7448-1/ISO 12135, JWES, and ASTM E1820 equations were compared to results obtained experimentally by SRC and from the FE modelling. From the results of the comparisons, the following conclusions were made:

- Due to the limited versatility of the 45° CTOD beyond crack initiation, in numerical models, CTOD is better defined as the opening of the original crack tip, as it gives better reliability regardless of the crack tip condition.
- The BS/ISO equation overestimates CTOD for strain hardening materials with yield to UTS ratios below 0.68.
- For $0.44 \leq \sigma_{ys}/\sigma_{uts} \leq 0.98$, the JWES and ASTM equations gave a consistent but conservative estimation of CTOD.
- The JWES equation shows promise as an improved rigid rotation approach to determine CTOD for inclusion into future international fracture toughness testing standards.
- The ASTM approach offers a method to determine CTOD from J without necessarily needing to measure the crack mouth displacement, while also ensuring reasonable accuracy across a range of strain hardening materials.

ACKNOWLEDGEMENTS

The authors wish to acknowledge the funding and facilities provided by TWI and NSIRC for this work, and thank Philip Cossey and Dan Bloom for assistance in the crack replication test. The authors also appreciate the updates and discussion on the silicone crack replication method with Prof Tetsuya Tagawa at JWES.

ORCID

W.L. Khor http://orcid.org/0000-0001-7699-8194
P. Moore http://orcid.org/0000-0002-2121-7669
C. Brown http://orcid.org/0000-0001-6155-0717

REFERENCES

1. Wells AA. Crack opening displacements from elastic-plastic analyses of externally notched tension bars. *Eng Fract Mech*. 1969;1:399-410.
2. BSI. BS 7448-1:1991 - Fracture mechanics toughness tests—part 1: method for determination of KIc, critical CTOD and critical J values of metallic materials. BSI 1991.
3. ISO. ISO 12135 - 16 Metallic materials—unified method of test for the determination of quasistatic fracture toughness. ISO 2016.
4. ASTM. ASTM E1820-13 - Standard measurement of fracture toughness. ASTM, 1–54 2014.
5. JWES. WES 1108: 2014 Standard test method for crack-tip opening displacement (CTOD) fracture toughness measurement. *The Japan Welding Engineering Society* 2014.
6. Wu S-X. Relationship between the J-integral and crack opening displacement for pure power hardening material. *Int J Fract*. 1981;17:R63-R66.
7. Lin IH, Anderson TL, de Wit R, Dawes MG. Displacements and rotational factors in single edge notched bend specimens. *Int J Fract*. 1982;20:R3-R7.
8. Ingham T, Egan GR, Elliott D, Harrison TC. The effect of geometry on the interpretation of COD test data. In: *Practical Application of Fracture Mechanics to Pressure-Vessel Technology, Institution of Electrical Engineers*. Savoy Place, London: Institution of Mechanical Engineers; 1971:200-208.
9. Wei L, Pisarski HG. ESIA9 - 9th International conference on engineering structural integrity assessment. *ESIA9 - 9th International Conference on Engineering Structural Integrity Assessment*. Beijing, China: EMAS; 2007.
10. Wang Y-Y, Reemsnyder HS, Kirk MT. Inference equations for fracture toughness testing: numerical analysis and experimental verification. *ASTM STP 1321* 1997;469–484.
11. Khor W, Moore PL, Pisarski HG, Haslett M, Brown CJ. Measurement and prediction of CTOD in austenitic stainless steel. *Fatigue Fract Eng Mater Struct*. 2016;39:1433-1442.
12. Shih CF. Relationships between the J-integral and the crack opening displacement for stationary and extending cracks. *J Mech Phys Solids*. 1981;29:305-326.
13. Tagawa T, Kayamori Y, Ohata M, et al. Difference between ASTM E1290 and BS 7448 CTOD estimation procedures. *Weld World*. 2010;54:R182-R188.
14. Tagawa T, Kawabata T, Sakimoto T, et al. Experimental measurements of deformed crack tips in different yield-to-tensile ratio steels. *Eng Fract Mech*. 2014;128:157-170.
15. Pisarski H, Malpas A, Horn A, Amadioha A, Tkach Y, Barron A. Experimental comparison of CTOD estimated according to BS7448 & ASTM E1820. *ASTM workshop on Critical Evaluation of Calculation Methods for Crack-Tip Opening Displacement (CTOD), San Antonio, TX:* 2010.
16. Kayamori Y, Inoue T, Tagawa T. Transformation of BS7448-CTOD to ASTM E1290-CTOD. *ASME Pressure Vessels and Piping Division Conference* 2008:1–8.
17. Kawabata T, Tagawa T, Sakimoto T, et al. Proposal for a new CTOD calculation formula. *Eng Fract Mech*. 2016;159:16-34.
18. Tagawa T, Haramishi Y, Minami F. Stress relaxation behavior of low carbon structural steels. *Q J Jpn Weld Soc*. 2011;29:48-54.
19. Spink GM, Worthington PJ, Heald PT. The effect of notch acuity on fracture toughness testing. *Mater Sci Eng*. 1973;11:113-117.
20. Taggart R, Wahi KK, Beeuwkes Jr. R. Relationship between the fracture toughness and the crack tip radius. *ASTM STP 605* 1976:62–71.
21. MacDonald M, Rhodes J, Taylor GT. Mechanical properties of stainless steel lipped channels. *15th International Specialty Conference on Cold-Formed Steel Structures*, St. Louis, Missiuri, U.S.A; 2000:673–686.

22. Ramberg W, Osgood WR. *Description of stress-strain curved by three parameters*. Washington, DC: National Advisory Committee for Aeronautics; 1943.

23. Hutchison E, Pisarski HG. Effects of crack front curvature on J and CTOD determination in fracture toughness specimens by FEA. *Proceedings of the ASME 2013 32nd International Conference on Ocean, Offshore and Arctic Engineering OMAE 2013*, Nantes, France; 2013.

24. Green G, Knott JF. On effects of thickness on ductile crack growth in mild steel. *J Mech Phys Solids*. 1975;23:167-183.

How to cite this article: Khor WL, Moore P, Pisarski H, Brown C. Comparison of methods to determine CTOD for SENB specimens in different strain hardening steels. *Fatigue Fract Eng Mater Struct*. 2017. https://doi.org/10.1111/ffe.12718